Modelling Moment Redistribution in Continuous Reinforced Concrete Beams

Abdul R. Azizi

BSc (Eng.) MSc (Eng.)

A Thesis submitted for the Degree of Ph.D. in the School of Engineering University of Durham

October 1996

ABSTRACT

This thesis investigates the relationship between ductility and moment redistribution in reinforced concrete beams. Parameters that reflect the relationship between the two are identified from both an experimental and a theoretical point of view, as well as in terms of the various provisions in national codes and standards.

The work described in this thesis is in two parts. Part One presents the experimental investigation made on seventeen test specimens of two-span continuous beams of various geometrical properties and ratios of reinforcement. The results were analysed by both existing software and software developed by the author. The test results and analyses for the seventeen beams are presented, with the reinforcement strains being measured by strain gauging the reinforcement internally. The concrete strains were measured using Demecs, and the deflections under the two point loads were measured by dial gauges. The experimental results indicate that redistribution may start even before development of any cracks on the surface of the beams. It was also found that the relative stiffness influenced the manner and degree of moment redistribution during all load stages.

Part Two presents the numerical model developed by the author which is based on the second moment area theorem applied to a propped cantilever centrally loaded, being the mirror image of the two-span continuous beams loaded in the middle of each span. The model employed multi-linear moment curvature relationships along the length of the beam, based on the reinforcement layout, to calculate forces, moments, deflection, rotation, curvatures and redistribution of the modelled beam. The modelled results were then compared with the experimental data along with other modelled results from various codes and standards. As a consequence of the experimental and modelling work, suggestions were made to vary the moment redistribution criteria used in the British Standard for reinforced concrete design. Further experimental work is proposed to materialise the work done into definite recommendations in design practice.

Special Gratitude
To
my Beloved Wife Taghrid
and my Beloved Children
Dimah
Danah and Mohammad

ACKNOWLEDGEMENTS

I am extremely grateful for the technical support given by the concrete laboratory technical staff. In particular, I thank Mr. Brian P. Scurr for his assistance during all my time in the Department, and Miss Deborah Dawes for the effort in installing several thousand strain gauges in the test beams.

But most of all, I would like to thank my supervisor, Dr. Richard H. Scott, for his continuous support and advice throughout the research program.

The experimental work described in this thesis was funded by the Science and Engineering Research Council, now the Engineering and Physical Science Research Council, and their support for this work is gratefully acknowledged.

I am grateful to Professor A. W. Beeby for his useful comments and
I am also extremely grateful for Miss Julie King for proof reading this thesis.

DECLARATION

No material in this thesis has previously been submitted for a degree in this or any other university.

The work in Part One was undertaken jointly with my supervisor Dr. Richard H. Scott as part of my contract as a Research Assistant in the University of Durham. The analysis of the results and the development of the new software were my own work

The work in Part Two is my own. I wrote all the computer software developed in this part.

STATEMENT OF COPYRIGHT

CONTENTS

LIST OF TABLES

LIST OF FIGURES

NOTATION

Δl_i	Gauge surrounding Length
A_s	Area of tension Steel
A_s'	Area of compression steel
b	Section breadth
a_v	Shear Span (distance from point load to the nearest free support)
d	Effective depth of a section
d'	Depth from top compression face to the centre of the compression reinforcement
$d_1..d_n$	Block lengths
d_x	Distance between tension and compression reinforcement
E_c	Concrete modulus of elasticity
E_{ci}	Tangent concrete Youngs modulus Model Code Eq 2.1-16
E_{co}	2.15×10^4 MPa
EI	Flexural stiffness of a section
$EI_{elastic}$	Elastic flexural stiffness of a section
E_s	Steel Modulus of Elasticity
f_c'	Cylinder compressive strength of concrete
f_c''	$0.85 f_c'$
F_{cc}	Forces in concrete in compression
f_{cmo}	10 MPa
f_{ct}	Concrete tensile strength (MPa)
F_{ct}	Forces in concrete in tension
$f_{ctk\ 0.05}$	Minimum (lower bound) strength of concrete in tension according to (Eurocode 2)
$f_{ctk\ 0.95}$	Maximum (upper bound) Strength of concrete in tension according to (Eurocode 2)
$f_{ctk,max}$	Maximum (upper bound) strength of concrete in tension according to (CEB-FIP Model Code)
$f_{ctk,min}$	Minimum (lower Bound) strength of concrete in tension according to (CEB-FIP Model Code)

$f_{ctko,max}$	1.85 MPa
$f_{ctko,min}$	0.95 MPa
f_{cu}	Cube compressive strength of concrete
f_s	Stress in the tension reinforcement
F_{sc}	Forces in reinforcement in compression
f_{st}	Rupture strength of the reinforcement.
F_{st}	Forces in tension reinforcement
f_y	Yield strength of the reinforcement
h	Total depth of a beam section
I_c	Cracked section modulus
I_e	Effective section modulus
I_g	Gross section modulus (uncracked neglecting reinforcement) $bh^3/12$
I_u	Uncracked section modulus (including reinforcement)
k	Neutral axis depth factor
k'	Constant used in EC 2 equal to $k' = 1.10E_c\left(\frac{\varepsilon_{ce}}{\left(f_c' + 8\right)}\right)$
K_{III}	Constant used in MC 90 equal to $K_{III} = \frac{\left(M_u - M_y\right)}{\left(\varphi_u - \varphi_y\right)}$
k_u	Neutral axis depth factor at ultimate
l	Total beam span (length)
l_1	Beam length from the propped end to Load position at midspan
l_2	Beam length from the load position to the fixed end support
l_p	Plastic hinge length
l_u	Distance from fixed end support to point of zero moment at ultimate
l_y	Distance from fixed end support to point of zero moment at yield
M	Applied moment on a section
M_{cr}	Cracking moment

M_{ctm}	The moment caused by the concrete in tension According to BS8110
M_{net}	Net applied moment which the moment
M_p	Plastic moment of resistance
$M_{span,cal}$	Modelled (*Calculated*) bending moment at span.
$M_{span,elastic}$	Elastic bending moment at span.
$M_{sup,cal}$	Modelled (*calculated*) bending moment at support
$M_{sup,elastic}$	Elastic bending moment at support
$M_{u,span}$	Moment at span when the support reaches ultimate
M_y	Yield moment
n	$\varepsilon_c/\varepsilon_{ce}$
$n_1..n_m$	Strip number up to n_m(maximum number of strips)
P	Applied load
P_u	Ultimate load
q	Tension reinforcement Index ($\rho f_y/f_c''$)
q'	Tension reinforcement Index ($\rho' f_y/f_c''$)
$R_1, R_2, R_3,$	Factors for (Baker equation for plastic hinge length)
R_{left}	Reaction at the left Side of the beam (propped End)
R_{right}	Reaction at the right Side of the beam (fixed Support)
x	Neutral axis depth
x_b	The neutral axis depth at the balanced condition.
x_{zero}	Distance from propped End to point of zero bending moment
x_u	Neutral axis depth at ultimate
y	Variable beam distance (integration length)
y_t	Distance from neutral axis Position to extreme fibre of concrete (neglecting reinforcement h/2)
z	Distance from section of maximum moment to section of zero moment.
γ	Factor relating the maximum compressive stress from flexure to the axial strength obtained from cylindrical test specimens 0.85.

μ_c, μ_t	Numerically calculated constants based on integrating functions of the ratios of compressive and tensile strain respectively.
γ_m	Concrete partial safety factor
δ	Deflection
ν	Factor in Baker Equation (0.57)
α	Modular Ratio $\alpha = \frac{E_s}{E_c}$
β	Percentage of moment redistribution
β_1	Bond Coefficient of the Bar (Using EC 2)
β_2	Duration of Load Coefficient (Using Eurocode 2)
β_b	Coefficients Representing Bond quality of the Steel Bars (Using the Model Code)
σ	Stress
ρ	Tension steel ratio A_s x100/bd
ρ'	Compression steel ratio A_s' x 100/bd
ρ''	Volumetric ratio of a stirrup to concrete enclosed by two stirrups
ρ_b	Balanced ratio of reinforcement
ε_{200}	Average Strain Calculated over 200 mm Length
ε_c	Concrete compression Strain
δ_{cal}	Modelled (calculated) deflection under the mid-span load
ε_{ce}	Compressive strain at the extreme edge of concrete, -2200 microstrain
$\varepsilon_{c,lim}$	Limiting concrete compressive strain on the descending branch of the concrete stress strain relationship.
ε_i	Strain from local strain gauges
ε_{cu}	Ultimate concrete compression strain
ε_g	Unit elongation
ε_s	Tension steel strain
ε_s'	Compression steel strain
ε_{us}	The tension reinforcement rupture strain

ζ	Distribution coefficient given by Eurocode 2
θ	Rotation
θ_p	Plastic rotation capacity.
θ_t	Total rotation capacity
φ	Curvature at a section
φ_u	Ultimate curvature
φ_y	Yield curvature
φ_1 , φ_{1r}	Uncracked curvatures corresponding to the action of the applied moment and the cracking moment.
φ_2, φ_{2r}	Cracked curvatures corresponding to the applied moment and cracking moment respectively.
κ	$0.85 - 0.008(f_c' - 30)$
ω	General parameter to be calculated adopted by Eurocode 2
ω_I	General parameter to be calculated at the uncracked state i.e. curvature
ω_{II}	General parameter to be calculated at the cracked state i.e. curvature

PART I

EXPERIMENTAL WORK ON TWO-SPAN CONTINUOUS REINFORCED CONCRETE BEAMS

CHAPTER ONE

1. INTRODUCTION

Studies on ductility and moment redistribution in reinforced concrete structures have been made in both experimental and theoretical fields, albeit with some shortcomings. The experimental approach depended on limited experimental techniques such that strains in reinforcement were not measured or investigated accurately, whilst the theoretical approach depended on empirical studies and lacked data. With the advent of the new European Concrete Code, interest increased in moment redistribution. It was therefore proposed that additional research was needed on this subject. The Science and Engineering Research Council (S.E.R.C), now the Engineering and Physical Science Research Council, granted support to carry out research into the subject of moment redistribution. The research carried out in this study provided new directions for the evaluation of deformations and moment redistribution in reinforced concrete continuous beams.

1.1 Objective

The objective of this research was to improve the development of a realistic method for predicting redistribution and deformational properties of reinforced concrete continuous beams, i.e. deflection, rotation, and curvature. This was to be accomplished in three stages.

(a) Testing of two-span continuous beams. These were loaded at mid-span and various reinforcement ratios and bar size diameters were used. Bars over the critical span and support sections were strain gauged to obtain accurate and detailed reinforcement strain distributions. Parameters investigated in the experimental work were loads, moments, strains and deflections.

(b) Numerical modelling of the experimental results by applying the moment area theorems to the curvature distribution of a propped cantilever having the same properties as the experimental beams. To find the curvature distribution, true stress strain relationships were used to formulate true moment curvature relationships for each portion of the modelled beam. Using an incremental

technique that employed the principles of moment area theorems, complete deformation profiles were formed.

(c) Comparison of modelled results with the experimental data. Major codes moment curvature assumptions were also tested using the new model. Throughout this research, experimental data acquired from the test beams were used to examine the validity of the proposed model and its procedure.

1.2 Scope

This thesis deals with the experimental and analytical aspect of moment redistribution of doubly reinforced rectangular cross-sections of two-span continuous beams. It is limited to under-reinforced beams made of normal weight concrete.

This thesis is divided into two parts. The first part comprises Chapters One to Five. Chapter One provides an introduction to moment redistribution and the factors influencing it. Chapter Two deals with an historical survey of both experimental and theoretical works carried out on the subject of moment redistribution since 1935 up to the present day. Chapter Three describes the new experimental work carried out on two-span continuous beams using the available testing technique of installing strain gauges in the reinforcing bars. Chapter Four describes the software that the author developed to process and analyse the data generated by the test beams. Chapter Five presents, analyses and discusses the experimental results.

The second part of this thesis comprises Chapters Six to Nine and deals with the numerical modelling procedure of a centrally loaded propped cantilever beam and its applications. Chapter Six describes the theoretical background and the programming technique of the numerical model, which is based on the principles of moment area theorems. This model was used to calculate loads, moments and deformations (i.e., curvatures, rotations and deflections). Chapter Seven presents the moment curvature relationship formulae according to the provisions in the following four reinforced concrete standards:

1. The British Standards BS 8110, The Structural Use of Concrete (1985)
2. Building Code Requirements for Structural Concrete (ACI 318-95)

3. Eurocode 2: Design of concrete structures: Part 1. General rules for buildings (1992)
4. Comité Euro-International Du Beton CEB-FIP Model Code (1990).

Furthermore, it presents the moment redistribution criteria used in the codes above and also in others.

Chapter Eight compares the experimental results with the modelled codes' moment curvature relationships. The variables considered were moment redistribution, load deflection, curvature distribution, plastic hinge lengths, rotations and neutral axis depth ratios. In this chapter, it is shown that the neutral axis depth ratio versus redistribution graphs suggest that the moment redistribution design criteria, particularly the BS 8110 code, should be altered. Chapter Eight also demonstrates the applicability and use of the model as a parametric tool. Chapter Nine presents the conclusions and suggestions for further research. Based on the experimental and modelled results, suggestions are made to vary the redistribution curve in BS 8110.

1.3 Preface

The realistic determination of the response of reinforced concrete structures in bending demands a knowledge of the inelastic flexural behaviour of reinforced concrete sections. This behaviour results from the non-linear stress strain characteristics of both the concrete and the reinforcement. These non-linear stress-strain relationships, and the development of cracks along a structure that occur due to increasing load, causes the moment curvature relationship along a beam to vary.

1.3.1 Moment Curvature Relationship

Reinforced concrete sections exhibit a non-linear moment curvature relationship. This best describes its behaviour since it accounts for the inelasticity of the concrete and the reinforcement. A typical moment curvature relationship for a reinforced concrete section up to failure is illustrated in **Figure 1-1,** for which the theoretical relationship is stated in the following **Equation 1-1**:-

$$M = E_C I \varphi \qquad \textit{Equation 1-1}$$

Where:-

M = The applied bending moment on the section.

E_C = Modulus of elasticity of the concrete.

I = The second moment of area of concrete section (including the reinforcement).

φ = Curvature of the section.

$E_C I$ = Flexural stiffness of the section.

The value of E_C is derived from the stress strain relationship of the concrete in compression. The value of (I) is the second moment of area of the beam section. This value is conventionally calculated based on the condition of the beam cross section being uncracked or fully cracked. **Figure 1-2** shows a diagram of both uncracked and cracked sections.

The effect of the reinforcement is taken into account by transforming steel areas to equivalent concrete areas using the ratio of the reinforcement modulus of elasticity to the concrete modulus. The ratio is represented in the following equation:

$$\alpha = \frac{E_s}{E_c} \qquad \textit{Equation 1-2}$$

Where:-

α = The modular ratio.

E_S= The reinforcing steel modulus of elasticity.

The bending moment acting on a section is caused by an applied load on the beam, (i.e., point load, uniformly distributed load, etc.). Calculating curvature at both uncracked and cracked sections is possible from the strain profile across the depth of the section as shown in **Figure 1-3**. Curvature of a section may conveniently be taken as the algebraic sum of the tension and compression strains on both sides of the neutral axis divided by the distance between them.

$$\varphi = \frac{\varepsilon_c}{x} = \frac{\varepsilon_s}{d-x} = \frac{\varepsilon_s - \varepsilon_s'}{d_x} \qquad \textit{Equation 1-3}$$

Where:-

ε_C= Concrete strain at the extreme compression face of the concrete.

ε_S= Tension steel strain.

ε_S' = Compression steel strain.

d = Effective depth of the cross section.

d_x = Distance between tension and compression reinforcement.

x = Neutral axis depth of the section.

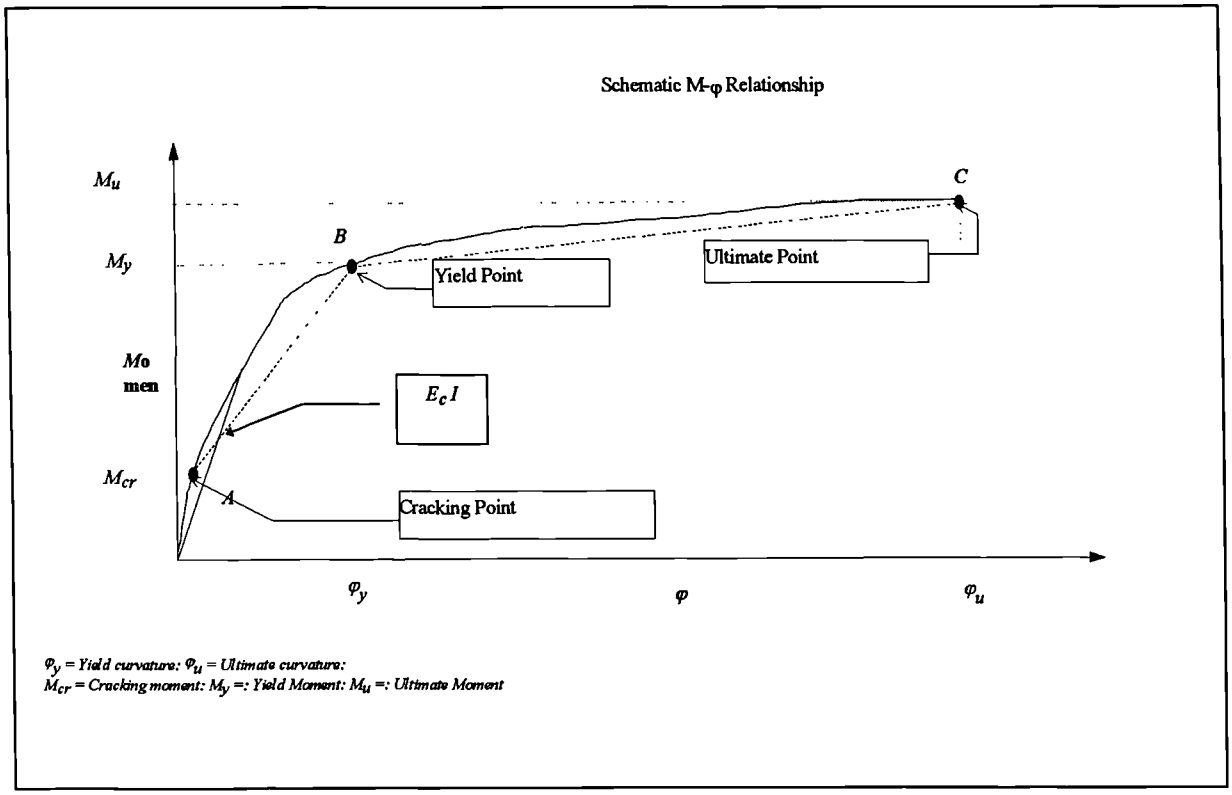

Figure 1-1: Moment curvature relationship of a reinforced concrete section

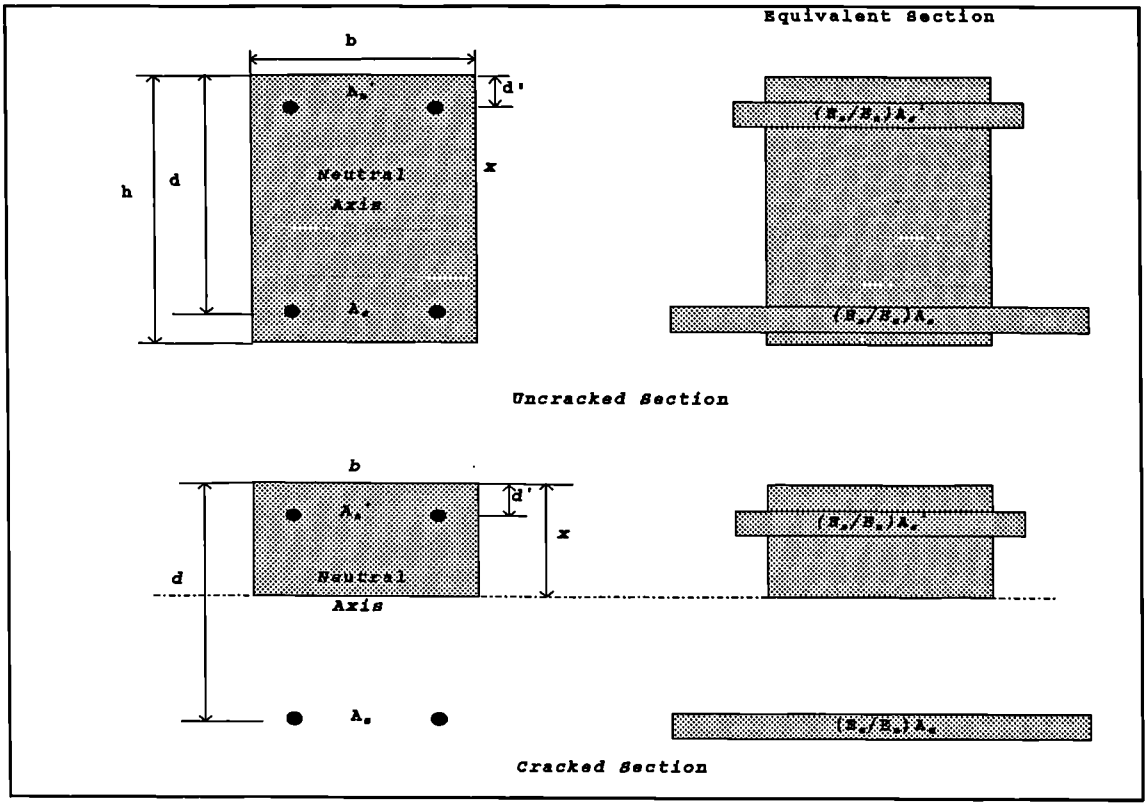

Figure 1-2: Equivalent sections for uncracked and cracked beam cross sections.

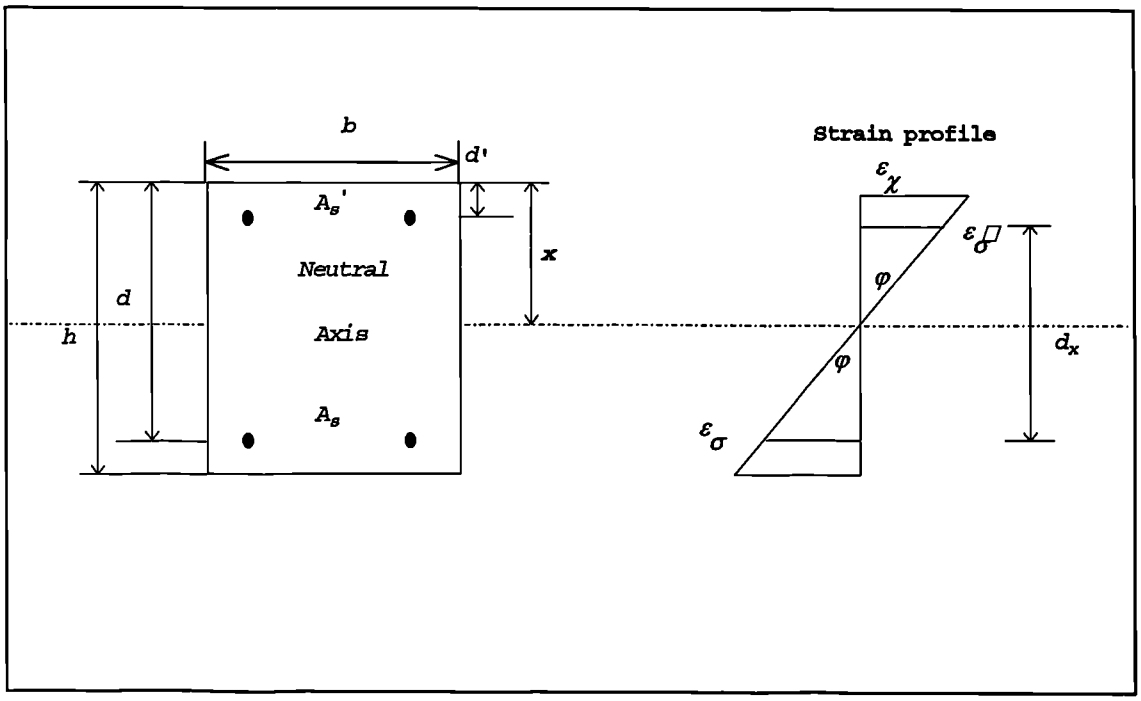

Figure 1-3: Strain distribution in a reinforced concrete section.

1.3.2 Flexural Stiffness

Flexural stiffness, (the slope the moment curvature relationship), is the product of two independent variables: the modulus of elasticity of the concrete (E_C), and the second moment of area (I) of the cross section including the reinforcement.

Calculations of the deformations of a member, (i.e. curvature, rotation, and deflection) require knowledge of its flexural stiffness. In the early stages of loading, when a reinforced concrete section is uncracked, the reinforcement has little effect and the stiffness is approximately equal to that of a plain concrete member (Regan and Yu, 1973).

$$EI = E_C I_g \qquad \text{Equation 1-4}$$

Where:-

I_g = The second moment of area of the concrete cross-section about its centroidal axis in the plane of bending neglecting the reinforcement.

EI = Flexural stiffness of a section

The curvature of any section at this early stage increases in direct proportion to the applied moment M.

As the load increases on the structure to a point beyond the tensile strength of the concrete, it causes the concrete to crack. Therefore, it is no longer possible to calculate the curvature based on the uncracked stiffness. The alternative is to base curvature calculation on the cracked stiffness which is the product of the cracked section modulus (I_C) and the concrete modulus of elasticity (E_C).

$$\varphi = \frac{M}{E_c I_c} \qquad \text{Equation 1-5}$$

Where:-

I_C = The cracked second moment of area including the reinforcement.

Flexural stiffness is not uniform. In a real situation, for example in the beam shown in **Figure 1-4**, cracks develop along the length of a beam as load is applied.

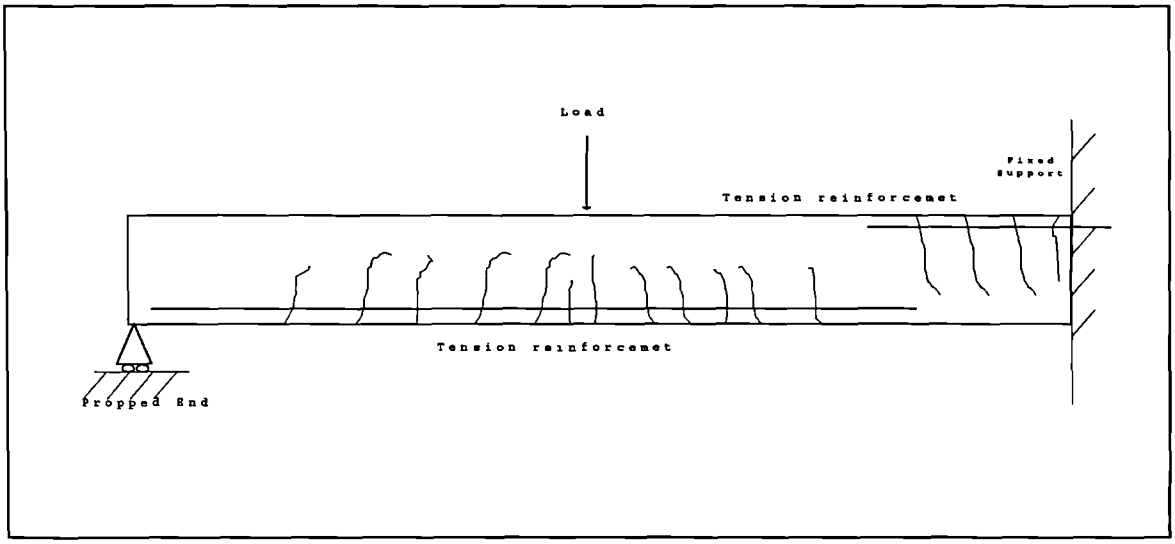

Figure 1-4: Crack development in a reinforced concrete beam in bending

The strain in the tension reinforcement peaks where it crosses a crack, and minimises away from the crack as load is shared with the surrounding concrete due to the action of bond. As a result, the stiffness of the beam varies along its length. It is a minimum at the crack positions, whilst between the cracks it increases due to the contribution of the concrete in tension. This contribution of the tensile concrete to the stiffness of a reinforced concrete member is called Tension Stiffening, (see Scott, 1985). The presence of this phenomenon makes the evaluation of the stiffness of a reinforced concrete member more complicated. However, it may be accounted for by using a non-linear moment curvature relationship for the beam's section as discussed next.

From **Figure 1-1**, it is seen that with the exception of a possible brief period when the section is initially uncracked, the moment curvature relationship over the rest of the load history is non-linear. Results from tests (see Burnett and Yu, 1964) indicated that the moment curvature relationship varies from section to section along a

reinforced concrete member. Before the reinforcing steel yields, the (M-φ) relationship is governed by the reinforcement and the concrete's behaviour. When the reinforcing steel reaches the yield point, the curvature then increases rapidly with little increase in moment as shown in **Figure 1-1.** At this stage, a plastic moment develops, and a plastic hinge is said to form at the yielded section. In a statically indeterminate beam, the flexural stiffness (E_cI), is considerably reduced when the bending moment at that section reaches levels of yield moment and beyond. This reduction in stiffness, albeit almost at a constant moment between the yield point up to failure, allows the tension reinforcement to undergo large plastic strains. The plastic strains result in rotations limited by the overall ductility of the section, (i.e. ductility of concrete and the reinforcement). This consequently causes a reduction from the elastic moment at the section i.e. hogging moment redistributes and increases the moment at the sagging section as a consequence. To account for this redistribution in full, knowledge of the moment curvature relationships of the sections of a reinforced concrete member and their flexural stiffnesses is required. Several approaches have been presented to model this non-linearity. Some approaches go beyond ultimate (maximum) and account for the descending branch of the moment curvature relationship, such as the work carried out by Rosenblueth and De Cossio (1964). They analysed a fixed-ended beam under two symmetrical concentrated loads near its supports. Two trilinear M-φ diagrams identical up to their peak points, but having different descending branches (one steeper than the other, and both having definite termination points) were assumed for all cross-sections of the beam. Cranston (1965) analysed a pin-ended portal frame subject to symmetrical two-point loading on the beam span, which he had tested earlier. Two moment curvature relationships with falling branch were considered: one at the central section of the beam, and the other in one column just below its intersection with the beam. Barnard and Johnson (1964) analysed two simply supported steel concrete composite beams subjected to symmetrical two-point loading. Non-linear moment-curvature relationships, analytically obtained, were used in computations. One common feature of the methods used by all the above researchers is that they are based, explicitly or implicitly, on an integration of curvatures along the structural member, associated with a non-linear moment curvature relationship. Another approach, adopted by the American Concrete Institute Code, ACI 318-95, BS 8110, 1985, the

European Code EC2 1992 and the CEB-FIP Model Code 1990 respectively, was to divide the moment curvature relationship into three linear sections, as shown in **Figure 1-1.** This thesis aims to show how the various codes and standard approaches to the moment curvature relationship compare with the author's own approach.

1.3.3 Ductility and Moment Redistribution

Reinforced concrete sections exhibit a non-linear behaviour with increasing load or moment that causes cracks to develop, thus making stiffness variable and non-linear along the beam. Indeterminate beams are designed to exhibit ductility under ultimate (maximum) loads. Ductility is the ability of reinforced concrete elements to deform, while maintaining their load carrying capacity. This ductility is a result of the yielding of the reinforcement under tensile load. Deformation is referred to as plastic and normally occurs over a short length of the beam (the plastic hinge length). The formation of enough plastic hinges eventually leads to the collapse of the structural element. This plastic hinge formation only occurs in flexural members. It is possible to utilise this ductility of flexural members in design. This is done by analysing the flexural member (a continuous beam) under the ultimate design loading, and then redistributing the bending moments within the beam. The resulting moments must still be in equilibrium with the design loading. Redistribution is made to reduce the moments, and hence the area of reinforcement required at the section with the highest moments. This is done by increasing the moments in the middle of the beam span, and consequently increasing the area of reinforcement required in the mid-span. This makes the structure easier to detail and construct.

Ductility ensures that the beam is capable of undergoing rotation after yielding of the tension steel reinforcement and before crushing of the concrete in compression. In **Figure 1-1**, the portion of the curve between points B and C corresponding to φ_y and φ_u represents ductility, where φ_y and φ_u are the curvature at yield and ultimate respectively. The principles of redistribution and ductility can be demonstrated by means of the example, (see Nilson, 1978, and Kong and Evans, 1990) shown in **Figure 1-5.**

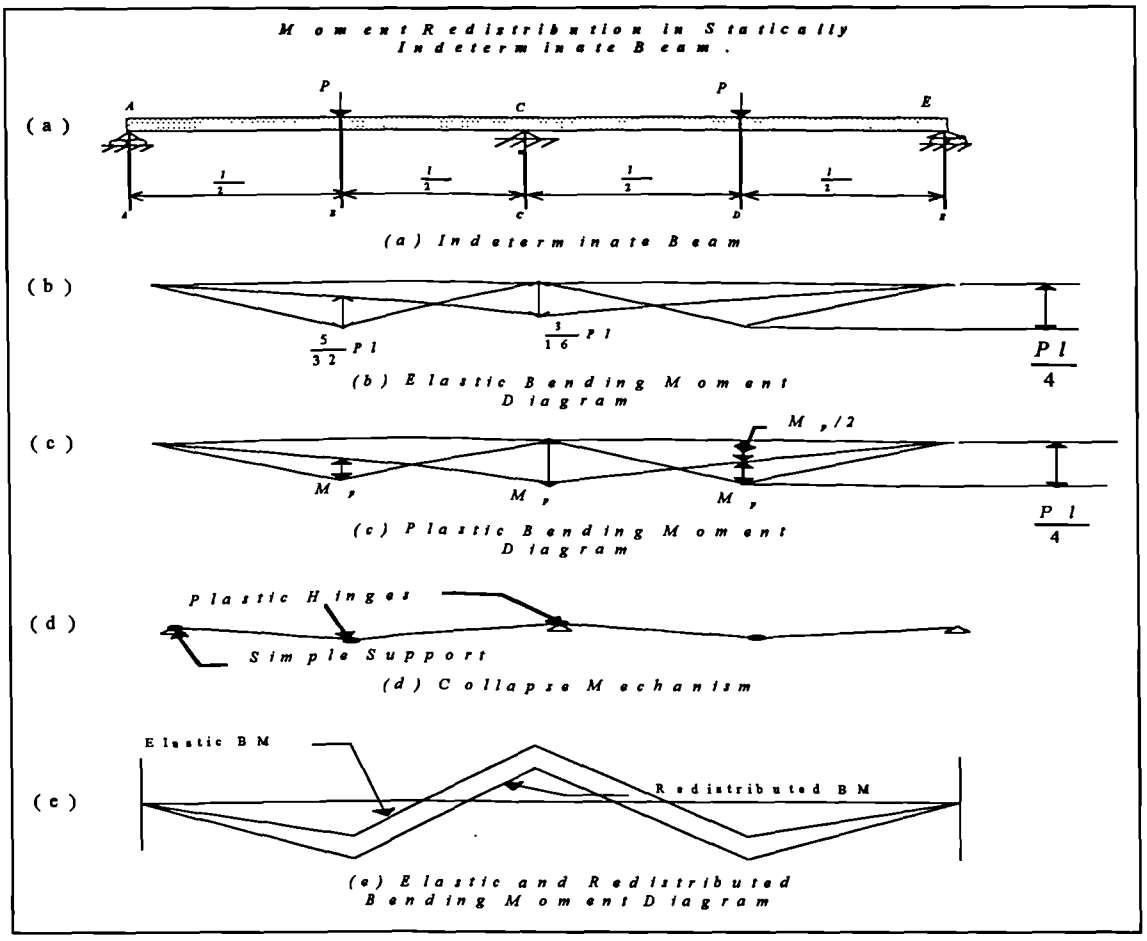

Figure 1-5: Moment redistribution and plastic hinge mechanism in a two-span continuous beam

Figure 1-5a shows a two-span continuous beam with hinged supports at points A, C and E. It carries a single concentrated load (*P*) at each mid-span. The beam has a reinforcement stress strain relationship and moment curvature relationship as shown in **Figure 1-6** (an ideally elastic-plastic beam section).

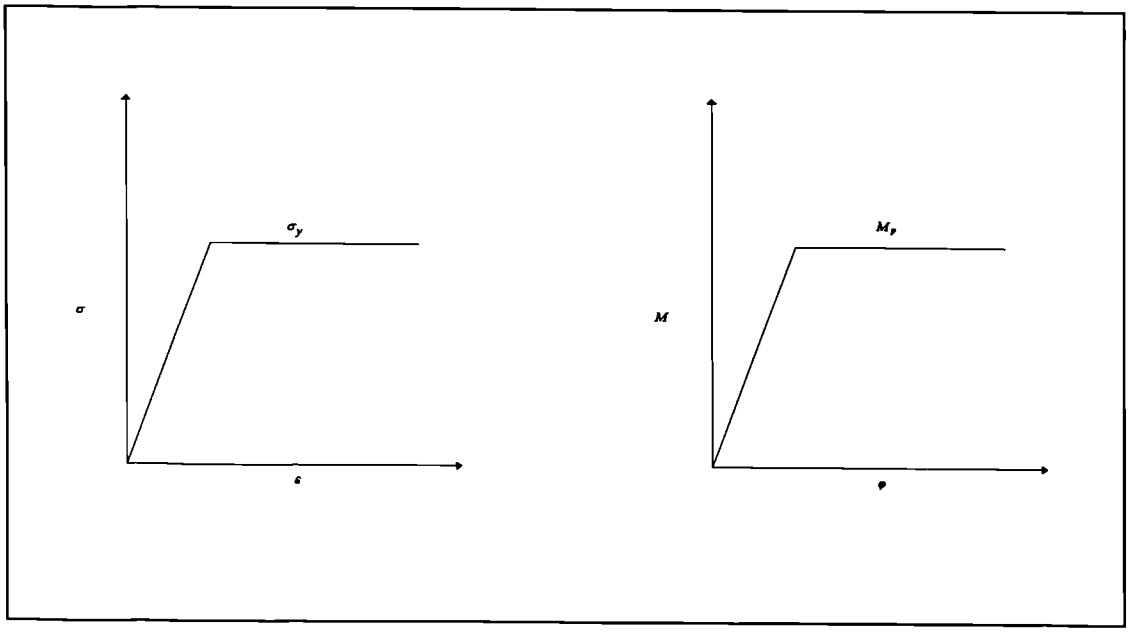

Figure 1-6: Idealised stress-strain and moment curvature relationships

Suppose that the load on the beam is increased gradually until the elastic bending moment at the middle support (Point C) reaches the value of $\left(\frac{3P\,l}{16}\right)$; which is just equal to the plastic moment capacity of the beam section (M_p called the plastic moment of resistance). Thus this load becomes:

$$P = \frac{16M_p}{3l} \qquad \textit{Equation 1-6}$$

Where:-

M_p= Plastic moment of resistance.

P = Applied load at mid-span.

l= Length of the beam.

At this stage the moment under the load at each mid-span is $\left(\frac{5P\,l}{32}\right)$, as shown in **Figure 1-5b.** With the increasing load, the beam still behaves elastically everywhere except at (point C), where moment reached its capacity and rotations are occurring. A plastic hinge is said to have developed at the support (point C), because after the moment at the section reaches M_p the beam behaves as though it is hinged there. At

this point the beam becomes statically determinate. The load can be increased further until the moment under the load also becomes equal to M_p (assuming that the beam has equal capacity in positive and negative bending), when the second hinge forms. The structure then forms a mechanism as shown in **Figure 1-5d** and collapse occurs. The moment diagram at the collapse load is shown in **Figure 1-5c.** From the geometry of **Figure 1-5c**, the magnitude of the load and moment causing collapse is calculated:

$$M_p + \frac{M_p}{2} = \frac{P_u l}{4} \qquad \textit{Equation 1-7}$$

From which:

$$M_p = \frac{P_u l}{6} \Rightarrow P_u = \frac{6M_p}{l} \qquad \textit{Equation 1-8}$$

Where:-

P_u= The ultimate load capacity of the beam at failure.

Had the beam remained elastic, the bending moment diagram at collapse would have been that of **Figure 1-5b.** With P_u substituted for P, and the (hypothetical) elastic moment at C ($M_{sup,elastic}$) would have been:

$$M_{sup,elastic} = \frac{3P_u l}{16} \Rightarrow P_u = \frac{16}{3l} M_{sup,elastic} \qquad \textit{Equation 1-9}$$

Where:-

$M_{sup,elastic}$= Elastic Support Bending Moment at the Middle at point C

Comparison of **Equations 1-8** and **1-9** shows that an increase in P from $5.33\frac{M_p}{l}$ to $6\frac{M_p}{l}$ (an increase of 12%) beyond that load which caused the formation of the first plastic hinge, before the beam will actually collapse. Because of the formation of plastic hinges, a redistribution of moments has occurred such that, at failure, the ratio between positive and negative moments is equal to the ratio of resisting moments provided in designing the beam, rather than the ratio of elastic moments. It is possible to calculate the moment redistribution at C as the ratio of the

elastic moment (**Equation 1-9**) to the plastic moment (**Equation 1-8**). The ratio of the latter to the first becomes *0.889*. This drop of the elastic moment by 11.1% is called the percentage of redistribution.

There is a direct relation between the amount of redistribution achieved and the amount of plastic rotation required at the critical sections of a beam to produce the desired redistribution. In general, the greater the modification of the elastic moment ratio, the greater the rotation capacity required to accomplish this change. If the beam of **Figure 1-5** had been designed with resisting moments consistent with the elastic moment diagram of **Figure 1-5b**, no rotation would have been required at the two critical sections, and the beam would have yielded at the same instant at the centre support and at mid-span. On the other hand, if the resisting moment at the mid support had been deliberately reduced (and correspondingly the mid-span increased), then substantial plastic rotation at the support would have been required before the mid-span sections reached their failure.

This example illustrates the difference between elastic and plastic analysis of moments, and the necessity for plastic rotation capacity at the location of hinges, if the failure load predicted by plastic analysis is to be achieved. Plastic analysis is widely used for steel structures where rotation capacity is usually adequate because of the larger amount of ductility of the steel as opposed to concrete. It has been partially accepted for reinforced concrete structures because a more limited amount of rotation can be achieved at the hinging sections, but there is the practical difficulty of predicting the ductility that is available in a given case.

When the beam has ductility, it has the potential to continue resisting load beyond the time of initial yield. Therefore, when a structural member has sufficient ductility to achieve a mechanism, it is possible for designers to use redistribution to achieve savings in materials and labour cost. Hence, reinforced concrete codes of practice recognise this advantage by permitting a certain amount of moment redistribution, albeit with limitations that insure equilibrium and strain compatibility within the structure. One of the objectives of this thesis is to compare the redistribution provisions of various codes. There are significant differences in the approaches used by different codes and these will be discussed in detail in Chapter Seven.

A reduction of the support moments in a continuous beam is an advantage, particularly in buildings at internal columns, where the beam reinforcement, typically in two directions, intersects the column reinforcement. Current British design practice in BS 8110 permits bending moments at support sections in continuous beams to be redistributed by up to 30 % of the elastic moment. The aim of such redistribution is to distribute bending moments away from peak moment regions, such as beam-column joints or supports of continuous members. By reducing beam moments, and thereby the amount of tension reinforcement, better concrete placement and compaction becomes possible. This reduces the congestion of the steel at the support regions and makes design more economical, hence, reducing the total construction cost, and simplifying reinforcement detailing.

The economic advantages of redistribution can be more understood through the bending moment envelope, which is a plot of the worst case bending moment resulting form the analyses of all possible loading arrangements. For example, **Figures 1-7a to c** show the elastic and redistributed bending moment diagrams (according to BS 8110 requirements) for a three-span continuous beam taking account of three loading arrangements (cases). Case 1 for maximum hogging moment at B, Case 2 for maximum sagging moment at span B and Case 3 is for maximum sagging moment at spans AB and CD. The elastic moment envelope is shown in Figure 1-7d, is constructed from the chain-dotted curves of the three loading cases. If the elastic moment envelope is used to proportion the beam sections for the ultimate limit state, peak moments of 1097 kNm would have to be catered for and this would result in congestion of steel at section B and C. Conversely, the use of the redistributed moments (solid lines in **Figure 1-7d**) leads to a more even distribution of reinforcement throughout the beam and also to some overall saving in steel at both the span and support sections respectively.

1-7a

1-7b

1-7c

1-7d

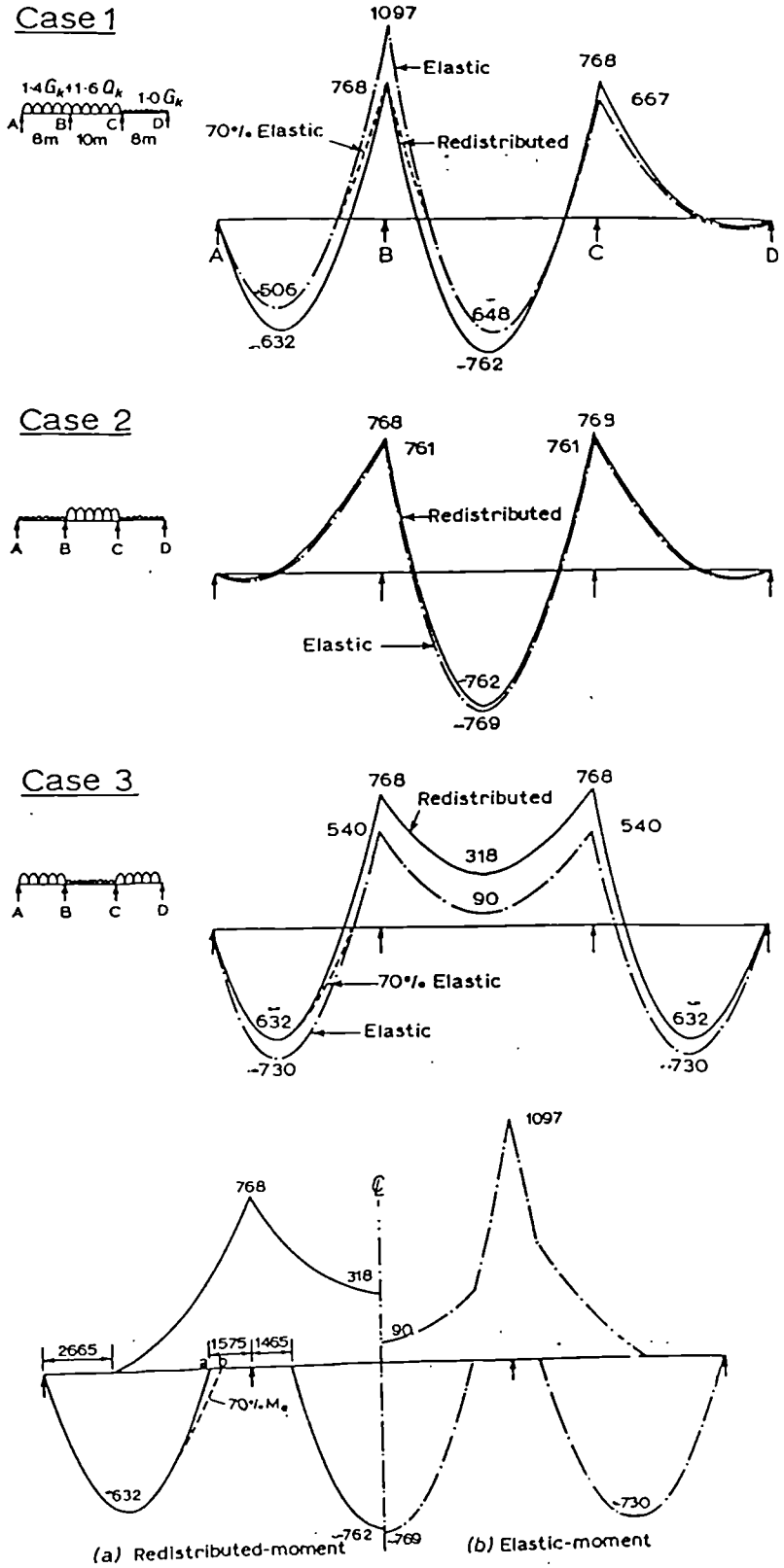

Figure 1-7: Elastic and redistributed bending moment envelope of a three-span continuous beam.(Ref : Kong and Evans, 1987)

In the next section, factors governing moment redistribution will be discussed.

1.3.4 Factors Governing Moment Redistribution

1.3.4.1 Reinforcement Ratio

For a given type of reinforcement and a given grade of concrete in an indeterminate beam, the moment curvature relationship at any section is most affected by the percentage of tension reinforcement. Textbooks identify three classes of reinforced concrete sections: balanced, over-reinforced and under-reinforced. The term balanced section refers to the situation where the beam is designed to fail simultaneously in flexural compression of the concrete and yielding of the tensile reinforcement. An over-reinforced section will fail in flexural compression of the concrete with the reinforcement still elastic, i.e. a brittle failure. An under-reinforced section will fail by the crushing of the concrete in the compression side after the tension reinforcement has already yielded. This causes the cracks to open up so that the depth of the beam available to resist flexural compression is reduced. An under-reinforced section contains less steel than the balanced (ideally) reinforced section. Therefore, the neutral axis depth is closer to the compressive face and the reinforcement yields, but the section still fails when the top fibre in the concrete reaches its limiting value. In a similar manner, an over-reinforced section contains more steel than the balanced, therefore compression in the concrete will reach its ultimate or failure strain while the tension steel is still elastic.

The effect of the amount of tensile reinforcement becomes more significant at yield and after yield. In an under-reinforced section, the percentage of reinforcement over the support relative to span sections becomes the main governing factor in the degree of redistribution. The higher the reinforcement ratio over the support relative to the span, the stiffer the beam becomes, and so the smaller the redistribution. On the other hand, a lower steel ratio over the support relative to the span decreases the stiffness, thus increasing redistribution. It is the relative reinforcement ratio that is important, thus making the relative stiffness of a beam or a structure the governing factor.

1.3.4.2 Reinforcement Types

Different stress strain curves for the various types of reinforcement affect the redistribution of moments in a number of ways. Eligehausen and Langer (1987), Eligehausen and Fabritius (1991) and Eligehausen and Longfie (1992), reported that the degree of redistribution is influenced by the amount of plastic strains that may be developed in the tensile reinforcement. Steel is a material that can undergo large deformation without fracture. The stress strain relationship is shown schematically in **Figure 1-8**. As strain in the reinforcement increases, more rotation will occur, thus increasing the amount of redistribution. The type of steel investigated in this research was high yield ductility steel classified as (hot rolled deformed bars BS4449). The specified yield stress of these bars falls between 425 and 460 MPa for small and large bar diameters respectively. However BS4449 specifies yield stress at 460 MPa for all bar diameters. An assumed yield point was computed at an off-set strain of 0.2 percent normally used for high ductility steel.

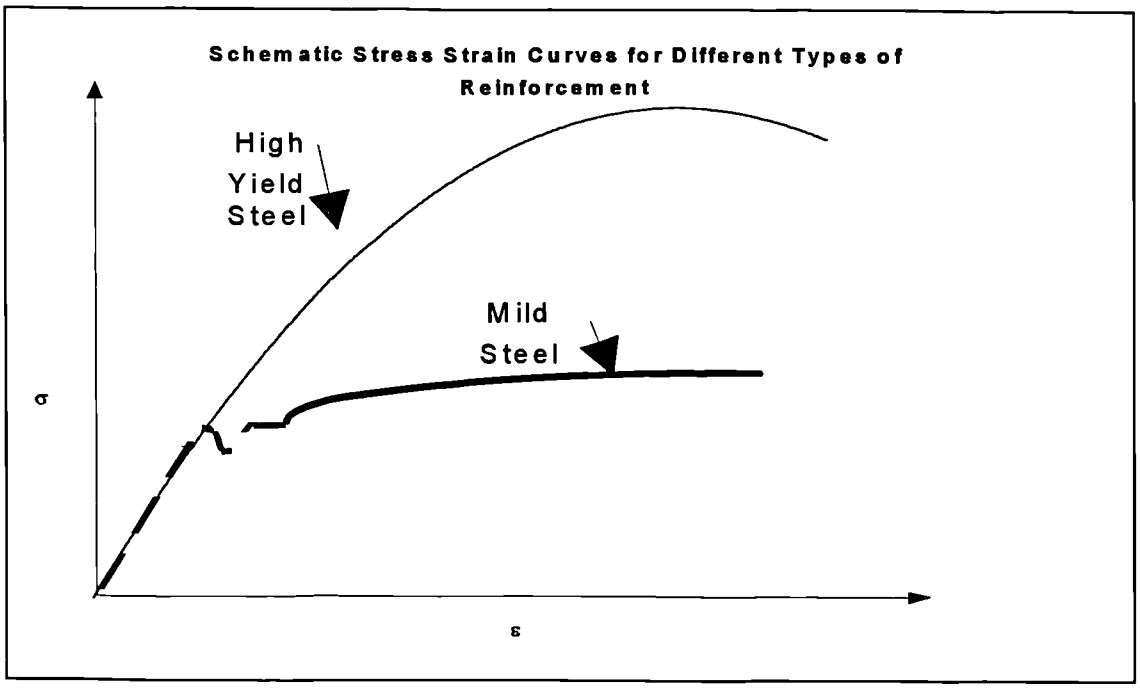

Figure 1-8: Stress-strain curves of two different types of steel

1.3.4.3 Concrete Stress Strain Relationship in Compression

Concrete in compression is a strain-softening material. In other words, the concrete stress-strain curve exhibits a distinct maximum stress after which stress decreases with increasing strain. After tests on simply supported concrete beams reported by Barnard (1964), it was found that the beams failed suddenly when the strain at maximum stress was reached in a compression specimen. This eventually led to the practice of limiting maximum concrete strain between 2000 and 3500 microstrain. However, earlier work by Baker (1949) suggested that with closely spaced stirrups and helical binding reinforcement in a beam or a column, maximum compressive strain in the concrete may be increased up to 10000 microstrain. Similar conclusions were reached by several researchers such as Kent and Park (1971) Roy and Sozen (1964) and Hognestad (1955). They proposed a general stress strain curve for concrete consisting of a second degree parabola up to a maximum stress, and a linear falling branch which depended on the quantity and degree of confining reinforcement (shear stirrups). The descending portion of the concrete stress strain curve has been excluded from the present analysis and similarly from the moment curvature relationship presented earlier for two main reasons. Firstly, there seems to be a considerable scatter in the descending portion even when agreement on the ascending branch is reasonable. Secondly, there is the problem as to which value to use on the descending portion in a functional relationship with moment-curvature relationship (average, minimum or maximum values). Therefore, in this study ascending stress strain relationship in subsequent analyses. **Figure 1-9** illustrates a typical stress strain diagram for a concrete specimen in compression. ε_{cu} is the ultimate strain that corresponds to the maximum compressive stress σ_c. The concrete modulus of elasticity is given by the slope of the stress strain curve of the concrete and its value decreases with increasing stress. The concrete modulus of elasticity is related to the concrete compressive strength. The ultimate concrete compressive strain ε_{cu} may be used to calculate curvature at ultimate in the following equation:

$$\varphi_u = \frac{\varepsilon_{cu}}{x_u} \qquad \textit{Equation 1-10}$$

Where:

φ_u = Curvature at ultimate.

ε_{cu} = Concrete ultimate compressive strain.

x_u = Neutral axis depth at ultimate.

Equation 1-10 shows that φ_u increases in proportion to increasing ultimate strain of concrete ε_{cu}, thereby increasing the ductility of a section. This was confirmed by tests carried out on reinforced concrete beams by Mattock (1964).

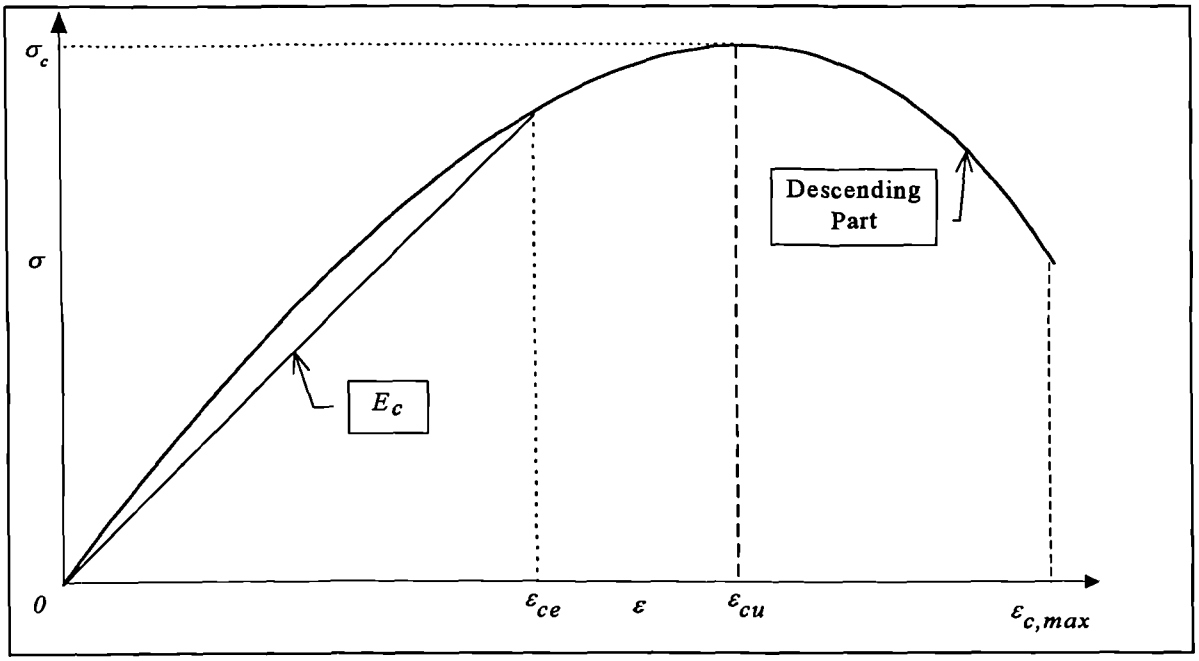

Figure 1-9: Stress strain curve of concrete with falling branch

1.3.4.4 Rotation Capacity

When a section reaches its yield moment and its yield strain in the tensile reinforcement, the reinforcement must undergo additional strain beyond yield with a small increase in the applied moment before the structure collapses completely. This additional plastic strain causes plastic rotation. Reinforced concrete sections have a reasonable amount of rotation capacity which is mainly dependent on the net reinforcement ratio (ρ-ρ') where ρ and ρ' are tension and compression reinforcement ratios respectively. If the net reinforcement ratio in a doubly reinforced concrete beam is less than the balanced amount, then the rotation capacity of the beam and moment redistribution increase. On the other hand, if the amount of the net reinforcement or

tensile reinforcement in the case of a singly reinforced section exceeds the balanced ratio, then the section is considered to be brittle and very little redistribution will take place.

In the case of the propped cantilever shown in **Figure 1-10,** the numerical value for rotation (slope of the beam) at any point along the beam is the summation (or the integral) of curvature from the fixed end up to the point where rotation needs to be evaluated. The deflection at the fixed support is zero and the value of rotation (slope of the beam) at the fixed end is also zero. However, this does not mean that the rotation capacity is zero, because as the bending moment increases, tensile strains in the reinforcement will continue to peak beyond yield and concentrate near the critical support and span sections under crack positions up to a certain length. This length is called the plastic length (l_p), and is calculated from the geometry of the bending moment diagram between yield and ultimate as shown in **Figure 1-10a.** This is proportional to the movement of the point of contraflexure (point of zero moment) between yield and ultimate. From the geometry in **Figure 1-10a,** the plastic hinge length l_p can be calculated by the following equation:

$$l_p = \frac{M_u - M_y}{M_u + M_{u,span}} l_2 \qquad \textit{Equation 1-11}$$

Where:-

l_p = The plastic hinge length.

l_2 = Distance between centre of the support to the centre of the span.

M_u = The ultimate moment.

M_y = The yield moment.

$M_{u,span}$ = Span moment when the support reaches ultimate moment.

Rotation capacity is calculated by integrating curvature over plastic hinge length l_p at ultimate (maximum load). **Figure 1-10b** shows a detailed schematic of the

rotation capacity in terms of the curvature distribution diagram over the support area. The plastic hinge length at yield is assumed to be the same at ultimate . The author defined the rotation capacity as the total rotation at ultimate that occurs under the plastic hinge length l_p. The elastic and plastic rotations respectively are defined as follows:-

Plastic rotation is the difference between total and elastic rotation referred, to as the plastic rotation capacity.

Total rotation is the rotation under peak load which is equivalent to the term rotation capacity.

Elastic rotation is equal to the integration of curvatures over the plastic hinge length under yielding moment (moment under which the reinforcing steel in the tension reaches its yield stress).

The *plastic rotation* is evaluated in terms of both yield and ultimate curvatures which may be expressed mathematically as:-

$$\theta_p = \int_0^{l_p} (\varphi_u - \varphi_y) dx \qquad \text{Equation 1-12}$$

Where:-

θ_p = The plastic rotation capacity (plastic rotation under l_p

φ_u = The ultimate curvature

φ_y = The yield curvature

This definition of plastic rotation capacity is however, one of the many which have been arrived at by various researchers relating the yield curvature at the yielding of the tensile reinforcement to the ultimate condition of the concrete reaching its ultimate strain ε_{cu}, (see Burnett 1972).

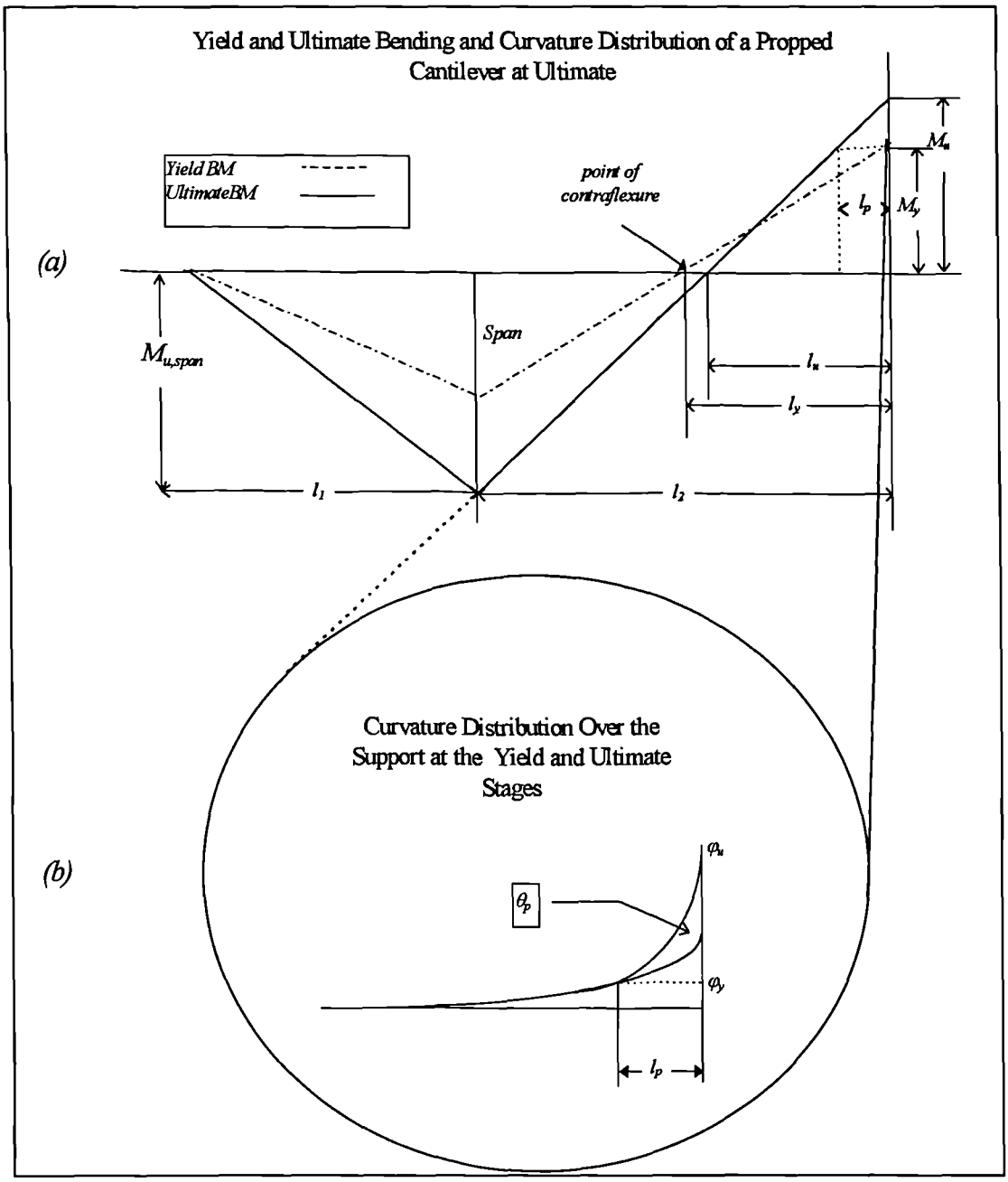

Figure 1-10: Propped cantilever yield and ultimate bending moment and curvature distributions

1.3.4.5 Flexural Ductility of Reinforced Concrete Beams

Flexural ductility is the ability of a structure to sustain strains under pure bending beyond the elastic range without a significant variation of the bending moment capacity. This thesis is concerned with the ductility of the reinforced concrete sections on the assumption that the properties of steel and concrete are known. Due to the

nature of the experimental work carried out in this thesis, the investigation is limited to pure bending on two span continuous beams centrally loaded at each span.

Ductility governs the rotation capacity of the hinging zones (plastic length region) and the redistribution of moment in a structure (Sozen, 1964). Ductility protects structures against sudden overloads by permitting plastic rotation to take place. It is therefore desirable that a structure has a reserve of ductility to withstand overloading conditions, such as earthquakes or excessive continuous repeated loads.

Reinforced concrete beams, unless under-reinforced, behave in a brittle manner when subjected to high bending moments. In order for a reinforced concrete structural element to undergo large deformations and rotations at loads close to its failure strains, limitations on the percentage of reinforcement and the neutral axis depth are necessary to allow sufficient deformation beyond the yield of the reinforcement without the failure of the beam. In continuous structures, redistribution of the bending moments from a region of higher stress at the supports to the less stressed regions along the span, depends upon the ductility and stiffness of the sections in the two regions. When the structure reaches yield at the support, plastic rotations commence at the steady increase of moment. This increase in rotation capability increases the ductility of the structure. Having defined ductility in a qualitative manner, it is necessary to further define it quantitatively. The conventional definition of ductility is in terms of the ductility factor seen as the ratio of ultimate to yield curvatures, that is φ_u/φ_y, (see Cohn and Ghosh 1973).

The yield curvature φ_y is defined as the curvature at which the tension steel reaches its yield point stress. The stress-strain relationships used for steel in the present investigation are characterised by an assumed yield point.

The ultimate curvature on the other hand, is defined as the curvature corresponding to where concrete reaches its limiting strain at the extreme fibre (ε_{cu}). Research carried out by Eligehausen and Langer (1987) suggested defining ultimate curvature based on high limiting tensile reinforcement strains, to exploit the ductility of a reinforced concrete section in order to achieve more redistribution by increasing the rotation capacity of a section. The ductility of reinforced concrete sections in bending

is primarily influenced by the tension and compression reinforcement, the strength of the concrete in compression and the yield strength of the tensile reinforcement. These factors directly affect the stiffness of a section, investigated in the context of this thesis.

In the next chapter, the historical background of the research carried out into moment redistribution will be presented.

CHAPTER TWO

2. HISTORICAL BACKGROUND

Moment redistribution in reinforced concrete members was first observed in 1920 when the results of tests on two beams fully fixed at the end were reported by the German Reinforced Concrete Committee (see Mattock, 1955). The first extensive series of tests demonstrating moment redistribution in reinforced concrete beam was carried out by Kazinczy and reported by Yu and Hognestad (1958). Glanville and Thomas (1935) conducted research on moment redistribution. Their tests were conducted on two-span continuous beams loaded with concentrated loads in the middle of each span. Until that time, there had not been any significant results that could relate redistribution to the percentage of reinforcement used in the research. Further experimental work was needed to enable engineers to predict the redistribution phenomenon and include it in design criteria. A survey on the history of moment redistribution is presented next.

2.1 Baker (1949)

Early work on moment redistribution was carried out by Baker at Imperial College, London and reported by Mattock (1959). Over twelve years of research, Baker derived the following equation from theoretical considerations for predicting the plastic rotation capacity over one side of a plastic hinge.

$$\theta_P = \frac{(\varepsilon_{cu} - \varepsilon_{ce}) l_p}{k_u d} \qquad \textit{Equation 2-1}$$

Where:-

ε_{cu} = Ultimate compressive strain of concrete.

ε_{ce} = Compressive strain at the extreme edge of concrete when tension reinforcing steel begins to yield.

$k_u d$ = Depth of neutral axis at ultimate stage.

l_p = Plastic hinge length.

Baker recommended ε_{cu}= 0.0035 for unconfined concrete and the following equation for concrete confined by closed stirrups.

$$\varepsilon_{cu} = 0.0035 + 0.0002\,(\rho'')^{0.5} \qquad \textit{Equation 2-2}$$

Where:-

ρ'' = Volumetric ratio of a stirrup to concrete enclosed by two stirrups.

The concrete strain at the yield stage, ε_{ce} equal to 0.002 was recommended for both bound and unbound concrete. The neutral axis depth $k_u d$ can be determined by considering equilibrium between tension and compression forces on the section.

The Research Committee Report of ICE (1964) suggested the following equation for the plastic hinge length. l_p :

$$l_p = R_1 R_2 R_3 \left(\frac{z}{d}\right)^{\frac{1}{4}} d \qquad \textit{Equation 2-3}$$

Where:-

R_1 = 0.7 for mild steel and 0.9 for cold worked steel.

R_2 = 1.0 for members without axial load.

R_3 = 0.6 for f_{cu} = 41.4 N/mm^2 and 0.9 for f_{cu} = 13.8 N/mm^2.

For a different value of f_{cu} , linear interpolation between the two values may be used.

z = Distance from the critical section to the point of zero moment.

Baker (1949) also put forward a trial and error method for calculating the amount of moment redistribution in continuous beams.

2.2 Lee (1953)

Lee (1953) tested a group of fixed ended reinforced concrete beams and assumed that redistribution started after the commencement of first crack at the fixed end support. He concluded that redistribution occurred due the variation in stiffness along the length of

the beam, and that ultimate redistribution occurred when the mid span section reinforcement had yielded.

2.3 Ernest (1957)

Ernest (1957) investigated the amount of plastic rotation that could occur in beam-column connections for both fast and slow loading. He concluded that the plastic rotation increased with a decreasing percentage of reinforcement.

Further tests were carried out by Ernest to investigate the manner and extent of moment redistribution in reinforced concrete beams. His results concluded that the ultimate strength of a section was controlled by the redistribution within the beam. In the analysis of two-span continuous beams centrally loaded at each mid span, Ernest derived equations for the plastic rotation at the central support and deflection at each mid-span of the continuous beam.

2.4 Macchi (1965)

Macchi (1965) tested two 3-span continuous beams 400 mm wide by 150 mm depth, one with a point load in the middle of the central span, and the other with four equal loads on the central spans. Loads, rotations and cracks were measured. Test results showed that redistribution on the two beams was 31% at ultimate load.

Macchi proposed a method of imposed rotations to analyse the beams. The method involved considering inelastic rotations as rotations artificially imposed on critical sections of a still elastic structure. Imposed rotations cause an equilibrated system of redistributed moments; by superposition of the latter and elastic moments due to loads the real distribution of moments is obtained. For full treatment of the method, see Macchi (1965), in which he concluded that elastic distribution of moments was not suitable a basis for design for reinforced concrete beams.

2.5 Mattock (1965)

Mattock (1965) conducted a series of tests on two-span continuous beams to investigate the redistribution of bending moments in continuous reinforced concrete beams. The first group consisted of four two-span continuous beams designed for the

same working load but using various distributions of design bending moments. The second group consisted of three continuous beams designed to simulate secondary beams in reinforced concrete framed buildings. One beam was reinforced with mild steel and was designed for the distribution of bending moment as predicted by an elastic analysis. The other two were designed using 25% reduction of support section moments with the appropriate increase in the mid span section.

Tests on the first group of beams showed that redistribution of moments started well before the yield point stress was reached. It was observed that the actual redistribution of bending moments at working load was about 27% of the assumed one in design. This was because moment curvature relationship was non-linear at high loads. In the second group of tests, observation revealed that redistribution was occurring at working loads at the same percentage as in group 1.

Mattock concluded that redistribution of design bending moments of reinforced concrete continuous beams did not affect the performance at the beam at service load or at failure. He also concluded that cracking and deflection of beams with redistributed design bending moments were not more severe than in those beams designed using elastic analysis. Furthermore, the factor of safety in design of these beams was unaffected by redistribution of design bending moment. His recommendation was to increase redistribution in British Standards (1957) from 15% to 25% to achieve economy in design and construction.

Mattock also investigated the rotational capacity of reinforced concrete beams. Thirty-seven beams were tested involving studying parameters such as concrete strength, depth, distance from point of maximum moment to point of zero moment and amount and yield point of reinforcement. The objective of these tests was to obtain a better understanding of the distribution of curvature around supports in continuous beams. Mattock established a model for the plastic rotational capacity over one side of the plastic hinge as:

$$\theta_p = \left(\varphi_u - \varphi_y \frac{M_u}{M_y} \right) l_p \qquad \textit{Equation 2-4}$$

From test results on the inelastic rotations, he recommended the following empirical equation for the plastic hinging length:

$$l_p = \frac{d}{2}\left[1+\left(1.14\sqrt{\frac{z}{d}}\right)\left(1-\frac{q-q'}{q_b}\right)\sqrt{\frac{d}{16.2}}\right] \qquad \textit{Equation 2-5}$$

Where:-

$$q = \frac{\rho f_y}{f_c'} \qquad \textit{Equation 2-6}$$

$$q' = \frac{\rho' f_y}{f_c'} \qquad \textit{Equation 2-7}$$

$$q = \frac{\rho f_y}{f_c'} \qquad \textit{Equation 2-8}$$

Mattock suggested that ε_{cu} to be calculated by the following equation:

$$\varepsilon_{cu} = 0.003+\frac{d}{2z} \qquad \textit{Equation 2-9}$$

Where:-

A_s = Tension steel reinforcement area.

A_s' = Compression steel reinforcement area.

b = Width of the cross section.

ρ = Tensile steel ratio = A_s/bd.

ρ' = Compression steel ratio = As'/bd.

f_c' = Concrete cylinder strength.

f_y = Yield point stress for the tensile reinforcement.

q' = Compression reinforcement index .= $\rho' f_y / f_c'$.

q = Tension reinforcement index = $\rho f_y / f'_c$.

z = Distance from section of maximum moment to section of zero moment.

2.6 Cranston (1965)

Cranston (1965) analysed a pin-ended portal frame subjected to symmetrical two point loading on the beam span. An experimental moment curvature relation was used derived from moment rotation curves. The flexibility method was used to analyse the frame. Cranston examined the falling branch of the moment curvature diagram. His analytical model showed consistency with the experimental results at all loading stages.

2.7 Barnard and Johnson (1965)

Barnard and Johnson (1965) analysed two simply supported steel-concrete composite beams subjected to symmetrical two point loads. They used analytical moment curvature diagrams for their computations. As the beam was a determinate structure, they employed the method of direct integration of curvatures to obtain deflections corresponding to the ultimate loads. Their modelled results turned out to be much greater than the experimental ones, and were attributed to an overestimation of curvatures in the inelastic regions.

2.8 Corley(1966)

Corley's (1966) research was an extension of Mattock's study, with the inelastic rotation model remaining the same. Rotations of forty simply supported beams were also measured in the same manner. Moments and curvatures at yield and ultimate stages were also determined. All beams were loaded with a concentrated load at the centre of the span. Primary variables were size of specimen and concrete confinement by stirrups, in addition to the variables in Mattock's tests. From the test results, Corley suggested the following equations:

$$\theta_p = \left(\varphi_u - \varphi_y \frac{M_u}{M_y}\right) l_p \qquad \textit{Equation 2-10}$$

$$l_p = \frac{d}{2}\left[1 + \frac{z}{d}\sqrt{\left(\frac{0.40}{d}\right)}\right] \qquad \textit{Equation 2-11}$$

$$\varepsilon_{cu} = 0.003 + 0.02\frac{b}{z} + \left(\frac{\rho'' f_y}{20.0}\right)^2 \qquad \textit{Equation 2-12}$$

2.9 Nawy et al (1968)

A joint experimental study carried out by Nawy et al (1968) was aimed at studying the effect of spiral shear reinforcement on plastic hinge rotation in reinforced concrete beams. The investigation aimed to increasing the rotational capacity of plastic hinges by the use of spiral stirrups to permit a better redistribution of moments. Two series of tests were conducted, the first investigated a plastic hinge in tension, the second investigated a plastic hinge in compression. A total of twenty simple beams loaded with a concentrated load at mid span were tested. Series one beams were subjected to pure bending while series two were subjected to an additional axial load to bending. They concluded that increasing spiral reinforcement would increase the rotational capacity in both tension and compression plastic hinges and that such an increase in ductility could improve moment redistribution.

2.10 Conner et al (1970)

Conner et al (1970) tested three precast concrete frames and observed that additional strength was developed by moment redistribution and strain hardening of the reinforcement. They stated that significant economy could be realised in construction of frames if moment redistribution and strain hardening effects were considered in design. It was reported that almost half of the total moment was redistributed at first yield, while tests carried out by Mattock reported 25% redistribution.

2.11 Snowdon (1970)

Snowdon (1970) reported on results of tests on several hundred specimens of nine different types made in an attempt to develop a simple method of test which could be used to compare and classify the bond strength of the different types of deformed bar

reinforcement used in the United Kingdom. He investigated the bond performance of high tensile deformed bars and its influence on cracking and deflection. Nine methods were used in the experimental work which he classified into two types: pull-out and transfer types. Snowdon concluded that it was possible to classify high bond bars in terms of the number of diameters of embedment necessary to develop and sustain the 0.2 percent proof stress. The work carried out by Snowdon on the bond performance of different bar diameters was one of the reasons which lead the author to choose the reinforcement layout in the experimental set-up where the same area of tensile steel was used, but with different number of bars and bar diameters in the test beams. This experimental procedure is presented in the next chapter, Chapter Three.

2.12 Ghosh and Cohn (1973)

Ghosh and Cohn (1973) developed an analytical technique to predict the load deformation characteristics of reinforced concrete sections in bending. The analysis proposed was based on known configuration and geometry ,and stress-strain relationships of concrete and steel. Moment curvature relationships were derived from the stress strain relationships of the concrete and steel using a computer model. Rotation and deflection were then calculated. The method was based on the concept of concentrated inelastic rotation at discrete sections. The method developed was claimed by the author to predict structural load deformation characteristics up to the point of collapse, in reasonable agreement with experimental results.

2.13 Kemp (1981)

Kemp (1981) assessed the theoretical moment redistribution capacity of reinforced concrete beams. He discussed the relevance of ductility on redistribution capacity and compared the theoretical formulation with the British Code CP 110 and the European Model Code MC 78. His main objective was to illustrate a quantitative procedure to evaluate the flexural ductility of reinforced concrete sections based on the determination of the moment curvature relationship up to the ultimate moment capacity of the section. In his theoretical analysis, Kemp adopted an idealised flat top elasto-plastic moment

curvature relationship. His model was constructed on the basis of a fixed ended beam under uniform distributed load.

Kemp stated that his theoretical formulation relating redistribution to curvature correlated very closely to criteria adopted in MC 78 and CP 110, but claimed that the British code was more conservative in its redistribution criteria by not exploiting the full ductility of reinforced concrete members.

2.14 Sakai et al (1984)

Sakai et al (1984) carried out joint research on the failure of two-span continuous beams. The purpose of the study was to investigate the calculation of energy absorption capacity of reinforced continuous beams in bending, which was derived from the load deflection relations. Four kinds of continuous beams were tested with different cross sectional properties and loaded symmetrically. Demec gauge readings measured the change in strain and curvature. They concluded that energy absorption capacity of continuous beams may be expressed in terms of the total rotation of the plastic hinges.

2.15 Hsu (1983)

Hsu (1983) presented a method that accounted for the load deflection and moment rotation curves for continuous under-reinforced concrete beams. The method of calculation developed was based on the derivation of a moment curvature relationship for singly and doubly reinforced sections based on the stress strain curve for the reinforcing steel. The model included both the ascending and the descending branches of the moment curvature relationship. The model developed by Hsu at the University of Illinois, was used to analyse the load deflection and load strain behaviour of 28 simply supported beams tested to failure. He calculated the slope, rotations and deflection at the relevant sections of the beams by using the following modified moment-area theorem:-

$$\theta = \int \varphi dy\ \theta \qquad \textit{Equation 2-13}$$

$$\delta = \int \varphi y dy\ \delta \qquad \textit{Equation 2-14}$$

Where:-

δ = Deflection of the beam at any point along the beam.

y = Distance over which the integration is desired.

Using the equations above with some minor modifications of the moment-area theorems, Hsu derived equations for the deflection of continuous beams before cracking, at yielding of the reinforcing steel and between yielding of the steel and ultimate.

2.16 Scott (1983)

Scott (1983) developed a `numerical model to calculate the moment curvature relationship for reinforced concrete beams using averaged linear strain distribution and linearised stress strain relationships for the reinforcement. The computer model analysed rectangular beams with inputs of section geometry, reinforcement areas, linearised stress strain data of the concrete and reinforcement and reinforcement strains. The model calculated iteratively the moment curvature relation of the beam based on the stress strain relationships of both the concrete and the reinforcement. The model outputted calculated stresses and strains in the top and bottom reinforcement, neutral axis depth, moment, curvature, flexural stiffness and forces on the cross section. The model developed by Scott is flexible since it can solve stresses, strains, forces and neutral axis depth for any rectangular section for a given moment, concrete or reinforcement strain or rotation. This model was used by the author as an analysis tool for part of the modelling procedure described and applied in this thesis.

2.17 Carriera and Chu (1986)

Carriera and Chu (1986) recommended a model for the moment curvature relationship for reinforced concrete members based on the calculation of stresses of a reinforced concrete section. They derived the following formula:

$$\frac{M}{bd^2} = \lambda k^2 \left[f_c{}' \mu_c + f_a \left(\frac{h}{kd} - 1 \right)^2 \mu_t \right] + \frac{\varepsilon_c E_s}{k} \left[\rho (1-k)^2 + \rho' \left(k - \frac{d'}{d} \right)^2 \right] \quad \textit{Equation 2-15}$$

Where:-

d' = Depth of the compression reinforcement.

k = Neutral axis depth factor.

f_c' = Concrete compression strength.

λ = A factor relating maximum compressive stress from flexure to axial strength of cylinder test specimens, = 0.85

ε_c = Strain in extreme concrete fibre in compression (face of the concrete).

μ_c, μ_t Are constants numerically calculated based on integrals or sum of the ratios of compressive and tensile strain respectively. For details of the calculations of all factors involved, see Carriera and Chu (1986).

Curvature was calculated according to the following formula:

$$\varphi = \frac{\varepsilon_c}{kd} \qquad \textit{Equation 2-15a}$$

The results for this formulation compared very closely with experimental data. They developed a general method to compute the location of the neutral axis depth. Their method consisted of the second degree equation above. The neutral axis depth factor k was determined by calculating a distinct value of the neutral axis depth for every value of the bending moment. The formulation they used included a non-linear concrete stress-strain relationship in both ascending and descending branches of the curve. They concluded that the effect of the concrete stress-strain relationship and the reinforcement ratio on the movement of the neutral axis depth could be accurately determined using their equations. They concluded that maximum moment at a section could occur even at elastic strain levels in the reinforcement, even after crack propagation has occurred. They endorsed a minimum level of reinforcement as recommended by the ACI 318-83 building code.

2.18 Mo (1986)

Mo (1986) used a non-linear iterative method in which the moment curvature relationships of the individual sections must be known. The actual section forces were predicted throughout the loading history. The iterative method developed recognises the

local failure. The work carried out by Mo included testing of three groups for frames of which results of the moment curvature relationship obtained experimentally were compared with analytical modelled results.

2.19 Krauthammer et al (1987)

Krauthammer et al (1987) presented an analytical/numerical method that can be used for predicting the complete load deflection behaviour of rectangular reinforced concrete beams under the combined action of bending, shear, and axial force. The numerical procedure was based on a linear strain distribution and an accurate description of stress strain relationships for steel, concrete and rational failure criteria. The beam cross section was divided into layers parallel to the neutral axis. The stresses and forces were determined for all layers of concrete and reinforcement based on material stress strain models. The numerical model developed was based on the equilibrium of internal tensile and compressive forces of the concrete and reinforcing steel. The procedure iterated the position of the neutral axis depth until equilibrium was obtained and then moments and curvatures were computed. This procedure was then repeated for incremental values of strain. They claimed that the method seems to simulate accurately experimental load deflection data for reinforced concrete beam and beam columns.

2.20 Eligehausen and Langer (1987)

Eligehausen and Langer (1987) developed an analytical model for the rotation capacity of plastic hinges and moment redistribution. The model is based on moment curvature, stress-strain and bond stress relationships all of which have been adopted from various sources. The research investigated the influence of the stress strain relationship of steel on the rotation capacity. Eligehausen concluded that the rotation capacity increases as f_{st}/f_y increases where f_{st} is the rupture strength of reinforcement and f_y is the yield strength. It was found that the influence of bond stress is significant in the determination of the rotational capacity of reinforced concrete beams. He reported that if it is assumed no bond stress exists between cracks at the onset of their formation, then the relationship between plastic rotation and size of bars infers higher rotational capacity. On the other

hand, if bond between cracks is considered, then plastic rotation decreases, with this influence only occurring with very low reinforced beams. Eligehausen and Langer proposed the revision of the model code MC 78 to classify reinforcement into two types: high rupture strength and low rupture strength steel based on test results. Conclusions were drawn that the type of steel, depending on its stress strain relationship, has a significant influence of the degree of moment redistribution. Therefore, they recommended altering the possible degree of moment redistribution in MC 78 to :-

$$0.30 \geq \beta \geq 0..56 - 1.25\frac{x}{d} \qquad \textit{Equation 2-16}$$

For continuous beams, braced frames reinforced with steel type 1. high ductility steel.

$$0.15 \geq \beta \geq 0.56 - 1.25\frac{x}{d} \qquad \textit{Equation 2-17}$$

For continuous beams, braced frames reinforced with steel type 2, normal ductility steel.

Where:-

β = Percentage of moment redistribution.

Steel type 1 : $\frac{f_{st}}{f_y} \geq 1.10$ *and* $\varepsilon_g \geq 6\%$

Steel type 2: $1.05 \leq \frac{f_{st}}{f_y} < 1.10$ *and* $2.5\% \leq \varepsilon_g \leq 6\%$

Where:-

f_{st} = Rupture strength of the reinforcement obtained in tests

ε_g = Unit elongation measured in tests.

Further work was also carried out by Eligehausen and Fabritius (1991), and Eligehausen and Longfie (1992) on the analysis of redistribution and rotation capacity in ordinary and precast reinforced concrete and compared experimental results with EC2 code requirements and CEB-FIP Model Code requirements.

2.21 Park and Ruitong (1988)

Park and Ruitong (1988) assessed the available ductility of doubly reinforced concrete beam sections with a range of tension and compression steel ratios and various strengths of steel and concrete. Ductility was assessed by determining curvature at first yield and at ultimate. Park defined yield as the point where the tension steel reaches a yield strain of f_y/E_s. Park derived a set of 22 equations which related the ductility factor φ_u/φ_y to ratio of tensile reinforcement computed for a range of combinations of concrete compressive strengths f_c', steel yield strengths f_y, and ratios of compression steel ratios to tension steel ratios ρ'/ρ.

2.22 Scholz (1993)

Scholz (1993) examined the aspect of moment redistribution for regular continuous beams. He suggested a new definition of moment redistribution for the Canadian code rules CAN3-A23.3 M84, and suggested new design recommendations. Scholz recommended the removal of the upper bound on redistribution and that ductility limitation should be governed by deflection and cracking under service loads.

2.23 Riva and Cohn (1994)

Riva and Cohn (1994) derived an expression for plastic rotations based on a non-linear analysis model. The effects of section shape, compression reinforcement and bending moment distribution were considered. Rotation capacity was modelled for rectangular, T and I sections with various points and distributed loading conditions of a simply supported beam and cantilevers. They compared rotation capacity formulae with their own recommendations. The research considered material parameters, (i.e. the stress strain relationship of concrete and reinforcement), geometric parameters, (shape of the section, ratio of tensile and compression reinforcement) and loading parameters (i.e. point

load, distributed, cantilevered) and finally structural layout (normal or prestressed concrete). They found that for lightly reinforced sections (steel failure) rotation capacity increases, while for highly reinforced sections (concrete failure) plastic rotation capacity decreases. Riva and Cohn's work was based on earlier research in non-linear analysis of concrete structures that resulted in the development of the analysis program STRUPL-IC, (see Riva and Cohn, 1989).

Other work has been carried out on redistribution in the numerical and experimental fields. However, those presented above have been selected by the author as being the most relevant to the contents and objective of this thesis.

2.24 Summary and Comments

From the previous review of the work on moment redistribution of reinforced concrete, it may be said that there is agreement in the following regarding redistribution:

1. Redistribution of moments due to inelastic action exists at any loading stage, even under service loads. Therefore, it should be considered in the analysis and design of concrete structures.
2. The inclusion of redistribution of moments requires knowledge of the moment curvature relationship and rotational capacity of hinging regions, and maximum tensile and compressive strain in the reinforcement and the concrete respectively. The results, conclusions and opinions expressed in the historical survey emphasise the importance of considering the following factors that affect redistribution:-

- Type of loading condition.
- Strength of concrete.
- Amount and type of tensile reinforcement.
- Moment curvature gradient
- Rotational capacity of the plastic hinges of members subjected to flexural loads.

The experimental program carried out in this research aimed to study one loading condition, i.e., centrally loaded two-span continuous beams, one concrete grade but with different amount tensile reinforcement. This therefore, resulted in a variety of moment curvature gradients and rotational capacities which were investigated here.

Finally, the author recognises that no survey can realistically include all the literature available in English language publications. However, to date no publication has been found by the author that has dealt with redistribution from the same perspective as used in this thesis.

In the next chapter, the experimental work carried out in this research is presented.

CHAPTER THREE

3. EXPERIMENTAL PROCEDURE

3.1 Preface

For some years, work at Durham University has been concerned with the measurement of reinforcement strain distributions by installing electric resistance strain gauges internally within the reinforcement (see Scott, 1989). When the author joined the department, funds were available to investigate the manner and degree of redistribution of internal moments in continuous reinforced concrete beams. With the basic expertise established in installing electric strain gauges in reinforcement, and the ability of the technique to provide detailed and reliable information proven, the possible application to investigate moment redistribution was encouraging. Therefore, it was decided to investigate moment redistribution employing this technique to its full capacity. This chapter describes the background to the experimental work, the strain gauging technique, the specimen details, the equipment and data processing tools and software that were used in the experimental procedure.

3.2 Background

The test program was intended to study moment redistribution in continuous reinforced concrete beams using the available testing technique of installing strain gauges in reinforcing bars. On the analytical front, the aim was to develop analysis and modelling software based on existing programs developed earlier at Durham University. With this in mind, the author selected the reinforcement percentages, layout, bar diameters and beam cross sectional areas. The choice was based on the following factors:

1. Previous knowledge of the influence of bar diameters on the flexural behaviour of reinforced concrete beams, (see Snowdon, 1970) and the possible effect it may have on moment redistribution. The author used different bar diameters to investigate their effect on redistribution.

2. The choice of specimen dimensions was intended to give a wide range of reinforcement percentages and examine the relationship between moment redistribution and ductility.

3. The availability of installing strain gauges in the reinforcement gave detailed information on the strain levels that would be developed in the different sizes of reinforcement. This enabled the author to relate redistribution to ductility.

These considerations were the reasons for the choice of specimen details. However the actual direction of the research program was reassessed after early test had been completed, and some adjustments were made. For instance, beams in series D and E were added to the series of tests later after the completion of series C tests.

3.3 The Strain Gauging Technique

A number of procedures have been developed over the years for measuring longitudinal reinforcement strains. One indirect approach is to interpolate values from surface strain measurements made either with a Demec gauge or with surface mounted strain gauges. This method is approximate, since it is difficult to perform the interpolation with any real degree of confidence or accuracy. Demec gauges can yield very useful data when used carefully, and for this reason they had been widely adopted for a whole range of strain measuring applications. Demec readings give average rather than local strain values. On the other hand, the use of electric resistance strain gauges to measure reinforcement strain is attractive since the data they yield is both more localised and more sensitive than Demec readings. A description of how each strain gauged rod was manufactured now follows.

3.4 Rod Manufacture

Each strain gauged rod was formed by milling two reinforcing rods down to a half round and then machining a longitudinal groove in each to accommodate the strain gauges and their wiring. **Figure 3-1** shows the process of rod manufacture. The strain gauges were installed using cyanoacrylic adhesive and protected with polyurethane varnish. Considerable care was needed in organising and successively bonding down the lead wires as these were added, starting at each end and working towards the middle. After installation of the gauges the two halves were glued together so that

outwardly they had the appearance of a normal reinforcing rod, but with the lead wires coming out at the ends. The rod lengths were 2.6 and 1.5 m long and either 20, 16, 12, 10, 8 or 6 mm diameter according to the specimen details, as will be presented later.

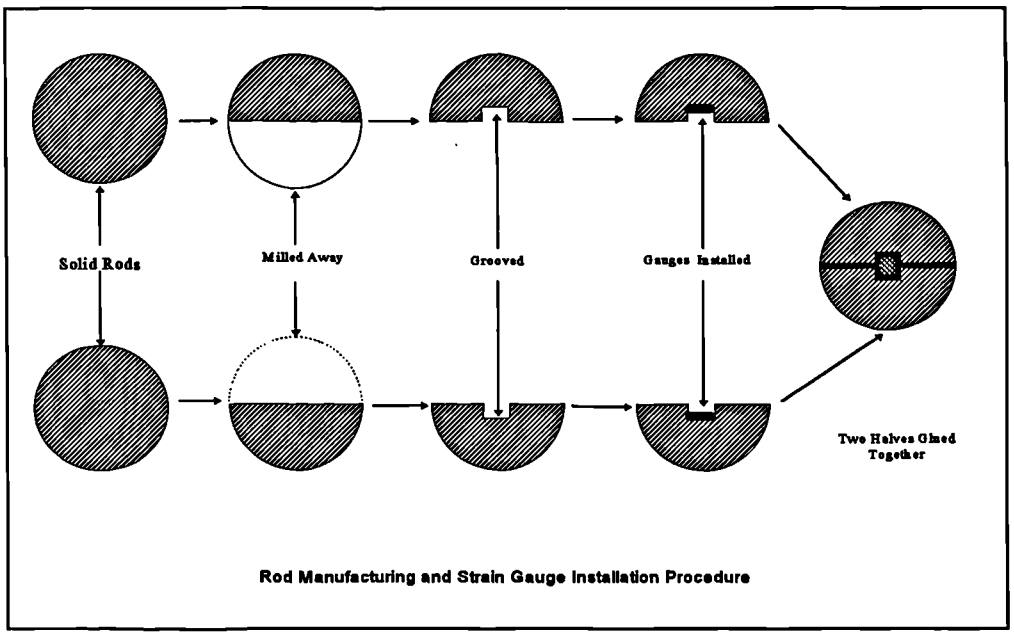

Figure 3-1: Rod manufacturing and strain gauge bedding procedure

The beams were constructed with four reinforcement bars in the left hand half strain gauged; two in the centre support (tension and compression sides) and two in the span. The technique was designed to be completely waterproof to avoid any damage to the embedded strain gauges. This technique left the steel-concrete interface completely undisturbed and a large number of gauges could be installed in quite a small duct (4 x 4 mm) for all bars down to 12 mm bar diameter, (3.2 x 3.2 mm) was for 10 mm bars only, and (2.5 x 2.5 mm) for 8 and 6 mm bars. Detailed and reliable measurements of reinforcement strains were obtained with no disturbance of the surrounding concrete since the gauges were sealed inside the rod. The duct wires were installed and tested to check the validity of the installation of the gauges before casting of the concrete. Occasionally some gauges failed during bar manufacture and at late

stages in a test around cracks in the concrete. However, this was expected. Failure rate was less than 3% when installed.

3.5 Beam Geometry

The test beams were chosen to be two-span continuous beams loaded centrally near the middle of each span. They were divided into six series (A, B, C, D, E and W). Each series contained three beams having the same ratios of tensile and compression reinforcement but with only bar diameter over centre support changed in each series. For instance, the beams in series D had the same amount of reinforcement in the support area, however each of the support sections in the three beams were reinforced with 12, 10, and 8 mm bars respectively. Four bars were strain gauged, two in the left hand span and two over the centre support; one each in the top and bottom of the beam at each of these locations.

The test beams were 5.2 metre long; each span was 2.6 metres. The cross sections were 300 mm wide with overall depths of 400, 250 and 150 mm for series A, B and (C, D, E and W) respectively. Specimen names were coded to identify type of reinforcement, number of bars, size and series. For example, with specimen B3T16A, B identified bar type reinforcement (W being used for wire); 3 was for the number of bars in the tension side over the support region. (T16) was for bar type and diameter (16 mm) and A was for series A. Beams were designed for 30% redistribution according to BS 8110 with adequate shear reinforcement. Shear reinforcement comprised twenty six 10 mm stirrups of high ductility steel for series A and B spaced at 200 mm centres along the length of the beam. For the other beam series, shear reinforcement was fifty one stirrups of 6 mm mild steel spaced at 100 mm centres along the length of the beam. **Figure 3-2** shows the left hand span beam longitudinal reinforcement layout, the right hand span being symmetrical but handed. Beams in Series W beams were reinforced with wire reinforcement (cold drawn, ribbed, high yield steel), which was thought to be less ductile than the bar reinforcement used in Series A,B,C, D and E.

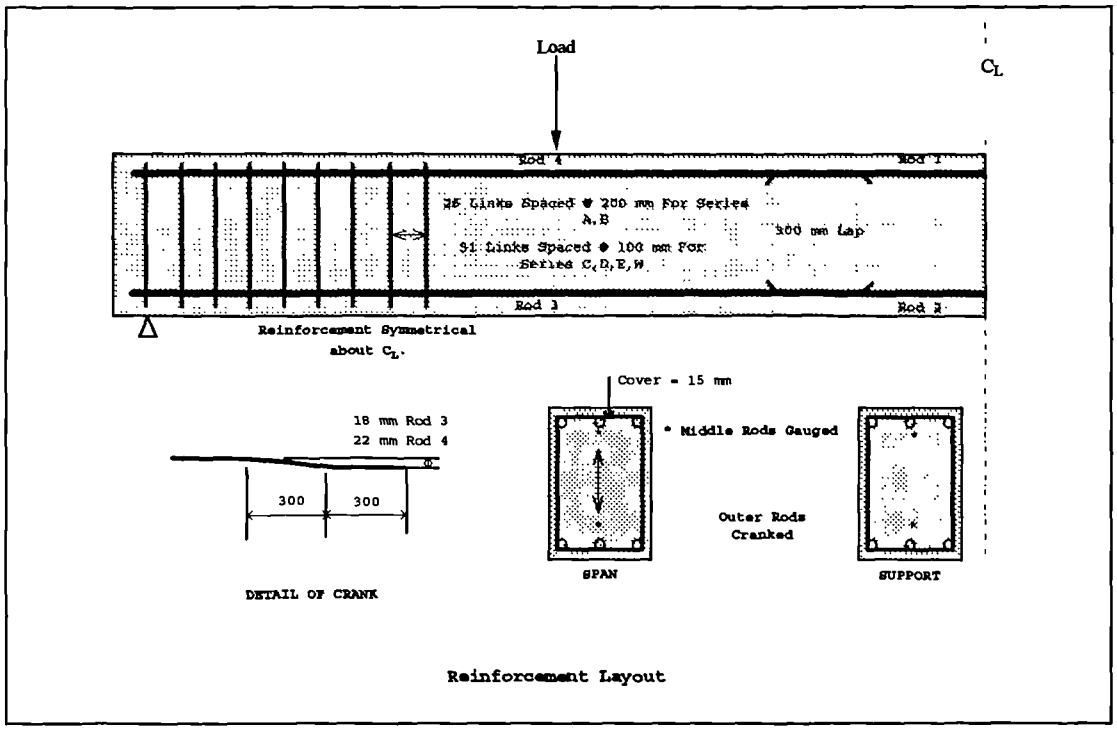

Figure 3-2: Longitudinal reinforcement layout for the test beams.

3.6 Reinforcement Layout and Percentages

The test beams were reinforced with 20, 16, 12, 10, 8 or 6 mm diameter rods. **Table 3-1** lists support and span reinforcement percentages overall cross section dimensions. **Figures 3-3 to 3-8** give detailed layouts of section reinforcement at the support and span areas respectively. Besides the main test specimens listed in **Table 3-1**, one trial specimen, similar to B3T16A but not gauged, was tested at the beginning of the test program to check the reliability of the test equipment. The author would like to point out that specimen B5T12C had faulty strain gauge wires and the load measuring instrumentation failed during the test. Therefore, this specimen was repeated and renamed as B5T12X. Furthermore, specimen B3T16B was repeated (B3T16BL) since the author had extra funds and time to build one more specimen near the end of the test program.

SPECIMEN		SUPPORT					SPAN				
Name	mm x mm	A_s mm^2	ρ %	A_s' mm^2	ρ' %	d mm	A_s mm^2	ρ %	A_s' mm^2	ρ' %	d mm
B3T16A	300 x 400	588	0.54	315	0.29	362	929	0.86	315	0.29	360
B3T16B	300 x 250	576	0.88	312	0.48	217	943	1.46	314	0.47	215
B3T16BL	300 x 250	604	0.93	313	0.49	217	927	1.44	321	0.50	215
B2T20B	300 x 250	625	0.97	322	0.50	215	945	1.46	318	0.49	215
B5T12B	300 x 250	543	0.83	315	0.48	219	934	1.45	314	0.49	215
B3T16C	300 x 150	595	1.64	316	0.87	121	941	2.72	314	0.91	119
B2T20C	300 x 150	625	1.75	311	0.87	119	932	2.70	317	0.92	119
B5T12C	300 x 150	547	1.48	314	0.85	123	931	2.70	339	0.98	119
B5T12X	300 x 150	547	1.48	317	0.86	123	933	2.70	319	0.92	119
B2T12D	300 x 150	201	0.54	229	0.62	123	321	0.87	226	0.61	123
B3T10D	300 x 150	228	0.61	223	0.60	124	321	0.87	230	0.62	123
B5T8D	300 x 150	247	0.66	229	0.61	125	228	0.62	230	0.62	123
B2T8E	300 x 150	91	0.24	94	0.25	125	150	0.40	149	0.40	125
B4T6E	300 x 150	108	0.29	95	0.25	126	146	0.39	148	0.39	125
W2T12D	300 x 150	216	0.59	218	0.59	123	320	0.87	218	0.59	123
W5T8D	300 x 150	241	0.64	225	0.60	125	320	0.87	218	0.59	123
W3T10D	300 x 150	216	0.58	227	0.61	124	325	0.88	215	0.58	123

A_s = Area of Tensile Steel, A_s' = Area of Compression Steel, b = Breadth, d = Effective Depth, $\rho = 100 \times A_s/bd$

$\rho' = 100 \times A_s'/bd$

Table 3-1: Test beam reinforcement percentages and dimensional details

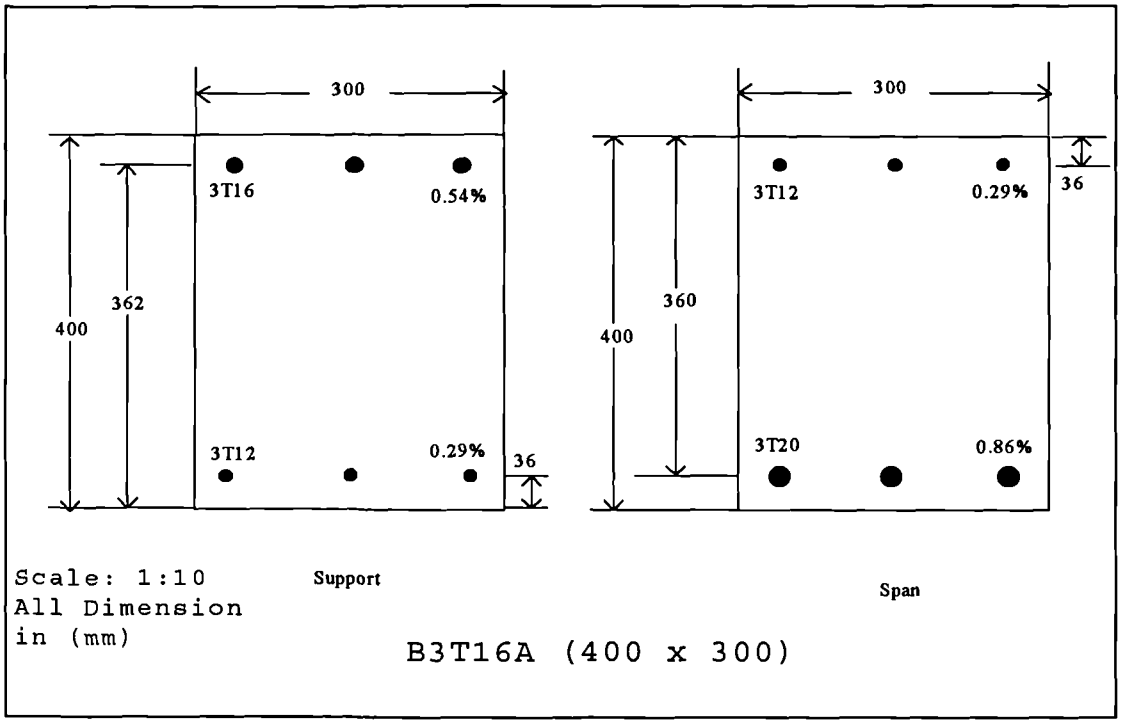

Figure 3-3: B3T16A reinforcement layout

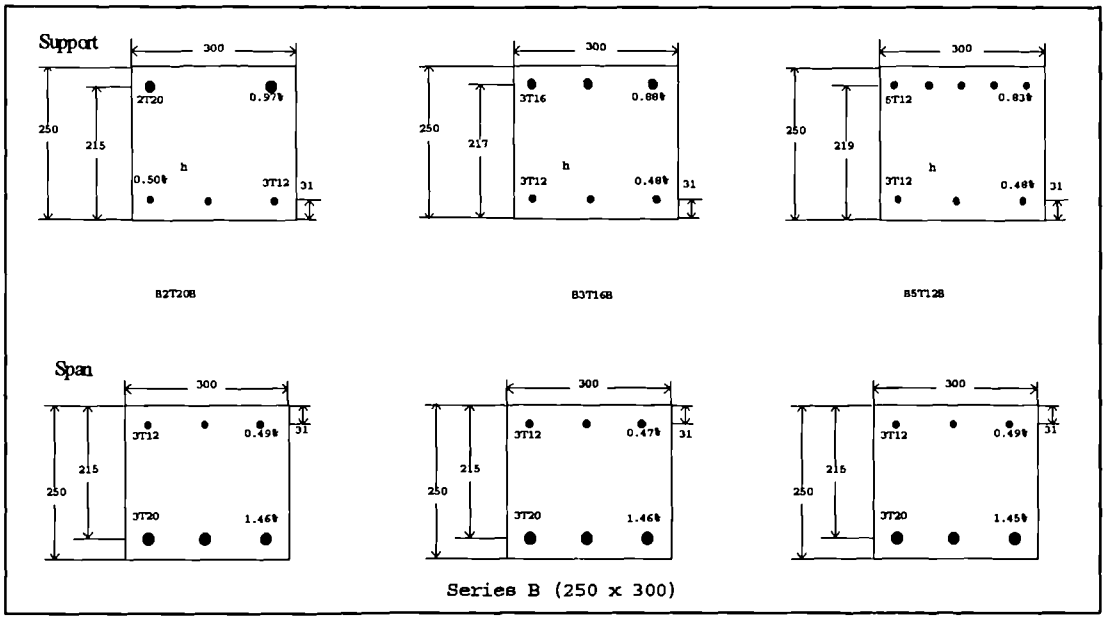

Figure 3-4: Series B test beam dimensions and reinforcement layout

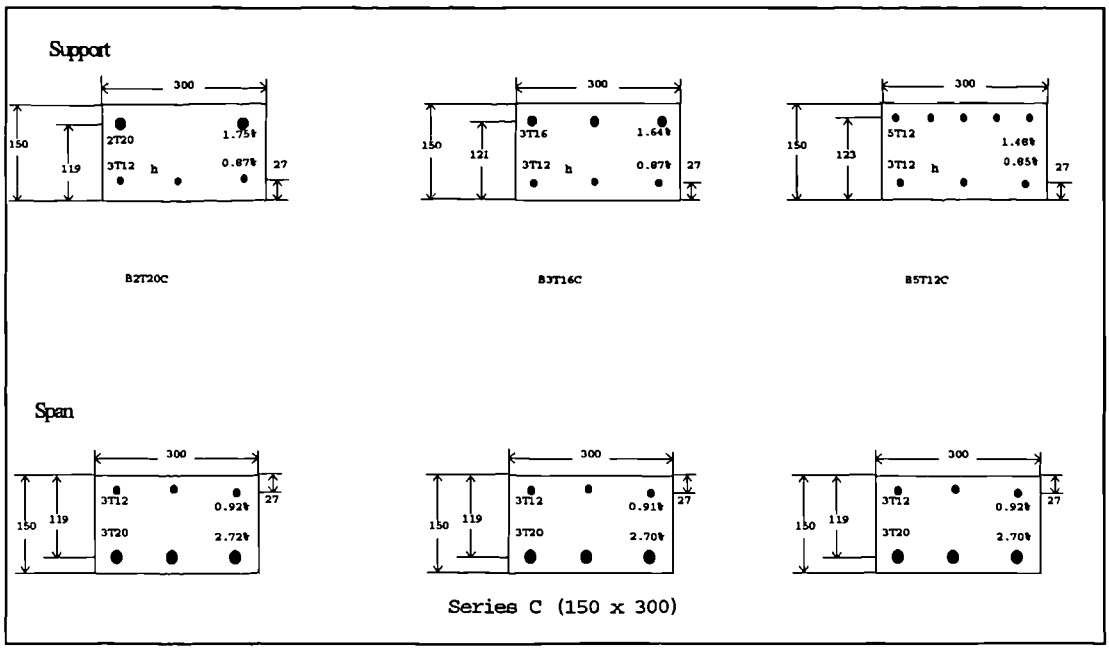

Figure 3-5: Series C test beams dimensions and reinforcement layout

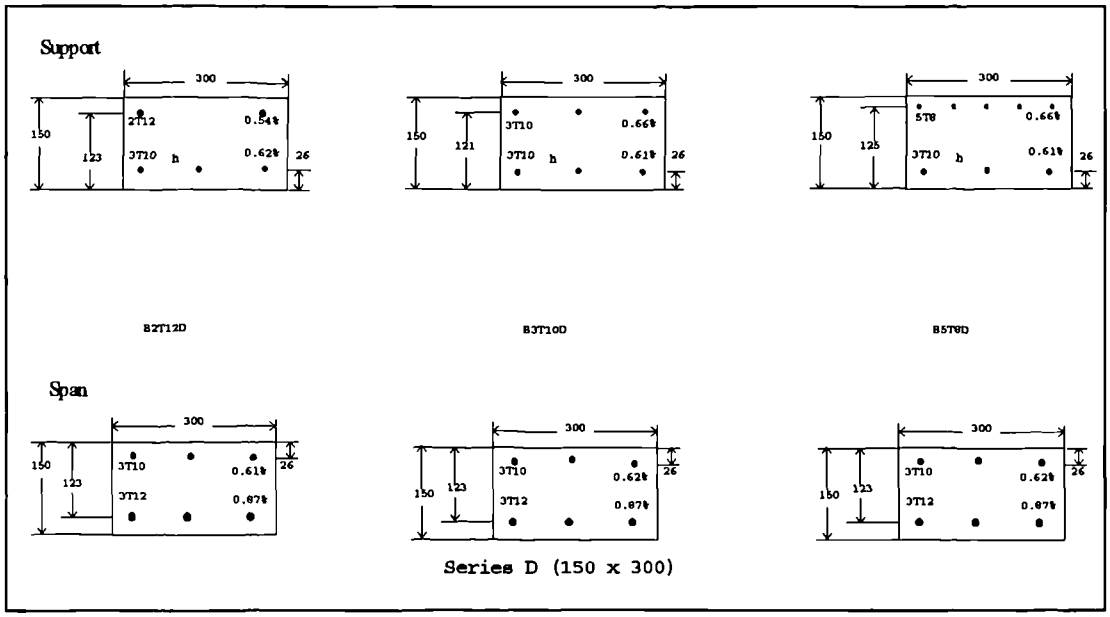

Figure 3-6: Series D test beams dimensions and reinforcement layout

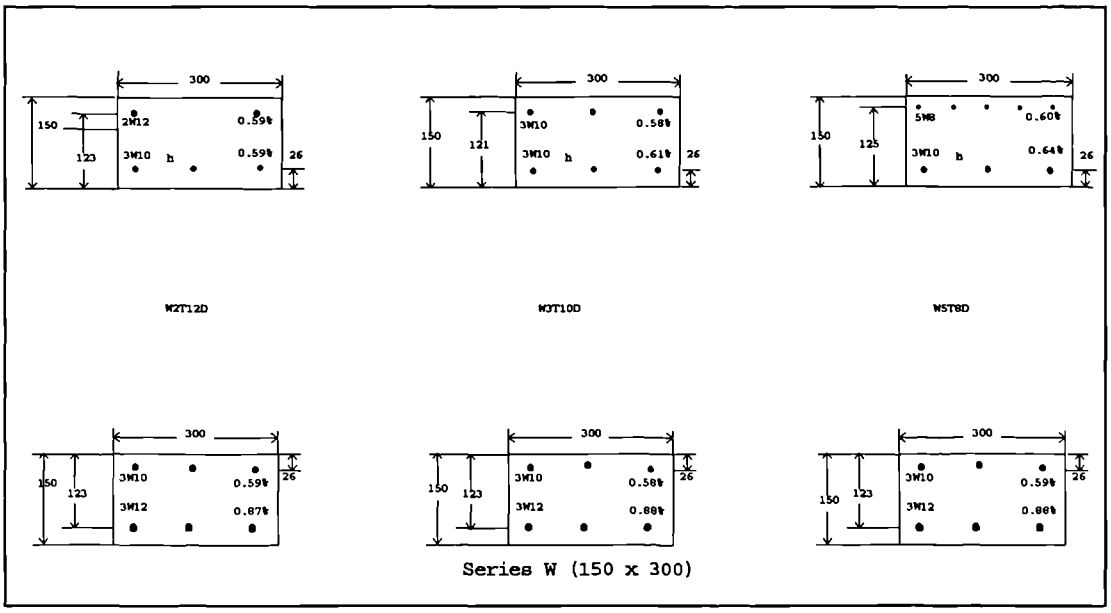

Figure 3-7: Series W test beams dimensions and reinforcement layout.

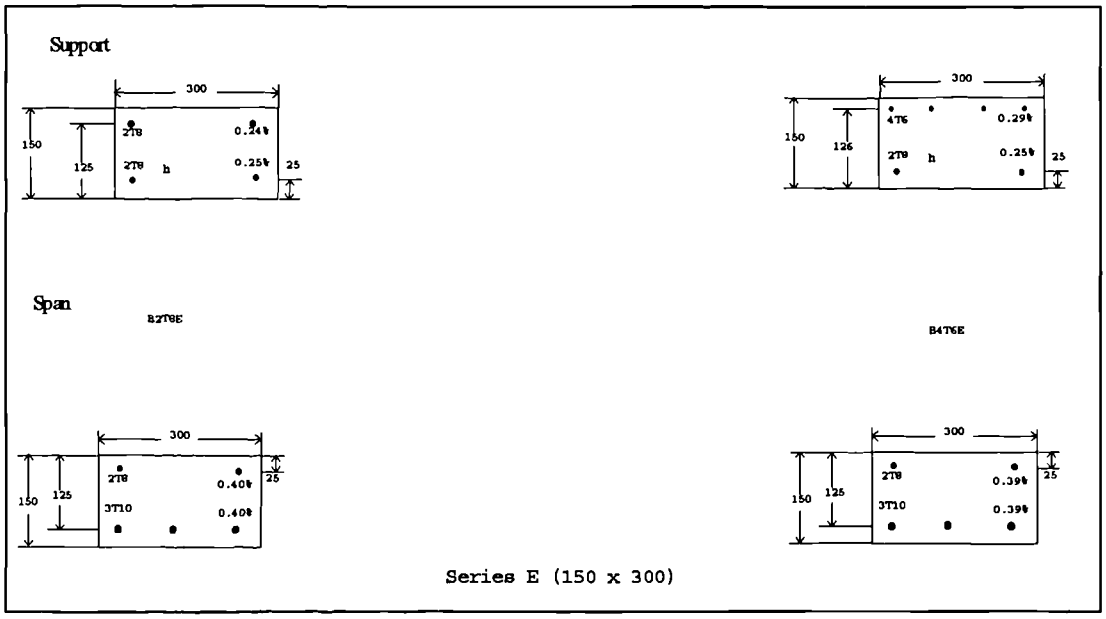

Figure 3-8: Series E test beam dimensions and reinforcement layout

3.7 Rod Gauging Layout

Bar strain gauging layout was influenced by bar diameter. All 20, 16, 12 and 10 mm bars contained 51 strain gauges, while 8 and 6 mm rods accommodated 30 strain gauges along the rods. Four gauged rods were used in each beam; two for the

tension and two for the compression in support and span regions. **Figure 3-9** to **Figure 3-12** show the strain gauge layout for both classes of bar diameters over the support and span areas. Rods numbered 1 and 2 were the support tension and compression rods respectively. Rods numbered 3 and 4 were the span compression and tension rods respectively. The gauges were staggered between both halves of the rod. The spacing decreased from 50 mm at the ends to 12.5 mm toward the centre. Where high strains were expected at the centre support and at the left side loading point, high elongation gauges were provided, having a strain capacity of 10-15%.

Before building the reinforcement cage, the rods were mounted in a test rig and load cycled to check the installation and minimise hysterisis. The results from this procedure were also used to calculate an average value of the cross-sectional area for each gauged rod, as described later.

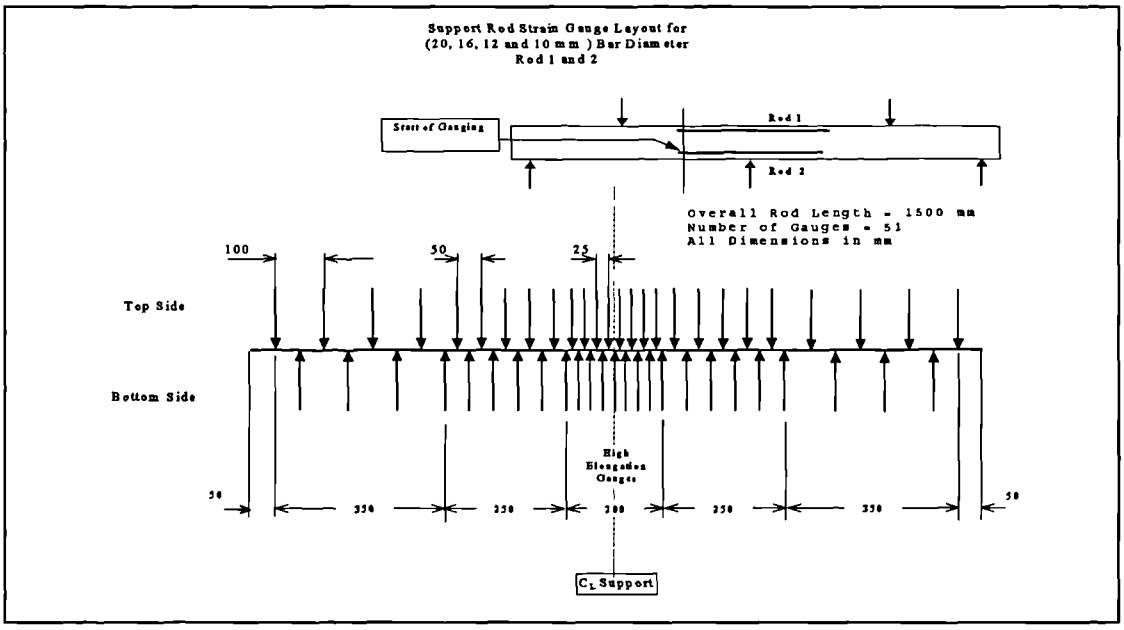

Figure 3-9: Strain gauge layout for support rods: Bar diameters (20 to 10 mm)

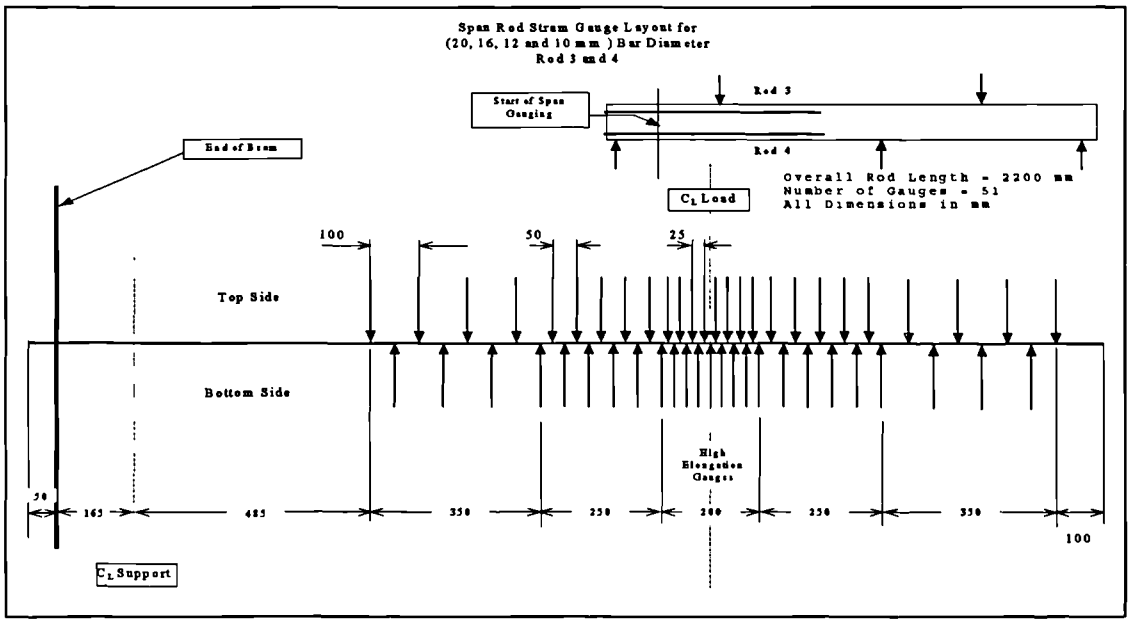

Figure 3-10: Strain gauge layout for span rods: Bar diameters (20 to 10 mm)

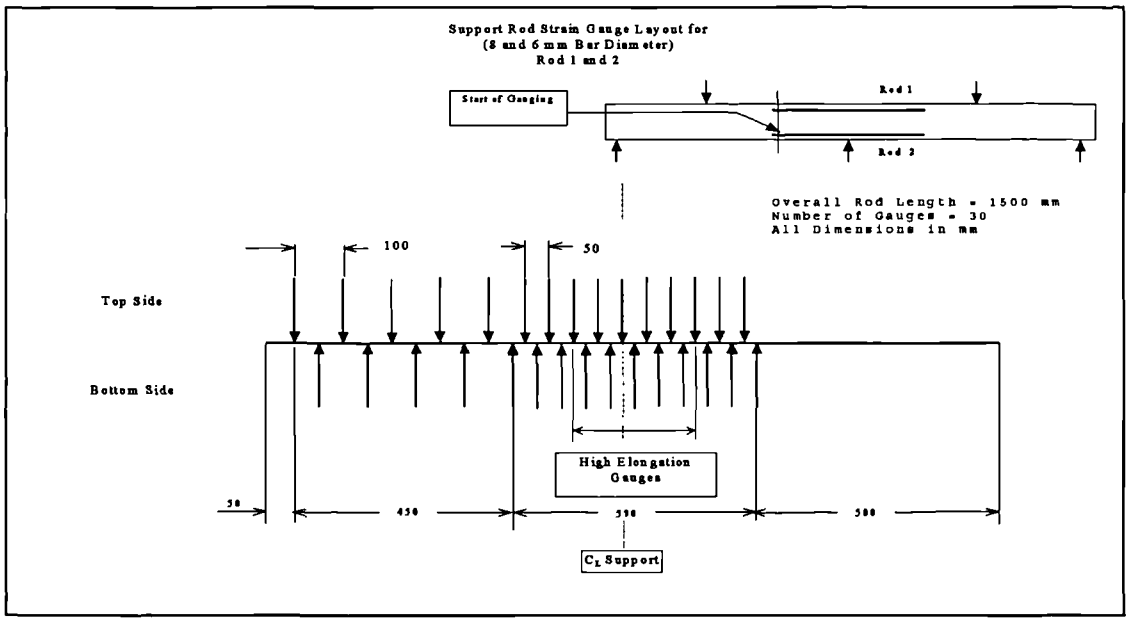

Figure 3-11: Strain gauge layout for support rods: Bar diameters (8 and 6 mm)

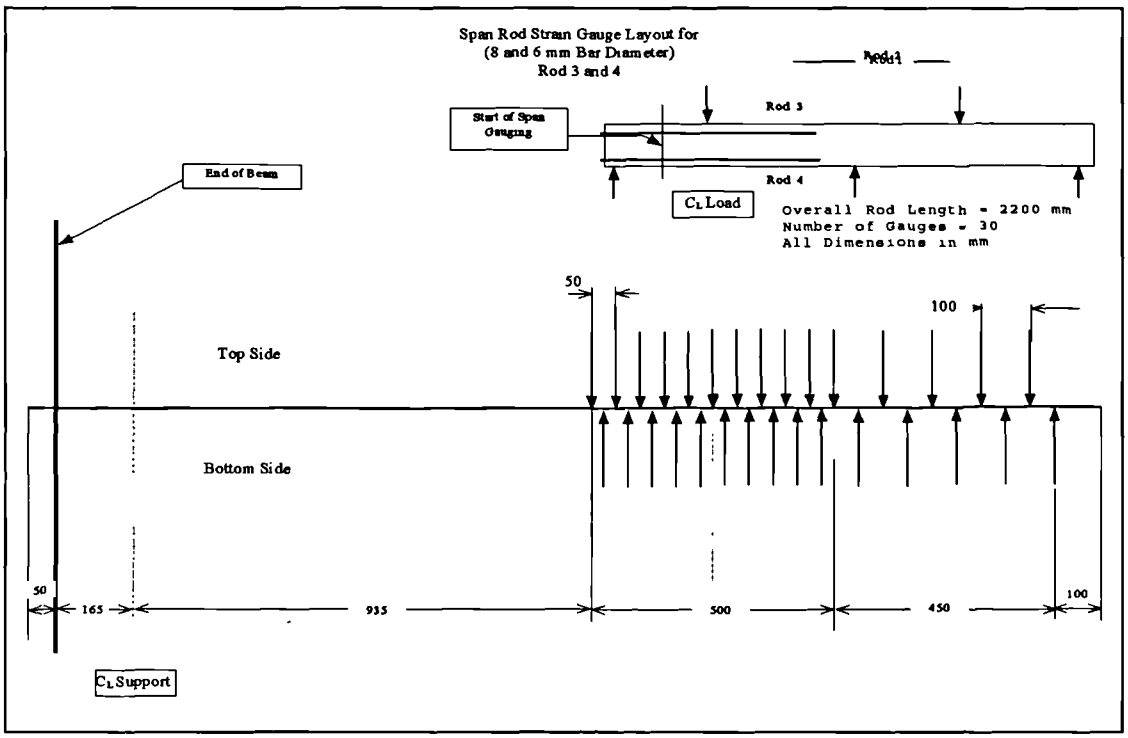

Figure 3-12: Strain gauge layout for span rods: Bar Diameters (8 and 6 mm)

3.8 Mix Design Details

Concrete for all the specimens had a maximum aggregate size of 10 mm, a water to cement ratio of 0.6 and an aggregate to cement ratio of 5.5. Three cubes and three cylinders (and with later specimens six cylinders) were cast with each specimen to determine compressive and tensile strength of the concrete. The extra cylinders were used to establish an experimental stress strain relationship for the concrete. Specimens were left for 24 hours to cure under damp hessian. **Table 3-2** lists measured cube compression failure tests, cylinder tension tests and age of test specimen in days at the time of testing.

SPECIMEN Name	Cube strength MPa	Cylinder Tensile Tests MPa	Age of Test Days	SPECIMEN Name	Cube strength MPa	Cylinder Tensile Tests MPa	Age of Test Days
B3T16A	27.8	3.0	39	**B2T12D**	48.9	2.9	34
B3T16B	47.7	2.9	39	**B3T10D**	41.8	3.00	33
B3T16BL	59.9	3.02	28	**B5T8D**	49.6	2.92	34
B2T20B	47.7	2.96	46	**B2T8E**	49.2	3.30	32
B5T12B	60.4	3.6	30	**B4T6E**	52.0	3.20	32
B3T16C	44.5	2.88	35	**W2T12D**	58.0	2.81	33
B2T20C	47.8	2.55	38	**W3T10D**	59.2	3.12	34
B5T12C	55.3	3.46	60	**W5T8D**	60.8	3.12	32
B5T12X	57.4	3.3	60	**Average**	**51 ≅ Grade 50**	**2.94 ≅ 2.90**	

Table: 3-2 Cube and cylinder test results of the test beams

3.9 Demec Gauging

The average concrete surface strains were measured using a Demec gauge. It was decided that a 200 mm gauge length would give sufficient details for the test beams. Demec studs were glued to one face of each specimen for the purpose of measuring average surface strains on the concrete, for comparison with electrical strain gauge readings. **Figure 3-13** shows a detailed layout of Demec gauges for all beam series. Series A, B and C had 11 columns of Demecs while the beams in series D, E, W had 19 columns. This alteration in the number of Demec columns was introduced to get a more exact curvature distribution along the beams.

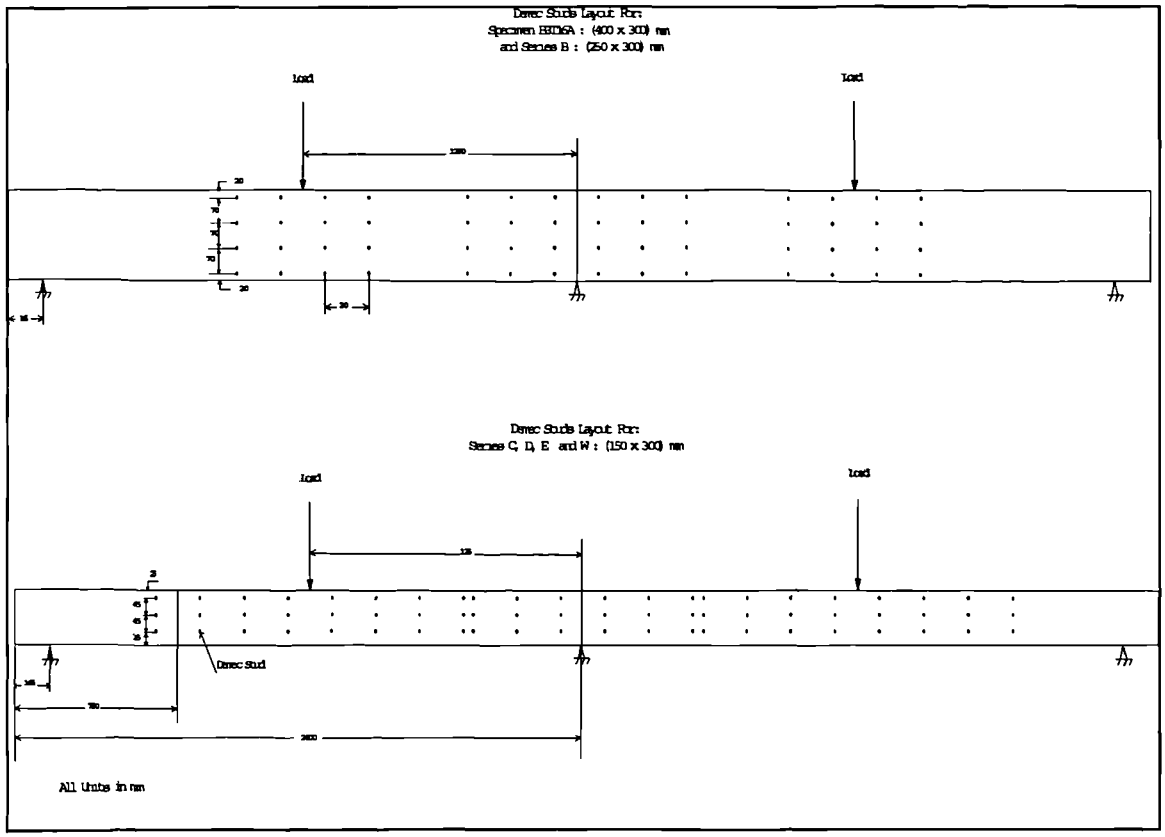

Figure 3-13: Demec gauge layout for all the beam series

3.10 Deflection Measurement

A specially constructed apparatus used for deflection measurement was built to fit on the test rig to carry the dial gauges. The dial gauges were placed under the beams at the two point loads to measure the deflection there. Usually deflection readings were taken at the same load stages as Demec readings. Deflection readings ceased when either the gauge would not translate any further or when the beam approached failure when it became unsafe to take any further readings. During the final load stages near the failure load, the author attempted to take further deflection readings using a steel ruler.

3.11 Testing

A test rig was purpose built to accommodate the test beams, as shown in the picture in Error! Number cannot be represented in specified format.. Loads were

applied using manually pumped hydraulic jacks, and load-cells were provided to measure beam loads and support reactions. The two load cells for applied load measurement at the centre of each span were connected to pre-set, pre-calibrated digital meters which displayed the load value in kN and were also connected to the data logger. Load cells measuring support reactions were directly connected to the logger. The specimens were loaded incrementally with the increment size varying depending on specimen size, reinforcement layout and the pattern of strains developed in the gauged rods as the test progressed. Typically load increments were 5 kN, but could be as fine as 0.5 kN.

Strain gauge and load cell readings were recorded at every load stage by a computer controlled data logger. Messages were also recorded when cracks occurred. Demec and dial gauge readings were also taken periodically at selected load stages. Cracks were marked on the beam face as the test progressed. Testing normally continued until it was not possible to increase the load any further. After testing and on the same day, the cubes and cylinders were tested and results were recorded.

During handling, around 28 days after casting, strain gauge wires of Rod 1 over the support in specimen B5T12C were severed. Therefore, the rod was dug out and another gauged rod was grouted in. Furthermore, in two exceptional cases beams B5T12C and B5T8D, a pump failure halted testing at 12.5 kN in each case. Testing was resumed later after repairing the faulty pump. Due to the grouting of another rod and the unfortunate pump failure in B5T12C, the author decided repeat B5T12C as B5T12X . The combination of these two event on B5T12C caused increased redistribution which is discussed in section 5.2.2.3.

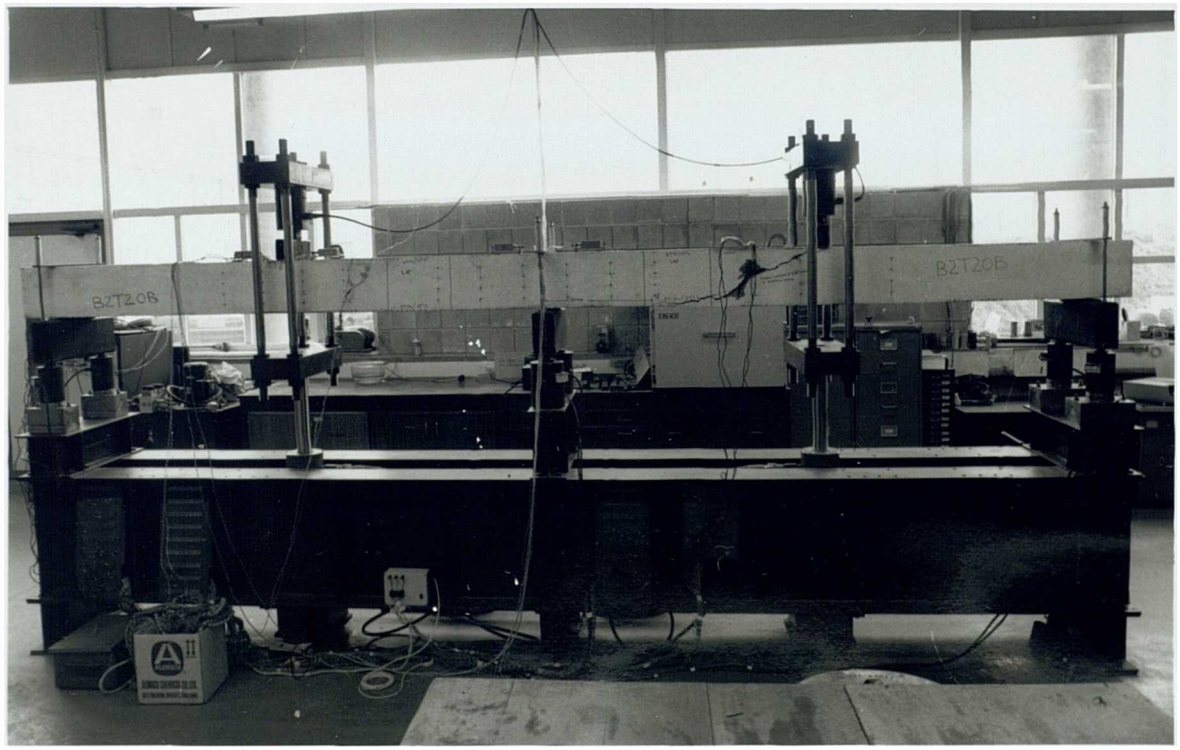

Figure 3-14: Picture of test beams rig.

3.12 Equipment and Data Processing Tools

3.12.1 Hardware

The data was collected through a 256 channel data logger that logged all the strain gauges and load cells. It was linked to a PC using purpose written interfacing software developed at Durham University see (Scott and Gill, 1984).

3.12.2 Software

3.12.2.1 LOGGER

LOGGER is a data collection program developed by Scott, (see Scott and Gill, 1984) especially for interfacing the data logger with a P. C. The program is very flexible in controlling data output and storage from the logger. A typical logging session normally starts with opening files on the hard disk. Data such as gauge factor, gauge resistance, number of active arms, calibrating loads and voltage for the load cells are entered interactively and later a double check can be conducted on all data entered. Groups of data can be scanned and saved on the hard disk with full records of date and time, and extra information may be entered interactively if needed. The software gives a display on the screen of strain and load data both with engineering units and in volts. Furthermore, it is possible to interrupt a logged session and reconnect again later should this prove to be necessary. Once a session is complete, data files can be easily transferred to other computer systems for further processing.

3.12.2.2 YMOD

An analytical program was developed by Scott (1985) for calculating actual areas of the gauged rods using the strain gauge readings generated by the bedding-in procedure. The bedding-in procedure involved load cycling each rod to around 500 microstrain about ten times to eliminate the effect of strain gauge hystersis. The first function of the program was to present this data in a compact and readily comprehensible form. Then, as part of the final part of the load cycling procedure, each rod was incrementally loaded until a strain level of about 500 microstrain (a strain level well within the elastic range of the stress-strain behaviour) and then unloaded using the same load steps. A linear regression analysis was performed by the program for both the loading and unloading curves using the average of all the strain gauge

readings for each load stage. The reason for this procedure was to calculate the average strains of the two loading and unloading regression lines which were proportional to the Young's modulus of the steel being used. Young's modulus was predetermined as 200 kN/mm^2 for both high ductility and wire reinforcement by tests of solid specimens. Given Young's modulus and the load/strain relationship for a particular bar, the actual average cross-sectional area of the gauged rods was easily calculated.

3.12.2.3 FASTLIST

FASTLIST was another program that was developed by Scott, (see Scott and Gill, 1984) in conjunction with the above two programs. After data has been logged, FASTLIST re-arranged the data into a compact form for subsequent output to the screen or to a file for hard-copy print-out. Output was displayed in a matrix-like form which listed load cell readings and strain gauge readings combined with extra information, date, time and messages. From FASTLIST it was possible to construct a load data file for later use in the analysis.

3.12.2.4 CONNECT

CONNECT was another data processing tool developed by Scott, (see Scott and Gill, 1986) which gave hard copy and screen display data output and graphics. Output consisted of strains, local and average bond stress and average strain. The software was written in such a way that faulty strain gauge readings were omitted from the output by giving them dummy values outside the range of acceptable ones. Furthermore, the software gave graphical output of strain and bond distribution at any desired loading stage through an interactive menu. This program was an important tool in the analysis as it was later developed by the author to calculate curvatures, redistribution, and neutral axis depth ratios. The development of CONNECT arose as the need for additional detailed analysis and insight into the beams' behaviour was identified. Full details of the development of CONNECT will come later.

CHAPTER FOUR

4. DATA ANALYSIS SOFTWARE

4.1 Introduction

The experimental work presented in Chapter Three created a need for a data processing system to record and analyse the Demec and strain gauge data. Previous software like CONNECT was written by Scott (1984) to cope with strain gauge data in any general layout. The author developed this program to analyse two-span continuous beams. This program (CONPCY) as developed by the author was a major piece of work in the analysis of the load and strain gauge data. The author also wrote a program to deal with the Demec data that were produced from the test beams. Both programs (CONPCY and NEWDEM) were written in the FORTRAN language and compiled on both the UNIX and p.c. systems. A detailed description of these two programs is presented next.

4.1.1 NEWDEM

After the Demec data were collected from each specimen (approximately 8000 readings in total were taken for all the specimens), the data were fed into NEWDEM in their raw form. NEWDEM incorporated a linear regression (least squares) analysis for each column of Demec data to obtain best fit strain values across the beam Demec depths at every load stage. The best fit lines were calculated based on a minimum of three data points. Whenever three points were not available for linear regression (due to faulty Demec studs), two points were considered. In addition, the program calculated at each Demec position the following:-

1. Strain values at each level corresponding to Demec positions including top and bottom face strains.
2. Neutral axis depth and neutral axis depth ratio ($\frac{x}{d}$).
3. From the load data, experimental and calculated bending moment and percentage of redistribution over the spans and the support sections.
4. From both load data and Demec calculated strains, curvatures and stiffness at each Demec position were calculated.

Two versions of the program could be used, one written to run on a p.c. and one on the UNIX computers at the university. The advantage of the latter one was the instant production of screen and hard-copy graphics. The graphical output of the data was flexible as it was possible to produce strain distributions at each Demec section. The PC version of NEWDEM was written and compiled to produce data compatible with the Microsoft Excel spreadsheet to make possible the graphical comparison between different specimens and for presentation graphics. A typical hardcopy output from the regression line analysis program is shown in **Figure 4-1**.

The results from NEWDEM were used in subsequent analyses in conjunction with results from the program CONPCY which is described next.

Figure 4-1: Sample output from NEWDEM

Calculated strains along the beam using linear regression
DEMEC TEST DATA: SPECIMEN B3T16A: 21/5/91
BEAM DEPTH = 400.00 mm
LOAD
60.00 (KN)

Position along the beam (mm)

	1150.00	1350.00	1550.00	2200.00	2400.00
	Strains down the beam depth (microstrain)				
0.000	-117.92	-128.79	-108.98	18.36	72.87
35.000	-95.18	-104.85	-87.80	12.00	60.47
145.000	-23.73	-29.62	-21.27	-8.00	21.49
255.000	47.73	45.62	45.27	-28.00	-17.49
365.000	119.18	120.85	111.80	-48.00	-56.47
400.000	141.92	144.79	132.98	-54.36	-68.87

****

Calculated strains along the beam using linear regression
DEMEC TEST DATA: SPECIMEN B3T16A: 21/5/91
BEAM DEPTH = 400.00 mm

LOAD
60.00 (KN)

Position along the beam (mm)

	2600.00	2800.00	3000.00	3650.00	3850.00
	Strains down the beam depth (microstrain)				
0.000	287.27	196.40	55.39	-117.89	-123.09
35.000	247.14	165.18	48.65	-97.26	-92.80
145.000	121.05	67.06	27.46	-32.42	2.40
255.000	-5.05	-31.06	6.27	32.42	97.60
365.000	-131.14	-129.18	-14.92	97.26	192.80
400.000	-171.27	-160.40	-21.66	117.89	223.09

****

Figure 4.1 (Sheet 1 of 2)

Calculated curvature from linear regression

DEMEC TEST DATA: SPECIMEN B3T16A: 21/5/91

	Curvature(e-6/mm)					
Distance(mm),	60.00,	100.00,	140.00,	200.00,	240.00,	300.00,
1150.00,	-0.65,	-1.35,	-2.90,	-4.62,	-5.83,	-7.73,
1350.00,	-0.68,	-2.24,	-3.60,	-5.74,	-7.54,	-9.55,
1550.00,	-0.60,	-1.42,	-3.17,	-5.32,	-6.54,	-8.21,
2200.00,	0.18,	0.19,	0.25,	0.26,	0.22,	0.86,
2400.00,	0.35,	0.67,	1.11,	7.33,	10.59,	17.59,
2600.00,	1.15,	4.65,	9.66,	15.09,	19.78,	19.78,
2800.00,	0.89,	0.55,	1.10,	1.40,	6.24,	10.54,
3000.00,	0.19,	0.27,	0.16,	0.44,	0.95,	1.19,
3650.00,	-0.59,	-1.49,	-3.69,	-8.82,	-11.60,	-15.74,
3850.00,	-0.87,	-2.80,	-4.37,	-6.55,	-7.94,	-9.90,
4050.00,	-0.59,	-1.44,	-3.06,	-4.90,	-6.35,	-8.11,

" Position 6 At position = 2600.00 mm along the beam"
"HSPAN = 324.00"
"HLAP = 325.00"
"HSUP = 325.99"

"Elastic" "mom",	" Exp" "mom",	"Top" "Strain",	"Bot" "Strain",	"Curv" "1e-6",	"EI" "KNmm2",	"x" "mm",	"x/d"	"%" "BETA"
0.267E+05,	0.228E+05,	287.,	-171.,	1.15,	19864.6,	149.40,	0.424,	-14.861
0.447E+05,	0.326E+05,	1492.,	-368.,	4.65,	7007.2,	79.08,	0.225,	-27.100
0.630E+05,	0.449E+05,	3299.,	-563.,	9.66,	4650.2,	58.34,	0.166,	-28.757
0.900E+05,	0.651E+05,	5323.,	-715.,	15.09,	4310.0,	47.35,	0.135,	-27.689
0.108E+06,	0.757E+05,	6902.,	-1010.,	19.78,	3824.3,	51.08,	0.145,	-29.953
0.133E+06,	0.933E+05,	7160.,	-752.,	19.78,	4718.5,	38.02,	0.108,	-30.043

Listing of Load Data matching Demec loads

Loads (kN) matching Demec loads

Load #	MATCH	LHS load	RHS load	DEMEC load
1	1	0.0	0.0	0.0
2	5	60.3	58.0	60.0
3	9	99.9	97.7	100.0
4	15	140.1	138.7	140.0
5	22	199.5	198.4	200.0
6	26	239.3	238.4	240.0
7	33	300.7	289.4	300.0

Figure 4.1 (Sheet 2 of 2)

4.1.2 CONPCY

CONPCY was a major piece of software developed by the author from CONNECT, which was described earlier in Chapter 3. The author carried out this development to enhance the level of analysis of the strain gauge data. The program first read the rod strains, load and geometry of the beam and the rods. Then CONPCY transformed the strain gauge data of separate rods to a beam configuration with rod strains identified by top and bottom strains along the beam. For instance, each beam had four rods laid out as shown in **Figure 4-2.** Rod 1 and rod 3 gave the top beam strains. Rod 4 and Rod 2 gave the bottom beam strains. In the area where the rods lapped, the arithmetic averages of the strains in each rod at both levels were computed, noting that during the gauging and construction of the beams, considerable care was taken to coincide the gauge positions in the lapped region.

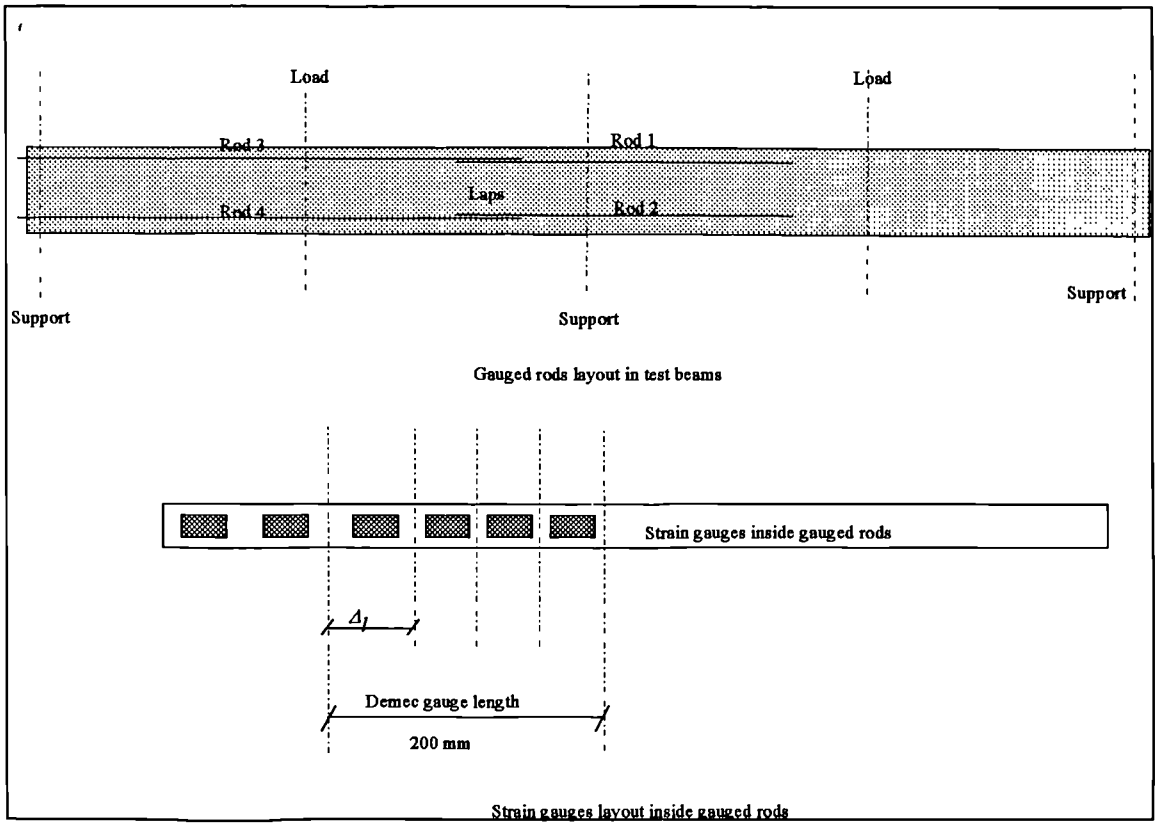

Figure 4-2: Strain gauge averaging technique and gauged rods layout

Once the beam strains had been defined, the program then calculated the average strains from the strain gauges over a length of 200 mm which corresponded to

measured strains from the Demec gages. The average strains were calculated according to the following expression and as shown schematically in **Figure 4-2.**

$$\varepsilon_{200} = \frac{\sum \varepsilon_i \Delta l_i}{\sum \Delta l_i} \qquad \textit{Equation 4-1}$$

Where:-

ε_i = The strain gauge reading falling in the Demec gauge range

Δl_i = The gauge surrounding length

n = The number of strain gauge readings within the Demec range

ε_{200} = The calculated average strain over the gauge length.

After the transformation to beam strains, further calculations were carried out to calculate local[1] and average moments, curvatures, flexural stiffness, neutral axis depth ratios and moment redistribution. In a similar manner to NEWDEM, the following graphical as well as hard-copy output could be obtained:-

1. Strain distribution along the beam (top and bottom).
2. Curvature distribution at any desired load stage.
3. Average strain distribution over Demec gauge length (200 mm) along the beam.
4. Average curvature distribution over 200 mm gauge length matching Demec positions.
5. Average moment curvature relationship matching Demec positions
6. Neutral axis depth ratio versus redistribution diagrams over the support and span sections.
7. Experimental moment or curvature versus percent of redistribution along any section of the beam.

Later during the course of the research, the author further developed the program to carry out calculation of measured average plastic hinge properties based on experimental yield strain values of the respective rods. Calculation of average strains,

[1] Local strains refer to strains produced from a single strain gauge.

curvatures, rotations and neutral axis depth over the plastic spread length were carried out. The details of these calculations are presented in Chapter Five. CONPCY was written and compiled for the PC user to produce output that was compatible with Microsoft EXCEL spreadsheet, to enable the comparison between the different test beams and to compare the results with the actual Demec data. The next chapter gives details of the experimental results.

The output form CONPCY is extensively presented in Chapters Five and Eight. All experimental strains, curvatures, moment redistribution and neutral axis depth and calculated rotations from strain gauge data were outputed using CONPCY.

CHAPTER FIVE

5. EXPERIMENTAL RESULTS AND ANALYSIS

5.1 Preface

This chapter presents the experimental results and analysis on the 17 two-span continuous reinforced concrete beams described in Chapter Three. The results of the laboratory work were analysed using software developed by the author as presented in Chapter Four. The beams' behaviour is described in terms of moments, strains, curvatures, neutral axis depth, crack pattern, plastic hinge rotations and lengths. The results presented here demonstrate the performance of the new software and the experimental techniques used in assessing measured moment curvature relationships of the tested beams. Moment redistribution is discussed here from an experimental point of view. For convenience and clarity, the results, tables, figures and charts are included at the end of the chapter.

5.2 Moment Redistribution and Load Data

The principal test data are summarised in **Table 5-1.** Loads, reactions, moments and moment redistribution of the specimens at the support and the two span sections are given for all the beams at maximum load. Maximum deflections listed in **Table 5-1** that developed under both spans were, in some cases, extrapolated from the last two measured points, since dial gauges were not mounted throughout the testing period. Moments over the support and in the spans were calculated from the measured forces and support reactions taking into account error adjustment of reaction load cells. Redistribution was calculated according to **Equation 5.1**

$$\beta = \frac{Measured\ Moment - Elastic\ Moment}{ElasticMoment} \times 100\% \qquad Equation\ 5\text{-}1$$

Where the *Elastic Moment* was calculated on the assumption of constant stiffness along the beam.

Redistribution started from very early loading stages, even before cracks appeared on the surface of the beams. The degree of redistribution was different in

each beam series. Furthermore, moment redistribution differed in beams reinforced with different bar diameters over the support. **Figures 5-1** to **6** show the experimental redistribution of all specimens in each series respectively, plotted against experimental bending moment at the centre support. With increasing load, redistribution increased to a point where it reached a plateau level up to and before the beginning of yield of the reinforcement over the centre support. After the reinforcement over the support yielded, more redistribution of the support moment took place. When the maximum moment over the support was reached the beam loads could still be increased, although the support moment stayed constant because the moment capacity in the spans had not been reached. Some redistribution values exceeded 35%. Redistribution behaviour of each beam series is presented next.

5.2.1 Specimen B3T16A

Specimen B3T16A developed constant redistribution with increasing moments after initial cracking. The left and right hand side spans' redistribution were very similar. The experimental redistribution curve in **Figure 5-1**, shows that in some instances, the moment at a higher load stage was lower than the previous one whereas the redistribution value had increased. This was mainly due to the waiting period during Demec reading that caused a relaxation of the bending moment. To overcome this effect, the author took several readings of the load data before, during and after Demec readings. Moment redistribution reached a maximum of 31.9% at the support and 16.2% and 20.3% for the left and right side spans respectively.

5.2.2 Series B

Throughout the load history, Series B developed higher redistribution (except B3T16BL) for the beams with bar diameters of 16 mm and 20 mm than for specimen B5T12B with 12 mm bars. See **Figure 5-2**. This was mainly due to increased crack development in the beams with larger bar diameters. Furthermore, when examining the redistribution trends for B3T16B and B2T20B, redistribution initially climbed and then dropped slightly. The curve then developed a flat plateau of redistribution. This slight decrease in redistribution may be attributed to the effect of tension stiffening. At maximum load, redistribution in B2T20B (20 mm bars) was around 10% lower than

the other specimens in the series. When observing the failure relative stiffness of the test beam series listed in **Table 5-2**, it can be seen that the relative stiffness (i.e. ratio of centre support stiffness to the left side span stiffness) of B2T20B at failure was higher than all the specimens apart from B3T16BL. Hence moment redistribution for B2T20B at maximum load was 10 % lower than the others except B3T16BL.

B3T16BL developed the highest value of relative stiffness at failure, therefore, redistribution was the lowest in the series. The behaviour of B3T16BL is interesting. Although the specimen was similar to B3T16B, the beam still developed different redistribution from that of B3T16B. Possible explanations for this are presented next.

The areas of tension steel in B3T16B over the support and span were 576 and 943 mm^2 respectively. This meant the ratio of support to the span areas of steel was 0.610. B3T16BL areas of tension reinforcement over the span and support sections were 604 and 927 mm^2 respectively. The ratio of support to span tension bars areas was 0.65, indicating that B3T16BL is approximately 5% stiffer at the support than B3T16B. Hence redistribution for B3T16BL was lower.

The average relative stiffness of B3T16BL listed in **Table 5-2** was greater than that of B3T16B. This may be the result of the difference in concrete strength of 59.9 and 47.7 MPa respectively **(see Table 3-2)**. In consequence, redistribution throughout the load history was lower in B3T16BL. Furthermore, it is noticeable that B3T16BL and B5T12B on one hand, and B3T16B and B2T20B on the other, developed similar redistribution curves for part of the load history. This could be attributed to the similar crack patterns which developed in each pair respectively.

5.2.3 Series C

Beams in series C developed similar trends to series B. See **Figure 5-3.** Before the support or the span cracked, the redistribution curves for three specimens B3T16C, B2T20C and B5T12C showed high initial redistribution. This may be attributed to the different degree of compaction of the concrete throughout the beam. Furthermore, the beams could take slightly more load stages before one or more of the supports were fully settled on the rig. Looking closely at the results of redistribution of specimen B5T12X shown in **Figure 5-3**, it is seen that at around 6 kNm of applied

moment (at 14.1 kN of applied load) over the support, redistribution in B5T12X was nearly zero, despite the fact the beam was already cracked, where the concrete top strain at the support and the concrete bottom strain at the span were 532 and 370 microstrain respectively. The stiffness at the support and span at this load stage were 1960 and 1751.9 $kNmm^2$ respectively. Therefore, the higher stiffness at the support relative to the span caused the redistribution to be at this very low level. After this, redistribution continued to climb with increasing moment, but at a lower level than the other specimens in the series. This may be caused by the small bar diameter (12 mm) used in B5T12X which caused fewer cracks to appear, than B3T16C (16 mm bars) and B2T20C (20 mm bars). As a result, redistribution stayed low. Although B5T12X was similarly reinforced as B5T12C, the latter developed higher redistribution than B5T12X. This was mainly due to rod 1 in the support area being replaced after casting and curing. This repair of the specimen meant the new concrete was bonding with already aged concrete. Therefore, at the time of testing, concrete in the support area comprised two different concrete ages, with the possibility being that bond failure occurred at the interface of the bar surface and the new and old concrete in the support area. This was a likely cause of the increased redistribution. B5T12C also had unexpected pump failure at 12.5 kN, after the beam had initially cracked, thereby forcing the testing to be restarted later. When the test was resumed, the beam was already cracked. The combination of the rod replacement and cracked beam may well have contributed to the increased redistribution in B5T12C when compared to the repeat specimen B5T12X. None of the beams in this series reached full moment capacities due to shear failure.

The relative stiffness of the test beams was investigated. **Table 5-3** lists the average and at failure relative stiffness and redistribution for the beams in series C. It can be seen that at failure, specimens with high values of moment redistribution had low values of relative stiffness. However, this was not the only factor affecting redistribution. The development of plastic strains in the specimens contributed little to the redistribution that took place, since only a few strain gauges developed plastic strains in the support and span areas.

5.2.4 Series (D, E, W)

In series D and W (**Figures 5-4** and **5**), redistribution was caused more distinctly by the development of a few or even a single cracks near the support. From **Figures 5-4** and **5** the effect of the reinforcement yielding is clearly visible, with the effect of the different bar diameters on redistribution being less significant. However, it was noticed that specimens with 8 mm bars developed slightly less redistribution over the support than the 12 and 10 mm bars. The beams in this series developed plastic strains in the tension reinforcement over both the span and support sections.

Table 5-4 lists relative stiffness values and redistribution of series D, E and W averaged over the full load history and at failure. The average of all load cases and maximum redistribution were very similar, except B5T8D and W5T8D which both developed less redistribution than the rest of the beams. This may be attributed to different crack patterns and the small bar diameter of these specimens, causing fewer cracks than the rest and hence lower redistribution. There was no noticeable difference between wire and bar specimens.

In Series E, specimen B2T8E, (**Figure 5-6**), developed high initial redistribution which may have been caused by a combination of the following factors:

1. Low value of initial relative stiffness (0.078) for the first load stage.
2. The support section was pre-cracked before the commencement of testing due to the very low percentage of reinforcement (0.39 and 0.25) in both the span and support areas respectively
3. Possible different degrees of concrete compaction throughout the length of the beam. It may be possible that concrete at the bottom of the beam developed higher strength than the top. In other words, there was stronger concrete in the span and so a stiffer span section. Higher redistribution developed as a result.
4. Unsettled support conditions at the early load stages. The beam required a few load stages to be applied before it was fully settled on the rig.

In both B2T8E and B4T6E (see**Table 5-4**) redistribution reached the high value of 39% at maximum applied moment, and the tension reinforcement at both the

span and support section exhibited gross yield. The author was not able to conclude any particular trend for this beam series since only two specimens were tested. Therefore, more testing would need to be done using these very low reinforcement ratios to establish any conclusive trends.

5.3 Strain Gauge Data

Three techniques were developed by the author and used to assess strains, curvatures, rotations of the test beams through the available data from strain gauges. The strains were assessed according to the following three methods:-

1. Strain gauge strains were averaged over a 200 mm gauge length. This method was used to compare strain gauge data with the Demec strains at corresponding load stages and positions along the beam to check the validity of the strain gauge results. The results of these calculations are covered in section 5.4.

2. Strains in both tension and compression bars at the support and span areas, where major cracks developed, were averaged. This involved taking the mean of strains that developed at crack positions. Summary results are presented in **Tables 5-5 to 10,** and will be discussed in the upcoming subsections.

3. Averaged strains over plastic hinge lengths. This method was used by the author in an attempt to calculate rotations and plastic hinge lengths from the strain gauge data. The results of this method together with a full description are presented in section 5.8.

Strains at failure using the three methods listed above gave different indications. Methods 1 and 3 gave lower strain values since the averaging technique included gauges under crack positions and those which were not (i.e. those which had been restrained by the surrounding concrete). The second method alone considered strains under cracks. Consequently, the strain values using method 2 were high. The third method may have exaggerated the plastic hinge length because strains peaked at every crack regardless of their position relative to the two critical sections (i.e. the support and span sections).

The strain gauge data produced detailed information regarding the strain distribution along the beam, specifically in the span and support areas. In **Figures 5-7 to 29**, the main results for each specimen from the strain gauges at selected load stages are plotted. In each figure three diagrams are presented. Diagram **a)** shows local top steel strain distribution along the beam. Diagram **b)** shows local bottom steel strain distribution. Diagram **c)** shows local curvature distribution calculated from the reinforcement strains. Measured curvature was based on the assumption of linear strain distribution over the section. **Figures 5-8, 13, 18, 22, 25, 29** show local strain distribution at maximum load for each test beam series respectively. These diagrams show yield strain levels for the tensile reinforcement in the test beams. Large and major cracks can be observed at positions of high strains in the tension bars, since strain values rose rapidly at major crack positions. Observations and discussions on each beam series are presented next.

5.3.1 Specimen B3T16A

Beam B3T16A developed a plateau of strain distribution across both support and span areas respectively. **Figure 5-7** shows small depressions of tensile strains under both the span and support areas. This phenomenon was due to the action of tension stiffening. Tensile strains at maximum load, under both span and support sections were nearly of equal magnitudes. **Table 5-5** lists average strains calculated using methods 1 and 2 described in 5.3. Specimen B3T16A failed in shear without developing any plastic strains at any point in the beam.

5.3.2 Series B

Once the support sections were cracked in series B, the specimens developed a plateau of strain at early loading stages. **Figures 5-9 to 12** demonstrate the development of strain distributions at selected load stages of each beam in series B. **Figure 5-13** shows top and bottom strain distribution at maximum load. The yield strain level of the tension reinforcement is shown for each bar diameter for both the support and span bars.

At failure, specimen B2T20B and B5T12B did not develop any yield strains. B3T16B (see **Figure 5-9**) began to yield, however post-yield strains were limited due

to the common failure of all the specimens in this series by shear. Unlike the other specimens in this series, B3T16BL developed large strains along most of the span as indicated by tensile strain distribution shown in **Figure 5-10b**. This may be attributed to bond failure initiated at major crack positions which consequently exposed the reinforcement causing a rapid climb in tensile strains. It should be noted that both specimens B3T16B and B3T16BL had some faulty strain gauges especially in the two critical sections of the support and span. Nevertheless, strain distribution for both specimens still produced an indication of where major crack formations had occurred. In both specimens the final crack formation caused shear failure. It is also noticeable that specimen B2T20B developed a similar strain level over both span and support areas. This indicates that more cracks developed when 20 mm diameter bars were used than when 12 or 16 mm were used. **Figure 5-11** shows strain and curvature distribution of selected load cases of B2T20B. This specimen did not develop any yield strains in either the support or the span areas, but was similar in the development of the strain plateau to B3T16B. The effect of tension stiffening can be observed around strain depressions under the span and support areas.

Figure 5-12 shows strain and curvature distributions for B5T12B. Maximum average strains at failure in this specimen exceeded 3500 microstrain over the support and 1500 microstrain over the span. Unlike strains in previous specimens, strains here tended to concentrate in the support region. This is because the specimen was reinforced with the smaller 12 mm bars, which meant smaller bar areas bearing higher forces. Diagonal cracks appeared in the beam between the support and span areas as well as major flexural crack development that caused the eventual shear failure.

Table 5-6 lists average strains over 200 mm gauge length and average strains under crack positions at maximum (failure) load. **Table 5-6** indicates the overall average strains assessed under crack positions to be slightly higher than the average strains over 200 mm gauge length. This is because the latter assessed strains under both cracked and uncracked portions in the beam.

5.3.3 Series C

Series C strain and curvature distributions are shown in **Figures 5-14 to 18.** At high loads, beams in this series developed strain plateaux similar to those in series B.

B3T16C (**Figure 5-14**) developed plastic strains at the support. However, later cracks developed shortly before failure approximately 100 mm away from the support due to the progression of shear cracks in that region. Most of the span stayed within elastic strains, only three strain gauges reached the yield strains of 3100 microstrain.

Table 5-7 lists average strains over 200 mm gauge length and the average of strains under major cracks. B2T20C (**Figure 5-15**) developed higher plastic strains in the span than in the support area. This may explain the low redistribution this specimen achieved, shown in **Figure 5-3**. At this point, this meant the support was stiffer than the span, therefore redistribution was lower than for other specimens.

As stated earlier, specimen B5T12C (see **Figure 5-16**) had a replacement tension bar grouted in the support area and an unexpected pump failure. These circumstances caused the specimen at the time of testing to fail earlier than expected. Therefore, strain levels in this specimen were relatively lower than the other specimens in the series, especially specimen B5T12X (**Figure 5-17**), the repeat specimen.

Strain distribution at maximum load for Series C, (**Figure 5-18**) suggests that the test beams that developed plastic strains could form a plastic hinge with a mechanism, had the beams failed in flexure rather than shear.

5.3.4 Series (D, E, W)

Series D, E and W were the only test beams that developed a desirable flexural failure. There were no noticeable differences in behaviour between high ductility bar specimens and wire reinforced specimens. **Figures 5-19** to **29** present the strain and curvature distribution for all the specimens in these series. The strain and curvature distributions show a concentration and peaking of strains near both the support and span sections. Specimen B2T12D (**Figure 5-19**) developed similar levels of strains at both support and span areas. At failure, B3T10D and B5T8D (**Figures 5-20** and **21**) strains over the span were higher than those over the support. **Table 5-8** lists average strains at the support and span sections at failure calculated over 200 mm gauge length and under crack positions for series D. It was observed that the strains assessed at crack positions were around 1.4 times higher than strains measured over 200 mm

gauge length. This was however expected, since this method averaged strains under crack positions only.

In Series E, specimens B2T8E and B4T6E had more than half of the strain gauges going off at the high load stages due to very high strains exceeding gauge capacity of 30000 microstrain. It was therefore difficult to assess the full strain distribution of the test beams in this series. **Figures 5-23 to 25** show both strain and curvature distributions of both specimens. Specimen B2T8E was initially pre-cracked, causing the rapid climb in strains at the support section. Specimen B4T6E (**Figure 5-24**) developed higher strains over support than the span. Compression strains in this beam series changed to positive tensile strains (i.e. neutral axis depth was in the cover) mainly as a result of the very low reinforcement ratios used.

Table 5-9 shows Series E average measured tensile and compressive strains over 200 mm gauge length and average strains under crack positions in the support and span areas respectively.

In series W, beams failed in flexure by the yielding of the reinforcement, and developed higher strains at the support than the span. See **Figures 5-26 to 29**. Levels of strains were comparable to those in series D. **Table 5-10** lists strains of series W in the same way.

5.4 Demec results

Using NEWDEM, written by the author and described in section **4.1.1,** the program performed linear regression (least squares) analysis to obtain strain and curvature distributions across the depth of the beam section for each column of Demec at every load stage. Linear regression for a column of Demec required a minimum of three points, but in some cases in series C, D, E and W, where one point was missing due to loss of a Demec stud, a straight line relationship through the remaining two points was taken. **Tables 5-11 to 26** show a comparison between actual Demec readings across the depth of the beam and the linear regression analysis lines. Strains at the top and the bottom of the section were extrapolated from the regression results. **Figures 5-30 to 45** show measured and calculated strain distributions for all specimens

at span and support sections respectively. Each regression line provided the following calculated values:

1. Top and bottom face strains.
2. Strains at the level of each line of Demec points.
3. Flexural stiffness.
4. Curvature.
5. Neutral axis depth ratio at each loading stage at each line of Demec points.

Measured strains correlated well with the regression lines at all loading stages. The results of the analysis enabled a comparison to be obtained between Demec and strain gauge curvatures. In most cases, the calculated curvatures from linear regression compared well with average strain gauge curvature over 200 mm gauge length. **Figures 5-46 to 61** illustrate the curvature distribution along the beam for all the specimens compared with the averaged strain gauge curvature distribution in all three beams. Solid connected lines represent average strain gauge curvature over 200 mm gauge lengths, and point symbols represent calculated Demec curvature from linear regression lines. Strain gauge data were compared with left side and support Demecs. The right hand span did not have any embedded strain gauges, and so could not be compared with the Demecs.

There was generally good agreement between values of curvatures at early load stages. At later load stages when major cracks developed on the surface, Demec readings started to diverge from values obtained from average strain gauge data. Demec data ceased at a few load stages before failure and so Demec data terminated. The basic assumption used for linear strain distribution across the section for both Demec and strain gauge readings was justified. **Figures 5-62 to 67** show support calculated Demec and averaged moment curvature relationship from strain gauge data over 200 mm gauge length for each beam series respectively. On the same diagrams the uncracked and cracked moment curvature relationships for each beam series are superimposed.

In specimen B3T16A (**Figure 5-62**), there was a marked difference between strain gauge and Demec data. As soon as the section cracked, the moment curvature relationship varied greatly. This could have been due to the development of large cracks in the concrete that caused the surface strain readings to deviate. Specimen

B3T16A failed in shear while the moment curvature relationship over the support area was still elastic, i.e. tension steel did not yield.

In Series B, (**Figure 5-63**), there was generally good agreement between both Demec and strain gauge data, except specimen B3T16BL. This was due to faulty Demec gauge , and with no Demec readings being taken for comparison, as with the other specimens.

Series C, D and W (**Figures 5-64, 65** and **67**) had good agreement between strain gauge and Demec moment curvature relationship for most of the loading history. The moment curvature relationships of the beam series from strain gauge data exhibited stepped curve and curvature softening, (a drop in curvature at increasing or constant moment) which normally occurred during the 15 minute Demec reading periods.

Figure 5-66 shows Series E Demec and average strain gauge moment curvature relationships. Specimen B2T8E Demec relationship exhibited a marked difference from the strain gauge relationship. This is because the specimen was pre-cracked at the support section before testing. The author was not able to get stable strain gauge data on the moment curvature relationship of this beam after the reinforcement yielded due to factors stated earlier in section **5.3.4**. On the other hand, specimen B4T6E had one strain gauge functioning steadily up to 22.1 kN load which was included as the last point on the moment curvature diagram shown in **Figure 5-66**.

Results of the regression line analysis and the strain gauge data provided analysis data of measured percentage redistribution and neutral axis depth ratio at both the span and support sections. **Figures 5-68** to **73** show plots of these two variables. Each figure shows two diagrams for both span and support sections respectively.

1. In B3T16A (**Figure 5-68**), the neutral axis depth at the support section decreased at the commencement of cracking. Later, redistribution increased slightly with decreasing neutral axis depth. Before failure, redistribution stayed constant with decreasing neutral axis depth. This was mainly due to crack developments over the support cross section which caused tensile strain over the support to increase and the neutral axis depth to decrease.
2. In Series B (**Figure 5-69**) the neutral axis depth versus redistribution over the support was different in each specimen. This was mainly due to the different strain

development in the reinforcement as presented earlier in section **5.3.2**. The neutral axis depth over the span section was constant, indicating that the increase of bending moment over the span does not greatly influence the neutral axis depth. Due to bond failure, specimen B3T16BL developed increasing neutral axis depth ratio at higher loads over the support section.

3. In Series C, (see **Figure 5-70**) B5T12C (12 mm bars) developed lower neutral axis depth ratio than B3T16C and B2T20C throughout the loading history. This may have been due to the grouting effect and pump failure which caused the beam at both the support and span sections to develop increasing tensile strains at crack positions in the reinforcing bars and the consequent reduction in the neutral axis depth ratio. This result could imply that 12 mm diameter bars had more ductility than 16 and 20 mm bars. However, this would not be conclusive since all the beams in the series failed in shear before developing any flexural failure mode. Similar to series B, the neutral axis depth ratio over the span in series C remained constant with increasing redistribution throughout most of the loading history. This implies that where moment at a section increases due to redistribution it does not affect the development of the neutral axis depth. This may justify why most standards do not put any limitation on neutral axis depth on span section when designing for redistribution.
4. Redistribution of specimens in Series D and W, (**Figures 5-71** and **72**) stayed constant with decreasing neutral axis depth ratio between cracking and yield of the tension bars. After yield of the support bars, redistribution increased drastically, but with constant neutral axis depth ratio. In these series neutral axis depth ratio was lower than beams of Series A, B and C. This was consistent with the level of plastic strains that developed in the beams which caused the low value of the neutral axis depth ratio. There was no noticeable significant difference between the behaviour of the two Series D and W.
5. In the early loading stages in Series E (**Figure 5-73**), redistribution appeared to be very high at high values of neutral axis depth. This was due to the different initial stiffness of the support and span sections discussed earlier and due to the supports requiring few load stages before they were fully settled. After the beams settled on the rig, moment redistribution was noticeably constant with decreasing neutral axis

depth. There were very few strain gauge data available at high load stages to assess the neutral axis depth ratio due to reasons presented earlier. Hence the data points on **Figure 5-73** do not show information of the full load history.

Table 5-27 shows experimental neutral axis depth values computed at failure over both the support and span sections. **Figure 5-74** shows an average view of the measured amount of redistribution over the support that occurred in the beam series with the measured neutral axis depth ratio. Series D, E, and W demonstrated more ductile behaviour because of the low neutral axis depth that developed during the loading history.

5.5 Load Deflection Relationship

Figures 5-75 to **79** show plots of the left side load versus deflection at mid-span as measured by dial gages. At a few load stages before failure, the dial gages reached their maximum travel and so deflection readings stopped. As far as was possible, the author continued to take approximate ruler readings of deflections. Therefore, to evaluate deflections at maximum load, extrapolated deflections from the last two load stages (ruler or dial gage readings) were used. No dial gage readings were done on specimen B3T16A. **Figure 5-75** shows series B measured load-deflection relationships. The three specimens in this series developed very similar deflections. Series C (**Figure 5-76**) specimens developed similar deflection throughout most of their load history, except specimen B2T20C which developed slightly higher deflections than the rest of the beams at lower loads. This may have been due to the increased crack development in this specimen. **Figure 5-77** shows the load deflection relationships for specimens in Series D. The curves, unlike the previous beams in Series B and C, exhibited a well-defined break at the onset of cracking and the slope of the curve decreased as cracking progressed. However, this did not occur in specimen B2T12D. This may suggest that the beam may have developed cracks due to creep and shrinkage before testing. For specimen B5T8D, it was possible to obtain a reasonable ruler reading at the maximum load shown in **Figure 5-77**.

Figure 5-78 shows Series E measured load deflection relationships which were not extrapolated at maximum load stages, since it was virtually impossible to take any readings once these beams began to yield. After yield of the reinforcement, failure of

the beams was very rapid so that neither ruler readings nor any reasonable extrapolations could be performed.

Series W (**Figure 5-79**) load deflection relationships were similar for all specimens. The curves show well-defined similar breaking points at cracking for all the specimens. This implies that the tensile strength concrete of these specimens compares well with each other (see **Table 3-2**).

5.6 Crack Formation

Major crack formation was recorded at failure. As the load increased, additional cracks formed on both sides of the beam. Crack spacing decreased with increasing tensile reinforcement ratio. In specimen B3T16A (**Figure 5-80**), a large diagonal crack formed between the left hand side load and the centre support which caused the beam failure in shear. Only a few cracks in this specimen formed over the support.

Cracks in Series B (**Figure 5-81**) were diagonal for most of the beams, except in specimen B3T16BL where a long diagonal shear crack extended along the line of the reinforcement over the span area thereby causing failure. This crack may have been the result of bond failure at the interface of the concrete and the reinforcement over the span, which may justify the high strains that developed in that specimen as presented earlier in section **5.3.2**.

The number of cracks in Series C (**Figure 5-82**) was greater than those in Series B. Cracks were spaced at around 100 mm apart. All the beams in this series developed diagonal cracks causing shear failure. Specimens that were reinforced with large diameter bars such as T20 and T16 bars over span and support developed larger number of cracks than B5T12C and B5T12X. The inclined cracks in both (B5T12C and B5T12X) specimens modified the manner in which the beams responded to the applied load. According to MacGregor and reported by Hawkin et al (1964), inclined cracks can be categorised into two types according to the condition of the beam before the formation of the inclined crack. If the portion of the beam in which the inclined crack formed was uncracked, the crack was called a shear crack. If the inclined crack was initiated by flexural cracked the crack was called a flexure-shear crack. For beams

with moderated reinforcement ratios like those in series B and C, flexure-shear cracks predominated the crack pattern. Crack formation in B3T16A, series B and C generally caused levelled plateaux of tensile strains before failure.

In Series D and W, (**Figures 5-83** and **84**) cracks were more concentrated near the support and mid-span sections. As load approached failure with the reinforcement already yielded, cracks near the two critical sections started to dominate, causing the beams to develop plastic strain leading to flexural failure.

Series E (**Figure 5-85**) failed with only a small number of cracks appearing at both support and span sections. Specimen B2T8E was pre-cracked during handling, however this did not seem to affect the way cracks developed in the beam at failure.

In summary, it could be concluded that the number of cracks varied directly with the ratio of tensile reinforcement. The heavier and larger the bar diameters used, the greater the number of cracks formed. The resultant crack distribution of the test beams presented may be summarised into two categories. The first category is crack formation which was due to shear failure and the second is crack formation due to flexural failure. **Figures 5-86** and **87** show pictures of test beams failing in shear and flexure respectively.

5.7 Mode of Failure

Although the tests were planned primarily to obtain information on moment redistribution of continuous beams failing in bending, shear failure dominated specimen B3T16A and the beams of Series B and C. Although specimens B3T16B, B3T16BL, B3T16C, B2T20C and B5T12X eventually failed because of shear cracks development, high plastic strains in these specimens developed. This is may be due to the failure of one span in shear thereby leading to the other span failing in bending. However this bending failure lacked the plastic hinge mechanism required, hence shear failure occurred. The factors influencing the behaviour and strength of concrete beams failing in shear are numerous and complex. They include the proportions and shape of the beam, the structural restraints and the interaction of the beam with other components in the system, the amount and arrangement of tensile and compressive and transverse reinforcement, and load distribution and history. The following paragraph

discusses the possible reasons which may have influenced the shear failure which occurred in specimens of Series A, B and C.

1. **Table 5-28** shows a listing of ultimate predicted flexural and shear loads as well as the failure load for both the left and right hand spans and failure modes. The predicted flexural failure load were determined based on 30% redistributed moment capacity at the support section using BSECT which is a section analysis program that is described in Chapter Eight. The predicted shear capacity was calculated according BS 8110 section 3.4.5.3 and 4. When the predicted shear failure load is greater than the predicted flexural failure load, then the predicted failure mode would be flexure; otherwise, if the predicted shear failure load is less than the predicted flexural failure load, then this would give a predicted shear failure. It can be seen from **Table 5-28** that all the beams were predicted to fail in flexure and that in all cases the actual failure loads exceeded the predicted flexure failure loads. Furthermore, the shear failure is also dependent on the shear-span/effective depth ratio a_v/d, where a_v is the distance between the point load and nearest support reaction. Beams with high value of a_v/d ratio usually fail in bending , i.e. $a_v/d > 6$. Values lower than 6 tend to fail in shear. B3T16A and Beams in Series B had this ratio averaged at 3.3 and 5.5 for B3T16A and Series B respectively. This indicates a possible reason for shear failure in this beam series. For beams in Series C a_v/d ratio was > 9.0. This ratio is relatively high, therefore, it may be possible that diagonal cracks rapidly spread to the position of the point load resulting in collapse by splitting the beam into two pieces. This mode of failure is called diagonal tension failure.

2. The tension steel ratio affects shear strength because a low value reduces the dowel shear capacity and lead to wider cracks. This in turn reduces the aggregate-interlock capacity, thus causing shear failure. See (Rajagopolan and Ferguson, 1967)

3. Although the test beams were simply supported at both ends on sliders, it is still possible that a small horizontal force caused by slider friction encouraged the development of inclined cracking which is an essential prerequisite to shear failure. See (Bresler and Macgregor, 1967). It is further reported by Bresler and

Macgregor (1967), that for a_v/d ratio between 3 and 6, inclined cracks develop in the shear span as an extension of a flexural crack which progressively bends over until the inclined crack is formed.

4. Clark and Thorgood (1985) reported test results for 64 reinforced concrete beams in shear which were reinforced similarly to beams in Series C, but with smaller bar diameters and an a_v/d ratio of 4.0. They investigated the effects of different concrete quality in the top regions compared with the bottom regions of the beams, the accuracy of steel fixing and the concrete quality around reinforcing bars. They concluded that the shear capacity of a beam was reduced by about 40% when the main tension bars were positioned in the top of the section (as is the case over an internal support) rather than in the bottom. It was suggested that the reduction in shear capacity was due to the inferior bond characteristic of the top bars caused by their proximity to a free surface. This could have contributed to the shear failures that occurred in Series C. Further attention should be given to these points in any future test programme.

In summary, beams can fail in combined bending and shear in at least five different ways: anchorage failure, bearing failure, flexure failure and arch and rib failure. These failure modes depend on the geometry and properties of the beams. Therefore, it is difficult to generalise about the nature of shear failures. Clearly to analyse the beams which failed in shear, a comprehensive consideration of such factors would be needed, which is a major task which goes beyond the scope of this research. Even when such factors are considered, definitive analysis and answers are not likely to be accurate due to the small number of specimens tested and failed in shear.

Beams in Series D, W and E, with low reinforcement, failed by the yielding of one or more of the bars. As load increased, the specimens developed plastic strains whereby an increase in load caused failure at the support. However, the beams continued to carry further load creating a plastic hinge failure.

5.8 Determination of Plastic Hinge Length and Measured Rotations

In an attempt to calculate plastic hinge length and total rotations of the test beams, the author developed a technique for this purpose using the available strain

gauge data. The technique, schematically shown in **Figure 5-88**, involved finding where the farthest and nearest strain gauge on both sides of the span and support area had exceeded the yield strains of the tension bars. Once this was established, it was possible to calculate maximum (corresponding to the farthest strain gauge) and minimum (corresponding to the nearest strain gauge) plastic spread length on both sides of the load and centre support. The difference between the left and right hand side plastic spread length halved, constituted the plastic hinge length over one side of the beam. After establishing the maximum and minimum plastic hinge length, average tensile and compressive strains and neutral axis depth were calculated. Curvatures were then integrated under the plastic hinge length at maximum load to give the total rotation values at both the span and support sections. The average values of the plastic hinge length, curvature, total rotation and neutral axis depth ratio were then computed by averaging both maximum and minimum values. All these calculations were done through further developments the author added to the program CONPCY described earlier in Chapter Four.

Tables 5-29 and **30** show plastic hinge lengths average strains, curvatures, total rotations, percentage redistribution and neutral axis depth ratios from strain gauge data using the technique that was developed by the author. As stated earlier, only series D, E and W failed by flexure. Therefore, the results presented in **Tables 5-28** and **29** are meaningful only for those beam series. The results of this technique were compared with numerically modelled results described in the second part of the thesis in Chapter Eight. The author proposes that more test data would be needed on beams failing in flexure before establishing any trends or conclusions on the evaluation of measured rotations.

5.9 Summary

This chapter has presented the following:

1. Principal load and redistribution results for each beam series.
2. Strain gauge data of the beams presented at selected load cases with special emphasis on maximum strains developing at both critical support and span sections. The strain distribution was further interpreted by the calculation of the curvature distribution along the beam and the crack development throughout the beams.

3. Demecs curvature distribution and moment curvature relationships were compared with average strain gauge data over the Demec range.
4. Measured load deflection history was presented and discussed for each beam series.
5. Crack formation of beam and its development and the final crack distribution at the failure of the beams was presented and discussed.
6. Mode of failure of each beam series was discussed with particular emphasis on the shear behaviour developed in some of the test beams.

The method of measurement of strain using strain gauges embedded in the reinforcing bars gave detailed distribution of longitudinal strains over the loading history of the beam. The strain measurement technique used in the test beams (by installing strain gauges inside the reinforcing bars) was further validated and supported by Demec readings which compared well with strain gauge data in early loading stages. The large quantity of data generated by the strain gauge technique was taken and assumed to represent actual strains in the beams, thus deriving curvature and neutral axis depth values. The graphs that were the output of the software developed by the author (and presented in Chapter Four) demonstrated strain and curvature distribution at selected load cases (matching Demec ones). The strain gauge data were used to determine the ductility limit (x/d) and its relationship to measured redistribution. Average strains were calculated by three methods to attain an accurate picture of the actual strains that were developing in the area of the critical sections. The measured plastic hinge lengths and rotations were presented. However, the author proposes more experimental work to be done before generalisation on the development of plastic rotations can be drawn.

The experimental results presented here form the basis for the new development described in this thesis. This is mainly the comparison of the experimental data with the analytical model developed by the author as the main tool for modelling redistribution, deflection, curvatures and rotations which is presented in the second part of this thesis.

SPECIMEN	LOAD (kN)		EXPERIMENTAL REACTION (kN)			EXPERIMENTAL BENDING MOMENT (kNm)			% REDISTRIBUTION			Deflection (mm)		
NAME	LH	RH	LH	CENTRE	RH	LH	CENTRE	RH	LH	CENTRE	RH	LH	RH	Rem.
B3T16A	349.8	319.1	136.5	409.4	122.4	-161.7	102.9	-145.8	16.2	-31.9	20.3	**	**	a*
B3T16B	221.4	214.7	88.4	262.8	84.6	-104.8	61.9	-100.3	20.9	-37.2	21.4	13.3	12.2	b*
B3T16BL	204.0	199.5	74.8	256.1	73.2	-88.7	71.9	-86.7	11.3	-21.1	12.7	**	**	b*
B2T20B	175.9	138.5	69.6	194.5	49.6	-82.4	51.3	-58.8	13.9	-27.8	18.5	10.7	7.9	b*
B5T12B	179.6	171.9	71.8	219.7	67.2	-83.2	53.9	-79.7	20.5	-36.5	20.9	11.2	10.1	b*
B3T16C	110.4	103.9	43.5	130.0	39.6	-51.6	32.7	-46.9	18.4	-32.5	18.4	23.5	25.8	ab
B2T20C	105.8	97.5	39.7	125.9	35.3	-47.0	35.8	-41.8	12.0	-22.2	13.2	28.5	24.3	b
B5T12C	93.9	86.4	38.2	108	33.1	-45.3	25.9	-39.2	21.5	-36.6	19.8	13.5	**	ab
B5T12X	103.8	101.8	39.2	128.9	38.4	-46.5	34.0	-45.5	14.7	-26.9	15.8	19.7	20.8	ab
B2T12D	45.5	42.9	17.4	55.1	15.9	-20.7	14.6	-18.9	15.1	-26.8	15.2	17.2	**	c
B3T10D	49.9	49.6	19.0	62.9	18.2	-22.5	16.9	-21.6	16.2	-25.1	12.2	40	34	c
B5T8D	49.7	52.3	18.1	65.1	19.2	-21.5	18.3	-22.7	13.0	-20.5	10.3	31.8	32.5	c
B2T8E	27.2	25.3	10.8	31.3	10.2	-12.8	7.2	-12.1	18.9	-39.1	25.7	11.2	11.2	c
B4T6E	24.9	23.2	10.1	29.2	9.2	-12.0	6.6	-10.9	21.3	-39.2	23.2	12.1	**	c
W2T12D	49.1	48.9	18.2	59.9	18.3	-21.6	16.7	-21.7	13.2	-24.5	14.6	45.5	45.5	c
W3T10D	46.6	47.2	18.0	59.4	18.3	-21.3	14.5	-21.7	18.2	-31.8	17.8	16.1	18.1	c
W5T8D	48.7	49.2	17.7	59.5	18.3	-21.0	17.4	-21.7	11.2	-21.5	13.1	14.9	13.9	c

a* Specimen failed in shear while neither support nor span reached any strains near yield.

b* Specimen failed in shear but strain over support reached values equal or above yield strains

ab* Specimen failed in shear but with obvious plastic strains developing

c* Specimen failed in flexure with plastic strains developing over support and span

Table 5-1 Loads reactions, moments and moment redistribution at maximum applied load

	Average of All Load Cases		At Failure Load	
Specimen	$\frac{EI(Support)}{EI(Span)}$	β	$\frac{EI(Support)}{EI(Span)}$	β
B3T16B	0.75	-24.2	0.38	-37.2
B3T16BL	1.05	-16.1	1.81	-21.1
B2T20B	0.72	-24.7	0.80	-27.8
B5T12B	0.73	-14.8	0.41	-36.5

Table 5-2: Series B relative stiffness and moment redistribution values

	Average of All Load Cases		At Failure Load	
Specimen	$\frac{EI(Support)}{EI(Span)}$	β Support	$\frac{EI(Support)}{EI(Span)}$	β Support
B3T16C	0.63	-21.9	0.40	-32.5
B2T20C	0.86	-15.2	1.31	-22.2
B5T12C	0.87	-21.4	0.53	-36.6
B5T12X	0.63	-10.6	0.32	-26.9

Table 5-3: Series C relative stiffness and moment redistribution values

	Average of All Load Cases		At Failure Load	
Specimen	$\frac{EI(Support)}{EI(Span)}$	β Support	$\frac{EI(Support)}{EI(Span)}$	β Support
B2T12D	0.79	-17.1	1.09	-26.8
B3T10D	0.57	-16.9	0.85	-25.1
B5T8D	0.72	-14.6	0.94	-20.5
W2T12D	0.72	-17.5	0.76	-24.5
W3T10D	0.61	-17.4	0.36	-31.8
W5T8D	0.94	-9.0	0.51	-21.5
B2T8E	0.62	-46.763	0.51	-39.1
B4T6E	0.713	-19.588	0.36	-39.2

Table 5-4: Series D, E and W relative stiffness and moment redistribution values

Tensile and Compressive Strains At Failure (microstrain)				
Support				
Strains	**Averaged Over 200 mm**		**Averaged Under Crack Positions**	
Specimen	**Tension**	**Compression**	**Tension**	**Compression**
B3T16A	2503.00	-607.00	2842.00	-563.00
Span				
Specimen	**Tension**	**Compression**	**Tension**	**Compression**
B3T16A	2327.00	-924.00	2480.50	-1009.50

Table 5-5: Specimen B3T16A average strains over 200 mm length and under crack positions over the support and span sections at maximum load.

Tensile and Compressive Strains At Failure (microstrain)				
Support				
Strains	**Averaged Over 200 mm**		**Averaged Under Crack Positions**	
Specimen	**Tension**	**Compression**	**Tension**	**Compression**
B3T16B	7190.00	--	3976.33	-205.33
B3T16BL	3777.00	-294.00	7694.00	188.00
B2T20B	2119.00	-137.00	2248.00	-175.00
B5T12B	3528.00	245.00	3470.00	360.75
Overall Avg.	**4153.5**	**-62**	**4347.08**	**42.11**
Span				
Specimen	**Tension**	**Compression**	**Tension**	**Compression**
B3T16B	3435.00	-995.00	5733.00	-1123.00
B3T16BL	8169.00	-1380.00	10282.00	-1344.33
B2T20B	2277.00	-614.00	2253.75	-561.25
B5T12B	1498.00	-535.00	1613.00	-632.00
Overall Avg.	**3844.75**	**-881**	**4970.44**	**-915.15**

Table 5-6: Series B list of average strains over 200 mm length and under crack positions over the support and span sections at maximum load.

Tensile and Compressive Strains At Failure (microstrain)				
Support				
Strains	**Averaged Over 200 mm**		**Averaged Under Crack Positions**	
Specimen	**Tension**	**Compression**	**Tension**	**Compression**
B3T16C	6861.00	-657.33	10831.00	-657.33
B2T20C	4819.00	-412.50	8821.00	-348.67
B5T12C	3424.03	442.1	4048.2	-223.7
B5T12X	8703.00	-21.0	11790.50	38.15
Overall Avg.	**5951.76**	**-162.18**	**8872.67**	**-297.89**
Span				
Specimen	**Tension**	**Compression**	**Tension**	**Compression**
B3T16C	3176.00	-1447.00	4014.50	-1415.00
B2T20C	7422.00	-1797.00	16502.25	-1868.25
B5T12C	2014.00	-1426.00	2066.00	-1306.00
B5T12X	2661.00	-1056.00	2873.50	-1082.00
Overall Avg.	**3818.25**	**-1431.5**	**6364.06**	**-1417.81**

Table 5-7: Series C list of average strains over 200 mm length and under crack positions over the support and span sections at maximum load.

Tensile and Compressive Strains At Failure (microstrain)				
Support				
Strains	**Averaged Over 200 mm**		**Averaged Under Crack Positions**	
Specimen	**Tension**	**Compression**	**Tension**	**Compression**
B2T12D	17155.00	1769.00	27283.50	2464.50
B3T10D	19030.00	1698.00	25349.00	1552.50
B5T8D	19647.00	686.00	25027.50	254.15
Overall Avg.	**18610.5**	**1384.67**	**25886.67**	**1423.72**
Span				
Specimen	**Tension**	**Compression**	**Tension**	**Compression**
B2T12D	25294.00	26.50	29998.67	13.27
B3T10D	19790.00	247.00	33805.25	256.05
B5T8D	20953.00	428.00	31048.00	446.17
Overall Avg.	**22012.33**	**233.83**	**31617.31**	**238.5**

Table 5-8: Series D list of average strains over 200 mm length and under crack positions over the support and span sections at maximum load.

Tensile and Compressive Strains At Failure (microstrain)				
Support				
Strains	**Averaged Over 200 mm**		**Averaged Under Crack Positions**	
Specimen	**Tension**	**Compression**	**Tension**	**Compression**
B2T8E	-**	1214.00	-**	-**
B4T6E	37609.00	2053.00	-**	-**
Overall Avg.	**37609**	**1633**	-**	-**
Span				
Specimen	**Tension**	**Compression**	**Tension**	**Compression**
B2T8E	10738.00	996.00	8521.00	656.00
B4T6E	10364.00	1217.00	14980.50	1192.00
Overall Avg.	**10551**	**1106.5**	**11750.75**	**924**
** No value could be obtained due to high strains exceeding strain gauge capacity				

Table 5-9: Series E list of average strains over 200 mm length and under crack positions over the support and span sections at maximum load

Tensile and Compressive Strains At Failure (microstrain)				
Support				
Strains	**Averaged Over 200 mm**		**Averaged Under Crack Positions**	
Specimen	**Tension**	**Compression**	**Tension**	**Compression**
W2T12D	11207.00	1215.00	20380.00	1284.00
W3T10D	20520.00	1263.00	33516.75	1519.00
W5T8D	14496.00	284.00	14066.00	243.50
Overall Avg.	**15407.67**	**920.67**	**22654.25**	**1015.5**
Span				
Specimen	**Tension**	**Compression**	**Tension**	**Compression**
W2T12D	10190.00	379.00	8948.00	242.00
W3T10D	10008.00	-187.00	19082.50	-217.60
W5T8D	8977.00	394.00	19075.00	124.90
Overall Avg.	**9725**	**195.33**	**15701.83**	**49.77**

Table 5-10: Series W average strains over 200 mm length and under crack positions over the support and span sections at maximum load.

Beam Depth(mm) B3T16A	60 kN		100 kN		140 kN		200 kN		240 kN		300 kN	
	Strain x 10^{-6} (microstrain)											
Span	Measured	Calculated	Measured	Calculated	Measured	Calculated	Measured	Calculated	Measured	Calculated	Measured	Calculated
0	-	-128.79	-	-312.15	-	-439.47	-	-681.45	-	-898.93	-	-1127.64
35	-104	-104.85	-240	-233.73	-344	-313.56	-560	-480.64	-712	-634.87	-912	-793.45
145	-32	-29.62	8	12.76	120	82.15	392	150.45	512	195.04	648	256.85
255	48	45.62	296	259.24	504	477.85	664	781.55	808	1024.96	1088	1307.15
365	120	120.85	480	505.73	840	873.56	1368	1412.64	1832	1854.87	2304	2357.45
400	-	144.79	-	584.15	-	999.47	-	1613.45	-	2118.93	-	2691.64
Support					-							
0	-	287.27	-	1491.56	-	3299.4	-	5322.65	-	6902.48	-	7160.04
35	272	247.14	1336	1328.89	2904	2961.4	3912	4794.39	4336	6210.1	4432	6467.74
145	72	121.05	840	817.63	2016	1899.13	3936	3134.13	5312	4034.03	4944	4291.91
255	-32	-5.05	216	306.37	752	836.87	1640	1473.87	2416	1857.97	3680	2116.09
365	-80	-131.14	-144	-204.89	-200	-225.4	-272	-186.39	-280	-318.1	-240	-59.74
400	-	-171.27	-	-367.56	-	-563.4	-	-714.65	-	-1010.49	-	-752.04

Table 5-11: Measured and calculated Demec strains using linear regression in the span and support sections for specimen B3T16A

Beam Depth(mm) B3T16B	20 kN		40 kN		70 kN		105 kN		135 kN		170 kN	
	Strain x 10^{-6} (microstrain)											
Span	Measured	Calculated	Measured	Calculated	Measured	Calculated	Measured	Calculated	Measured	Calculated	Measured	Calculated
0	-	-179.4	-	-439.99	-	-846.95	-	-895.72	-	-1608.35	-	-1960.78
20	-120	-148.46	-232	-344.63	-456	-643.6	-712	-676.52	-984	-1188.45	-1296	-1435.86
90	-72	-40.15	-72	-10.88	32	68.13	176	90.67	368	281.18	600	401.38
160	64	68.15	208	322.88	488	779.87	808	857.85	1224	1750.82	1664	2238.62
230	184	176.46	720	656.63	1632	1491.6	-	1625.04	3456	3220.45	4312	4075.86
250	-	207.4	-	751.99	-	1694.95	-	1844.23	-	3640.35	-	4600.78
Support												
0	-	263.64	-	955.88	-	1907.36	-	3416.04	-	3112.31	-	4098.56
20	208	227.22	792	843.9	1544	1702.02	2112	3043.88	2536	2766.02	3336	3663.59
90	96	99.74	440	451.97	872	983.34	1200	1741.29	992	1554.01	1896	2141.2
160	16	-27.74	184	60.03	664	264.66	1864	438.71	1216	341.99	1464	618.8
230	-176	-155.22	-392	-331.9	-584	-454.02	-816	-863.88	-952	-870.02	-1176	-903.59
250	-	-191.64	-	-443.88	-	-659.36	-	-1236.05	-	-1216.31	-	-1338.56

Table 5-12: Measured and calculated Demec strains using linear regression in the span and support sections for specimen B3T16B

92

Beam Depth(mm) B2T20B	15 kN		40 kN		60 kN		120 kN		140 kN		160 kN	
	Strain x 10^{-6} (microstrain)											
Span	Measured	Calculated	Measured	Calculated	Measured	Calculated	Measured	Calculated	Measured	Calculated	Measured	Calculated
0	-	-238.69	-	-493.08	-	-780.52	-	-1179.14	-	-574.27	-	-763.05
50	-152	-135.21	-296	-264.65	-384	-353.91	-496	-434.68	192	36.24	168	-17.83
100	16	-31.74	40	-36.22	144	72.7	416	309.77	480	646.75	552	727.39
150	56	71.74	168	192.22	464	499.3	1048	1054.23	1216	1257.25	1376	1472.61
200	160	175.21	400	420.65	920	925.91	1760	1798.68	1920	1867.76	2304	2217.83
250	-	278.69	-	649.08	-	1352.52	-	2543.14	-	2478.27	-	2963.05
Support												
0	-	64	-	1522.83	-	2908.84	-	7104	-	7360	-	8480
50	-	56	-	1110.33	-	2124.12	-	5064	-	5400	-	6320
100	48	48	728	697.83	1400	1339.39	3024	3024	3440	3440	4160	4160
150	40	40	192	285.33	336	554.67	984	984	1480	1480	2000	2000
200	-	32	-	-127.16	-	-230.06	-	-1056	-	-480	-	-160
250	-	24	-	-539.66	-	-1014.78	-	-3096	-	-2440	-	-2320

Table 5-13: Measured and calculated Demec strains using linear regression in the span and support sections for specimen B2T20B

93

Beam Depth(mm) B2T20B	15 kN		60 kN		90 kN		120 kN		140 kN		160 kN	
	Strain x 10^{-6} (microstrain)											
Span	Measured	Calculated	Measured	Calculated	Measured	Calculated	Measured	Calculated	Measured	Calculated	Measured	Calculated
0	-	-113.14	-	-492.22	-	-598.04	-	-802.73	-	-935.12	-	-1098.2
50	-40	-55.09	-200	-184.13	-240	-202.03	-320	-260.04	-360	-289.07	-400	-322.92
100	-16	2.97	136	123.96	368	193.99	560	282.65	688	356.98	864	452.36
150	64	61.03	560	432.04	472	590.01	656	825.35	800	1003.02	960	1227.64
200	120	119.09	616	740.13	968	986.03	1320	1368.04	1592	1649.07	1936	2002.92
250	-	177.14	-	1048.22	-	1382.04	-	1910.73	-	2295.12	-	2778.2
Support												
0	-	128.67	-	1243.53	-	2053.26	-	2823.72	-	3301.8	-	9135.63
50	48	82	904	896.52	1528	1525.55	2144	2126.23	2512	2489.88	7008	6502.18
100	56	35.33	560	549.51	1008	997.85	1376	1428.74	1608	1677.96	1840	3868.73
150	-40	-11.33	144	202.49	440	470.15	776	731.26	928	866.04	1240	1235.27
200	-16	-58	-104	-144.52	-40	-57.55	24	33.77	40	54.12	120	-1398.18
250	-	-104.67	-	-491.53	-	-585.26	-	-663.72	-	-757.8	-	-4031.63

Table 5-14: Measured and calculated Demec strains using linear regression in the span and support sections for specimen B2T20B

94

Beam Depth (mm) B3T16C	20 kN		30 kN		42 kN		62 kN		70 kN		90 kN	
	Strain x 10^{-6} (microstrain)											
Span	Measured	Calculated	Measured	Calculated	Measured	Calculated	Measured	Calculated	Measured	Calculated	Measured	Calculated
0	-	-399.35	-	-626.68	-	-850.39	-	-1376.64	-	-1348.77	-	-2253.41
25	-224	-228.16	-368	-366.68	-488	-479.06	-784	-796.41	-920	-853.73	-1312	-1306.72
70	72	80	104	101.33	208	189.33	224	248	248	37.33	408	397.33
115	392	388.16	568	569.34	848	857.72	1304	1292.41	784	928.4	2096	2101.38
150	-	627.83	-	933.35	-	1377.58	-	2104.74	-	1621.45	-	3426.76
Support												
0	-	895.13	-	1464.94	-	2075.59	-	3206.71	-	3652.45	-	5014.22
25	672	670.68	1112	1109.37	1576	1573.36	2456	2444.31	2800	2783.24	3832	3832
70	264	266.67	464	469.33	664	669.33	1048	1072	1184	1218.67	1704	1704
115	-136	-137.35	-168	-170.7	-232	-234.69	-288	-300.31	-328	-345.91	-	-424
150	-	-451.58	-	-668.5	-	-937.82	-	-1367.67	-	-1562.8	-	-2079.11

Table 5-15: Measured and calculated Demec strains using linear regression in the span and support sections for specimen B3T16C

95

Beam Depth (mm) B2T20C	20 kN		30 kN		40 kN		50 kN		62 kN		80 kN	
	Strain x 10^{-6} (microstrain)											
Span	Measured	Calculated	Measured	Calculated	Measured	Calculated	Measured	Calculated	Measured	Calculated	Measured	Calculated
0	-	-721.93	-	-1030.87	-	-1215.9	-	-1704.46	-	-2168.5	-	-3014.7
25	-360	-476.48	-560	-660.8	-616	-751.17	-984	-1060.49	-1272	-1335.94	-1808	-1878.02
70	-184	-34.67	-144	5.33	-112	85.33	-32	98.67	48	162.67	40	168
115	440	407.15	720	671.47	984	921.84	1312	1257.82	1712	1661.28	2272	2214.02
150	-	750.78	-	1189.57	-	1572.46	-	2159.39	-	2826.86	-	3805.38
Support												
0	-	1337.84	-	2106.75	-	2776.18	-	3510.5	-	4320.46	-	4215.66
25	1024	1026.7	1624	1620.05	2136	2129.45	2704	2694.84	3352	3324.11	3224	3254.83
70	472	466.67	736	744	952	965.33	1208	1226.67	1472	1530.67	1584	1525.33
115	-96	-93.37	-128	-132.05	-192	-198.78	-232	-241.51	-232	-262.77	-232	-204.16
150	-	-528.96	-	-813.43	-	-1104.2	-	-1383.43	-	-1657.67	-	-1549.32

Table 5-16: Measured and calculated Demec strains using linear regression in the span and support sections for specimen B2T20C

96

Beam Depth (mm) B5T12C	30 kN		40 kN		50 kN		62 kN		70 kN		90 kN	
	Strain x 10^{-6} (microstrain)											
Span	Measured	Calculated	Measured	Calculated	Measured	Calculated	Measured	Calculated	Measured	Calculated	Measured	Calculated
0	-	-734.22	-	-976.89	-	-1200	-	-1550.22	-	-1773.33	-	-2365.33
25	-432	-432	-568	-568	-680	-680	-888	-888	-960	-960	-1352	-1352
70	112	112	168	168	256	256	304	304	504	504	472	472
115	-	656	-	904	-	1192	-	1496	-	1968	-	2296
150	-	1079.11	-	1476.44	-	1920	-	2423.11	-	3106.67	-	3714.67
Support												
0	-	1372.44	-	2039.11	-	2937.78	-	3802.67	-	4793.78	-	7902.22
25	-	1048	-	1568	-	2280	-	2976	-	3776	-	6320
70	464	464	720	720	1096	1096	1488	1488	1944	1944	3472	3472
115	-120	-120	-128	-128	-88	-88	0	0	112	112	624	624
150	-	-574.22	-	-787.56	-	-1008.89	-	-1157.33	-	-1312.89	-	-1591.11

Table 5-17: Measured and calculated Demec strains using linear regression in the span and support sections for specimen B5T12C

Beam Depth (mm) B5T12x	20 kN		30 kN		40 kN		50 kN		60 kN		80 kN	
	Strain x 10^{-6} (microstrain)											
Span	Measured	Calculated	Measured	Calculated	Measured	Calculated	Measured	Calculated	Measured	Calculated	Measured	Calculated
0	-	-317.07	-	-519.28	-	-721.01	-	-948.45	-	-1171.56	-	-1701.8
25	-176	-167.64	-272	-268.11	-376	-372.08	-496	-497.34	-616	-616	4520	-908.3
70	120	101.33	192	184	264	256	312	314.67	384	384	2040	520
115	360	370.31	632	636.11	880	884.08	1128	1126.67	1384	1384	-152	1948.3
150	-	579.51	-	987.74	-	1372.58	-	1758.23	-	2161.78	-	3059.2
Support												
0	-	823.31	-	1361.23	-	1884.38	-	2450.65	-	3008.99	-	5774.38
25	616	612.13	1032	1025.55	1440	1428.53	1880	1861.13	2344	2306.73	4520	4474.96
70	224	232	408	421.33	584	608	760	800	960	1042.67	2040	2136
115	-144	-148.13	-176	-182.89	-200	-212.53	-240	-261.13	-176	-221.4	-152	-202.96
150	-	-443.78	-	-652.84	-	-850.71	-	-1086.46	-	-1204.56	-	-2022.15

Table 5-18: Measured and calculated Demec strains using linear regression in the span and support sections for specimen B5T12X

Beam Depth (mm) B2T12D	10 kN		15 kN		20 kN		25 kN		30 kN		40 kN	
	Strain x 10^{-6} (microstrain)											
Span	Measured	Calculated	Measured	Calculated	Measured	Calculated	Measured	Calculated	Measured	Calculated	Measured	Calculated
0	-	-521.25	-	-712.52	-	-925.54	-	-1185.61	-	-1582.22	-	-2862.33
25	-144	-136.59	-200	-179.85	-256	-240.91	-336	-320.71	-424	-409.8	-240	-197.21
70	208	192	480	434.67	640	608	800	768	1016	986.67	4688	4600
115	512	520.59	1024	1049.19	1440	1456.91	1840	1856.71	2368	2383.13	9352	9397.21
150	-	776.15	-	1527.14	-	2117.17	-	2703.48	-	3469.27	-	13128.38
Support												
0	-	4194.67	-	5524.44	-	6297.78	-	7106.67	-	8502.22	-	17322.67
25	1568	1568	2640	2640	3240	3240	3880	3880	5000	5000	12096	12096
70	-3160	-3160	-2552	-2552	-2264	-2264	-1928	-1928	-1304	-1304	2688	2688
115	-	-7888	-	-7744	-	-7768	-	-7736	-	-7608	-	-6720
150	-	-11565.3	-	-11782.2	-	-12048.9	-	-12253.3	-	-12511.1	-	-14037.3

Table 5-19: Measured and calculated Demec strains using linear regression in the span and support sections for specimen B2T12D

Beam Depth (mm) B3T10D	10 kN		15 kN		20 kN		25 kN		30 kN	
	Strain x 10^{-6} (microstrain)									
Span	Measured	Calculated	Measured	Calculated	Measured	Calculated	Measured	Calculated	Measured	Calculated
0	-	-162.07	-	-444.33	-	-628.95	-	-842.94	-	-1058.96
25	-104	-99.43	-200	-230.4	-256	-298.61	-320	-381.89	-416	-496
70	24	13.33	104	154.67	224	296	344	448	384	517.33
115	120	126.1	560	539.73	920	890.61	1320	1277.89	1584	1530.67
150	-	213.8	-	839.23	-	1353.09	-	1923.36	-	2318.81
Support										
0	-	223.11	-	1063.11	-	2085.33	-	2936	-	3848.89
25	152	152	792	792	1632	1632	2296	2296	3040	3040
70	24	24	304	304	816	816	1144	1144	1584	1584
115	-	-104	-	-184	-	-	-	-8	-	128
150	-	-203.56	-	-563.56	-	-634.67	-	-904	-	-1004.44

Table 5-20: Measured and calculated Demec strains using linear regression in the span and support sections for specimen B3T10D

100

Beam Depth(mm) B5T8D	15 kN		20 kN		25 kN		30 kN		35 kN		40 kN	
	Strain x 10^{-6} (microstrain)											
Span	Measured	Calculated	Measured	Calculated	Measured	Calculated	Measured	Calculated	Measured	Calculated	Measured	Calculated
0	-	-387.01	-	-602.43	-	-767.66	-	-869.96	-	-1155.22	-	-1638.92
25	-168	-173.56	-248	-257.75	-288	-304.92	-280	-308.78	-416	-436.93	-520	-645.97
70	200	210.67	344	362.67	496	528	648	701.33	816	856	928	1141.33
115	600	594.89	992	983.09	1376	1360.92	1736	1711.45	2168	2148.93	3016	2928.64
150	-	893.73	-	1465.64	-	2008.75	-	2497.1	-	3154.54	-	4318.77
Support												
0	-	1265.85	-	2151.2	-	2854.23	-	3527.14	-	4288.38	-	5985.79
25	992	994.71	1696	1700.06	2264	2265.34	2800	2802.68	3464	3332.05	4784	4781.34
70	512	506.67	896	888	1208	1205.33	1504	1498.67	1072	1610.67	2608	2613.33
115	16	18.62	72	75.94	144	145.33	192	194.65	296	-110.72	448	445.32
150	-	-360.97	-	-555.66	-	-679.12	-	-819.58	-	-1449.58	-	-1240.91

Table 5-21: Measured and calculated Demec strains using linear regression in the span and support sections for specimen B5T8D

101

Beam Depth(mm) B2T8E	5 kN		10 kN		15 kN		20 kN	
Strain x 10^{-6} (microstrain)								
Span	Measured	Calculated	Measured	Calculated	Measured	Calculated	Measured	Calculated
0	-	-171.4	-	-513.1	-	-746.61	-	-963.84
25	-136	-132.09	-184	-172.71	-208	-195.2	-184	-174.85
70	-32	-61.33	464	440	824	797.33	1264	1245.33
115	-16	9.42	1040	1052.71	1776	1789.87	2656	2665.52
150	-	64.45	-	1529.25	-	2561.84	-	3770.1
Support								
0	-	639.77	-	1866.85	-	3315.8	-	6437.35
25	496	485.57	1472	1466.79	2648	2640.16	5168	5170.68
70	184	208	736	746.67	1408	1424	2896	2890.67
115	-56	-69.57	32	26.55	216	207.84	608	610.66
150	-	-285.45	-	-533.54	-	-738.06	-	-1162.68

Table 5-22: Measured and calculated Demec strains using linear regression in the span and support sections for specimen B2T8E

102

Beam Depth(mm) B4T6E	5 kN		10 kN		15 kN		20 kN	
	Strain x 10^{-6} (microstrain)							
Span	Measured	Calculated	Measured	Calculated	Measured	Calculated	Measured	Calculated
0	-	-195.73	-	-365.82	-	-841.02	-	-1122.01
25	-104	-94.4	-184	-161.84	-264	-258.75	-296	-312.72
70	112	88	264	205.33	800	789.33	1888	1144
115	256	270.4	536	572.5	1832	1837.41	1840	2600.72
150	-	412.27	-	858.08	-	2652.59	-	3733.72
Support								
0	-	290.67	-	1527.11	-	5936.46	-	8656.89
25	224	224	1216	1216	4888	4760.1	7208	7208
70	104	104	656	656	2304	2642.67	4600	4600
115	-16	-16	96	96	736	525.23	1992	1992
150	-	-109.33	-	-339.56	-	-1121.66	-	-36.45

Table 5-23: Measured and calculated Demec strains using linear regression in the span and support sections for specimen B4T6E

Beam Depth(mm) W2T12D	10 kN		15 kN		20 kN		25 kN		30 kN		35 kN	
	Strain x 10^{-6} (microstrain)											
Span	Measured	Calculated	Measured	Calculated	Measured	Calculated	Measured	Calculated	Measured	Calculated	Measured	Calculated
0	-	-320.94	-	-553.74	-	-678.12	-	-843.25	-	-983.92	-	-1162.61
25	-224	-225.36	-304	-282.64	-312	-287.36	-376	-350.66	-424	-398.24	-480	-455.01
70	-56	-53.33	256	205.33	472	416	592	536	712	656	872	818.67
115	120	118.7	664	693.31	1088	1119.36	1392	1422.66	1680	1710.24	2064	2092.34
150	-	252.5	-	1072.85	-	1666.42	-	2112.29	-	2530.2	-	3082.98
Support												
0	-	545.8	-	2289.69	-	2957.4	-	3378.92	-	4104.39	-	5571.18
25	400	415.63	1808	1820.51	2360	2364.04	2720	2712.16	3336	3300.44	4536	4493.85
70	208	181.33	1000	976	1304	1296	1496	1512	1776	1853.33	2464	2554.67
115	-64	-52.97	120	131.49	224	227.96	320	311.84	448	406.23	664	615.48
150	-	-235.2	-	-525.35	-	-602.75	-	-621.62	-	-719.3	-	-892.77

Table 5-24: Measured and calculated Demec strains using linear regression in the span and support sections for specimen W2T12D

104

Beam Depth(mm) W3T10D	10 kN		15 kN		20 kN		25 kN		30 kN		35 kN	
	Strain x 10^{-6} (microstrain)											
Span	Measured	Calculated	Measured	Calculated	Measured	Calculated	Measured	Calculated	Measured	Calculated	Measured	Calculated
0	-	-155.41	-	-405.51	-	-531.97	-	-803.95	-	-1028.92	-	-1195.24
25	-48	-64.67	-184	-194.02	-232	-244.84	-304	-325.4	-400	-410.97	-408	-440.75
70	72	98.67	168	186.67	248	272	496	536	680	701.33	856	917.33
115	272	262	576	567.35	800	788.84	1416	1397.4	1824	1813.64	2304	2275.41
150	-	389.04	-	863.44	-	1190.82	-	2067.37	-	2678.77	-	3331.7
Support												
0	-	408.57	-	2209.94	-	2396	-	4366.69	-	5458.93	-	7572.11
25	320	308.36	1760	1742.58	1944	1871.71	3488	3461.44	4336	4325.5	6056	6020.16
70	96	128	864	901.33	680	928	1776	1832	2264	2285.33	3152	3226.67
115	-32	-52.36	80	60.09	160	-15.71	232	202.56	256	245.17	472	433.17
150	-	-192.65	-	-594.21	-	-749.71	-	-1064.79	-	-1341.63	-	-1739.55

Table 5-25: Measured and calculated Demec strains using linear regression in the span and support sections for specimen W3T10D

105

Beam Depth(mm) W5T8D	5 kN		10 kN		15 kN		20 kN		25 kN	
	Strain x 10^{-6} (microstrain)									
Span	Measured	Calculated	Measured	Calculated	Measured	Calculated	Measured	Calculated	Measured	Calculated
0	-	-78.14	-	-261.49	-	-476.54	-	-847.16	-	-980.48
25	-56	-53.09	-144	-141.43	-256	-247.3	-472	-469.36	-512	-509.36
70	0	-8	80	74.67	184	165.33	216	210.67	344	338.67
115	32	37.09	288	290.77	568	577.97	888	890.7	1184	1186.69
150	-	72.16	-	458.84	-	898.91	-	1419.61	-	1846.27
Support										
0	-	99.72	-	409.24	-	1470.16	-	1905.99	-	2214.51
25	72	70.77	280	302.13	1080	1131.77	1336	1466.23	1504	1708.37
70	16	18.67	144	109.33	608	522.67	864	674.67	1072	797.33
115	-32	-33.44	-96	-83.46	-120	-86.44	-176	-116.9	-184	-113.71
150	-	-73.96	-	-233.41	-	-560.18	-	-732.56	-	-822.29

Table 5-26: Measured and calculated Demec strains using linear regression in the span and support sections for specimen W5T8D

106

Values are based on average strains over 200 mm gauge length				
	Support Values		LH Span Values	
Specimen	% Redistribution	$\frac{x}{d}$	% Redistribution	$\frac{x}{d}$
B3T16A	-31.9	0.275	16.2	0.361
B3T16B	-37.2	0.167	20.9	0.344
B3T16BL	-21.1	0.215	11.3	0.272
B2T20B	-27.8	0.196	13.9	0.333
B5T12B	-36.5	0.206	20.5	0.374
B3T16C	-32.5	0.291	18.4	0.47
B2T20C	-22.2	0.288	12.0	0.385
B5T12C	-36.6	0.309	21.5	0.554
B5T12X	-26.9	0.221	14.7	0.45
B2T12D	-26.8	0.261	15.1	0.213
B3T10D	-25.1	0.287	16.2	0.224
B5T8D	-20.5	0.237	13.0	0.233
B2T8E	-39.1	0.252	18.9	0.28
B4T6E	-39.2	0.245	21.3	0.311
W2T12D	-24.5	0.307	13.2	0.241
W3T10D	-31.8	0.261	18.2	0.232
W5T8D	-21.5	0.224	11.2	0.252

Table -5-27: Moment redistribution and neutral axis depth ratio at ultimate

107

Test beam predicted and actual failure load and mode of failure							
Specimen	Ultimate Predicted Flexural Failure Load kN	Predicted PredictedShear Failure Load kN	Ultimate Actual Failure Load (LH) kN	Ultimate Actual Failure Load (RH) kN	a_v/d	Predicted Failure mode*	Actual Failure mode**
B3T16A	288	321	350	319	3.27	Flexure	Shear
B3T16B	162	215	221	215	5.46	Flexure	Shear
B3T16BL	162	215	204	200	5.46	Flexure	Shear
B2T20B	162	215	176	139	5.51	Flexure	Shear
B5T12B	162	215	180	172	5.41	Flexure	Shear
B3T16C	88	99	110	104	9.79	Flexure	Shear
B2T20C	88	99	106	98	9.96	Flexure	Shear
B5T12C	88	99	94	86	9.63	Flexure	Shear
B5T12X	88	99	104	102	9.63	Flexure	Shear
B2T12D	39	78	46	43	9.63	Flexure	Flexure
B3T10D	39	78	50	50	9.56	Flexure	Flexure
B5T8D	39	78	50	52	9.48	Flexure	Flexure
B2T8E	21	67	27	25	9.48	Flexure	Flexure
B4T6E	21	67	25	23	9.40	Flexure	Flexure
W2T12D	42	80	49	49	9.63	Flexure	Flexure
W3T10D	42	80	47	47	9.48	Flexure	Flexure
W5T8D	42	80	49	49	9.56	Flexure	Flexure
*If predicted shear failure load < predicted flexural failure load, then failure mode is shear. **If predicted shear failure load is > predicted flexural failure load, then failure mode is flexure.							

Table -5-28: Ultimate predicted and actual failure loads and modes of failure.

Specimen (Support)	Plastic Hinge Length (mm)	Avg. Tensile Strain (10^{-6})	Avg. Compressive Strain (10^{-6})	Avg. Curvature (10^{-6}/mm)	Total Rotation (rad x 10^{-6})	% Redistribution	$\frac{x}{d}$
B3T16A	a	a	a	a	a	-31.9	a
B3T16B	71.4	9711	421.3	54.5	2812.65	-37.2	0.179
B3T16BL	19.85	5349.20	900.70	33.60	222.0	-21.1	0.27
B2T20B	a	a	a	a	a	-27.8	a
B5T12B	a	a	a	a	a	-36.5	a
B3T16C	61.88	8312.55	-311.45	85.10	5817.75	-32.5	0.25
B2T20C	246.95	4282.50	-236.10	44.00	5050.05	-22.2	0.27
B5T12C	a	a	a	a	a	-36.6	a
B5T12X	80.25	7987.55	-2.00	83.20	2228.00	-26.9	0.22
B2T12D	167.35	10956.80	1339.80	126.80	15111.20	-26.8	0.30
B3T10D	162.35	15378.20	1487.40	172.10	23409.20	-25.1	0.28
B5T8D	181.05	8256.60	299.40	86.40	14891.90	-20.5	0.24
B2T8E	108.6	12227.10	1403.60	136.30	3259.90	-39.1	0.28
B4T6E	136.50	2160.00	b	b	2698.90	-39.2	0.65
W2T12D	120.78	6398.05	955.15	75.80	3885.80	-24.5	0.31
W3T10D	110.15	12484.60	1323.30	140.90	6840.30	-31.8	0.29
W5T8D	112.45	12804.70	205.90	131.40	6650.90	-21.5	0.22
a* No plastic hinge formed at the support							

Table -5-29: Average deformational properties over plastic spread length over support section based on strain gauge data

109

Specimen (Span)	Plastic Hinge Length (mm)	Avg. Tensile Strain (10^{-6})	Avg. Compressive Strain (10^{-6})	Avg. Curvature (10^{-6}/mm)	Total Rotation (rad x 10^{-6})	% Redistribution	$\frac{x}{d}$
B3T16A	ab	ab	ab	ab	ab	16.2	ab
B3T16B	142.58	2943.10	-659.40	12.40	-2308.30	20.9	0.40
B3T16BL	213.60	3774.80	-1205.40	14.00	-5109.60	11.3	0.55
B2T20B	ab	ab	ab	ab	ab	13.9	ab
B5T12B	ab	ab	ab	ab	ab	20.5	ab
B3T16C	54.38	2913.55	-795.25	23.05	-1764.50	18.4	0.56
B2T20C	121.60	3706.00	-718.55	32.45	-5780.05	12.0	0.41
B5T12C	b	b	b	b	b	21.5	b
B5T12X	b	b	b	b	b	14.7	b
B2T12D	234.50	12824.30	-131.90	130.80	-25536.50	15.1	0.22
B3T10D	163.95	11376.35	159.45	118.95	-11865.65	16.2	0.22
B5T8D	140.73	16534.05	189.35	172.40	-22539.60	13.0	0.22
B2T8E	114.85	6146.00	326.80	64.70	-727.40	18.9	0.24
B4T6E	97.28	8198.20	838.55	90.35	-6029.70	21.3	0.28
W2T12D	182.45	2135.00	116.60	76.60	-2527.80	13.2	0.25
W3T10D	143.78	7221.70	-135.15	73.05	-7989.35	18.2	0.23
W5T8D	186.35	5826.80	203.20	62.20	-8761.10	11.2	0.24

a* No plastic hinge formed at the support, b* No plastic hinge formed at the span, ab* No plastic hinge at the support and the span

Table -5-30: Average deformational properties over plastic spread length over span section based on strain gauge data

110

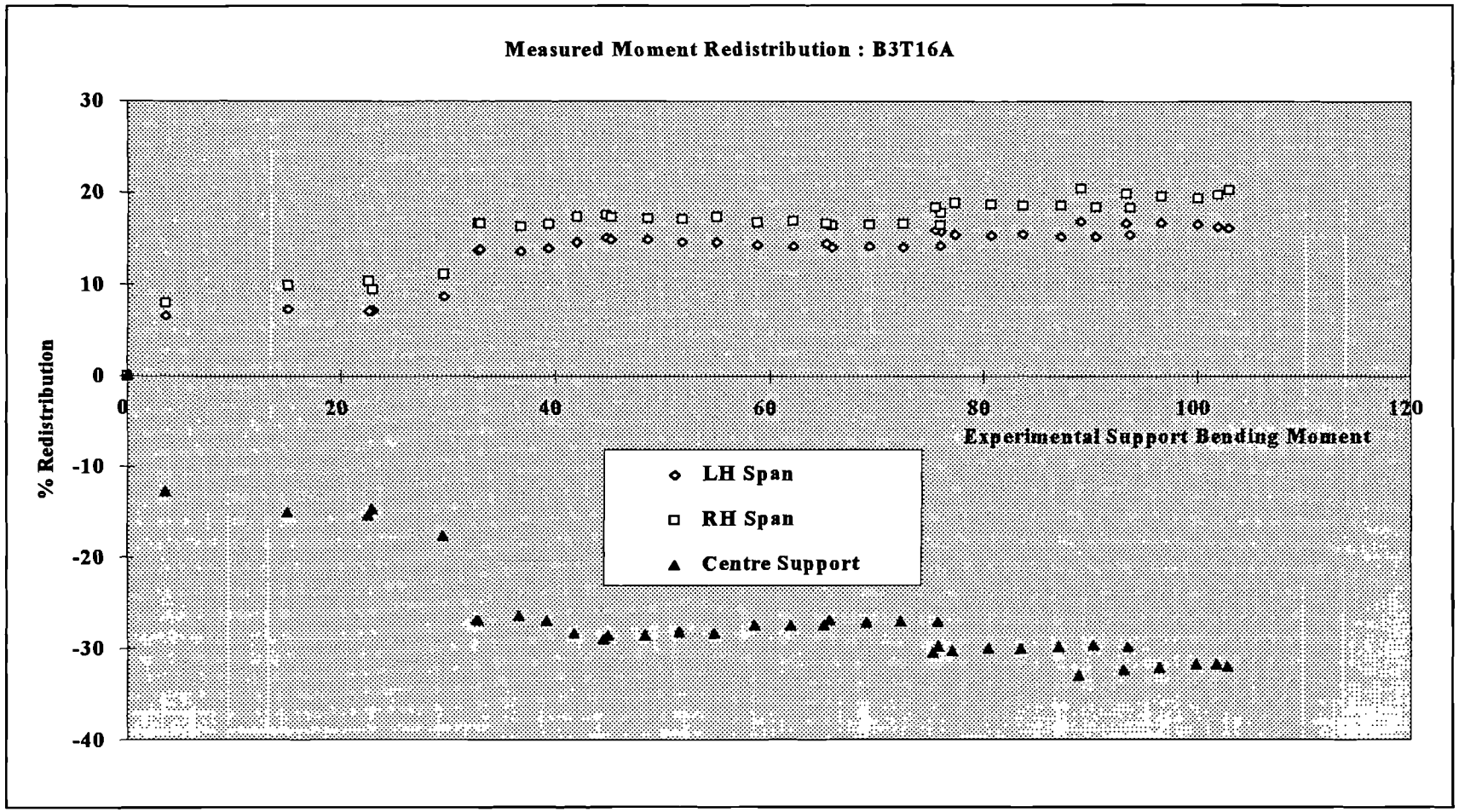

Figure 5-1: B3T16A measured moment redistribution of both spans and the support

111

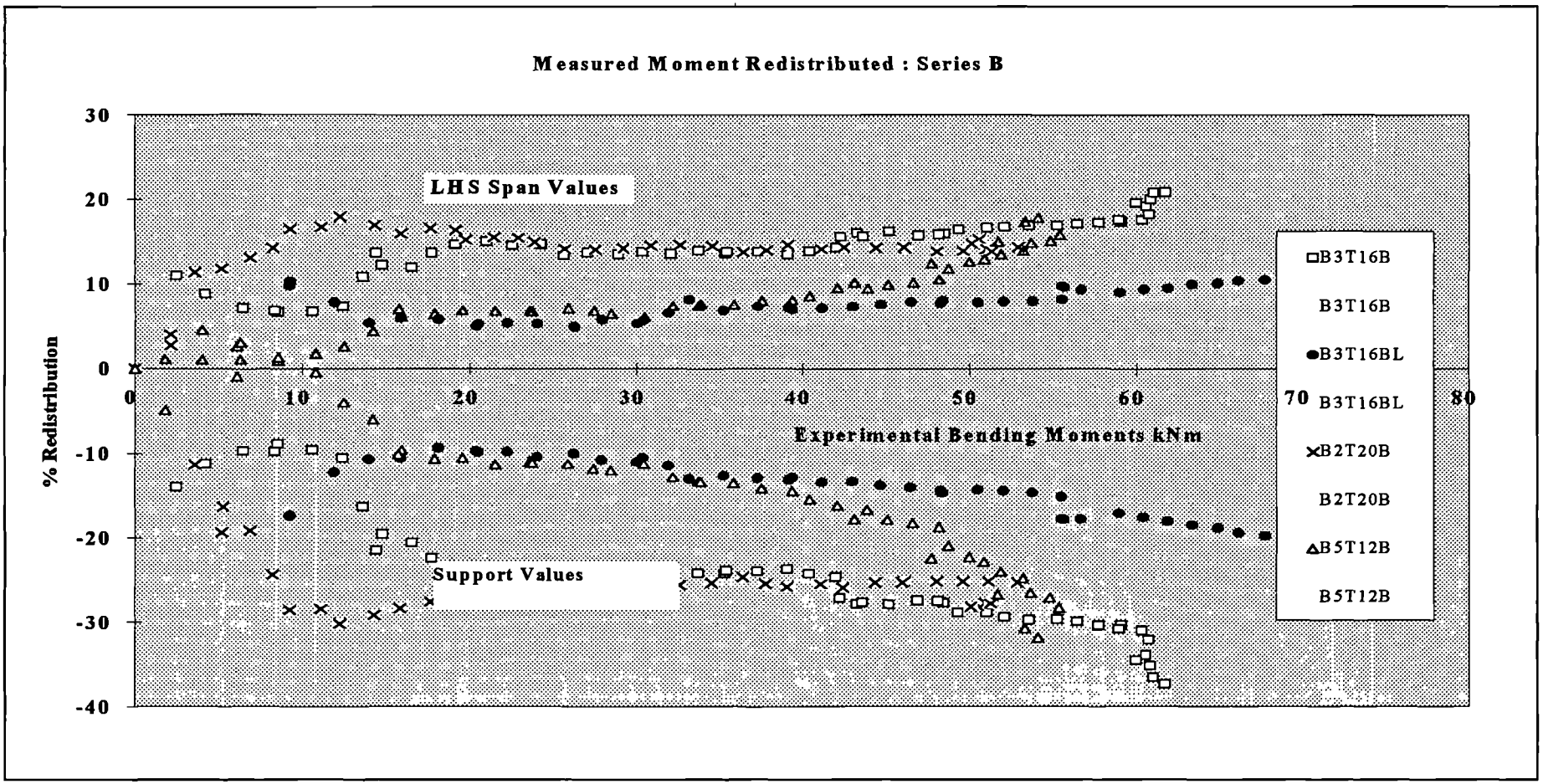

Figure 5-2:Series B measured moment redistribution of both spans and the support

112

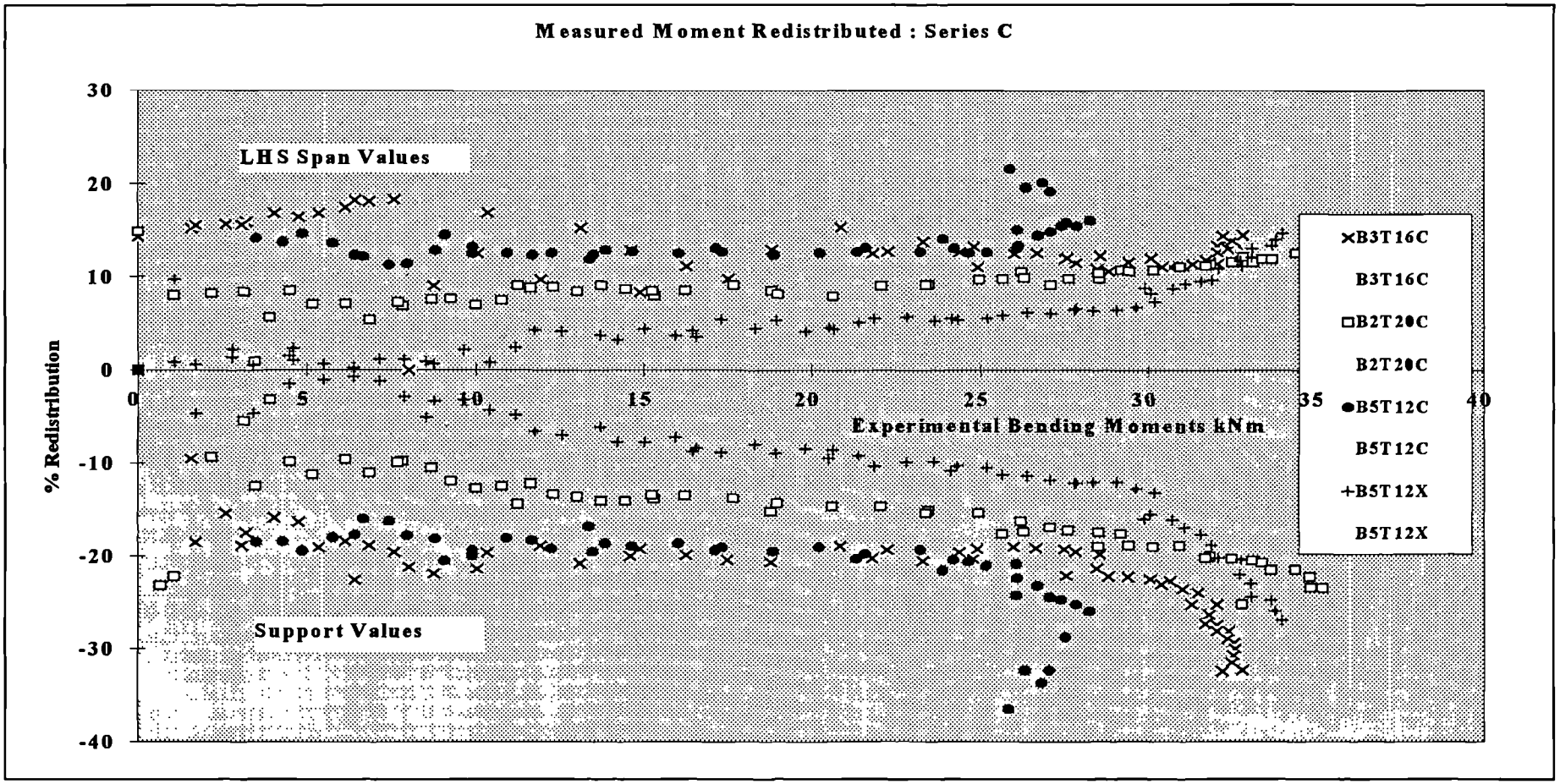

Figure 5-3: Series C measured moment redistribution of both spans and the support

113

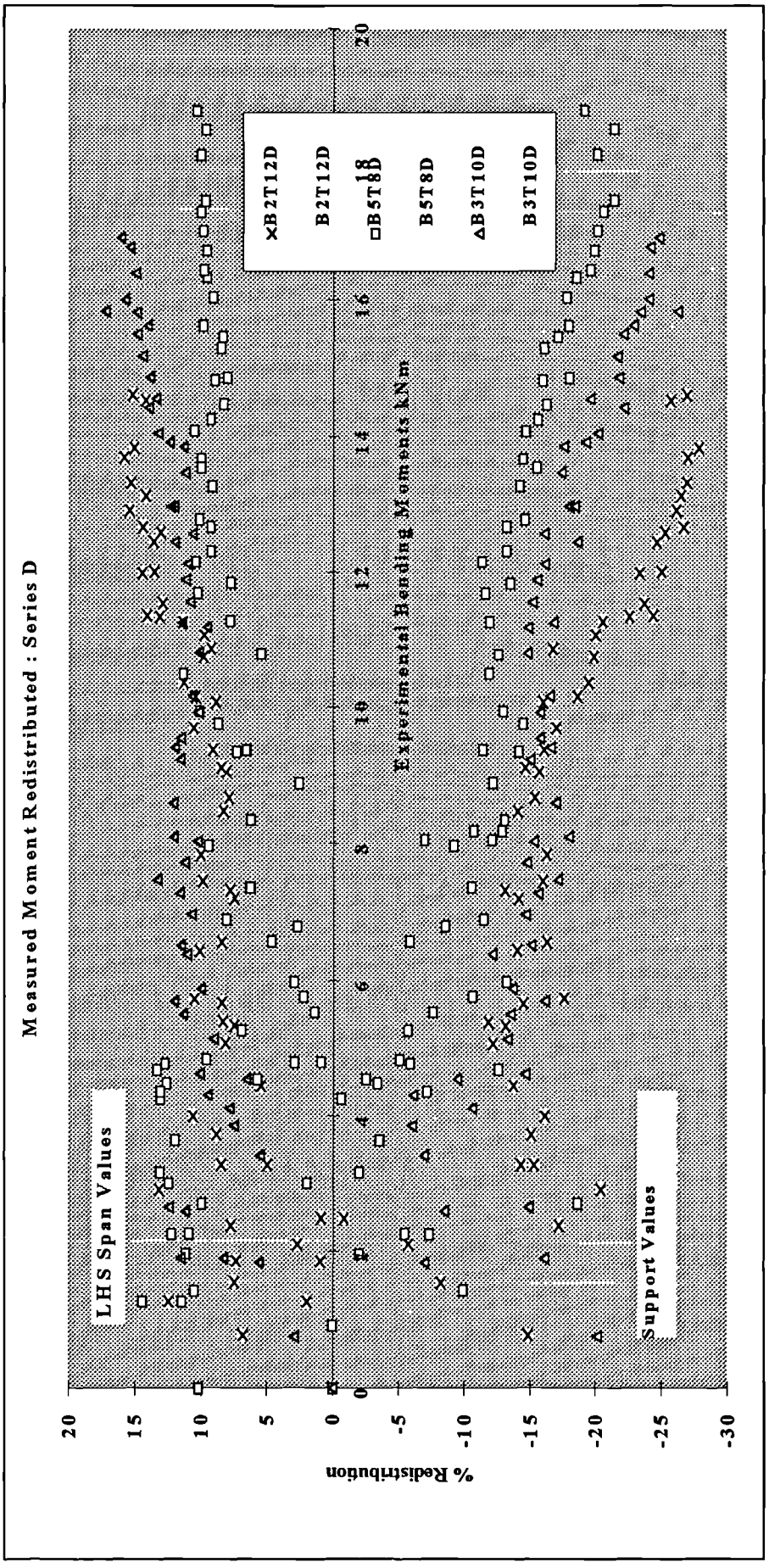

Figure 5-4: Series D measured moment redistribution of both spans and the support

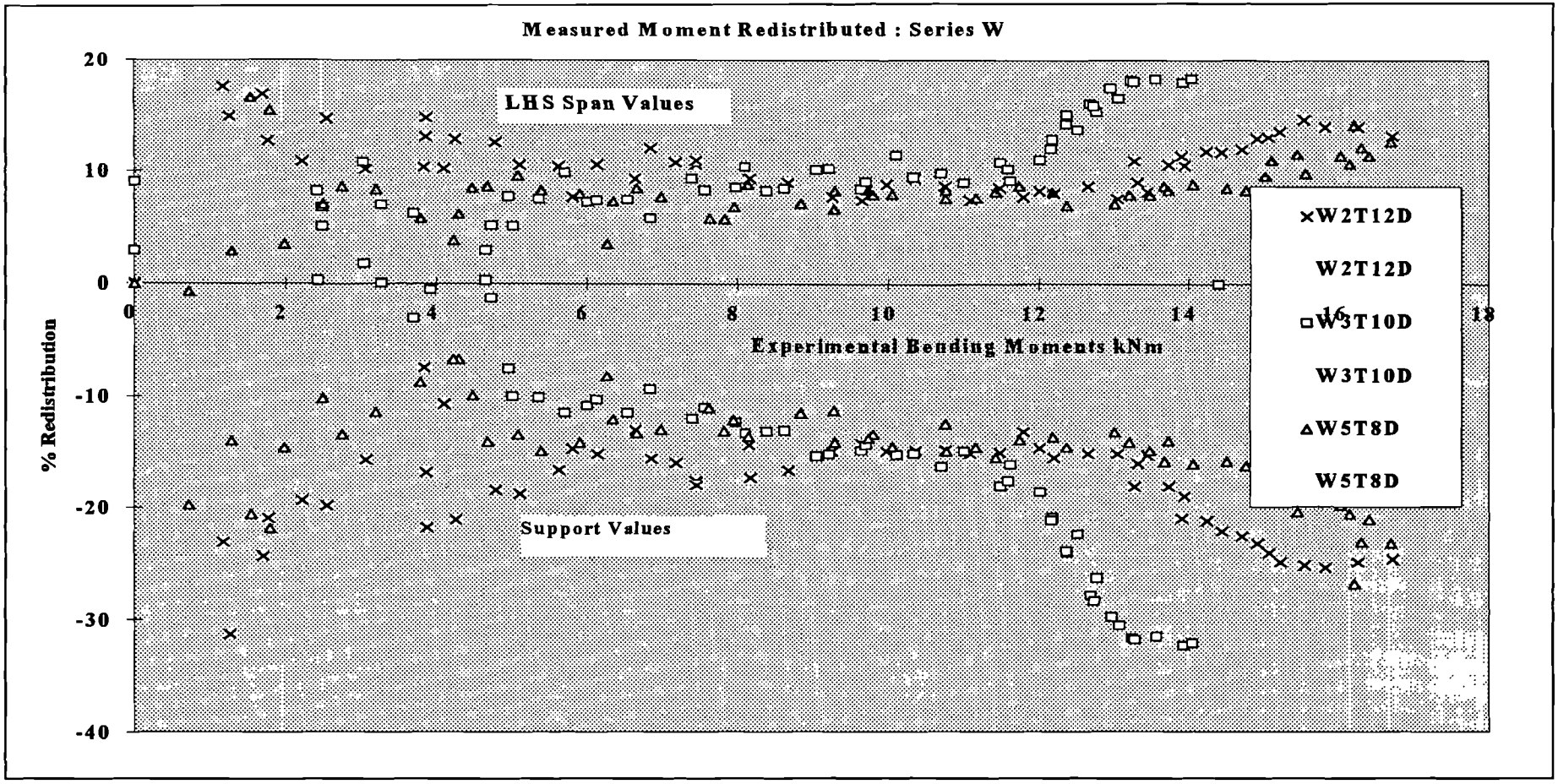

Figure 5-5: Series W measured moment redistribution of both spans and the support

115

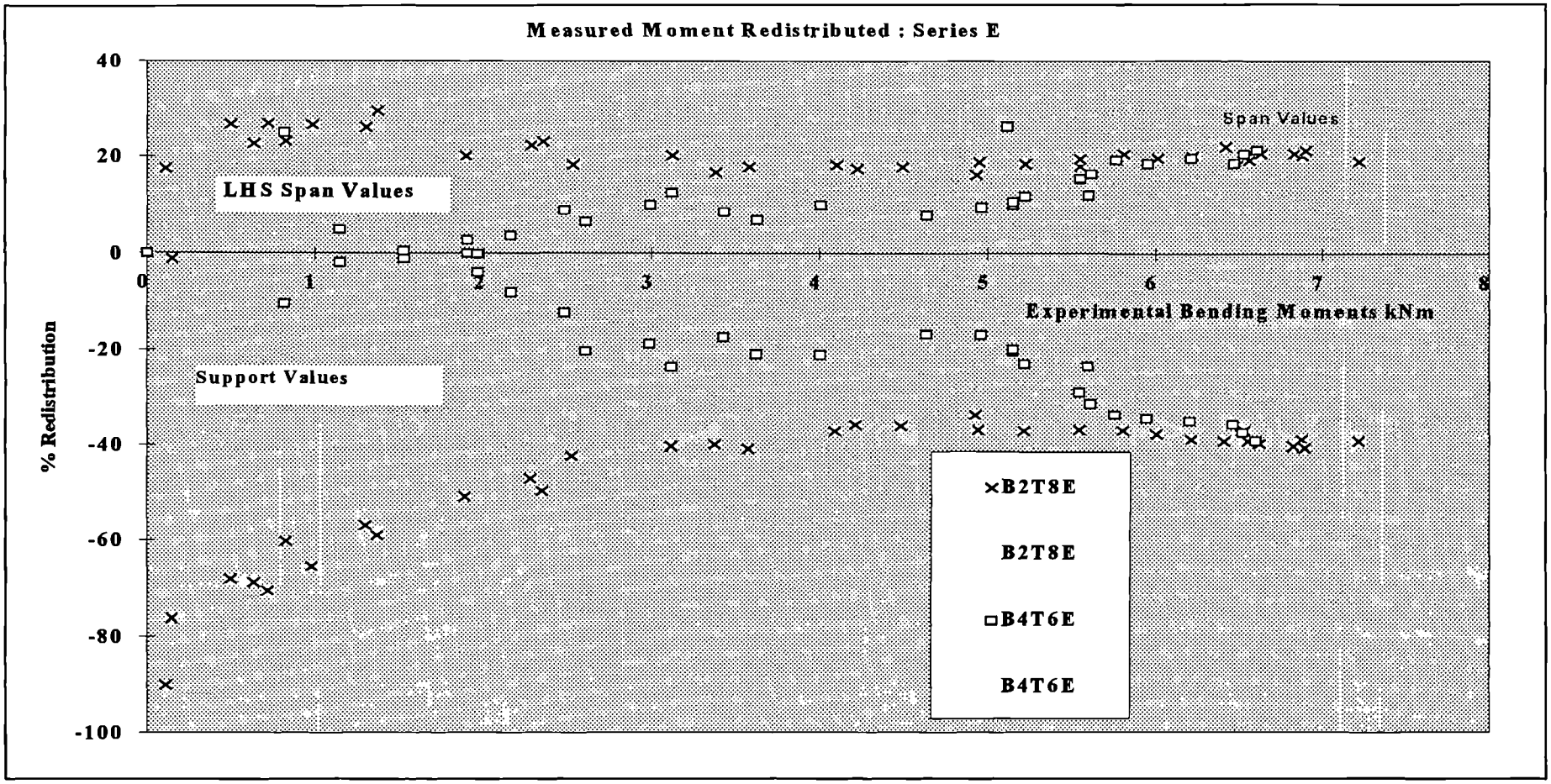

Figure 5-6: Series E measured moment redistribution of both spans and the support

116

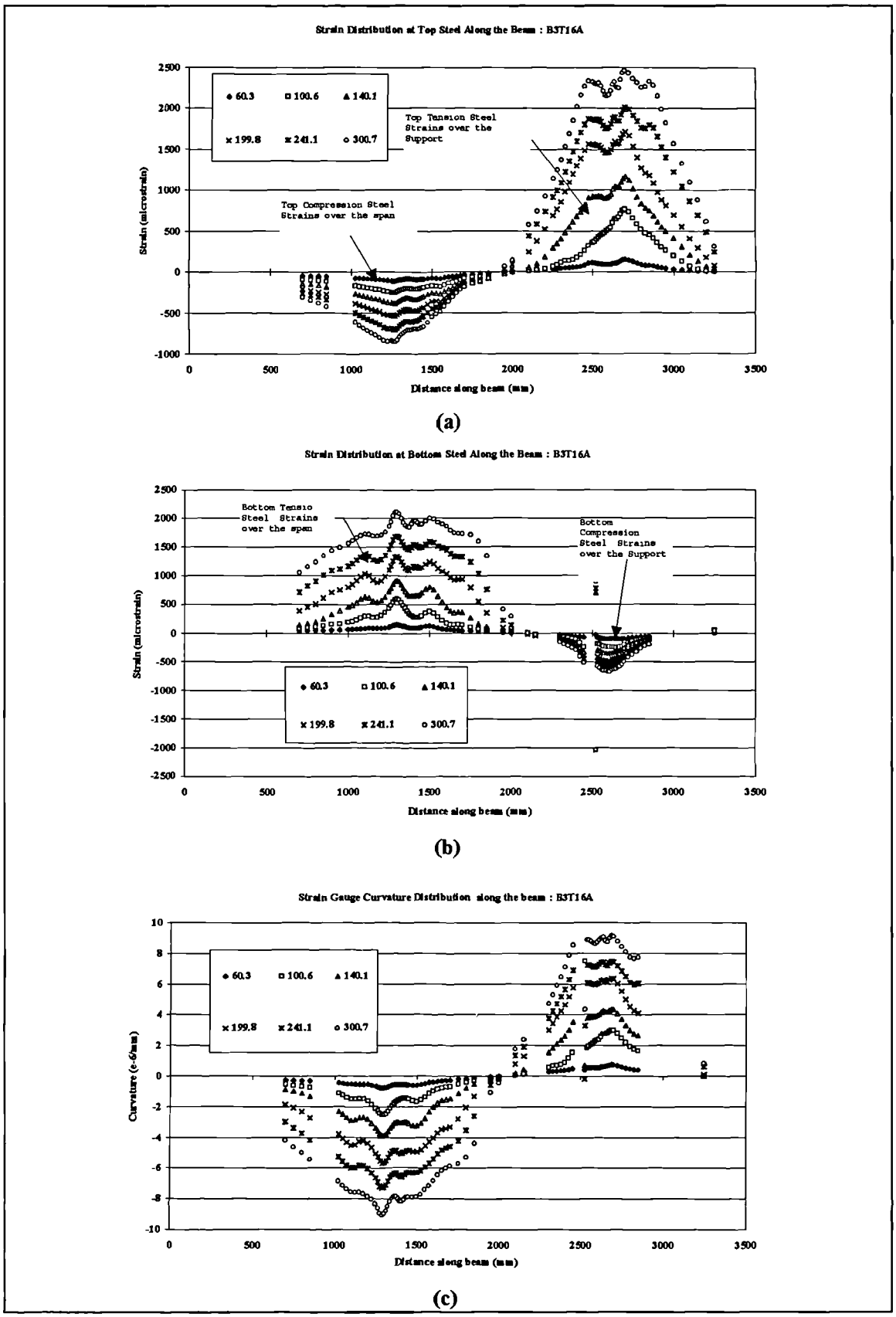

Figure 5-7:Specimen B3T16A(a) Top steel strain distribution (b) Bottom steel strain distribution (c) Curvature distribution

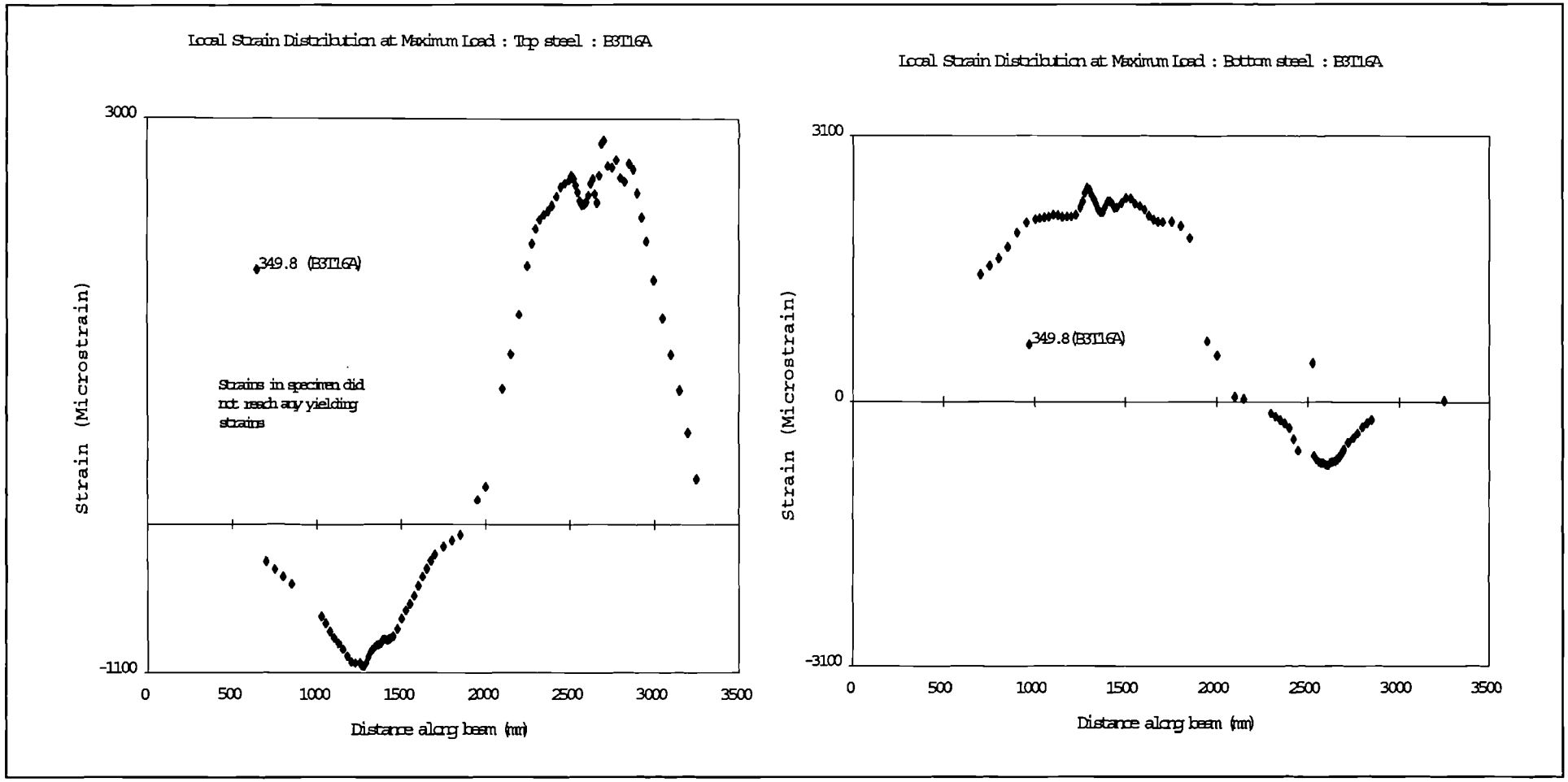

Figure 5-8: Specimen B3T16A local top and bottom steel strain distributions at failure loads

118

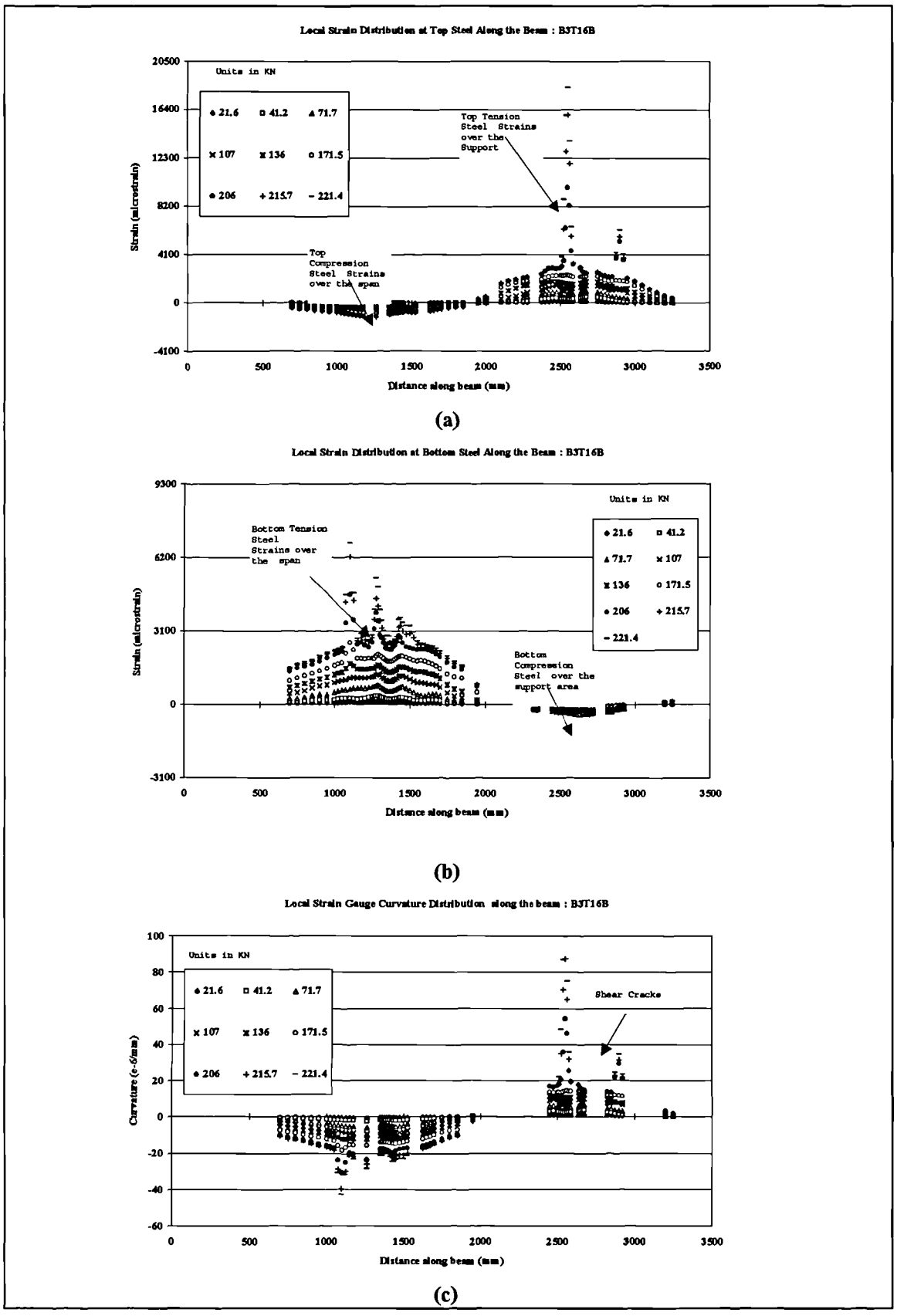

Figure 5-9:Specimen B3T16B (a) Local top steel strain distribution (b) Local bottom steel strain distribution (c) Local Curvature distribution

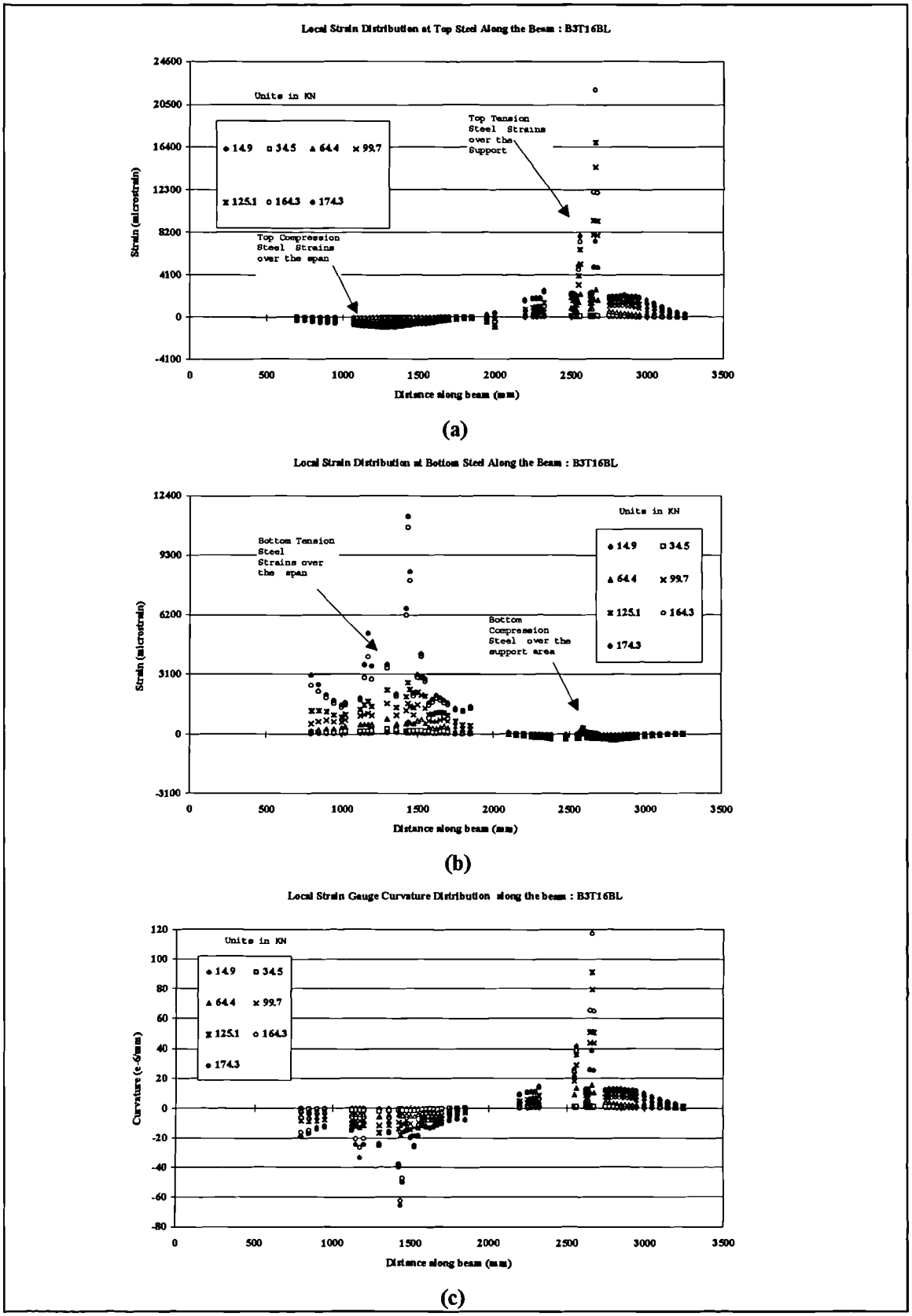

Figure 5-10:Specimen B3T16BL (a) Local top steel strain distribution (b) Local bottom steel strain distribution (c) Local Curvature distribution

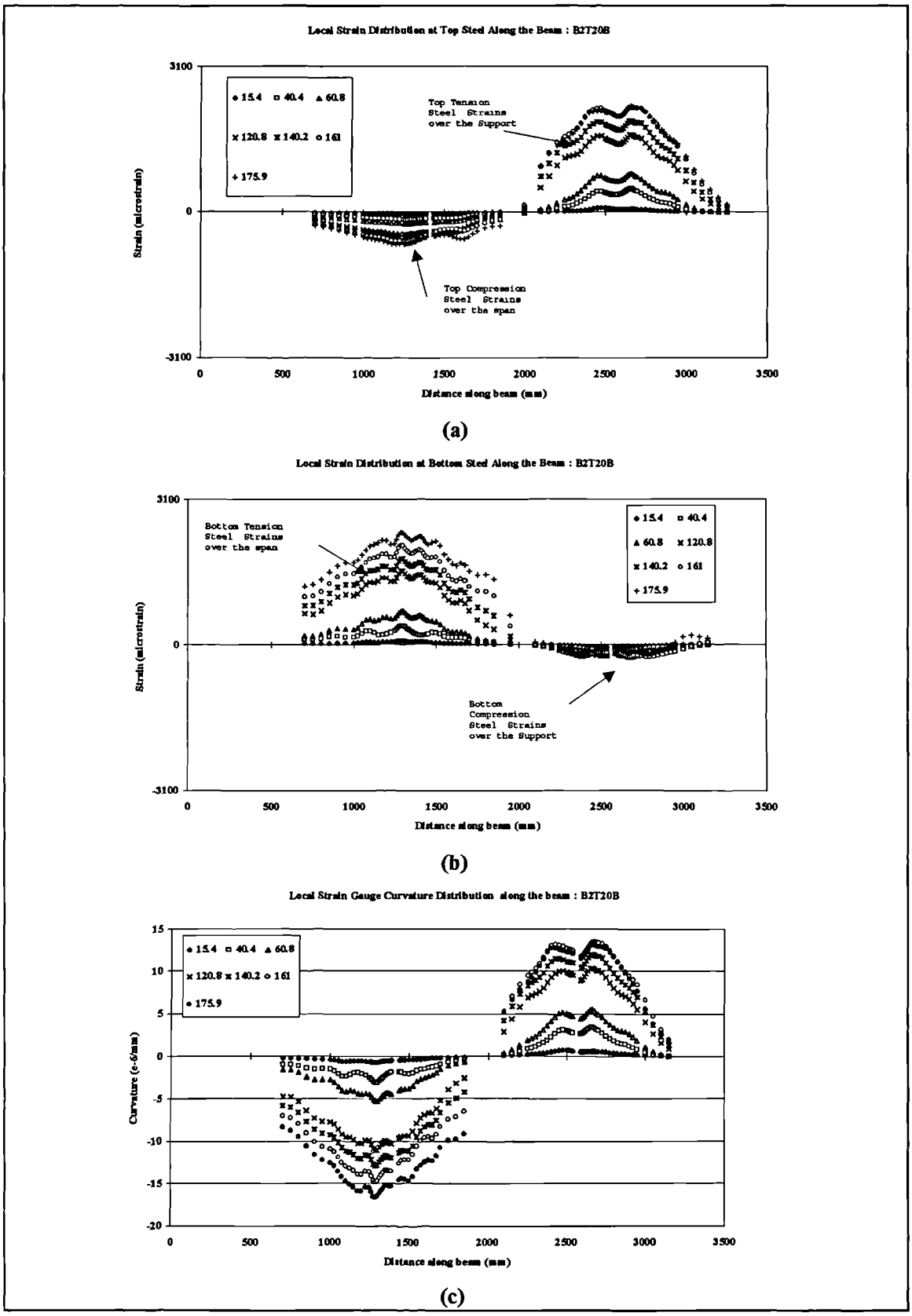

Figure 5-11:Specimen B2T20B (a) Local top steel strain distribution (b) Local bottom steel strain distribution (c) Local Curvature distribution

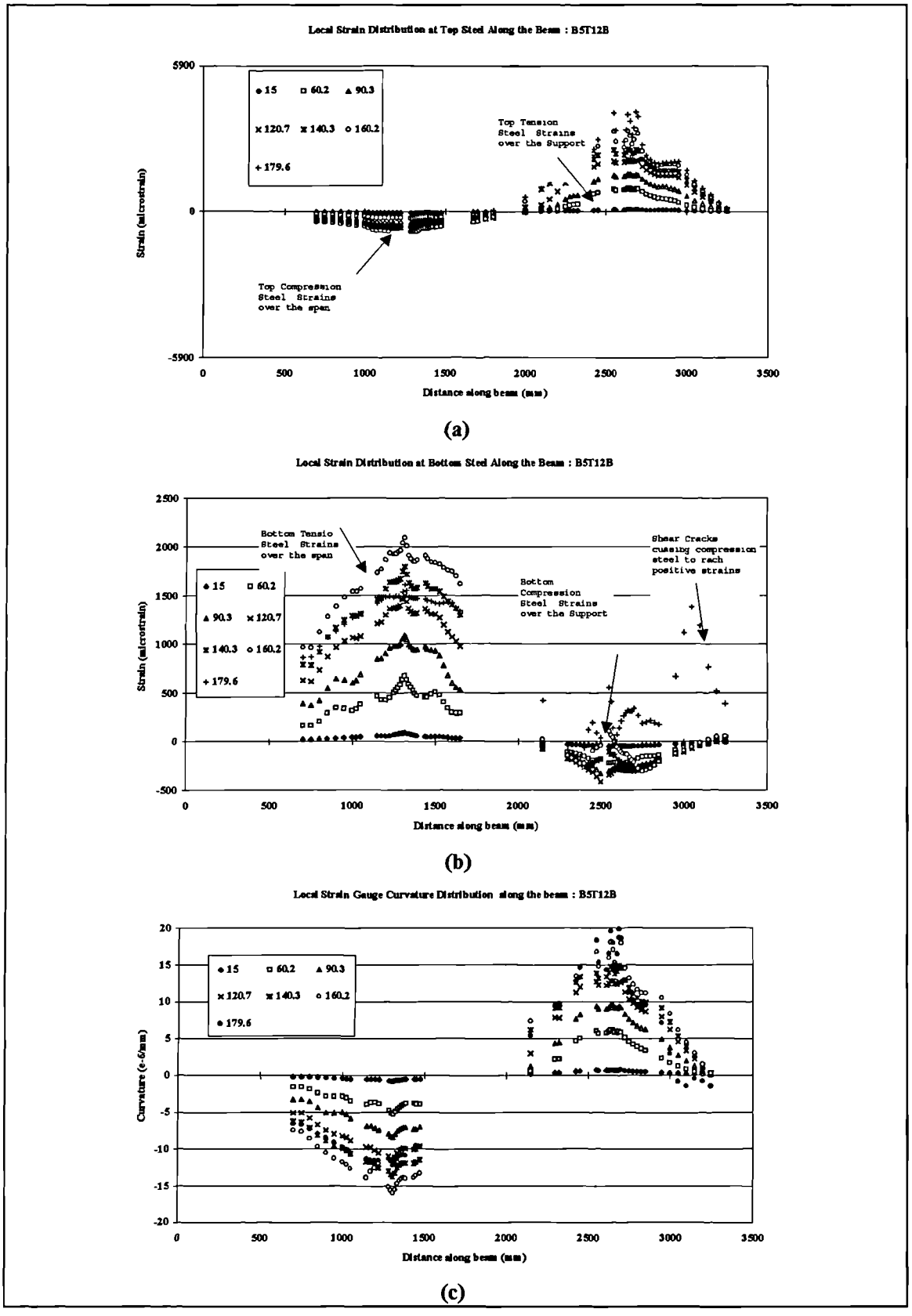

Figure 5-12:Specimen B5T12B (a) Local top steel strain distribution (b) Local bottom steel strain distribution (c) Local Curvature distribution

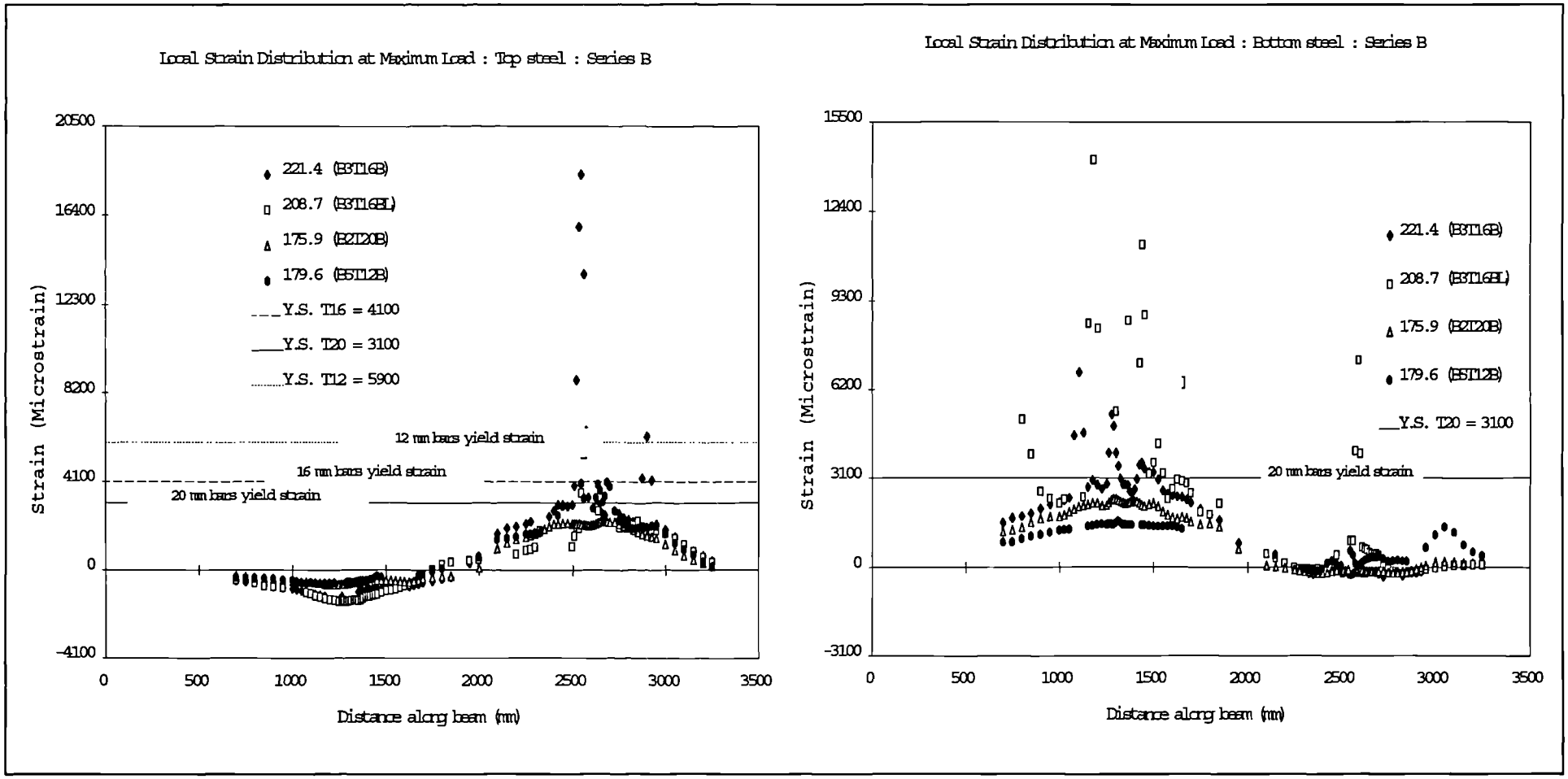

Figure 5-13: Series B local top and bottom steel strain distributions at failure loads

123

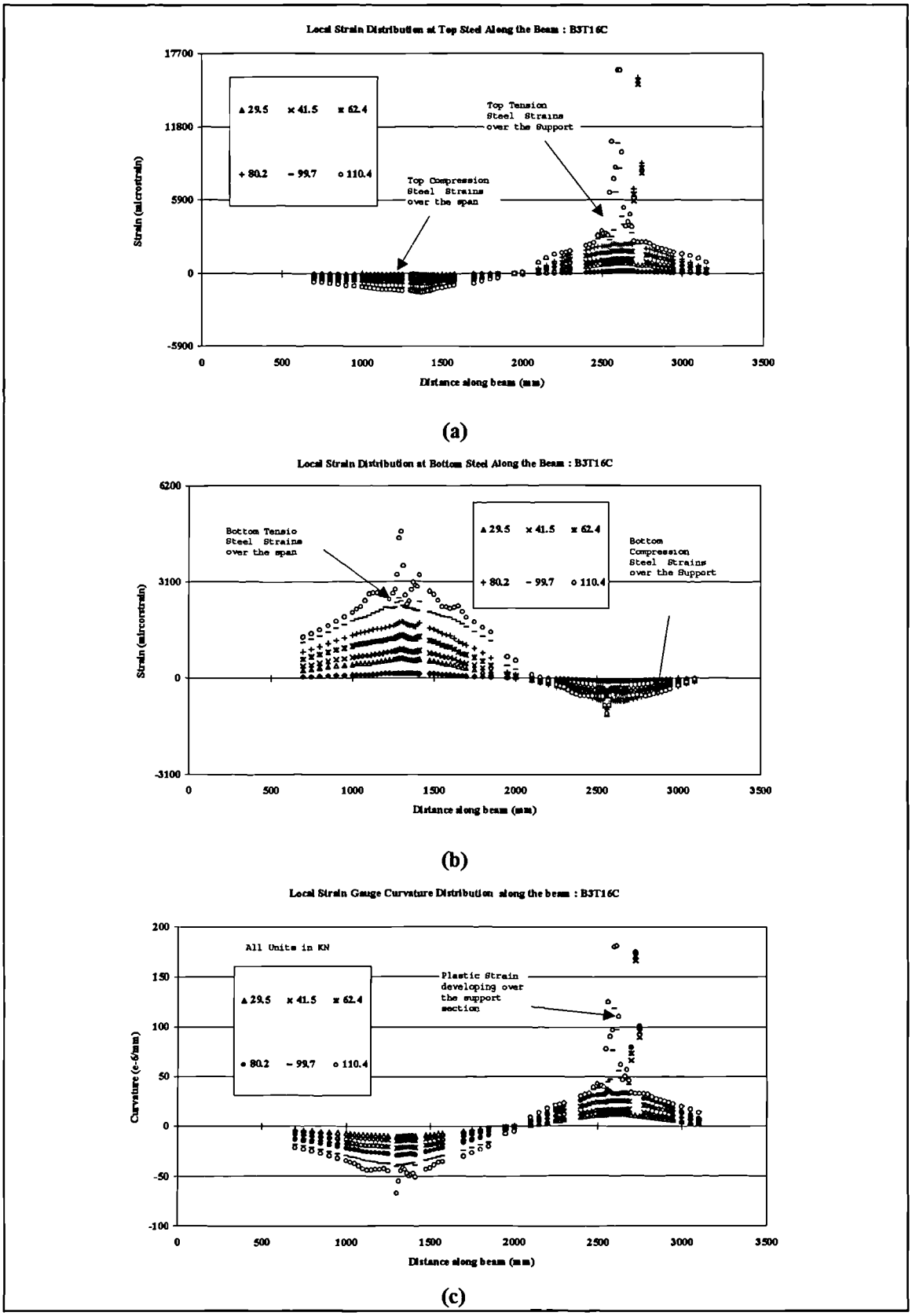

Figure 5-14:Specimen B3T16C (a) Local top steel strain distribution (b) Local bottom steel strain distribution (c) Local Curvature distribution

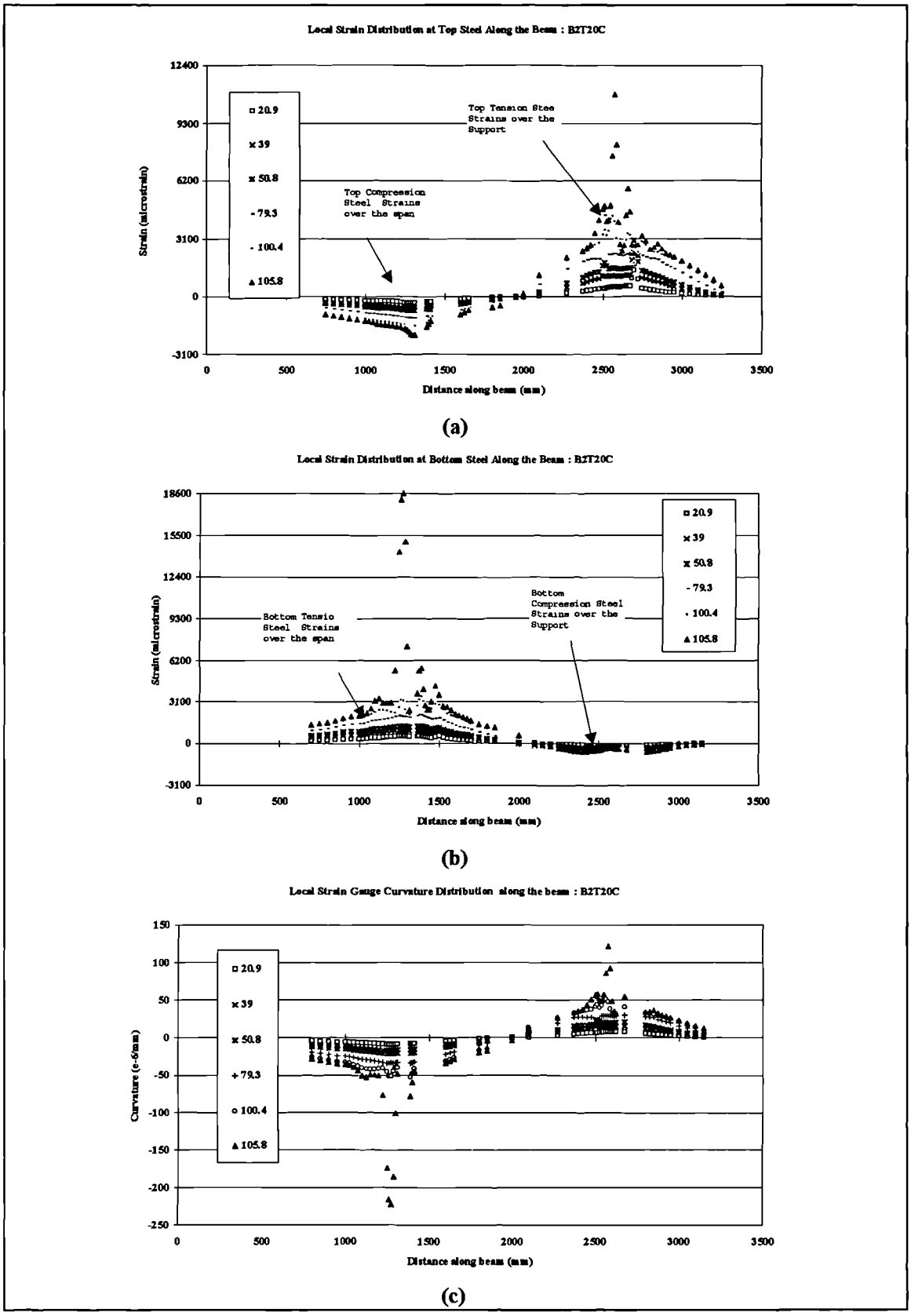

Figure 5-15:Specimen B2T20C (a) Local top steel strain distribution (b) Local bottom steel strain distribution (c) Local Curvature distribution

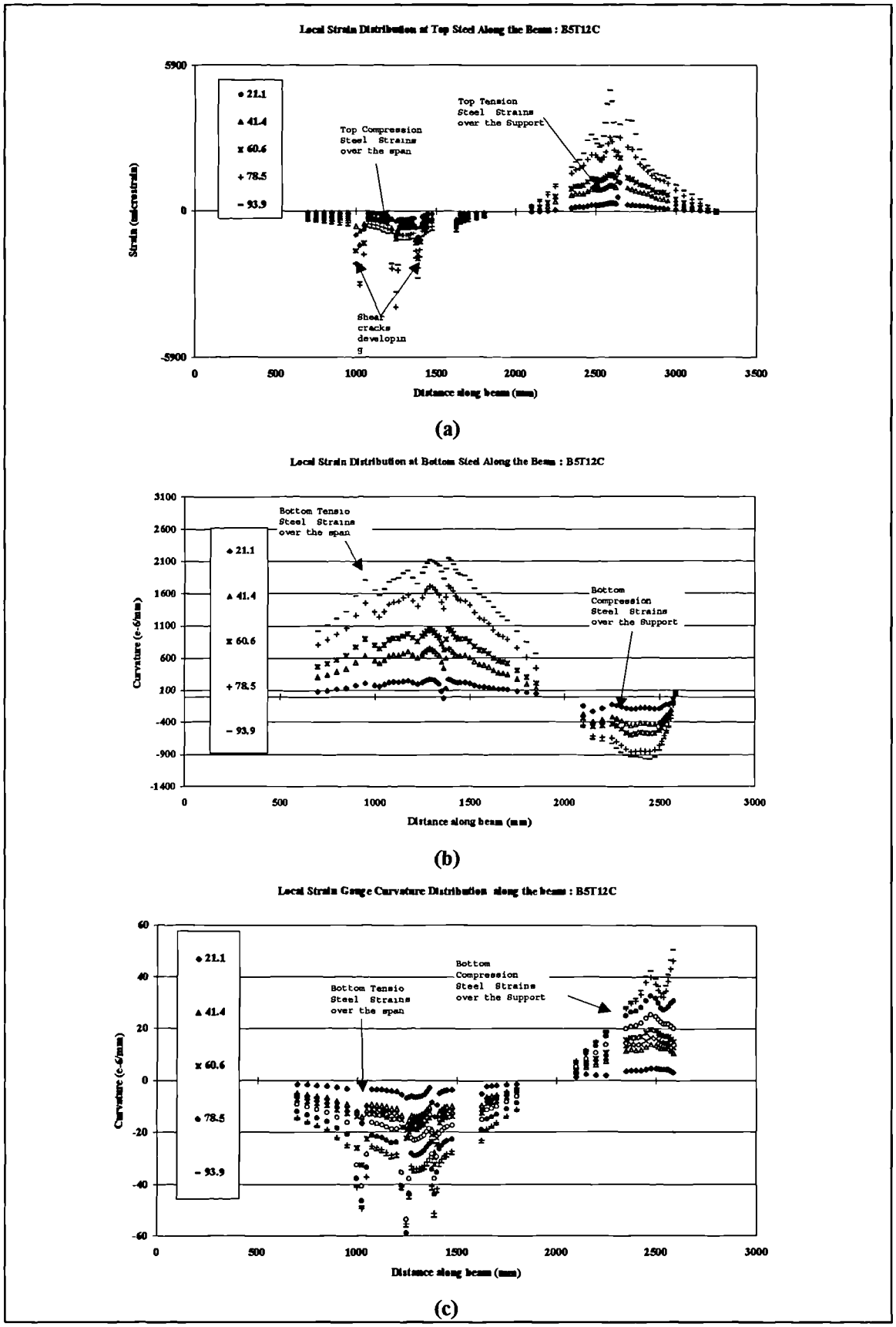

Figure 5-16:Specimen B5T12C (a) Local top steel strain distribution (b) Local bottom steel strain distribution (c) Local Curvature distribution

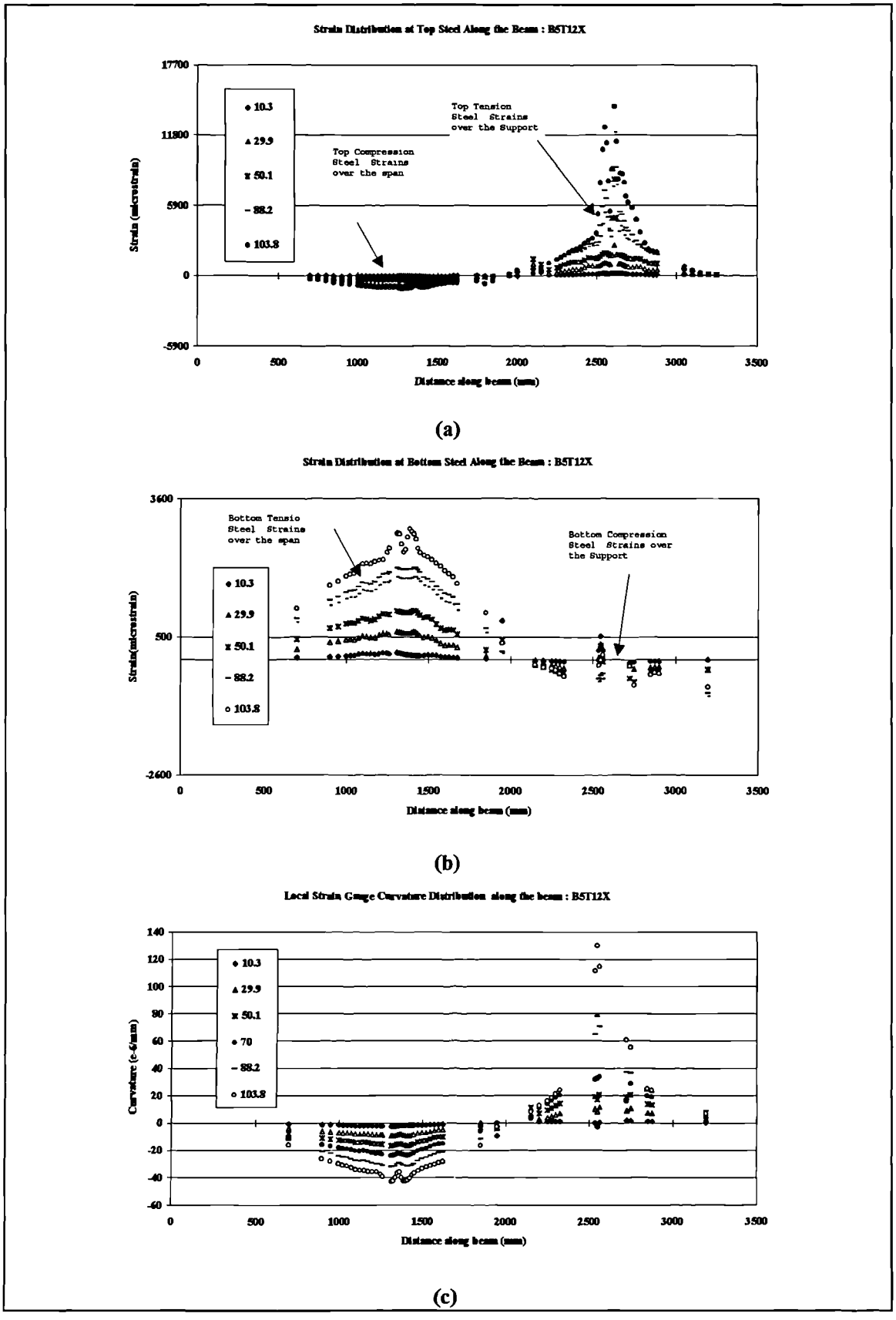

Figure 5-17:Specimen B5T12X (a) Local top steel strain distribution (b) Local bottom steel strain distribution (c) Local Curvature distribution

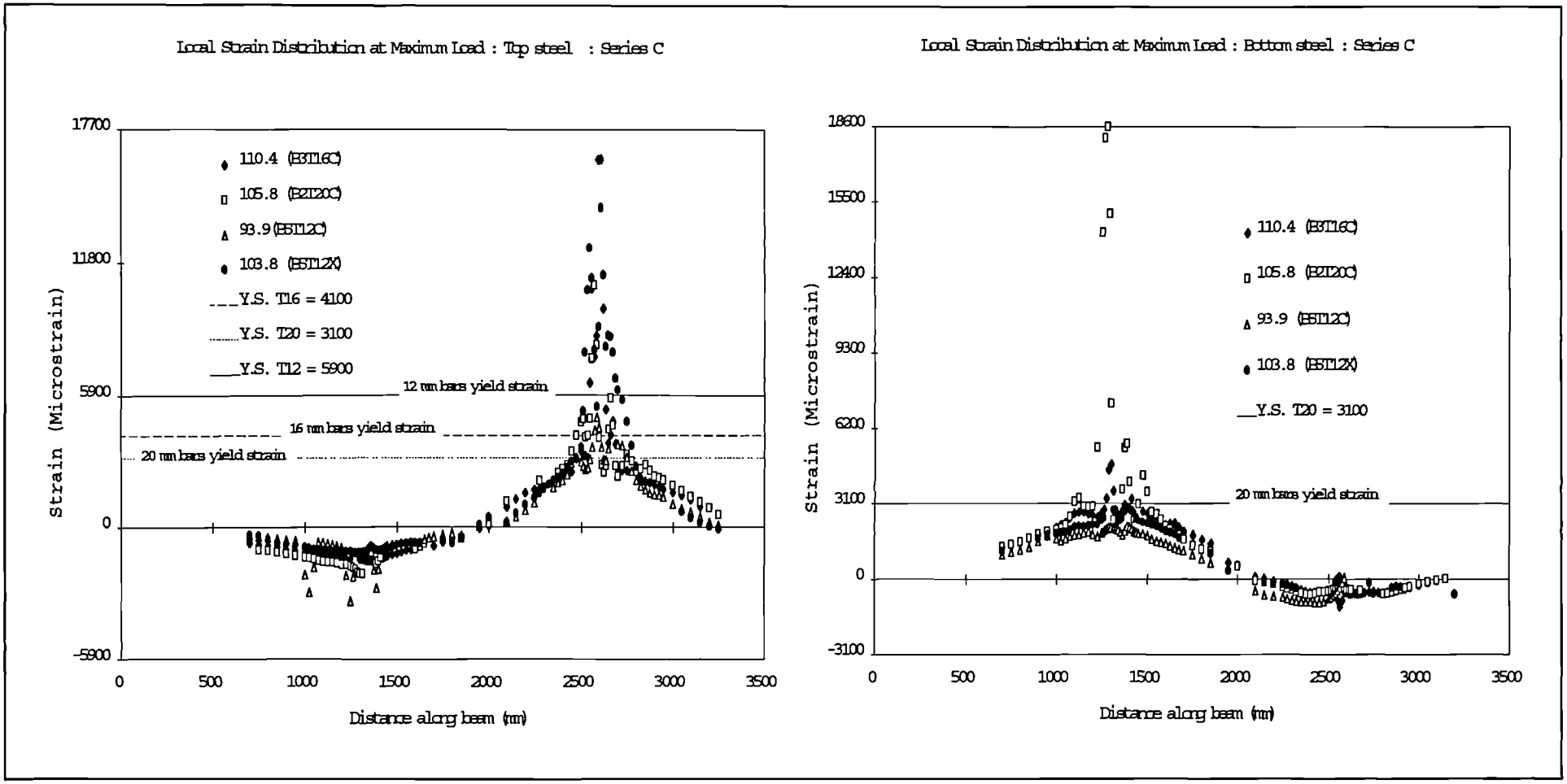

Figure 5-18: Series C local top and bottom steel strain distributions at failure loads

128

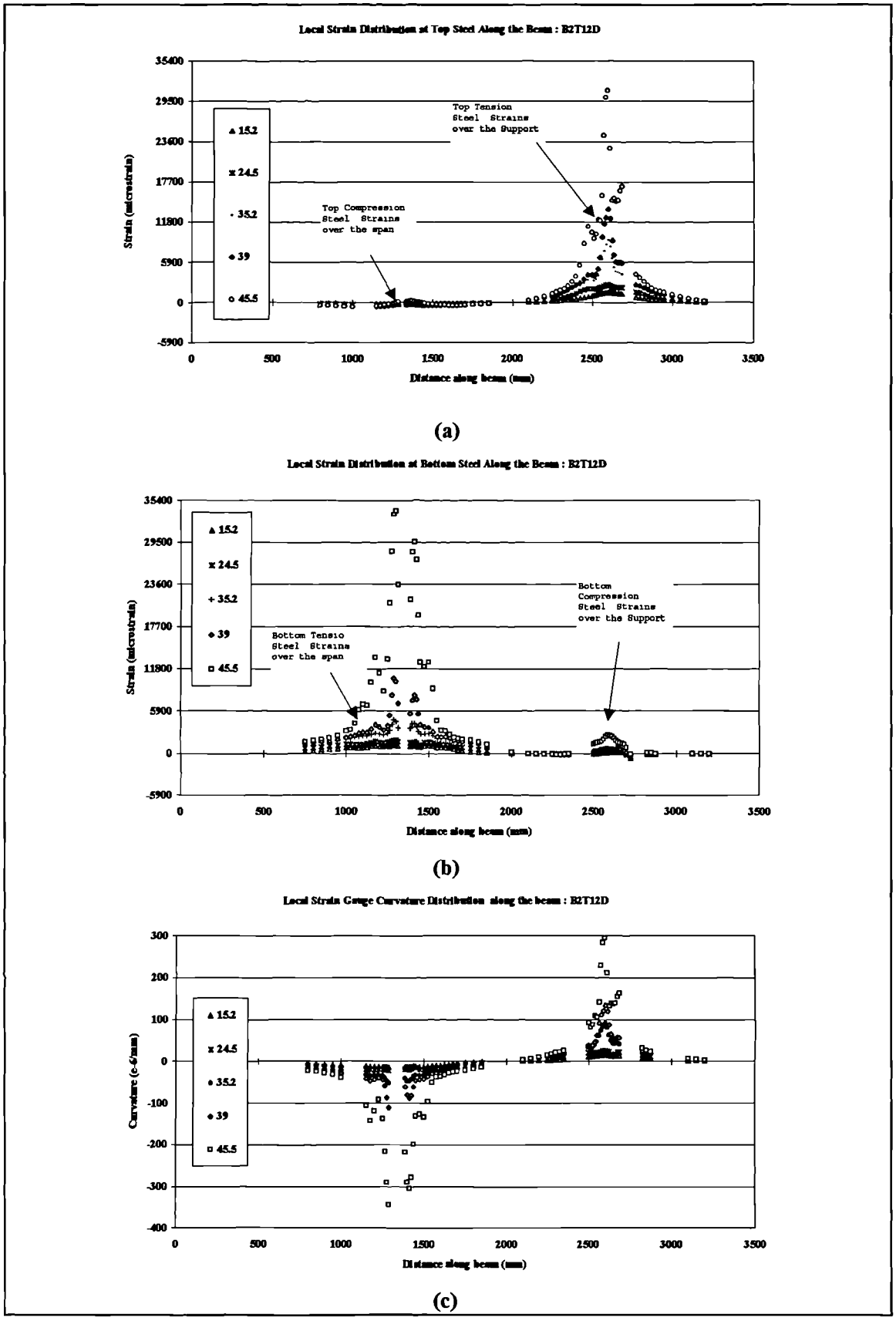

Figure 5-19:Specimen B2T12D (a) Local top steel strain distribution (b) Local bottom steel strain distribution (c) Local Curvature distribution

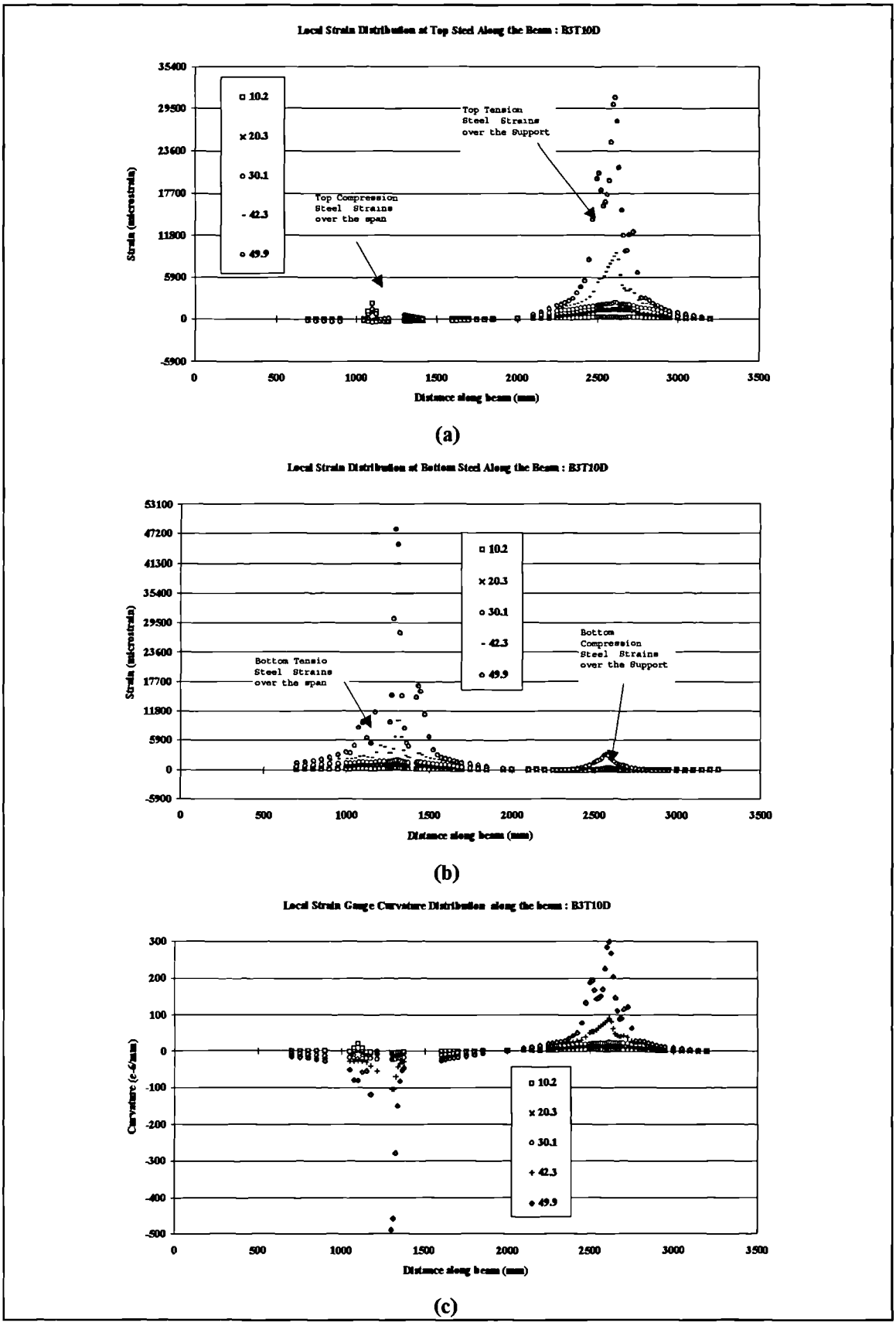

Figure 5-20:Specimen B3T10D (a) Local top steel strain distribution (b) Local bottom steel strain distribution (c) Local Curvature distribution

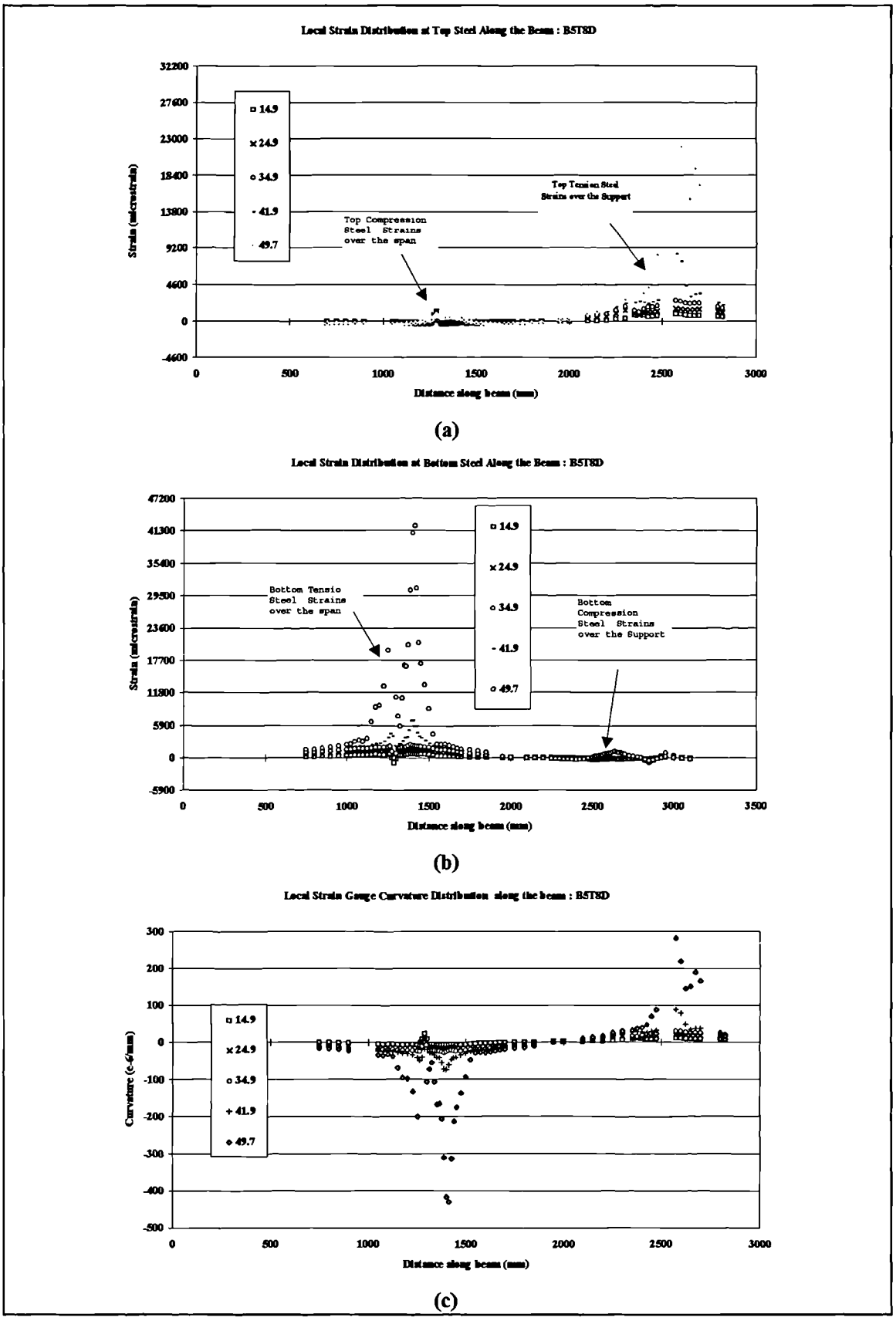

Figure 5-21:Specimen B5T8D(a) Local top steel strain distribution (b) Local bottom steel strain distribution (c) Local Curvature distribution

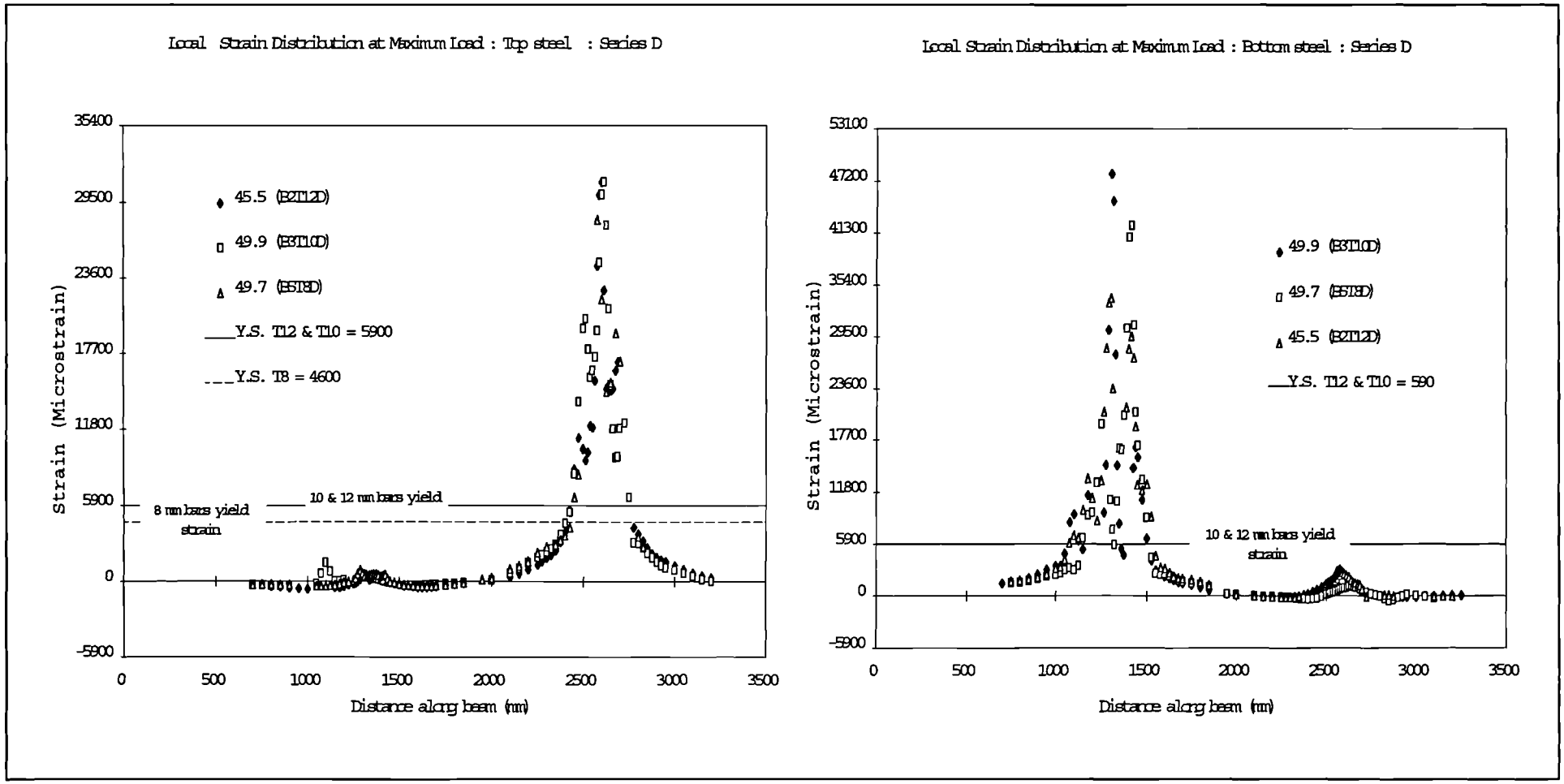

Figure 5-22: Series D local top and bottom steel strain distributions at failure loads

132

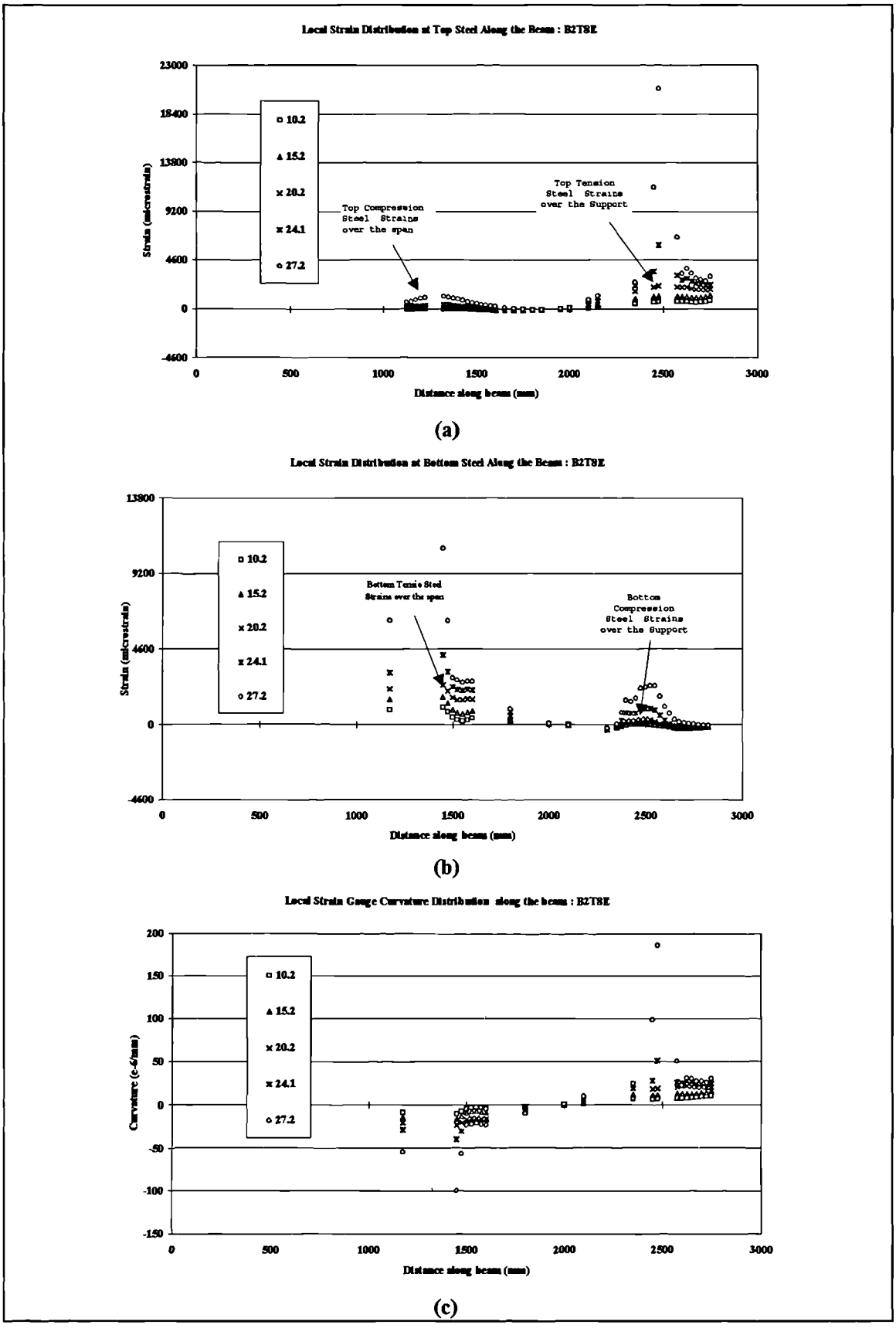

Figure 5-23:Specimen B2T8E (a) Local top steel strain distribution (b) Local bottom steel strain distribution (c) Local Curvature distribution

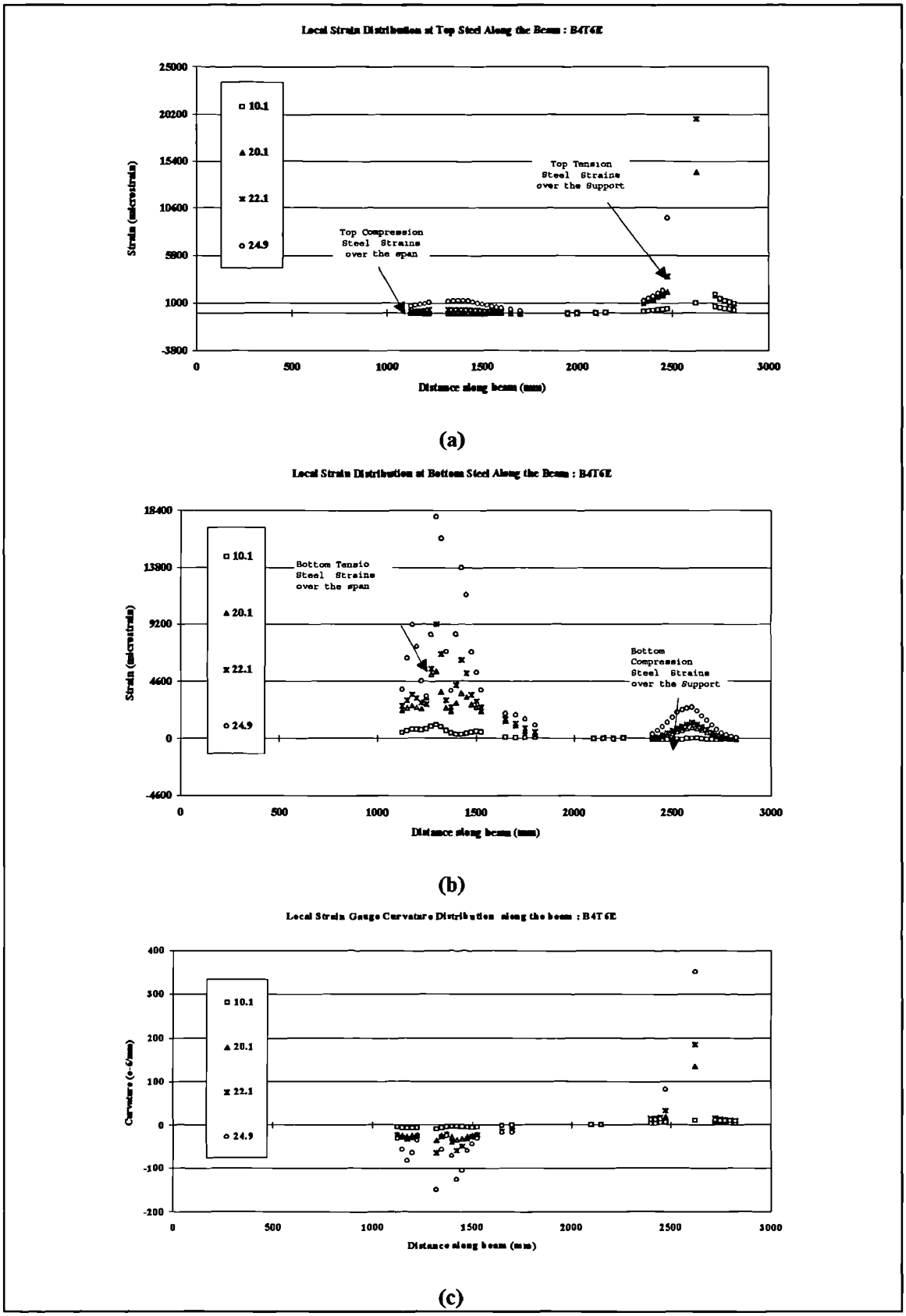

Figure 5-24:Specimen B4T6E (a) Local top steel strain distribution (b) Local bottom steel strain distribution (c) Local Curvature distribution

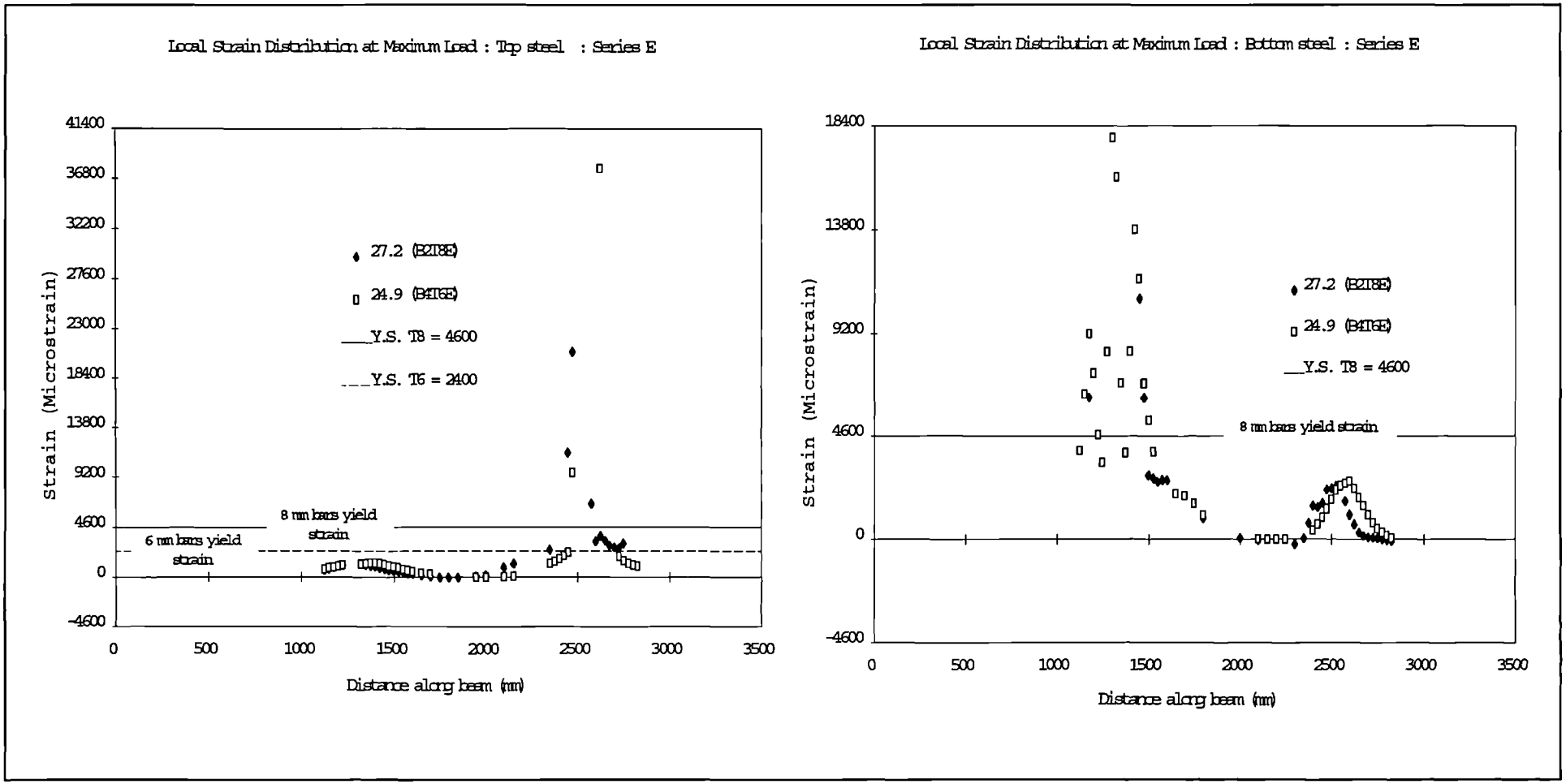

Figure 5-25: Series E local top and bottom steel strain distributions at failure loads

135

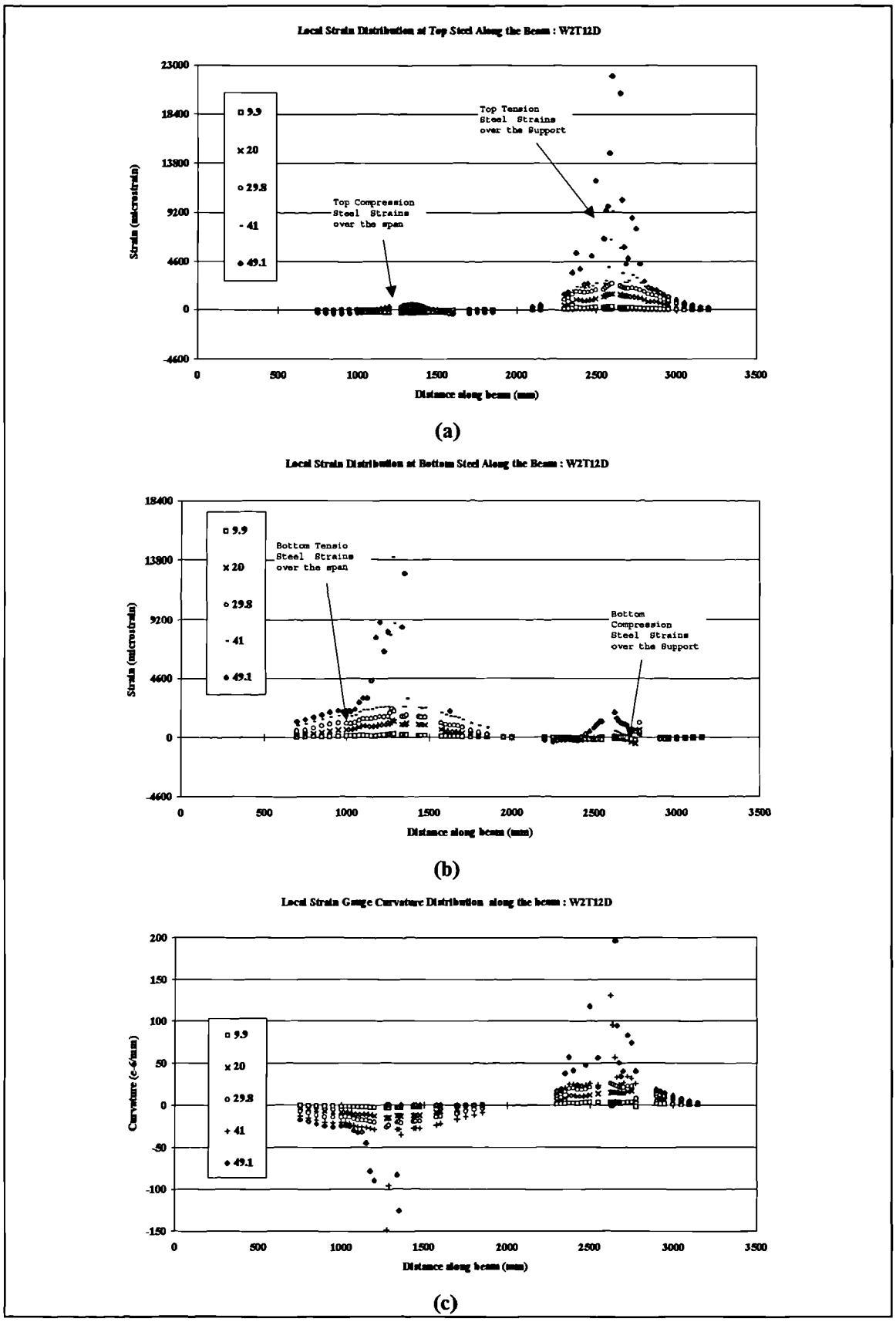

Figure 5-26:Specimen W2T12D (a) Local top steel strain distribution (b) Local bottom steel strain distribution (c) Local Curvature distribution

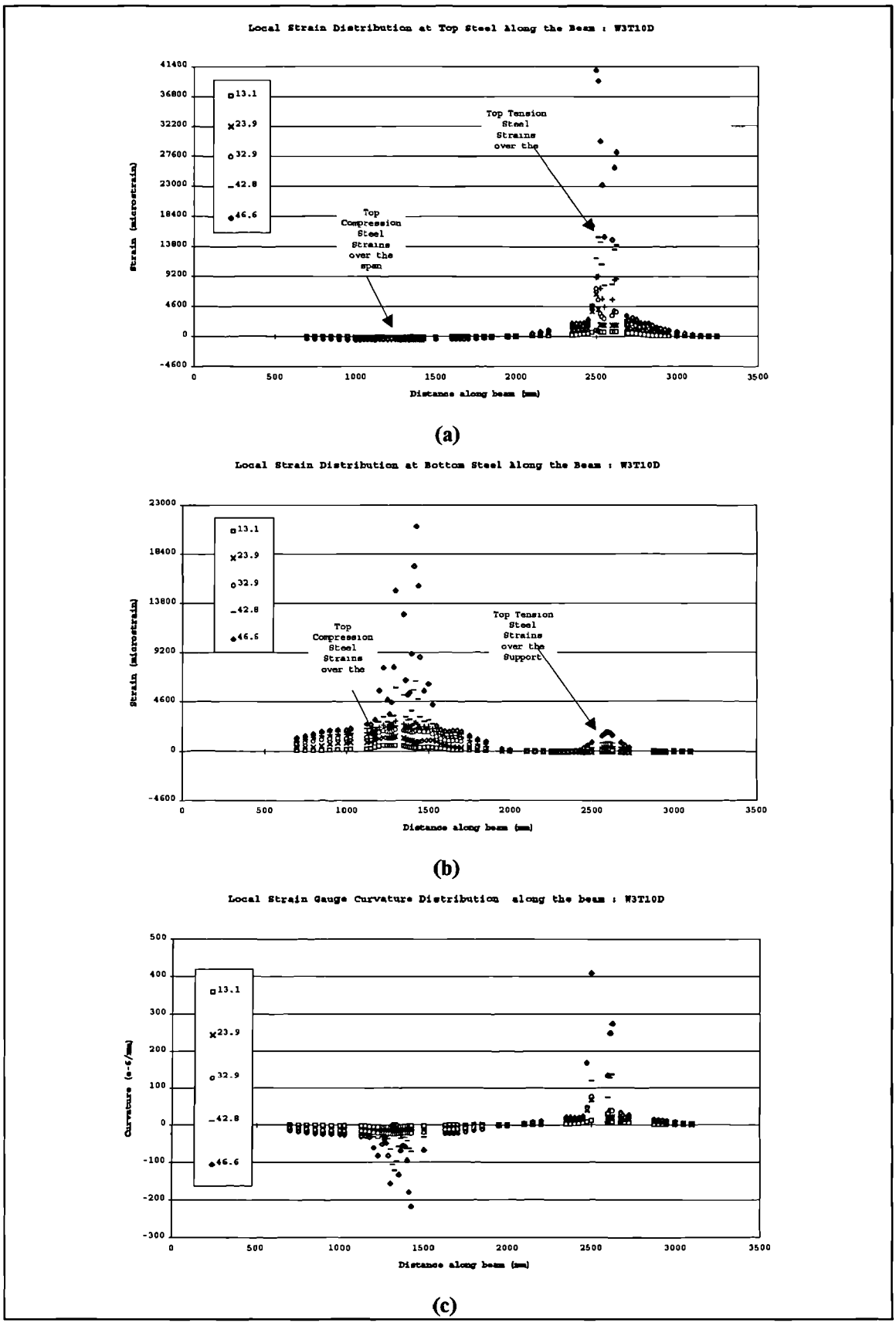

Figure 5-27:Specimen W3T10D (a) Local top steel strain distribution (b) Local bottom steel strain distribution (c) Local Curvature distribution

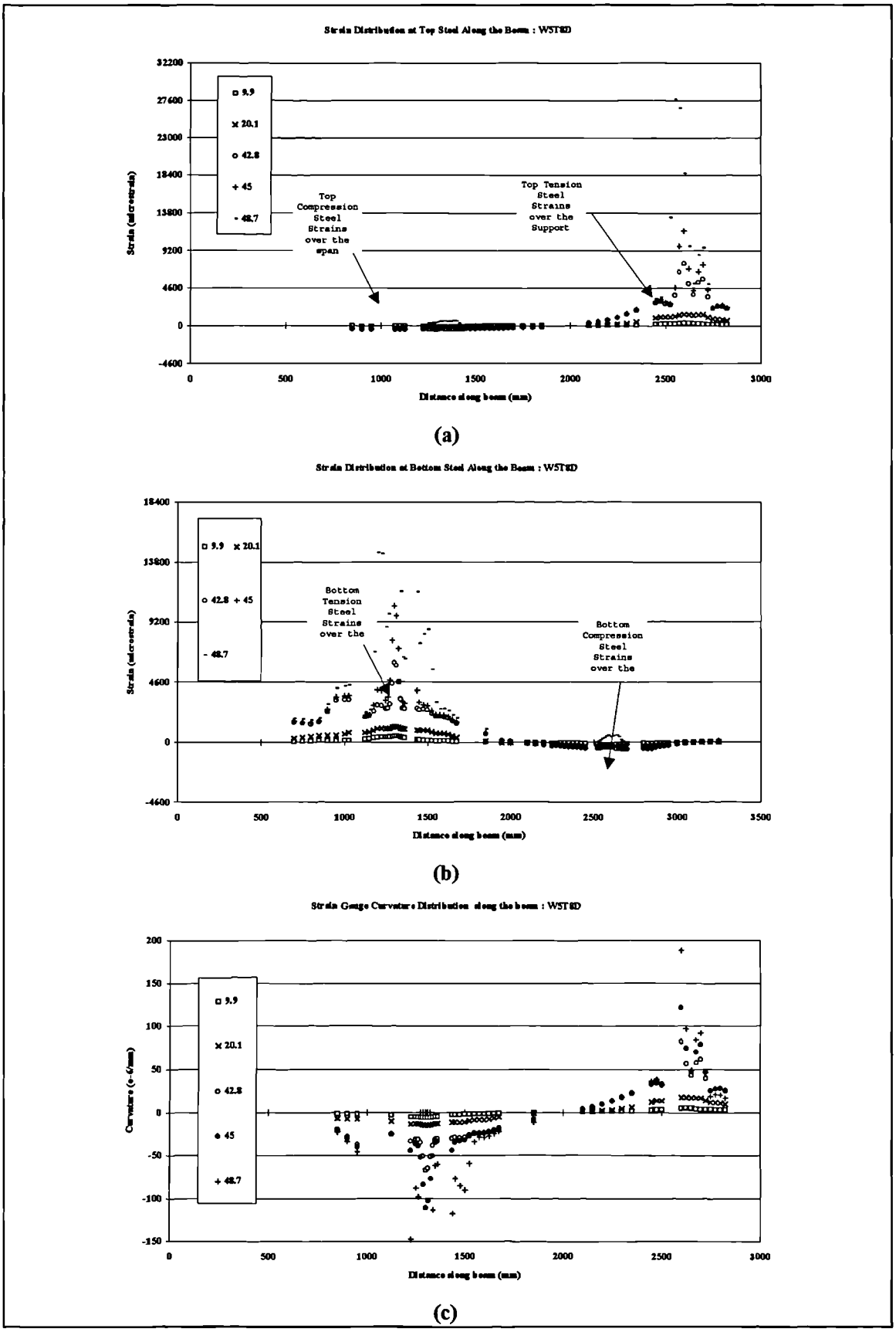

Figure 5-28:Specimen W5T8D (a) Local top steel strain distribution (b) Local bottom steel strain distribution (c) Local Curvature distribution

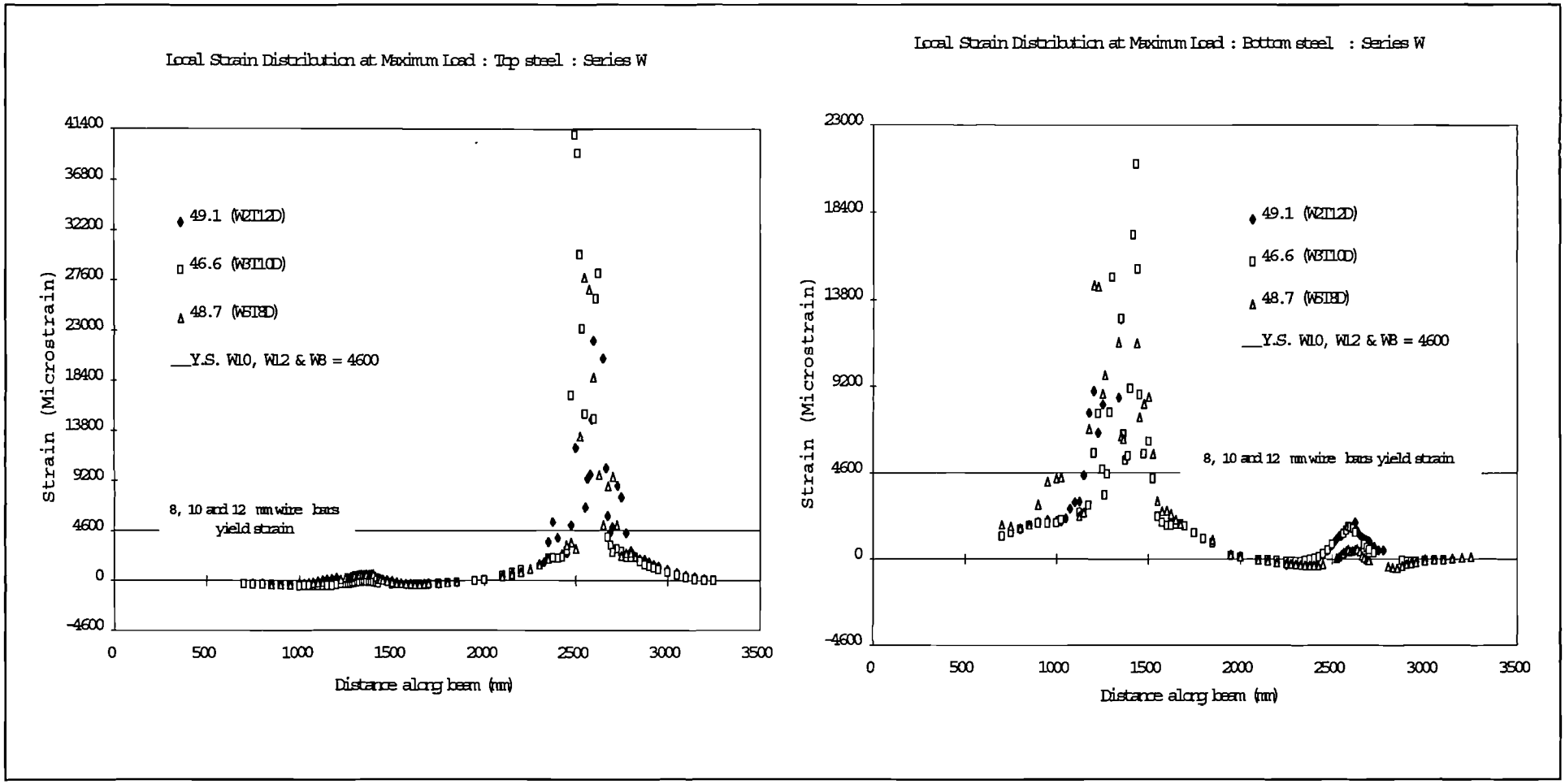

Figure 5-29: Series W local top and bottom steel strain distributions at failure loads

139

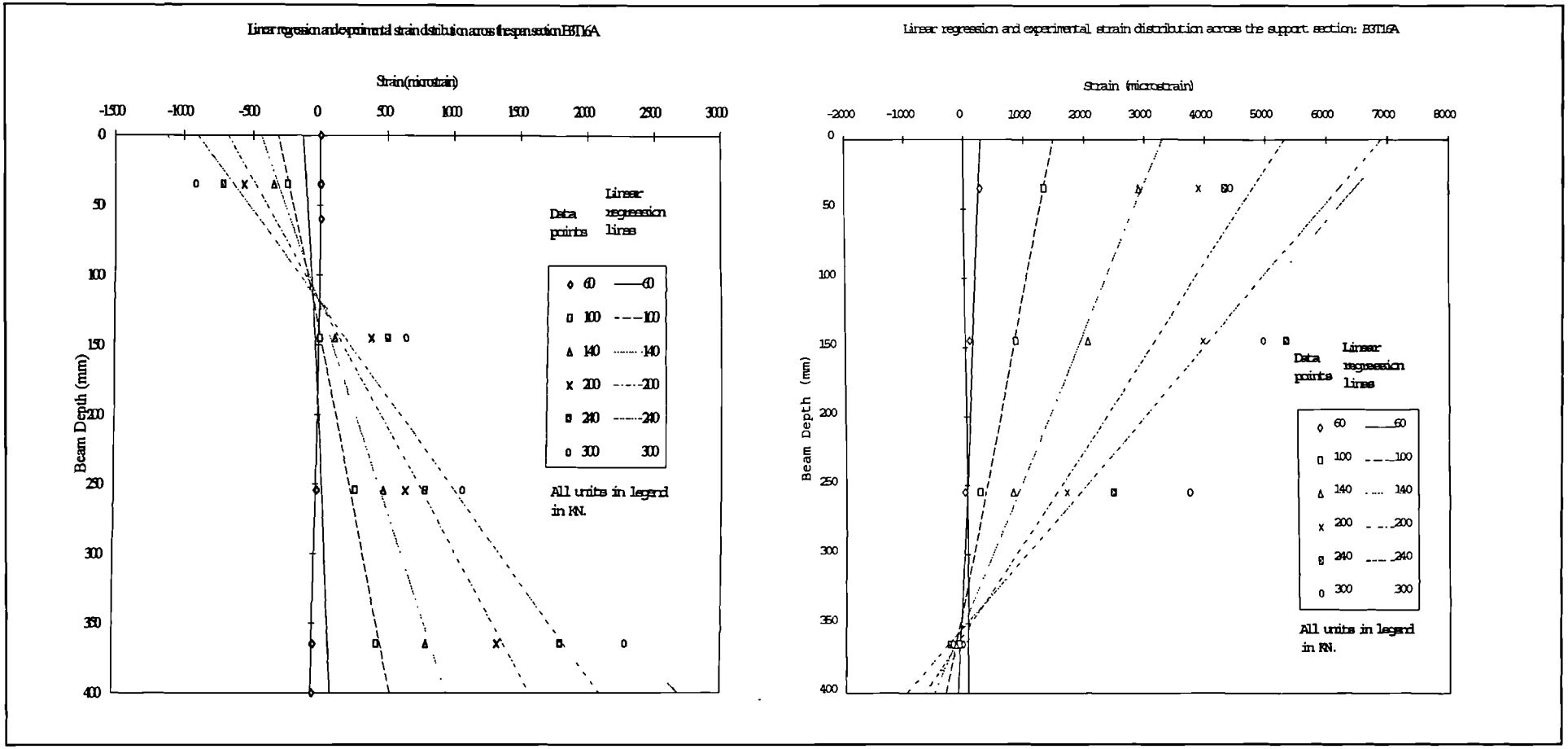

Figure 5-30: Specimen B3T16A calculated and measured strain across the depth of the span and support section

140

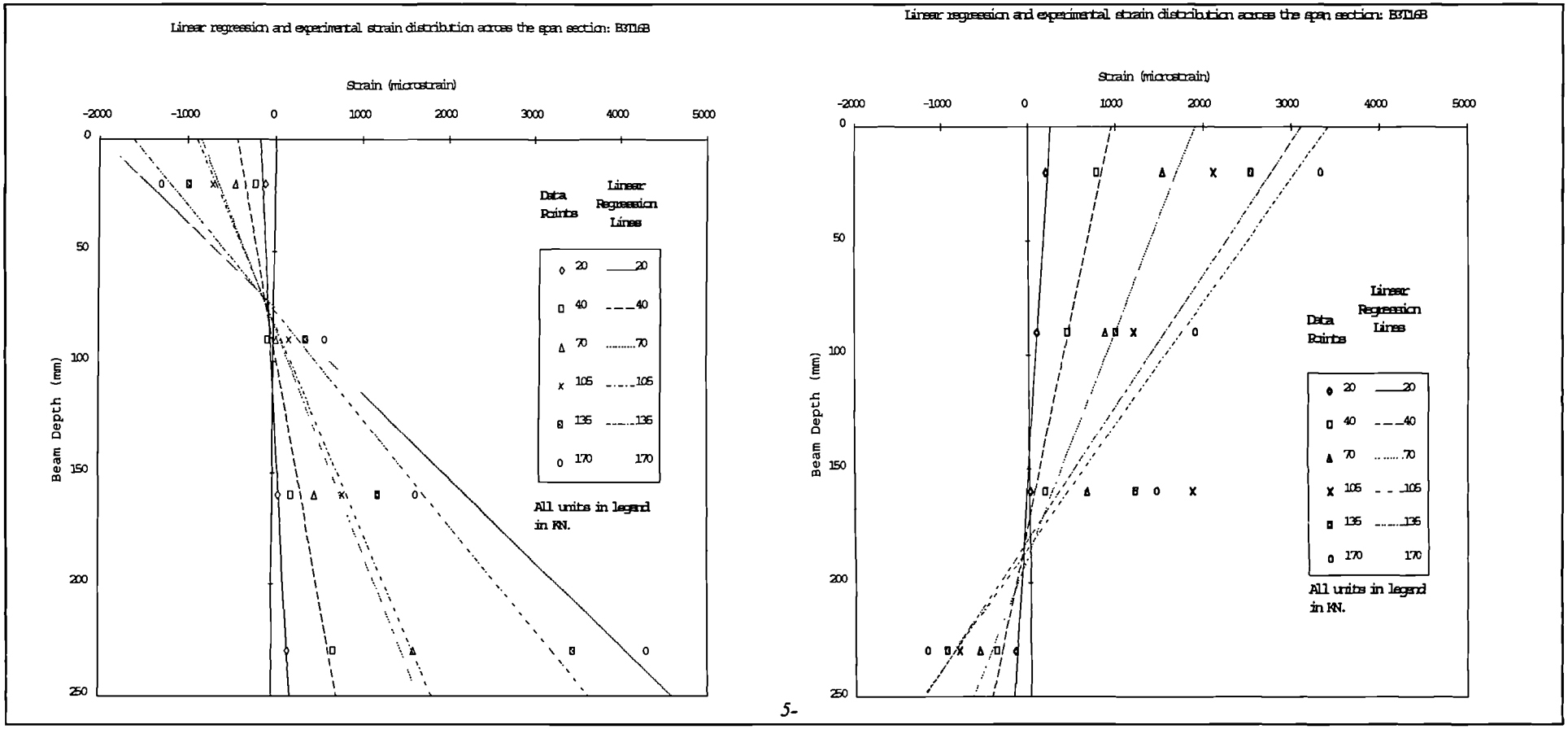

5-

Figure 5-31: Specimen B3T16B calculated and measured strain across the depth of the span and support sections

141

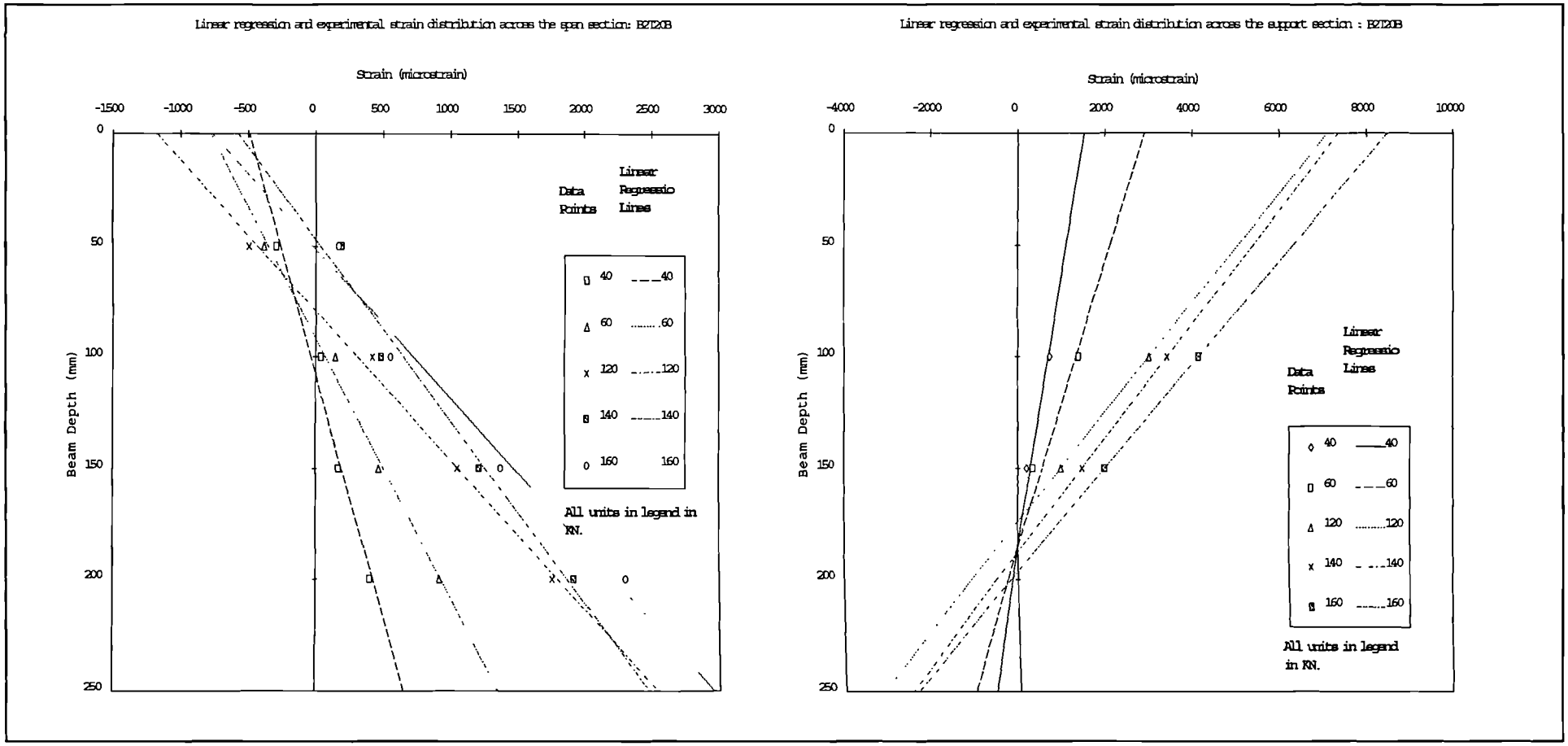

Figure 5-32: Specimen B2T20B calculated and measured strain across the depth of the span and support sections

142

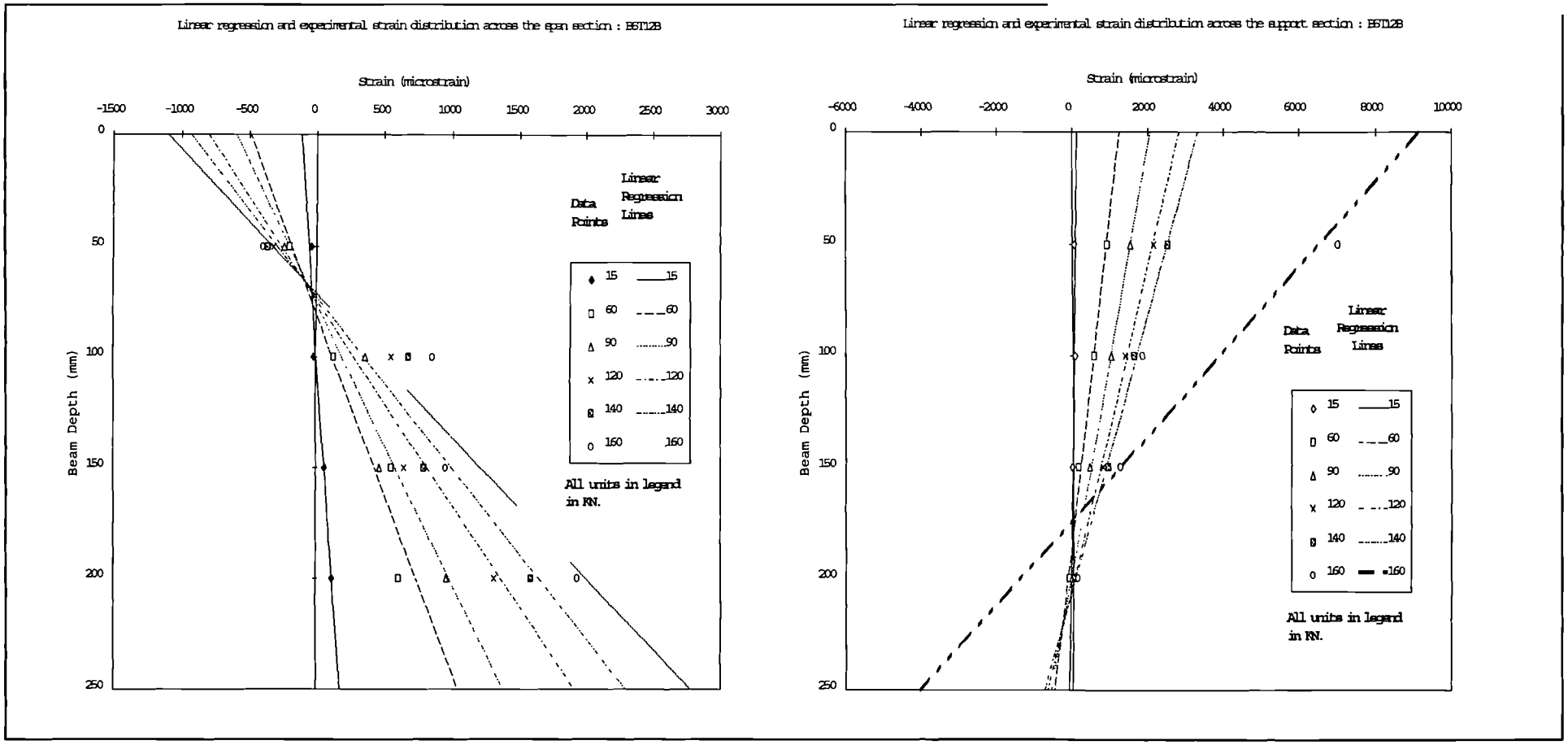

Figure 5-33: Specimen B5T12B calculated and measured strain across the depth of the span and support sections

143

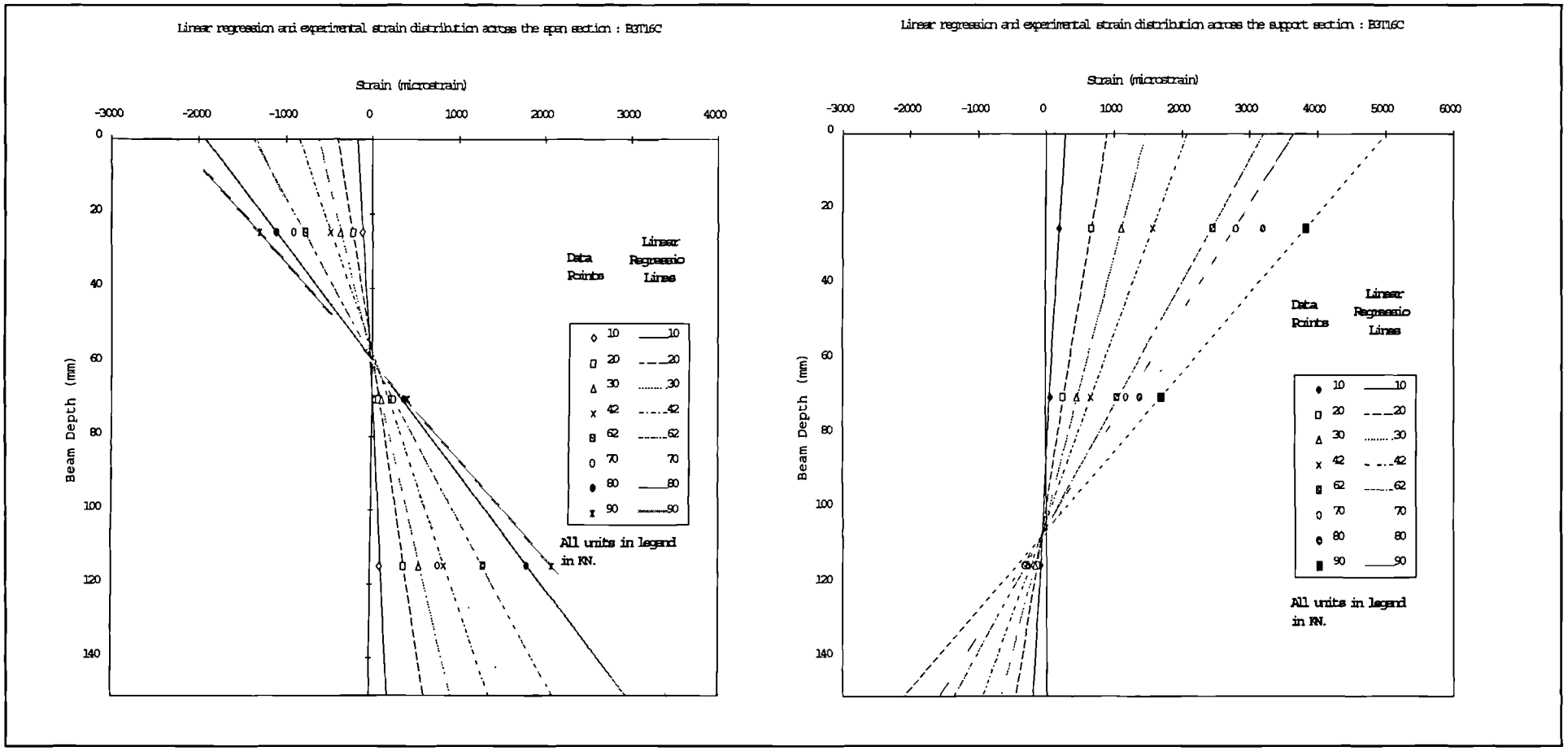

Figure 5-34: Specimen B3T16C calculated and measured strain across the depth of the span and support sections

144

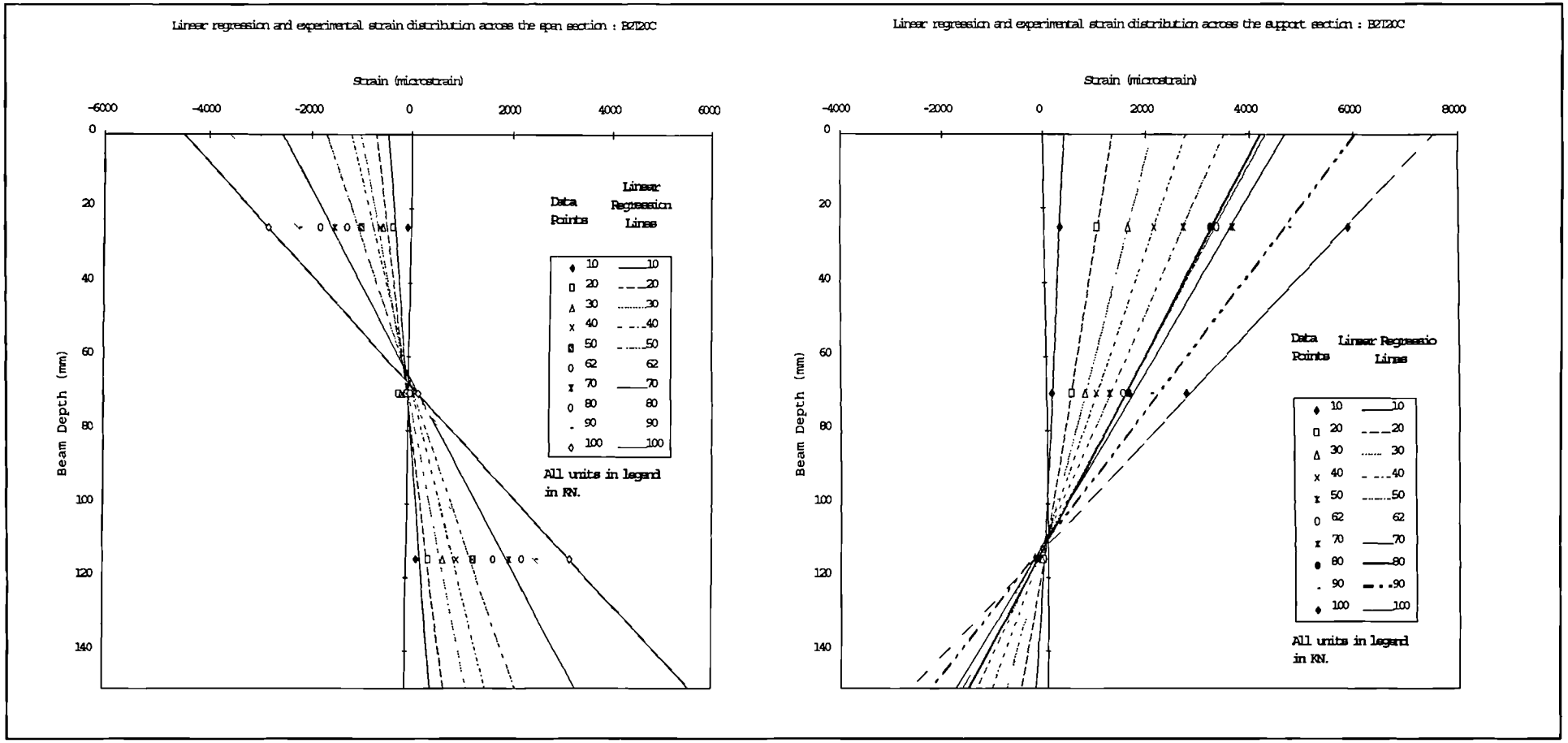

Figure 5-35: Specimen B2T20C calculated and measured strain across the depth of the span and support sections

145

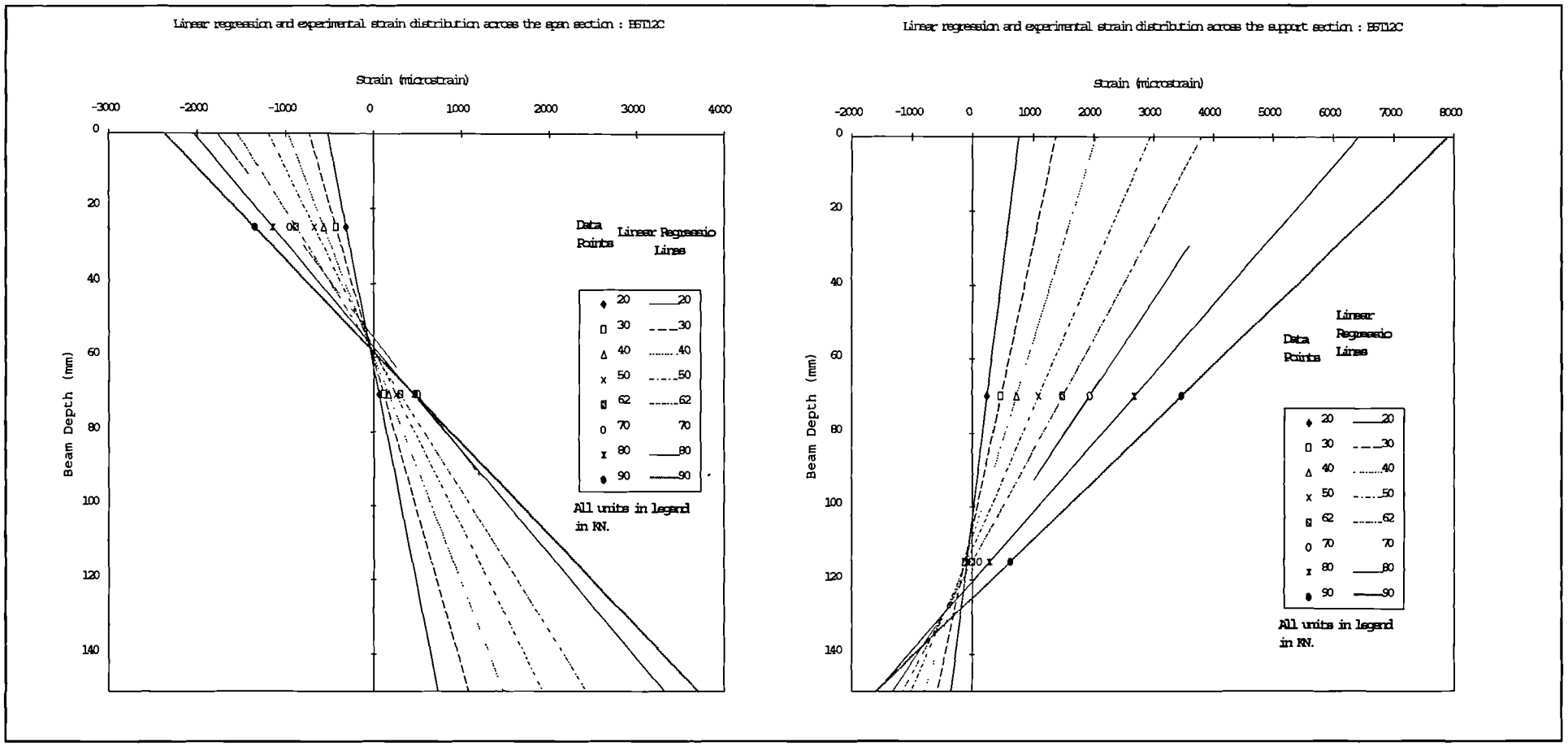

Figure 5-36: Specimen B5T12C calculated and measured strain across the depth of the span and support sections

146

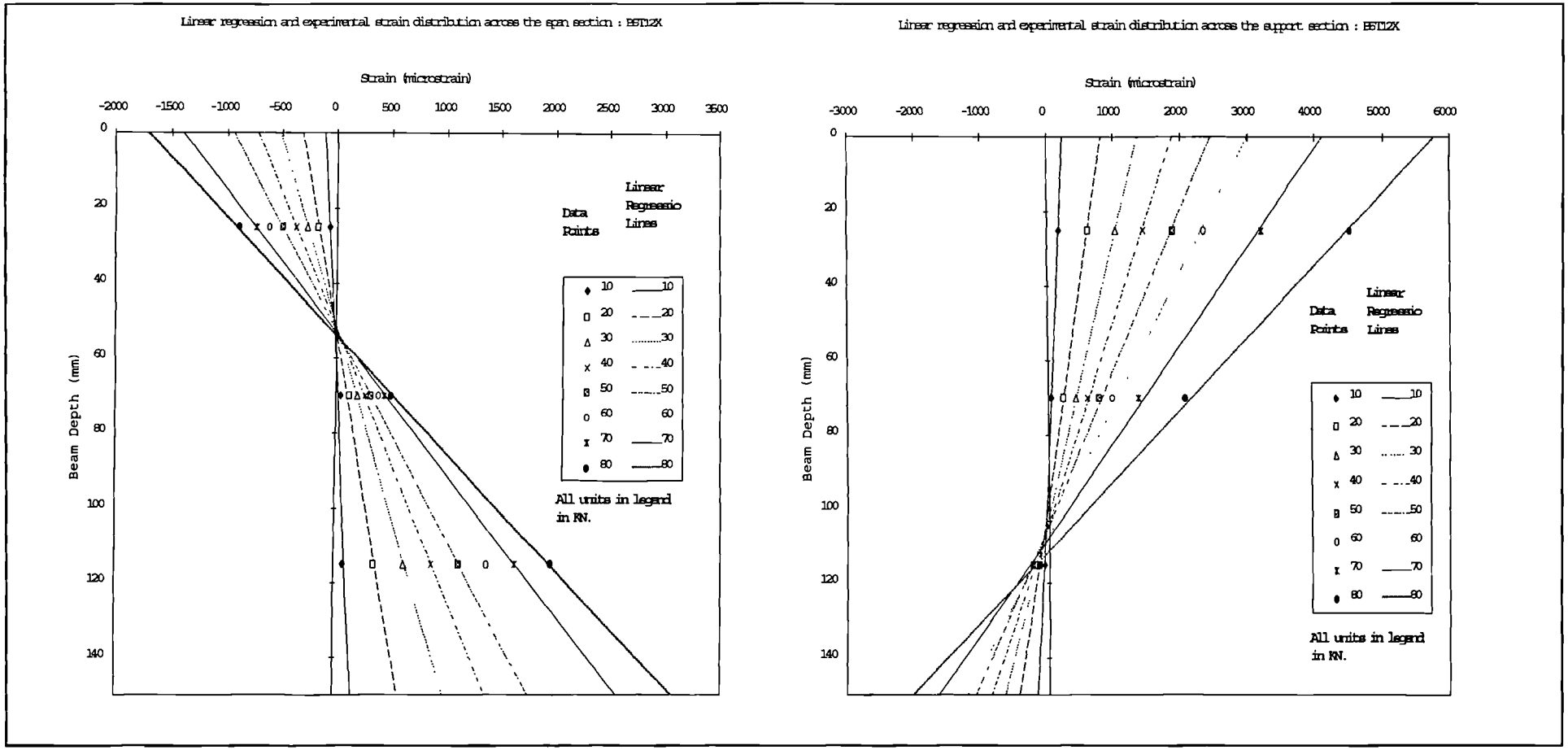

Figure 5-37: Specimen B5T12X calculated and measured strain across the depth of the span and support sections

147

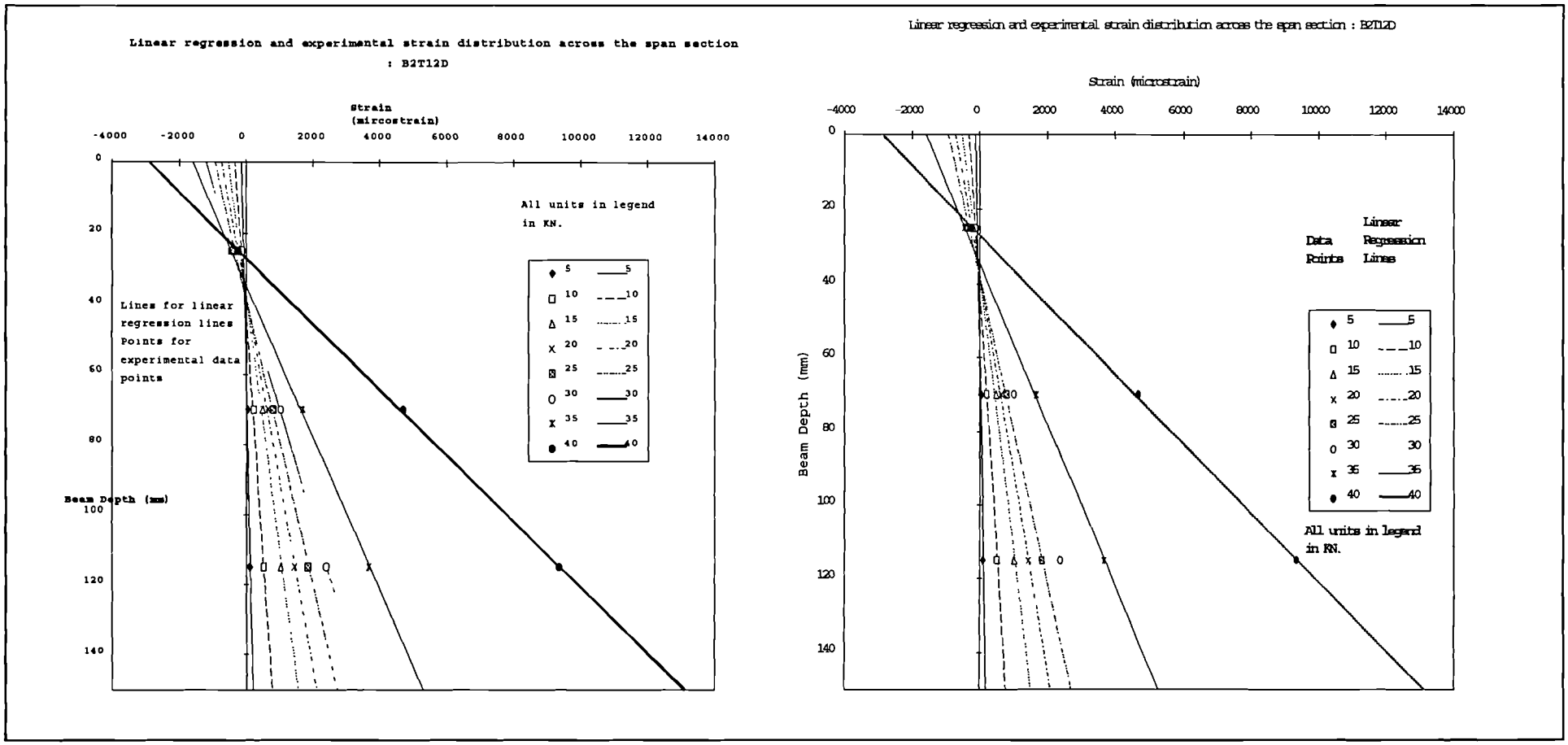

Figure 5-38: Specimen B2T12D calculated and measured strain across the depth of the span and support sections

148

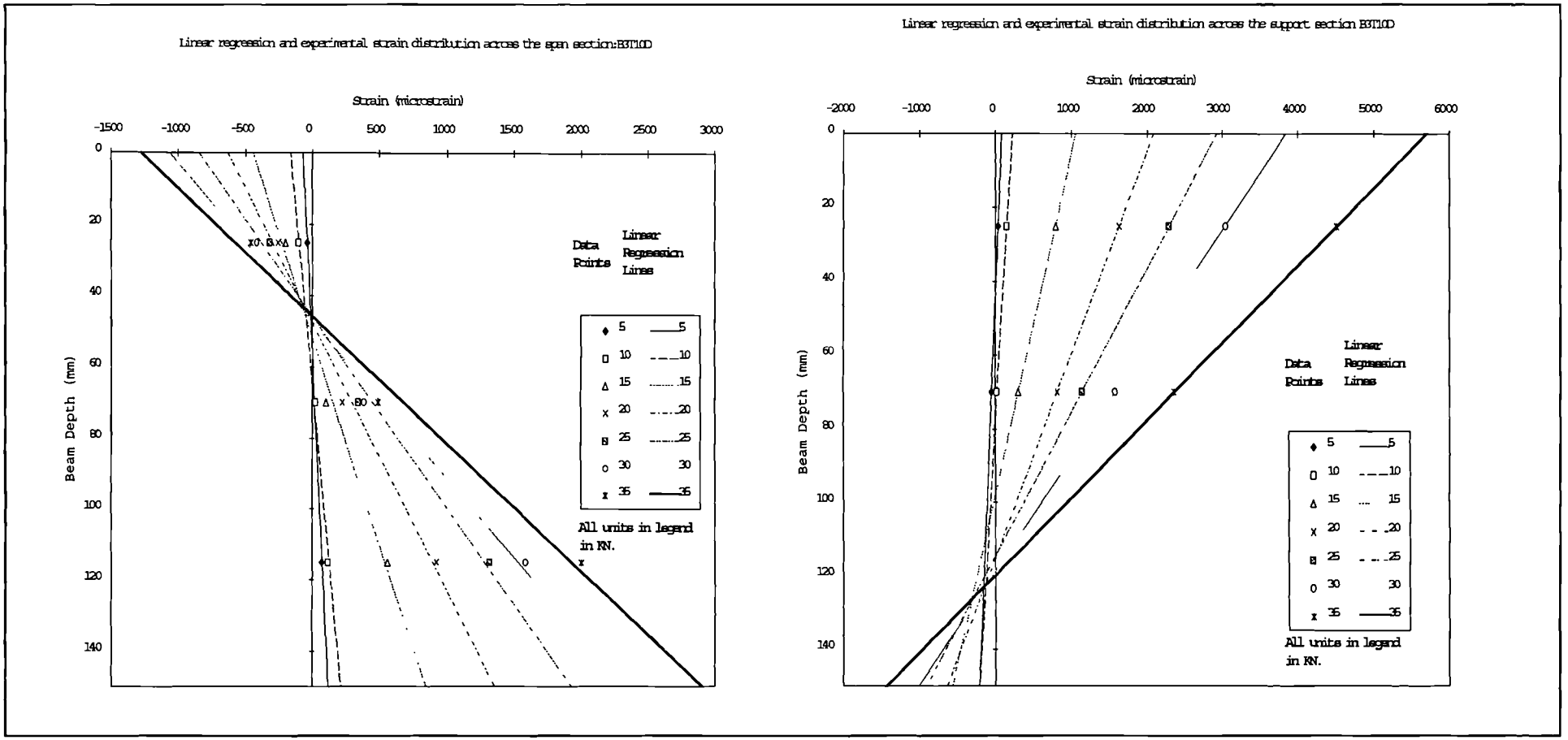

Figure 5-39: Specimen B3T10D calculated and measured strain across the depth of the span and support sections

149

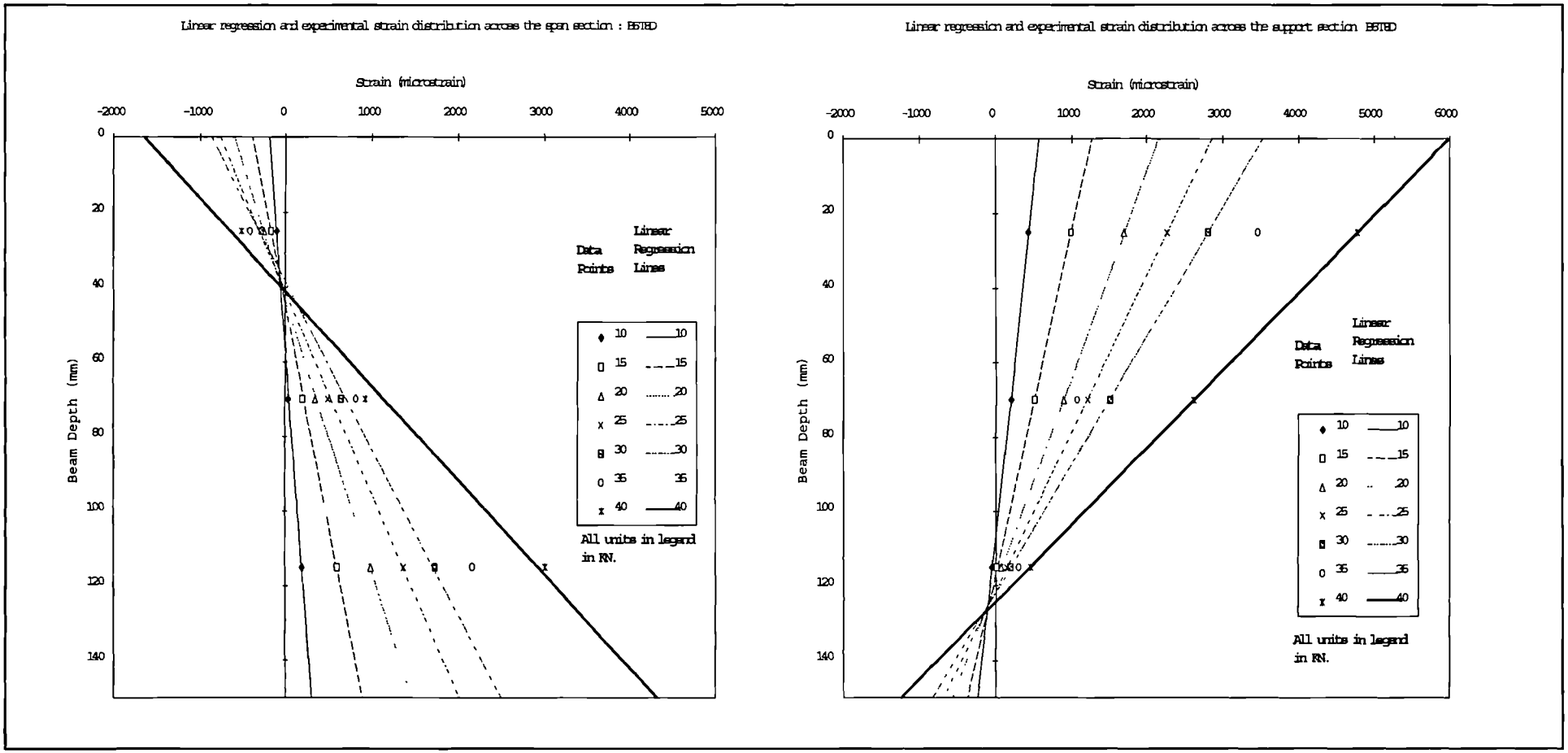

Figure 5-40: Specimen B5T8D calculated and measured strain across the depth of the span and support sections

150

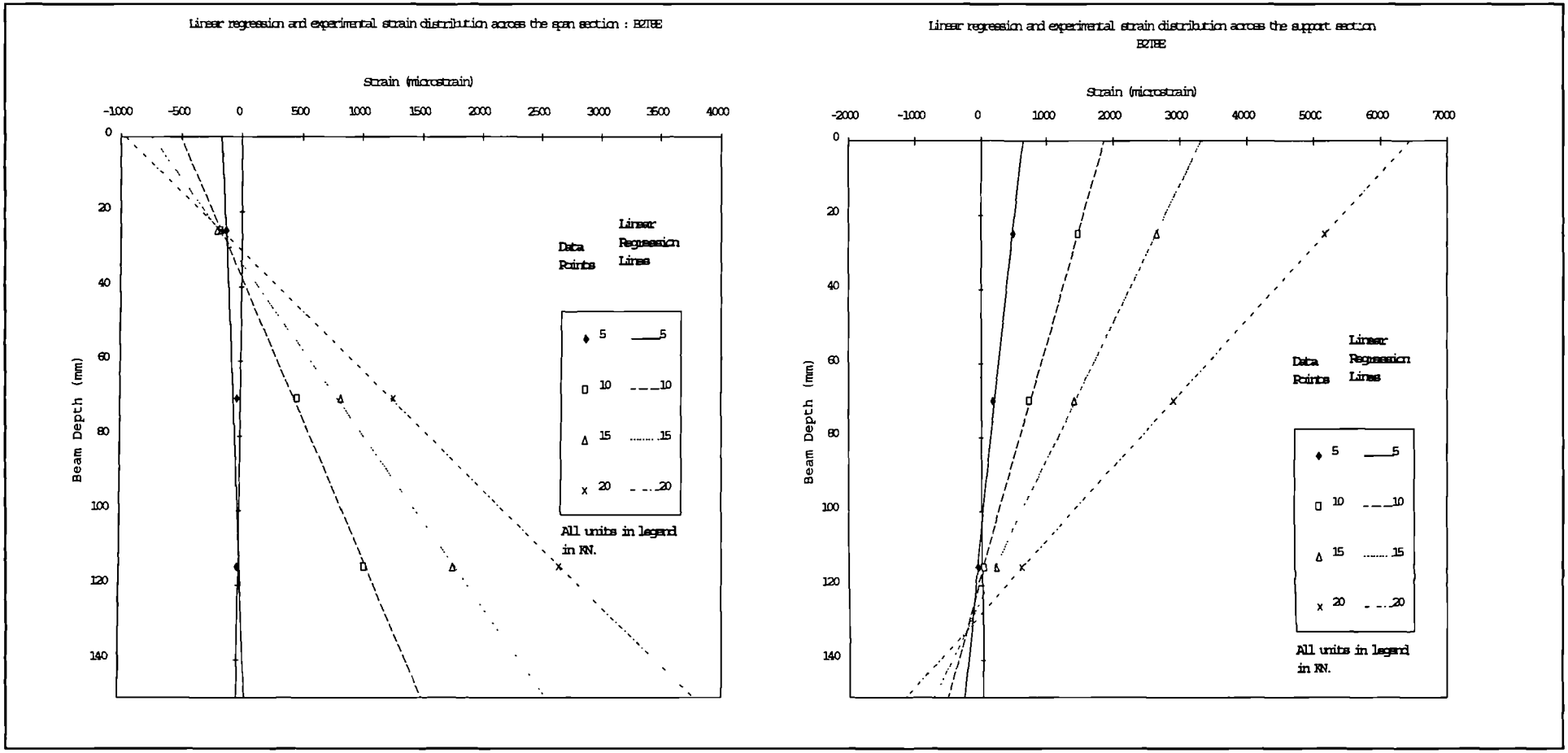

Figure 5-41: Specimen B2T8E calculated and measured strain across the depth of the span and support sections

151

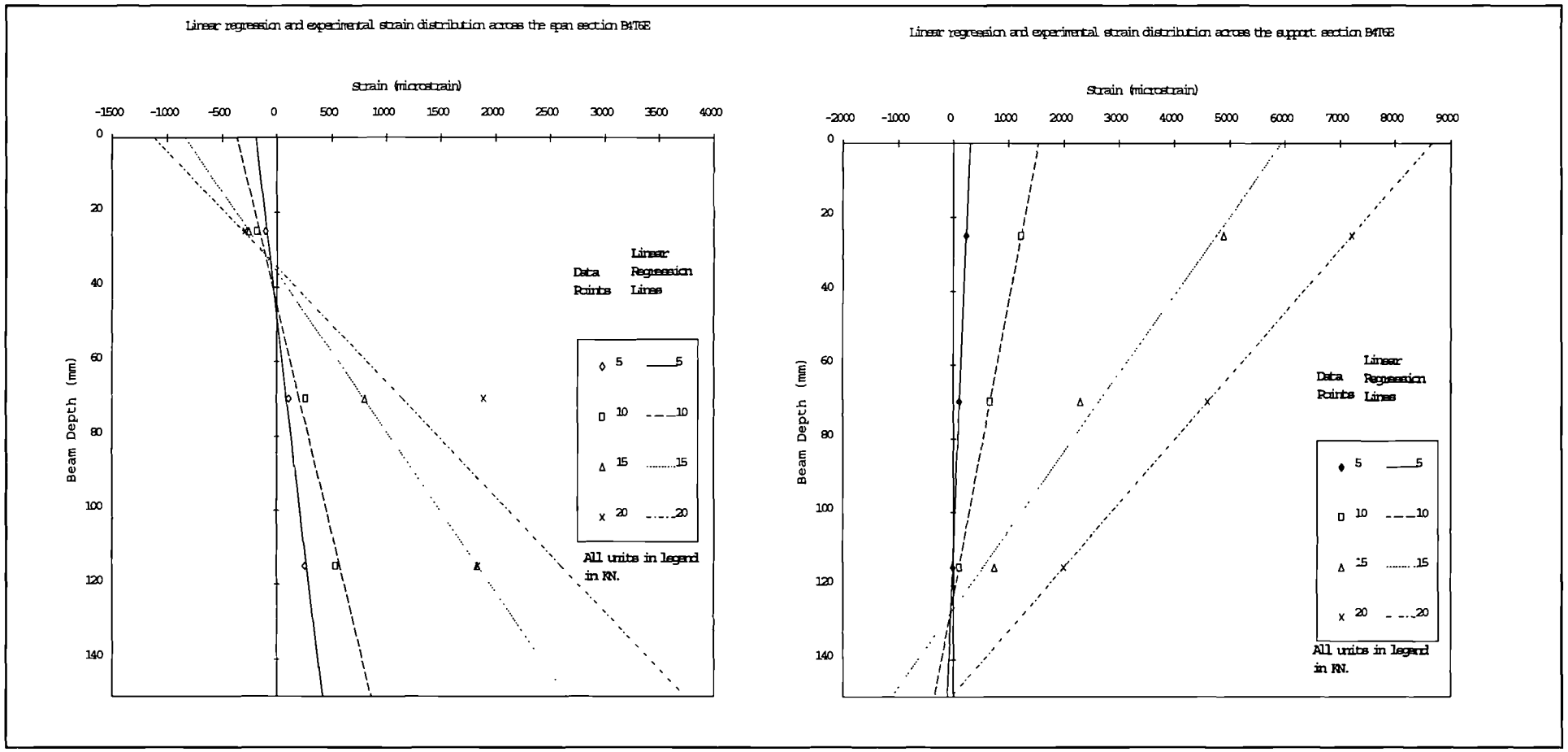

Figure 5-42: Specimen B4T6E calculated and measured strain across the depth of the span and support sections

152

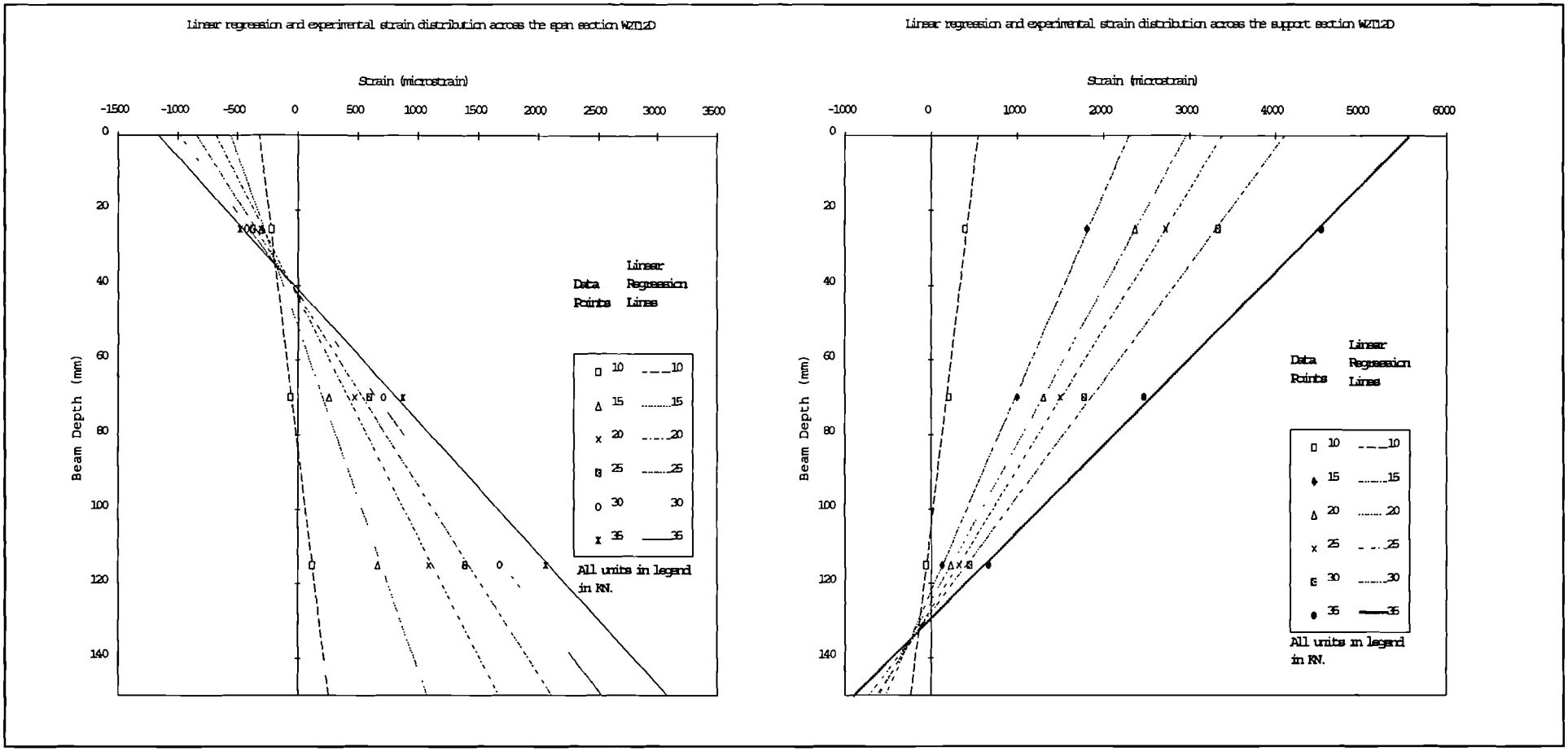

Figure 5-43: SpecimenW2T12D calculated and measured strain across the depth of the span and support sections

153

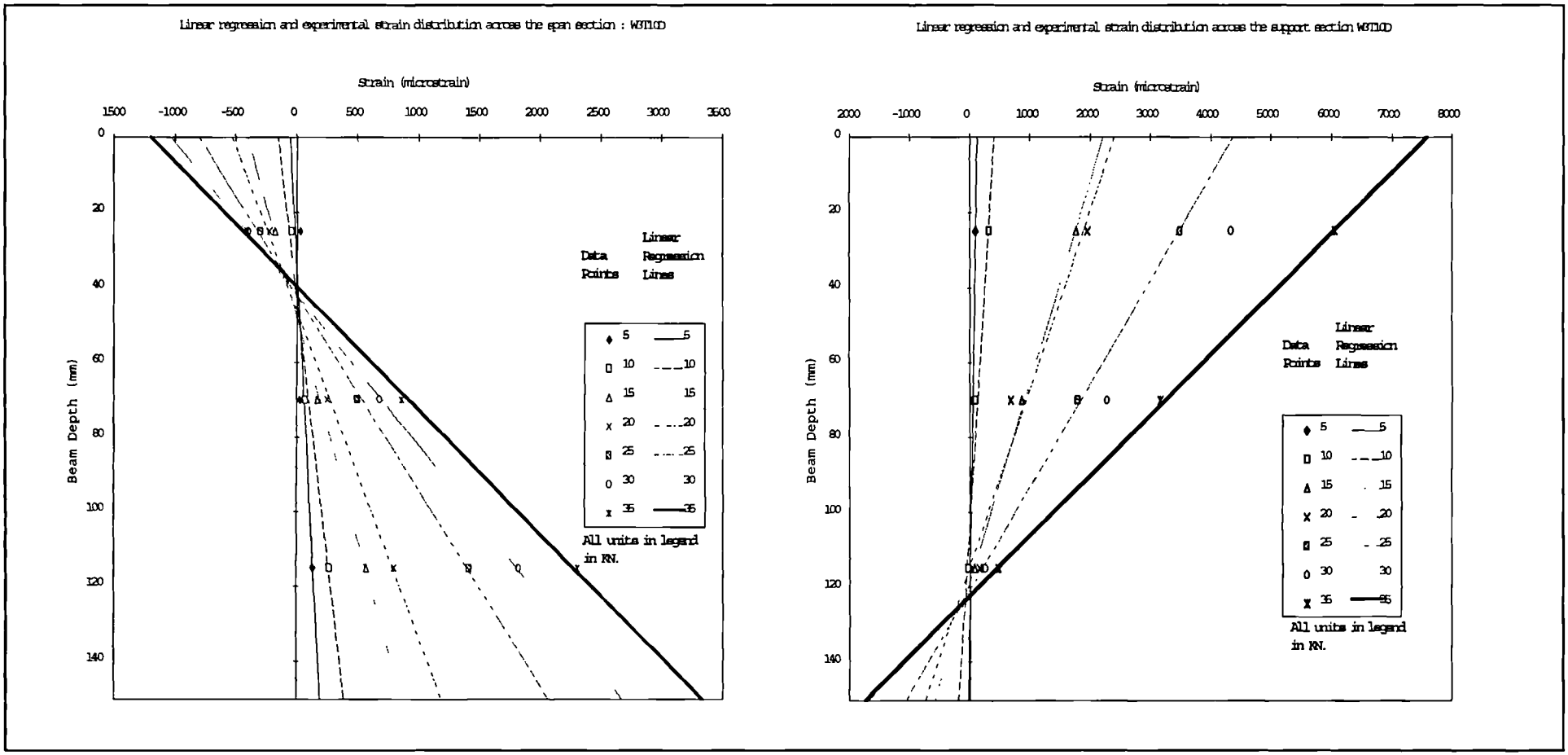

Figure 5-44: Specimen W3T10D calculated and measured strain across the depth of the span and support sections

154

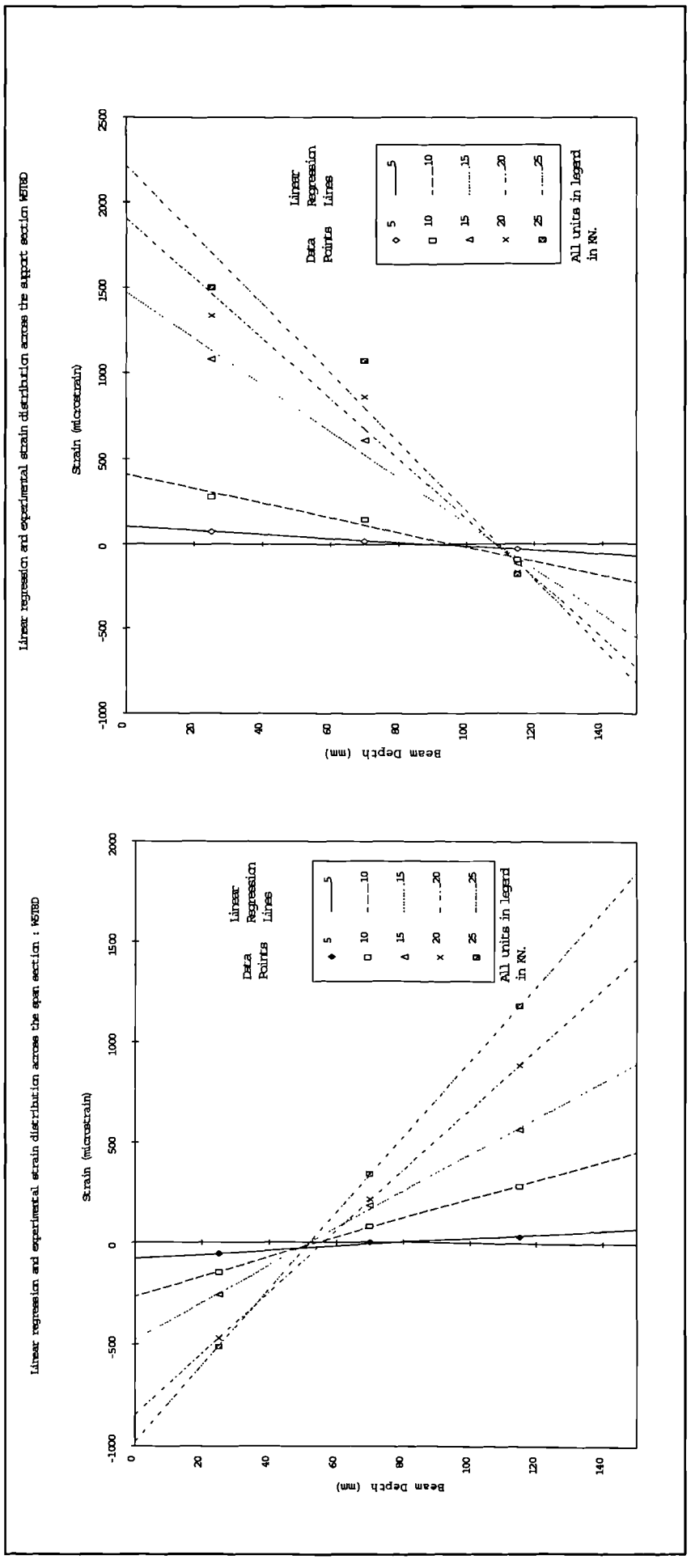

Figure 5-45: Specimen W5T8D calculated and measured strain across the depth of the span and support sections

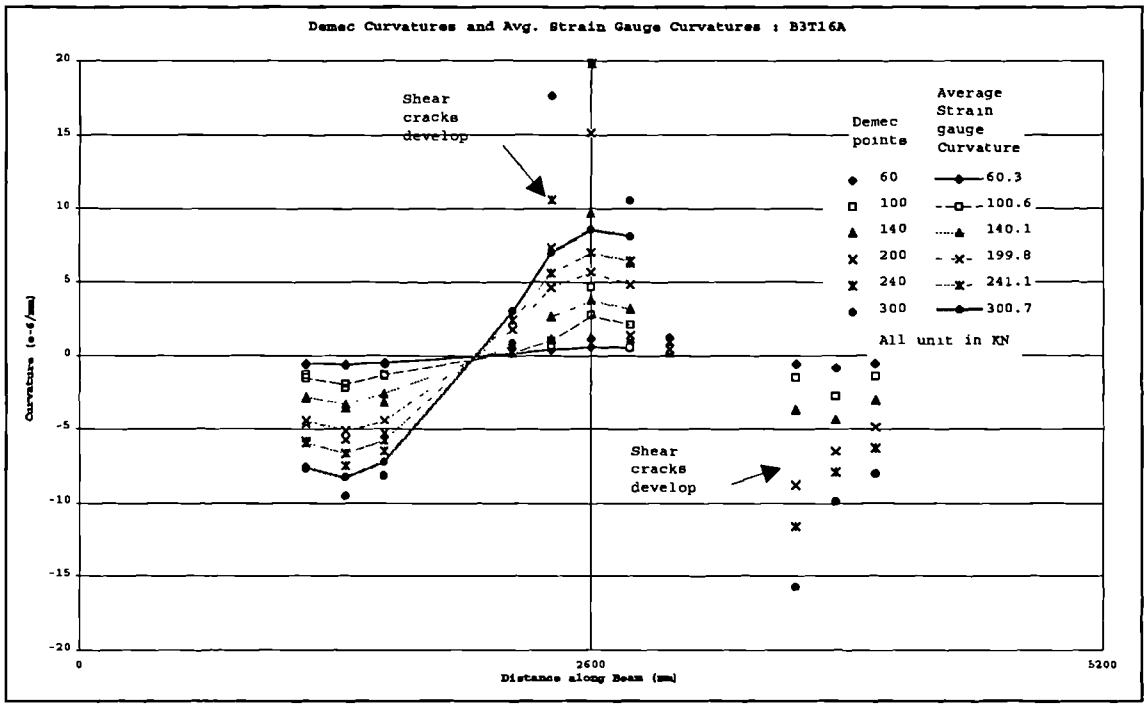

Figure 5-46: B3T16A Demec and average strain gauge curvatures

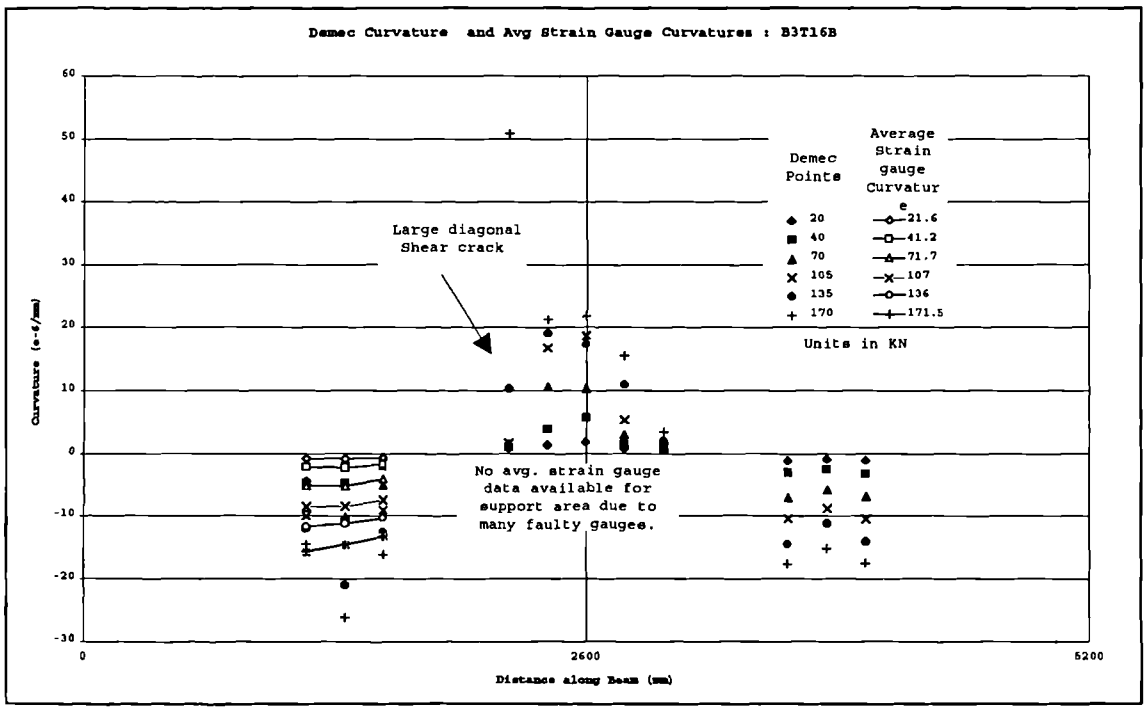

Figure 5-47: B3T16B Demec and average strain gauge curvatures

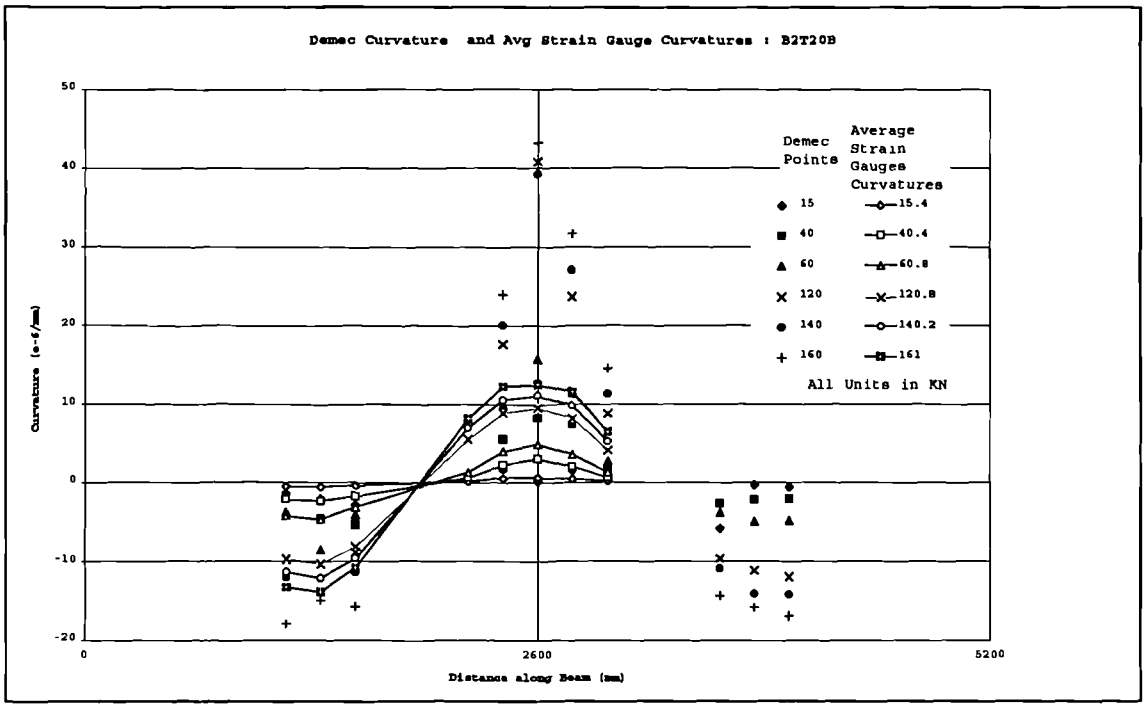

Figure 5-48: B2T20B Demec and average strain gauge curvatures

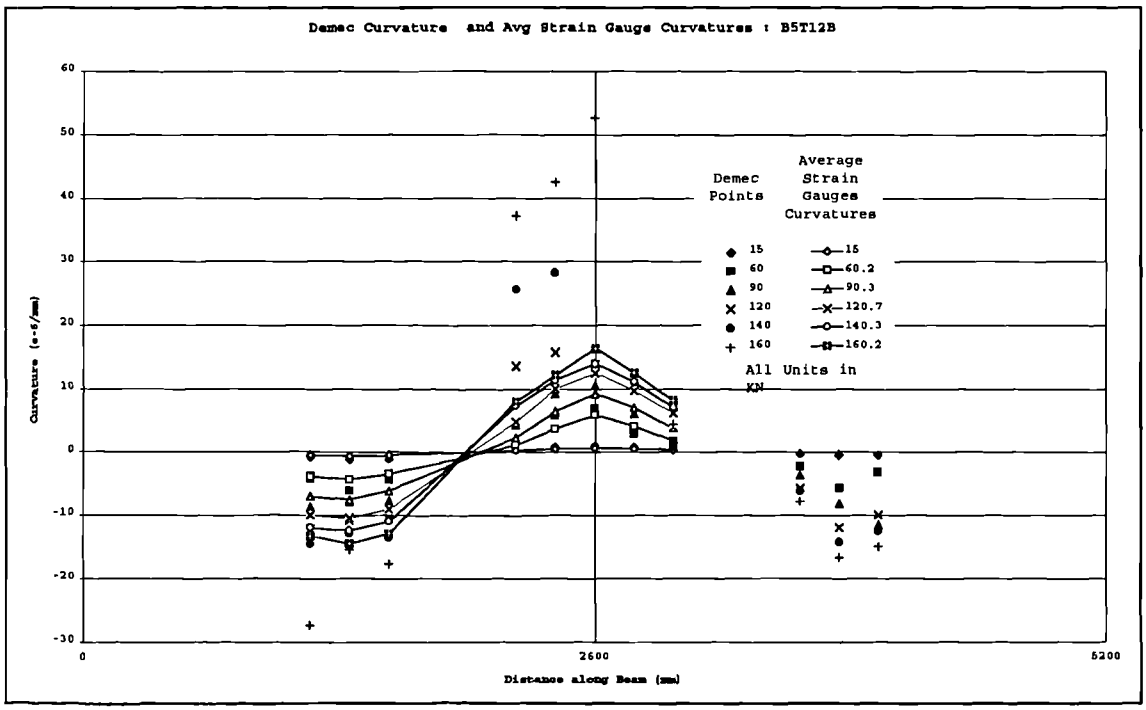

Figure 5-49: B5T12B Demec and average strain gauge curvatures

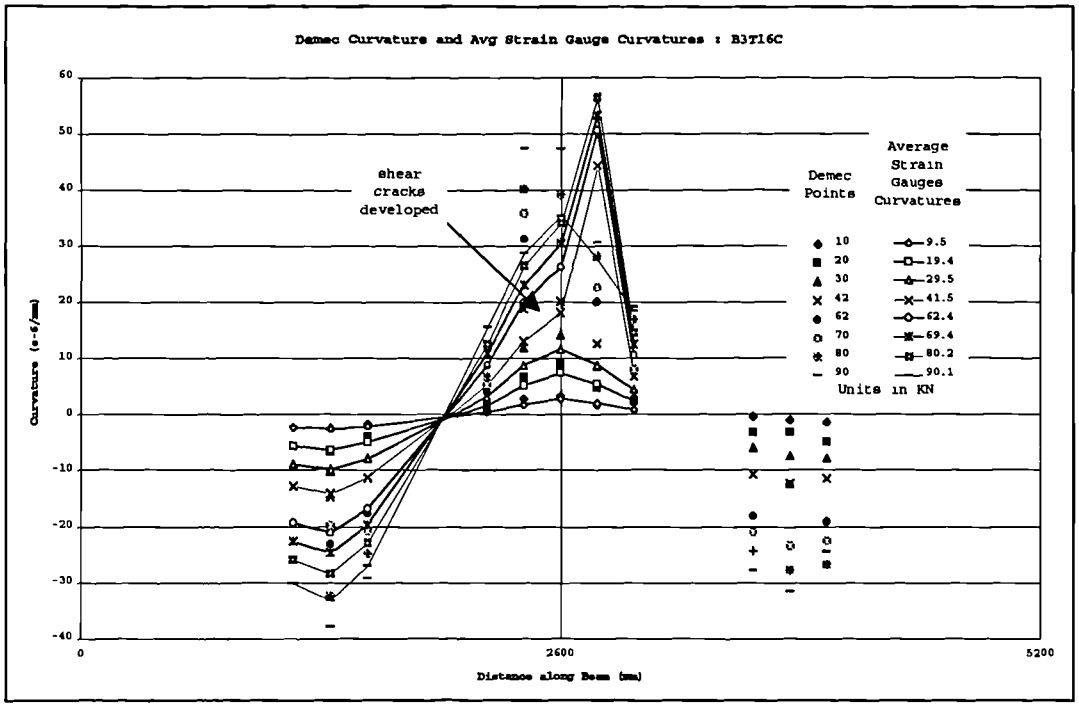

Figure 5-50: B3T16C Demec and average strain gauge curvatures

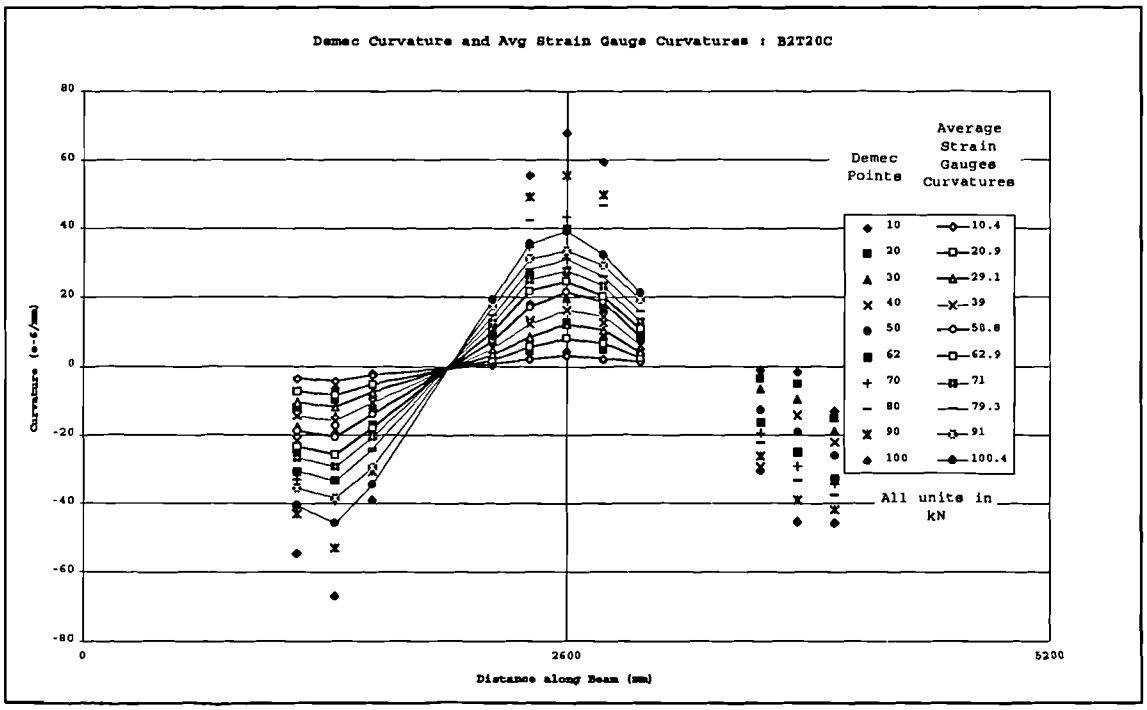

Figure 5-51: B2T20C Demec and average strain gauge curvatures

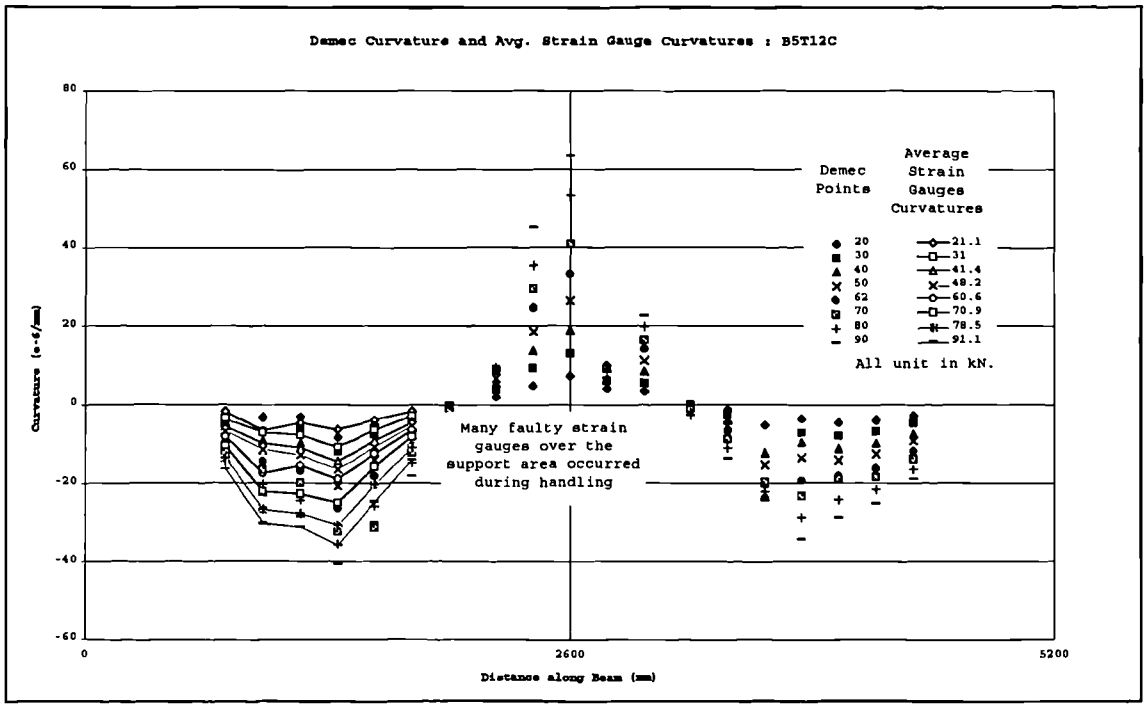

Figure 5-52: B5T12C Demec and average strain gauge curvatures

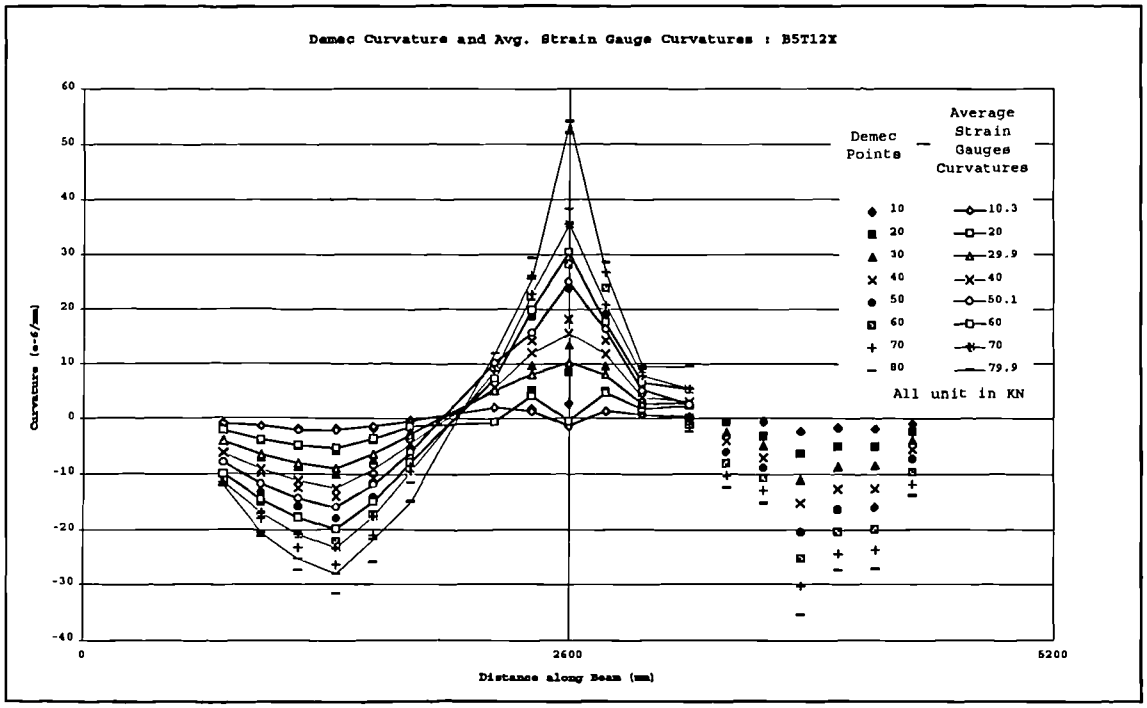

Figure 5-53: B5T12X Demec and average strain gauge curvatures

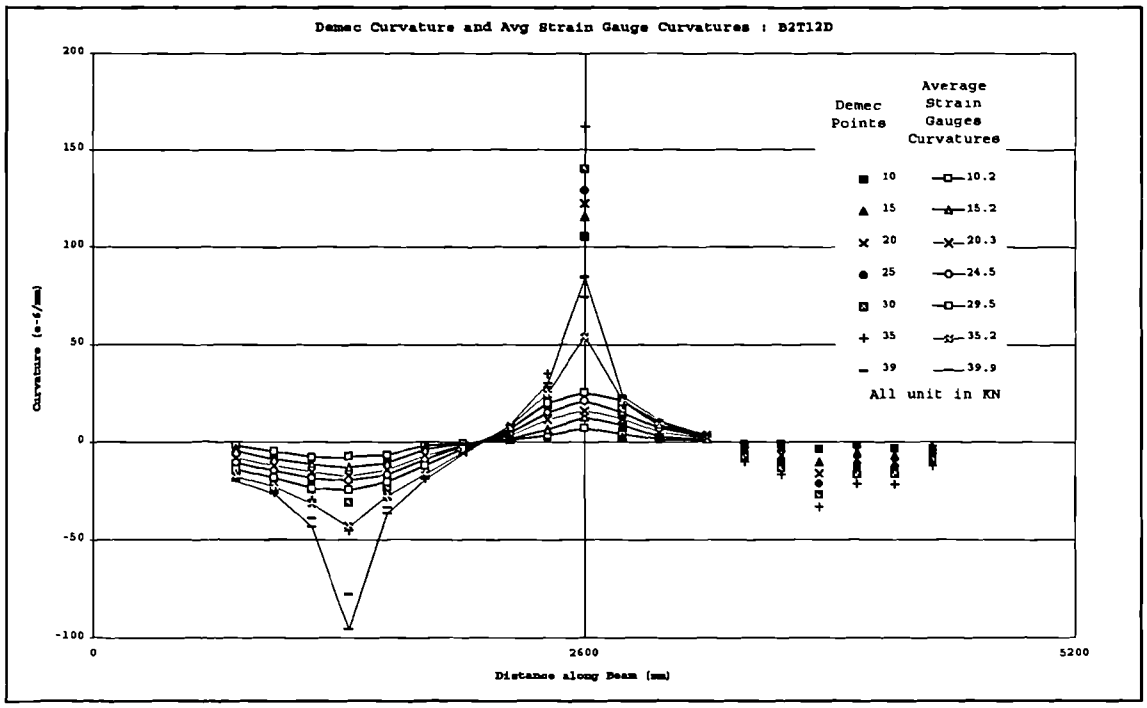

Figure 5-54: B2T12D Demec and average strain gauge curvatures

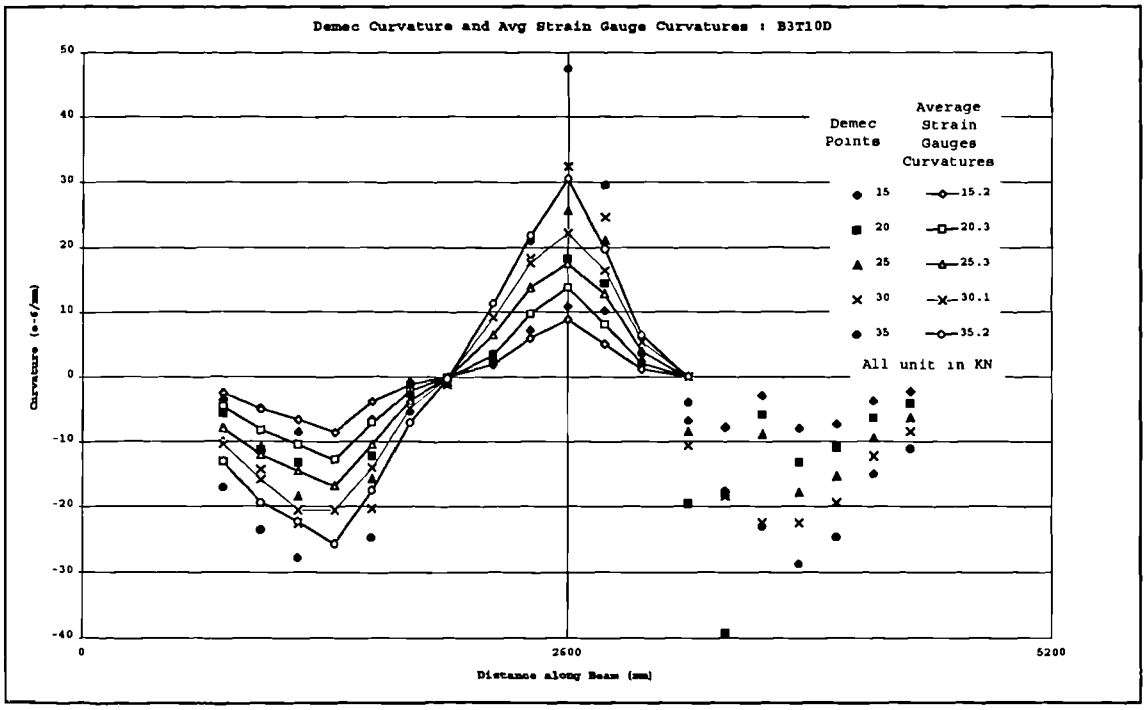

Figure 5-55: B3T10D Demec and average strain gauge curvatures

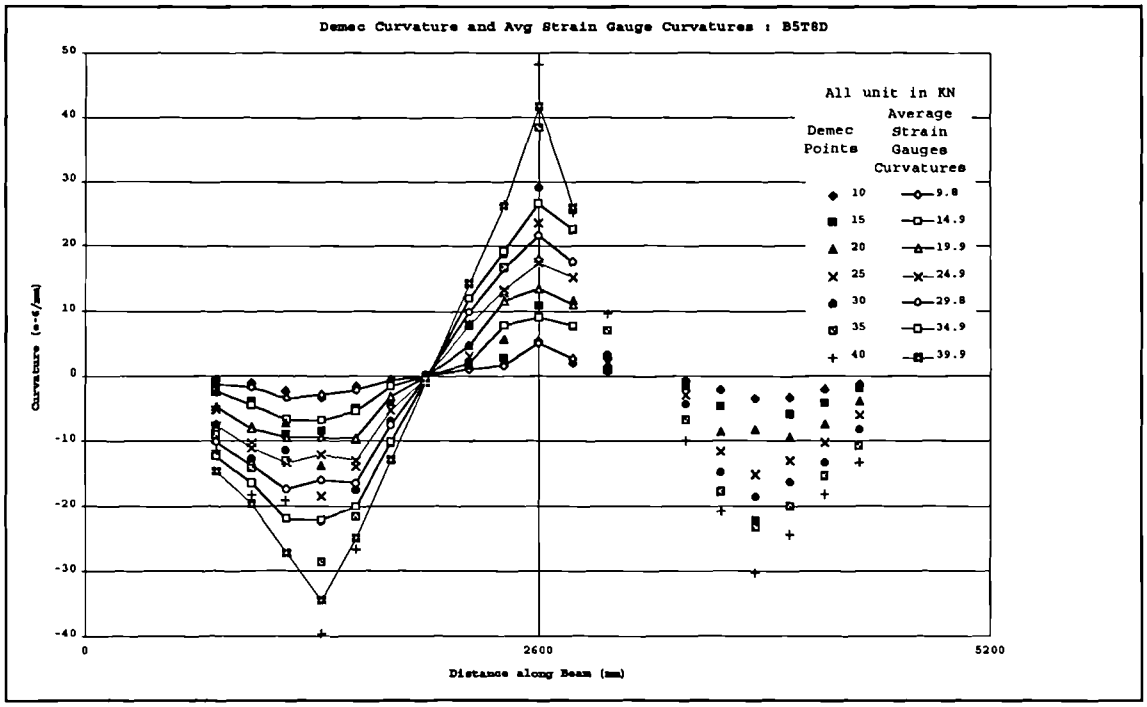

Figure 5-56: B5T8D Demec and average strain gauge curvatures

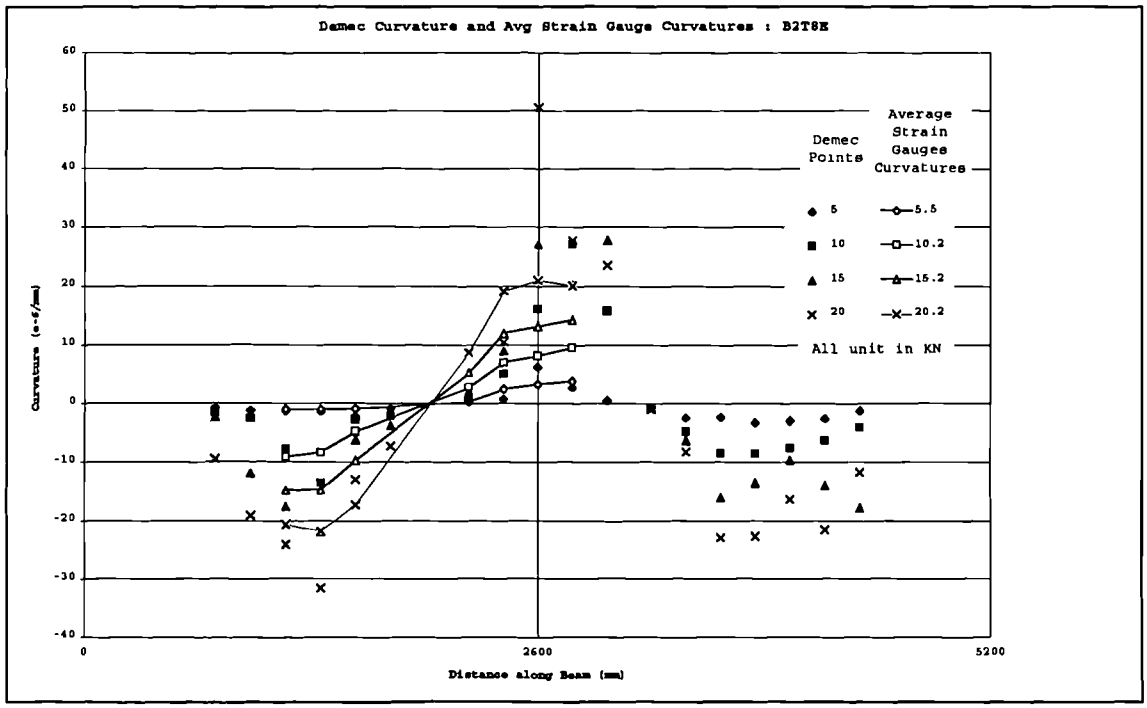

Figure 5-57: B2T8E Demec and average strain gauge curvatures

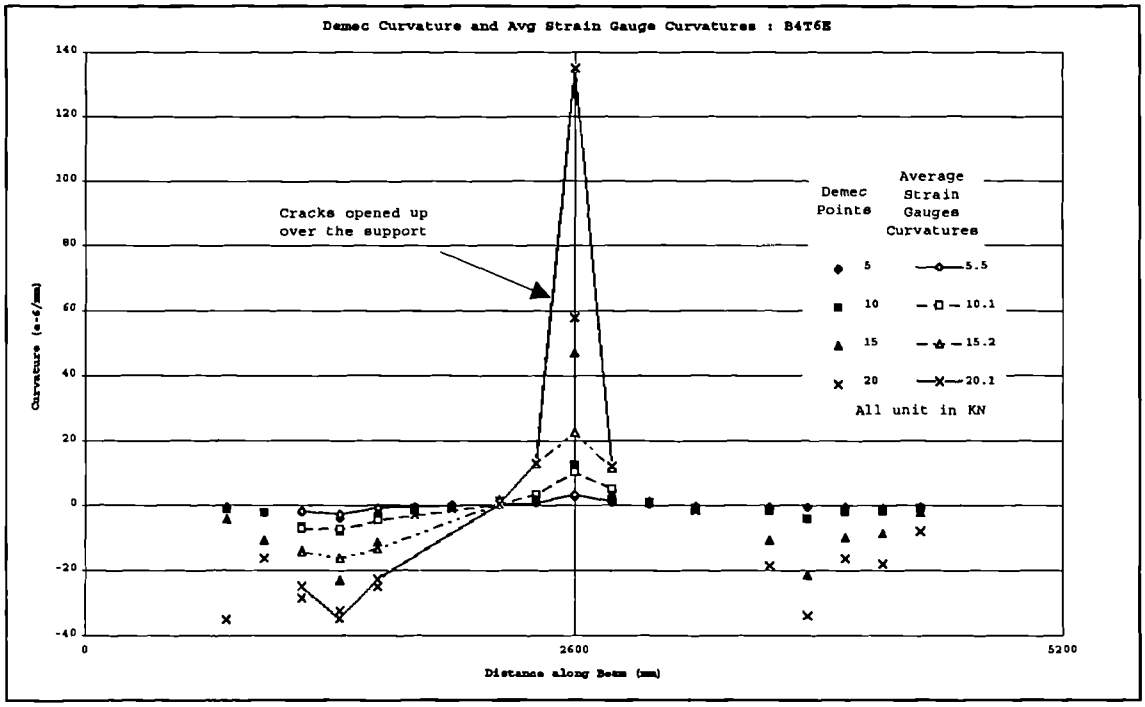

Figure 5-58: B4T6E Demec and average strain gauge curvatures

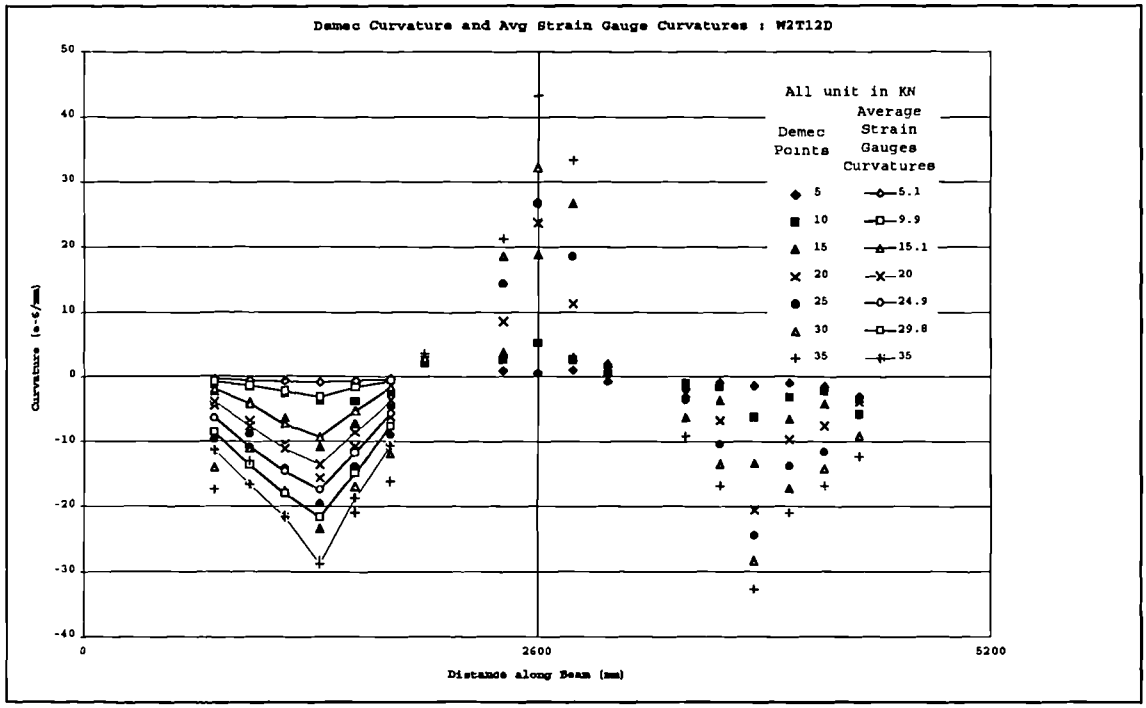

Figure 5-59: W2T12D Demec and average strain gauge curvatures

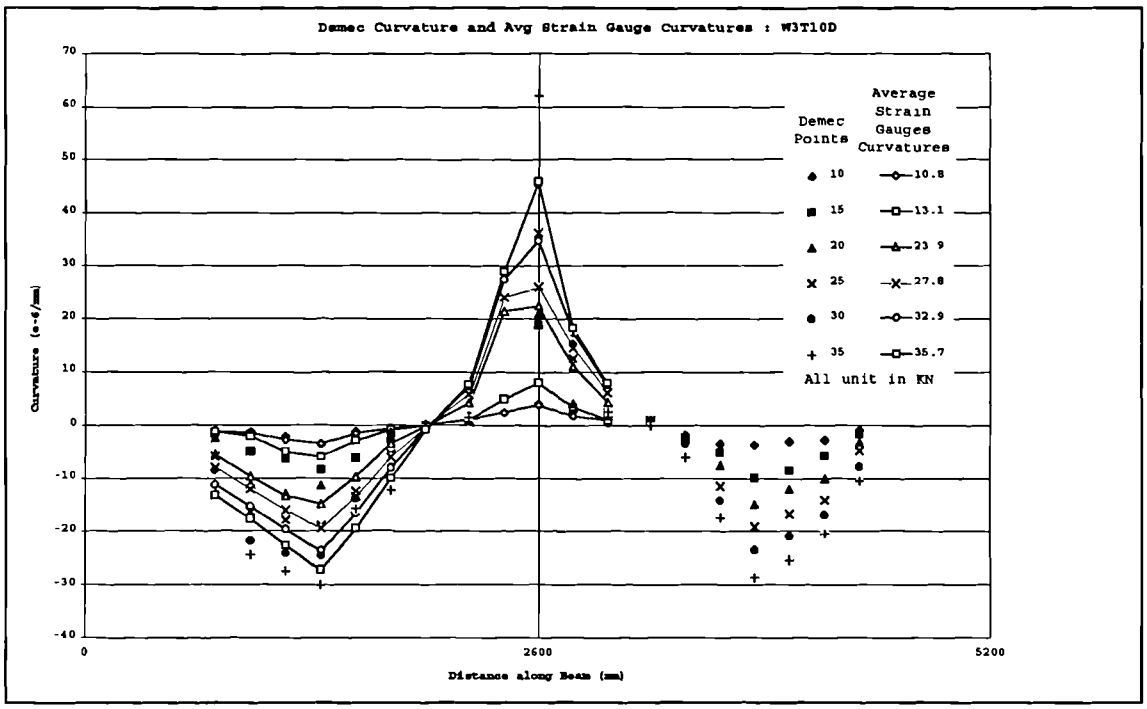

Figure 5-60: W3T10D Demec and average strain gauge curvatures

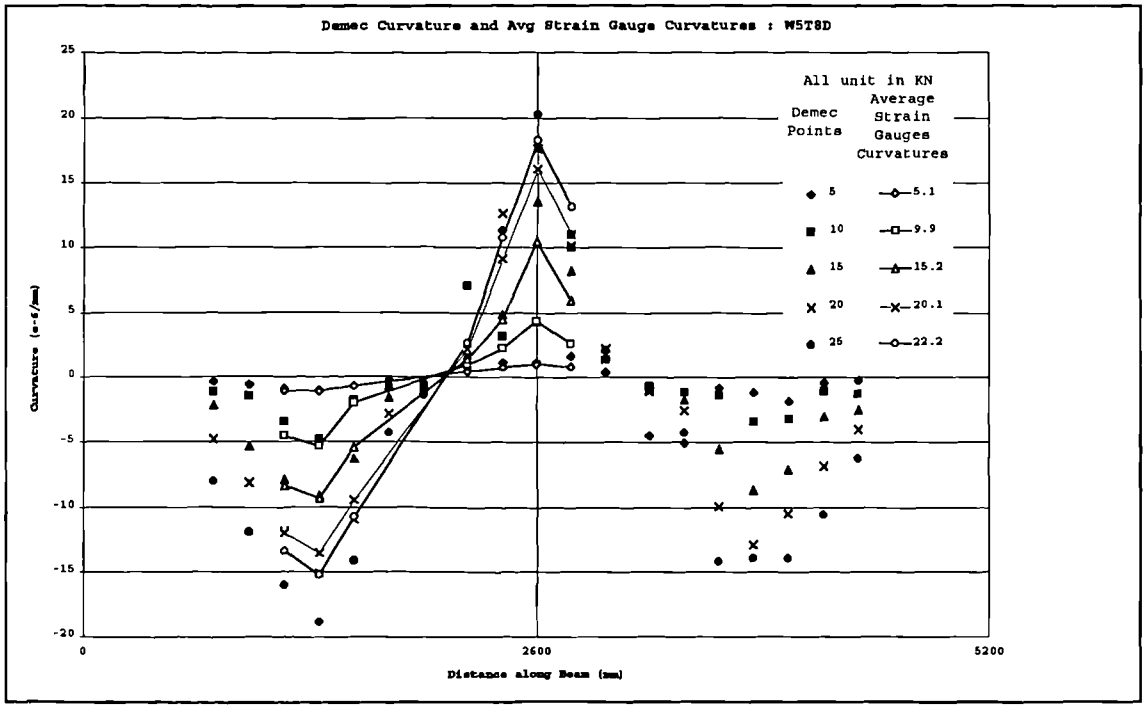

Figure 5-61: W5T8D Demec and average strain gauge

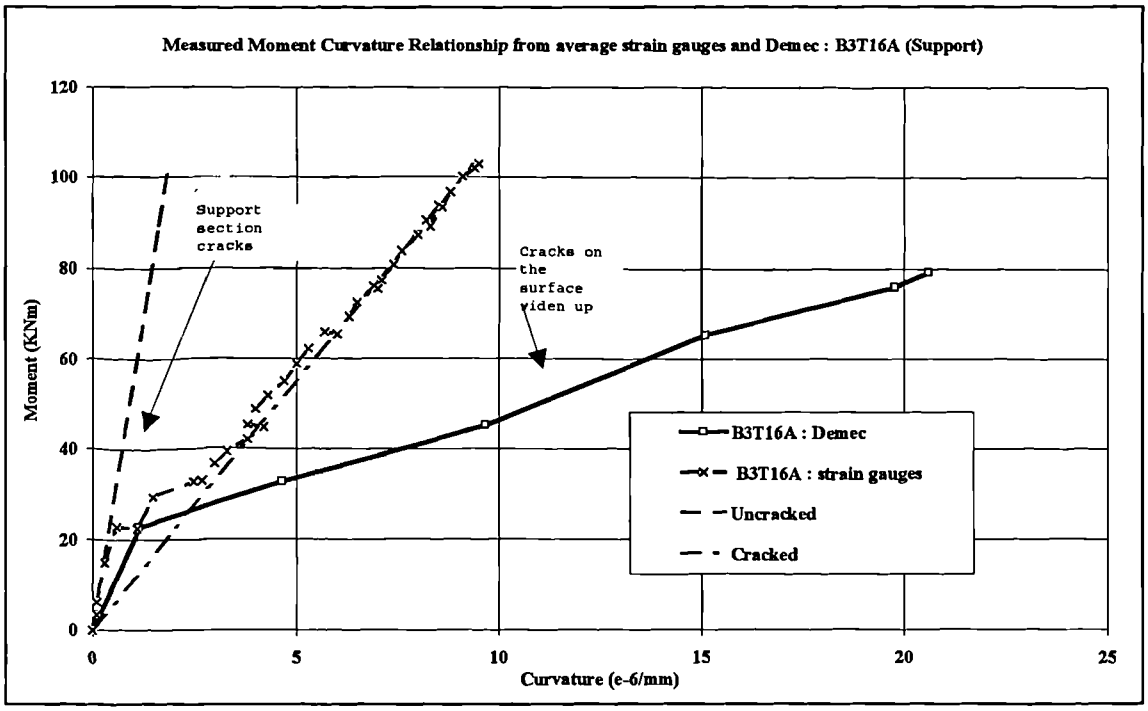

Figure 5-62: Specimen B3T16A measured moment curvature relationship over the support area from calculated Demec curvatures and averaged local strain gauges over 200 mm gauge length

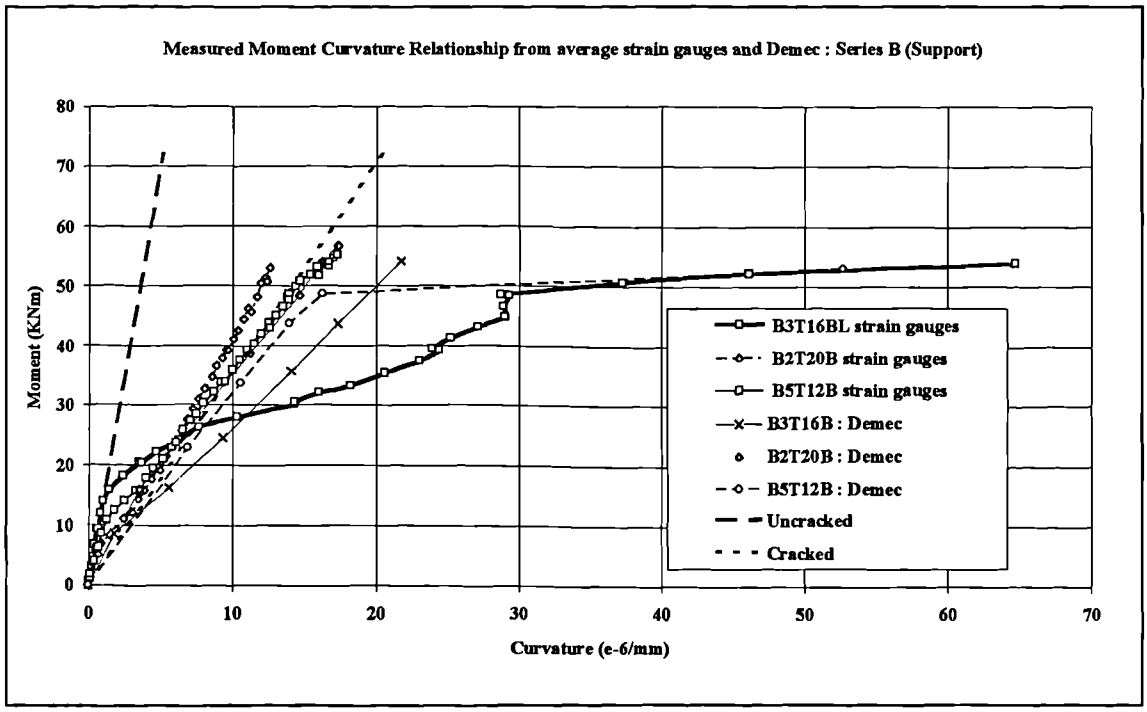

Figure 5-63: : Series B measured moment curvature relationship over the support area from calculated Demec curvatures and averaged local strain gauges over 200 mm gauge length

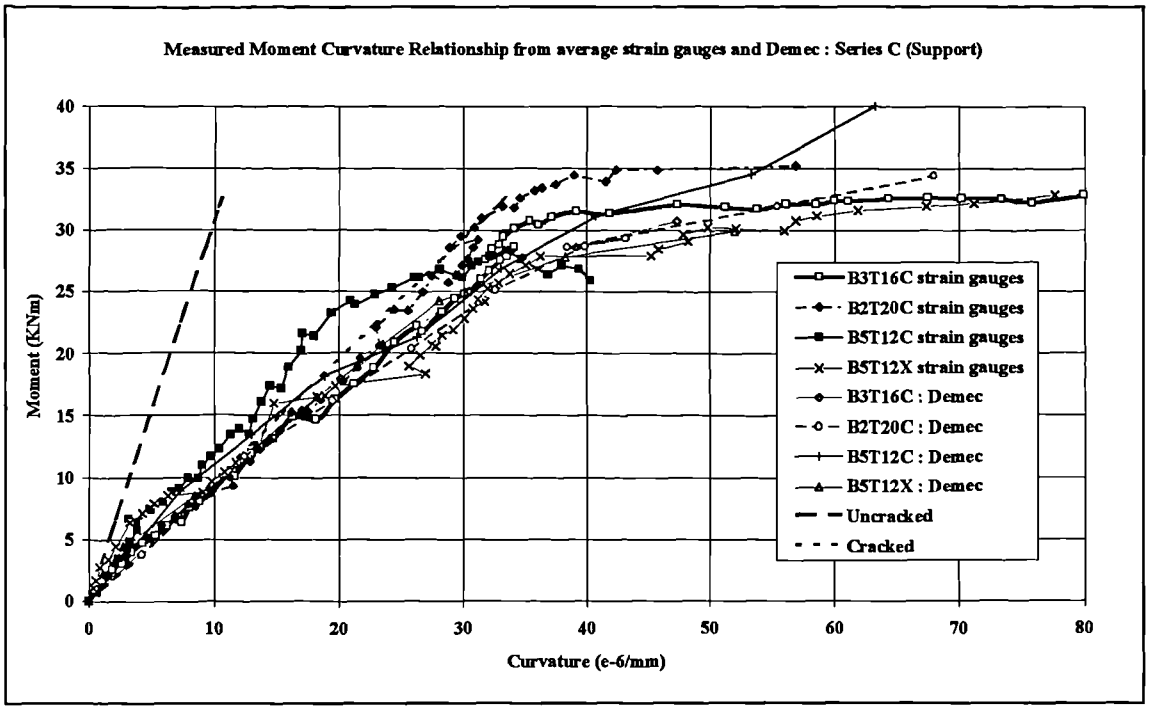

Figure 5-64: Series C measured moment curvature relationship over the support area from calculated Demec curvatures and averaged local strain gauges over 200 mm gauge length

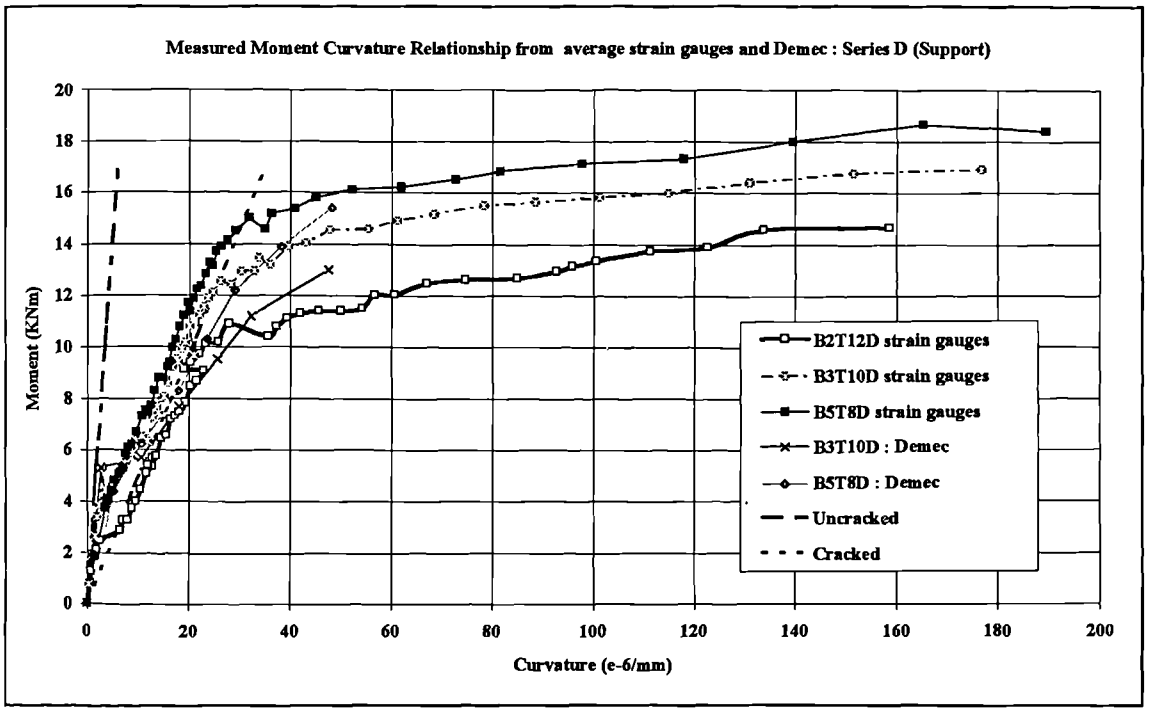

Figure 5-65: Series D measured moment curvature relationship over the support area from calculated Demec curvatures and averaged local strain gauges over 200 mm gauge length

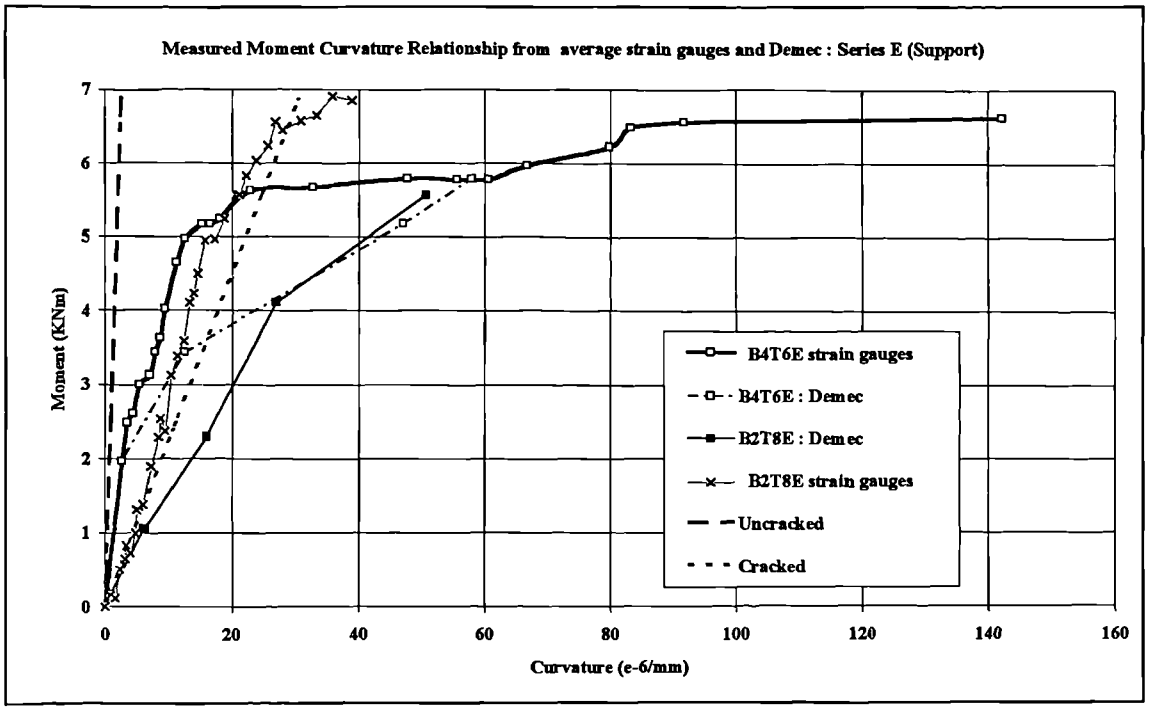

Figure 5-66: Series E measured moment curvature relationship over the support area from calculated Demec curvatures and averaged local strain gauges over 200 mm gauge length

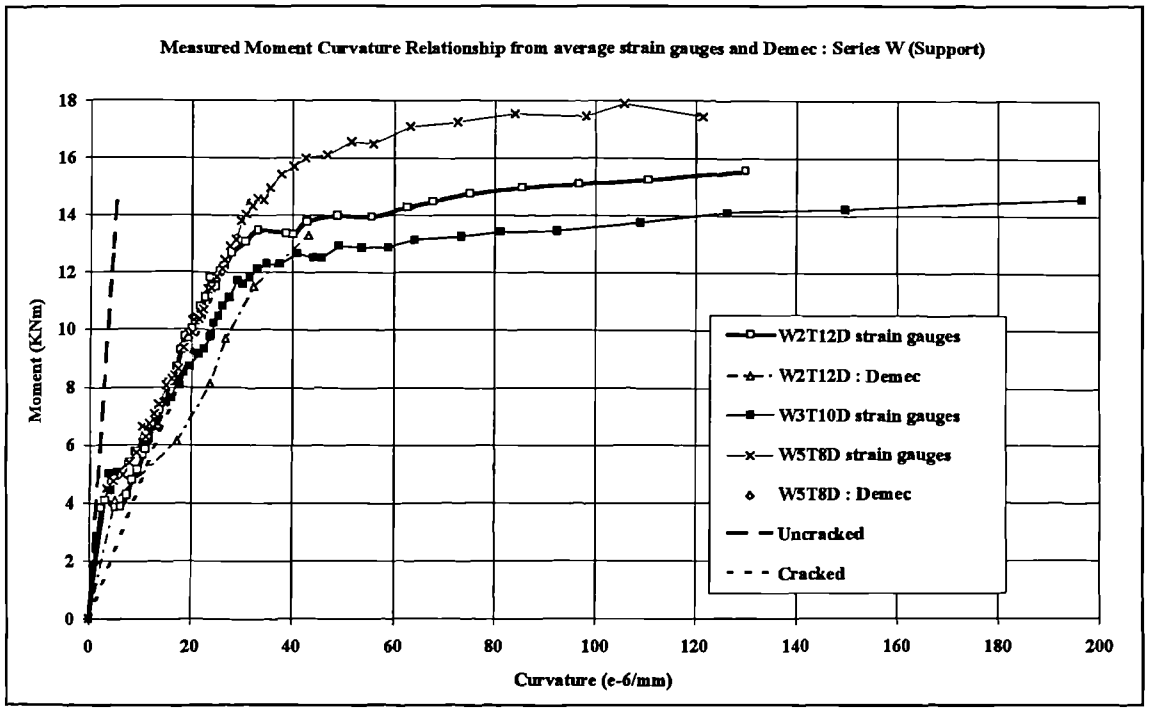

Figure 5-67: Series W measured moment curvature relationship over the support area from calculated Demec curvatures and averaged local strain gauges over 200 mm gauge length

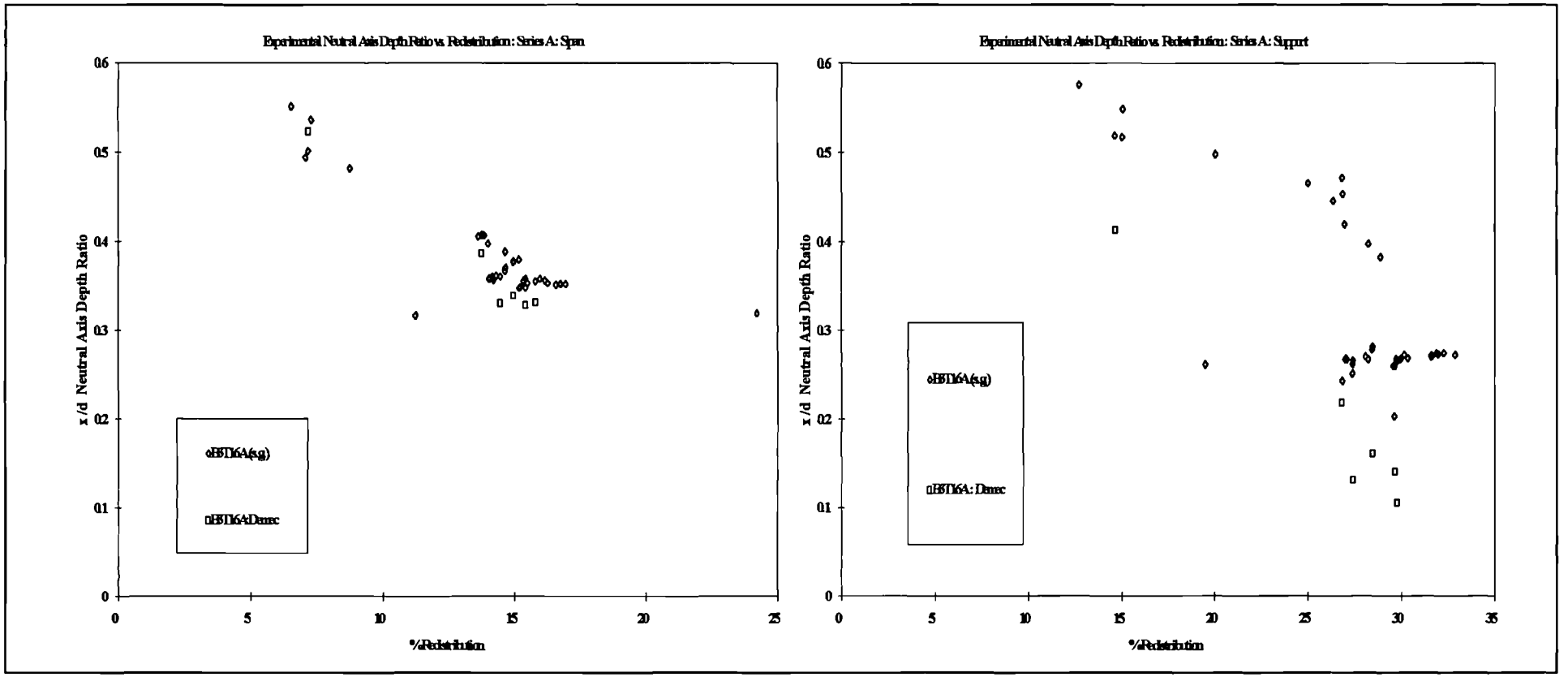

Figure 5-68: B3T16A Measured neutral axis depth ratio versus redistribution from Demec and averaged strain gauge data for both span and support sections.

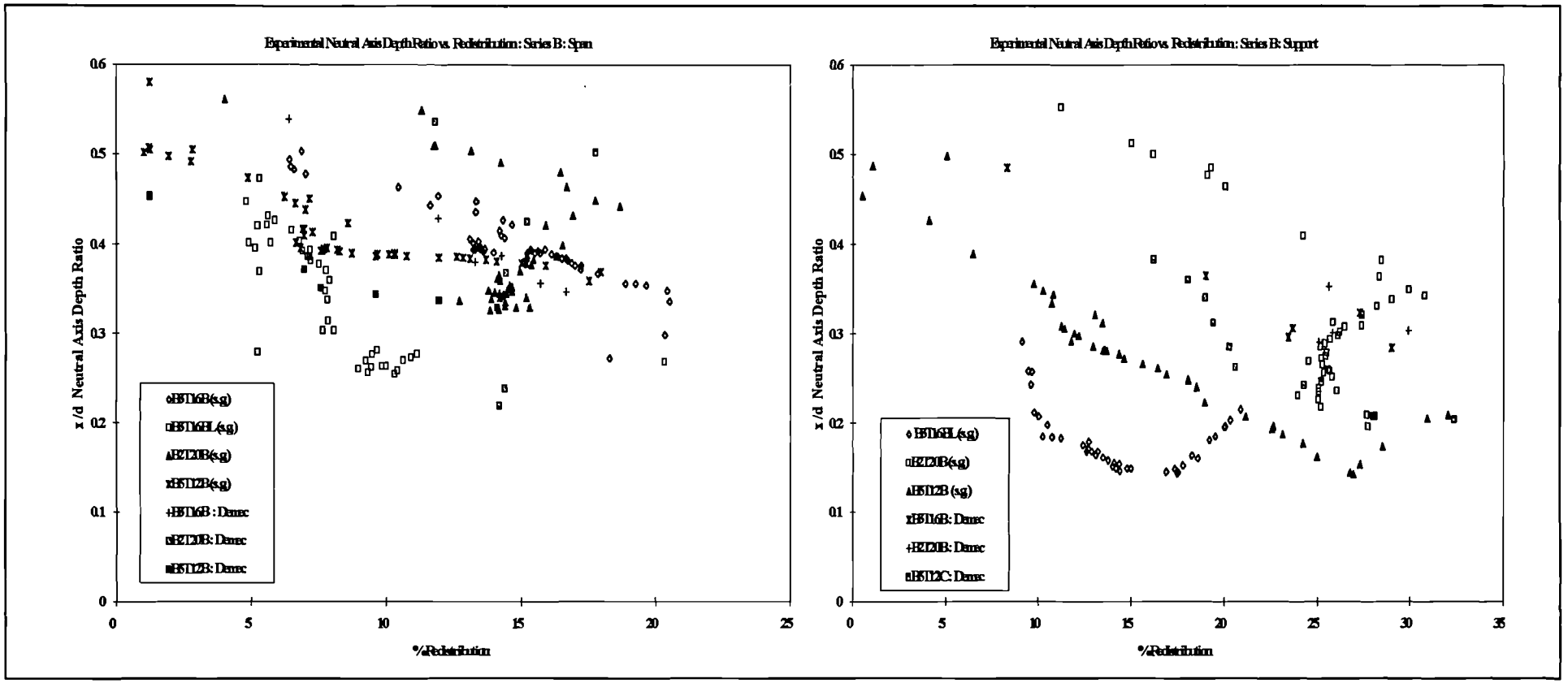

Figure 5-69: Series B Measured neutral axis depth ratio versus redistribution from Demec and averaged strain gauge data for both span and support sections

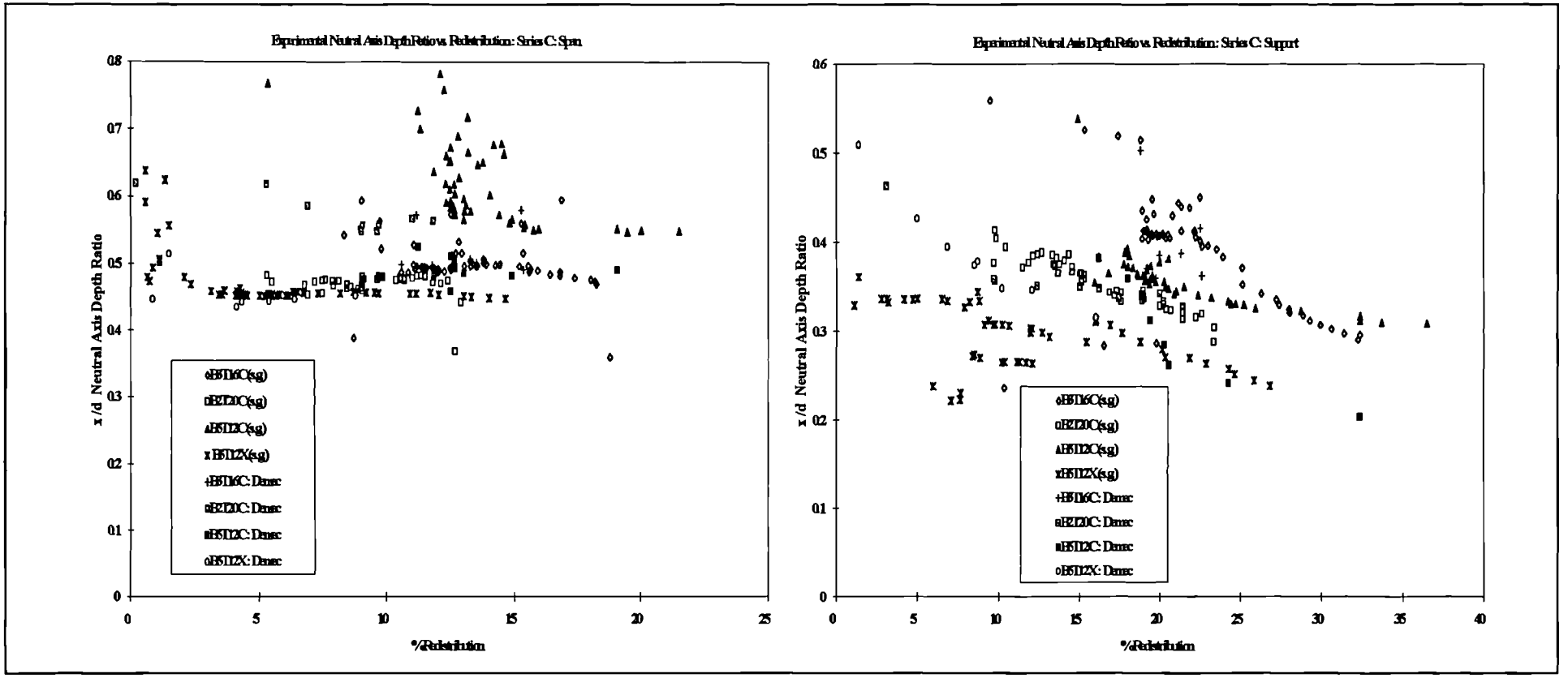

Figure 5-70: Series C Measured neutral axis depth ratio versus redistribution from Demec and averaged strain gauge data for both span and support sections

169

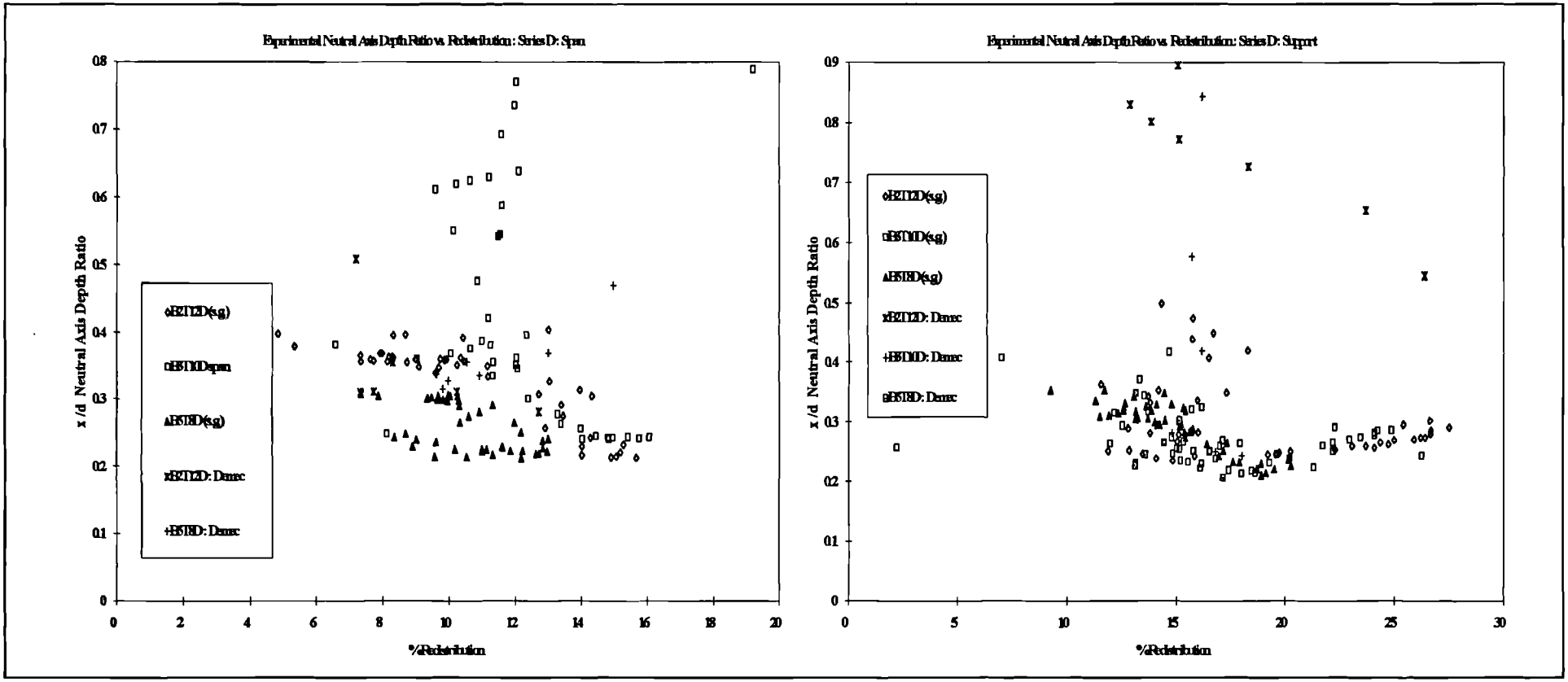

Figure 5-71: Series D Measured neutral axis depth ratio versus redistribution from Demec and averaged strain gauge data for both span and support sections

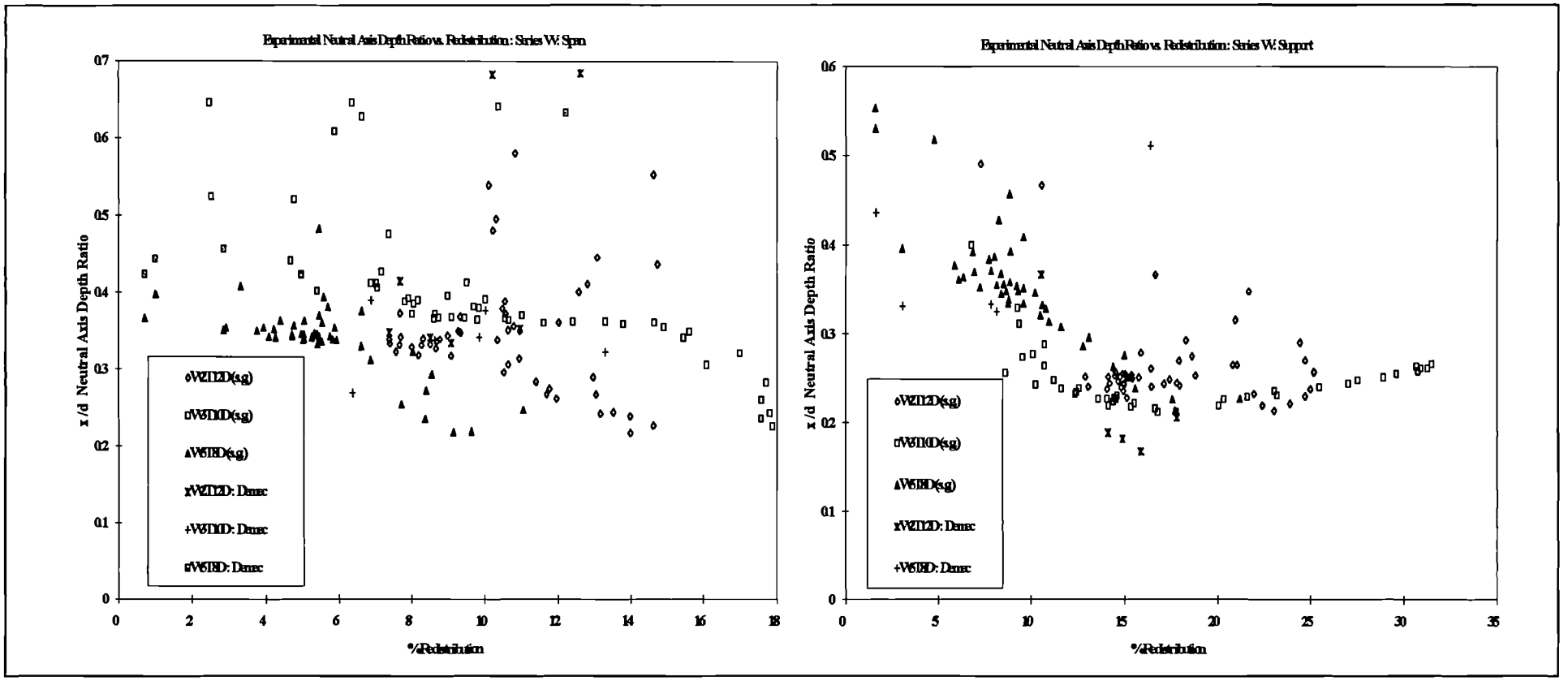

Figure 5-72: Series W Measured neutral axis depth ratio versus redistribution from Demec and averaged strain gauge data for both span and support sections

171

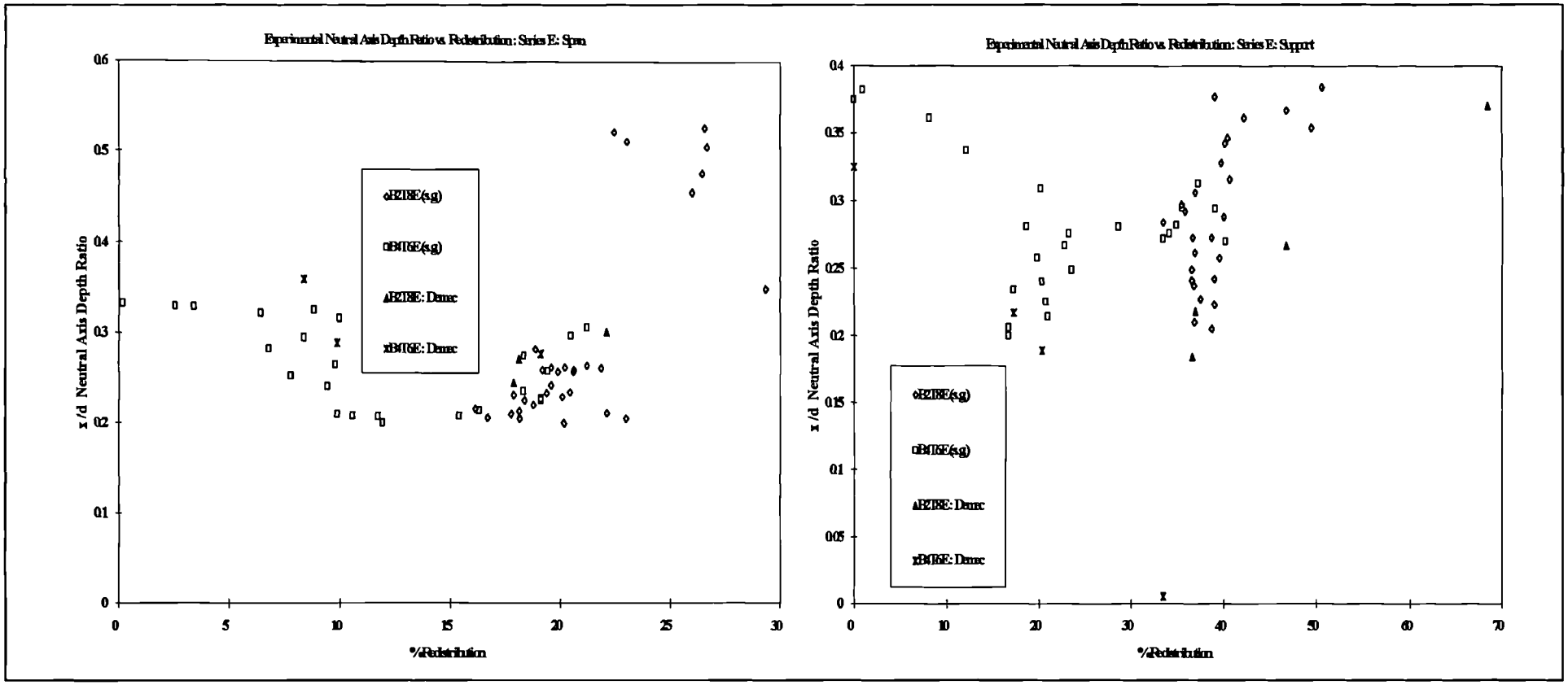

Figure 5-73: Series E Measured neutral axis depth ratio versus redistribution from Demec and averaged strain gauge data for both span and support sections

172

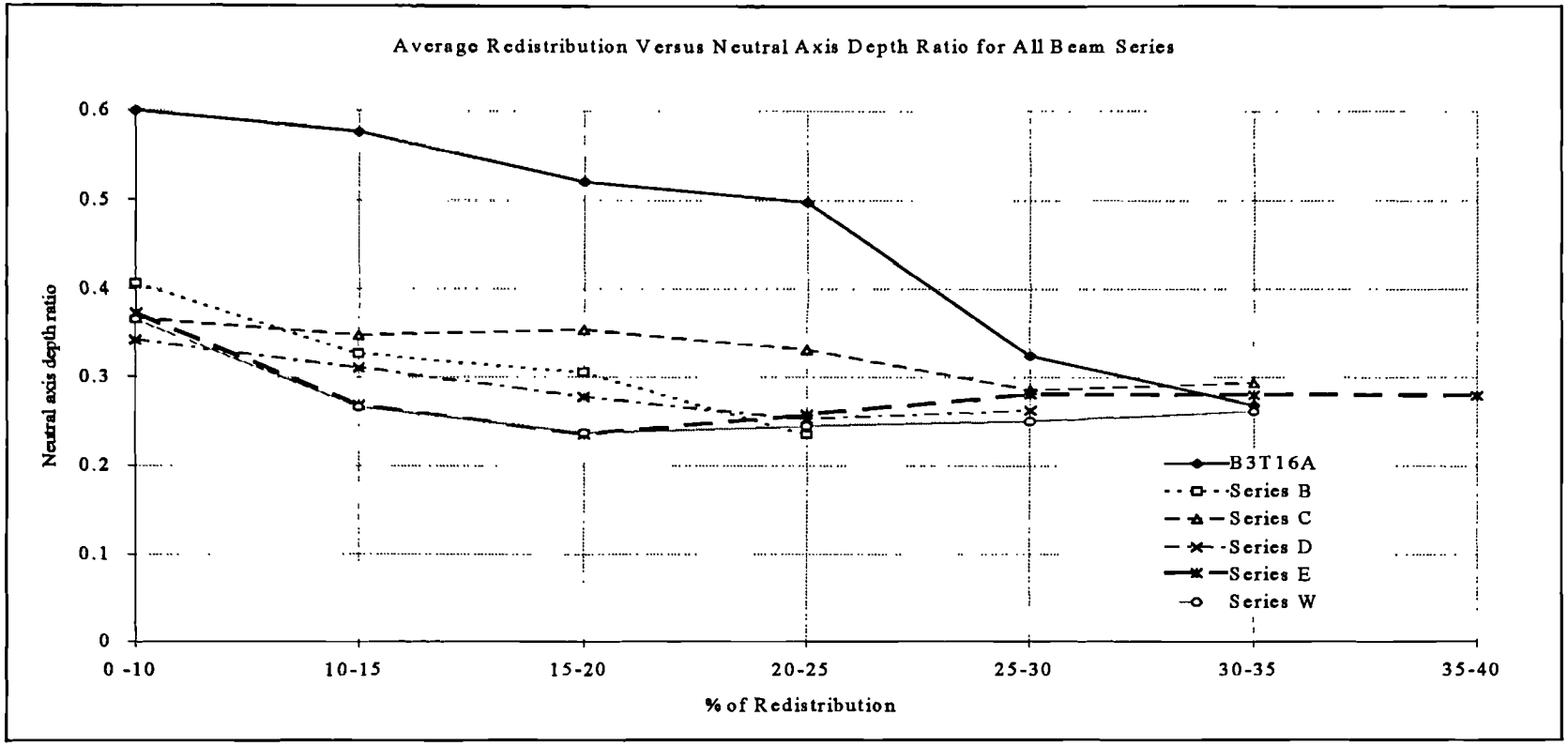

Figure 5-74: Shows a comparison between beam series range of redistribution development with the neutral axis depth ratio

173

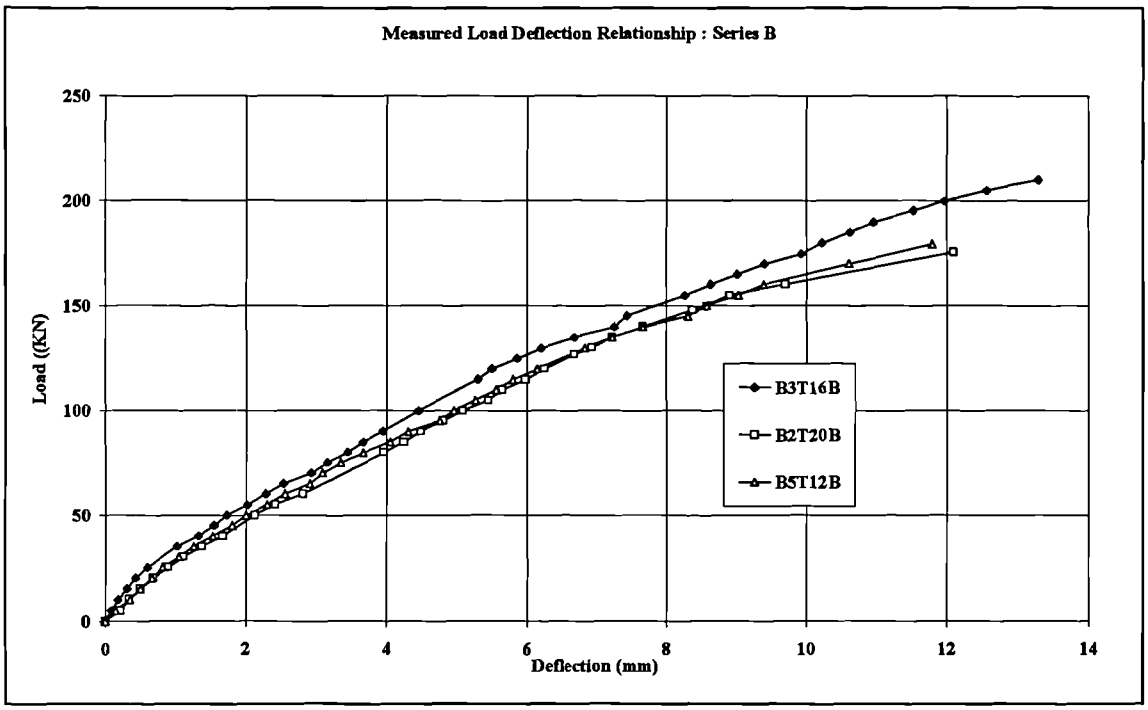

Figure 5-75: Series B experimental load deflection diagram over the gauged half (left side of the test beams)

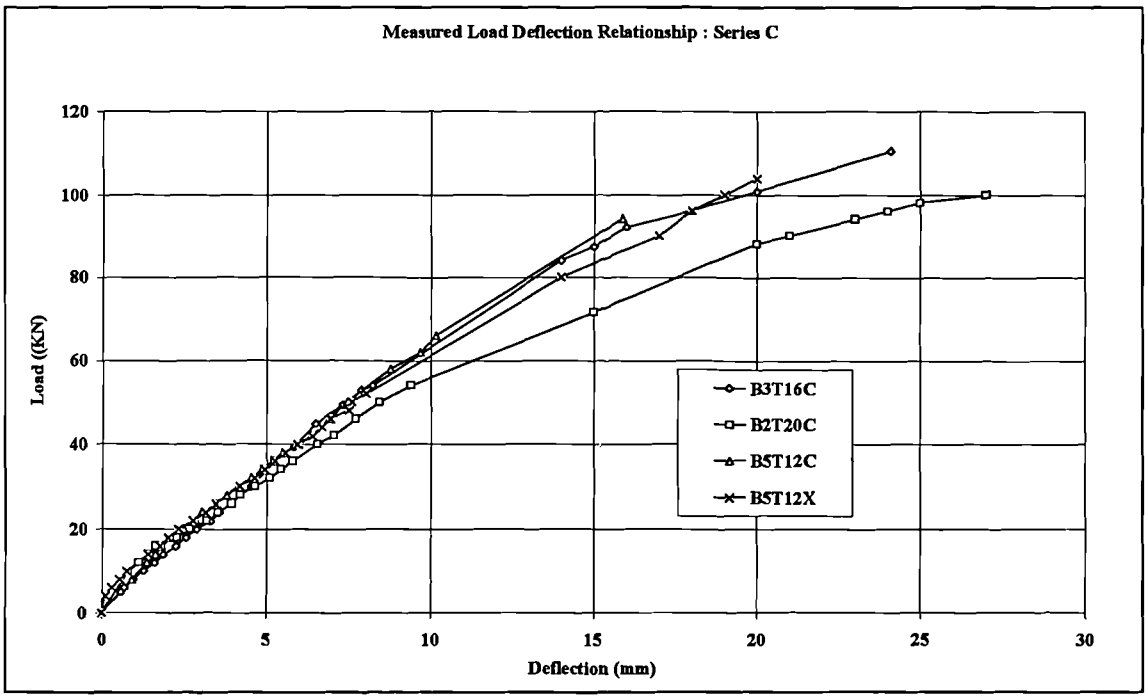

Figure 5-76: Series C experimental load deflection diagram over the gauged half (left side of the test beams)

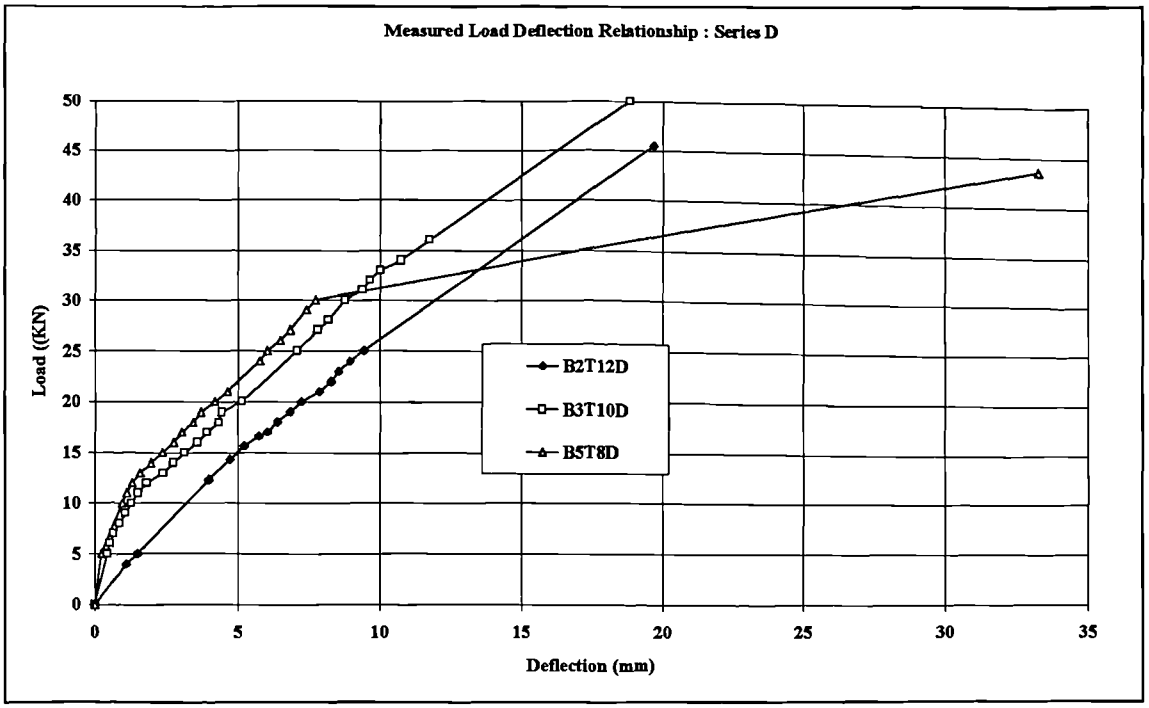

Figure 5-77: Series D experimental load deflection diagram over the gauged half (left side of the test beams)

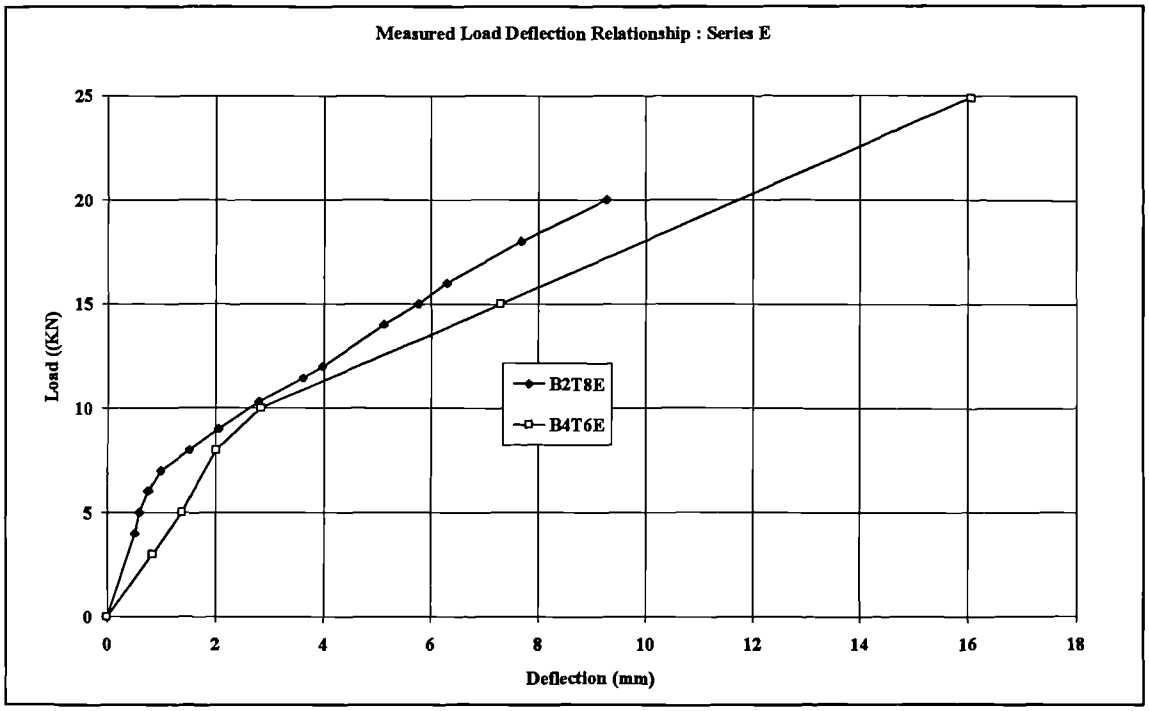

Figure 5-78: Series E experimental load deflection diagram over the gauged half (left side of the test beams)

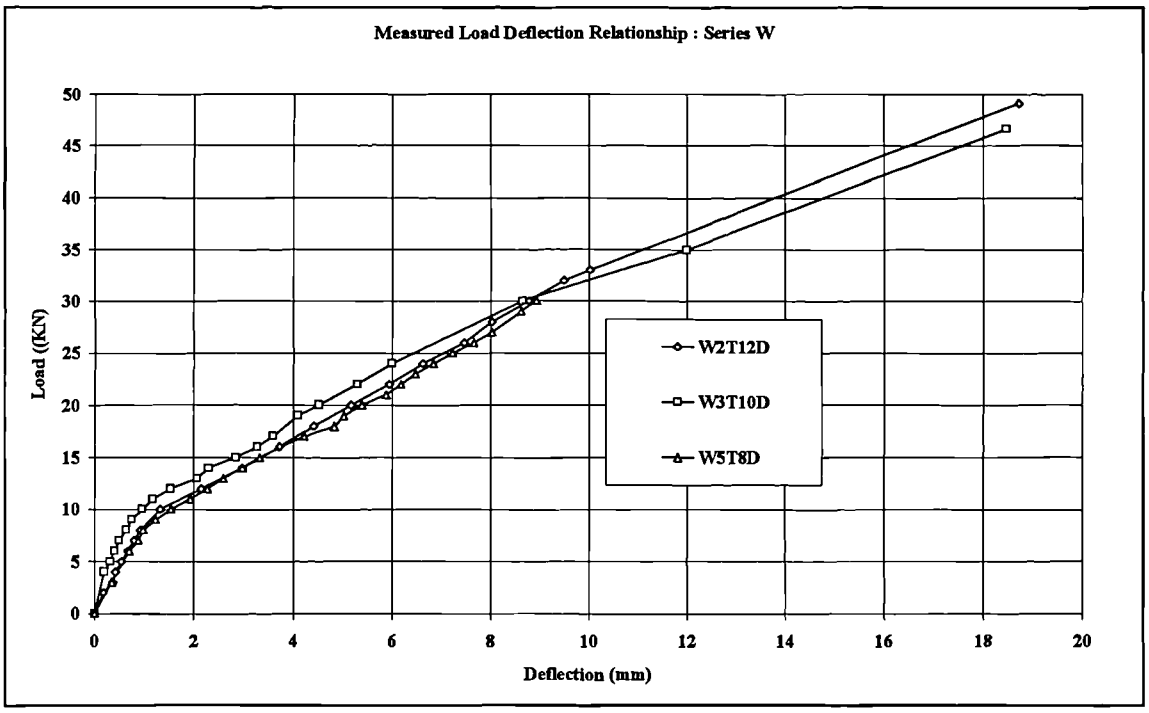

Figure 5-79: Series W experimental load deflection diagram over the gauged half (left side of the test beams)

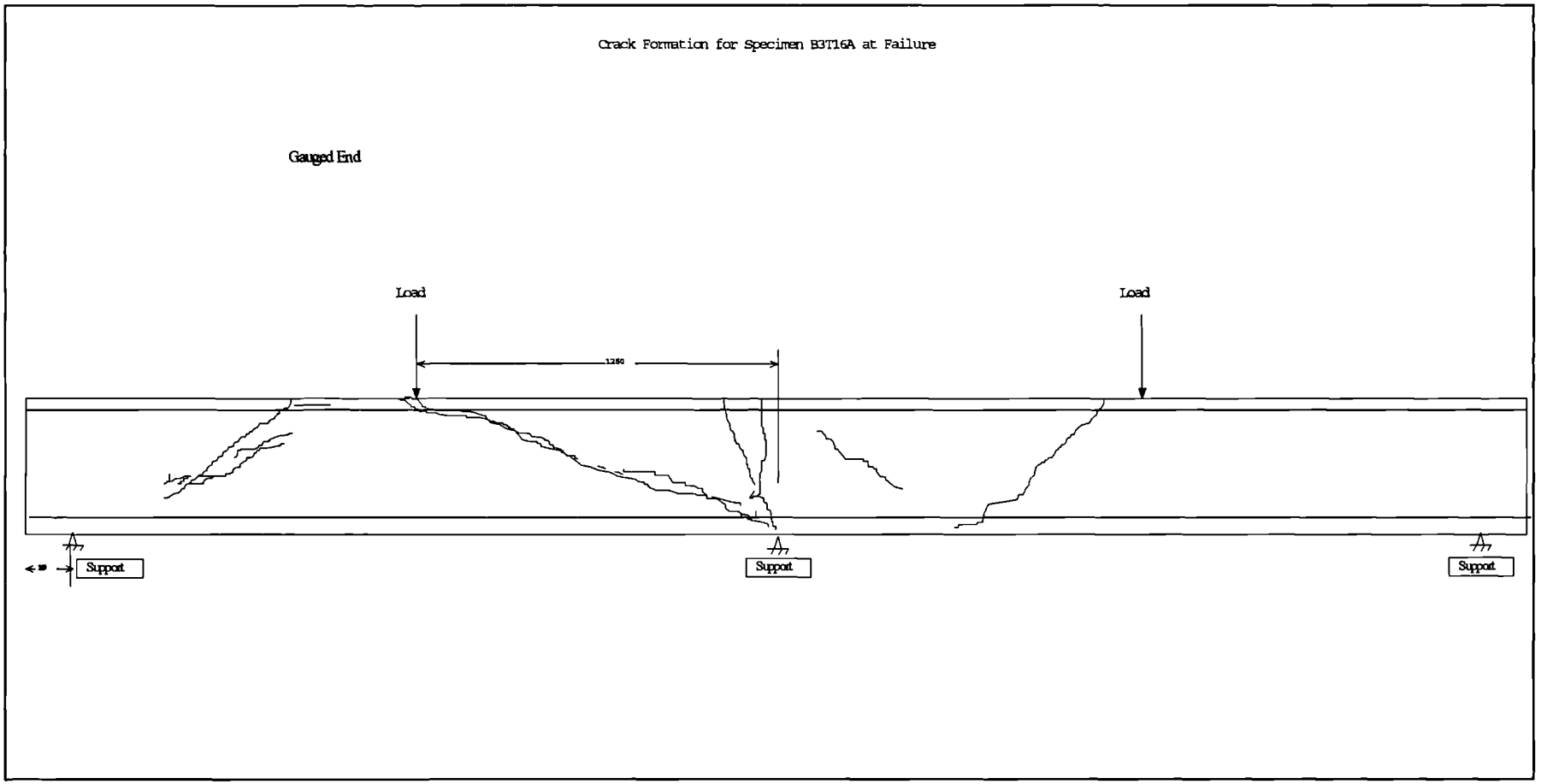

5-80:Specimen B3T16A final major crack formation at failure

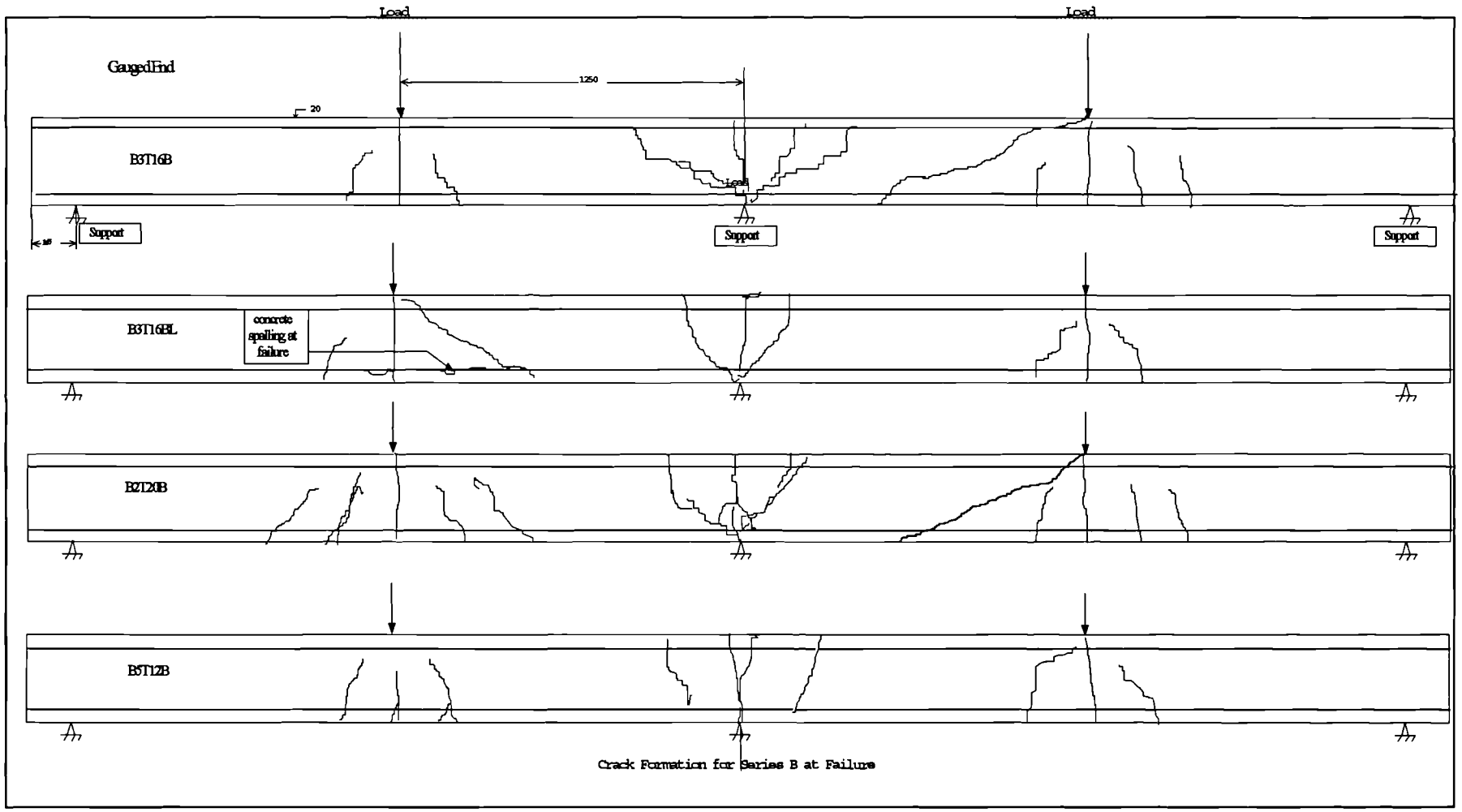

Figure 5-81: Series B final major crack formation at failure

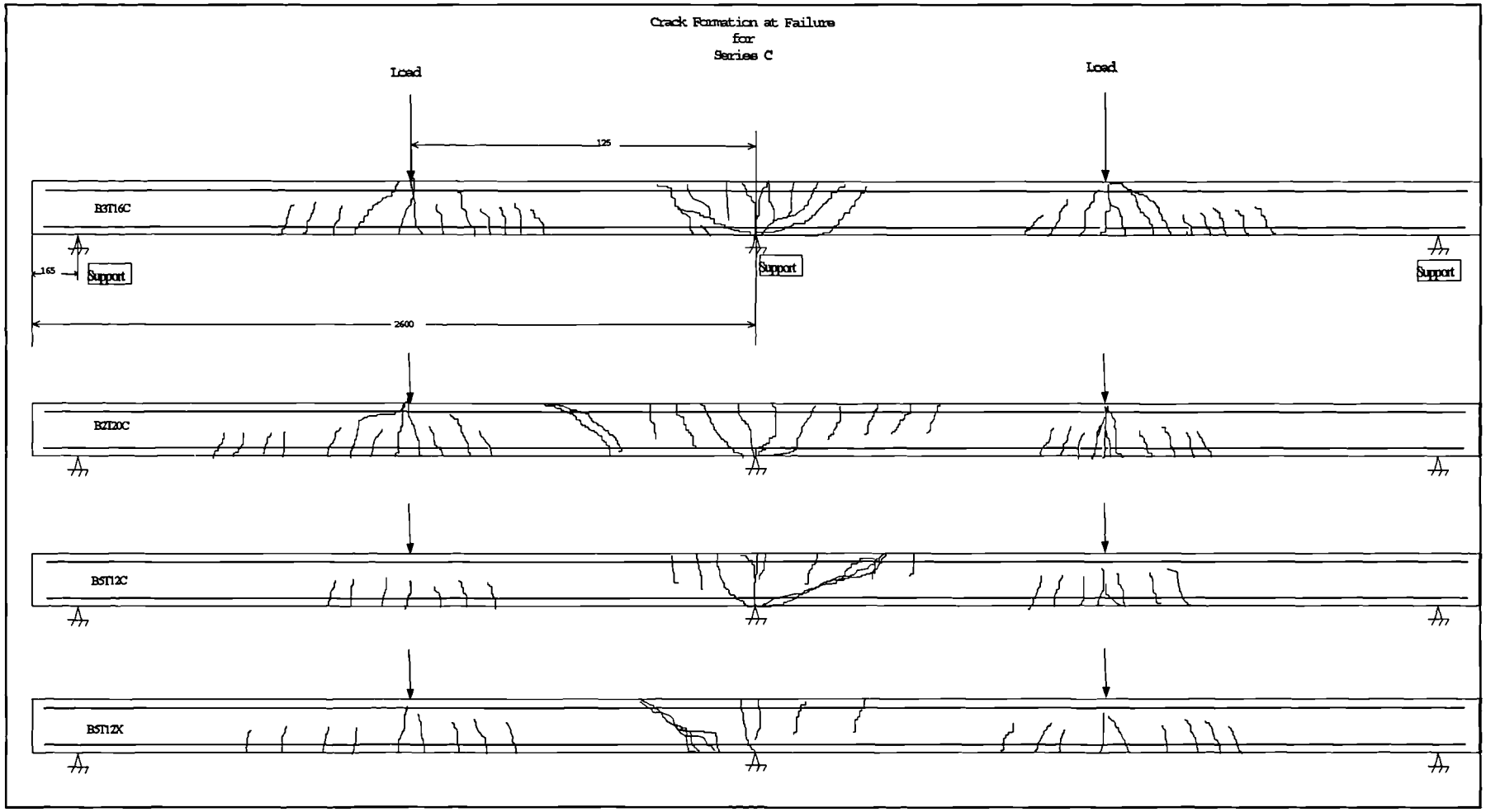

Figure 5-82: Series C final major crack formation at failure

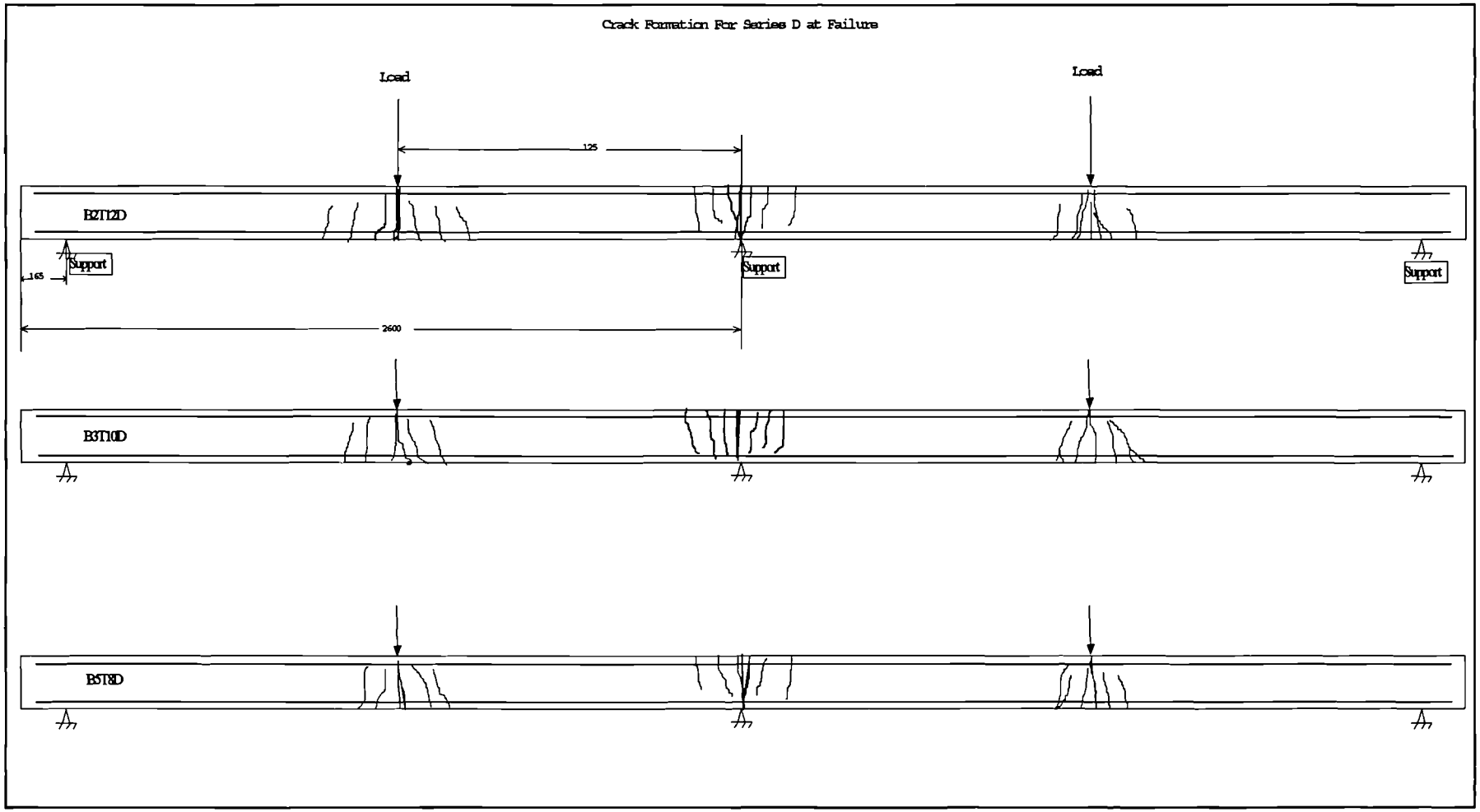

Figure 5-83: Series D final major crack formation at failure

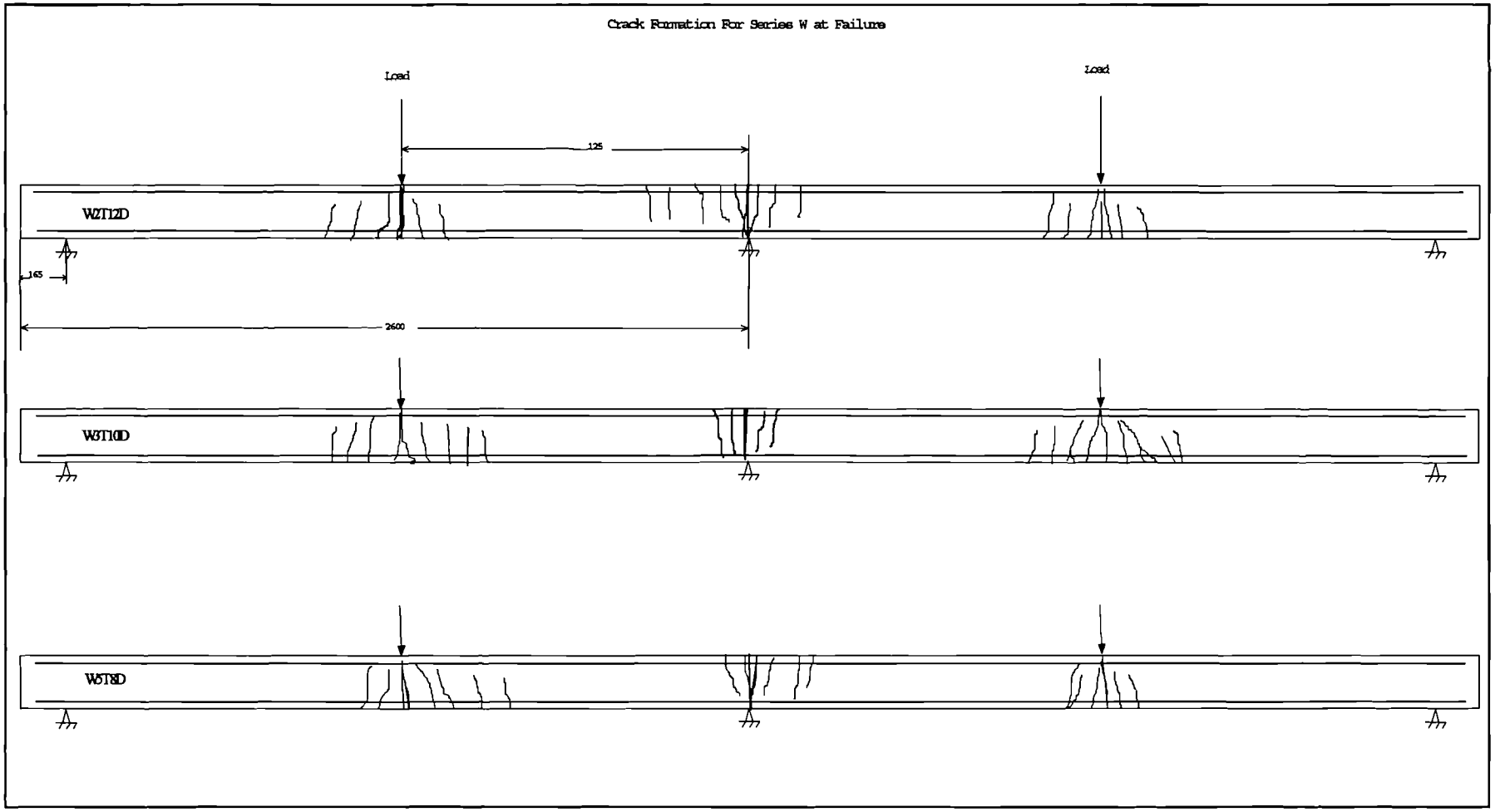

Figure 5-84: Series W final major crack formation at failure

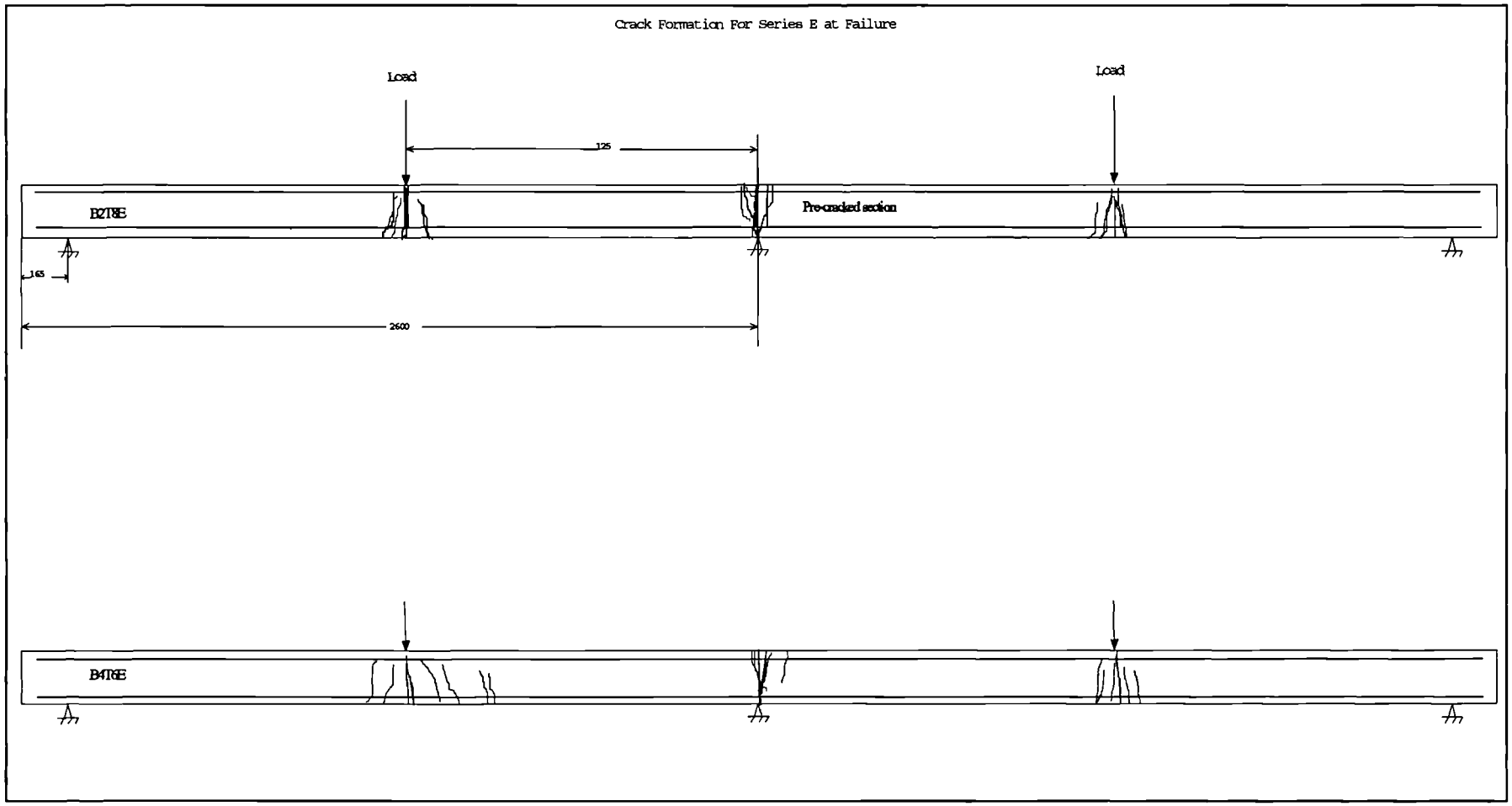

Figure 5-85: Series E final major crack formation at failure

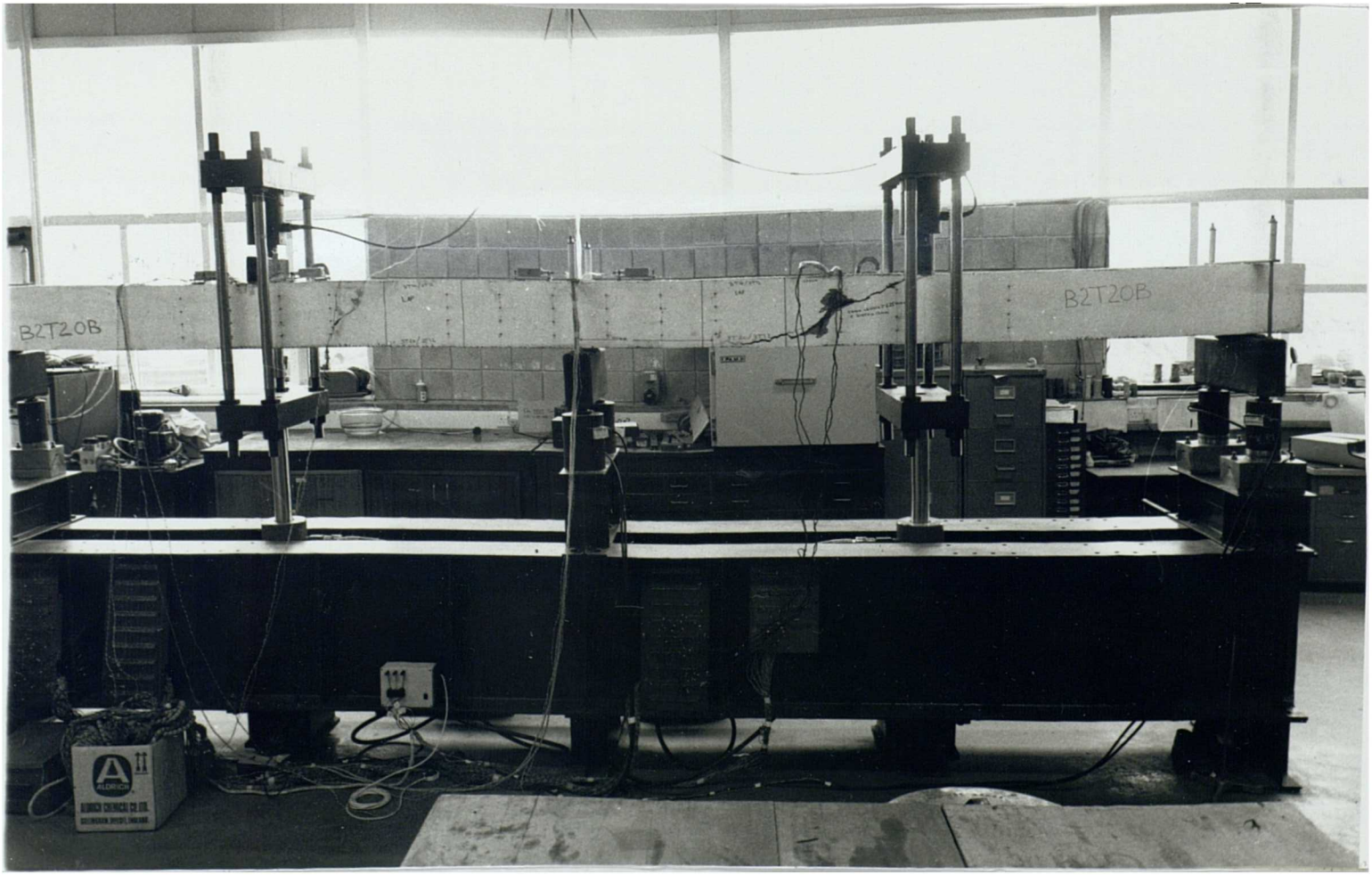

Figure 5-86: Picture of beam failing in shear

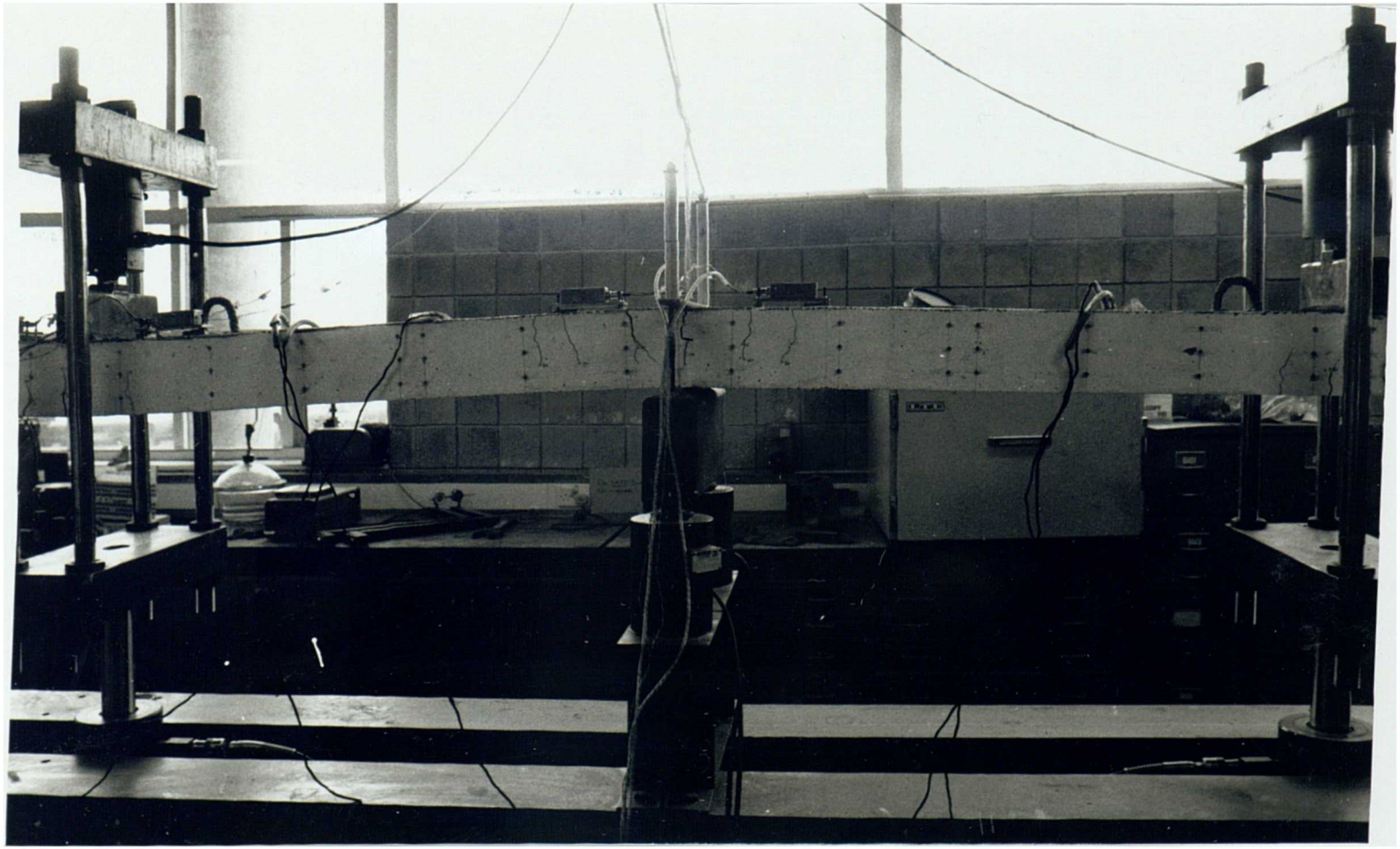

Figure 5-87: Picture of beam failing in flexure

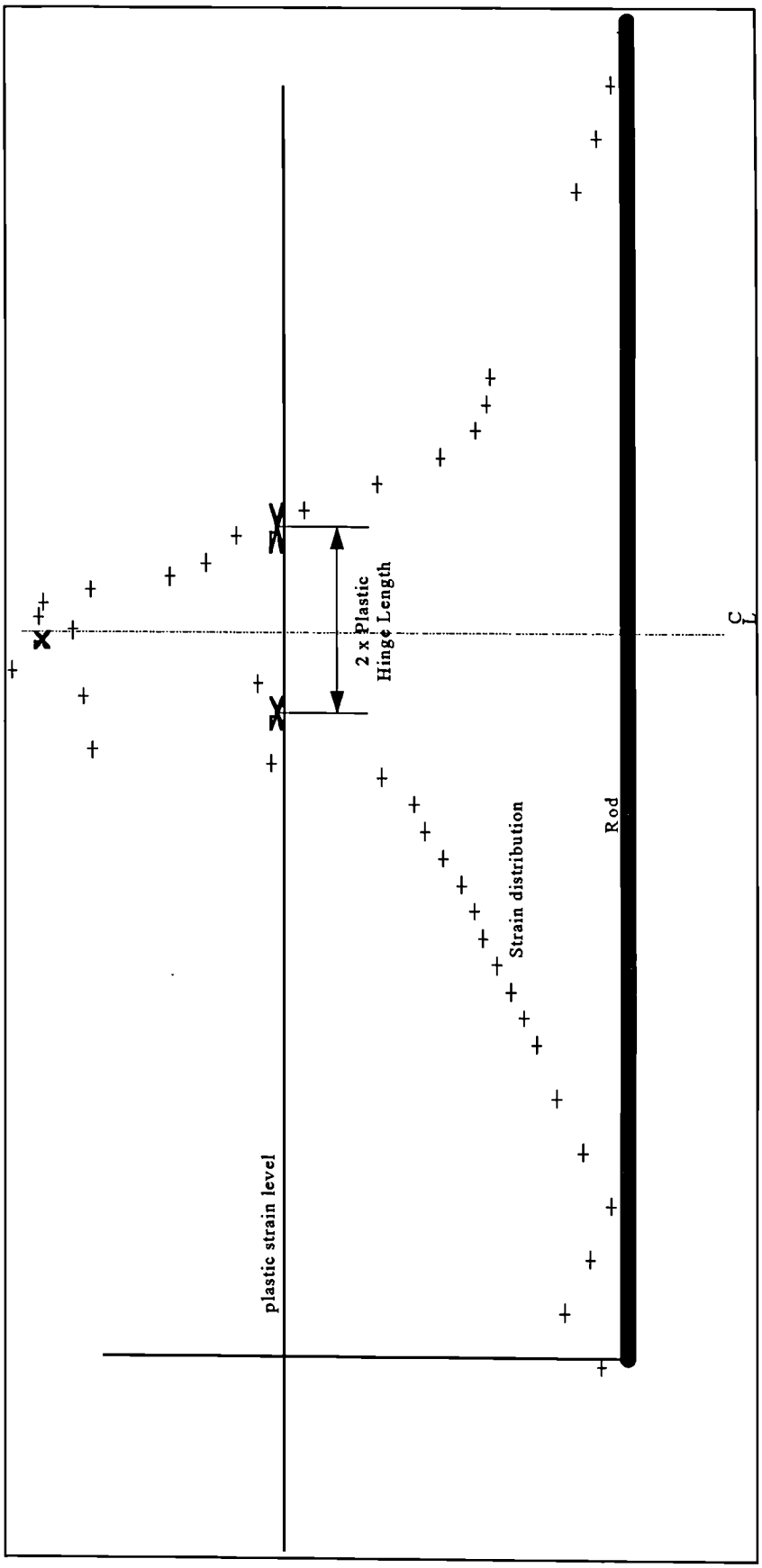

Figure 5-88: Schematic of strain distribution indicating method in which plastic length was calculated.

PART II

NUMERICAL MODELLING
AND
COMPARISON WITH EXPERIMENTAL RESULTS

CHAPTER SIX

6. BEAM MODELLING

6.1 Introduction

Besides testing the beams described in Chapter Three, one of the main objectives of this research was the development of a numerical procedure to model moments, redistribution, curvatures and deflections of the test beams. This chapter describes the numerical model that was used as the main tool for modelling the experimental results. The numerical model provided a complete history of redistribution and other deformation parameters by applying the moment area theorems to a propped cantilever beam loaded in the middle of the span. The non-linear approach developed by the author was simple and versatile since it is flexible in accommodating any moment curvature relationship.

The model has the following limitations:-

1. Only centrally loaded propped cantilever beams could be modelled.
2. It ignored dynamic response. This limitation was mandatory, since any investigation to include dynamic response demanded further experimental verification that was beyond the scope of this research program.
3. The analytical model was limited because it assumed that during bending, plane sections would remain plane. This is particularly important in the vicinity of the fixed support at maximum load.

Despite these limitations, the model was useful in the analysis and investigation of moment redistribution. Furthermore, the model can be used as the basis for the further development of a practical engineering tool.

6.2 Theory and Background

The second theorem of moment area states that deflection at point (A) relative to the tangent at point (B) (see **Figure 6-1**) equals the sum of moments of the curvature between (A) and (B) about point (A). It can be expressed mathematically as:

$$\delta = \int_B^A \varphi y dy \qquad \textit{Equation 6-1}$$

Where:-

δ = Deflection at point A

φ = $\frac{M}{EI}$ = Curvature along the beam at distance *(y)* from A

y = Moment arm or distance from the pinned end to the centre of the sectioned curvature diagram

M = Moment at the section distance y from A

EI = Stiffness of the member at distance *(y)* from A

Two-span continuous beams were tested and loaded near the centre. Symmetry permitted half of the beam to be represented as a propped cantilever under a point load, as shown in the **Figure 6-1.** As shown earlier in Chapter One, redistribution in a propped cantilever took place from the support section towards the span. As the load increased on the beam, the point of zero bending moment moved towards the fixed support. This movement caused the bending moment at some sections in the area of zero bending moment to go from a hogging to a sagging moment. This phenomenon is called unloading and is presented next.

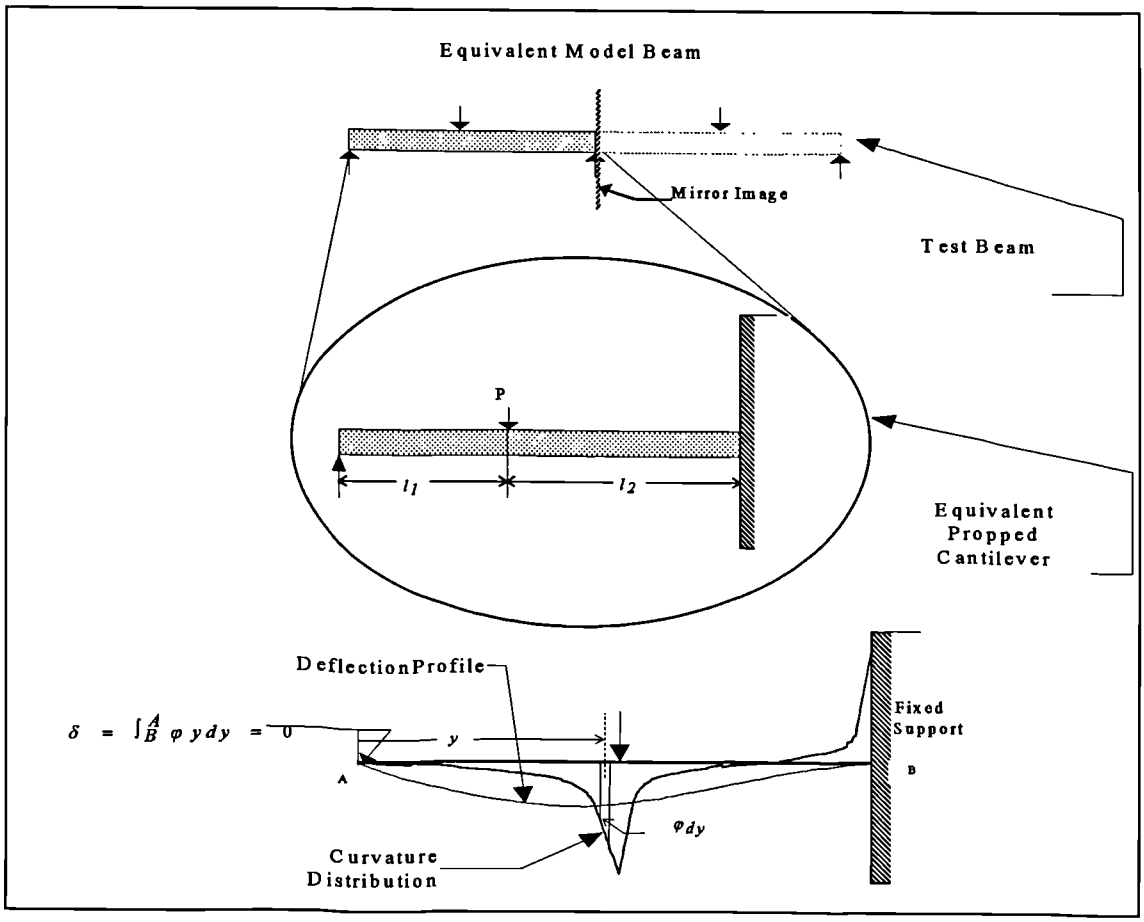

Figure 6-1: Propped cantilever equivalent beam

6.2.1 Unloading

In the case of a perfectly elastic beam, the moment curvature relationship would be linear. Furthermore, the bending moment diagram would pass through the same point of zero moment at any two consecutive load stages shown in **Figure 6-2a.** In reality, the beam is not perfectly elastic and the moment curvature relationship is non-linear. The zero bending moment point along the beam at any two consecutive load stages would shift toward the support as shown in **Figure 6-2b**. This shift causes some sections to unload and change from a hogging to a sagging bending moment. There are very few data available on how unloading occurs. **Figure 6-2b** shows a schematic diagram of three possible unloading paths near the point of contraflexure (zero bending moment). Path 1 unloads through an approximate mirror image, path 2 unloads on the same loading curve and path 3 unloads linearly from a point on the moment curvature diagram through the origin.

The possibilities are numerous, therefore, assumptions and approximations on the nature of unloading are needed. Since the effect of unloading on the overall behaviour of the beam is small, then it is tempting to ignore this effect. However, the author decided to examine the programming problem involved.

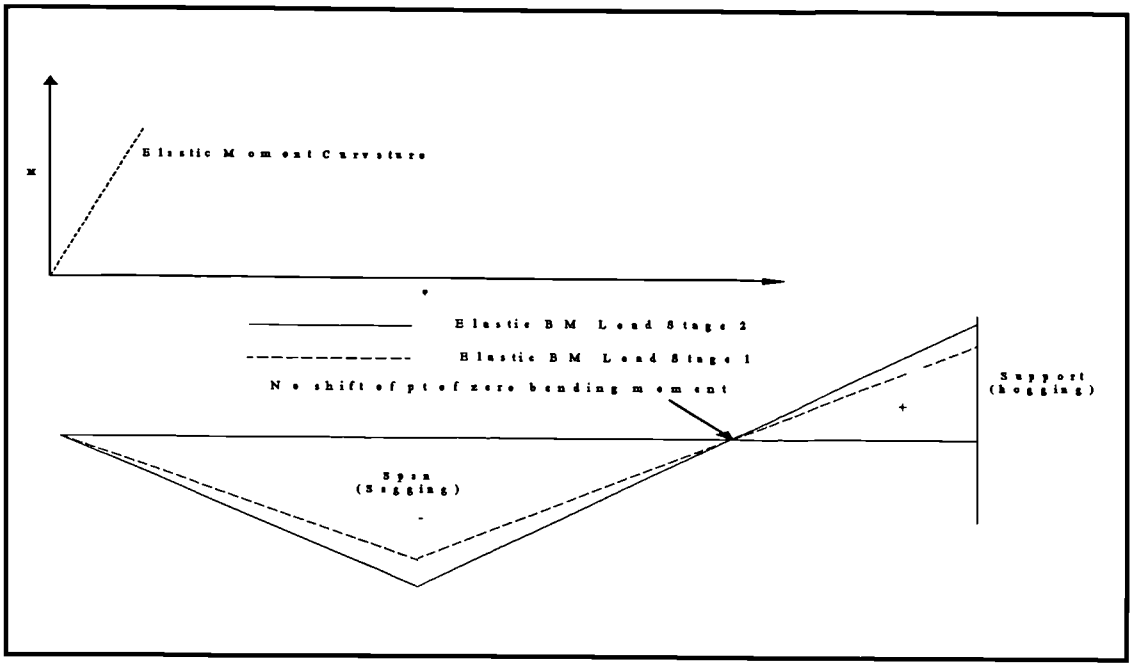

Figure 6-2a: Bending moment diagram for perfectly elastic situation

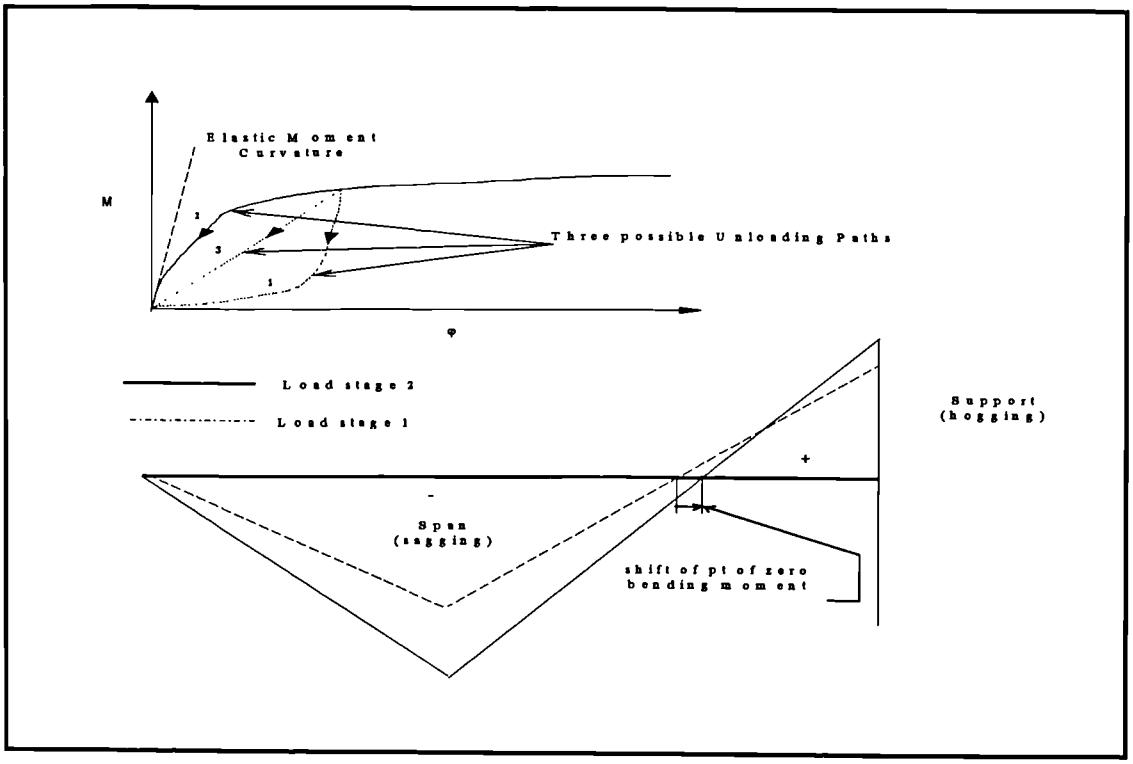

Figure 6-2b:. Bending moment diagram if the moment curvature relationship is not perfectly elastic showing possible modes of beam sections unloading

6.3 Objectives

The main objective of the software was to produce a numerical model of a propped cantilever for all values of loading from zero to collapse. The model would calculate the moment, stiffness, curvature, rotation and deflection at any point along the beam taking account of its non-linear stiffness. Despite the small effect of unloading on the overall behaviour of the beam, the author decided to include unloading in the structure of the program. The model was initially intended for a propped cantilever, however the model concept and procedure could be used to model the behaviour of other beams.

6.4 Method of Analysis

To achieve the objectives stated in 6.2, the author used the FORTRAN language to write the program of the model. The program contained 4500 lines of code which, during the period of the research, were written for different compilers that were available on the university computers. The author was forced to write the software for an MTS (a multi user time sharing system), UNIX and p.c. systems due to the change in computer systems used on the university site. This consequently produced a variety of output programs written to suit the different compilers. However, for this thesis, the author decided to use the p.c. option since readily available application software could be used for the presentation graphics. Each run of the model on a 100 MHz 486 PC took approximately ten minutes depending on the number of load cases tested at each run of the program. The beam model constituted the main tool of modelling in a chain of other software programs written by the author and some developed earlier in the School of Engineering.

6.5 Beam Geometry

The model developed was formulated to accept variable non-linear moment curvature relationships in a linearised form along a propped cantilever beam. The propped cantilever was divided into blocks of lengths d_1, d_2, d_3, d_4,....d_n. The

purpose of dividing the beam into blocks was to facilitate and account for the inclusion of a multi moment curvature relationship along the beam according to any beam reinforcement layout as shown in **Figure 6-3.** Block boundaries were made to coincide with the point load position. However, putting the boundaries at any point along the beam was immaterial as was found later when the program was complete. Each block contained n_1, n_2, n_3, n_4,....n_m strips or elements of equal length respectively, therefore, each block (i.e. all strips in a block) had the same moment curvature relationship. The purpose of dividing each block into strips was to control the level of accuracy of the subsequent calculations, and the runtime for the program. It was found that increasing the number of strips beyond 1000 would not affect the level of precision and used unnecessary run time. To facilitate the increase or decrease of the number of blocks or strips in each run of the analysis, moment curvature relationships were inputted for each block with their sizes, number of strips in a block, number of points, and load cases to be solved. The program calculated the following necessary geometrical parameters before it started the iteration process:

1. Block number for each strip
2. Strip numbers
3. Length of each strip in each block
4. Moment arm from the propped end of the beam to the middle and edge of each strip
5. Checked if boundaries of the beam coincided with the total length of the beam. If they did not match, the user had the option of terminating the program.

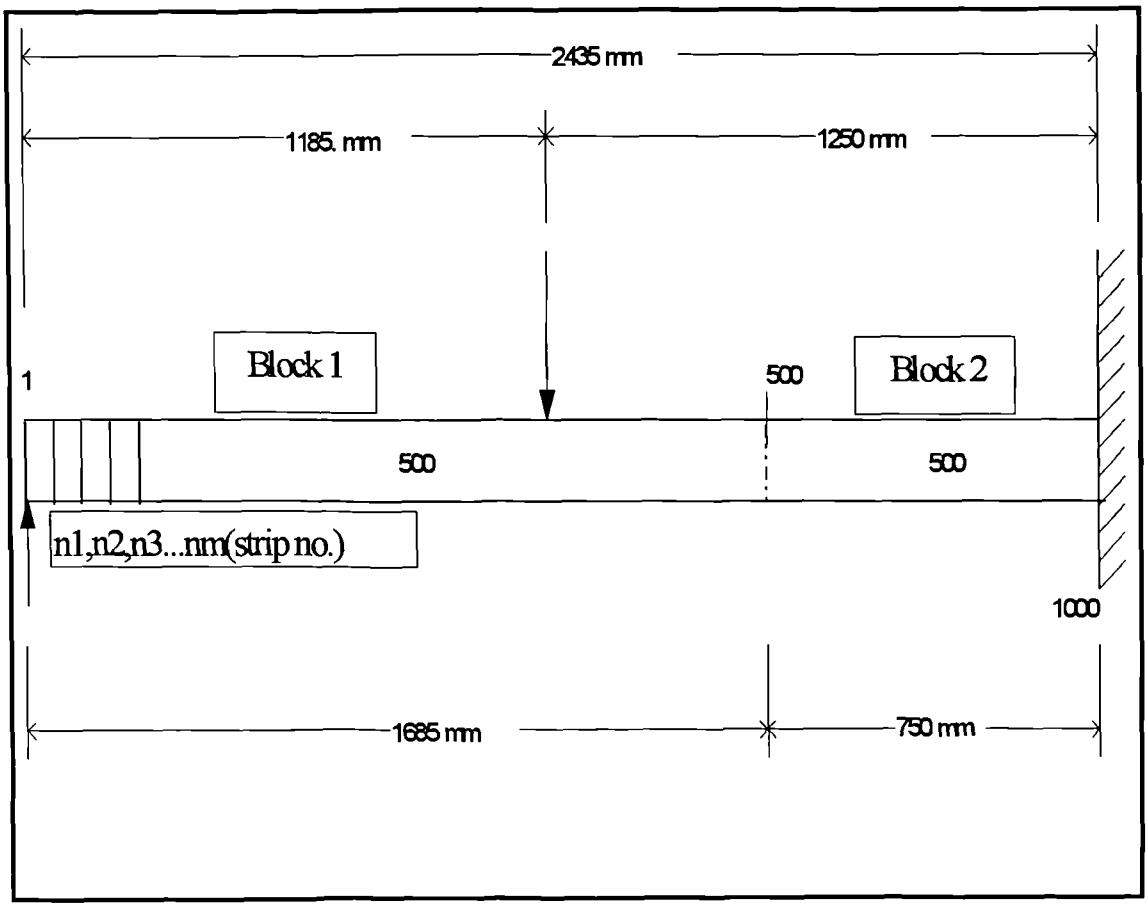

Figure 6-3: Beam geometry with block and strip layout

6.6 Program Algorithm and Details

The aim of the program was to find the fixed moment at the support for each load stage which satisfied the condition laid in **Equation 6-1**, namely zero deflection at the simple end relative to the tangent at the fixed support. To achieve this, the bending moment diagram for the support effect of a propped cantilever was superimposed onto the bending moment for a simply supported beam as shown in **Figure 6-4.**

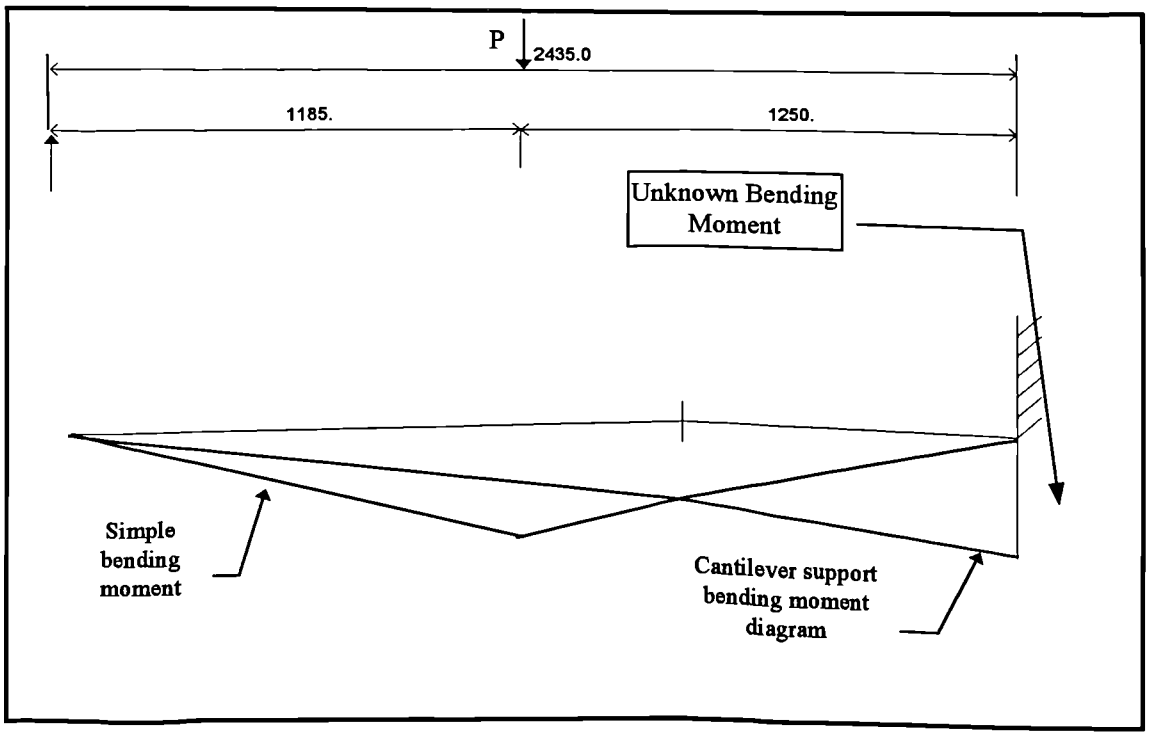

Figure 6-4: Superimposed bending moment diagram of the propped cantilever beam

The model assumed that since the value of the point load was known, the simple bending moment in **Figure 6-4** would also be known. The only unknown value then, would be the support bending moment at the fixed end. The procedure used an iterative technique employing the existing known moment curvature relationships of the beam to find the value of the fixed end moment. This required the model to be structured in a pyramidal manner. Arrays were built in three dimensions in the main program, then reduced in subroutines to two dimensions, then to one dimension, and finally to a single variable. The reason for this technique was to translate the input data from the moment curvature relationships to each strip along the beam. This methodology designed by the author made the programming more efficient and easier to follow and debug. **Figure 6-5** shows a detailed flowchart of the program. The program algorithm started in the following order:-

1. All the input, working and output arrays were dimensioned and initialised.
2. The first load increment was started, assuming the beam was loading since there was no previous loading history.

3. The program read in a tolerance for the residual deflection at point A that needed to be satisfied. The tolerance level was the value of deflection at point A in **Figure 6-1**, which theoretically should be zero. The author chose to use {1.00 x 10^{-6}mm} for this value. This tolerance level was not fixed; it could be varied at the discretion of the user. To choose a higher value than $1x10^{-6}$ mm could affect the accuracy of the results. It was possible to choose a very low value of tolerance, which meant greater accuracy down to the value of $1x10^{-10}$mm.
4. In a separate subroutine, the program calculated the simple bending moment at each strip.
5. The program then incremented the support bending moment; a tentative value was assumed to be half that of the elastic one and each iterative step toward the real value was incremented at half the step of the previous one.
6. The program then calculated deflection at the simple end relative to the fixed one by summing moments of the curvature strips. If the summation (residual deflection) were less than or equal to the tolerance, the calculation would terminate. If not, the support moment would be incremented up or down depending on the sign of the summation. If the summation were greater than the tolerance, the support moment would be incremented down, otherwise it would be incremented up, until a solution was found within the specified tolerance.
7. Once the first load stage iteration was completed, the program would proceed to calculate the final bending moment diagram, curvatures, rotations, deflections at each strip along the beam. All these calculation were carried out in separate subroutines. When the calculated bending moment diagram had been established, redistribution was calculated at the support and span sections respectively.

Since there was no previous load history, it was necessary to set the initial load case as the first record of loading history of the beam. The process then started again, but this time each strip during each loading stage and at each iteration was checked to establish whether the strip or section had changed from hogging to sagging bending moment. If unloading had occurred, then the fixed end moment was determined by

assuming unloading to occur on the same loading curve of the moment curvature relationship as shown in **Figure 6-2b** path 2. The author also investigated an assumed linear unloading through the origin of the moment curvature relationships, (see **Figure 6-2b**, *path 3*). However, the inclusion of unloading in this manner did not contribute any further accuracy to the modelled results. Therefore, unloading down the loading curve (path 2 in **Figure 6-2b**) was used to calculate the bending moment diagram as it took less time to run. After the iteration process was complete, all the calculated variables were stored and outputted by employing a menu driven screen.

The interactive procedure of the model made it flexible enough to examine a wide variety of moment curvature relationships. Calculations of deflections, rotations and curvatures at any point along the beam were straightforward once a true bending moment diagram had been established. The model was numerically stable while values were within the region of the moment curvature relationship. If moments fell outside this region, the program displayed an appropriate message stating the moment curvature relationship was out of range. This validity check helped choose an appropriate moment curvature relationship.

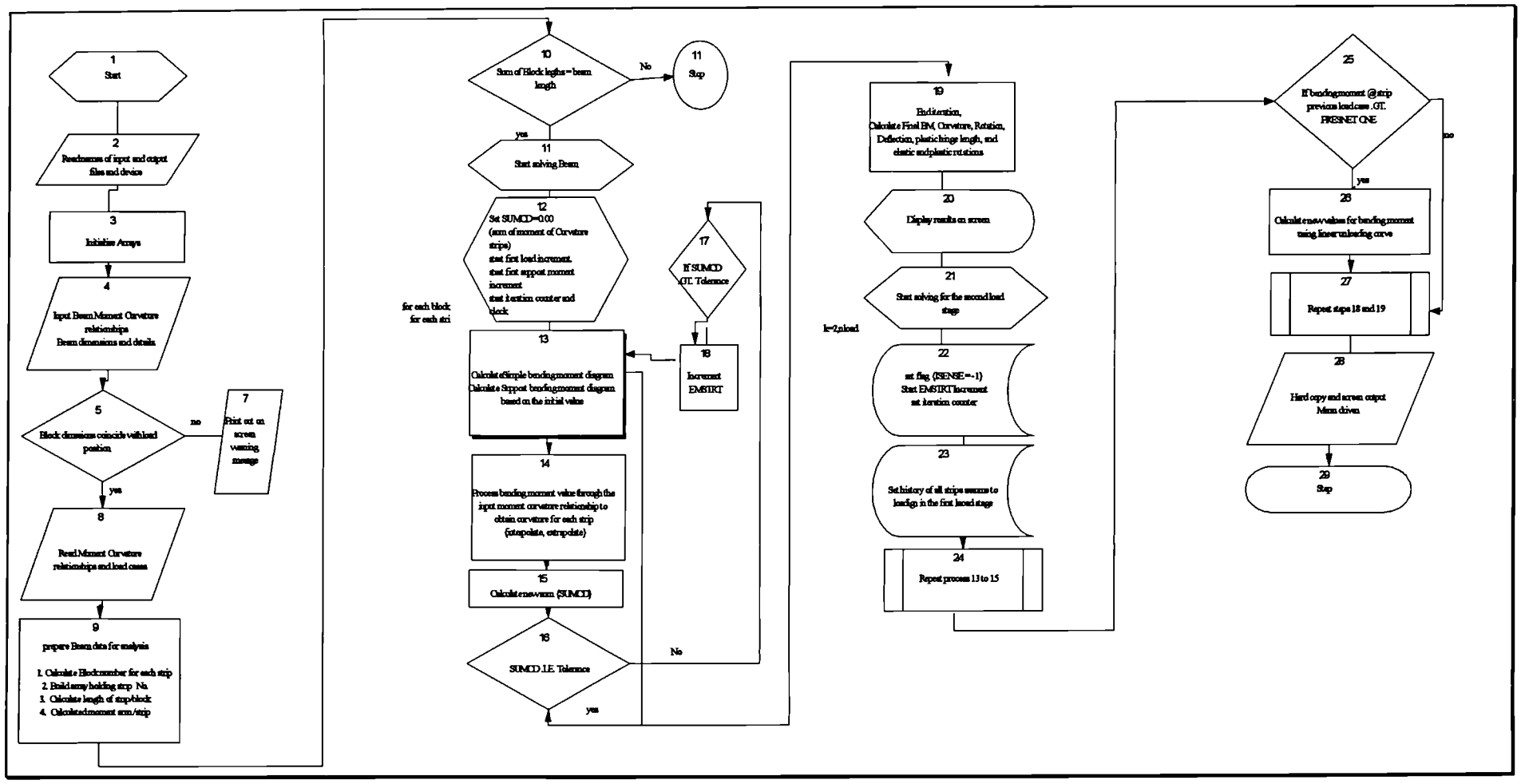

Figure 6-5: Detailed flow chart of the beam model program

197

6.7 Calculation of Moments, Reactions, Redistribution and Deflection

Redistribution was defined as:

$$\beta = \frac{Modelled\ Moment - Elastic\ Moment}{Elastic\ Moment} \times 100\% \qquad Equation\ 6\text{-}2$$

Redistribution was determined numerically by calculating the support and span bending moments corresponding to the moment at a section after redistribution as shown by the above equation (6.2). The moment at the section before redistribution was taken as the elastic moment calculated according to the theory of elasticity. Elastic bending moments at support and span were calculated according to the following formulae:-

$$M_{sup,elastic} = \frac{Pl_1}{2l^2}\left(l^2 - l_1^2\right) \qquad Equation\ 6\text{-}3$$

$$M_{span,elastic} = \frac{Pl}{4} - \frac{Pl_1}{4l^2}\left(l^2 - l_1^2\right) \qquad Equation\ 6\text{-}4$$

Where:-

l_1 = Length of beam from propped end to load position.

l = Total length of beam

P = Force at mid-span of the propped cantilever

$M_{sup,elastic}$ = Elastic Bending moment at support

$M_{span,elastic}$ = Elastic Bending moment at span.

After the establishment of the support and span moments, the elastic and calculated (modelled) position of the point of contraflexure (point of zero moment), was calculated for each load case by similar triangles from the bending moment diagrams. Elastic and modelled deflection at mid-span under the concentrated load, and shear force distribution were also determined. The following are the equations used for the calculations:

$$x_{zero} = \frac{M_{span,cal}(l - l_1)}{(M_{span,cal} + M_{sup,cal})} + l_1 \qquad \textit{Equation 6-5}$$

Where:-

$M_{span,cal}$ = Calculated span bending moment from model

$M_{sup,cal}$ = Calculated support bending moment from model

x_{zero} = Distance from propped end to point of zero bending moment

Deflection under the load was calculated based on the deflection of the nearest strip to the position of the load, termed NMID. The value of deflection at each strip according to the second theorem of moment area was the moment of the area under the curvature diagram of all previous strips about the position of the strip from the fixed support up to the middle of the strip.

Elastic Deflection was:

$$\delta_{cal.} = \frac{Pl_1^2(l - l_1)^3(l_1 + 3l)}{(l - l_1)l^3 \times (EI)_{elastic}} \qquad \textit{Equation 6-6}$$

Calculated reactions were:

R_{left} = $M_{span,cal} / l_1$ *Equation 6-7*

R_{right} = $P - R_{left}$ *Equation 6-8*

Similarly elastic values for reactions and the elastic point of contraflexure were calculated.

6.8 Example

The computer model described here was developed to accommodate any number of moment curvature relationship along a propped cantilever beam. The beam shown in **Figure 6-3** was analysed using two linearised moment curvature relationship, as plotted in **Figure 6-6** one for each block. The total number of strips used was one thousand (1000).

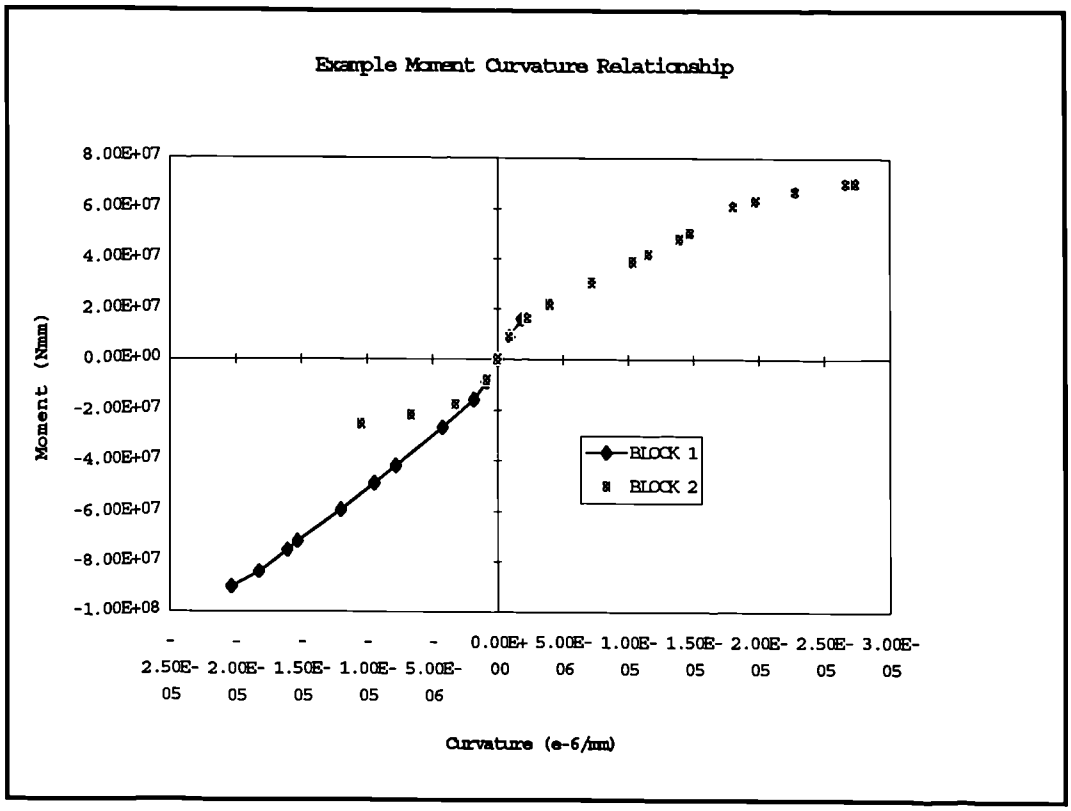

Figure 6-6 : Example linearised moment curvature relationships

6.8.1 Example Input

The following were the example program input:-

1. Beam length (2435 mm).
2. No. of blocks, [NBLOCK = 2].
3. No of strips [NSTRIP = 1000].
4. Size of each block, [DEL (1) = 1685.00], [DEL (2) = 750.00].
5. No. of points in each moment curvature relationship, (Curve 1: 14 points) and (Curve 2: 20 points).
6. The moment curvature relationship for each block contained a negative and positive part as shown in **Figure 6-6** and listed in **Figure 6-8**. The extent to which each relationship extended in the negative or positive side depended on whether the relationship was over the support area (mainly positive) or the span area (mainly negative). The relationship in **Figure 6-6** shows that for the span area (block 1), the moment curvature relationship extended mainly in the negative side since strips

in that region were not expected to reload from negative to positive moments, while the support area moment curvature relationship (block 2) extended more than (block 1) in the negative side of the diagram since it was expected to unload from the positive to the negative side of the bending moment diagram. The two moment curvature relationships used here were produced for specimen B3T16B (using BS 8110 assumptions which is presented later in Chapter Seven).

7. No. of load cases (NLOAD = 25), and load cases to be solved for were paramaterised to a maximum of 100 load cases. As much as possible, the author examined load cases that related closely to the actual experimental load cases.
8. Accuracy level or level of tolerance for calculations (1 x 10^{-6} mm).

6.8.2 Example Calculations

The program first prepared the problem for solving by calculating prerequisite parameters such as the moment arm to the middle and end of each strip position, strip number and block number for each strip. For the initial load of 10,000 N, the program first tried a support bending moment equal to half the elastic bending moment at that load stage, i.e. 2.261x10^{6} Nmm. After 17 iterations trying values in that region, it would achieve a residual deflection at the propped end less than or equal to (1.00 x 10^{-6} mm). This would give a bending moment at the support of 4.448 x10^{6} Nmm and redistribution of -1.636 % over the support. The support bending moment having been established at the first load stage, the program would then proceed to calculate the curvatures, rotations and deflections at the middle of each strip position. Once the first load stage had been established, the program set the history record for the first load stage and assumed that no unloading had occurred (HISTORY = FALSE.). In the following load stage, a new value of support bending moment (EMSTRT) was selected at half the elastic one. However, this time and at every load stage thereafter, the program would check for unloading for each strip at each iteration. If a strip was found to unload, the program would use the unloading path specified and would look for a new (EMSTRT) value that would satisfy the tolerance level. Once this was completed, and the new value for the support bending moment was found at the second load stage, the curvatures, rotations and deflections at each strip would be determined.

Once the calculations were all completed, the program calculated the percentage error in the residual deflection at the propped end. For instance, when the 20th load stage was taken, the percentage of error was ($-0.2724422 \times 10^{-5}$ %) at a residual deflection of (-0.838×10^{-6} mm). This load stage took 36 iterations.

Later development in the program calculated the plastic hinge length over the support. This is presented in the analysis in Chapter Eight.

6.8.3 Example Output

The output structure of the program was very flexible and wide. Numerical output of moment, curvature, rotation and deflection was possible at every load stage giving the opportunity to examine results very closely. The program was menu driven, it had the flexibility of directing all output to a file or to the screen. Once the program started running it gave screen output of fixed end moments, elastic, modelled and redistribution percentage at each load stage. Furthermore, it gave output of execution time for each load case and displayed any event of unloading that occurred during each load stage. Once the run was complete, it was possible to look at various options of output. Modelled results output were suitable for use in conjunction with other packages like EXCEL.

Figures 6-7a to 6-7d show the example moment redistribution, bending moment, rotation and deflection diagrams. **Figure 6-8** shows a summary output of the example.

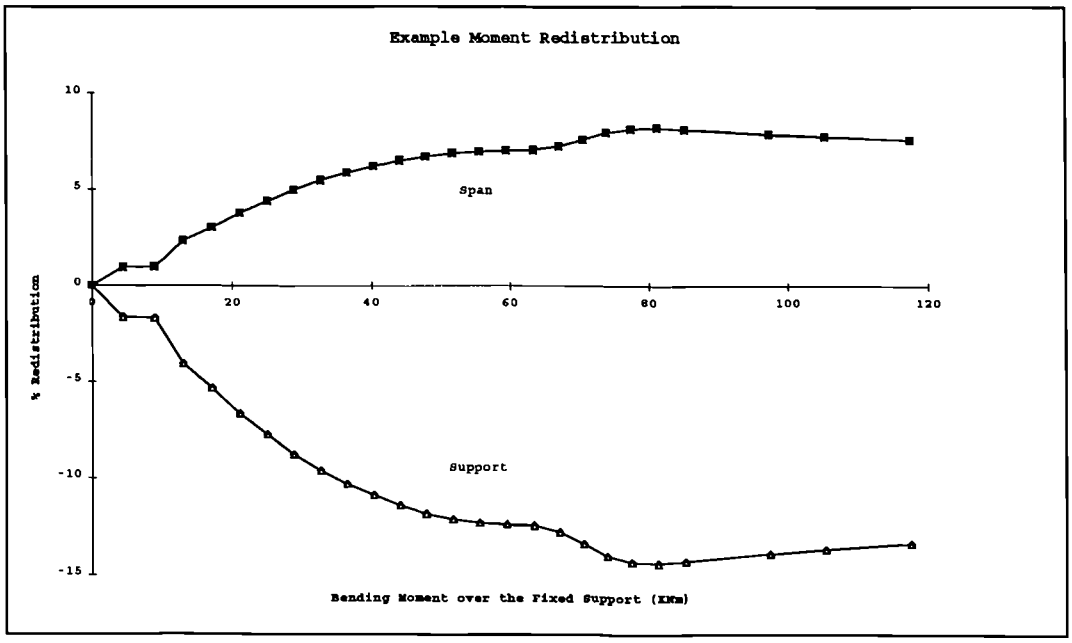

Figure 6-7a: Example moment redistribution curve

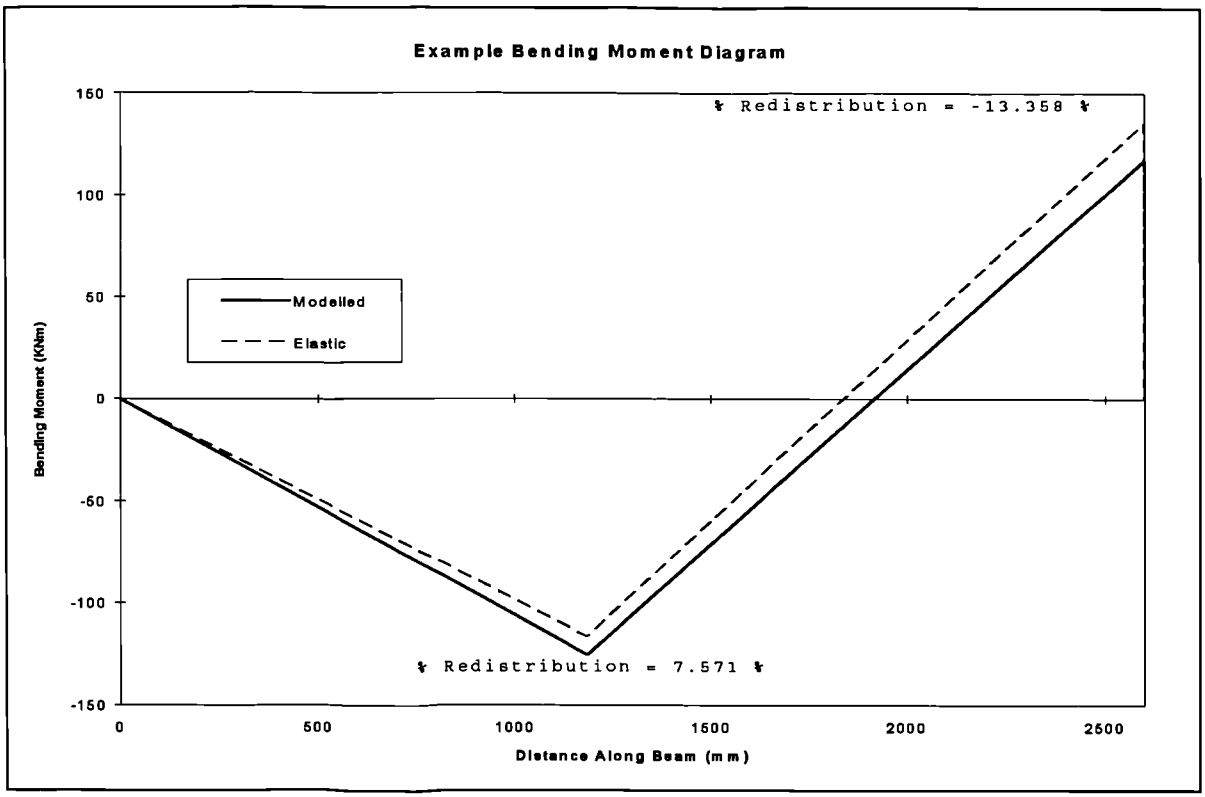

Figure 6-7b: Example bending moment diagram

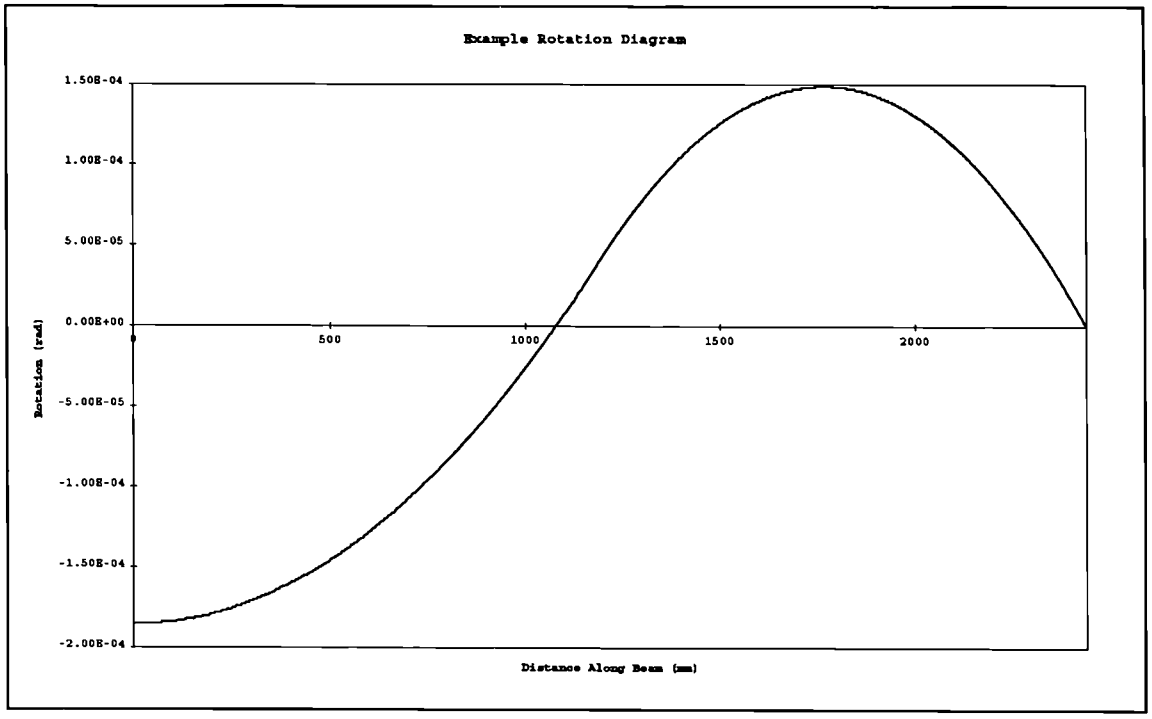

Figure 6-7c: Example rotation diagram

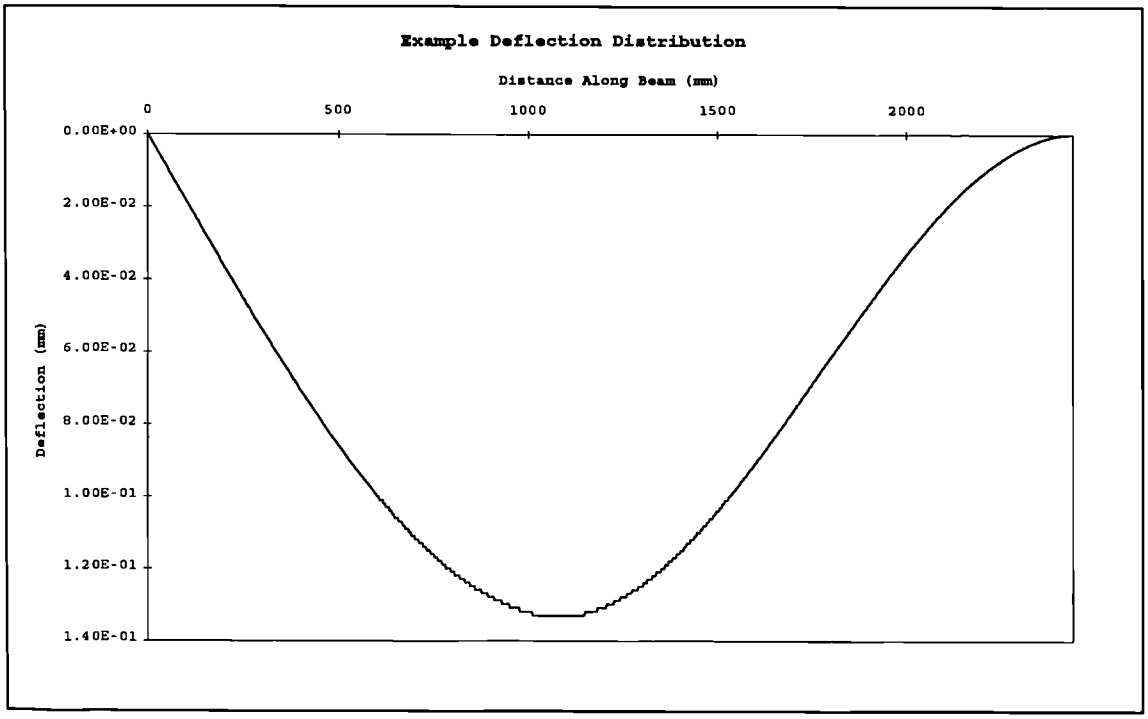

Figure 6-7d: Example Deflection Diagram

Figure 6-.7: (a) Example moment redistribution(b) Example bending moment diagram, (c)Example rotation diagram and (d) Example deflection diagram

6.9 Summary

The purpose of the model was to find the true bending moment diagram of a propped cantilever based on a multi moment curvature relationship applied across the length of the beam. Once this had been established, it was possible to compute the moment redistribution at the centre and at the mid-span, and the deformational properties along the length of the beam (Curvatures, rotations and deflections). The procedure consisted of dividing the beam into segments with different moment curvature relationships derived from the reinforcement properties and layout. The moment curvature relationship varied along the beam. An iterative numerical integration procedure was then applied employing the second theorem of moment-area to establish the bending moment diagram. Results of the calculations gave a full profile of modelled bending moment, curvature, rotation and deflection distribution. Furthermore, the model included on-screen and hard-copy graphics written for a UNIX and p.c. system.

In the next chapter the author will present and describe the moment curvature relationships and the redistribution criteria of the codes and standards used for the application of the model.

Figure 6-8: Example hardcopy input and output

```
FILE: SERIESB2.DAT
No. of blocks to the left, No of blocks, No. of strips, No. of load cases
1    2   1000
Length of span 1, length of span 2
1185.00            1250.00
No. of strips in a block, No. of points, length of each Block
500   14    1685.
   Curvature    ,     Moment
   -20.333e-4   ,    -89.95e10
   -20.333e-6   ,    -89.95e6
   -18.24e-6    ,    -83.86e6
   -16.082e-6   ,    -75.13e6
   -15.302e-6   ,    -71.85e6
   -11.997e-6   ,    -59.22e6
   -9.471e-6    ,    -48.95e6
   -7.821e-6    ,    -42.09e6
   -4.246e-6    ,    -26.99e6
   -1.843e-6    ,    -16.09e6
   -0.872e-6    ,    -9.06e6
     0.0        ,    0.0
   0.872e-6     ,    9.06e6
   1.843e-6     ,   16.09e6
No. of strips in a block, No. of points, length of each Block
500    20        750.
 Curvature      ,     Moment
   -100.e-6     ,    -150.e6
   -10.447e-6   ,    -25.58e6
   -6.630e-6    ,    -22.18e6
   -3.244e-6    ,    -17.94e6
    -.817e-6    ,    -8.21e6
    0.0         ,    0.0
   0.852e-6     ,    8.47e6
   2.283e-6     ,    16.53e6
   4.000e-6     ,    21.84e6
   7.22e-6      ,    30.57e6
   10.358e-6    ,    38.65e6
   11.557e-6    ,    41.69e6
   13.975e-6    ,    47.72e6
   14.746e-6    ,    50.30e6
   18.093e-6    ,    61.06e6
   19.807e-6    ,    63.24e6
   22.819e-6    ,    66.98e6
   26.687E-6    ,    70.16e6
   27.406E-6    ,    70.22E6
   .1E-3        ,    200.E8
  Tolerance level
  1.e-6
Yield and ultimate moments
9.598600E+07    9.958000E+07    6.925000E+07    7.104000E+07
  No. of load cases
25
  Load case values
  10000


  100000
  110000
  120000
  130000
  140000
  150000
  160000
  170000
  300000
```

Figure 6-8 (Sheet 1 of 3)

UMMARY RESULTS

Load case 23 : 250000.000

	Simple Support	Span	Fixed Support
Calc. BM	-	-0.10472E+09	0.97324E+08
Elastic BM	-	-0.97066E+08	0.11304E+09
Redistribution (%)		7.881	-13.906
Calc. reactions	0.88368E+05		0.16163E+06
Elastic reactions	0.81912E+05		0.16809E+06

Calculated deflection (mm) .7946029E+01 at strip 353
Elastic deflection/EI .3359977E+14

Zero BM position (Calc.) from LH Support 1832.8654
Zero BM position (Elastic) from LH Support 1762.4692

Load case 24 : 270000.000

	Simple Support	Span	Fixed Support
Calc. BM	-	-0.11295E+09	0.10540E+09
Elastic BM	-	-0.10483E+09	0.12209E+09
Redistribution (%)		7.748	-13.670
Calc. reactions	0.95319E+05		0.17468E+06
Elastic reactions	0.88465E+05		0.18154E+06

Calculated deflection (mm) .8392900E+01 at strip 353
Elastic deflection/EI .3628775E+14

Zero BM position (Calc.) from LH Support 1831.6253
Zero BM position (Elastic) from LH Support 1762.4692

Load case 25 : 300000.000

	Simple Support	Span	Fixed Support
Calc. BM	-	-0.12530E+09	0.11753E+09
Elastic BM	-	-0.11648E+09	0.13565E+09
Redistribution (%)		7.571	-13.358
Calc. reactions	0.10574E+06		0.19426E+06
Elastic reactions	0.98294E+05		0.20171E+06

Calculated deflection (mm) .8907714E+01 at strip 353
Elastic deflection/EI .4031972E+14

Zero BM position (Calc.) from LH Support 1829.9838
Zero BM position (Elastic) from LH Support 1762.4692

Figure 6-8 (Sheet 2 of 3)

ITERATION DETAILS

Load #	Sum(+)	Sum(-)	% Error	Res. Def.	Its.
1	0.3290530E+00	-0.3290534E+00	-0.5620212E-04	0.3699E-06	17
2	0.6585666E+00	-0.6585661E+00	0.3572711E-04	0.4706E-06	24
3	0.1040822E+01	-0.1040822E+01	0.1359086E-04	0.2829E-06	34
4	0.1490297E+01	-0.1490297E+01	-0.3742699E-05	-0.1116E-06	33
5	0.2047500E+01	-0.2047500E+01	0.6197823E-05	0.2538E-06	27
6	0.2716179E+01	-0.2716178E+01	0.7734878E-05	0.4202E-06	30
7	0.3453152E+01	-0.3453151E+01	0.6340774E-05	0.4379E-06	33
8	0.4240906E+01	-0.4240905E+01	0.6211827E-05	0.5269E-06	37
9	0.5066253E+01	-0.5066254E+01	-0.6891503E-05	-0.6983E-06	31
10	0.5917805E+01	-0.5917805E+01	-0.8616485E-06	-0.1020E-06	36
11	0.6791357E+01	-0.6791358E+01	-0.2662967E-05	-0.3617E-06	37
12	0.7683264E+01	-0.7683265E+01	-0.2502870E-05	-0.3846E-06	36
13	0.8583749E+01	-0.8583749E+01	0.9551547E-06	0.1640E-06	34
14	0.9486390E+01	-0.9486390E+01	0.8644303E-06	0.1640E-06	36
15	0.1039231E+02	-0.1039231E+02	-0.1494230E-06	-0.3106E-07	33
16	0.1131443E+02	-0.1131443E+02	0.3683613E-05	0.8336E-06	33
17	0.1228773E+02	-0.1228773E+02	0.4236256E-06	0.1041E-06	37
18	0.1331785E+02	-0.1331785E+02	0.1190163E-06	0.3170E-07	35
19	0.1436232E+02	-0.1436232E+02	0.6826870E-06	0.1961E-06	36
20	0.1537942E+02	-0.1537942E+02	-0.2724422E-05	-0.8380E-06	36
21	0.1638250E+02	-0.1638250E+02	-0.5503702E-06	-0.1803E-06	39
22	0.1736329E+02	-0.1736329E+02	0.8256810E-06	0.2867E-06	36
23	0.1981965E+02	-0.1981966E+02	-0.1511936E-05	-0.5993E-06	40
24	0.2114086E+02	-0.2114086E+02	0.1279834E-05	0.5411E-06	37
25	0.2278075E+02	-0.2278075E+02	-0.1135028E-05	-0.5171E-06	36

Figure 6-8 (Sheet 3 of 3)

CHAPTER SEVEN

7. MOMENT CURVATURE RELATIONSHIPS ACCORDING TO CODES OF PRACTICE

7.1 Introduction

Most present reinforced concrete standards recognise the non-linear behaviour of concrete structures in section design by allowing limited moment redistribution. A common parameter governing moment redistribution used by many codes is $\frac{x}{d}$, the neutral axis depth ratio, x being the neutral axis depth, and d the effective depth of a section. The neutral axis depth may be expressed as a function of the curvature and concrete compressive strain of a section, that is:

$$x = \frac{\varepsilon_c}{\varphi} \qquad \textit{Equation 7-1}$$

Where:-

ε_c = Concrete compressive strain at the outermost fibre.

φ = Curvature of the section.

The neutral axis depth ratio is used by many standards as a ductility indicator to limit the amount of redistribution allowed. Any evaluation of the neutral axis depth and redistribution requires knowledge of the moment curvature relationship of the sections in a reinforced concrete structure. In this chapter, the moment curvature relationship and moment redistribution requirements of three major European codes and the American code are identified and presented.

The four standards stated below were chosen by the author for their influential role in reinforced concrete design practice throughout Europe and the United states. The author considered the moment curvature relationship provisions in the following codes:

1. The British Standard BS 8110, The Structural Use of Concrete (1985)
2. ACI 318-95 Building Code Requirements for Structural Concrete.

3. Eurocode 2: Design of concrete structures: Part 1. General Rules and Rules for Buildings (1992).
4. Comité Euro-International Du Beton CEB-FIP Model Code (1990).

The purpose was to investigate moment redistribution that resulted from the codes moment curvature relationships when applied to the author's propped cantilever model described in Chapter Six. The modelled redistribution values resulting from these moment curvature relationships were then compared with the standards' own moment redistribution criteria. This comparison is presented and discussed in Chapter Eight. Before this, the four codes' moment curvature relationships and redistribution provisions will be presented next in this chapter.

In all the aforementioned codes, the moment curvature relationships can be divided into three parts; the uncracked, cracked and yielded sections. **sixth** shows a general schematic of a moment curvature relationship with the main stages considered by the various codes. In each segment of the curve in **Figure 7-1**, each code has its assumptions regarding material properties, stiffness and stress-strain relationship of the concrete and the reinforcement.

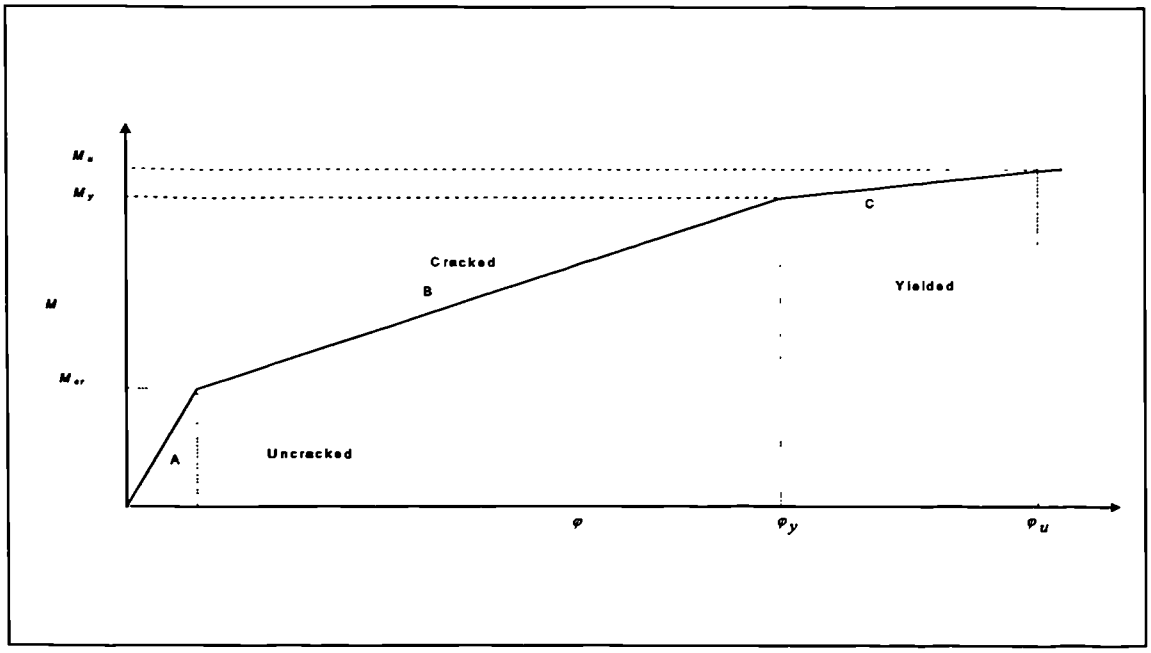

Figure 7-1: Schematic Moment Curvature Relationship

Moment curvature relationships generated by the codes' provisions up to yield, have for their upper and lower limits, the curves for the uncracked and cracked sections respectively. **fifth** shows a sample of codes' moment curvature relationship

falling between the cracked and the uncracked curves from zero loading up to yield. The uncracked section analysis is relevant when an applied bending moment is small enough for the maximum concrete tensile stress not to exceed the modulus of rupture of the concrete. To evaluate the uncracked portion of the moment curvature relationship shown in **Figure 7-2**, the following equation of the section modulus and the associated neutral axis depth was used in this study. See Kong and Evans (1978):

$$I_u = \frac{bh^3}{12} + bh\left(x - \frac{h}{2}\right)^2 + \alpha A_s'\left(x - d'\right)^2 + \alpha A_s\left(d - x^2\right) \qquad \textit{Equation 7-2}$$

$$x = \frac{\frac{bh^2}{2} + \alpha A_s' d' + \alpha A_s d}{\left(bh + \alpha A_s + \alpha A_s'\right)} \qquad \textit{Equation 7-3}$$

$$\varphi = \frac{M}{E_c I_u} \qquad \textit{Equation 7-4}$$

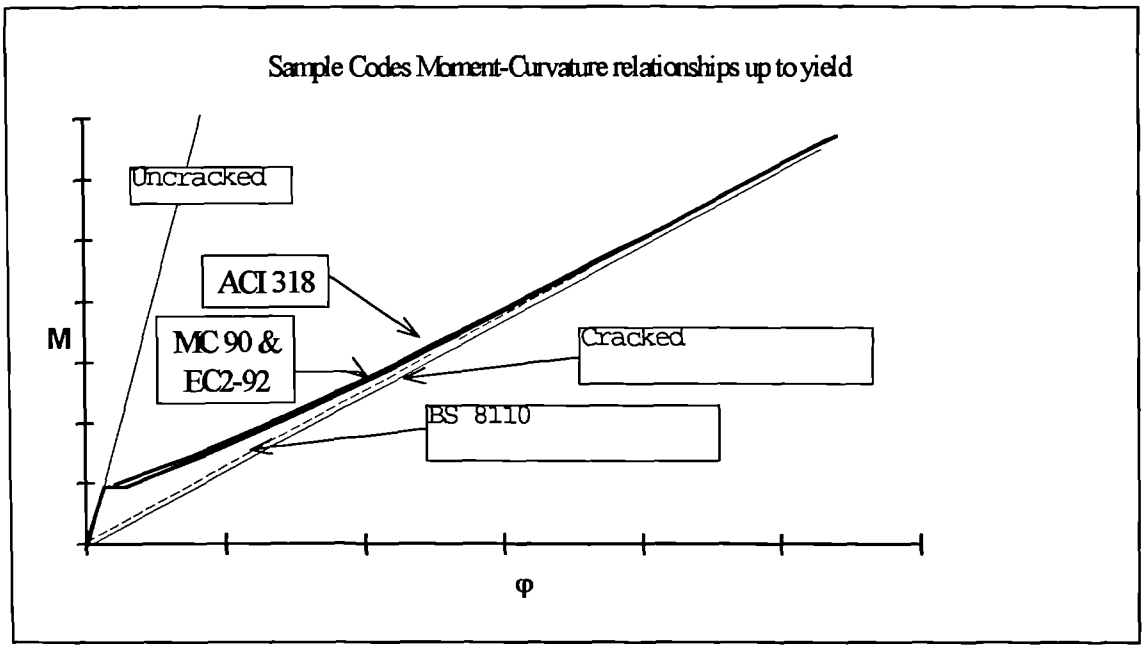

Figure 7-2: Shows sample moment curvature relationships for codes of practice

The cracked section modulus, neutral axis depth and curvature can be calculated according to the following equations. See Kong and Evans (1978):-

$$I_c = \frac{bx^3}{3} + \alpha A_s (d-x)^2 + \alpha A_s^{'} (x-d')^2 \qquad \textit{Equation 7-5}$$

$$\frac{x}{d} = -\alpha(\rho+\rho') + \sqrt{\alpha^2(\rho+\rho')^2 + 2\alpha\left(\rho + \frac{\rho d'}{d}\right)} \qquad \textit{Equation 7-6}$$

$$\varphi = \frac{M}{E_c I_c} \qquad \textit{Equation 7-7}$$

The parameters listed below were required by the author to formulate the moment curvature relationship between zero moment and up to yield:

1. Compressive Strength of Concrete.
2. Tensile Strength of Concrete.
3. Steel and Concrete Modulus of Elasticity.
4. Calculation of Moments Curvatures and Stiffness.

Each parameter is now considered in turn in the context of the provision of the four codes listed above.

7.2 Compressive Strength of Concrete

In all the codes considered, except BS 8110 which uses cube crushing strength f_{cu}, the cylinder compressive strength of concrete $f_c^{'}$ is used. The relationship which was used to relate cylinder strength is as follows: (see Wang and Salmon, 1979)

$f_c^{'} = 0.80 f_{cu}$ *Equation 7-8.*

Where:-

$f_c^{'}$ = Concrete Cylinder Compressive Strength.(MPa).

f_{cu} = Concrete Cube Compressive Strength. (MPa).

The average value for the cube compression test for all specimens was 50 MPa (see **Table 3-1**). The ACI 318, EC 2 and MC 90 codes relate cube to cylinder test according to **Equation 7-8**. Therefore the concrete compressive strength used for all the codes is 50 and 40 MPa for cube and cylinder compression strength respectively.

7.3 Tensile Strength of Concrete

BS 8110 recognises that some concrete in tension is still active below the neutral axis and can be incorporated into section analysis. For short term loading, the concrete is assumed to carry a small tensile stress of 1.0 MPa at the level of the tension steel.

In the ACI[1] code, the tensile strength of concrete is based on an estimated split cylinder strength. Based on statistical data the ACI code expresses the modulus of rupture of the concrete (concrete tensile strength) in terms of cylinder compressive strength f_c' as accepted by ACI (9.5.2.3) in the following equation:-

$$f_{ct} = 0.62\sqrt{f_c'} \qquad \textit{Equation 7-9}$$

Where:-

f_{ct} = Concrete Tensile Strength (MPa)

The tensile strength of concrete is covered by EC 2 cl 3.1.2.3 and EC 2 cl 3.1.2.3(4). The relationship between the characteristic cylinder compressive strength f_c' and the mean concrete tensile strength f_{ct} is given in EC 2 cl 3.1.2.3 (4).

$f_{ct} = 0.30 f_c'^{2/3}$

$f_{ct} = f_{ctk\,0.05} = 0.70 f_{ct}$ (lower characteristic strength).

$f_{ct} = f_{ctk\,0.95} = 1.3\ f_{ct}$ (upper characteristic strength).

The author used the lower limit of the characteristic tensile strength since it was closer to the actual measured values.

The Model Code (MC 90), section 2.1.3.3.1, in a similar manner to EC 2, gives two equations for determining axial tensile strength f_{ct} which is determined according to RILEM CPC 7. Without more accurate data for a particular concrete, the lower and upper bound values of the characteristic tensile strength are used according to the following codes' equations 2.1-2 and 2.1-3:

$$f_{ct} = f_{ctk,\min} = f_{ctko,\min}\left(\frac{f_c'}{f_{cko}}\right)^{\frac{2}{3}} \qquad \textit{(MC Eq. 2-1-2) Equation 7-10}$$

[1] All ACI formulae used by the author are expressed in SI units

$$f_{ct} = f_{ctk,\max} = f_{ctko,\max}\left(\frac{f_c'}{f_{cko}}\right)^{\frac{2}{3}} \qquad \textit{(MC Eq. 2-1-3) Equation 7-11}$$

Where:-

$f_{ctko,min}$ = 0.95 MPa.

$f_{ctko,max}$ = 1.85 MPa.

f_{cmo} = 10 Mpa.

$f_{ctk,min}$ = Lower bound tensile strength of the concrete.

$f_{ctk,max}$ = Upper bound tensile strength of the concrete.

The author used the lower bound tensile strength since it was more appropriate and compared well the average experimental values listed in **Table 3-2**

7.4 Steel and Concrete Modulus of Elasticity

For all the four codes, the steel modulus used in the analysis was 200 GPa based on the experimental stress strain curve of the reinforcement shown later in **Figure 7-6.**

In BS 8110 the concrete modulus of elasticity is a function of the concrete crushing strength. If an accurate calculation of deformation is required, BS 8110 recommends the determination of the modulus of elasticity based on actual cube crushing tests. The BS 8110 mean values for E_c is calculated from the following expression:

$$E_c = 20 + \frac{f_{cu}}{5} \qquad \textit{Equation 7-12}$$

Where:-

E_c = Concrete Modulus of Elasticity.

The modulus of elasticity of concrete has been approximated in the ACI code as the result of a statistical analysis of available data in the following empirical formula presented here in SI units:

$$E_c = 4.73\sqrt{f_c'} \qquad \textit{Equation 7-13} \text{ (Eq. ACI(8.5.1))}$$

The EC 2 modulus of elasticity used in the modelling of the moment curvature relationship is stated in EC 2 cl 3.1.2.5.2. Typical values of E_C is given in EC 2 Table

3.2 , based on the concrete compressive strength classes in EC 2 cl 3.1.2.5.2 (3). The values listed in EC 2 Table 3.2 are based on the following equation:

$$E_c = 9.5(f_c' + 8.0)^{\frac{1}{3}} \qquad \textit{Equation 7-14}$$

The Model Code proposes two values of the modulus of elasticity for normal weight concrete that can be estimated from the specified characteristic strength. These values can be found in the code's **Table 2.1.6**. Where the actual compressive strength of concrete at an age of 28 days is known E_c is determined from the following formula:-

$$E_c = \left[\frac{\left(f_c' + 8\right)}{0.0022 \times 1000}\right] \qquad \textit{Equation 7-15}$$

7.5 Calculation of Moments, Curvatures and Stiffness

7.5.1 BS 8110 (1985)

Before cracking, BS 8110 prescribes the uncracked transformed section and the associated neutral axis depth ratio for the calculation of curvature in the uncracked state, which were presented earlier in **Equations 7-2** to **7-4**. After cracking, the moment curvature relationship in BS 8110 is based on the partially cracked section. **Figure 7-3** shows the stress and strain profile of a partially cracked section. In the tension zone and below the neutral axis, it assumes that concrete carries some tension. Such assumptions have a direct impact on the evaluation of the neutral axis depth which in varies with the magnitude of the applied moment. However, for practical applications, a simplified assumption may be used where the neutral axis depth is assumed to be the same for both partially cracked and fully cracked sections respectively. See Kong and Evans (1987). Therefore, it is determined using **Equation 7-6.**

The small concrete tensile stress of 1.0 MPa causes a small moment due to the concrete in tension that is:

$$M_{ctm} = \frac{b(h-x)^3 f_{ct}}{3(d-x)}$$ *Equation 7-16*

Where:-

M_{ctm} = The moment caused by the concrete in tension.

The latter assumptions of stress strain distribution shown in **Figure 7-3** gives the following expression for the effective second moment of area to be used in the calculation of curvature at the section. See Reynolds and Steedman (1988).

$$\frac{I_e}{bd^3} = \left[\frac{1}{3}\left(\frac{x}{d}\right)^3 + \alpha\rho\left(1-\frac{x}{d}\right)^2 + (\alpha-1)\rho'\left(\frac{x}{d}-\frac{d'}{d}\right)^2\right]$$ *Equation 7-17*

It follows that when a moment M is applied to the partially cracked section, part of it is resisted by the concrete tension (M_{ctm}). The net moment (M_{net}) to be resisted by the concrete compression and by the forces in the reinforcement is

$M_{net} = M - M_{ctm}$ *Equation 7-18*

$$\varphi = \frac{M_{net}}{E_c I_e}$$ *Equation 7-19*

Where:-

I_e = The effective Second moment of area

M = The applied bending moment on the section

M_{net} = Net applied Moment which the moment M_{ctm} is subtracted from the applied moment. *($M_{net} = M - M_{ctm}$)*

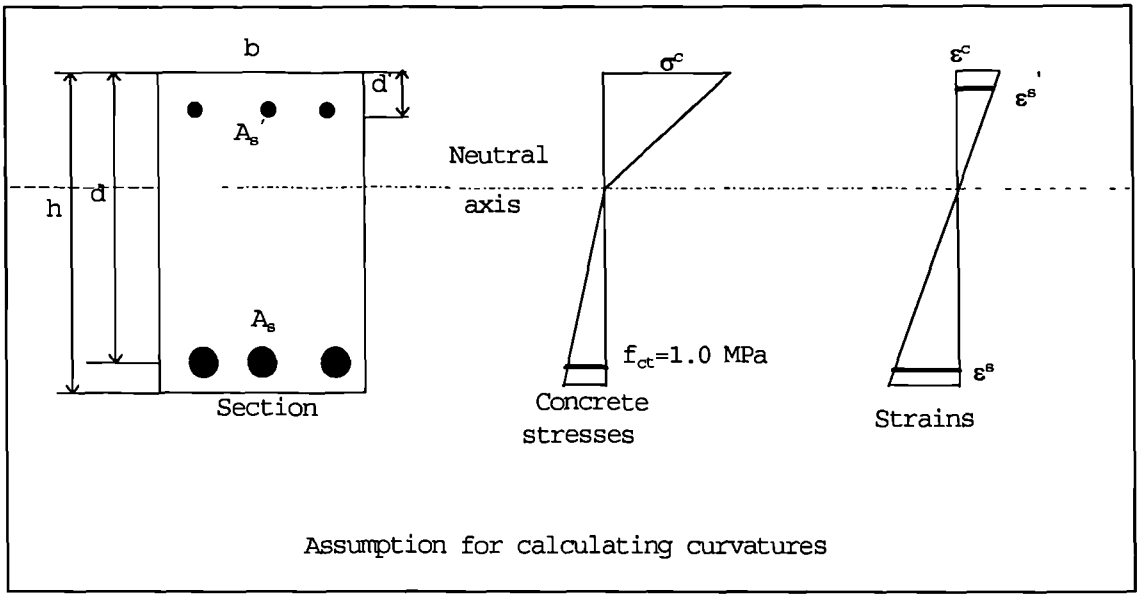

Figure 7-3: Shows stress and strain profile of partially cracked section

7.5.2 ACI 318 (1995)

The American Concrete Institute Code allows for the uncracked portion of the moment curvature relationship to be calculated based on the following equation. Notice all constants have been redefined by the author in S.I. units to facilitate comparison with the other codes being considered:-

$$\varphi = \frac{M}{E_c I_g} \qquad \textit{Equation 7-20}$$

Where:-

I_g = ($bh^3/12$) Gross second moment of area neglecting reinforcement.

After cracking, the ACI code section 9.5.2.3 formula 9-7 uses the expression below **(Equation 7-21)** to calculate the effective second moment of area, which includes the effects of load level and degree of cracking developed by Branson. See Wang and Salmon (1979):-

$$I_e = \left(\frac{M_{cr}}{M}\right)^3 I_g + \left(1 - \frac{M_{cr}}{M}\right)^3 I_c \qquad \textit{Equation 7-21}$$

Where:-

$$M_{cr} = \frac{f_{ct} I_g}{y_t}$$ *Equation 7-22*

E_C = $4.730\sqrt{f_c'}$

f_{ct} = $0.62\sqrt{f_c'}$

f_C' = $0.80 f_{cu}$

y_t = Distance from neutral axis to extreme fibre of concrete in tension neglecting reinforcement i.e. (h/2).

The cracked second moment of area is calculated based on **Equation 7-5**, with the only difference being that the ACI code prefers the rounding up of the modular ratio (α) to the nearest integer. To compensate for the voids in the concrete in compression 2α-1 is used. Furthermore, the neutral axis depth can also be calculated using the following polynomial formula derived from the force equilibrium of the cross section:

$$\frac{bx^2}{2} + (2\alpha - 1)A_s'(x - d') = \alpha A_s(d - x)$$ *Equation 7-23*

From the above equations it is possible to evaluate stiffness as it varies under the applied load up to yield. Using the ACI 318 formulae, the moment curvature relationship is calculated, with the curvature being:-

$$\varphi = \frac{M}{E_c I_e}$$ *Equation 7-24*

7.5.3 Eurocode 2 (1992)

EC 2 recommends two alternatives to determining the moment curvature relationship, a refined and a simplified approach, EC 2 clauses A2.2 (3) and A2.2(1) respectively. The code gives a generalised equation for calculating curvature, rotation and strains or deflection. Equation EC 2 Equation A4.1 is shown below:

$$\omega = \xi\omega_{II} + (1 - \zeta)\omega_I$$ *Equation 7-25 (EC 2 Equation A4.1)*

Where:-

ω_I, ω_{II} Are the parameter curvatures at the uncracked and cracked state respectively

ζ is a distribution coefficient given by equation EC 2 A4.2

ζ Is zero for an uncracked section.

$$\zeta = 1 - \beta_1 \beta_2 \left(\frac{M_{cr}}{M} \right)^2$$ *Equation 7-26* (EC 2 Equation A4.2)

ω = The parameter which to be calculated at a particular applied load. In this case, it is curvature.

β_1 = Coefficient taking into account the bond properties of the bar 1.0 for High bond bars and 0.5 for plain bars.

β_2 = Coefficient taking account of load duration. β_2 =1.0 for a single short -term loading and 0.5 for sustained loads or cyclic loading.

$$M_{cr} = \frac{f_{ct} I_u}{(h - x)}$$ *Equation 7-27*

7.5.4 CEB-FIP Model Code (1990)

The CEB-FIP Model Code, like the EC 2 code, for the uncracked section, the same principles apply. Curvatures are calculated based on the uncracked modulus. After cracking, the following MC 90 equation 3.6-2a applies:-

$$\varphi = \varphi - (\varphi_{2r} - \varphi_{1r}) \beta_b \left(\frac{M_{cr}}{M} \right)$$ *Equation 7-28* (MC eq. 3.6-2a)

For moments greater than the yield moments the following MC equation 3.6-2c applies:

$$\varphi = \varphi - (\varphi_{2r} - \varphi_{1r}) \beta_b \left(\frac{M_{cr}}{M} \right) + \frac{(M - M_y)}{2K_{III}}$$ *Equation 7-29* (MC eq. 3.6-2c)

Where:-

$$K_{III} = \frac{(M_u - M_y)}{(\varphi_u - \varphi_y)}$$ *Equation 7-30*

M_{cr} = $(E_c I_g f_{ct})$

φ_1 , φ_{1r} = Uncracked curvatures corresponding to the action of M and M_{cr} respectively.

φ_2, φ_{2r} = Cracked curvatures corresponding to M and M_{cr} respectively.

The calculation of the cracked and uncracked state are established by using correction coefficients κ_{s1} and κ_{s2} , which can be found from graphs in the CEB Manual on Cracking and Deformation (1985), or alternatively can be calculated from formulae stated in the manual. The author chose to calculate these factors through a purpose written program.

β_b = Coefficients representing the bond quality of the bars and the influence of duration of application or repetition of loading. The values of these coefficients are 1.0 and 0.8 for β_1 and β_2 respectively. The two coefficient are combined to give the value of β_b

7.6 Concrete Stress Strain Relationship

BS 8110 recommends the following formula:

$$\sigma = 5500\varepsilon_c\left(\frac{\sqrt{f_{cu}}}{\gamma_m} - \frac{\varepsilon_c}{4125.0}\right) \qquad \textit{Equation 7-31}$$

Where:-

f_{cu} = Cube strength.

Υ_m = Concrete Partial Safety Factor taken as 1.0 for the concrete stress-strain relationship.

σ , ε_c = Stress and strain respectively.

The ACI code allows the use of any stress strain relationship for the concrete in compression as long as this relationship is compatible with compressive test results. ACI 318 states in Article 10.2.6:

> "Relationship between concrete compressive stress distribution and concrete strain may be assumed to be rectangular, trapezoidal, parabolic or any other shape that results in prediction of strength in substantial agreement with results of compressive tests."

Many equations for the stress-strain curve of concrete under uniaxial compression were proposed in the past. See Hognestad (1955) and Popovics (1970). After consideration of the ACI code's recommendations and design textbooks that have been reviewed, and based on ACI article 10.2.6, Hognestad equation was used in the analysis. See Wang and Salmon (1979)

Hognestad's equation for ACI 318-95 is:

$$\sigma = f_c''\left(\frac{2\varepsilon_c}{\varepsilon_{ce}} - \left(\frac{\varepsilon_c}{\varepsilon_{ce}}\right)^2\right) \qquad \textit{Equation 7-32}$$

Where:-

ε_{ce} = 0.0022

f_c'' = $0.85f_c'$ *Equation 7-33*

The EC 2 code stress strain relationship for concrete subjected to uniaxial compression is stated in section 4.2.1.3.3 of the code. For short term loading, EC 2-92 recommends the following formula in (EC 2 cl 4.2.1.3.3 (5) equation 4.2):-

$$\sigma = \frac{\left(k'n - n^2\right)}{\left(1+\left(k'-2\right)n\right)} f_c' \qquad \textit{Equation 7-34}$$

Where:-

n = $\varepsilon_c/\varepsilon_{ce}$

f_c' = Characteristic compressive strength of the concrete.

$$k' = 1.10E_c\left(\frac{\varepsilon_{ce}}{\left(f_c' + 8\right)}\right) \qquad \textit{Equation 7-35}$$

EC 2 code allows the use of other stress strain diagrams (e.g. bi-linear), (refer to EC 2 4.2.1.3.3 clauses 8 to 10) provided they are equivalent to the above equation (7-34)

The CEB-FIP Model Code uses three stress strain curves for the concrete in compression.

1. Section 2.1.4.4.1 using uniaxial compression.
2. Section 6.2.2.2 parabola rectangle diagram.

3. Section 6.2.2.2 the uniform stress diagram..

The first consists of a complete profile of relationship approximated by equation 2.1-18 in the Model Code and includes a descending portion. This stress strain relationship is used for short term analysis. The ultimate strain varies according to the concrete grade as specified by the codes table 2.1.7. For this analysis, the author used the first option stated above in order to be consistent with the choices made in the other codes of practice for a coherent comparison. The following stress strain relationship of the concrete in compression was used:-

$$\sigma = \frac{\frac{E_{ci}}{E_c}\frac{\varepsilon_c}{\varepsilon_{ce}} - \left(\frac{\varepsilon_c}{\varepsilon_{ce}}\right)^2}{1+\left(\frac{\varepsilon_c}{\varepsilon_{ce}}\right)\left(\frac{E_{ci}}{E_c}-2\right)}(f_c'+8) \quad for \quad |\varepsilon_c| \subset |\varepsilon_{c,\lim}| \text{ (MC 2.1-18) Equation 7-36}$$

Where:-

$$E_{ci} = E_{co}\left(\frac{\left(f_c'+8\right)}{f_{cmo}}\right)^{\frac{1}{3}} \text{ Tangent modulus Equation } MC\ 2.1\text{-}16\ Equation\ 7\text{-}37$$

Where:-

f_{cmo}= *10 MPa*

E_{co}= *2.15 x 10⁴*

The value of ($\varepsilon_{c,lim}$) is calculated using Model Code equation 2.1-19:

$$\frac{\varepsilon_{c,\lim}}{-0.0022} = \frac{1}{2}\left(\frac{1}{2}\frac{E_{ci}}{E_c}+1\right)+\left[\frac{1}{4}\left(\frac{1}{2}\frac{E_{ci}}{E_c}+1\right)^2-\frac{1}{2}\right]^{\frac{1}{2}} \qquad Equation\ 7\text{-}38$$

Where:-

$\varepsilon_{c,lim}$ = Limiting concrete compressive strain on the descending branch of the concrete stress strain relationship.

7.7 Application of Codes Equations for the Concrete in Compression

All the standards show idealised stress strain curves for the concrete in compression. BS 8110, the CEB-FIP Model code and Eurocode 2 allow the use of parabolic rectangular curves with a flat top simplification for the descending branch. The concrete in compression stress strain equations presented in 7.6 were used to calculate moments and curvatures at the ultimate state. **third** illustrates the various concrete stress strain curves used. All codes recommend a flat top idealisation of the stress-strain relationship at a certain concrete ultimate compression strain ε_{cu}. The condition for determining the ultimate strain at the compressive edge of the concrete (ε_{cu} = 3500 microstrain) is the same for all codes except the ACI which uses a value of 3000 microstrain.

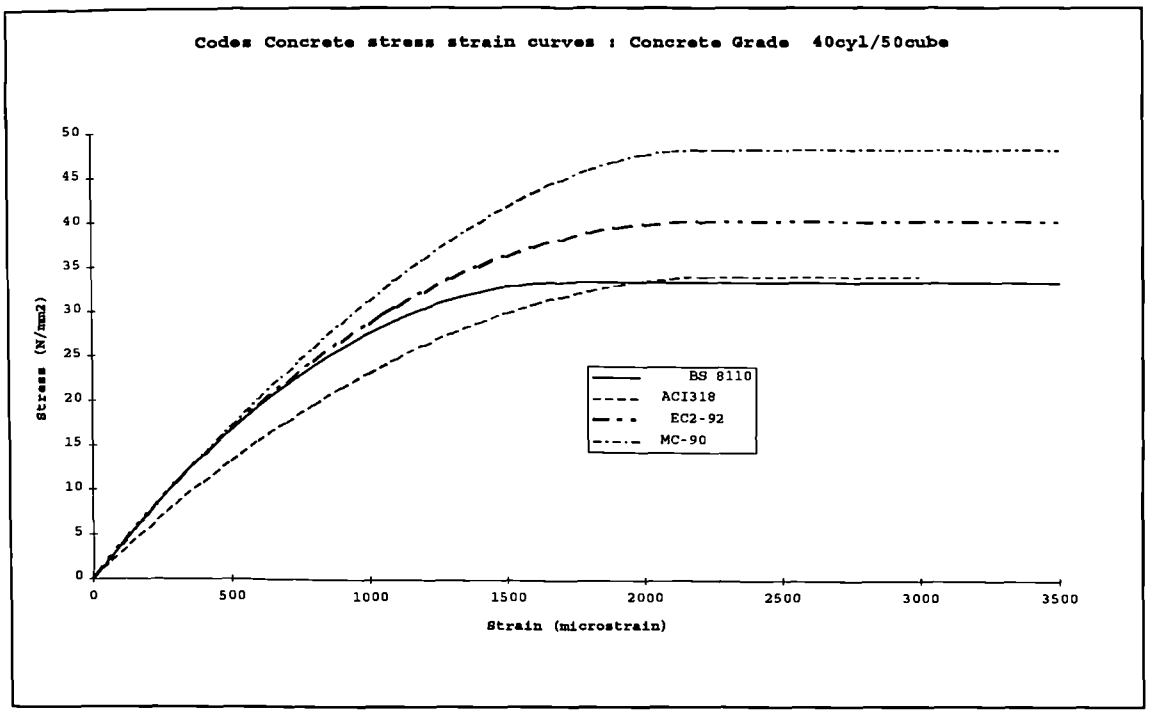

Figure 7-4: Codes Concrete Stress-Strain Relationship of Concrete in Compression

7.8 Application of the Stress Strain Relationship for the Reinforcement

All four standards allow bilinear idealisation of reinforcement stress strain curves. Compression reinforcement stress strain relationships are not clearly specified except in BS 8110 design curves, where curves for steel in compression are the same as in tension. The author used measured stress strain relationships for all codes except

Eurocode 2, where a flat top horizontal idealisation was used according to EC 2 clause [4.2.2.3.2. p(3)] and shown in **Figure 7-5.**

Neither the ACI or BS 8110 codes give any direct information on ductility requirements for tension reinforcement yield strains. The yield strain were taken at 0.2% offset strain. **Figure 7-6** shows the experimental stress strain curves used for the reinforcement in the analysis and a schematic superimposed showing how the yield point was determined. For the yield point of the high yield bars, it was calculated by taking a parallel line at 0.2 percent strain for each bar stress-strain curve in **Figure 7-5.** At the point of intersection of this line with the stress-strain curve, lines were projected to both the stress and strain axes to determine the yield stress and strain for each different bar diameter. **sixth** lists experimental yield stress and strain for all rod diameters. Since the yield stress and strain are known, it is possible to calculate the yield moments and curvatures. These calculations were made numerically using the purpose written software presented later in Chapter Eight.

Rod type	Rod Diameter (mm)	Yield Strain (microstrain)	Yield Stress (MPa)
High Yield Bar	6	2400	500
High Yield Bar	8	4600	540
High Yield Bar	10 & 12	5900	460
High Yield Bar	16	4100	613
High Yield Bar	20	3100	545
Wire	8	4600	464
Wire	10	4600	532
Wire	12	4600	504

Table 7-1: Yield strain for reinforcing bars used in the test beams

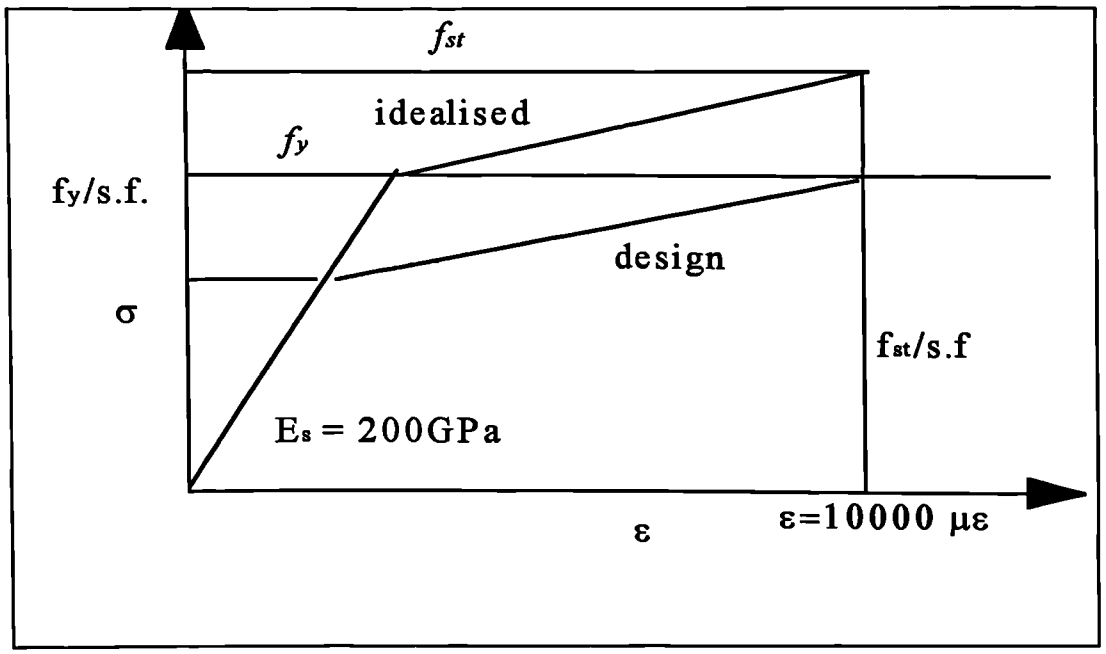

Figure 7-5: EC 2 Design and idealised stress-strain diagram for reinforcing steel

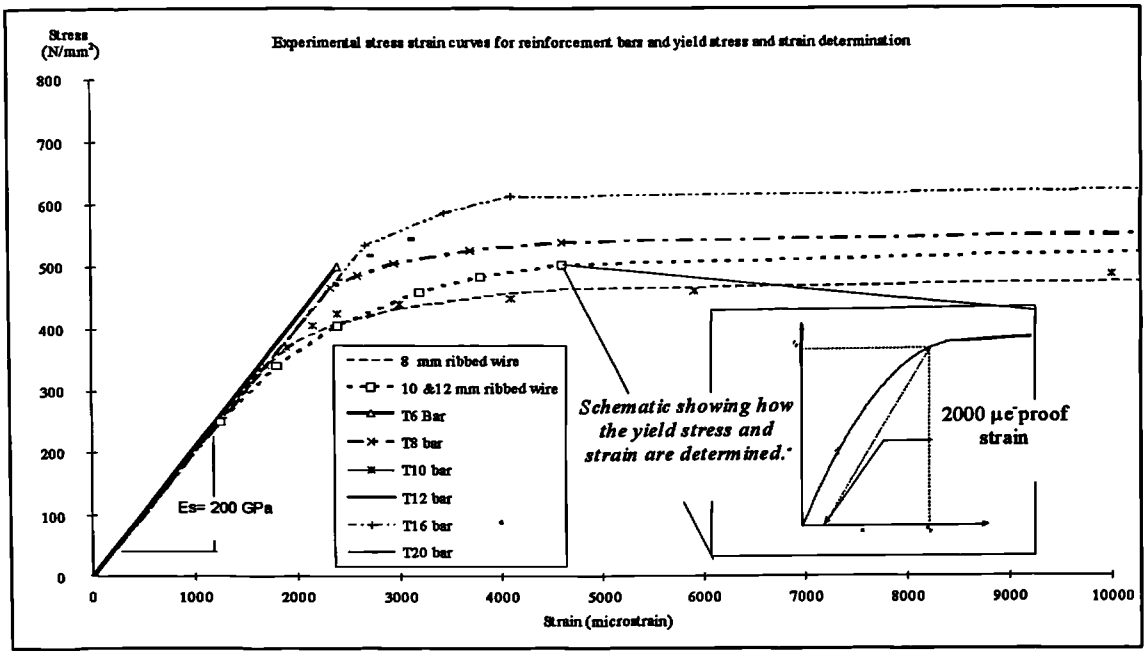

Figure 7-6: Experimental stress strain curves of bars used in test beams

7.9 Summary and Comments

This chapter up to section 7-8 illustrates how the different codes of practice (BS 8110, the ACI 318-95, EC 2-92 and CEB-FIP MC 90) treat material properties and moment curvature relationships.

In summary, the methods for specifying the characteristic concrete compressive strength are very similar in all the codes except BS 8110 which favours the use of cube

test results. The other three codes ACI, EC 2 and MC 90 relate the cylinder to cube strengths at an approximate ratio ($f_c' = 0.80\, f_{cu}$). Both EC 2 and MC 90 use dual notation of concrete strength which is useful to avoid the problems associated with the conversion of cube to cylinder test results and vice versa.

As the tensile strength of concrete is quite small, it is mostly ignored in the assessment of the moment curvature relationship as it does not appreciably affect section ductility. See Cohn and Gosh (1973). There are considerable difficulties in the measurement of concrete tensile strength, and it is normally measured indirectly. The two main methods of indirect measurement are the cylinder splitting test and the flexural modulus of rupture test.

Unlike the other codes, (ACI 318, EC 2 and MC 90), BS 8110 deals with concrete in tension by suggesting that a 1.0 MPa tensile stress be used rather than by presenting a formula for direct calculation of stiffness. However, this method used by the BS 8110 leads to some complexity in the ensuing calculations of the neutral axis depth and the associated section modulus.

In the absence of accurate data, the two European codes EC 2 and MC 90 give similar upper and lower limits on the concrete tensile strength as a function of the concrete compressive strength. This is advantageous especially with the limited number of test specimens the author examined.

The ACI code gives an approximate but fixed equation for the concrete tensile strength which may lead in some instances to overestimation of the concrete tensile strength. All concrete tensile strength relations allowed by the ACI, EC 2 and MC 90 codes depend on the type and grading of the aggregate and the age of the concrete.

Both EC 2 and MC 90 use a variety of concrete moduli depending on the purpose for which they are required (i.e. design or analysis). The provisions for concrete moduli in EC 2 and MC 90 are flexible and based on concrete age, cement content, concrete moisture and load history. BS 8110 gives typical values in Part 2 Section 7.2 based on concrete compressive strength. If an accurate calculation of deflection is required, BS 8110 recommends the determination of the modulus of elasticity of the actual concrete mix being used. The value of E_c is important in determining the serviceable ductility level available in a beam before yielding. The results of using different E_c values reflect heavily on redistribution at service loads,

shown later in Chapter Eight. The reinforcement modulus of elasticity used in the analysis is the same for each code.

For the yield condition the author used yield criteria based on the experimental stress strain relationships of the reinforcement. The reason for this is that all codes allow very similar idealisation of the stress strain relationship of the reinforcement. If accurate calculations are desired, the codes allow the use of experimental stress strain relationship for the reinforcement. Since the various codes base the steel stress-strain curve on steel manufactured in the specific country in which the code is used, the author decided that it was more suitable to use the experimental stress strain relationships of the steel when determining the moment curvature relationships.

For the ultimate condition, a maximum concrete compressive strain of 3500 microstrain was used for all the codes apart from the ACI where 3000 microstrain is recommended. The author would like to point out that the effect of reinforcement ductility was not experimentally tested, however the numerical model which was developed did examine ductility effects in the reinforcement, as presented later in section 8.13.

The moment curvature relationships according to the codes were calculated using purpose written programs. These are described in detail in section 8.2

Table 7-2 gives a summary of the code provisions used by the author to calculate the moment curvature relationships.

Summary Table of Codes Provisions for Determining The Moment Curvature Relationship				
CODES	**ACI 318-1995**	**BS 8110 1985**	**EUROCODE 2 1992**	**CEB-FIP MODEL CODE 1990**
f_{cu} = ** f_c' =**	*50 MPa Cube* *40 MPa Cylinder*	*50 MPa Cube* *40 MPa Cylinder*	*50 MPa Cube* *40 MPa Cylinder*	*50 MPa Cube* *40 MPa Cylinder*
f_{ct} =	$f_r = 0.62\sqrt{f_c'}$	*1.0 MPa*	$f_{ctk\,0.05} = 0.70 f_{ctm}$	$f_{ctk,\min} = f_{ctko,\min}\left(\frac{f_c'}{f_{cko}}\right)^{\frac{2}{3}}$
E_c=	$E_c = 4730.0\sqrt{f_c'}$	$E_c = 20 + \frac{f_{cu}}{5}$	$E_c = 9.5\left(f_c' + 8.0\right)^{\frac{1}{3}}$	$E_c = \frac{\left(f_c' + 8.0\right)}{0.0022}$
M_{cr} =	$M_{cr} = \frac{f_{ct} I_g}{y_t}$	$M_{ctm} = \frac{b(h-x)^3 f_{ct}}{3(d-x)}$	$M_{cr} = \frac{f_{ct} I_u}{(h-x)}$	$M_{cr} = \frac{f_{ct} I_u}{(h-x)}$
Concrete σ-ε *Relationship*	$\sigma = f_c''\left(\frac{2\varepsilon_c}{\varepsilon_o} - \left(\frac{\varepsilon_c}{\varepsilon_o}\right)^2\right)$	$\sigma = 5500\varepsilon_c\left(\frac{\sqrt{f_{cu}}}{\gamma_m} - \frac{\varepsilon_c}{41250}\right)$	$\sigma = \frac{(kn - n^2)}{(1+(k-2)n)} f_c'$	$\sigma_c = \frac{\frac{E_{ci}}{E_c}\frac{\varepsilon_c}{\varepsilon_e} - \left(\frac{\varepsilon_c}{\varepsilon_e}\right)^2}{1+\left(\frac{\varepsilon_c}{\varepsilon_e}\right)\left(\frac{E_{ci}}{E_c} - 2\right)}\left(f_c' + 8\right)$ for $\left\|\frac{\varepsilon_c}{\varepsilon_e}\right\| \subset \left\|\frac{\varepsilon_{c,lim}}{\varepsilon_e}\right\|$
E_s	*200GPa*	*200GPa*	*200GPa*	*200GPa*
M_y*** φ_y	*Figure 7-6*	*Figure 7-6*	*Figure 7-5*	*Figure 7-6*
M_u φ_u	$\varepsilon_{cu} = .0030$	$\varepsilon_{cu} = .0035$	$\varepsilon_{cu} = .0035$	$\varepsilon_{cu} = .0035$
** *The values for the concrete compressive strengths are based on the average experimental values (see Table 3-1)*				
***Yield moment and curvature are calculated at points corresponding to the yield points in figure 7-5 and 7-6 for the reinforcing bars*				

Table 7-2: Lists Codes provision used to calculate moments and curvature at cracking, yield and ultimate state.

7.10 Codes of Practice Moment Redistribution Criteria

Due to the non-linear behaviour of reinforced concrete structure and the occurrence of moment redistribution as explained in Chapter One, some deviations from the linear elastic design are permitted by all four structural codes being considered. The common idea in all codes is that for each possible loading scheme the elastic moments at a critical section may be modified by a selected amount provided that this amount does not exceed specified permissible limits and equilibrium is maintained through the structure.

7.10.1 British Code BS 8110 (1985)

Redistribution first appeared in the British Code of Practice CP 114 in 1957. For the design of continuous beams it stated that:

> ".. the negative moment at the supports for any assumed arrangement of loading may each be increased or decreased by not more than 15 % provided that these modified negative moments are used for the calculation of the corresponding moments in the spans."

Up to 1972, the criteria for redistribution did not change. During this period extensive research was carried out on the ultimate limit state behaviour, which caused the British code to alter its redistribution criteria to the present form given in BS 8110. The present criteria in BS 8110 clause 3.2.2 lay down three conditions for redistribution.

A. Equilibrium must be maintained between the applied loading and the internal moments and shears at all times under all combinations of loading

B. At the point of maximum moment, the neutral axis depth must satisfy $\frac{x}{d} < 0.6 - \beta$, where β is the percentage of moment redistribution at the section.

C. The moment at any section after redistribution should be at least 70% of the elastic moment envelope.

The British Code criteria imply that where elastic moments are reduced, the beam must be sufficiently ductile to enable plastic hinges to develop and rotation to take place. Increased ductility is ensured for a given strain in the concrete by reducing

further the limiting value of x/d. Neutral axis depth ratio limitation is not required where elastic moments are increased. According to BS 8110, in these regions, the beam does not reach the ultimate limit state until the full design load is applied. Failure of the beam is progressive, requiring rotation at the plastic hinges before collapse occurs. It is not necessary therefore to place restrictions on the value of (x/d), where moments have been increased. Where the full 30% redistribution is utilised, the effect of condition B above, which states that the depth of neutral axis should not be greater than *(0.6-β) d,* is to limit the depth of neutral axis to *0.3d.*

zeroth shows that when redistribution is carried out, there will be regions where the service load produces a hogging moment. However, theoretically no hogging reinforcement would be required at the ultimate limit state (between a and b). This situation is prevented by condition C above which states that the moment of resistance at any section must be at least 70% of the moment derived from elastic analysis.

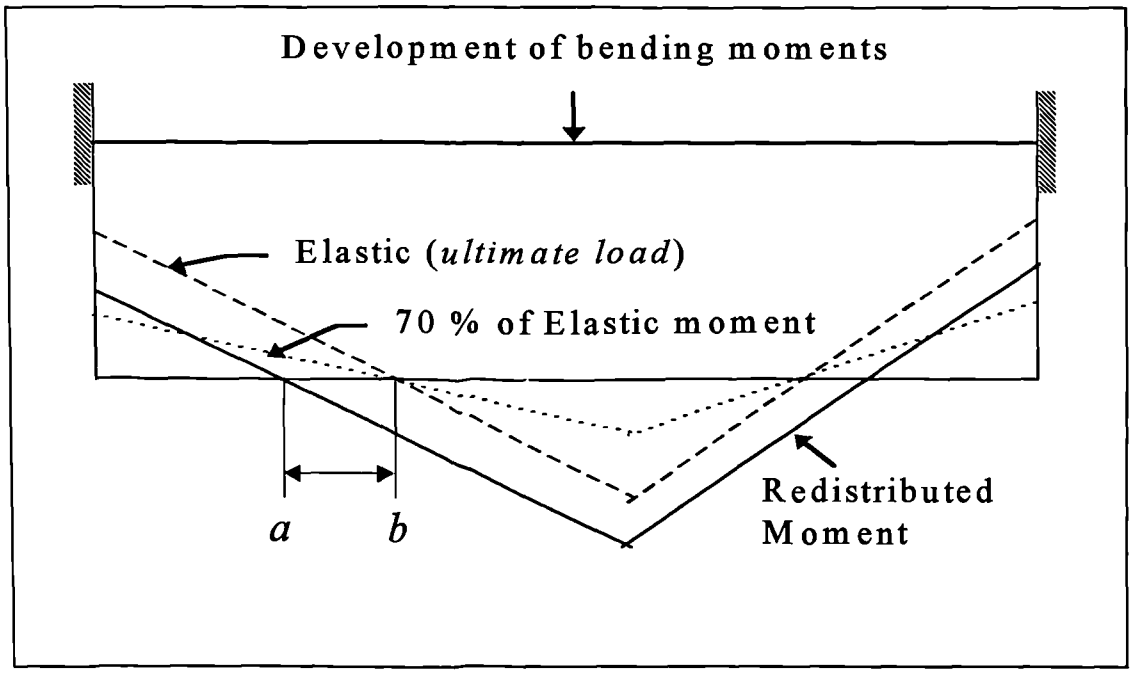

Figure 7-7: Development of bending moment

Redistribution ≤ 10% implies maximum x/d = 0.5; redistribution between 10% and 30% implies maximum $\frac{x}{d} = 0.6 - \beta$, where β ≤ 0.30.

In a structure over four stories high, in which the structural frame provides the lateral stability, the maximum reduction in moment allowed in BS 8110 is limited to 10%. The calculation of the neutral axis depth is not specifically identified, but it is a complicated calculation dependent on the shape of the concrete stress-strain curve and is commonly obtained from standard design charts. It is interesting to note that the code does not place any limitation on redistribution in slabs that are analysed by the yield line method. This could probably be accounted for by the small values of x/d that generally exist in slabs. Furthermore, BS 8110 does not take into consideration the type and distribution of reinforcing steel when checking for redistribution. Additionally, the New Zealand Code of Practice NZ 3101 1982 adopts the same redistribution criteria for continuous beams as BS 8110. **Figure 7-8** demonstrates graphically BS 8110 and NZ 3101 design criteria for redistribution.

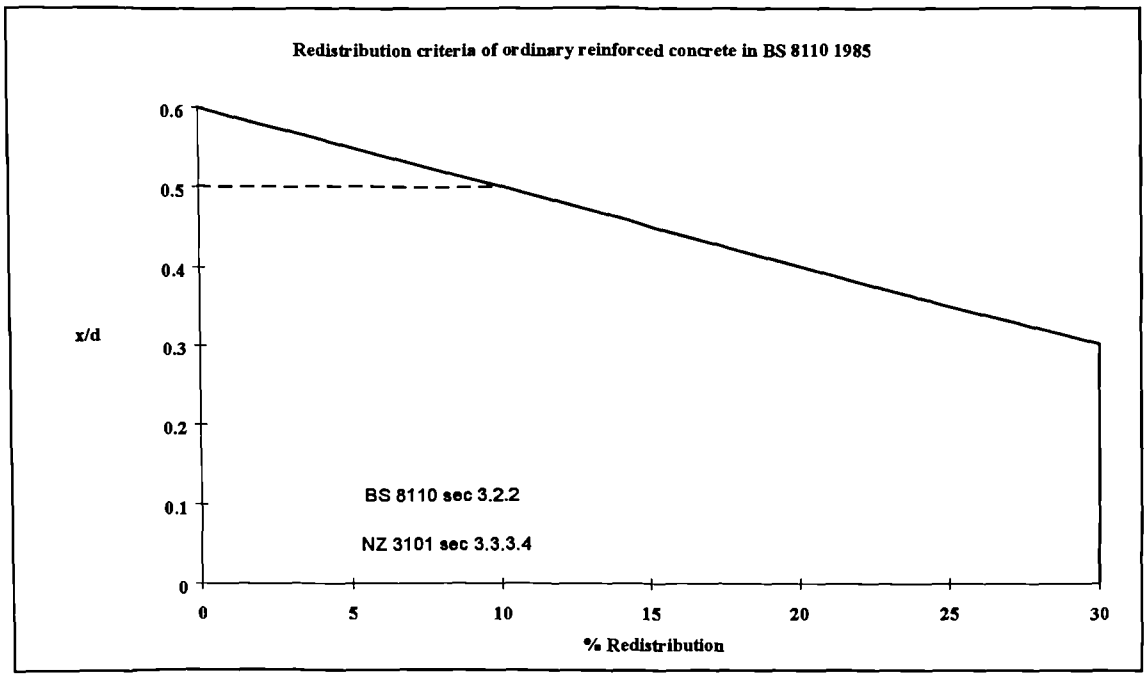

Figure 7-8: Redistribution Criteria in both BS 8110 and Nz-3101 Codes

7.10.2 American Code ACI Code 318-95

The concept of moment redistribution was first introduced into the ACI code in 1963 after considerable research into the limit state behaviour of reinforced concrete continuous beams, (see Wang and Salmon, 1979). Thereafter, concrete design in the American practice moved toward limit state design.

The ductility of reinforced concrete is controlled by the ACI code in a simple and direct manner. For a continuous beam, it specifies the maximum percentage of moments at the supports that can be redistributed. This maximum percentage change of moment is a function of the tension and compression steel ratios. ACI 318 clause 8.4 allows the moments at the supports of continuous beams, calculated by elastic theory, to be increased or decreased by not more than:

$$20\left(1-\frac{\rho-\rho'}{\rho_b}\right)\% \qquad \textit{Equation 7-39}$$

ρ_b is specified in the following equation:-

$$\rho_b = \frac{0.85 f_c'}{f_y}\kappa\left(\frac{0.003}{0.003+\frac{f_y}{E_s}}\right) \qquad \textit{Equation 7-40}$$

Where:

$\kappa = 0.85 - 0.008(f_c' - 30)$

κ is a function of the concrete grade only. See Cohn and Lounis(1991)

Redistribution criteria in the ACI code can be graphically illustrated as shown in **Figure 7-9** in terms of net reinforcement ratio as specified by the code. **Figure 7-10** shows the neutral axis depth ratio and percentage redistribution. The author derived the conversions in **Figure 7-10** to neutral axis depth ratio (described shortly) to facilitate the comparison of the ACI criteria with the other codes. The value of the balanced neutral axis depth ratio $\left(\frac{x_b}{d}\right)$ associated with the (ρ_b) is:

$$\frac{x_b}{d} = \frac{0.003}{0.003+\frac{f_y}{E_s}} \qquad \textit{Equation 7-41}$$

Where:-

x_b = The neutral axis depth at the balanced condition.

The value of the net reinforcement ratio when expressed in terms of the neutral axis ratio becomes:

$$\rho - \rho' = \frac{0.85 f_c' \kappa \left(\frac{x}{d}\right)}{f_y} \qquad \textit{Equation 7-42}$$

Having established the ratio between net reinforcement ratio and the neutral axis depth, it is possible to convert **Equation 7-38** in terms of neutral axis depth ratio as follows:

$$20\left(1 - \frac{\frac{x}{d}}{\frac{x_b}{d}}\right)\% \qquad \textit{Equation 7-43}$$

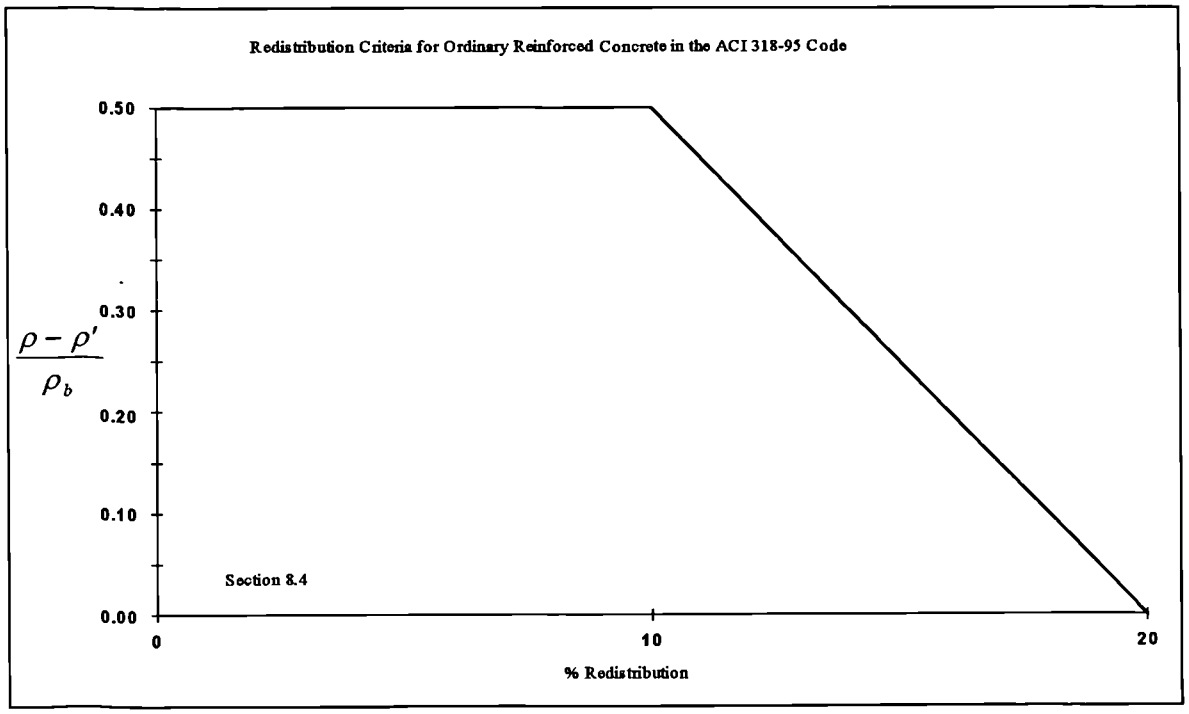

Figure 7-9: ACI 318-95 Redistribution criteria in terms of net reinforcement ratio

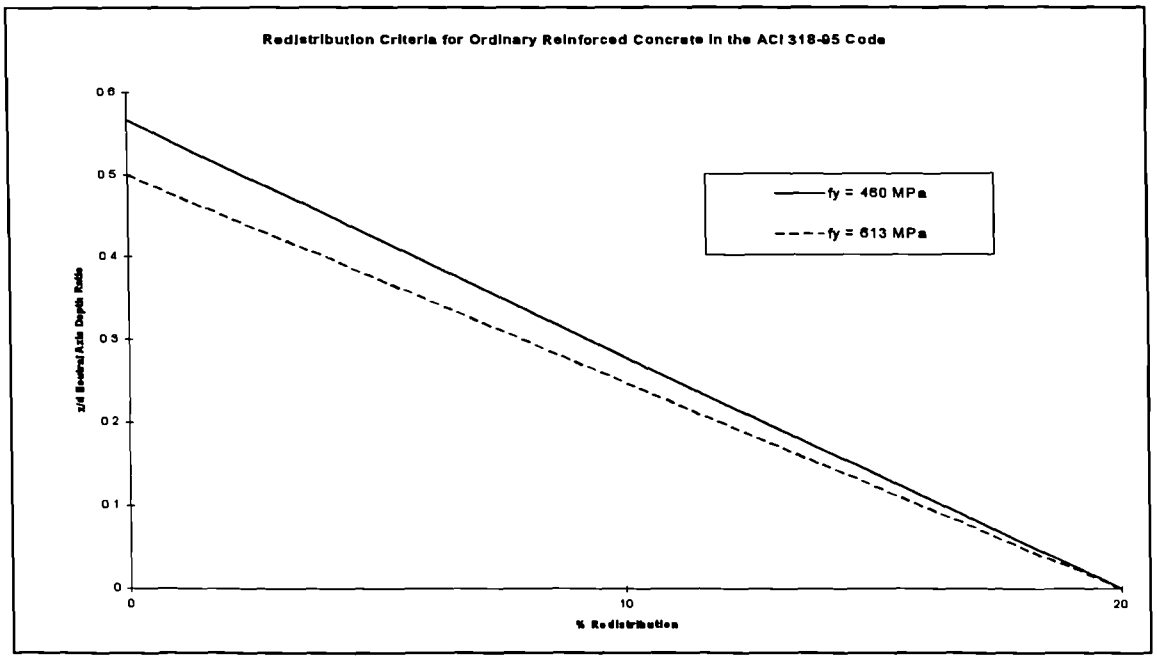

Figure 7-10: ACI 318-95 Redistribution criteria in terms of neutral axis depth ratio

The two curves shown in **Figure 7-10** suggest that the ACI code criteria are dependent on the yield strength of reinforcing steel. Using a value of yield stress such as 613 MPa, completely alters the design curve. However, the ACI code ignores this difference and prefers to relate redistribution independently from steel yield strength. Cohn and Lounis (1991) reported that the neutral axis depth ratio in the ACI code is independent of the steel yield strength. The author would like to point out that such a conclusion may not be fully justified, and has proven, in the derivation above, that moment redistribution in the ACI code is dependent on the steel yield strength of the reinforcement. It is interesting to note that when the ACI code criteria are expressed in these terms, there is no derivable realistic limitation on the neutral axis depth at 20 percent redistribution. Even when assuming that the minimum neutral axis depth ratio is associated with the minimum reinforcement ratio of $1.379/f_y$, (equivalent to the codes' $200/f_y$), the values of (x/d) obtained are 0.0525 and 0 .0670 for 460 and 613 yield strength respectively. These values are not realistic when compared with other codes. The author has shown that the affect of the neutral axis depth ratio and the yield strength of the reinforcement is masked by the use net reinforcement ratio which the ACI code prefers.

The limitations of moment redistribution are summarised as follows. They are expressed in terms of net reinforcement ratio as the code prefers:

1. Application is limited to continuous flexural members.
2. No more than 20 % of the negative moments for any given loading arrangement may be adjusted.
3. Bending moments used in such an adjustment must be obtained by an elastic analysis. Moments from use of coefficients or other approximate methods may not be adjusted.
4. The net reinforcement $(\rho - \rho')$ at the cross section where the moment is reduced must not exceed one half of the balanced percentage ρ_b, as defined by the ACI formula 8-1.

The author questioned and searched for the basis on which the ACI (and other codes) derived their criteria. The conclusion is that most of these criteria are rather subjective and arbitrary, and no information is given in the code or elsewhere to justify the criteria as they are in their present form.

7.10.3 Eurocode 2 1992

This code allows moments calculated by linear elastic analysis to be redistributed provided that the resulting distribution of moments remains in equilibrium with the applied loads. In continuous beams, in non sway frames and in elements subjected to pure bending, rotation capacity of the critical section can be neglected provided that conditions (a) and (b) given below are satisfied.

a. For concrete grades not greater than C35/45: $\beta \leq 0.56 - 1.25\frac{x}{d}$

b. For concrete grades greater than C35/45: $\beta \leq 0.44 - 1.25\frac{x}{d}$

For high ductility steel: $\beta \leq 30\ \%$

For normal ductility steel: $\beta \leq 15\ \%$

EC 2 does not allow redistribution in sway frames. In elements defined above where no redistribution has been carried out, the ductility factor x/d should not exceed 0.45 for concrete not greater that C35/45, and 0.35 for concrete grades C40/50. Further, the code does not recommend redistribution to be carried out in circumstances where the rotation capacity cannot be defined with confidence (for example in the corners of prestressed frames). The code allows a maximum redistribution of 35% in rigid supports in continuous spans provided there is full fixity at the faces of the rigid

support. Error! Number cannot be represented in specified format. illustrates more clearly the redistribution criteria in EC 2 by means of a design chart.

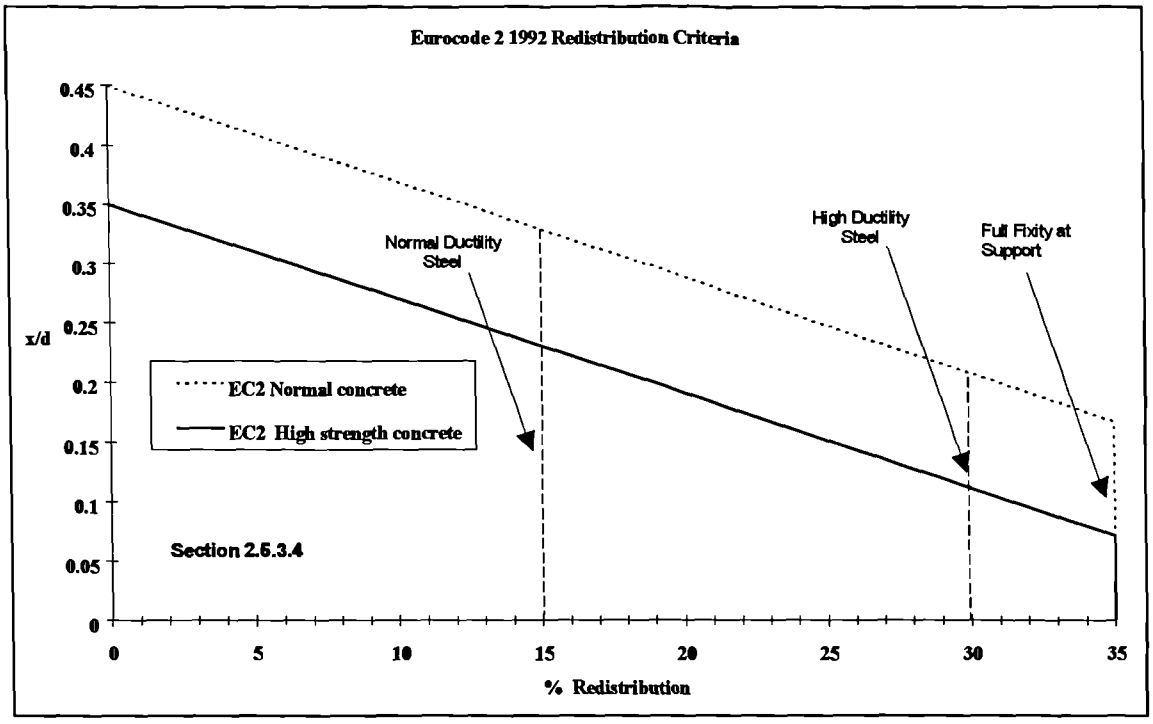

Figure 7-11 Eurocode 2 Moment Redistribution Criteria

7.10.4 CEB-FIP Model Code (1990)

The Model Code allows moments calculated by elastic analysis to be reduced in continuous beams and frames to a maximum of 25 %. **fourth** list redistribution criteria in the new Model Code 1990. The design criteria are further illustrated in Error! Number cannot be represented in specified format..

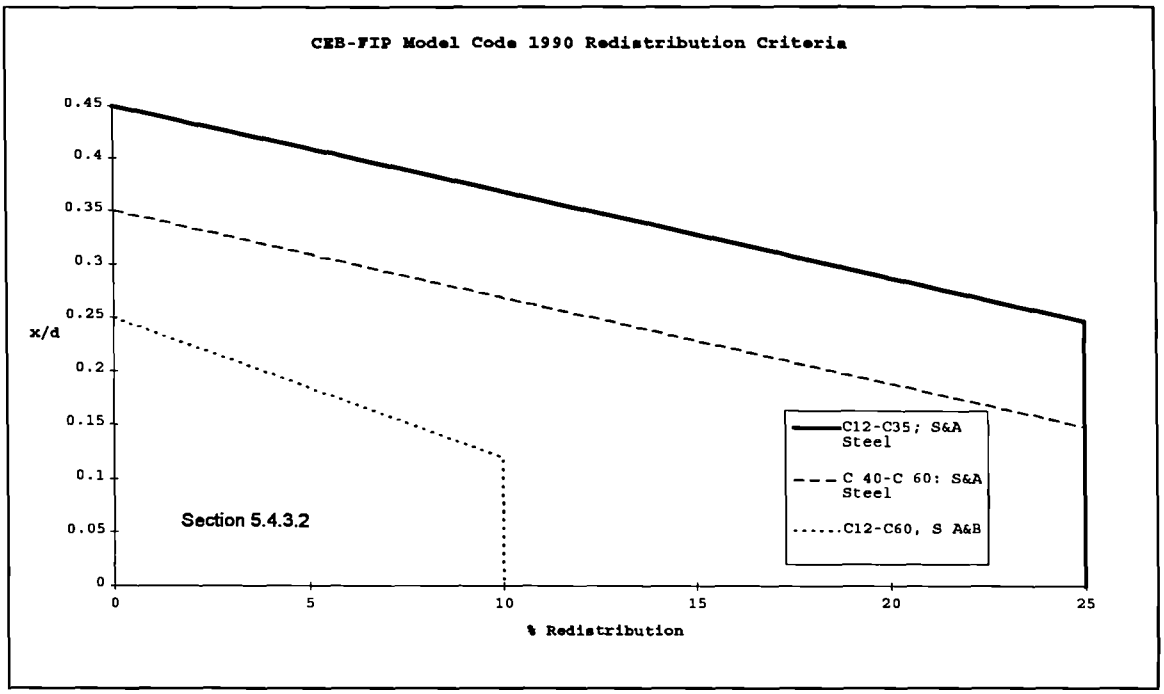

Figure 7-12 CEB-FIP Model Code 90 Redistribution Criteria

Steel type	Concrete grade for Continuous Beams, and Non-sway Frames	Allowed Redistribution	Ductility Limit
S &A*	C12-C35**	0.56-1.25x/d $0.0 \leq \beta \leq 25\%$	$x/d \leq 0.45$
S & A*	C40-C80**	0.44-1.25x/d: $0.0 \leq \beta \leq 25\%$	$x/d \leq 0.35$
B*S & A	C12-C80** Sway frames	0.25-1.25x/d: $0.\leq \beta \leq 10\%$	$x/d \leq 0.25$
* Steel type A: post-tensioned steel, steel type B : pre-tensioned steel type S: high strength. ** Number associated with grade refer to characteristic strength of concrete.			

Table 7-3: Redistribution Criteria in Model Code MC 90

In addition to concentrating on the four codes already discussed, the author obtained details of some additional codes which are presented here to widen the perspective on moment redistribution criteria.

7.10.5 Australian Code AS-3600-88

The Australian Code AS-3600 allows redistribution in continuous beams provided that the following requirements are met:

a. Overall equilibrium is maintained in a structure.

b. Where the neutral axis depth is less than or equal to 0.2 in a peak moment region, the redistribution must not exceed 30%.

c. Where x/d > 0.2 in one or more peak moment regions, but does not exceed 0.4, the redistribution must not exceed 75(0.4 - x/d)%.

d. Where x/d > 0.4 no redistribution shall be made.

The same criteria also apply in the design of continuous prestressed concrete members. The Australian criteria can be expressed graphically in Error! Number cannot be represented in specified format..

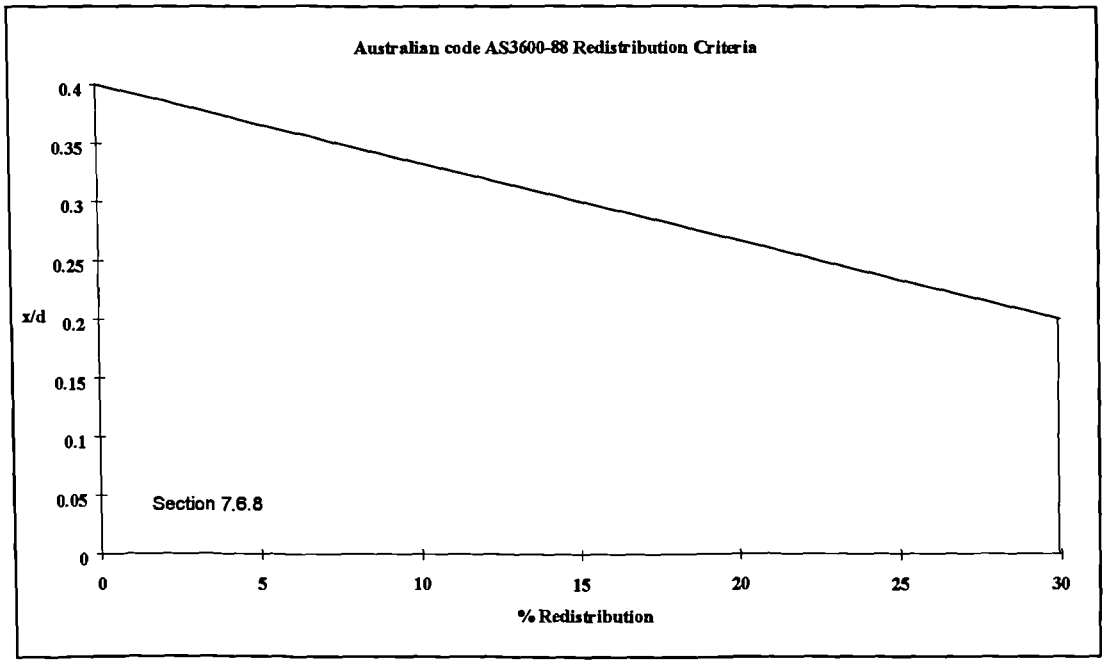

Figure 7-13: Australian Code AS 3600 Redistribution Criteria

7.10.6 Canadian Code CAN3-M84

The design criteria in the Canadian Code CAN3-M84, section A23.3 allows maximum redistribution of 20 % according to the following formula:

$$\beta = 30 - 50\frac{x}{d} \leq 20\% \qquad \textit{Equation 7-44}$$

Error! Number cannot be represented in specified format. illustrates this criteria graphically.

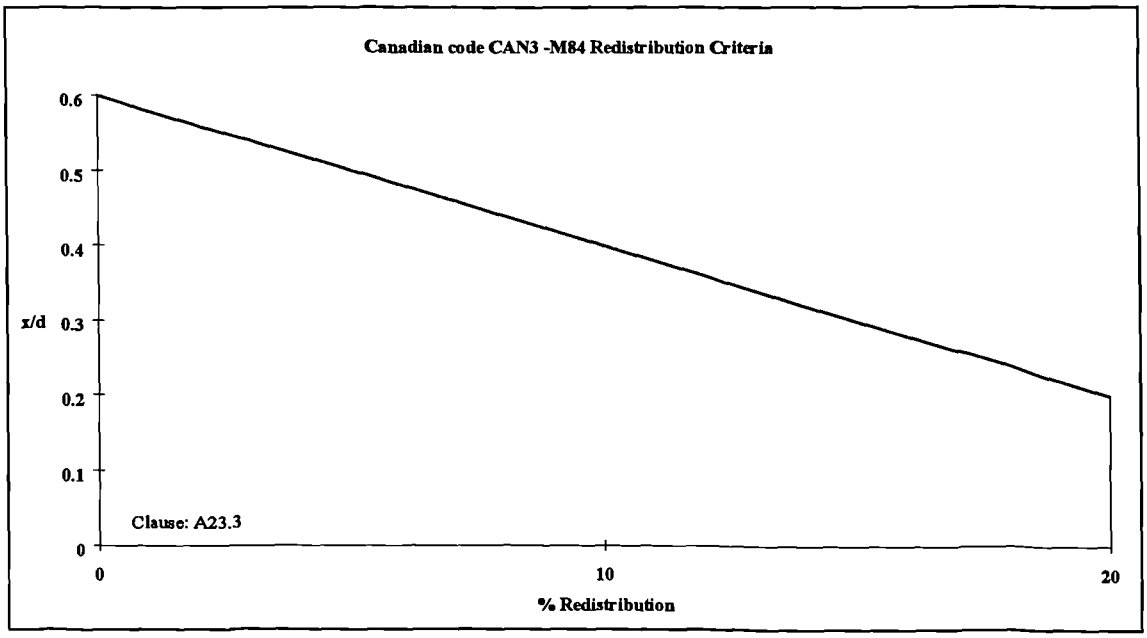

Figure 7-14: Canadian code redistribution criteria (CAN3-M84 Clause A23.3)

7.10.7 Russian Code of Practice

Unlike other codes, the design criteria in I123-50, Russian Code do not allow a linear increase of the permissible redistribution with x/d. The Russian code places the highest restriction on the neutral axis depth ratio by limiting it to 0.3 regardless of the amount of moment redistribution allowed. Maximum value for redistribution is limited to 25%. The design criteria for redistribution is plotted in Error! Number cannot be represented in specified format..

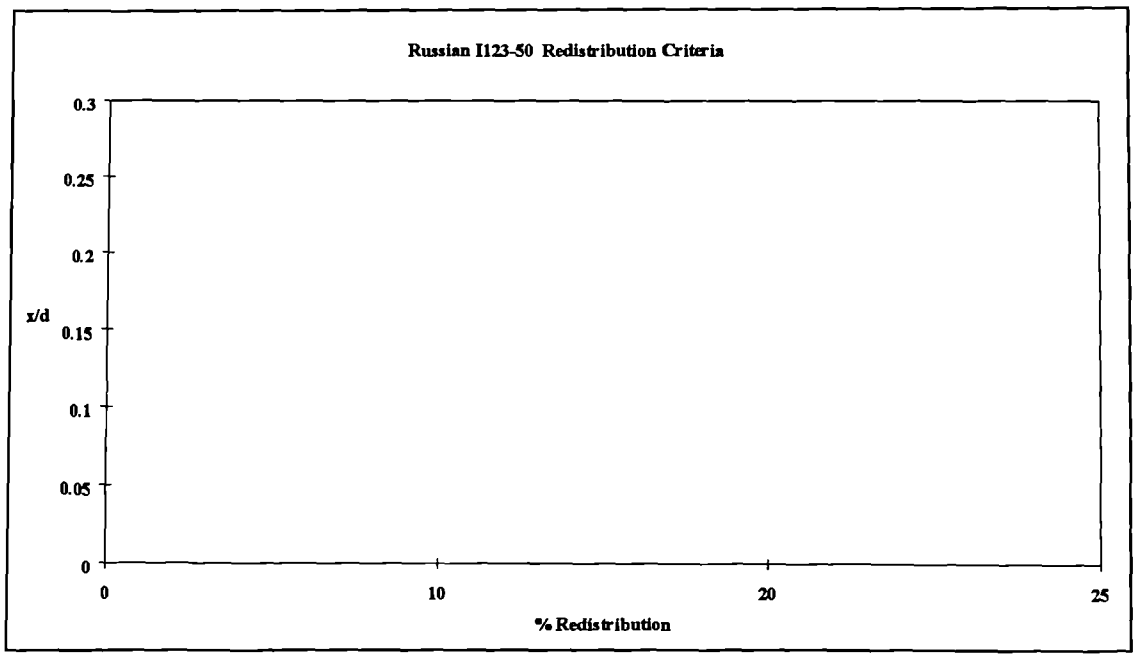

Figure 7-15 Russian code redistribution criterion as stated in i123-50

7.11 Summary and Comments on Redistribution Criteria

The rather arbitrary moment redistribution criteria permitted by the major standards for reinforced concrete beams have been presented. It is noted that permitted redistribution varies from 20 % in the American code up to 35% in Eurocode 2. At the same time the code provisions indicate that all but the Russian code allow a linear increase of redistribution with decreasing value of x/d. The BS 8110 provisions allow a certain redistribution of the elastic moments at the critical sections obtained from a linear analysis of the structure. The maximum permissible redistribution is a function of the relative neutral axis depth ratio (x/d) at ultimate and the type of concrete structure (pre-cast or ordinary reinforced) concrete. Moment redistribution may be of arbitrary magnitude, and within the permissible limit, but without an explicit check on the rotation capacity or plastic rotation of the structure. It should be pointed out that all codes apart from Eurocode 2 and CEB-FIP Model Code 90 codes have some differences when considering the major limits that influence redistribution, namely the concrete grades and the type of steel. For example, in BS 8110 the permissible moment redistribution is independent of the concrete grade and type of steel. On the other hand, in the CEB-FIP Model code there is a 12% reduction in the permissible redistribution as the concrete grade increases from 35 to 40 MPa

which is a very small range. Similarly, the CAN M3-84 and AS 3600 codes criteria are independent of the type of steel and concrete grade and differ in the degree of maximum redistribution permitted against x/d.

Finally, the author sees the EC 2 code restrictions on redistribution as more severe than all other codes and more complicated. Higher strength concrete has a lower allowable redistribution than lower strength concrete. All grades of concrete in EC 2 have a lower neutral axis limit than those given in BS 8110. The 70% redistribution envelope for hogging bending moments is not found in EC 2 and the other codes. The lower EC 2 limits on neutral axis depth at maximum redistribution is a concept which the author supports as it agrees with the findings of this research which are presented in Chapter Eight and Nine.

In summary, the intention of the redistribution rules are very similar in all the codes, The aim is to ensure that equilibrium is maintained and that there is sufficient ductility in the section. However, the codes use different procedures to achieve this. All codes control the section ductility by limiting the neutral axis depth ratio.

In the next chapter, the moment curvature relationships calculated according to four codes' provisions presented here, will be applied using the author's numerical model described in Chapter Six to model redistribution and deformations in the test beams presented in Chapter Five. These values are compared with the earlier experimental results described in Chapter Five.

CHAPTER EIGHT

8. APPLICATION OF THE NUMERICAL MODEL

8.1 Introduction

This chapter describes the application of the numerical model developed by the author and presented earlier in Chapter Six. The need for the numerical model resulted from the experimental work described in Chapters Three and Five of this thesis. One of the objectives set by the author was to apply the numerical model to the current codes of practice moment curvature relationships presented in Chapter Seven. The reason for this was to model moment redistribution using these codes' provisions and to compare the results with the experimental work and the codes' own limitations on neutral axis depth ratio and redistribution. This required more purpose written software to be developed. Therefore, the author wrote the program "CODACI" which calculated the moment curvature relationships of the test beams using criteria from ACI 318-95, BS 8110 1985, CEB-FIP Model Code 1990 and Eurocode 2 1992. A chain of analysis took place using CODACI as a pre-processor for ARMUNY (the numerical model program described in Chapter Six), and another program "BSECT" developed earlier by Scott (1985). Details of this chain are presented in the next section. The results of this were output of modelled moment curvature relationships, moment redistribution, load deflection relationships, plastic hinge properties and neutral axis depths. All these calculated parameters were compared with the experimental results described in Chapter Five of the thesis.

8.2 Modelling Procedure and Software

To apply the model described in chapter Six, a knowledge of the moment curvature relationship at every section along the propped cantilever was required. Two types of moment curvature relationship were used. The first type was based on the four aforementioned codes of practice. The second type was derived from the experimental results. The first type was a straightforward application of the codes' prescribed criteria processed and calculated using CODACI, which will be described shortly. The second type required a manual evaluation of the moment curvature relationship from average strain gauge data. The process involved vetting each

moment curvature relationship for the span and the support sections to avoid repetition of any irregularities that might have occurred in testing. Although the experimental relationships were averaged over 200 mm gauge lengths, the author took on the task of validating the model's capability to use any moment curvature relationship. Interestingly, the results using the experimental averaged moment curvature relationships were an accurate representation of the test beams' behaviour.

To produce the moment curvature relationships according to the four codes, the two programs CODACI and BSECT were used. After the moment curvature relationships had been computed, they were used in the numerical model program ARMUNY (described in detail in Chapter Six) to produce modelled results. The two programs are presented next.

8.2.1 BSECT

The program (BSECT) was only used to analyse and calculate the yield and ultimate moment and curvatures of the test beams. The moments and curvatures calculated using BSECT were based on a numerical iterative technique, which is described in some detail below.

The program BSECT was written for rectangular sections, dealing with both the uncracked and cracked sections and included provision for the effects of compression reinforcement. It assumed a linear strain distribution across the section and allowed non-linear stress-strain relationships to be used for the concrete in compression and the reinforcement in tension and compression. Concrete in tension could be ignored completely, but if included, the stress-strain relationship was assumed to be linear. In contrast, the codes moment curvature relationships in the uncracked and cracked stages were based on exact formulas, hence the need to write CODACI. To evaluate moments and curvatures at yield and ultimate, the following data were fed into the program BSECT:

1. Section geometry and reinforcement areas.
2. Stress strain data for both concrete and reinforcement in tension and compression.

3. A list of required solution parameters. The program would solve the section subject to any one of the following being specified at the section:-

    a) Reinforcement tension strain

    b) Bending moment

    c) Concrete compression strain

    d) Concrete tension strain

    e) Reinforcement compression strain

    f) Rotation

    g) Neutral axis depth

Any number of parameters could be specified in any order during a single run of the program.

Program Output

BSECT first listed the stress-strain data and geometrical properties of the section and then output the following data for each solution parameter:-

Stresses and Strain for the top face of concrete, reinforcement in compression, reinforcement in tension and bottom face of concrete.

Neutral axis depth, lever arm, applied bending moment, curvature, flexural stiffness, and forces in the concrete and reinforcement.

Program Details

The problem was reduced to that of finding a strain distribution across the section which satisfied two conditions:

1. The forces acting on the section must be in equilibrium

$$F_{cc} + F_{sc} = F_{st} + F_{ct} \qquad \textit{Equation 8-1}$$

Where:-

F_{cc} = Forces in concrete in compression

F_{sc} = Forces in reinforcement in compression

F_{st} = Forces in tension reinforcement

F_{ct} = Forces in concrete in tension

2. The specified value of the solution parameter must be achieved.

A double iteration procedure was performed which satisfied the conditions above. For detailed information on the iterative procedure, see Scott (1985).

8.2.2 CODACI

CODACI was written by the author to calculate the short-term moment curvature relationship up to and before yield of the test beams series based on the requirements of ACI 318-95, BS 8110-85, CEB-FIP Model Code 90 and Eurocode 2 1992. Data entry to the program was:

1. The respective test beams series' geometric properties together with concrete tensile and compressive strengths and modulus of elasticity.
2. Yield and ultimate moments calculated by BSECT.

From the input data, the program used the respective codes' formulae to calculate the moment curvature relationship at uncracked and cracked stages. Each code formula was programmed in a separate subroutine. The program calculated the negative and positive moment curvature relationships for the span and support sections. The program output was suited to a format readable by ARMUNY (numerical model program described in Chapter six). Output of CODACI was:

- Hardcopy and screen graphic output of the moment curvature relationship according to each of the codes of practice for the span and support sections.
- Data inputs for ARMUNY.

8.3 Beams Moment Curvature Relationships

Moment curvature relationships for sections at the support and span of the test beams were determined by averaging strains over 200 mm gauge length in both tension

and compression reinforcement using the program CONPCY described earlier. Using the various codes' idealised concrete stress strain curves for concrete, and the actual properties of material and loading conditions, the test beams' moment curvature relationships at the span and support sections were computed accordingly.

8.3.1 Calculation of Yield and Ultimate Moments and Curvatures

Applying the procedure presented in 8.2.1, moments and curvatures at yield and ultimate were calculated for each test beam using stress strain curves that were obtained experimentally for the reinforcement, and the concrete stress strain relationships specified by the four codes. The experimental yield and ultimate (maximum) moments and curvatures were taken from the measured averaged relationships from the strain gauge data. The yield strains were taken from experimental stress strain curves shown in **Figure 7-5** at 2% proof stress listed in **Table 7-2**. **Tables 8-1** and **2** show a comparison of measured and calculated support yield and ultimate moments. A comparison of measured and calculated curvatures at yield and ultimate are shown in **Tables 8-3** and **4**. The span values shown in **Tables 8-1** to **4** were calculated based on the support reaching yield and ultimate.

The average ratios of measured to calculated yield and ultimate moments are shown in **Table 8-5**. The average ratios of measured to calculated yield moments ranged from 1.025 to 1.685 with a standard deviation between 0.135 to 0.867. For the yield curvatures, the average ratios were between 1.000 to 1.025 with standard deviations between 0.145 to 0.183.

Calculated curvatures at yield related well to the measured values for the specimen of series C, D, E and W. At ultimate, curvatures were approximately 70% of those calculated. The average ratio of measured to calculated at ultimate curvatures varied from 0.412 to 0.634.

Ultimate and yield moments and curvatures from the four codes were not sensitive to the shape of the concrete stress strain curves. This was noticeable since the values of moments and curvatures using the various concrete curves were very similar. However, ultimate curvatures were sensitive to the shape of the concrete stress strain curves, as indicated in **Table 8-4** which shows the varying curvatures

calculated using each code. This could imply that the strength of the concrete would affect the ductility of reinforced concrete sections. This implication is not wholly conclusive, since the test data available were analysed and modelled on the basis of one class of concrete strength only.

Figures 8-1 to 6 show a comparison of measured and calculated moment curvature diagrams according to the four codes. Each figure contains five curves: four for the codes plus the experimental curve calculated from averaged strains. The codes' curves are shown using points while the experimental curves are shown using points on continuous lines.

With specimen B3T16A (see **Figure 8-1**), the measured and codes' values were in close agreement as far as the initial uncracked and cracked loading were concerned. However, the computed curves deviated from the point of yield onwards. This was mainly because B3T16A had failed in shear before developing any yield strains at any point on the support and span sections.

Figure 8-2 shows the comparison between measured and computed values for specimens in Series B. The measured moment curvature relationships were refined by eliminating repetitive points to show a clear comparison between the computed and measured values. The agreement was satisfactory for the uncracked and cracked portions of the moment curvature relationship. Measured curvatures were lower than those predicted by the codes' moment curvature relationships. This was due to the following:

1. The failure of the beams in shear preventing the development of deformations comparable with those associated with flexural failures.
2. The measured curvatures were averaged from curvatures over 200 mm gauge length.

Series C beams' moment curvature relationships shown in **Figure 8-3**, demonstrate a close correlation of the moment curvature relationships for all specimens with the computed ones. Series C beams developed shear failure, with strains over the support exceeding yield values. Average measured tensile strains over the support were 6861, 4819, and 8704 microstrain for B3T16C, B2T20C and

B5T12X respectively. Flexural failure did not occur due to the combination of two factors: the relatively large amount of tension steel and the redundancy of the beam.

Series D, E and W beams were lightly reinforced with 12,10, 8 and 6 mm bars over the support as described in Chapter Three. All the beams of these series reflected a certain amount of ductility as evidenced through the measured ductility factors listed in **Table 8-6.** The development of plastic strains in the reinforcement allowed for the formation of plastic hinge in the support section. **Table 8-7** illustrates the level of tensile strains developed over the support. In all specimens of this series, the span reached yield and developed plastic strains before failure of the support.

8.4 Modelling Moment Redistribution

Comparison of measured redistribution with that calculated from the four codes at yield and ultimate over both span and the support are listed in **Tables 8-8** and **9. Figures 8-7 to 21** show the results of the test beams modelled and measured redistribution curves. In each figure six curves are plotted, of which four are for the various modelled codes. The curve labelled with the specimen's name refers to the experimental redistribution curve, whilst the curve labelled "analytical" is a modelled curve using averaged experimental moment curvature relationships derived from measured strains. Positive values of redistribution are for redistribution over the span, while negative ones are for the support. The author used positive redistribution where moments increased numerically, i.e. over the span area, while negative redistribution was where moments decreased numerically, i.e. over the support. The curves on these diagrams do not go beyond maximum load since no allowance was made in the model for the descending part of the moment curvature diagram.

8.4.1 Experimental Redistribution

Experimental redistribution of all the test beams may be summarised in the following stages:-

1. Redistribution before cracking. Although short-lived, this phenomenon occurred because of the different initial stiffnesses at the support and the

span areas. The support sections were approximately 50% less reinforced than the span and so initial redistribution occurred. However, this redistribution is not significant. Furthermore, part of this redistribution was caused by unsettled support conditions at the early load stages.

2. Redistribution after cracking. After cracking, the concrete between two adjacent cracks was still capable of developing tensile forces, thereby increasing the stiffness of the beam relative to that of the cracked section. As a result, the level of redistribution during this stage decreased due to this effect of tension stiffening. As the load increased on the beams, the tension stiffening effect declined and redistribution was almost constant with increasing moments over the support.

3. Redistribution at yield of the tension reinforcement and beyond. This redistribution was more noticeable with the specimens of low reinforcement ratios of series D, E and W. As the reinforcement yielded, the effect of tension stiffening declined and more redistribution of the support moments took place. When the support reached maximum moment, load on the beams could still be increased slightly, although the support moment remained constant as the moment capacity of the span had not reached ultimate.

8.4.2 Modelled Redistribution

Moment redistribution from the codes recorded some initial redistribution before cracking. The change in reinforcement layout along the beam introduced some minimal redistribution due to the different initial stiffnesses of the span and support sections. This may be viewed as an indirect recognition by the codes' of the effect of variation in initial stiffnesses. Redistribution resulting from codes of practice moment curvature relationships was similar, except the British Code BS 8110-85 whose initial assumption was that the moment curvature followed that for a cracked section. Furthermore, redistribution calculated using ACI 318-95 moment curvature relationships, was generally less in the uncracked and cracked portions than the other curves. This is because the ACI cracking moment was higher than the other codes, due to its use of a high value of concrete tensile strength and concrete modulus of

elasticity. (**Equations 7-9** and **7-13** respectively). Moreover, throughout the load history of the test beams, the codes predicted less redistribution than the experimental redistribution. This may be due to overestimation of the flexural stiffnesses by the codes.

8.4.3 Analytical Redistribution

The more representative redistribution behaviour was expressed through the analytical curves derived from moment curvature relationships from measured load and strain gauge data. The results showed interesting redistribution trends very similar to the experimental ones. The analytical curves predicted the large redistribution values observed at early load stages of the tests which occurred due to the greater initial stiffnesses at the span than at the support areas. This was because the moment curvatures used were based on actual measured strains.

8.5 Post Yield Redistribution

Tables 8-10 and **11** list average calculated and measured redistribution for each beam series at the support and span sections at yield of the support. The listed redistribution varied in each series due to the different degree of cracking over the support and span. Specimen B3T16A never reached yield and failed in shear while reinforcement strains were in the elastic range. Consequently, no value for redistribution was obtained near yield.

Tables 8-12 and **13** list average redistribution for each beam series at ultimate over the support and span sections respectively. The results presented indicate that the amount of redistribution occurring after yield varied with the ratio of tensile reinforcement. As the amount of tensile reinforcement at the support decreased, redistribution due to the yield of the reinforcement increased. **Table 8-14** shows the average percentages of the total redistribution that occurred after yield for each beam series.

8.6 Modelling Load Deflection

Deflections were measured under the point load near the middle of each span. The left hand span load deflection plots for each specimens are shown in **Figures 8-22**

to 36. Each graph contains six plots, four for the various codes, as well as measured deflection and an analytical plot based on derived experimental moment curvature relationships. The results indicated the following:

1. Modelled results according to the codes gave deflections smaller than those measured. The large discrepancies between the modelled and experimental curves reflect the high flexural stiffness resulting from the moment curvature relationships derived from the four codes.
2. Differences in deflection curves indicated that the moment curvature relationship for the codes underestimated deflections of the beams at ultimate.
3. The modelled results based on moment curvature relationships derived from experimental data gave a better prediction of the beams' deflections throughout the beams' load history.
4. Both experimental and modelled curves showed a distinct break (change of slope of the deflection curve) when cracking occurred.
5. The analytical plots indicated the validity of the numerical model in predicting deflections using any moment curvature relationship.

The modelling procedure used gave a complete load deflection history of the test beam up to maximum applied load. The resultant load deflection curves reflected the sensitivity of these results to the change in the flexural stiffnesses of the moment curvature relationships.

8.7 Modelling Curvature Distribution

Figures 8-37 to 44 show experimental and modelled curvature distributions along the propped cantilever at failure. Modelled curvature diagrams were based on moment curvature relationships derived from average strain gauge data. The curvature distributions were modelled for the beams in series D, E and W which failed in flexure. Curvature distributions compared well at maximum load in specimens of series D, E and W. Series A, B and C curvature distribution could not be modelled at failure since all beams in these series failed in shear.

8.8 Evaluation of Plastic Hinge Length

The experimentally determined plastic hinge lengths exceeded values determined from the modelled bending moment diagrams. The reason for this additional spread of plastic hinge length was that the longitudinal steel had reached yield even at some distance beyond the zone where moments were at or above the yield moment. This behaviour can be attributed to local bond failure at positions of cracks and microcracking. (See Rosenblueth and Diaz De Cossio, 1964).

When modelling plastic hinge length, the author assumed the length to be zero where yield first occurred. Thus, the first step for determining the plastic hinge length was the determination of the bending moment distribution at yield and ultimate. The plastic hinge length in the model was derived from the position of the point of contraflexure (point of zero bending moment) at ultimate, (see **Figure 8-45**). From similar triangles of the bending moment diagram at yield and ultimate, the following was derived (**Equation 8-2**):

$$l_p = \frac{(M_u - M_y) l_u}{M_u} \qquad \textit{Equation 8-2}$$

Where:

M_u = Ultimate bending moment at the support section

M_y = Yield bending moment at the support section

l_u = Distance from support to point of zero moment at ultimate.

l_p = Plastic hinge length

Figure 8-45 shows a schematic distribution of bending moment at yield and ultimate where the plastic hinge length was calculated. Measured and modelled plastic hinge lengths for all the specimens using the four codes are listed in **Table 8-15**. The modelled values based on moment curvature relationship derived from the strain gauge data gave closer values to the experimental values, mainly due to the use of the more representative moment curvature relationships. Averaged values of plastic hinge lengths for each beam series are listed in **Table 8-16.** The experimental results

suggests that the plastic hinge length is approximately equal to *1.1d* for the beams of series D, E, and W, which is agreeable with plastic hinge length prediction by Baker and Amarkone (1962), where they related l_p ranging from *0.4d* to *2.4d* depending on material properties and loading conditions of the beam. Other expressions (see Naaman et al(1986), Mattock(1983), Riva and Cohn (1994)) related the plastic hinge length to the effective depth, but with extremely varied results based on similar experimental tests on simply supported beams, with different loading conditions. This suggests that the influence of testing procedure and experimental set-up on the plastic hinge length is significant for the related formulations of the above to be considered generally valid. Similarly, analytical expressions of the plastic hinge length developed by the above and others, give different results in relating the plastic hinge length to the effective depth, depending on the number of parameters considered. This only adds to the complexity involved in developing a realistic expression for the plastic hinge length. However, the author found that the following expressions by Baker (1964), Mattock (1964) and Corley (1964) gave similar results:-

$$l_p = R_1 R_2 R_3 \left(\frac{z}{d}\right)^{\frac{1}{4}} d \text{ (Baker Equation)} \qquad \text{Equation 8-3}$$

$$l_p = \frac{d}{2} + 0.2\sqrt{d}\left(\frac{z}{d}\right) \text{ (Corley Equation)} \qquad \text{Equation 8-4}$$

$$l_p = \frac{d}{2} + 0.05z \text{ (Mattock Equation)} \qquad \text{Equation 8-5}$$

The parameters in the above equation have been defined earlier. The results using these equations for the plastic hinge length and the experimental values are listed in **Table 8-17.** The values for the constant R_1, R_2 and R_3 in **Equation 8-3** were R_1 = 0.9 for high yield steel, R_2= 1.0 and R_3 values were interpolated between 0.6 and 0.9 depending on the concrete compressive strength. The value of z was determined from the experimental bending moment diagram of the test beams at maximum moment. It can be seen that the experimental values are greater than those predicted by the above formulae. This is mainly because of the development of cracks some distance away from the support section causing tensile strains to increase beyond yield. To give a

reasonable approximation in relating plastic hinge length to the effective depth, and based on the experimental results and values calculated by the expressions above, the author suggests a value for the plastic hinge length equal to *0.8d.*

8.9 Evaluation of Total Rotation

Total rotation was assumed to equal the sum of the curvatures over the plastic hinge length at the ultimate (maximum) moment. The equation used to determine rotation was:

$$\theta_t = \int_{z_1}^{z_2} \varphi_u dy \qquad \textit{Equation 8-6}$$

Where:-

φ_u = Curvature distribution at ultimate.

θ_t = Total rotation calculated between z_1 and z_2 *(i.e. plastic hinge length)*

z_1 , z_2 = Length which defined the plastic hinge length i.e., the integral limits. In this case the integral limits were the plastic hinge length. $l_p = (z_1 - z_2)$

Irrespective of the shape of the curvature diagram, it was possible to calculate the rotation at any point along the beam using the beam model. Calculated curvatures were numerically integrated over the plastic length to give values of total rotation (rotation capacity) over the support sections. **Table 8-18** lists values of total rotation calculated according to the various codes' moment curvature relationships. Analytical values were obtained from modelling moment curvature relationships derived from strain gauge data. Experimental total rotations were calculated using strain gauge data as described in Section 5.8. Experimental values demonstrated large deviations from calculated ones due to the following:

1. Plastic hinge lengths from the codes were lower than those derived from measured data due to crack development and plastic strains forming further away from the support section due to crack development some distance from the support.
2. The calculated values, using the four standards listed, varied in their prediction of total rotation at ultimate due to the use of different stress strain assumptions for

concrete and reinforcement. This consequently affected the slope of the moment curvature diagram between yield and ultimate, and influenced the amount of rotation. Averaged total rotations for each beam series are listed in **Table 8-19.**

The results presented in **Table 8-19** indicate the following:

1. The assumption of a partially cracked section, as in BS 8110, increased the rotation available in the beams.
2. Rotations were sensitive to the reinforcement stress-strain relationships. The use of idealised flat-top stress-strain curves for the reinforcement as in the case of the EC2, decreased the total rotations.
3. The use of a concrete stress strain curve with a lower modulus of elasticity for the concrete as in the Model Code 90 calculations, increased the total rotation.

8.10 Test Beams Ductility factors

Ductility factor is defined as the ratio of ultimate to yield curvatures (φ_u/φ_y) for sections subjected predominantly to flexural moments under static loading (see Cohn and Ghosh 1973). The yield curvature (φ_y) was defined as the curvature at which the tension steel reached its yield strain. There are three definitions for ultimate curvature (φ_u) of a section. The three definitions presented next are illustrated schematically in **Figure 8-46:**

1. In the codes used here, the ultimate curvatures are at a limiting value of concrete strain (corresponding to the onset of crushing) attained at the extreme compression fibre ε_{cu}= 3500, 3000, 3500, 3500 microstrain for the BS 8110, ACI 318, EC2 and the Model Code MC 90 respectively, corresponding to point (x_1) on **Figure 8-46**
2. The experimental ultimate curvature is defined as the curvature corresponding to the attainment of maximum moment, shown by point (x_2) on **Figure 8-46.**
3. A third definition of ultimate curvature (φ_u) is when the beam reaches curvature beyond that corresponding to maximum moment, i.e., curvature

on the end of the descending part of the moment curvature relationship, shown by point (x_3) on **Figure 8-46**. This definition was beyond the scope of the research, as the numerical model only modelled the ascending part of the moment curvature relationship.

The codes' conventional definition of failure at point (x_1) underestimated the ductility of a section, because limiting values of concrete strain at the extreme fibre had either to be arbitrarily fixed or based on visual observations of the onset of crushing in experiments. The definition of ultimate curvature corresponding to point x_3 accounted for the ductility of a section to a fuller extent than the codes or the adopted experimental curvatures at maximum moment. However, this definition was still arbitrary since there was not a mathematically well-defined point on the descending part of the moment curvature relationship. Therefore, the author based the definition of the ultimate experimental curvature as where the section reached its maximum moment, clearly defined as the maximum point in the moment curvature diagram.

Averaged measured and calculated (according to codes) ductility factors (φ_u/φ_y) are listed in **Table 8-20.** The experimental ductility of unity was assumed for the beams that failed in shear, since no real ultimate flexural curvature was reached (see Cohn and Ghosh, 1973). The codes' calculations gave higher ductility values than the measured ones. This was because the reinforcement stress strain relationship used for the codes' moment curvature modelling did not account for the influence of tension stiffening at ultimate.

Figure 8-47 shows a comparison between measured and computed ductility factors versus the neutral axis depth ratio. The ductility of lightly reinforced sections with low neutral axis depth ratio was high, while more heavily reinforced beams developed lower ductility, evidenced by the brittle failures that occurred in Series A, B and C. This confirmed that ductility decreased with increasing neutral axis depth ratio. High neutral axis depth ratios at failure were a characteristic of beams with high tensile reinforcement ratio. **Figure 8-48** shows the influence of ductility on the amount of tensile reinforcement. Ductility decreased with increasing amount of tension reinforcement. Little ductility developed in sections in some beams which had very

high percentages. This is why, for example, the ACI code of practice imposes an upper limit on the amount of tension reinforcement that should be used in design.

8.11 Relative Stiffness and Redistribution

The author defined relative stiffness as the ratio of stiffness (EI) of the support to that of the span at any particular stage. **Tables 8-21** and **22** show measured and calculated stiffnesses at yield and ultimate over the support and span sections. **Table 8-23** lists relative stiffness values when the support reached its yield and ultimate conditions respectively. The beams' relative stiffness directly affected the amount of moment redistribution that took place in continuous beams. As the relative stiffness approached unity, redistribution decreased. **Figure 8-49** shows the relationship between the support moment redistribution (shown positive for clarity) and relative stiffness at yield and ultimate respectively.

8.12 Neutral Axis Depth and Redistribution

Neutral axis depth was defined as the point or level on the cross section where the strain equalled zero. By inputting the modelled moments from ARMUNY for both the support and span sections into BSECT, the program gave neutral axis depth values at every corresponding moment. Therefore, full history of the neutral axis depth development was available for comparison with the calculated redistribution over the support. **Table 8-24** shows neutral axis depth ratios calculated at ultimate over the support using codes' moment curvature relationships compared with the experimental values obtained from strain gauge data. **Figures 8-50** to **55** show an historical development of neutral axis depth ratio versus redistribution for each beam series over the support area. Each figure contains two types of curves: the first type using continuous lines represented the four codes' computed values according to the codes' stress strain curves, and the second type, using points of the experimental curves for each specimen was calculated from average strains and Demecs.

The computed curves for the codes were segmented into three parts, uncracked cracked and yielded. In the uncracked part very little redistribution occurred, with a decrease in the neutral axis depth ratio. This portion was governed by the concrete tensile strength. The codes' predictions of the uncracked portion were similar except

for BS 8110 where a partially cracked section was assumed. Therefore, the sections modelled according to BS 8110 had initial redistribution while the other three codes' redistribution was nearly zero. In the cracked portion of the curves, the support sections' redistribution continued to increase, but at a constant neutral axis depth ratio. At yield, redistribution increased with a drop in the neutral axis depth ratio. At failure of the support, when it reached its ultimate moment, redistribution was at maximum and the neutral axis depth ratio reached its minimum value.

The degree of moment redistribution showed different patterns of development of neutral axis depth ratio depending on the percentage of tensile reinforcement used in each beam series. The lower the percentage of tensile reinforcement the more redistribution occurred, due to the yield of the reinforcement. With a higher reinforcement ratio, redistribution mainly occurred as a result of cracking of the concrete. The neutral axis depth ratio stayed constant once the section had cracked, but when yield was reached, it decreased with an increased redistribution. The modelled solutions shown illustrate that the value of neutral axis depth ratio between cracking and ultimate fell between 0.43 and 0.05, and redistribution boundaries were between zero and 40%. **Figure 8-56** shows the codes' redistribution criteria superimposed on the modelled results.

The envelope boundaries of the codes' redistribution criteria represent neutral axis depth ratio versus redistribution at ultimate. The modelled curves show the full historical moment redistribution and neutral axis depth ratio. The author superimposed the curves as they were of particular importance and interest, and gave a picture of the codes' redistribution criteria and the codes' modelled results based on their moment curvature relationships.

At the cracked portion (serviceable loads), the calculated neutral axis depth ratio was below the codes' limits. **Figure 8-56** shows that the codes' criteria under-estimated the amount of redistribution that took place before the reinforcement yielded. The modelled and the experimental results indicated that more redistribution could occur while the structure is still in the serviceability range without the excessive cracking that might cause failure. For instance, BS 8110 allows 30% redistribution provided that the neutral axis depth ratio is not greater than 0.30. The modelled results

shown in **Figures 8-50 to 55**, and the experimental results shown in **Figure 8-57**, suggest that redistribution may exceed 30% at a neutral axis depth ratio below 0.25 experimentally, and below 0.2 analytically, even before reaching ultimate. Furthermore, examining the results presented in **Table 8-24**, it can be seen that the average experimental neutral axis depth ratios for specimens of series D, E and W (which failed in flexure) is 0.259, while the analytical average (modelled results from the codes), varies between 0.076 and 0.109. At the same time, the modelled and experimental average strains in the tensile reinforcement of series D, E and W shown in **Table 8-7**, indicate that the codes modelled strains are higher than the experimental strains. Higher strains mean lower neutral axis depth ratios, suggesting some contradiction in the codes, especially BS 8110, when such high strains may be required in the reinforcement, while the neutral axis depth ratio is limited to 0.3 at maximum redistribution (the low end of the design curve). Therefore, based on the experimental and modelled results of strains, neutral axis depth ratios and redistribution, it maybe possible to reduce the neutral axis depth ratio to 0.25 in the BS 8110 design curve. This finding is in partial agreement with the design curves of both the EC 2 and MC 90 codes. The neutral axis depth at 30% redistribution in the EC 2 code is limited to 0.208 and 0.112 for normal and high strength concrete respectively, using high ductility steel. The CEB-FIP Model Code MC 90 however, limits redistribution to a maximum 25% at a neutral axis depth ratio of 0.248 and 0.152 for normal and high strength concrete respectively. Therefore, this suggests that the results reached by the author are more agreeable with the CEB-FIP MC 90 design curve than the EC 2 code. This indicates that the EC 2 restrictions are much more severe and rather complicated than those given in BS 8110. Higher strength concrete has a lower allowable redistribution than the low strength concrete. All grades of concrete in EC 2 have a lower neutral axis depth value than that given in BS 8110. The results the author reached, however, cannot be conclusive as more experimentation would be needed before finalising the results into firm recommendations.

8.13 The use of the Model as a Parametric Tool

This section will demonstrate that the numerical model developed by the author can be used to model other beams' behaviour, as well as laying down the foundations

for further development of the model into a parametric analysis and design tool for practicable values of moment redistribution of continuous beams.

The numerical model used in this research was based on multi-linearised moment curvature relationships for a propped cantilever. The model gave results of deformational properties (i.e. curvatures, deflections and rotations). A result of particular interest was the rotation capacity (total rotation) at the support sections in continuous beams. Other researchers (Eligehausen and Langer, 1978), through a series of tests on simply supported beams under point loads, modelled rotation capacity and related it to amount of tensile reinforcement. Eligehausen studied the steel quality and suggested a modification to the CEB-FIP Model Code 1990 to account for the different behaviour of such sections when brittle or ductile steel were used. He assumed two criteria of failure: crushing of the concrete and rupture of the reinforcement. The result of his work was the development of a curve that related the percentage of reinforcement to rotation capacity of reinforced concrete beams.

The author used the numerical model developed to calculated the rotation capacity of idealised beams using several reinforcement ratios. This semi-parametric study has been conducted to assess the influence of the basic limits governing the rotation capacity of reinforced concrete beams (that is, the percentage of tensile reinforcement). Another reason was to illustrate the model's capabilities as a tool to investigate the different parameters which influence redistribution. **Figure 8-58** shows the stress strain curves for the concrete in compression and the reinforcement in both tension and compression that were used to model the beams. The stress strain relationship of the steel in tension given in **Figure 8-58** shows the following parameters that were assumed:

$$\frac{f_{st}}{f_y} = 1.09 \quad \varepsilon_{us} = 30000 \text{ microstrain}$$

$$\frac{f_{st}}{f_y} = 1.15 \quad \varepsilon_{us} = 50000 \text{ microstrain}$$

$$\frac{f_{st}}{f_y} = 1.21 \quad \varepsilon_{us} = 70000 \text{ microstrain}$$

Where:-

$\frac{f_{st}}{f_y}$ = The ratio of the reinforcement rupture stress (f_{st}) to yield stress (f_y)

ε_{us} = The tension reinforcement rupture strain

Table 8-25 lists the material variables as well as the geometry of the idealised beams. The range of reinforcement ratios used was ρ = 0.1% to 0.6% over the support with a fixed span reinforcement ratio of 0.65%. Two failure criteria were tested: concrete crushing at 3500 microstrain, and steel rupture at 30000, 50000 and 70000 microstrain. Beam geometry was based on Series D beams of 150 mm overall height and 300 mm width, with an effective depth of 123 mm with no compression reinforcement being used in the span and support sections of the idealised beams. It was assumed that sufficient shear reinforcement was provided to prevent shear failure. Steel modulus of elasticity of 200 GPa was assumed. Concrete strength of 40 MPa and a parabolic rectangular stress strain curve in accordance with BS 8110 with a maximum strain of 3500 microstrain was assumed. The modelling procedure required 356 input and output files to be used in the chain of programs, described earlier in this chapter.

Tables 8-26 to **29** present the modelled neutral axis depth ratios, plastic hinge lengths and total rotations (rotation capacity) calculated using the various failure criteria for the range of reinforcement ratios specified.

Rotation capacity was determined as the total rotation that took place after the yield of the steel. Yield strain was assumed at 5900 microstrain at 2% proof stress. **Figure 8-59** shows the rotation capacity (total rotations) for all the idealised beams plotted against the percentage of tensile reinforcement. The graph contains eight plots representing the intersections of the rotations caused by the rupture of the steel and the concrete crushing. Any point to the left of a pointed curve signifies failure through the rupture of the reinforcement. Any point to the right represents failure through crushing of the concrete in compression. The experimental values of series D,W and E were also plotted. The resulting total rotations (from the modelled idealised beams) versus percentage of tensile reinforcement were compared with the curve developed by

Eligehausen. There was generally an agreement between the shape of the Eligehausen curve and the resultant curves of the idealised beams. However, values of plastic rotations do not compare because of the different geometric, material and loading properties and conditions used in the idealised beams. Whilst the author used a propped cantilever loaded in the middle (one degree of redundancy), Eligehausen used a simply supported beam loaded in the middle. Furthermore, the range of steel percentages considered was lower than that used by Eligehausen: range of reinforcement used by the author was 0.1 to 0.6 %, Eligehausen used 0.2 to 1.2%. Rotations obtained by the author were therefore higher.

In **Figure 8-59** the predicted and measured rotation capacities of the idealised beams are plotted as a function of the percentage of reinforcement. The roof shaped behaviour was captured in a similar way to the Eligehausen curve. The critical reinforcement ratio using the author's model differed from that developed by Eligehausen for the above-stated reasons. For reinforcement percentages smaller than a critical value (dependent on the stress strain relationship of the steel and concrete and the beam cross section), a beam may fail due to rupture of the reinforcement, (that is, the ductility of the reinforcement was fully utilised). For this failure mode, the rotation capacity decreases with decreasing reinforcement ratio. For reinforcement ratios larger than a critical value, a beam may fail due to crushing of the concrete. It is important to note that the author's curves showed several critical values (in contrast to Eligehausen's curve) of tensile reinforcement depending on the failure criteria used which consequently gave the failure mode of the beam. Any point to the right hand side of a peak was seen to represent the values at which concrete fails, while any point to the left represented the steel reaching its failure strain.

Tables 8-30 and **31** show the modelled percentage of redistribution that occurred in the idealised beams using the various failure criteria.

The amount of redistribution increased with decreasing reinforcement ratios over the support. **Figure 8-60** shows the relationship between the two variables.

The idealisation demonstrated the following:

1. Material, geometric and loading conditions affect the degree of rotation capacity that may occur in a structure or a beam, thus affecting the ductility of the beam.

2. Reinforcing steel strains control the amount of rotation capacity that a beam can undergo, i.e., different strain capacities imply different ductility levels for various kinds of steel.

3. The ratio of tensile reinforcement used in the idealised beams influenced the degree of ductility and moment redistribution in reinforced continuous beams.

8.14 Summary

A method of modelling has been described and presented using available and newly developed software to process and model the data generated by the strain gauges. Four codes' moment curvature relationships were modelled and discussed using different concrete and reinforcement stress-strain relationships. Moments and curvatures were compared at yield and ultimate. Experimental and computed moment curvature relationships were also compared. In the uncracked portion close agreement with experimental results was evident. However, the codes' computed curves began to deviate near the point of yield and beyond. Total rotations were calculated and compared with available measured rotations. The experimental measured plastic hinge lengths were higher than those predicted by the numerical model using the codes moment curvature relationships, because cracks in beams developed some distance away from the support section. Based on the experimental and numerical modelling results of plastic hinges, it is suggested that a safe value of the plastic hinge length may be taken to equal *0.8d*. The use of idealised flat top stress-strain curve for the steel as used in EC 2, decreased the total rotations of the beams. An historical development of neutral axis depth ratios was calculated up to ultimate and compared with the modelled percentages of redistribution. The modelled neutral axis depth ratio versus redistribution indicated that the values of (x/d) were less than those expressed in the redistribution design curves of the codes. This implied more redistribution could occur at lower neutral axis depth ratios while the beam was still in serviceable loads. It was found that the ratio of tensile reinforcement was proportional to the movement of neutral axis depth, thus influencing the amount of redistribution that may occur at any loading stage. Codes' curves predicted redistribution less than the experimental in the uncracked and cracked portions. More important was the occurrence of redistribution before cracking, resulting from overlooking the initial relative stiffnesses of the beams, whereas current practices are based on redistribution starting on the commencement of yield. Post yield redistribution varied from as low as 11% to 28% experimentally and 4% to 64% analytically. The amount of redistribution due to yield increased with decreasing tension reinforcement.

Load deflections under the point load were modelled. The analysis showed that the computed values were smaller than the experimental ones. This is perhaps a result of over-estimation of the beams' flexural stiffness by the codes. The analytical curves derived from strain gauge data show closer correlation to the experimental curves.

Curvature distributions along the beam were modelled using moment curvature relationships derived from strain gauge data. The use of derived moment curvature relationship from experimental data gave very close approximation of the actual curvature diagram along the beam. It was also found that ductility factors increased with decreasing ratios of tension reinforcement and neutral axis depth ratios.

Finally, the author conducted a semi-parametric study to evaluate the effect of tensile reinforcement on the rotation capacity of idealised beams with certain geometric and material properties. The idealisation was compared with similar work carried out by Eligehausen in Germany. The results of the study showed that the model developed relating rotation to steel percentages was reasonable and comparable with the work carried out by Eligehausen in capturing the 'roof-topped' curve with a critical value for tensile reinforcement percentage. However, numerical values do not compare well due to the different geometric and material properties used by the author. Furthermore, the modelling of the idealised beams indicated that more than one critical value of tensile reinforcement ratio could exist due to the use of different failure criteria of the concrete and the reinforcement.

The author suggests more experimental work is required on the effect of other variables influencing the rotation capacity (i.e. compression reinforcement, shear reinforcement, concrete grade) by testing more under-reinforced sections under various loading conditions. The model developed by the author could be used to examine these variables. The author suggests altering the limit of the neutral axis depth ratio by reducing the required neutral axis depth ratio from 0.3 to 0.25 at a maximum of 30% redistribution in the BS 8110 moment redistribution criteria, this being based on the curves presented earlier. Furthermore, the reduction of the neutral axis depth ratio to 0.25 is in general agreement with the current CEB-FIP Model Code 90 and the EC 2 code moment redistribution criteria.

The author based the conclusion and recommendations presented in the next chapter on the experimental and modelling work undertaken combined with a philosophy adopting practicality in design.

Modelled Results Tables and Figures

	Yield Moments kNm at the Support					Moments at the Span kNm				
SPECIMEN	**BS 8110**	**ACI 318-95**	**EC2-92**	**Model Code**	**Measured at Yield**	**BS 8110**	**ACI 318-95**	**EC2-92**	**Model Code**	**Measured at Yield**
B3T16A	121.1	120.6	121.3	121.4	a	-165.3	-164.3	-165.6	-166.0	a
B3T16B	69.2	68.8	69.5	69.8	60.6	-96.0	-96.6	-96.3	-97.2	-102.0
B3T16BL	69.2	68.8	69.5	69.8	63.4	-96.0	-96.6	-96.3	-97.2	-58.0
B2T20B	65.7	65.3	65.9	66.1	a	-96.0	-96.6	-96.3	-97.2	a
B5T12B	50.8	50.5	51.0	51.1	a	-96.0	-96.6	-96.3	-97.2	a
B3T16C	37.5	37.4	38.1	38.6	31.7	-48.8	-48.8	-49.4	-50.8	-51.3
B2T20C	34.4	34.3	34.8	35.2	34.0	-48.8	-48.8	-49.4	-50.8	-45.6
B5T12C	27.5	27.4	27.9	28.1	a	-48.8	-48.8	-49.4	-50.8	a
B5T12X	27.5	27.4	27.9	28.1	31.9	-48.8	-48.8	-49.4	-50.8	a
B2T12D	10.8	10.7	10.8	10.8	12.0	-16.9	-16.8	-17.0	-17.1	-14.6
B3T10D	12.2	12.2	12.3	12.3	15.6	-16.9	-16.8	-17.0	-17.1	-16.8
B5T8D	15.5	15.3	13.3	15.5	15.8	-16.9	-16.8	-17.0	-17.1	-18.7
B2T8E	5.9	5.9	5.9	5.9	6.5	-9.6	-9.5	-9.6	-9.6	-11.6
B4T6E	6.7	6.4	6.4	6.4	5.2	-9.6	-9.5	-9.6	-9.6	-10.0
W2T12D	12.5	12.4	12.5	12.5	14.4	-18.3	-18.2	-18.4	-18.5	-20.9
W3T10D	13.3	13.2	13.3	13.3	12.4	-18.3	-18.2	-18.4	-18.5	-19.3
W5T8D	13.1	13.0	13.1	13.1	16.5	-18.3	-18.2	-18.4	-18.5	-18.5
a* No yield strain reached										

Table 8-1: Computed and experimental yield bending moments when the support reached yield strains

Ultimate Moments at the Support* kNm						Moments at the Span kNm*				
SPECIMEN	BS 8110	**ACI 318-95**	**EC2-92**	**Model Code**	**Measured at failure**	**BS 8110**	**ACI 318-95**	**EC2-92**	**Model Code**	**Measured at Failure**
B3T16A	126.4	125.3	124.9	128.9	102.9	-192.3	-141.3	-130.5	-133.3	-161.7
B3T16B	71.0	70.7	71.2	73.0	61.9	-79.2	-77.4	-80.1	-84.4	-104.8
B3T16BL	71.0	70.7	71.2	73.0	71.9	-79.2	-77.4	-80.1	-84.4	-98.3
B2T20B	69.4	68.7	68.2	71.7	51.3	-79.5	-76.3	-76.6	-86.4	-82.4
B5T12B	55.0	54.3	52.0	57.1	53.9	-76.3	-71.6	-63.0	-86.5	-83.2
B3T16C	37.8	37.6	38.5	39.5	32.7	-39.5	-38.5	-40.1	-39.4	-51.6
B2T20C	35.2	34.9	35.6	36.9	35.8	-35.7	-36.1	-35.6	-37.8	-47.0
B5T12C	28.8	28.3	28.2	30.1	25.9	-30.8	-29.6	-29.5	-35.7	-45.3
B5T12X	28.8	28.3	28.2	30.1	34.0	-30.8	-29.6	-29.5	-35.7	-46.5
B2T12D	12.0	11.8	11.0	12.5	14.6	-15.7	-16.9	-14.4	-18.2	-20.7
B3T10D	13.5	13.3	12.5	14.1	16.9	-17.7	-17.0	-14.9	-17.8	-22.5
B5T8D	16.5	16.1	13.6	16.7	18.3	-17.5	-16.8	-15.6	-17.9	-21.5
B2T8E	6.6	6.5	6.0	6.9	7.2	-10.0	-10.0	-8.8	-10.6	-12.8
B4T6E	6.7	6.7	6.7	6.7	6.6	-6.7	-9.5	-10.6	-9.8	-12.0
W2T12D	13.9	13.6	12.9	14.6	16.7	-18.9	-17.9	-15.9	-19.9	-21.6
W3T10D	14.1	13.9	13.7	14.6	14.5	-17.9	-14.1	-16.4	-19.2	-21.3
W5T8D	13.8	13.7	13.4	14.3	17.4	-17.4	-16.1	-15.5	-18.7	-21.0
* measured at maximum load										

Table 8-2: Computed and experimental ultimate bending moments when the support reached maximum moment

269

Curvature at the Support 10^{-6}/mm						Curvature at the Span 10^{-6}/mm				
SPECIMEN	**BS 8110**	**ACI 318-95**	**EC2-92**	**Model Code**	**Measured at Yield**	**BS 8110**	**ACI 318-95**	**EC2-92**	**Model Code**	**Measured at Yield**
B3T16A	70.87	14.48	14.18	13.99	a	-11.65	-12.08	-11.75	11.51	a
B3T16B	25.26	26.03	25.43	24.87	b	-21.76	-21.49	-21.93	21.17	-22.00
B3T16BL	25.26	26.03	25.43	24.87	21.54	-21.76	-21.49	-21.93	21.17	-21.06
B2T20B	19.87	20.60	20.06	19.60	a	-21.76	-21.49	-21.93	21.17	a
B5T12B	33.05	33.74	33.15	32.72	a	-21.76	-21.49	-21.93	21.17	a
B3T16C	52.49	53.89	52.59	50.05	51.52	-48.46	-50.10	-48.66	44.62	-49.26
B2T20C	41.42	42.99	41.72	39.88	38.18	-48.46	-50.10	-48.66	44.62	-50.60
B5T12C	64.99	66.26	64.67	63.12	a	-48.46	-50.10	-48.66	44.62	a
B5T12X	64.99	66.26	64.67	63.12	65.32	-48.46	-50.10	-48.66	44.62	a
B2T12D	56.62	57.91	56.58	56.25	57.23	-59.83	-61.32	-59.58	58.97	-65.31
B3T10D	56.83	58.19	56.76	56.38	57.08	-59.83	-61.32	-59.58	58.97	-64.63
B5T8D	46.15	47.37	45.19	45.68	48.35	-59.83	-61.32	-59.58	58.97	-63.33
B2T8E	41.88	42.75	41.93	41.75	43.17	-43.62	-44.71	-43.64	43.40	-42.74
B4T6E	44.86	23.64	22.96	22.76	22.12	-43.62	-44.71	-43.64	43.40	-43.80
W2T12D	45.80	47.11	45.78	45.46	58.64	-48.28	-49.58	-48.18	47.66	-59.20
W3T10D	45.69	47.00	45.65	45.32	45.73	-48.28	-49.58	-48.18	47.66	-52.91
W5T8D	45.14	46.35	45.10	44.78	51.37	-48.28	-49.58	-48.18	47.66	-51.28
a* Support bars did not reach yield strains										
b* Reached yield strain shortly before failure										

Table 8-3: Computed and experimental yield curvature when support reached yield

270

	Ultimate Curvature at the Support 10^{-6}/mm					Curvature at the Span* 10^{-6}/mm				
SPECIMEN	**BS 8110**	**ACI 318-95**	**EC2-92**	**Model Code**	**Measured at Failure**	**BS 8110**	**ACI 318-95**	**EC2-92**	**Model Code**	**Measured at Failure**
B3T16A	85.00	67.24	93.09	105.22	9.54	-111.35	-9.30	-8.24	-10.79	-10.04
B3T16B	91.17	71.72	96.47	110.06	39.8	-15.82	-15.20	-17.90	-16.51	-24.07
B3T16BL	91.17	71.72	96.47	110.06	18.7	-15.82	-15.20	-17.90	-16.51	-51.98
B2T20B	92.37	73.11	99.67	110.74	12.26	-15.90	-14.96	-17.06	-17.15	-15.72
B5T12B	110.68	89.04	133.53	142.55	17.46	-15.19	-13.98	-13.84	-17.04	-11.05
B3T16C	93.56	72.97	95.18	113.25	79.95	-32.65	-33.61	-36.56	-30.46	-50.26
B2T20C	97.84	76.79	101.26	117.76	56.87	-28.78	-31.16	-31.69	-29.07	-100.21
B5T12C	118.30	95.21	132.63	146.38	40.27	-24.23	-24.89	-25.59	-27.39	-37.39
B5T12X	118.30	95.21	132.63	146.38	90.88	-24.23	-24.89	-25.59	-27.39	-40.40
B2T12D	118.30	224.05	360.93	371.53	158.60	-30.92	-63.11	-50.21	-119.35	-260.49
B3T10D	255.27	198.98	318.00	331.26	176.85	-93.04	-66.00	-51.74	-86.46	-201.47
B5T8D	212.60	164.56	293.54	278.58	191.52	-85.02	-61.52	-54.40	-90.04	-211.48
B2T8E	182.62	423.28	678.72	695.61	107.18	-340.86	-202.37	-40.18	-396.94	-97.42
B4T6E	1.23	414.88	611.74	717.73	142.3	-340.86	-44.68	-412.00	-94.28	-91.47
W2T12D	246.00	193.09	306.53	316.31	103.00	-89.76	-45.70	-41.29	-157.77	-101.14
W3T10D	244.40	189.57	290.40	319.24	196.49	-43.96	-26.14	-42.76	-90.43	-105.10
W5T8D	251.30	194.90	298.43	328.47	143.50	-39.23	-34.02	-40.24	-46.25	-88.48
*Curvature at span was evaluated when support reached failure										

Table 8-4: Computed and experimental ultimate curvature when support reached maximum moment

271

Averaged Ratios of Measured to Calculated Moments and Curvatures at Yield and Ultimate at the Support					
		BS 8110 -85	**ACI 318 - 95**	**EC2 - 92**	**MC-90**
M_y	**Average**	1.025	1.461	1.572	1.685
	S. D.	0.135	0.279	0.551	0.867
M_u	**Average**	1.030	1.226	1.220	1.096
	S. D.	0.183	0.169	0.195	0.145
φ_y	**Average**	0.99	0.99	1.015	1.025
	S. D.	0.150	0.085	0.089	0.085
φ_u	**Average**	0.581	0.634	0.444	0.412
	S. D.	0.371	0.373	0.279	0.265

Table 8-5: Comparison of average ratio of measured to calculated moments and curvatures.

272

Ductility Factor for the support section φ_u/φ_y					
SPECIMEN	**BS 8110**	**ACI 318-95**	**EC2-92**	**Model Code**	**Measured**
B3T16A	1.20	4.64	6.56	7.52	1(a)
B3T16B	3.61	2.76	3.79	4.43	1(a)
B3T16BL	3.61	2.76	3.79	4.43	1.15
B2T20B	4.65	3.55	4.97	5.65	1(b)
B5T12B	3.35	2.64	4.03	4.36	1(b)
B3T16C	1.78	1.35	1.81	2.26	1.55
B2T20C	2.36	1.79	2.43	2.95	1.49
B5T12C	1.82	1.44	2.05	2.32	1(b)
B5T12X	1.82	1.44	2.05	2.32	1.39
B2T12D	2.09	3.87	6.38	6.61	2.77
B3T10D	4.49	3.42	5.60	5.87	3.10
B5T8D	4.61	3.47	6.50	6.10	3.96
B2T8E	4.36	9.90	16.19	16.66	2.48
B4T6E	0.03(c)	17.55	26.64	31.53	6.42
W2T12D	5.37	4.10	6.70	6.96	1.76
W3T10D	5.35	4.03	6.36	7.04	4.30
W5T8D	5.57	4.21	6.62	7.33	2.79
a* Assumed ductility to be unity as a result of shear failure and lack of plastic hinge mechanism.					
b* Section did not reach ultimate moment capacity and did not develop any plastic strains.					
c* Concrete crushing before reinforcement yielded					

Table 8-6: Computed and measured ductility factors

273

Tensile Strain over the support at ultimate (mircrostrain)					
SPECIMEN	**BS 8110**	**ACI 318-95**	**EC2-92**	**Model Code**	**Measured at Failure**
B3T16A	27272	21341	30197	34591	2503
B3T16B	16283	12563	17433	20383	7190
B3T16BL	16283	12563	17433	20383	3777
B2T20B	16360	12718	17930	20310	2119
B5T12B	20739	16499	25742	27718	3528
B3T16C	7821	5829	8017	10203	6861
B2T20C	8143	6174	8550	10514	4819
B5T12C	11050	8711	12813	14505	3424
B5T12X	11050	8711	12813	14505	8704
B2T12D	31793	24558	40895	42199	17155
B3T10D	28154	21673	35933	37576	19030
B5T8D	23078	17570	33193	31322	19647
B2T8E	63970	49910	81340	83451	*
B4T6E	64635	49275	73579	86934	37609
W2T12D	26760	20795	34203	35406	11207
W3T10D	26804	20508	32509	36085	20521
W5T8D	27917	21362	33804	37559	14495
Average D, E and W	**25183.06**	**19456.47**	**30375.53**	**33155.53**	**20958**
*Realistic average value could not be obtained due to strains exceeding gauge capacities.					

Table 8-7: Computed and average experimental tensile strains at the support over 200 mm gauge length

274

% Redistribution at Yield of Support							% Redistribution (span)					
SPECIMEN	BS 8110	ACI 318	EC2-92	Model Code	Analytical at Yield Moment	Measured	BS 8110	ACI 318	EC2-92	Model Code	Analytical at experiment Yield Moment	Measured
B3T16A	-37.7	-13.3	-18.6	-17.6	a	a	21.36	7.54	10.5	10.01	a	a
B3T16B	-13.3	-13.8	-13.4	-12.6	-20.3	-33.9	7.5	7.8	7.6	7.1	11.5	20.8
B3T16BL	-13.3	-13.8	-13.4	-12.6	-20.3	-18.5	7.5	7.8	7.6	7.1	11.5	8
B2T20B	-10.7	-10.3	-11.1	-9.9	a	a	6.2	5.8	6.3	5.6	a	a
B5T12B	-14.9	-13.6	-16.2	-14.4	a	a	8.5	7.7	9.2	8.2	a	a
B3T16C	-11.9	-10.8	-12.1	-9.9	-15.9	-26.7	6.7	6.1	6.9	5.6	9.0	18.4
B2T20C	-10.9	-10.4	-12.1	-10.6	-8.5	-21.5	6.2	5.9	6.8	6.0	6.5	12.2
B5T12C	-13.5	-12.1	-12.2	-11.5	-15.0	-18.9	7.7	6.9	6.9	6.5	8.5	14.5
B5T12X	-13.5	-12.1	-12.2	-11.5	-15.0	-18.9	7.67	6.9	6.9	6.5	8.5	14.50
B2T12D	-14.2	-13.3	-17.5	-15.7	-15.0	-23.3	8.1	7.5	9.9	8.9	8.5	13.4
B3T10D	-11.6	-9.4	-12.3	-10.9	-15.4	-16.4	6.6	5.4	7.0	6.2	8.7	14.7
B5T8D	-7.9	-7.6	-8.3	-7.1	-12.6	-17.4	4.5	4.3	4.7	4.0	7.1	12.7
B2T8E	-16.3	-16.5	-12.8	-12.7	-25.6	-37.3	9.2	9.4	7.3	7.2	14.5	21.7
B4T6E	-10.2	-7.3	-10.3	-10.4	-19.9	-20.1	5.8	4.1	5.8	5.9	11.3	21.3
W2T12D	-13.1	-10.8	-13.1	-12.4	-15.5	-22.0	7.4	6.1	7.4	7.0	8.8	14.1
W3T10D	-12.3	-10.1	-12.5	-11.7	-13.2	-23.6	7.0	5.7	7.1	6.6	7.5	17.2
W5T8D	-8.6	-7.7	-8.9	-8.3	-7.3	-14.1	4.9	4.4	5.1	4.7	4.1	8.5
a* support did not reach yield												

Table 8-8: Moment redistribution over the support and spans at when the support reached yield moment

275

% Redistribution at Failure of Support							% Redistribution (span)					
SPECIMEN	BS 8110	ACI 318	EC2-92	Model Code	Analytical at experiment failure load	Measured	BS 8110	ACI 318	EC2-92	Model Code	Analytical at experiment failure load	Measured
B3T16A	-39.3	-16.8	-19.1	-18.7	-24.3	-31.9	22.3	9.5	10.8	10.6	16.2	16.2
B3T16B	-15.9	-14.9	-13.9	-18.1	-20.3	-37.2	9.0	8.5	7.9	10.2	20.9	20.9
B3T16BL	-15.9	-14.9	-13.9	-18.1	-20.3	-21.1	9.0	8.5	7.9	10.2	11.3	11.3
B2T20B	-17.6	-15.8	-16.4	-20.5	-21.7	-27.8	10.0	8.9	9.3	11.6	13.9	13.8
B5T12B	-28.2	-25.4	-20.6	-32.8	-20.1	-36.5	16.0	14.4	11.7	18.6	20.5	18.0
B3T16C	-12.1	-10.9	-12.3	-10.1	-25.5	-32.5	6.8	6.2	7.0	5.7	18.4	18.0
B2T20C	-11.2	-11.7	-12.6	-11.2	-9.0	-22.2	6.3	6.6	7.1	6.3	12.0	12.7
B5T12C	-14.2	-12.5	-12.3	-19.4	-17.4	-36.6	8.0	7.1	7.0	11.1	21.5	21.5
B5T12X	-14.2	-12.5	-12.3	-19.4	-21.9	-26.9	8.0	7.1	7.0	11.1	14.7	14.7
B2T12D	-25.1	-29.9	-25.2	-32.4	-20.2	-26.8	14.2	16.9	14.3	18.4	15.1	15.1
B3T10D	-24.9	-23.6	-19.6	-24.7	-19.6	-25.1	14.1	13.4	11.1	14.0	16.2	16.1
B5T8D	-13.1	-12.3	-17.4	-13.4	-11.6	-20.5	7.4	7.0	9.9	7.6	13.0	13.0
B2T8E	-32.8	-34.0	-31.0	-33.6	-18.7	-39.1	18.	19.3	17.5	19.1	18.9	18.9
B4T6E	-13.1	-29.9	-35.4	-31.0	-40.0	-39.2	7.4	16.9	16.9	17.6	21.3	21.3
W2T12D	-27.1	-25.3	-21.6	-27.5	-18.4	-24.5	15.4	14.3	12.2	15.6	13.2	13.2
W3T10D	-23.3	-12.3	-20.3	-25.5	-27.5	-31.8	13.2	6.9	11.5	14.4	18.2	18.2
W5T8D	-22.6	-19.1	-18.0	-25.8	-14.7	-21.5	12.8	10.8	10.2	14.6	11.2	11.2

Table 8-9: Moment redistribution over the support and spans at ultimate

276

Support % Redistribution at Yield						
Beam Series	**BS 8110**	**ACI 318**	**EC2-92**	**MODEL CODE**	**Analytical**	**Measured**
B3T16A	-37.68	-13.30	-18.58	-17.65	-	-
SERIES B	-13.09	-12.86	-13.54	-12.37	-20.31	-26.20
SERIES C	-12.47	-11.37	-12.12	-10.85	-13.57	-21.50
SERIES D	-11.23	-10.12	-12.70	-11.24	-14.30	-19.03
SERIES E	-13.28	-11.91	-11.56	-11.55	-22.74	-28.70
SERIES W	-11.34	-9.53	-11.49	-10.79	-12.00	-19.90
Over all avg.	**-16.52**	**-11.51**	**-13.33**	**-12.41**	**-16.59**	**-23.07**

Table 8-10: Average redistribution over the support for all beam series at yield

277

Span % Redistribution at Yield						
Beam Series	**BS 8110**	**ACI 318**	**EC2-92**	**MODEL CODE**	**Analytical**	**Measured**
B3T16A	21.36	7.54	10.53	10.01	-	-
SERIES B	7.42	7.29	7.68	7.01	11.51	14.40
SERIES C	7.07	6.44	6.87	6.15	8.13	14.90
SERIES D	6.37	5.74	7.20	6.37	8.11	13.60
SERIES E	7.53	6.75	6.55	6.55	12.89	21.50
SERIES W	6.43	5.40	6.51	6.12	6.80	13.27
Over all Avg.	**9.36**	**6.53**	**7.56**	**7.03**	**9.49**	**16.10**

Table 8-11: Average redistribution over the span for all beam series at yield

278

Support % Redistribution at Ultimate						
Beam Series	**BS 8110**	**ACI 318**	**EC2-92**	**MODEL CODE**	**Analytical at failure load**	**Measured at failure**
B3T16A	-39.32	-16.81	-19.13	-18.73	-24.29	-31.95
SERIES B	-19.40	-17.76	-16.24	-22.36	-20.63	-30.65
SERIES C	-12.90	-11.92	-12.37	-15.03	-18.46	-29.86
SERIES D	-21.03	-21.93	-20.73	-23.49	-17.10	-24.07
SERIES E	-22.95	-31.96	-33.19	-32.33	-29.35	-39.13
SERIES W	-24.36	-18.90	-19.98	-26.23	-20.20	-25.92
Over all avg.	**-23.33**	**-19.88**	**-20.27**	**-23.03**	**-21.67**	**-30.26**

Table 8-12: Average redistribution at ultimate over the support

279

Span % Redistribution at Ultimate						
Beam Series	**BS 8110**	**ACI 318**	**EC2-92**	**MODEL CODE**	**Analytical at Failure load**	**Measured at failure**
B3T16A	22.29	9.52	10.84	10.62	13.77	16.18
SERIES B	11.00	10.07	9.20	12.67	15.96	16.01
SERIES C	7.31	6.76	7.01	8.52	10.46	16.85
SERIES D	11.92	12.43	11.75	13.31	9.69	14.75
SERIES E	13.01	18.10	17.24	18.32	16.63	20.12
SERIES W	13.81	10.71	11.32	14.87	11.45	14.20
Over all avg.	**13.22**	**11.27**	**11.23**	**13.05**	**12.99**	**16.35**

Table 8-13: Average redistribution at ultimate over the Span

280

% of Redistribution Due to Yield						
Beam Series	**BS 8110**	**ACI 318**	**EC2-92**	**MODEL CODE**	**Analytical at Failure load**	**Measured at failure**
B3T16A	4.17	20.88	2.88	5.77	-	-
SERIES B	32.53	27.59	16.63	44.68	1.55	11.37
SERIES C	3.33	4.61	2.02	27.81	26.49	28.00
SERIES D	46.60	53.85	38.74	52.15	16.37	20.94
SERIES E	42.14	62.73	65.17	64.27	22.52	26.65
SERIES W	53.45	49.58	42.49	58.86	40.59	23.23
Over all avg.	**30.37**	**36.54**	**27.99**	**42.26**	**21.51**	**22.04**

Table 8-14: Average percentage of total redistribution occurring due to yield

281

Plastic Hinge length over the support (mm)						
SPECIMEN	**BS 8110**	**ACI 318**	**EC2-92**	**Model Code**	**Analytical**	**Measured**
B3T16A	20.7	17.8	17.6	35.4	5.74	x
B3T16B	14.9	15.4	14.4	25.5	x	71.4
B3T16BL	14.9	15.4	14.4	25.5	82.22	19.8
B2T20B	30.5	28.8	19.9	44.1	30.53	x
B5T12B	40.5	38.0	11.1	52.1	607.36	x
B3T16C	5.5	3.4	6.3	14.2	17.69	61.9
B2T20C	13.8	12.1	12.8	28.5	21.97	246.95
B5T12C	27.2	19.1	6.8	37.6	x	x
B5T12X	27.2	19.1	6.8	37.6	35.49	80.3
B2T12D	56.9	47.3	11.4	69.1	100.68	167.4
B3T10D	52.4	46.5	11.9	69.5	42.67	162.4
B5T8D	27.1	27.9	15.3	43.8	82.56	181.1
B2T8E	55.6	45.9	12.3	71.2	49.45	108.6
B4T6E	1.1	18.9	22.6	24.7	97.28	136.5
W2T12D	52.9	45.0	14.8	73.2	81.72	120.8
W3T10D	31.6	12.1	14.9	45.5	74.34	110.5
W5T8D	32.5	30.1	15.3	45.0	31.86	112.5
x : No plastic hinge formed						

Table 8-15: Computed and measured plastic hinge length over the support area.

282

Average Plastic Hinge lengths (mm)						
Code Beam Series	BS 8110	ACI 318	EC2-92	MC 90	Analytical	Measured
B3T16A	20.68	17.82	17.56	35.36	5.74	-
Series B	25.19	24.43	14.93	36.82	240.04	45.6
Series C	18.46	13.39	8.17	29.50	25.05	88.53
Series D	45.49	40.57	12.88	60.79	75.30	170.25
Series E	28.38	32.39	17.45	47.98	73.37	122.53
Series W	39.01	29.10	14.98	54.58	62.64	114.58

Table 8-16: Computed and experimental plastic hinge lengths of the beam series

283

Plastic Hinge Length Expressions (mm)				
Specimen	**Baker**	**Mattock**	**Corley**	**Experi-mental**
B2T12D	76.15	87.45	70.86	167.4
B3T10D	77.23	88.79	71.62	162.4
B5T8D	79.16	91.37	72.83	181.1
B2T8E	74.45	85.08	70.58	108.6
B4T6E	74.67	85.31	70.95	136.5
W2T12D	77.12	88.79	71.34	120.8
W3T10D	76.23	87.42	71.13	110.5
W5T8D	78.84	90.90	72.66	112.5
Average	**76.73**	**88.14**	**71.5**	**137.48**

Table 8-17: Computed and experimental plastic hinge lengths of the beam series

284

Total Rotation over the support radians. 10^{-6}						
SPECIMEN	**BS 8110**	**ACI 318-95**	**EC2-92**	**Model Code**	**Analytical**	**Measured**
B3T16A	1611.80	728.17	941.64	2107.99	x	x
B3T16B	867.17	754.51	875.70	1723.49	3100.00	2812.65
B3T16BL	867.17	754.51	875.70	1723.49	3100.00	222.00
B2T20B	1709.56	1349.74	1191.72	2872.95	x	x
B5T12B	2910.17	2334.34	922.30	4564.34	x	x
B3T16C	401.21	216.03	467.52	1158.91	940.00	5817.00
B2T20C	963.38	722.30	913.50	2247.87	1000.00	5050.05
B5T12C	2496.97	1538.56	670.29	3943.65	x	x
B5T12X	2496.97	1538.56	670.29	3943.65	2700.00	2228.00
B2T12D	4979.42	6673.99	2388.41	14777.00	9900.00	15111.20
B3T10D	8182.82	5981.21	2227.05	13461.00	4300.00	23409.20
B5T8D	3503.92	2951.39	2592.09	7104.00	10000.00	14891.90
B2T8E	12227.44	10687.42	4442.04	26254.79	3700.00	3259.90
B4T6E	327.78	4148.23	7165.95	9160.54	18000.00	2698.90
W2T12D	7722.55	5409.67	2600.99	13248.11	6500.00	3885.80
W3T10D	4585.21	1434.43	2505.81	8299.74	8900.00	6840.30
W5T8D	4815.46	3632.60	2623.21	8391.29	3100.00	6650.90
x : No plastic hinge formed						

Table 8-18: Computed and measured total rotation values over the support section.

285

Average Total rotation X 10^{-6} radian						
Code Beam Series	BS 8110	ACI 318	EC2-92	MC 90	Analytical	Measured
B3T16A	1612.	728.	942.	2108.	-	-
SERIES B	1589.	1298.	966.	2721.	3100.	1517.
SERIES C	1590.	1004.	680.	2824.	1547.	4365.
SERIES D	5555.	5202.	2403.	11781.	8067.	17804.
SERIES E	6278.	7418.	5804.	17708.	10850.	2979.
SERIES W	5708.	3492.	2577.	9980.	6167.	5792.

Table 8-19: Average measured and calculated total rotations of test beams series

286

Ductility Factor : Support					
SPECIMEN	**BS 8110**	**ACI 318-95**	**EC2-92**	**MODEL CODE**	**d**
B3T16A	1.20	4.64	6.56	7.52	1.00
Series B	3.80	2.92	4.15	4.71	1.00
Series C	1.95	1.50	2.08	2.46	1.36
Series D	3.73	3.59	6.16	6.19	3.28
Series E	10.77	13.72	21.41	24.10	15.91
Series W	5.43	4.11	6.56	7.11	2.95

Table 8-20: Average ductility factor for all specimen series

287

	Support Stiffness at Yield (kNm^2)					Yield stiffness span (kNm^2)				
SPECIMEN	**BS 8110**	**ACI 318-95**	**EC2-92**	**Model Code**	**Measured**	**BS 8110**	**ACI 318-95**	**EC2-92**	**Model Code**	**Measured**
B3T16A	1709.27	8325.71	8553.18	8679.69	a	14190.52	13599.96	14089.29	14418.26	a
B3T16B	2741.60	2644.96	2733.16	2806.57	b	4412.14	4497.78	4389.01	4594.08	4639.55
B3T16BL	2741.60	2644.96	2733.16	2806.57	2945.68	4412.14	4497.78	4389.01	4594.08	2756.89
B2T20B	3309.84	3171.77	3286.58	3373.25	a	4412.14	4497.78	4389.01	4594.08	a
B5T12B	1536.20	1495.78	1538.44	1561.23	a	4412.14	4497.78	4389.01	4594.08	a
B3T16C	714.67	694.74	723.75	770.76	615.68	1007.22	974.67	1016.39	1139.61	1041.82
B2T20C	831.78	797.09	834.82	881.85	890.52	1007.22	974.67	1016.39	1139.61	901.78
B5T12C	423.77	413.90	431.62	445.92	b	1007.22	974.67	1016.39	1139.61	a
B5T12X	423.77	413.90	431.62	445.92	488.06	1007.22	974.67	1016.39	1139.61	a
B2T12D	189.95	184.90	190.38	191.72	210.20	283.26	274.63	285.44	289.51	224.31
B3T10D	215.38	209.51	216.18	217.99	274.00	283.26	274.63	285.44	289.51	261.02
B5T8D	336.08	323.75	294.08	340.08	327.61	283.26	274.63	285.44	289.51	295.44
B2T8E	140.57	137.38	140.51	140.87	151.26	219.43	213.16	219.61	220.73	270.71
B4T6E	148.46	271.45	279.96	280.86	233.23	219.43	213.16	219.61	220.73	228.77
W2T12D	273.36	264.35	273.93	276.17	246.08	379.91	366.78	382.33	387.99	353.04
W3T10D	291.31	281.35	291.82	294.38	271.81	379.91	366.78	382.33	387.99	364.01
W5T8D	289.24	280.03	290.13	292.55	320.81	379.91	366.78	382.33	387.99	361.35
a* Support did not reach yield strains. b* No experimental data available										

Table 8-21: Computed and experimental flexural stiffness calculated when the support reached yield

	Support Stiffness at Failure (kNm^2)					Stiffness at Span When Support Reached Failure (kNm^2)				
SPECIMEN	**BS 8110**	**ACI 318-95**	**EC2-92**	**Model Code**	**Measured at Failure**	**BS 8110**	**ACI 318-95**	**EC2-92**	**Model Code**	**Measured at Failure**
B3T16A	1487.21	1863.93	1341.63	1224.66	10786.16	3020.14	2790.89	1918.37	1647.75	16105.58
B3T16B	779.24	985.40	738.58	663.36	1556.60	1189.45	1093.26	1172.20	1028.20	4353.55
B3T16BL	779.24	985.40	738.58	663.36	3859.64	1189.45	1093.26	1172.20	1028.20	2134.60
B2T20B	751.10	939.30	684.54	647.46	4188.42	1194.92	1077.20	1121.04	1052.36	5244.27
B5T12B	497.14	609.90	389.54	400.29	3091.64	1145.80	1010.85	921.57	1054.32	7536.65
B3T16C	404.55	515.95	404.03	348.54	409.07	564.87	720.49	576.83	456.32	1026.64
B2T20C	360.12	455.16	351.16	313.12	618.78	510.28	675.64	512.04	437.15	472.31
B5T12C	243.80	297.33	212.82	205.83	642.17	440.41	554.01	424.37	413.55	1211.82
B5T12X	243.80	297.33	212.82	205.83	373.79	440.41	554.01	424.37	413.55	1150.74
B2T12D	101.61	52.64	30.49	33.59	92.5	87.69	118.07	64.33	75.65	84.4
B3T10D	53.08	66.93	39.41	42.45	95.39	98.40	118.63	66.22	73.89	111.88
B5T8D	77.61	97.65	46.49	60.12	95.84	97.50	117.76	69.47	74.25	101.56
B2T8E	16.67	15.31	8.90	9.88	67.47	29.45	37.96	21.45	23.88	131.49
B4T6E	12.34	16.06	11.02	9.37	46.60	19.73	35.93	25.75	22.20	130.68
W2T12D	56.54	70.36	42.02	46.09	162.31	110.88	134.35	77.63	90.17	213.67
W3T10D	57.77	73.55	47.11	45.64	73.65	104.98	106.16	80.27	86.85	202.67
W5T8D	55.19	70.28	45.04	43.52	121.11	101.84	121.24	75.69	85.28	236.95

Table 8-22: Computed and experimental flexural stiffness calculated when the support reached maximum moment

	$EI_{(Support)}/EI_{(Span)}$ at Yield					$EI_{(Support)}/EI_{(Span)}$ at Ultimate				
SPECIMEN	**BS 8110**	**ACI 318-95**	**EC2-92**	**Model Code**	**Measured at Failure**	**BS 8110**	**ACI 318-95**	**EC2-92**	**Model Code**	**Measured at Failure**
B3T16A	0.12	0.61	0.61	0.60	a	0.49	0.67	0.70	0.74	0.67
B3T16B	0.62	0.59	0.62	0.61	b	0.66	0.90	0.63	0.65	0.38
B3T16BL	0.62	0.59	0.62	0.61	1.07	0.66	0.90	0.63	0.65	1.81
B2T20B	0.75	0.71	0.75	0.73	a	0.63	0.87	0.61	0.62	0.80
B5T12B	0.35	0.33	0.35	0.34	a	0.43	0.60	0.42	0.38	0.41
B3T16C	0.71	0.71	0.71	0.68	0.59	0.72	0.72	0.70	0.76	0.40
B2T20C	0.83	0.82	0.82	0.77	0.99	0.71	0.67	0.69	0.72	1.31
B5T12C	0.42	0.42	0.42	0.39	a	0.55	0.54	0.50	0.50	0.53
B5T12X	0.42	0.42	0.42	0.39	a	0.55	0.54	0.50	0.50	0.32
B2T12D	0.67	0.67	0.67	0.66	0.94	1.16	0.45	0.47	0.44	1.09
B3T10D	0.76	0.76	0.76	0.75	1.05	0.54	0.56	0.60	0.57	0.85
B5T8D	1.19	1.18	1.03	1.17	1.11	0.80	0.83	0.67	0.81	0.94
B2T8E	0.64	0.64	0.64	0.64	0.56	0.57	0.40	0.41	0.41	0.51
B4T6E	0.68	1.27	1.27	1.27	1.02	0.63	0.45	0.43	0.42	0.36
W2T12D	0.72	0.72	0.72	0.71	0.70	0.51	0.52	0.54	0.51	0.76
W3T10D	0.77	0.77	0.76	0.76	0.75	0.55	0.69	0.59	0.53	0.36
W5T8D	0.76	0.76	0.76	0.75	0.89	0.54	0.58	0.59	0.51	0.51
a* Support or span bars did not reach yield b* Experimental data not available										

Table 8-23: Relative stiffness ratios over the support at both yield and ultimate stages.

290

Neutral Axis Depth Ratios(Support)						
SPECIMEN	**Depth (mm)**	**BS 8110**	**ACI 318-95**	**EC2-92**	**Model Code**	**Measured at Failure**
B3T16A	362	0.114	0.123	0.104	0.092	0.275
B3T16B	217	0.177	0.193	0.167	0.147	0.167
B3T16BL	217	0.177	0.193	0.167	0.147	0.215
B2T20B	215	0.176	0.191	0.163	0.147	0.196
B5T12B	219	0.144	0.154	0.120	0.112	0.206
B3T16C	121	0.309	0.340	0.304	0.255	0.291
B2T20C	119	0.301	0.328	0.290	0.250	0.288
B5T12C	123	0.241	0.256	0.215	0.194	0.309
B5T12X	123	0.241	0.256	0.215	0.194	0.221
B2T12D	**123**	**0.099**	**0.109**	**0.079**	**0.077**	**0.261**
B3T10D	**124**	**0.111**	**0.122**	**0.089**	**0.085**	**0.287**
B5T8D	**125**	**0.132**	**0.146**	**0.095**	**0.100**	**0.237**
B2T8E	**125**	**0.052**	**0.057**	**0.041**	**0.040**	**0.252**
B4T6E	**126**	**0.051**	**0.057**	**0.045**	**0.039**	**0.245**
W2T12D	**123**	**0.116**	**0.126**	**0.093**	**0.090**	**0.307**
W3T10D	**124**	**0.111**	**0.128**	**0.097**	**0.088**	**0.261**
W5T8D	**125**	**0.111**	**0.123**	**0.094**	**0.085**	**0.224**
Average		*159.47*	*0.157*	*0.171*	*0.14*	*0.1269*
Average was taken for highlighted values of Series D, E and W						

Table 8-24: Computed and experimental neutral axis depth ratios at ultimate.

291

<table>
<tr><td>f_c= 40Mpa
E_s=200
E_c= 30</td><td>Section Dimensions</td><td colspan="6">b= 300
d=123 h = 150
ρ @ support variable
 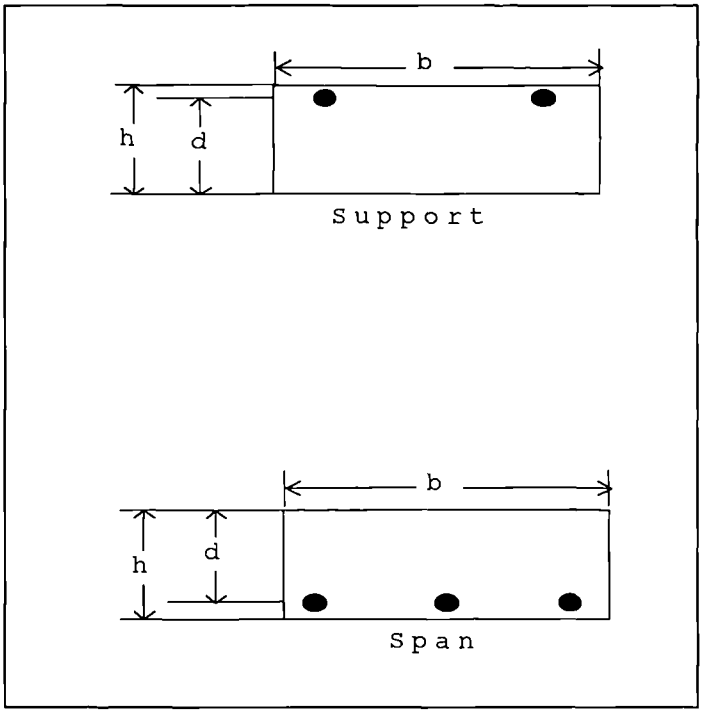

Span reinforcement fixed at 0.65% b= 300 ,d=123, h =150</td></tr>
<tr><td colspan="2">ρ @ Support (%)</td><td>0.1</td><td>0.2</td><td>0.3</td><td>0.4</td><td>0.5</td><td>0.6</td></tr>
<tr><td>Loading</td><td colspan="7">Propped cantilever loaded at centre by a point load
 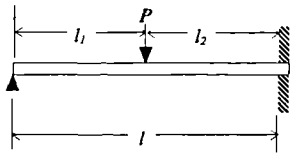
</td></tr>
</table>

Table 8-25: Idealise beam properties

% ρ Tensile Reinforcement ratio.	0.6	0.5	0.4	0.3	0.2	0.1
Yield and Failure Strains (microstrain)	**Neutral Axis Depth Ratio at Ultimate**					
5900 (Yield condition)	0.164	0.146	0.130	0.112	0.091	0.064
30000	0.106	0.093	0.078	0.063	0.049	0.031
50000	0.070	0.069	0.067	0.059	0.043	0.026
70000	0.053	0.052	0.051	0.050	0.041	0.023
3500 (Concrete failure)	0.112	0.092	0.075	0.058	0.041	0.018

Table 8-26: Calculated Neutral Axis depth ratios for the idealised beams

Plastic Hinge Lengths (mm)				
%r	**3%**	**5%**	**7%**	ε_{cu} **=0.35%**
0.6	54	89.09	114.21	49.11
0.5	47.46	75.03	98.01	52.08
0.4	43.68	63.02	83.88	55.01
0.3	41.22	56.35	72.53	60.92
0.2	39.95	55.81	69.42	76.93
0.1	28.87	24.09	25.67	36.29

Table 8-27: List of all plastic hinge length of the idealised beams

Plastic Rotations X 10^{-6}(radians)				
%r	**3%**	**5%**	**7%**	ε_{cu} **=035%**
0.6	5473	17224	30958	4709
0.5	5049	14466	26224	6600
0.4	4507	11234	21044	7954
0.3	4056	9402	17947	11423
0.2	4132	9646	16287	21418
0.1	566	1979	2879	12054

Table 8-28: Plastic rotation calculated based on the four failure criteria

Total Rotations x 10^{-6} (radians)				
%r	3%	5%	7%	ε_{cu} =0.35%
0.6	8771	22232	37163	7779
0.5	7759	18509	31312	9600
0.4	6972	14650	25434	11010
0.3	6454	12592	21828	14824
0.2	6406	12620	19866	25323
0.1	3163	4726	5697	15368

Table 8-29: Total rotation calculated based on the basis four failure criteria

% Redistribution at Yield				
%r	3%	5%	7%	ε_{cu} =0.35%
0.6	30.3	30.3	30.32	30.3
0.5	35.67	35.69	35.7	35.69
0.4	39.31	39.31	39.31	39.31
0.3	43.3	43.3	43.3	43.3
0.2	47.21	47.21	47.21	47.21
0.1	51.89	51.89	51.89	51.89

Table 8-30: Percent redistribution at yield using the four failure criteria

% Redistribution at Ultimate				
%r	3%	5%	7%	ε_{cu} =0.35%
0.6	29.2	27.26	25.77	29.32
0.5	37.8	37.31	36.18	38.22
0.4	44.38	45.88	45.56	45.78
0.3	48.3	50.65	51.52	51.14
0.2	50.88	51.7	52.28	52.47
0.1	52.2	52.27	52.31	52.56

Table 8-31: Percent redistribution at ultimate using the four failure criteria

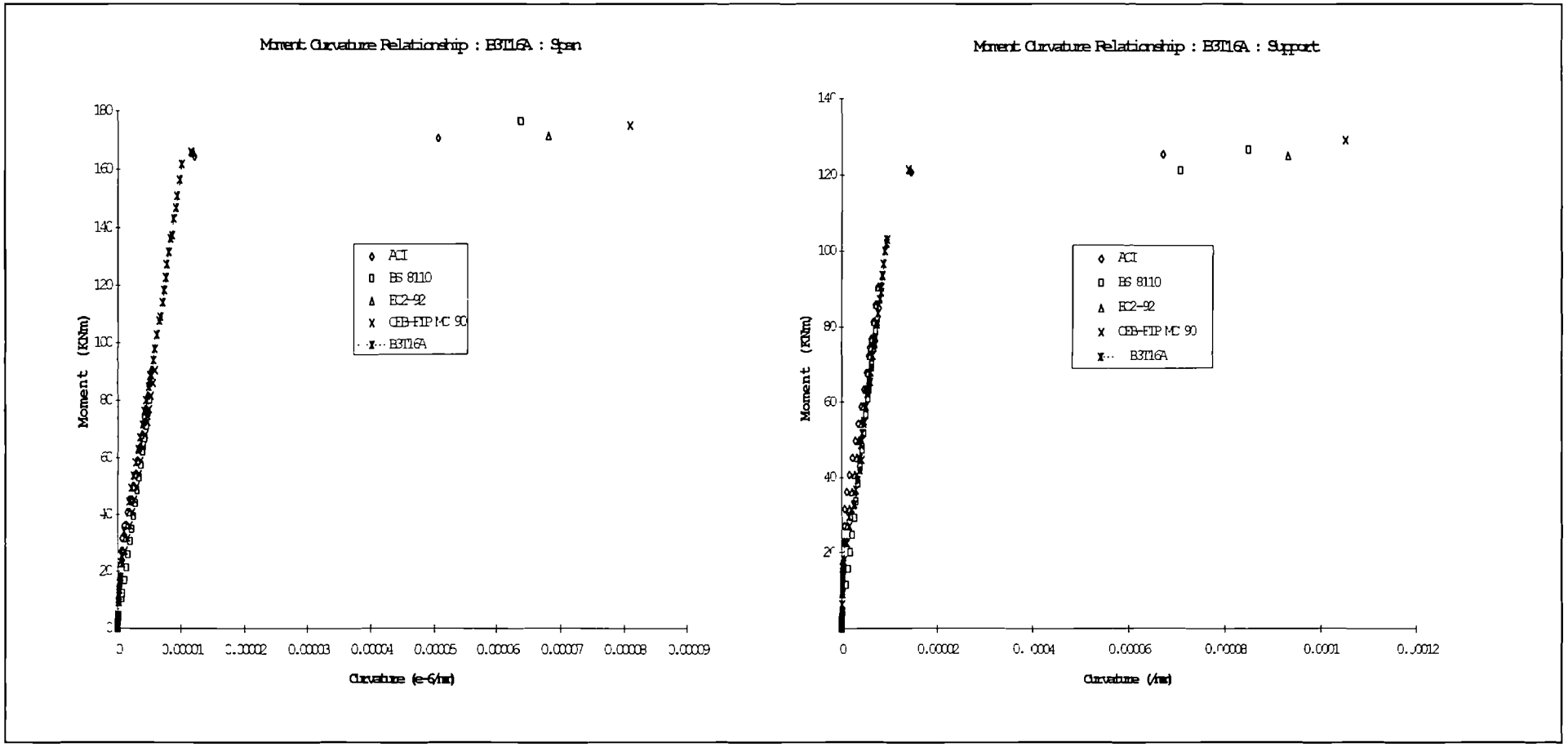

Figure 8-1: Specimen B3T16A measured and modelled codes moment curvature relationship over span and support sections.

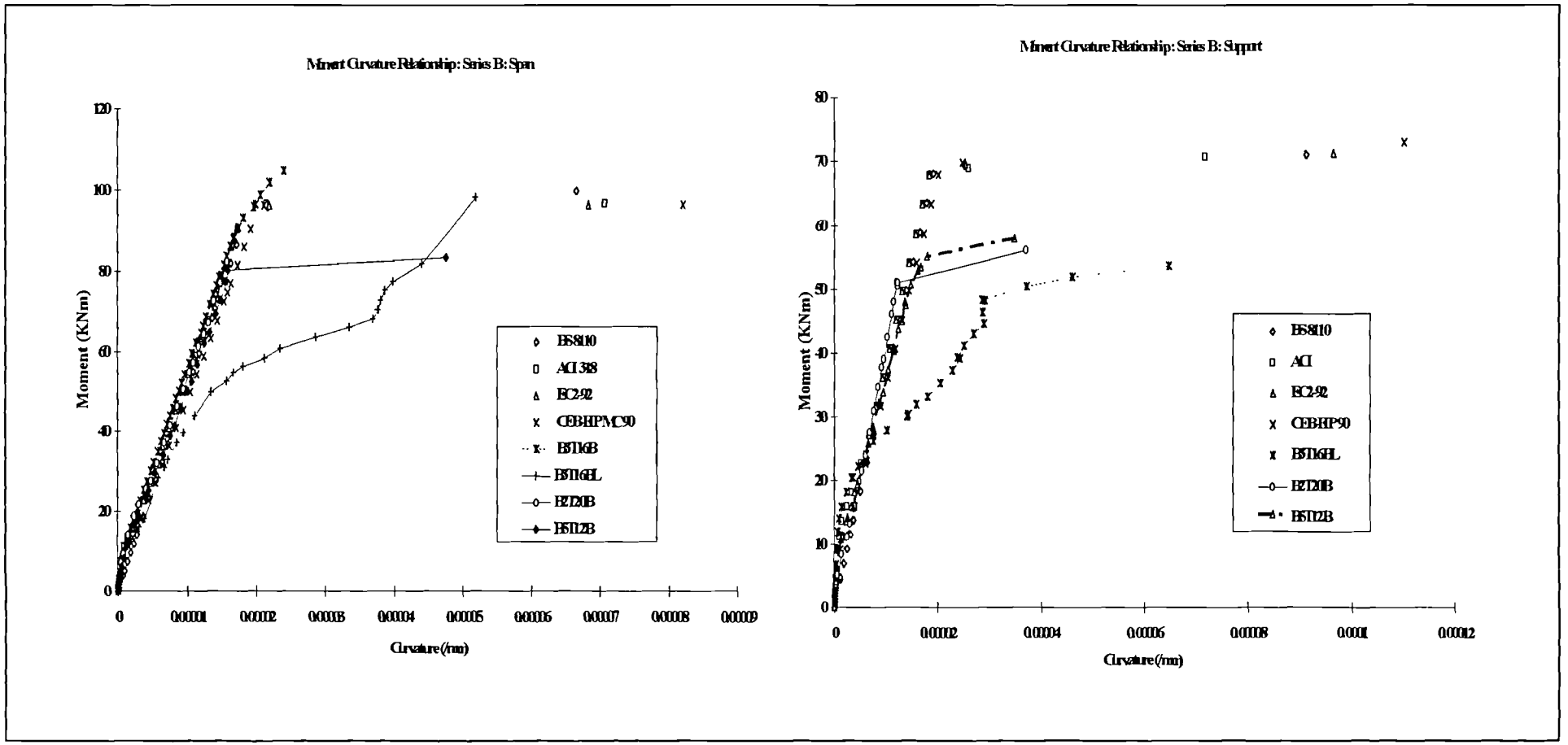

Figure 8-2: Series B measured and modelled codes moment curvature relationship over span and support sections

296

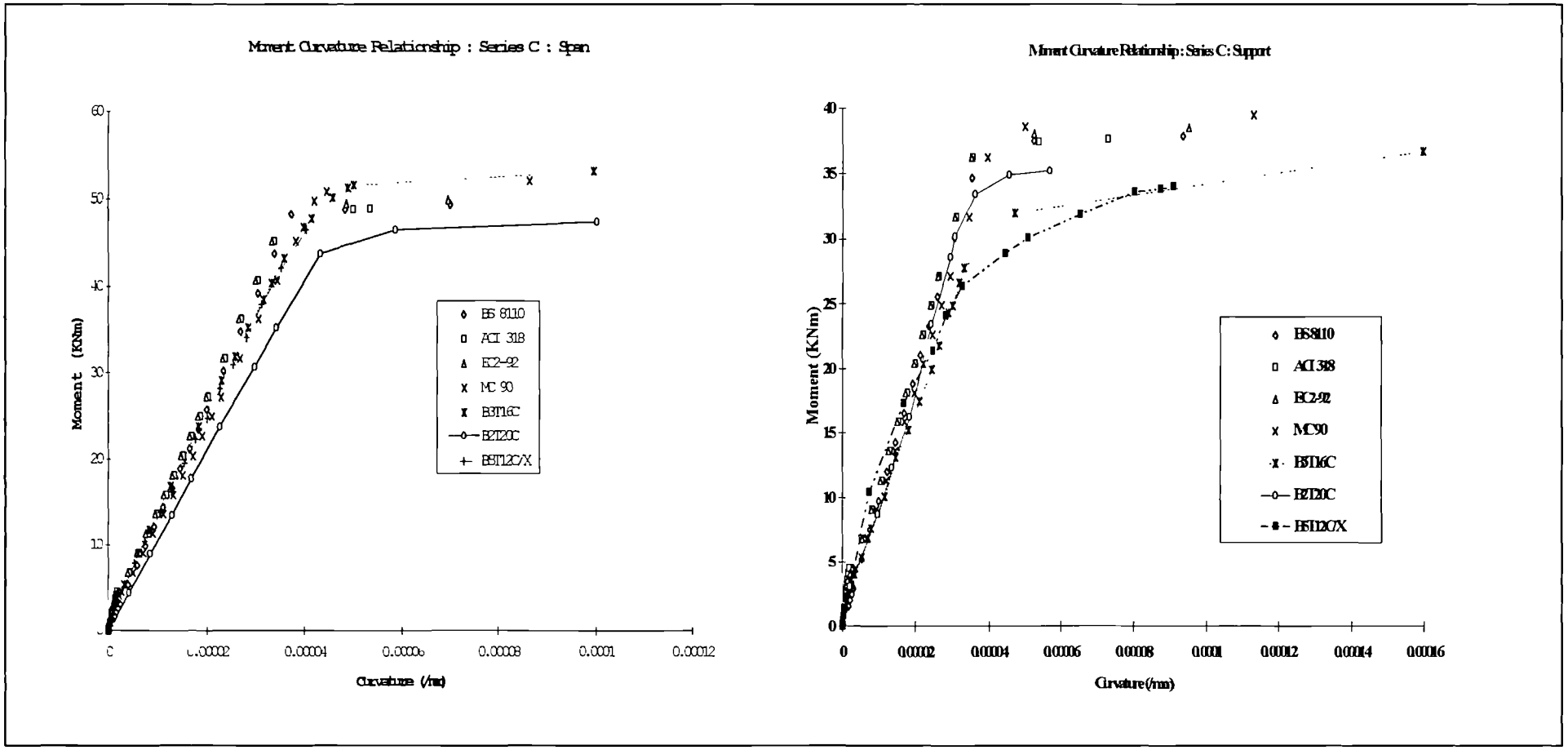

Figure 8-3: Series C measured and modelled codes moment curvature relationship over span and support sections

297

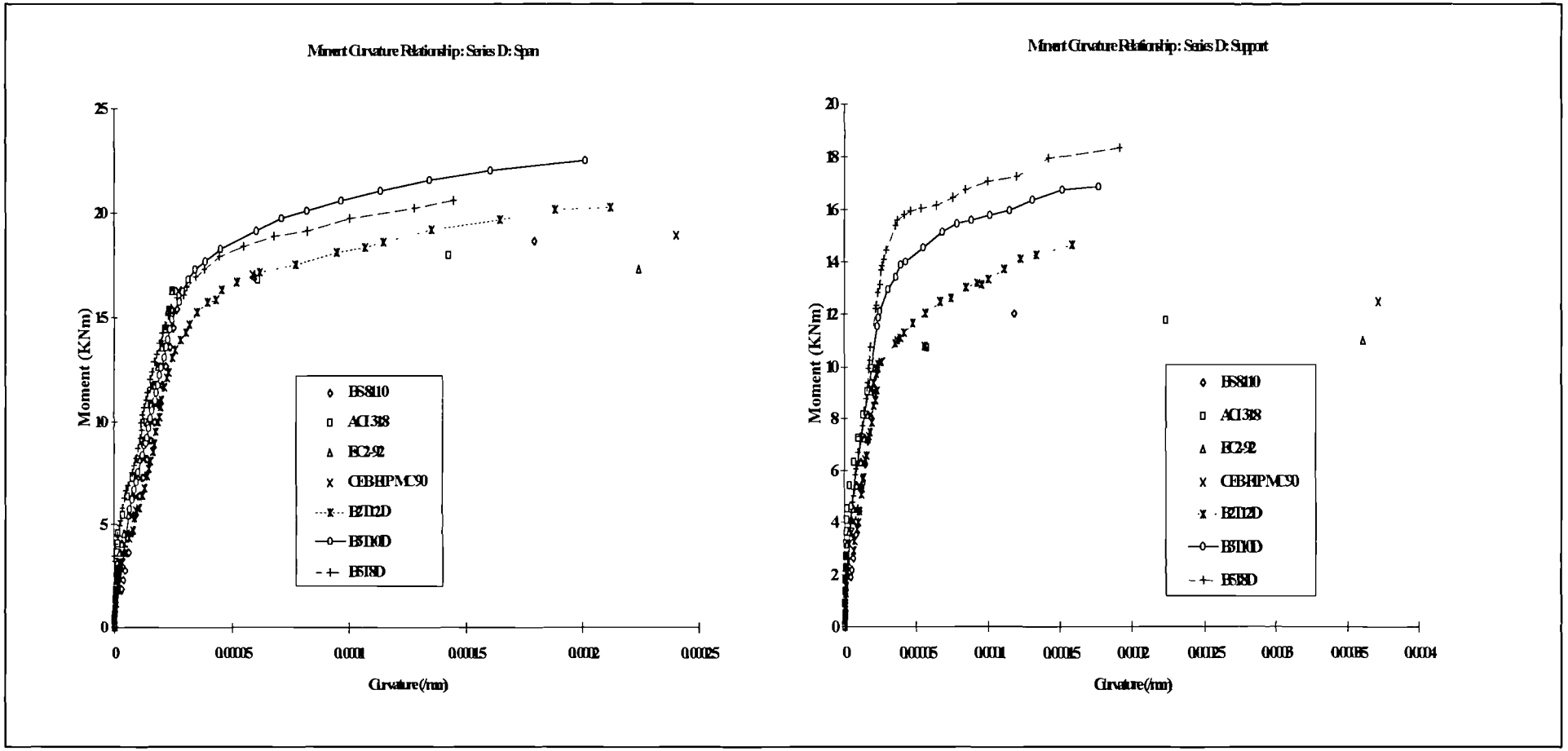

Figure 8-4: Series D measured and modelled codes moment curvature relationship over span and support sections

298

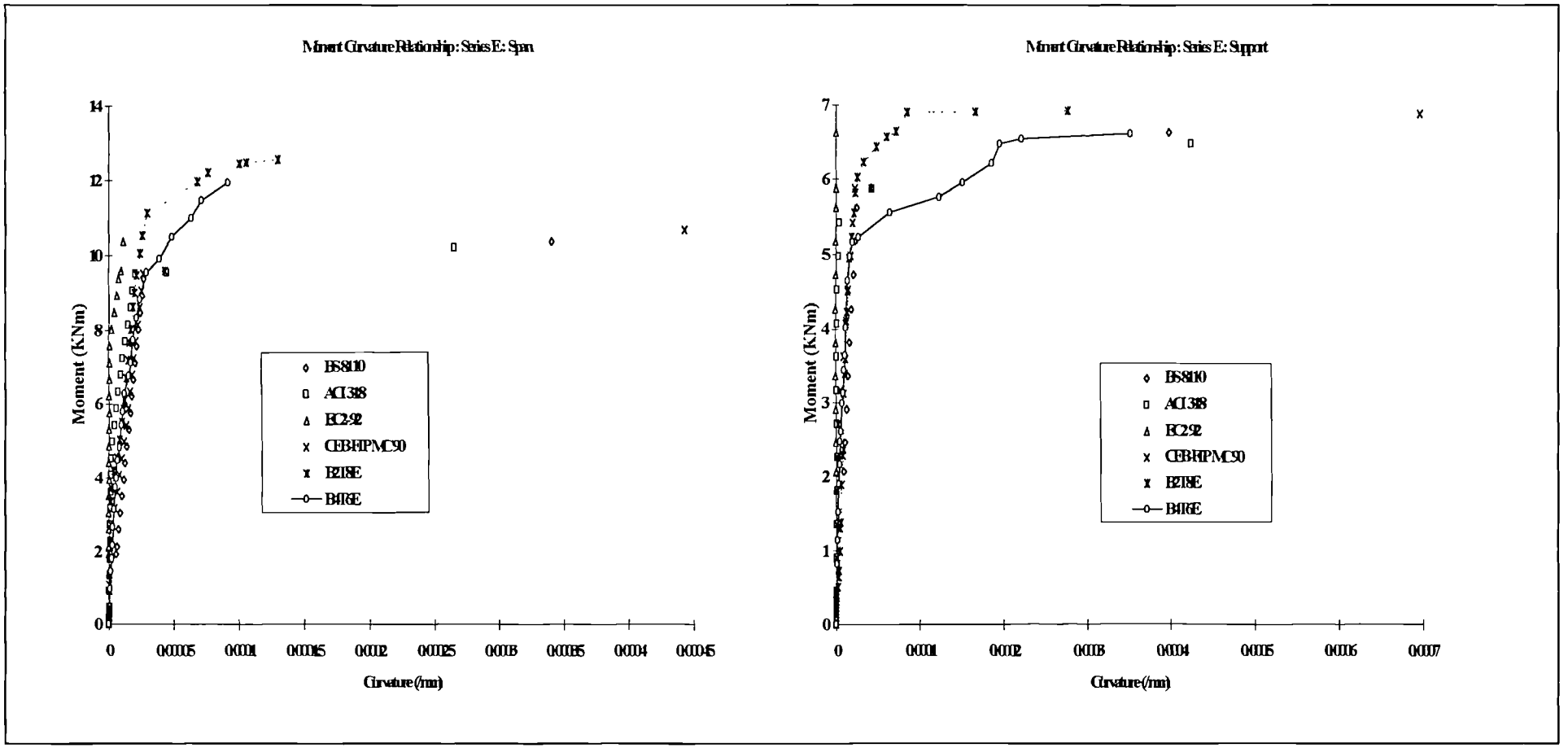

Figure 8-5: Series E measured and modelled codes moment curvature relationship over span and support sections

299

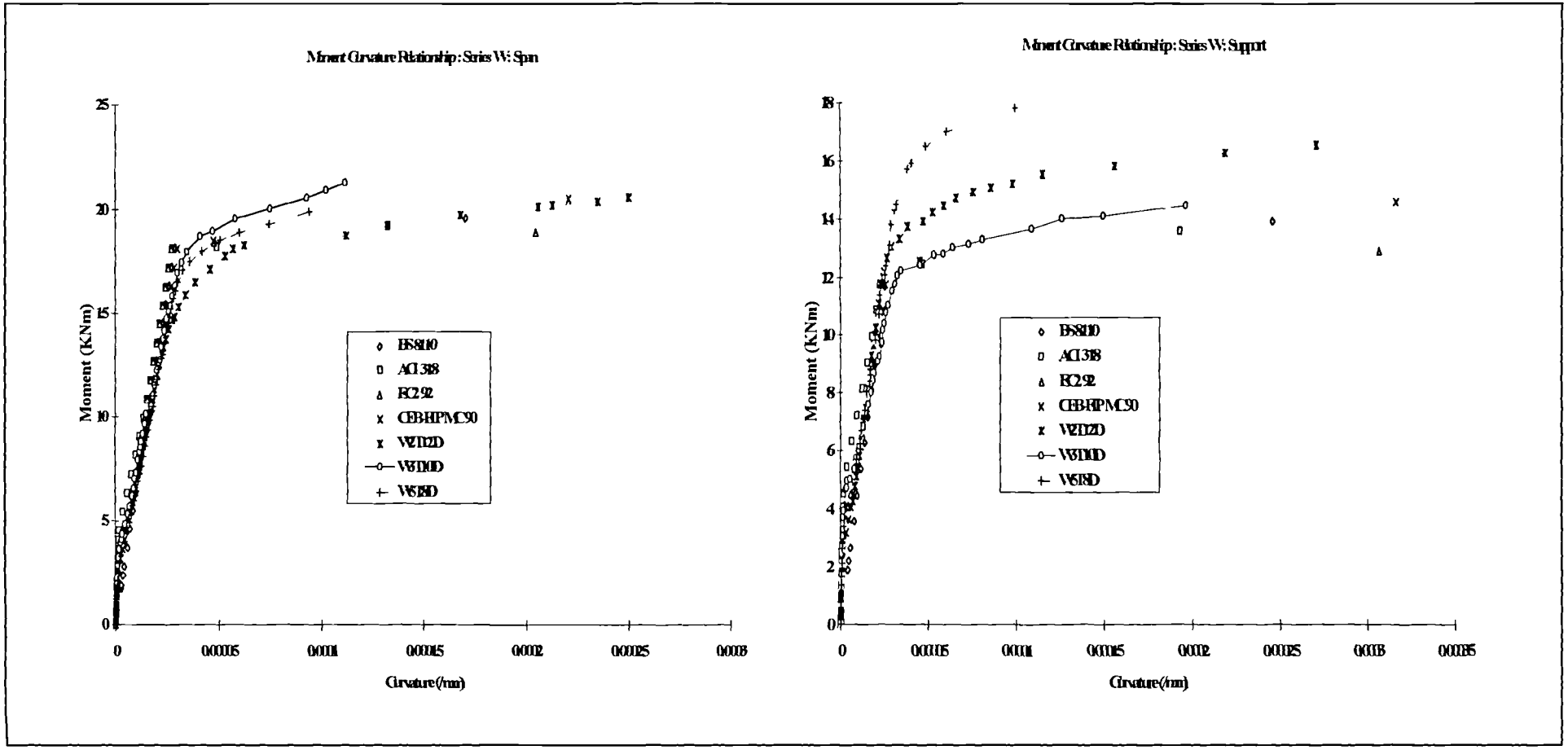

Figure 8-6: Series W measured and modelled codes moment curvature relationship over span and support sections

300

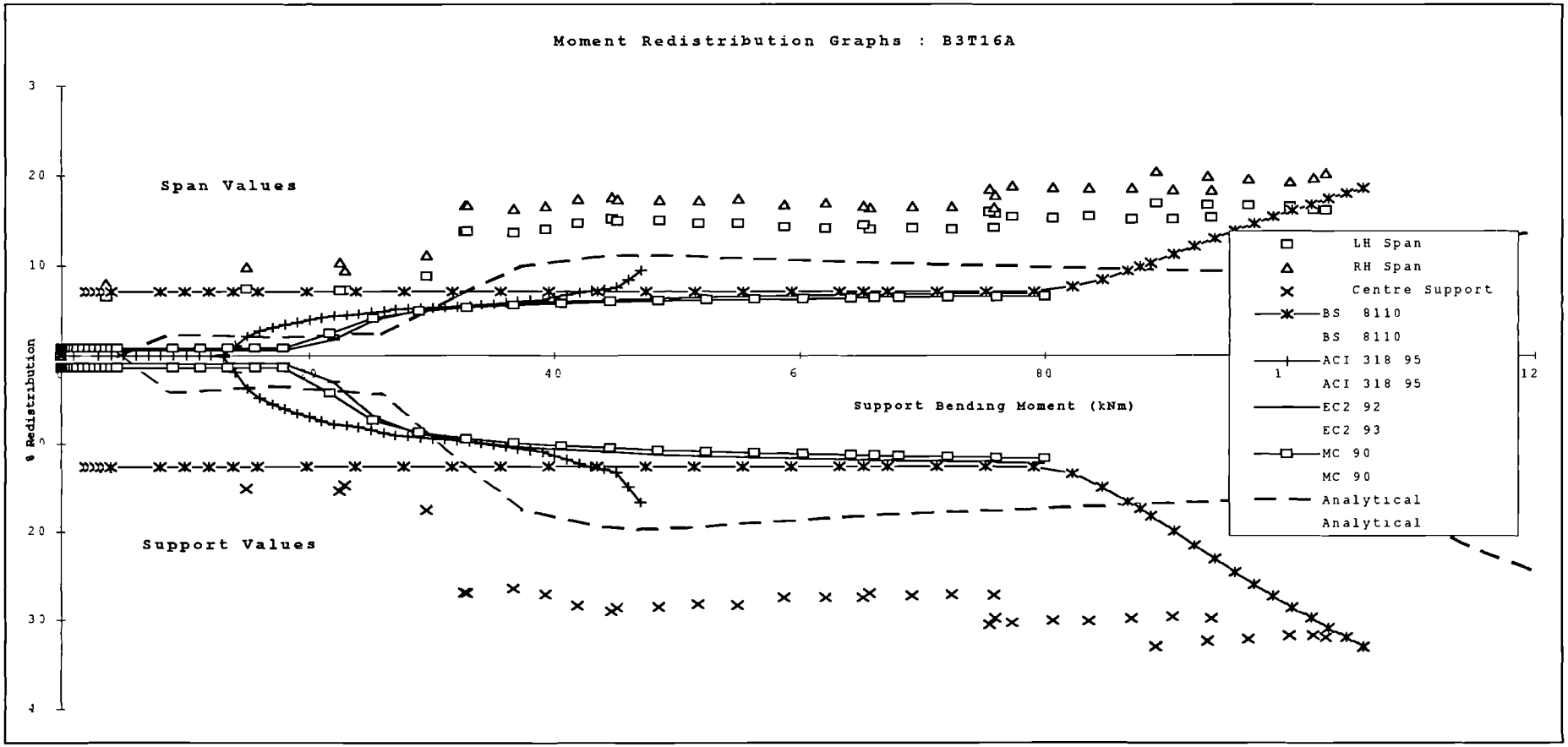

Figure 8-7: B3T16A measured and modelled moment redistribution versus support moment.

301

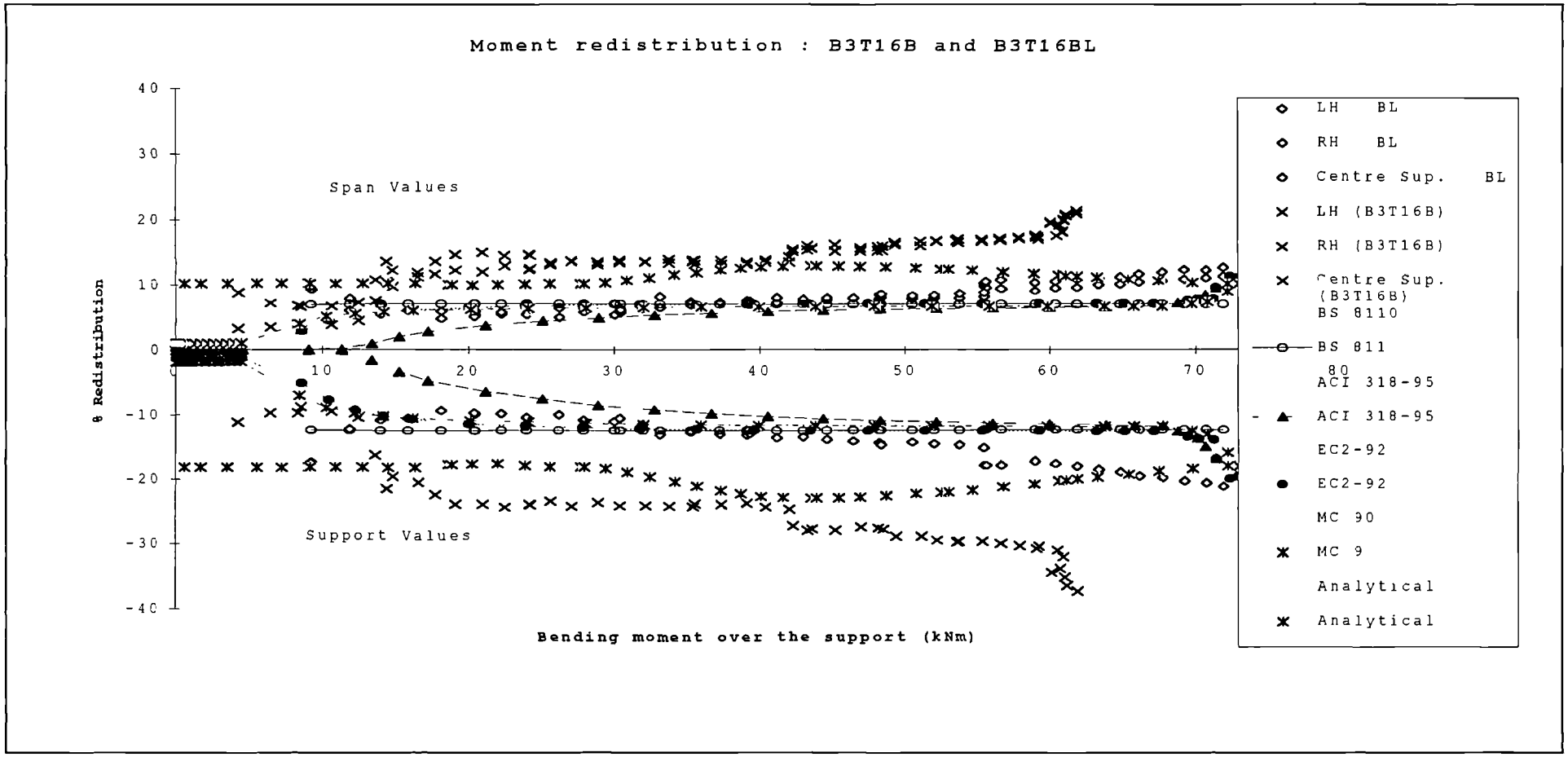

Figure 8-8: B3T16B measured and modelled moment redistribution versus support moment.

302

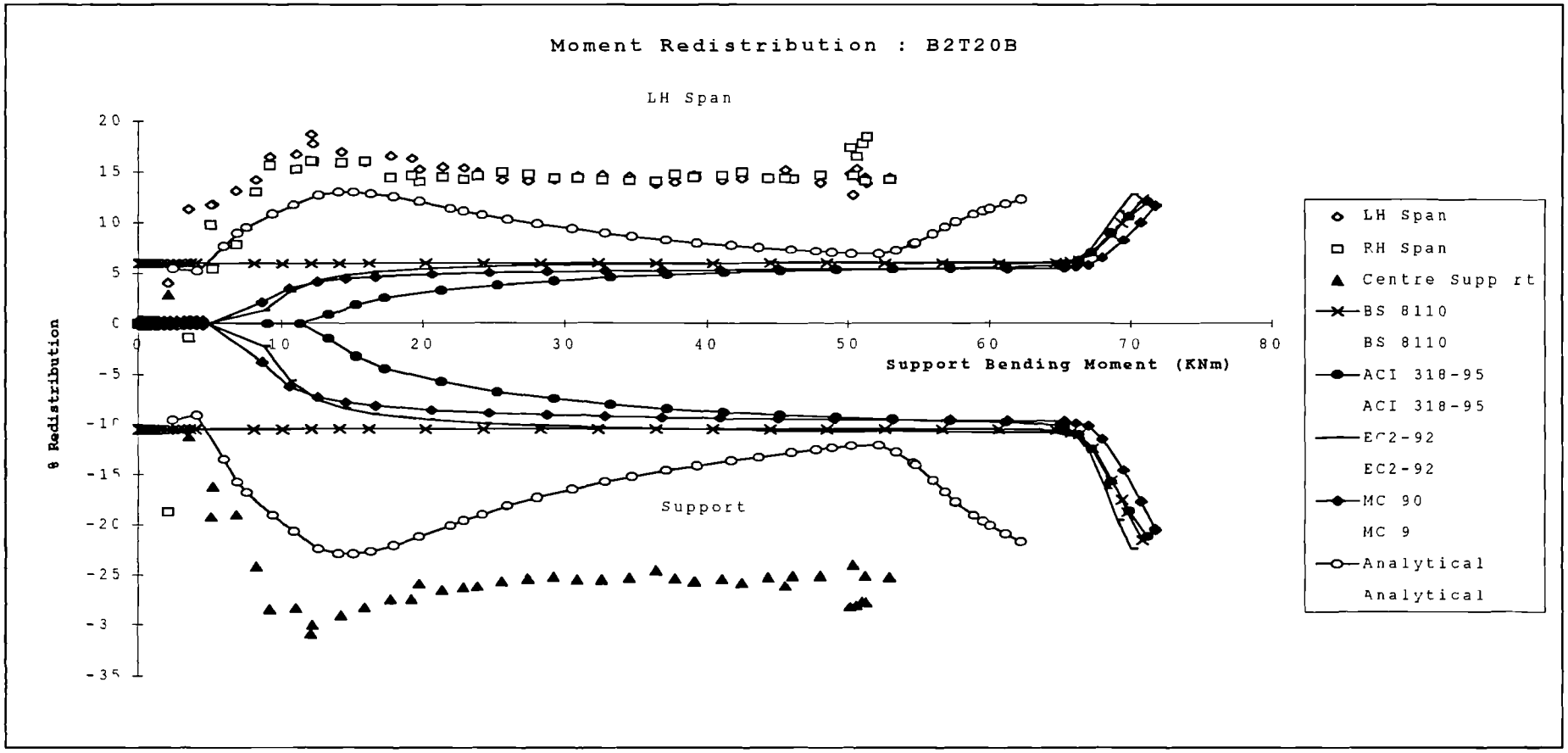

Figure 8-9: B2T20B measured and modelled moment redistribution versus support moment.

303

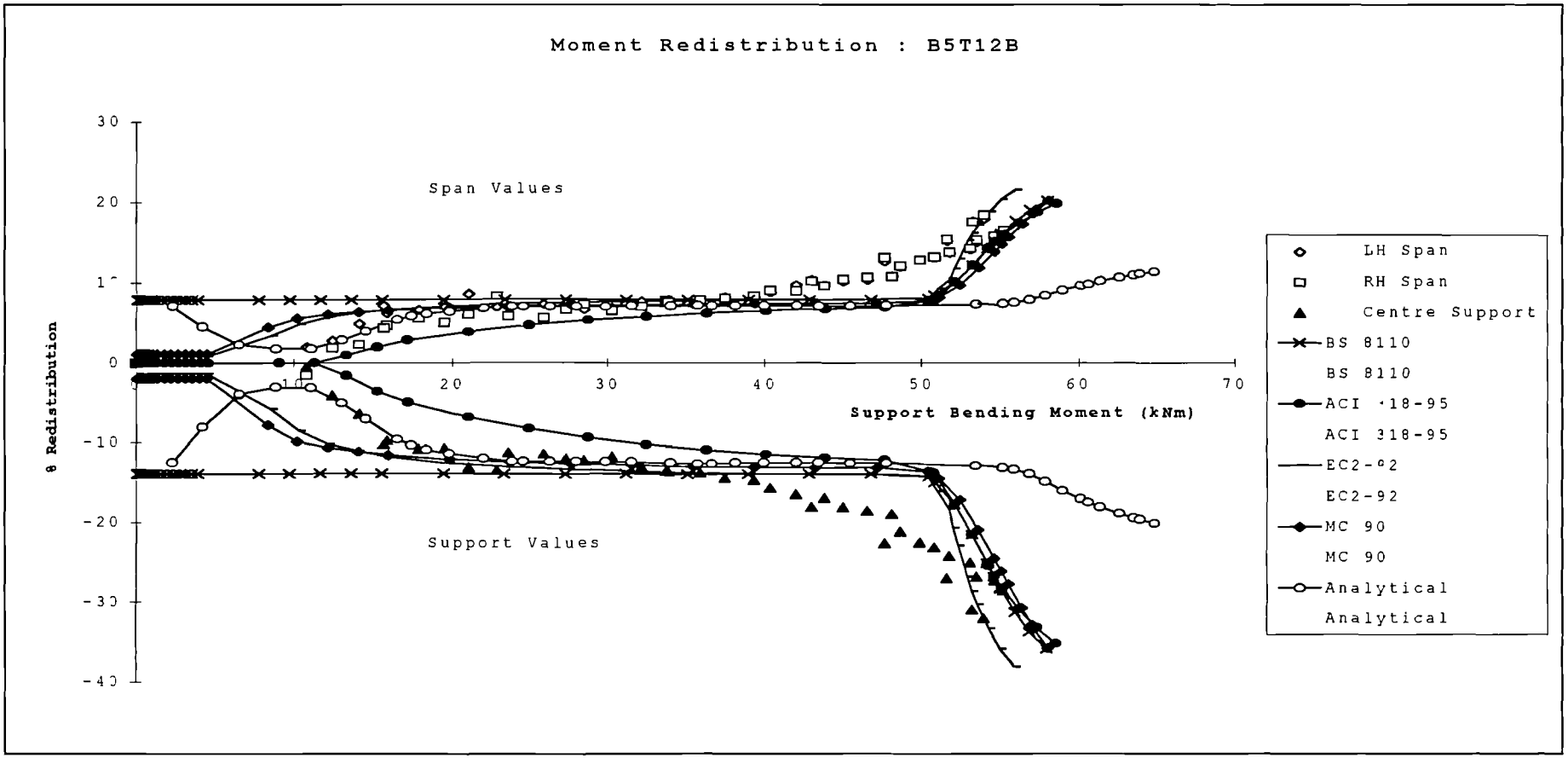

Figure 8-10: B5T12B measured and modelled moment redistribution versus support moment.

304

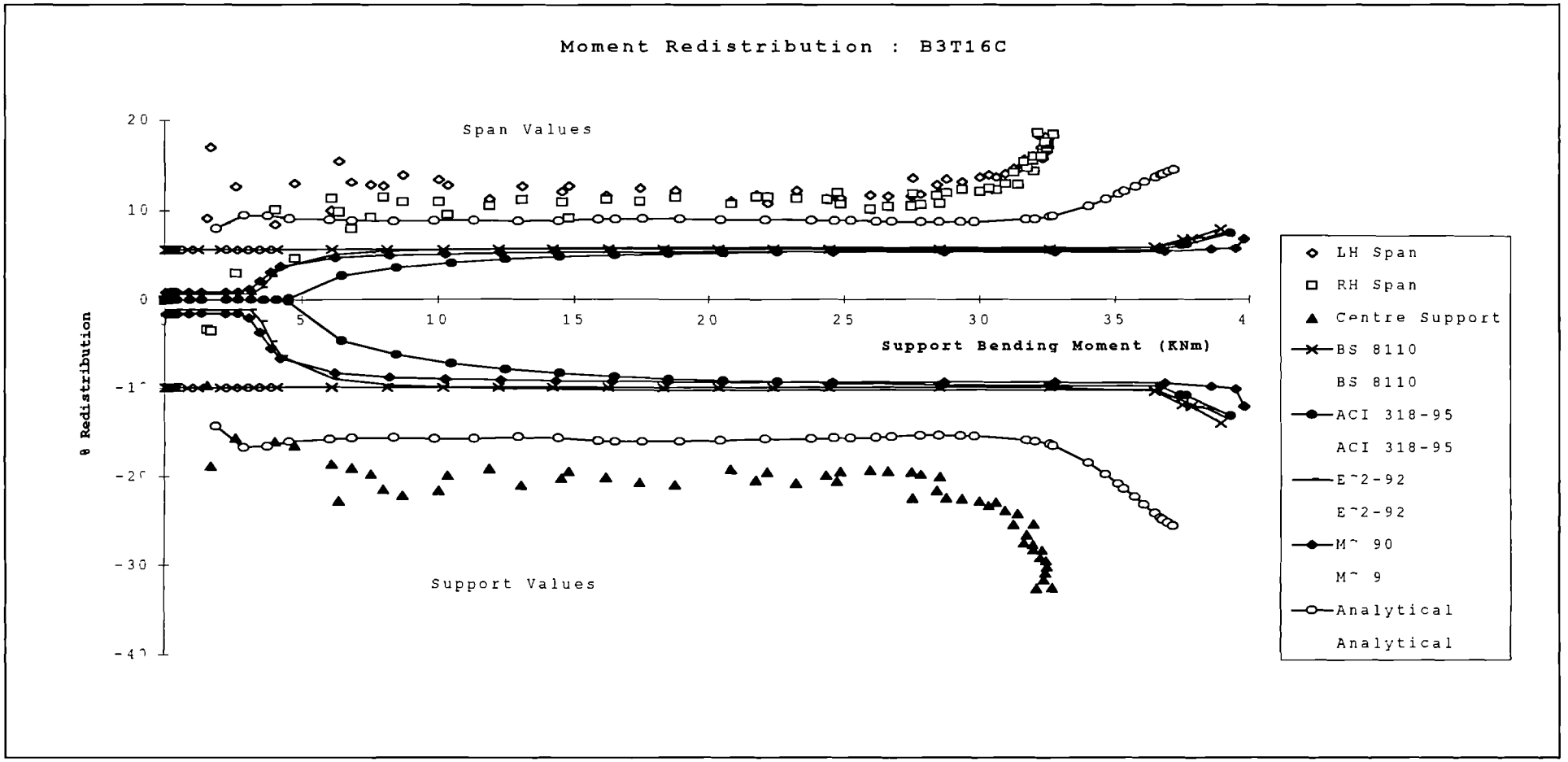

Figure 8-11: B3T16C measured and modelled moment redistribution versus support moment.

305

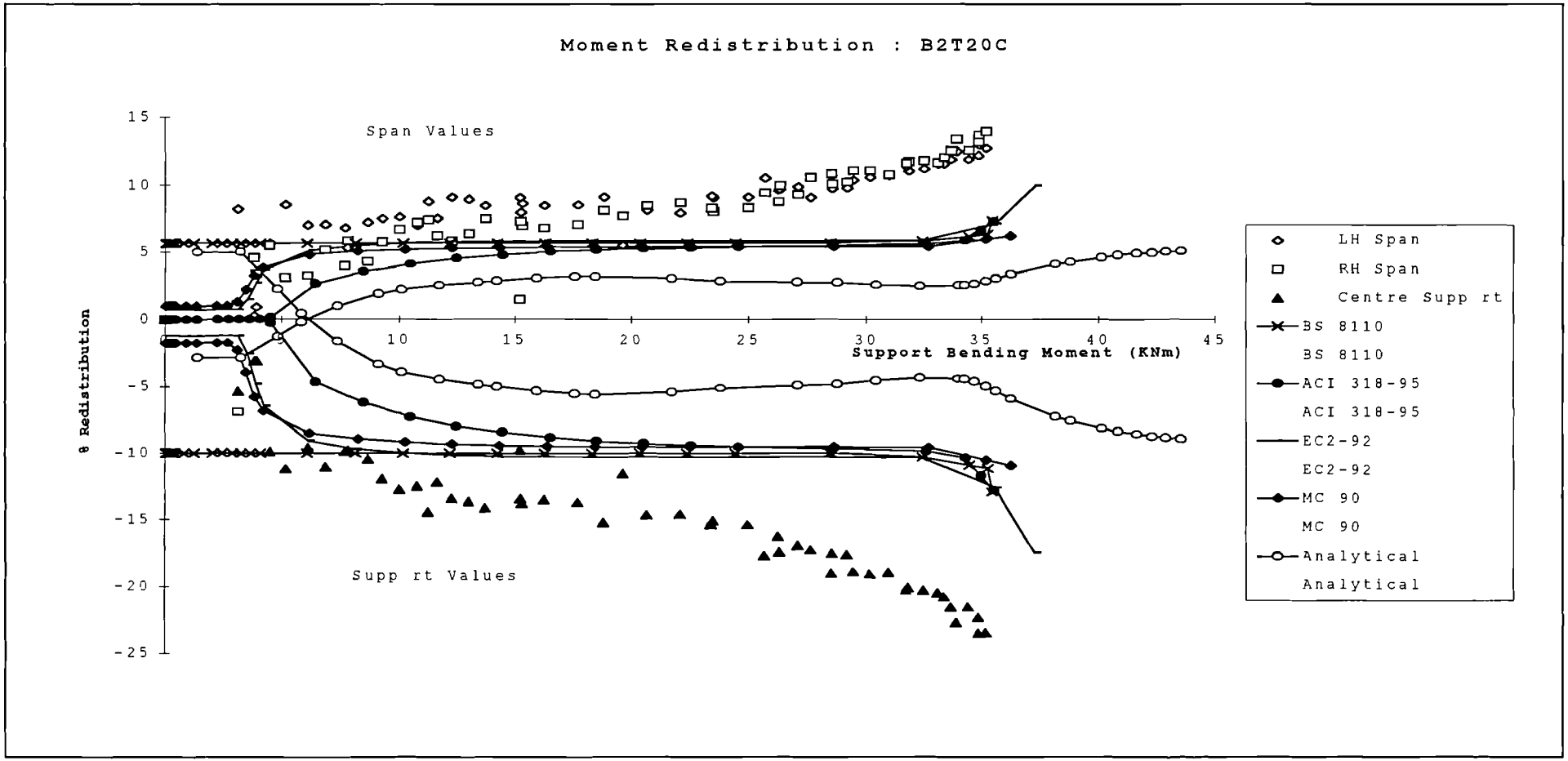

Figure 8-12: B2T20C measured and modelled moment redistribution versus support moment.

306

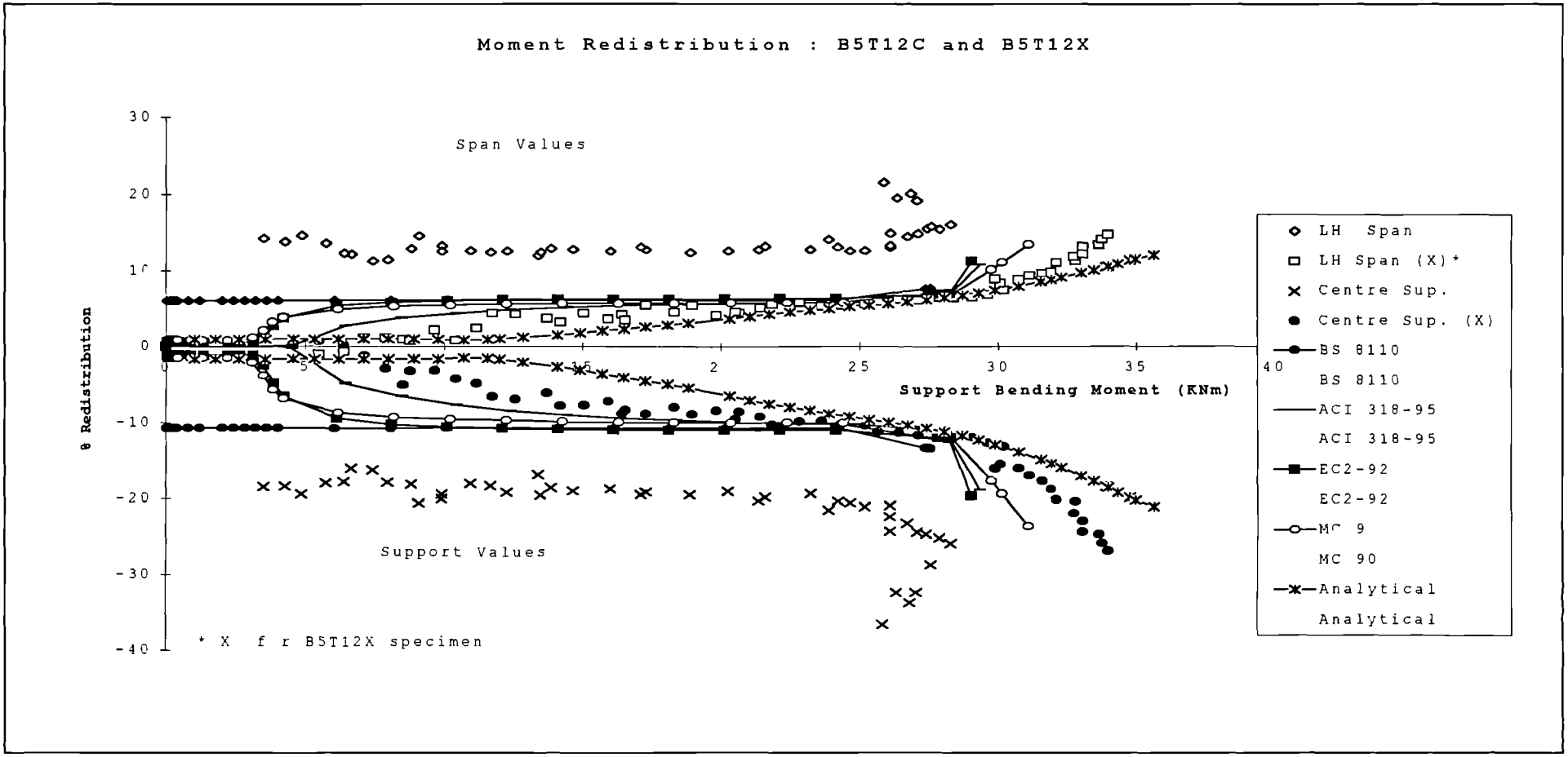

Figure 8-13: B5T12C and B5T12X measured and modelled moment redistribution versus support moment.

307

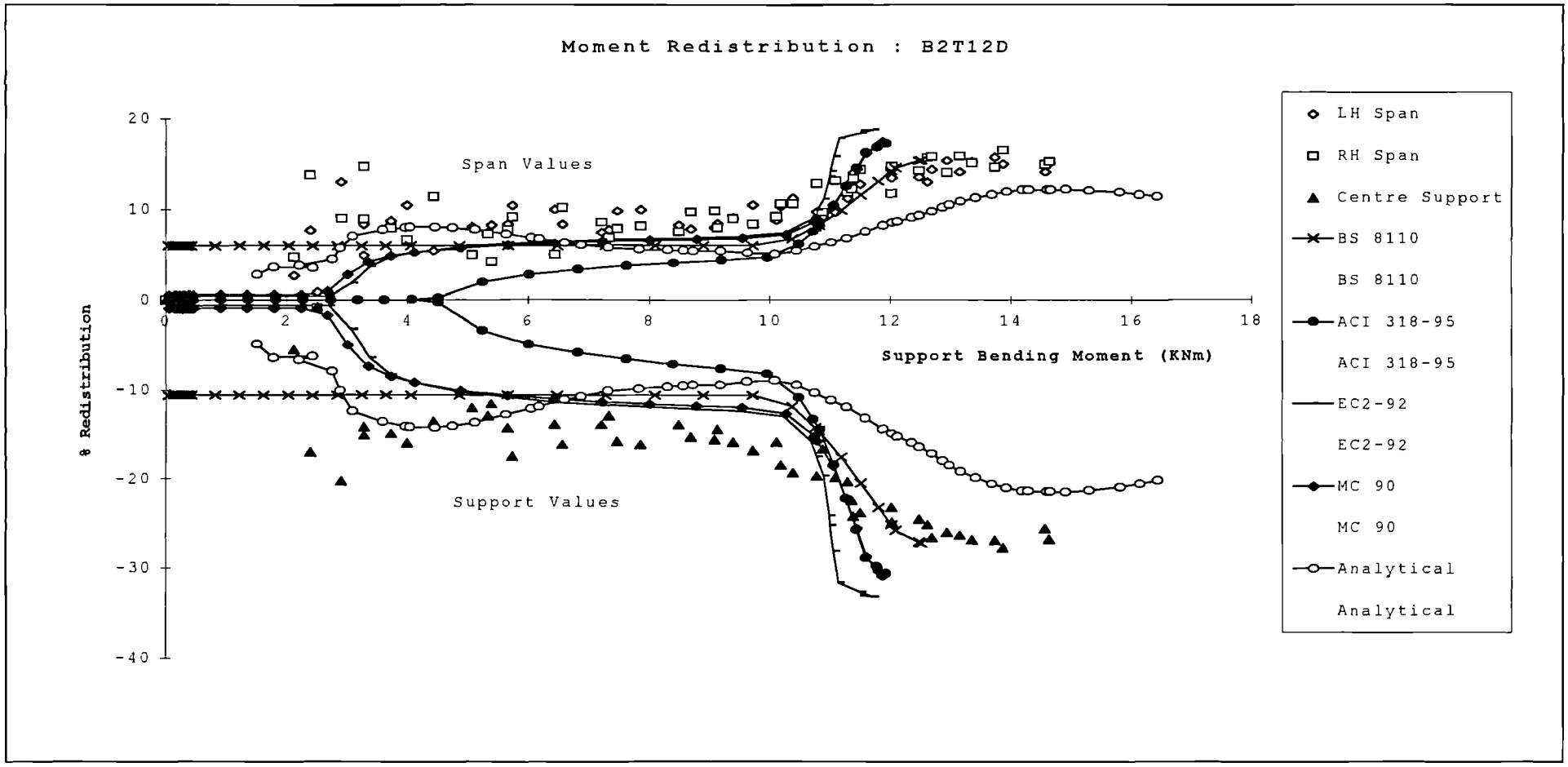

Figure 8-14: B2T12D measured and modelled moment redistribution versus support moment.

308

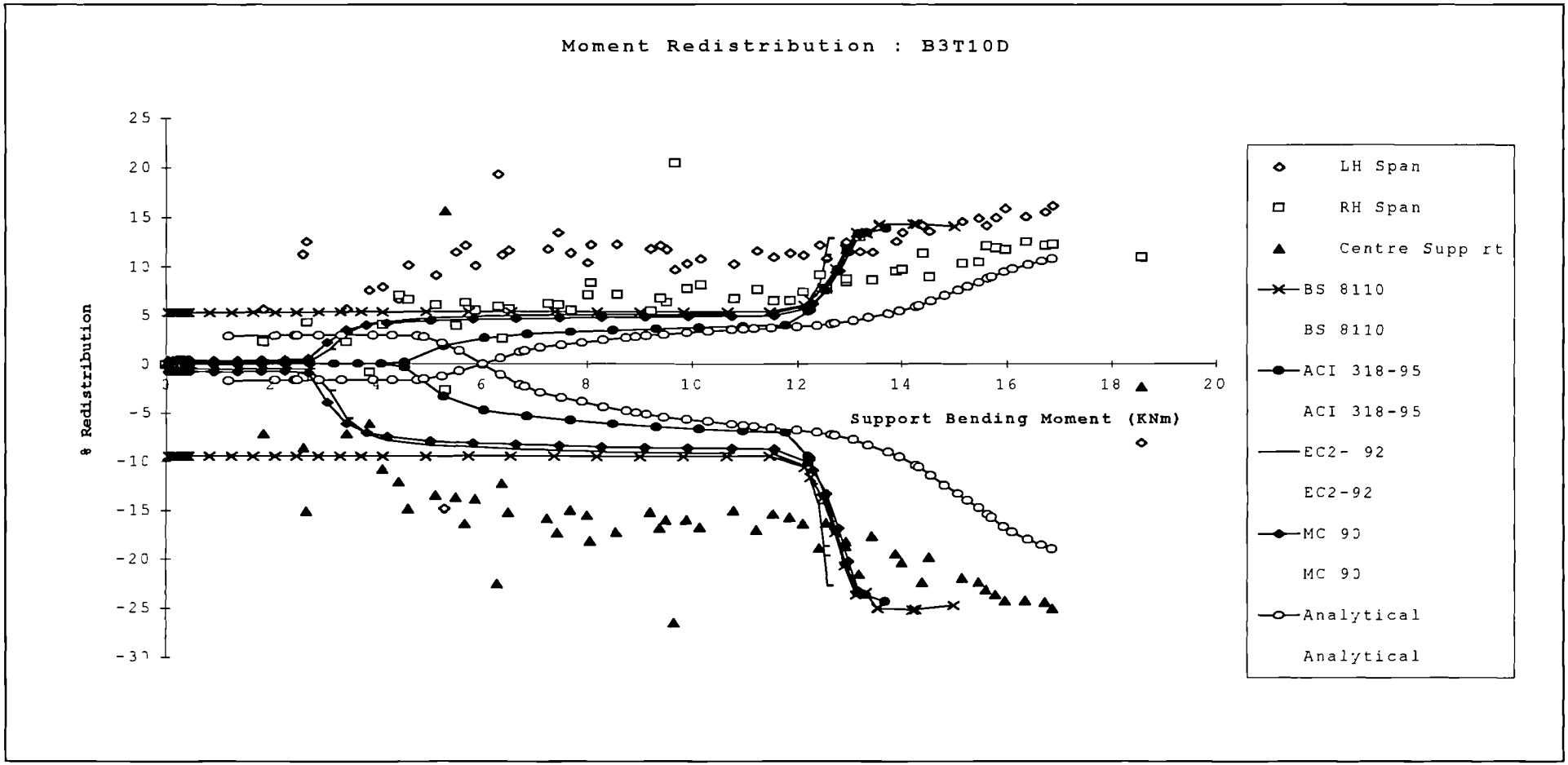

Figure 8-15: B3T10D measured and modelled moment redistribution versus support moment.

309

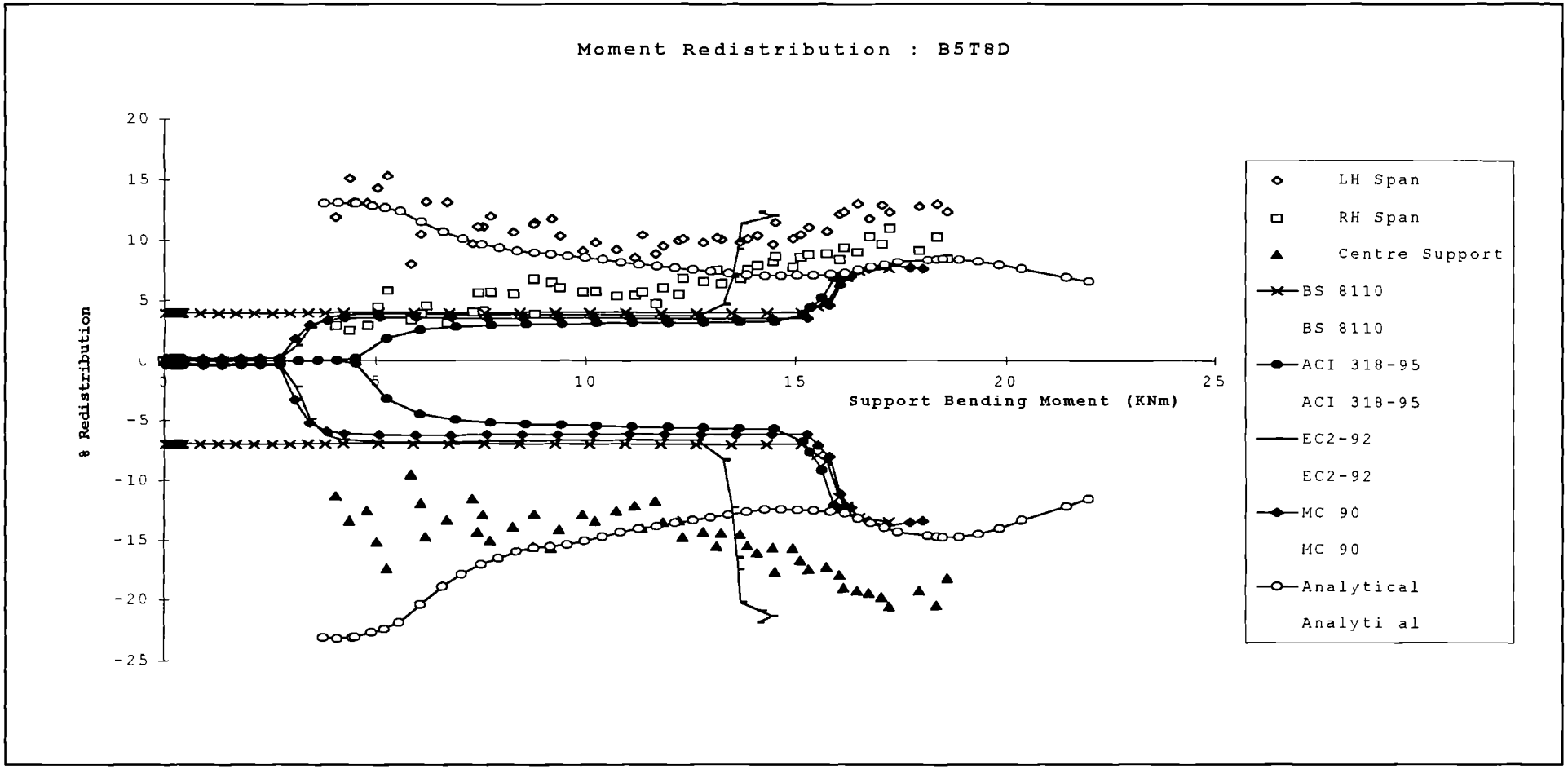

Figure 8-16: B5T8D measured and modelled moment redistribution versus support moment.

310

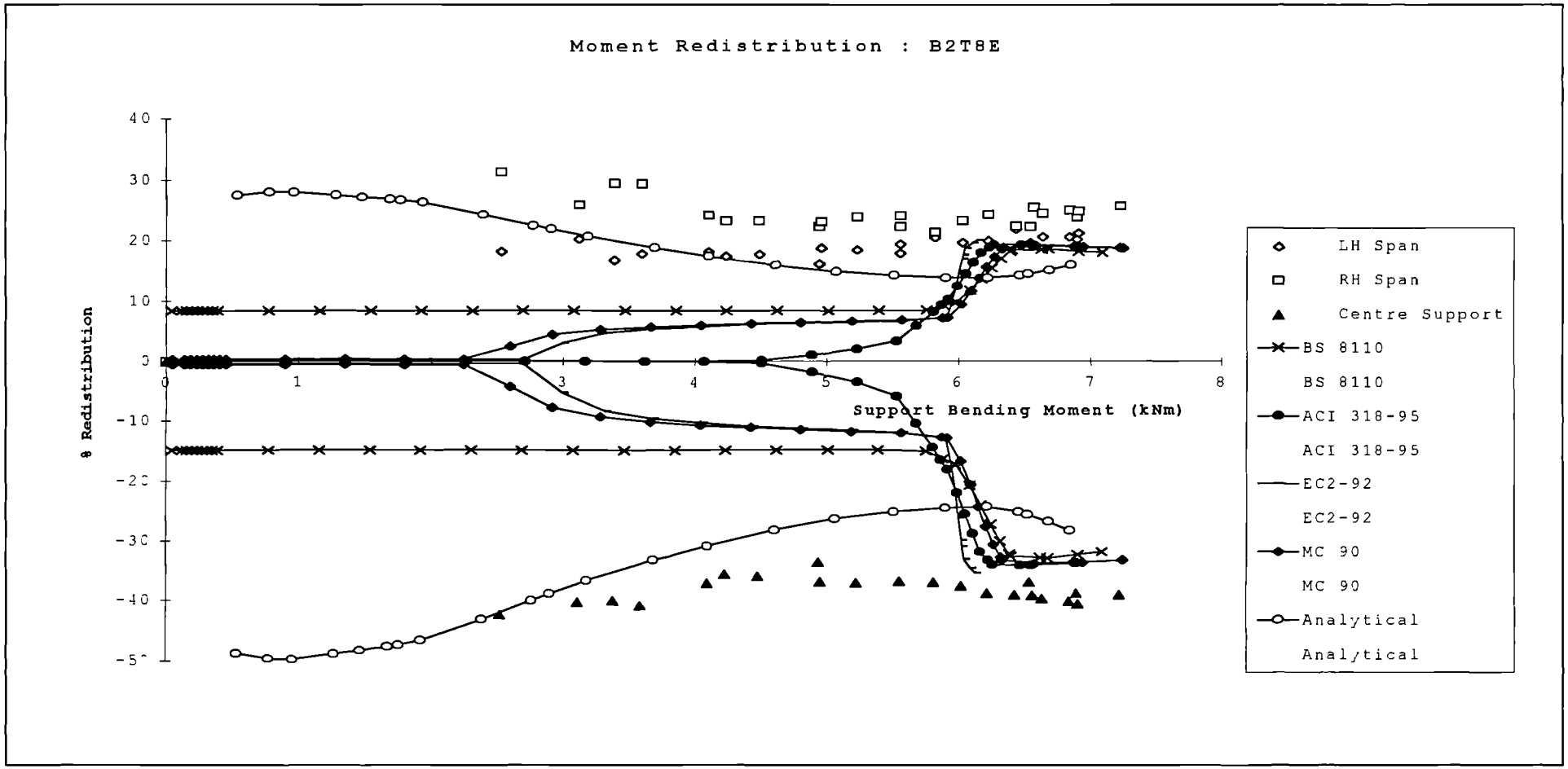

Figure 8-17: B2T8E measured and modelled moment redistribution versus support moment.

311

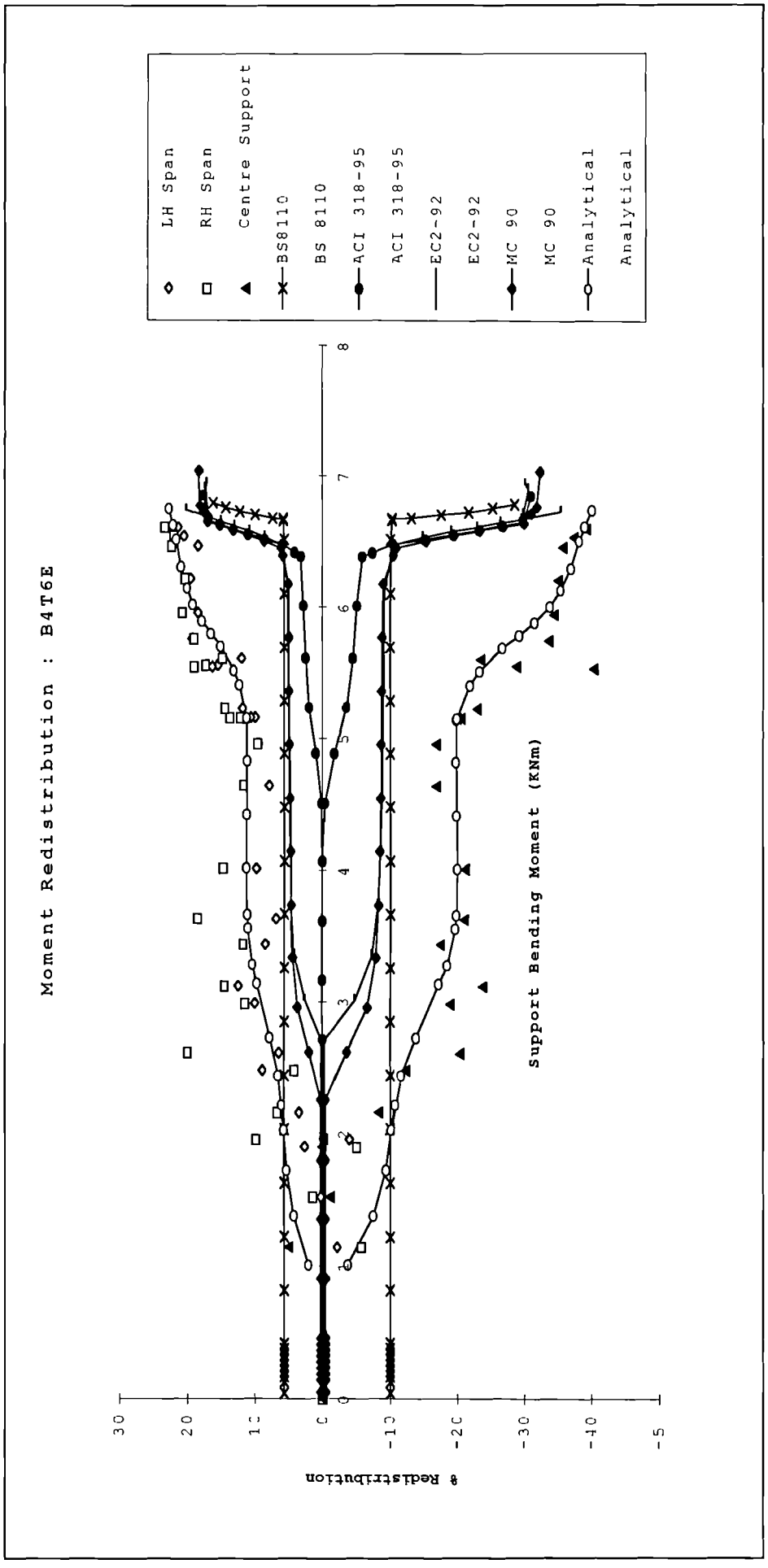

Figure 8-18: B4T6E measured and modelled moment redistribution versus support moment.

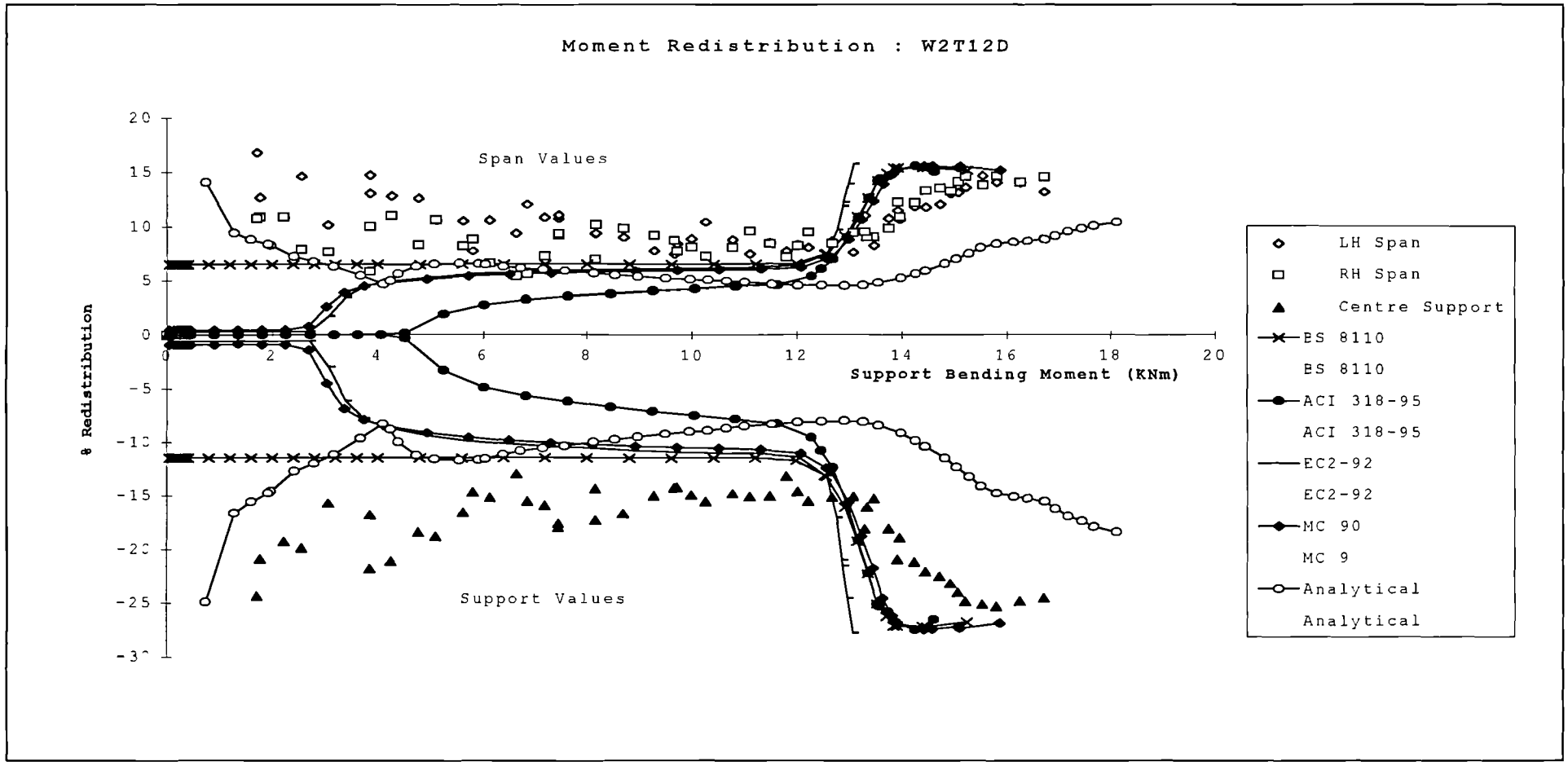

Figure 8-19: W2T12D measured and modelled moment redistribution versus support moment.

313

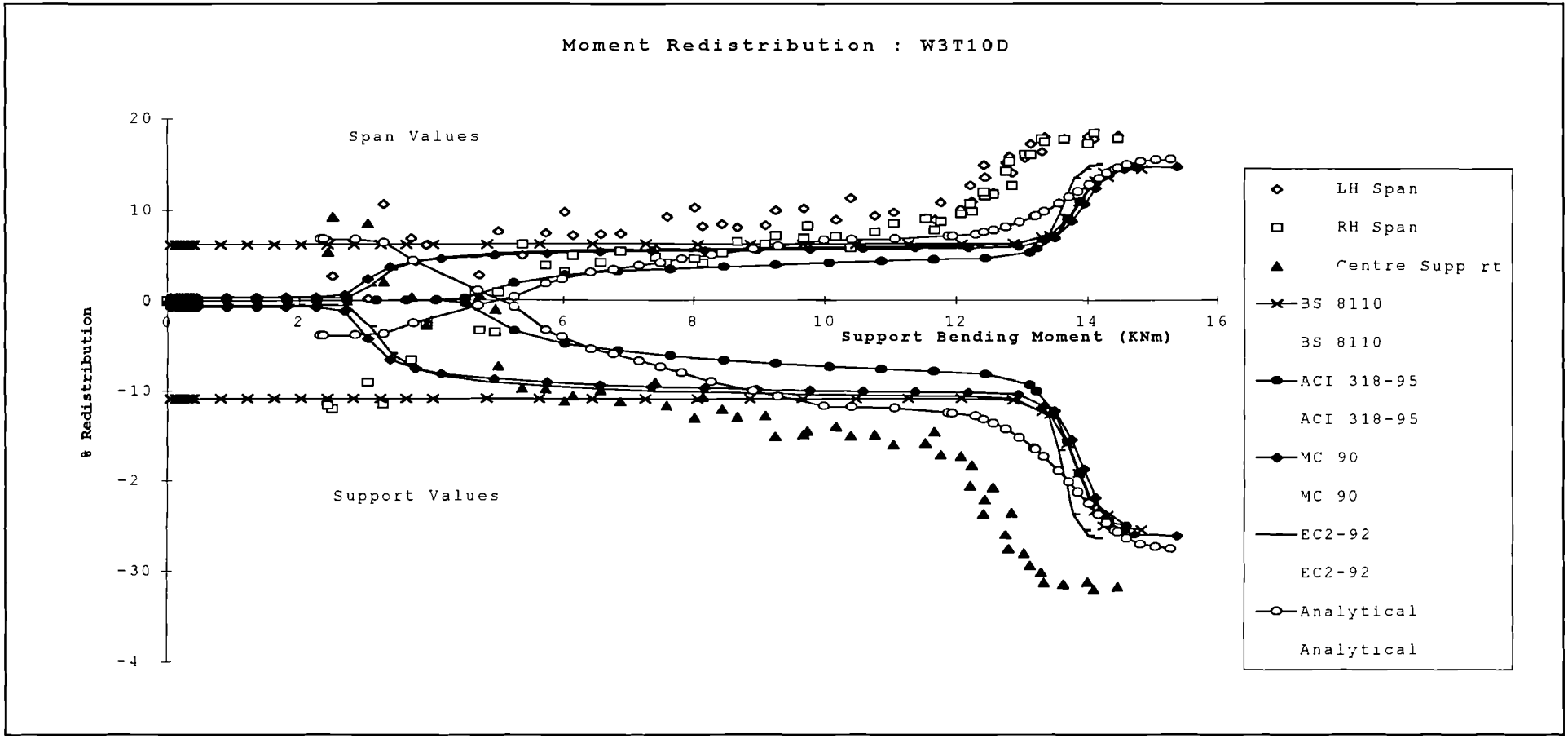

Figure 8-20: W3T10D measured and modelled moment redistribution versus support moment.

314

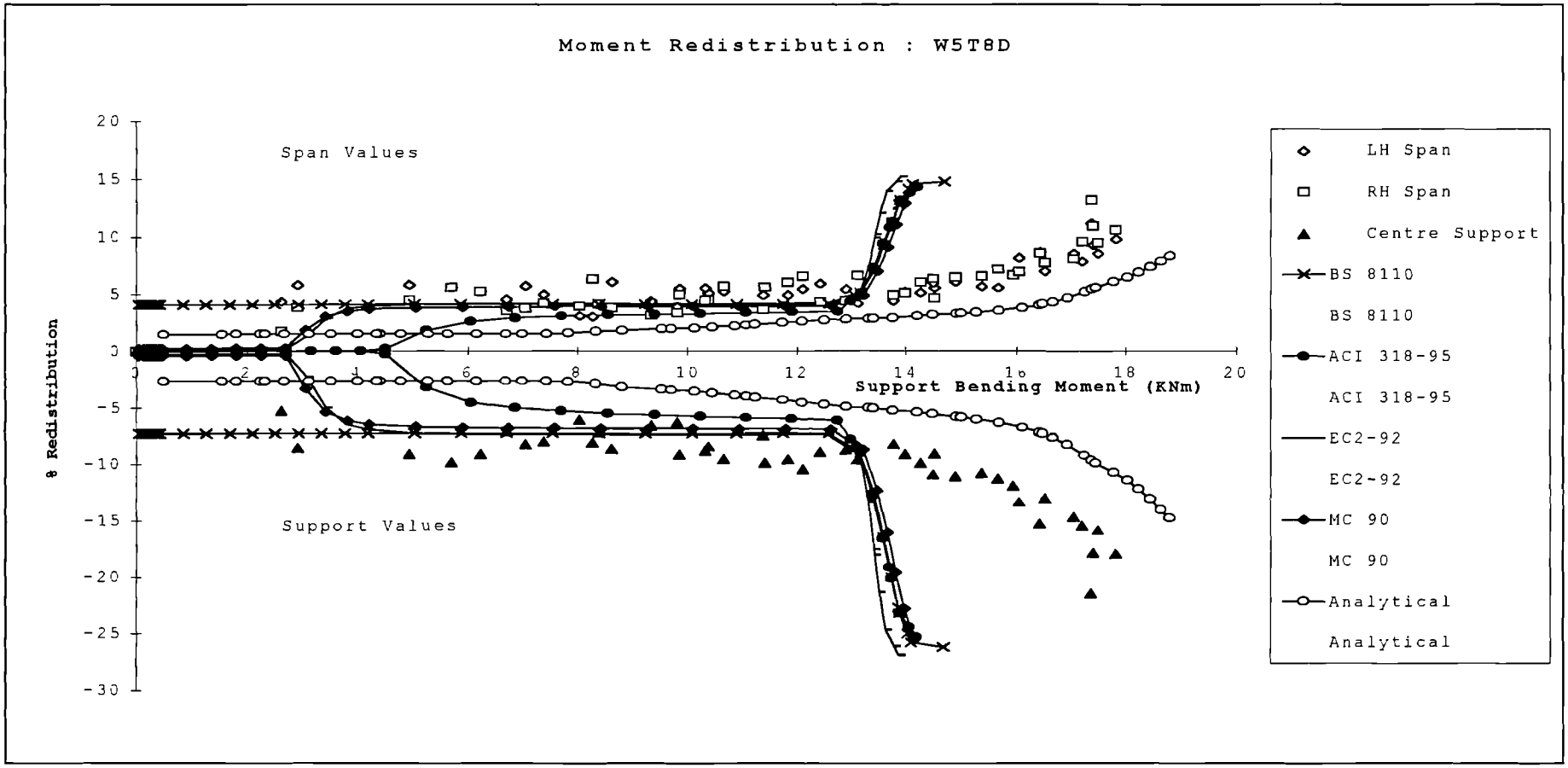

Figure 8-21: W5T8D measured and modelled moment redistribution versus support moment.

315

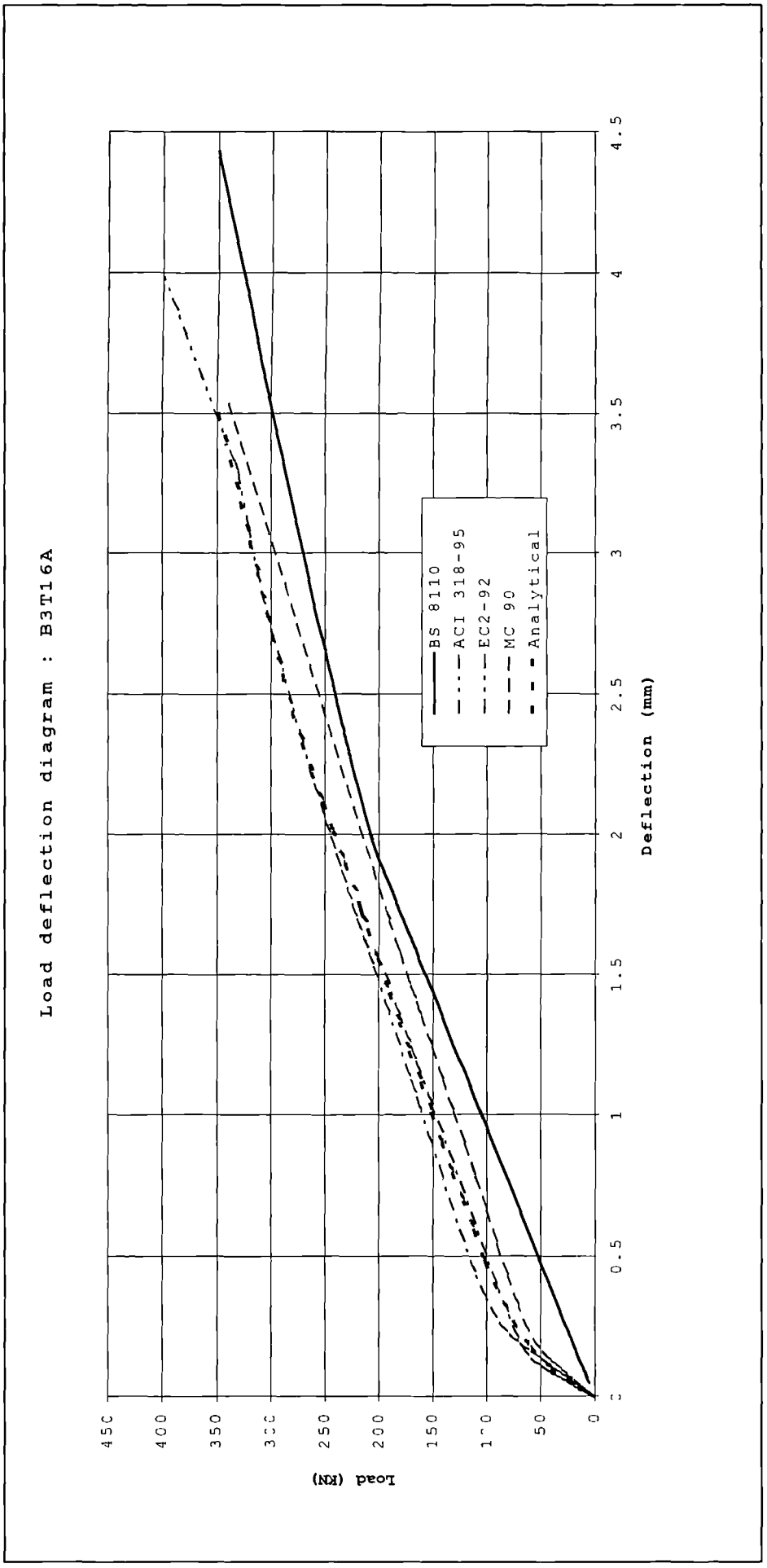

Figure 8-22: B3T16A measured and modelled load deflection curves.

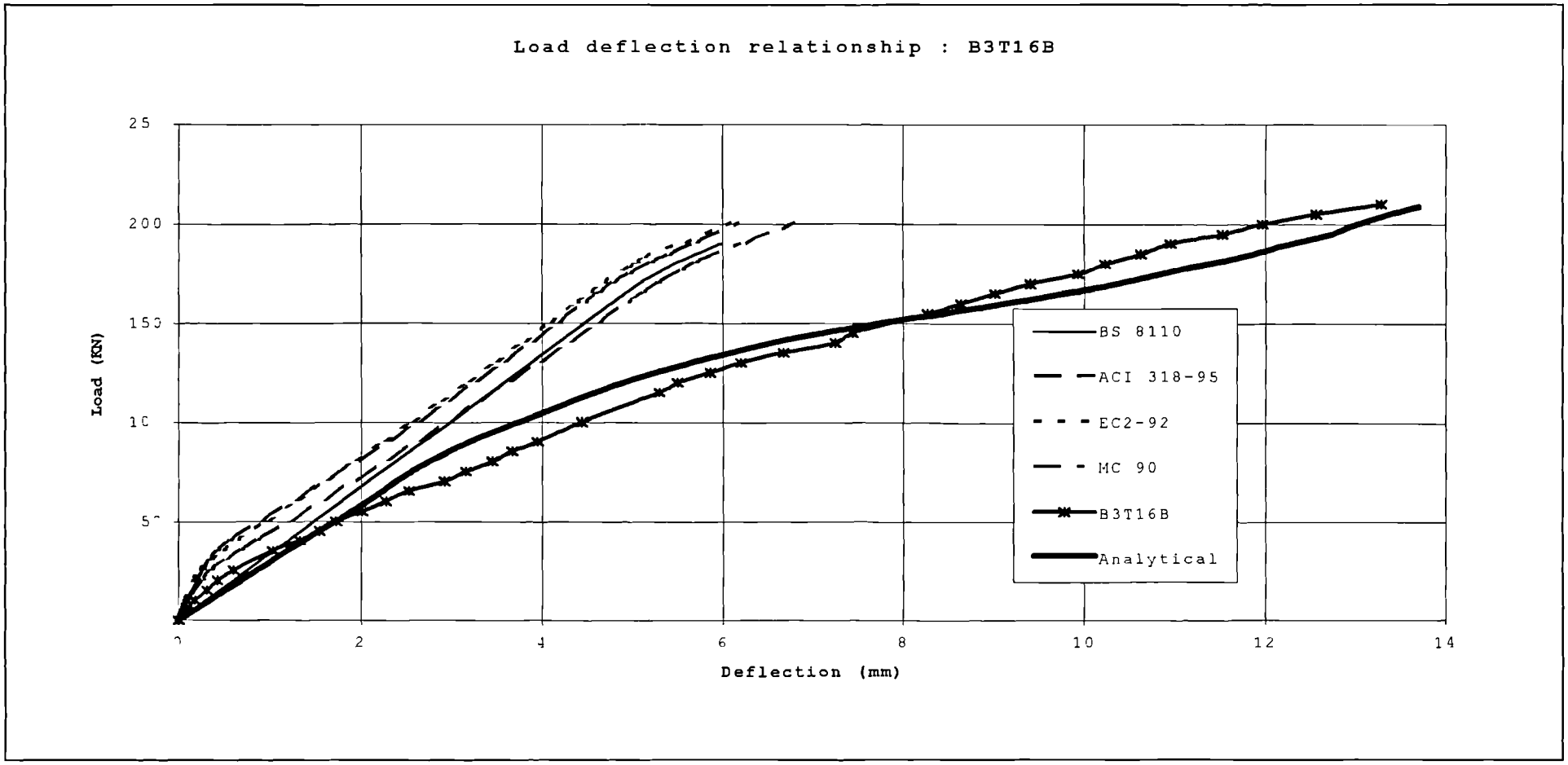

Figure 8-23: B3T16B measured and modelled load deflection curves.

317

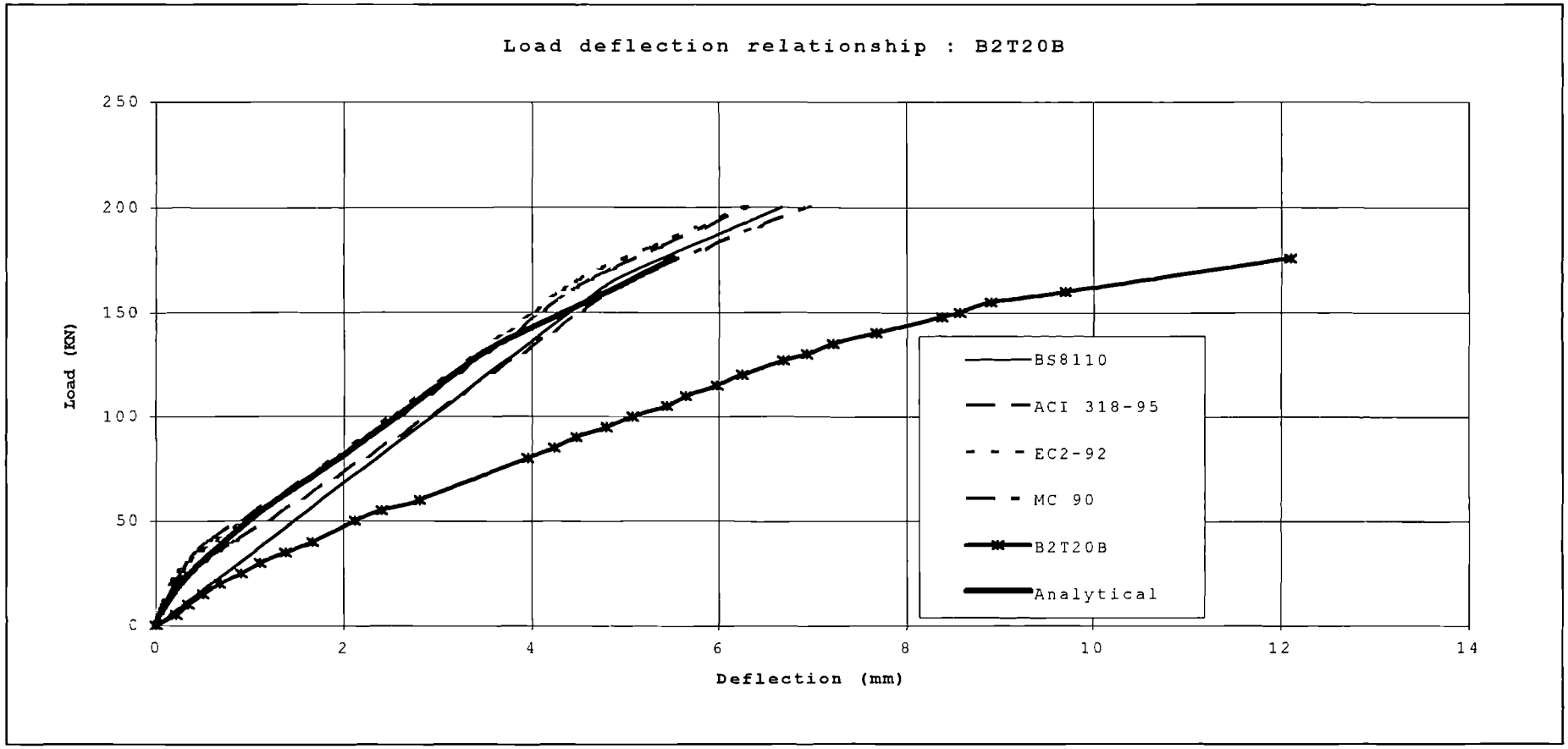

Figure 8-24: B2T20B measured and modelled load deflection curves.

318

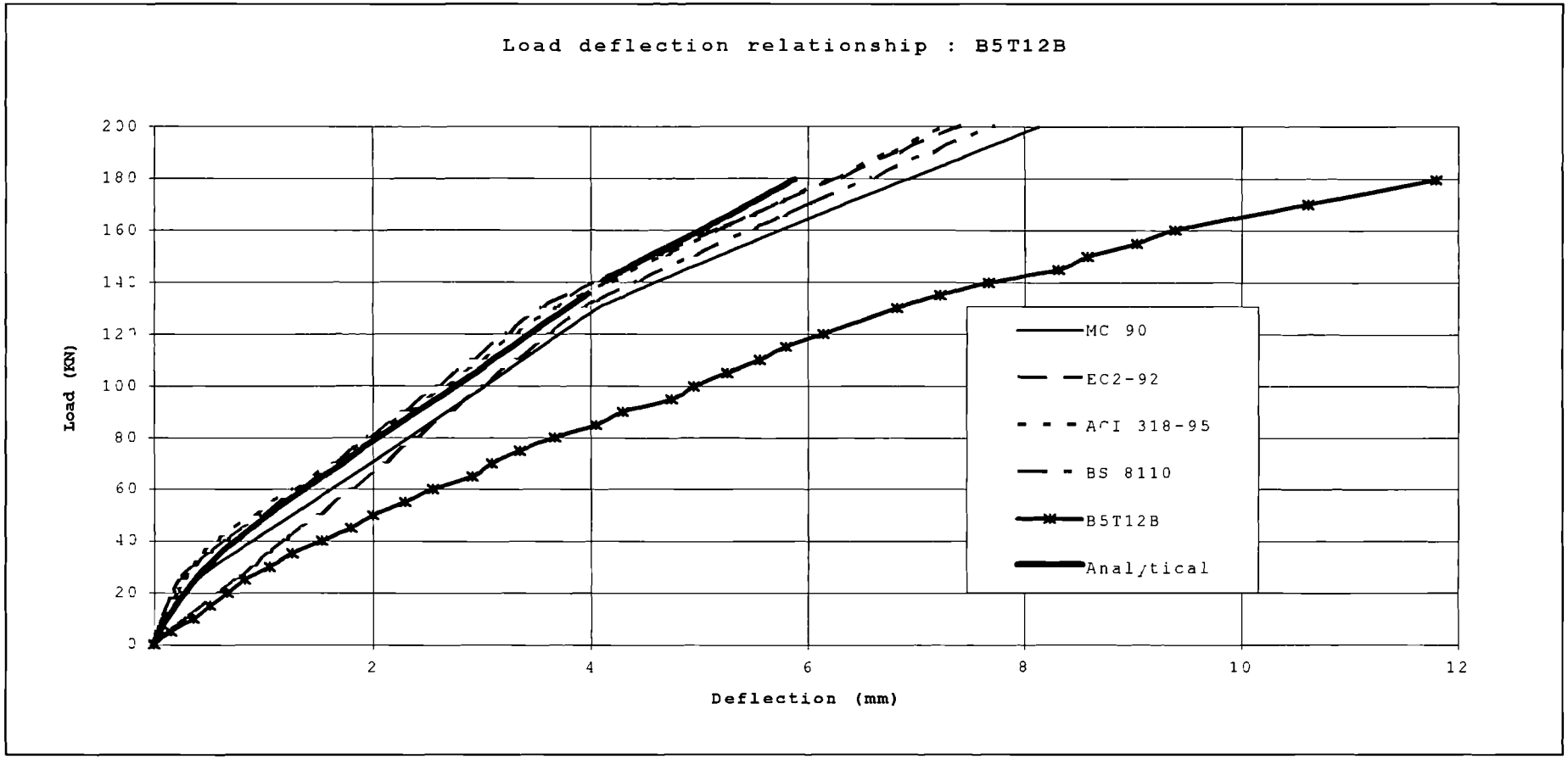

Figure 8-25: B5T12B measured and modelled load deflection curves.

319

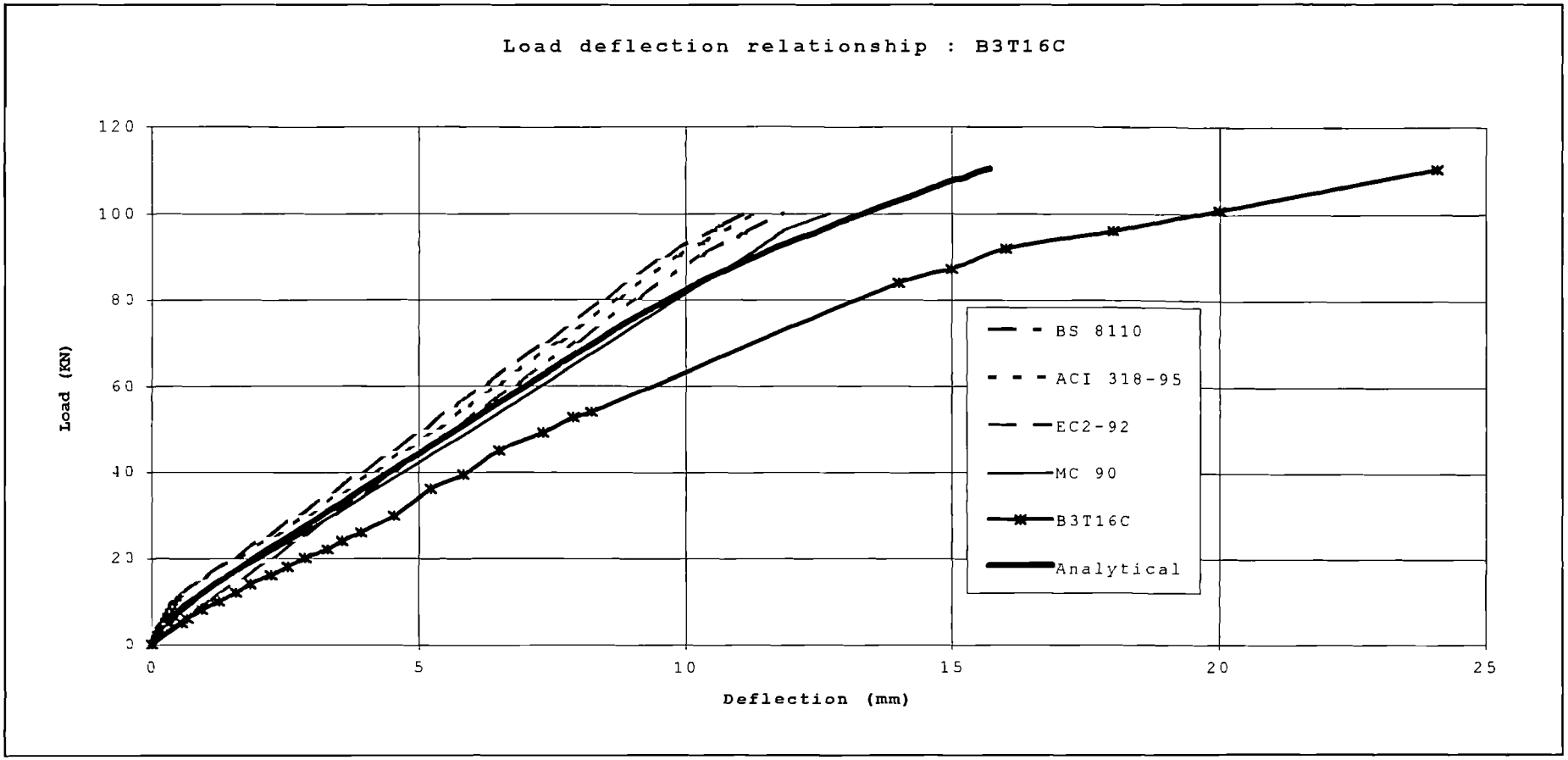

Figure 8-26: B3T16C measured and modelled load deflection curves.

320

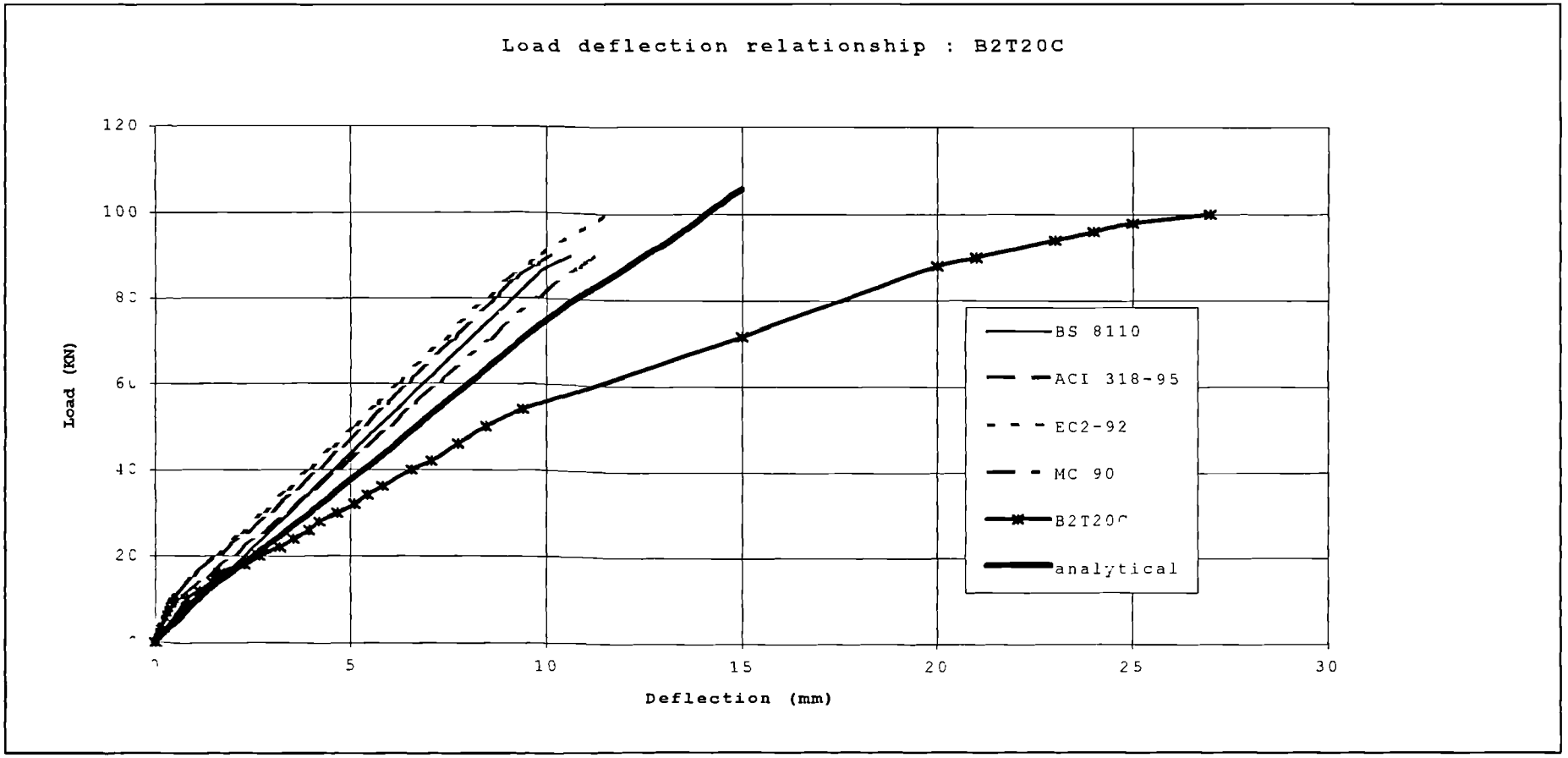

Figure 8-27: B2T20C measured and modelled load deflection curves.

321

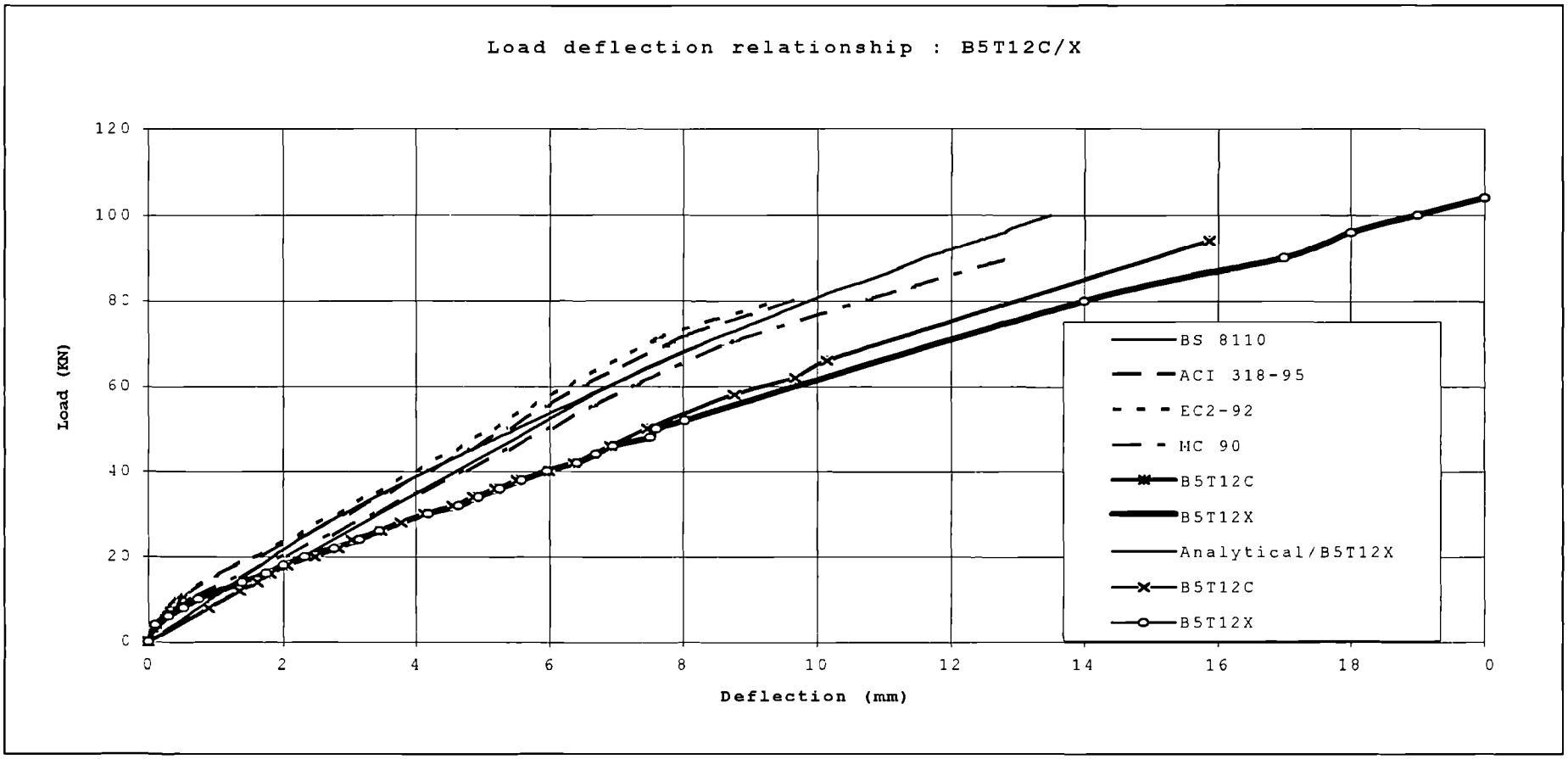

Figure 8-28: B5T12C and B5T12X measured and modelled load deflection curves.

322

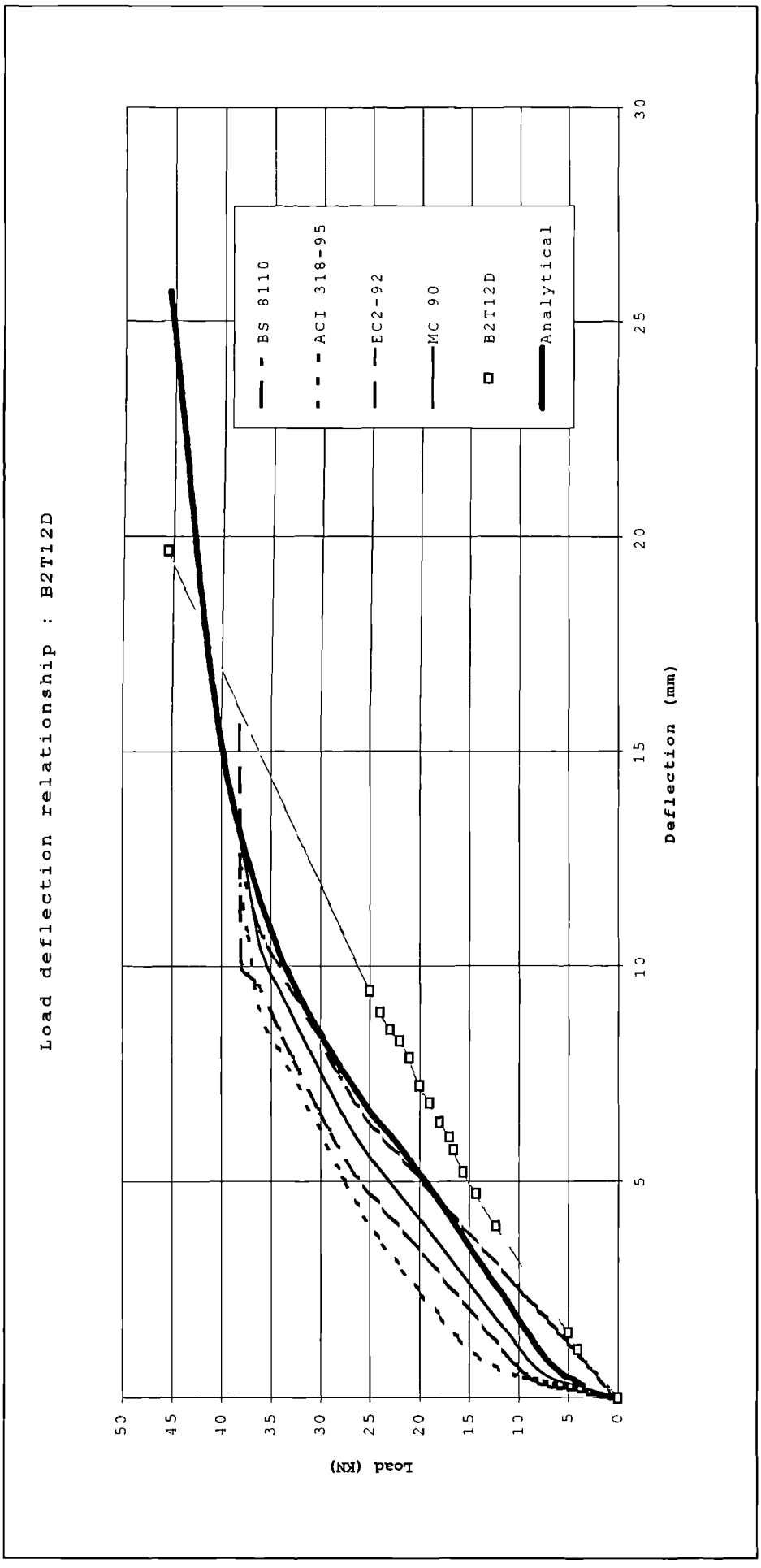

Figure 8-29: B2T12D measured and modelled load deflection curves.

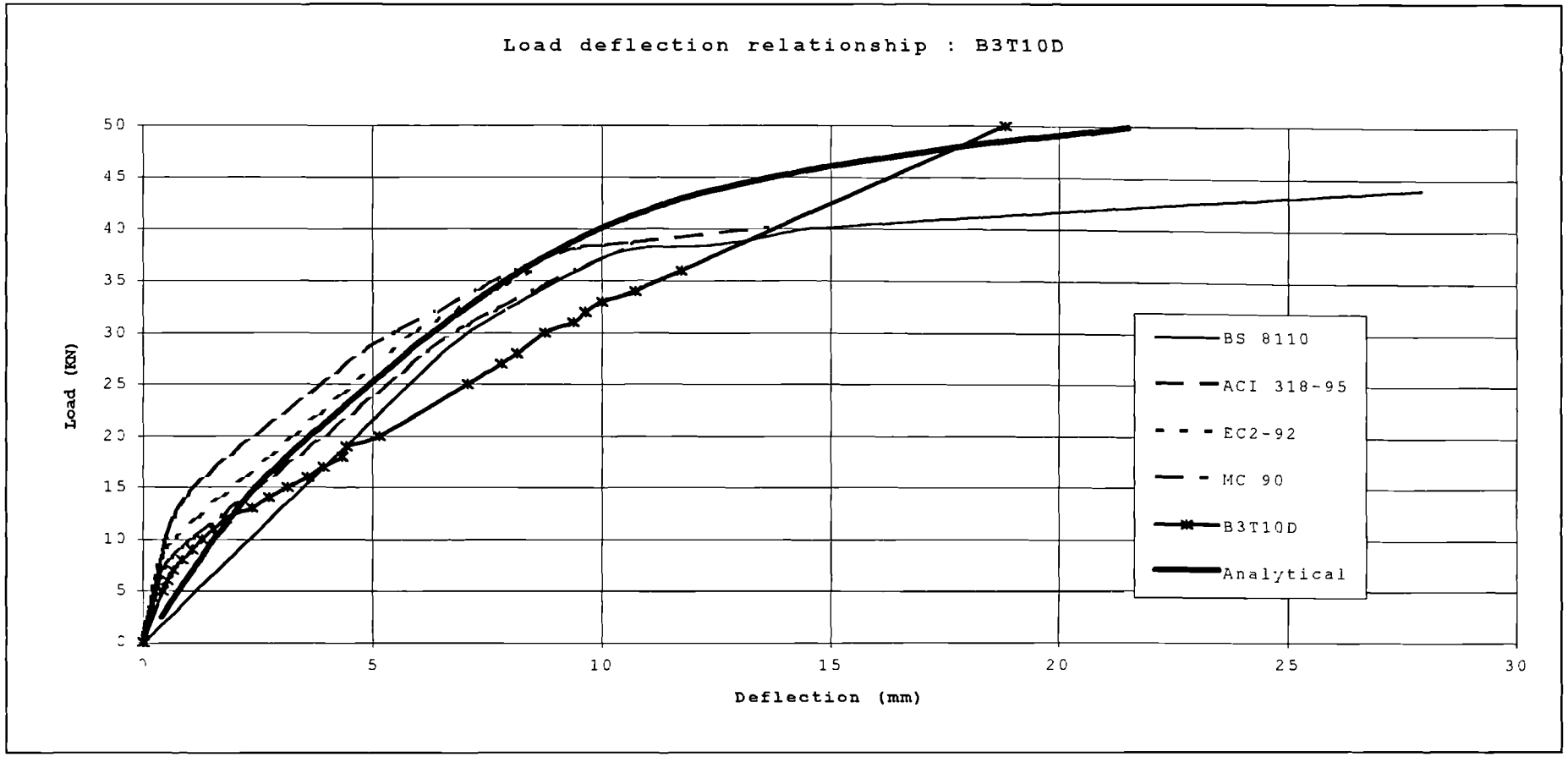

Figure 8-30: B3T10D measured and modelled load deflection curves.

324

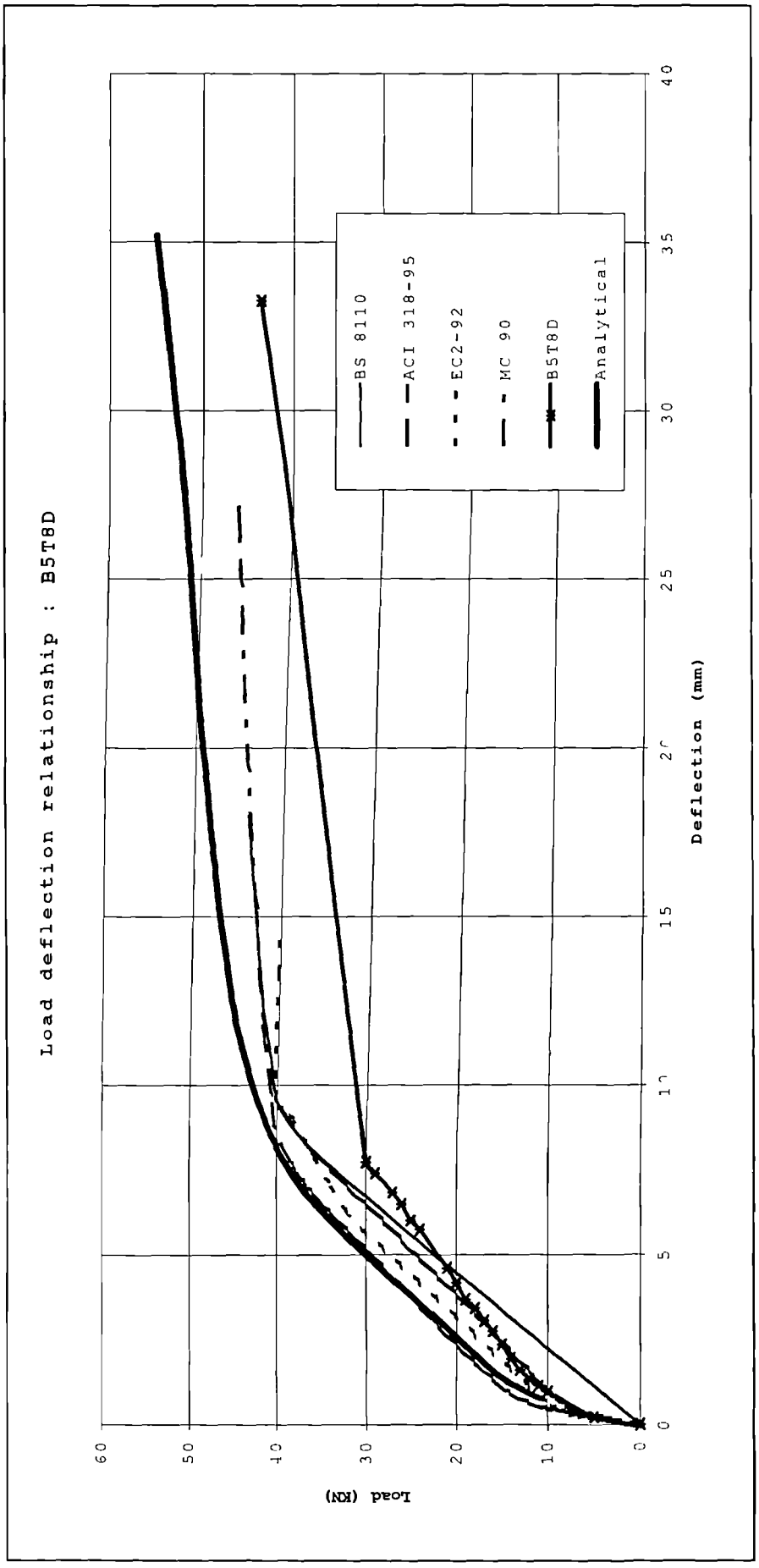

Figure 8-31: B5T8D measured and modelled load deflection curves.

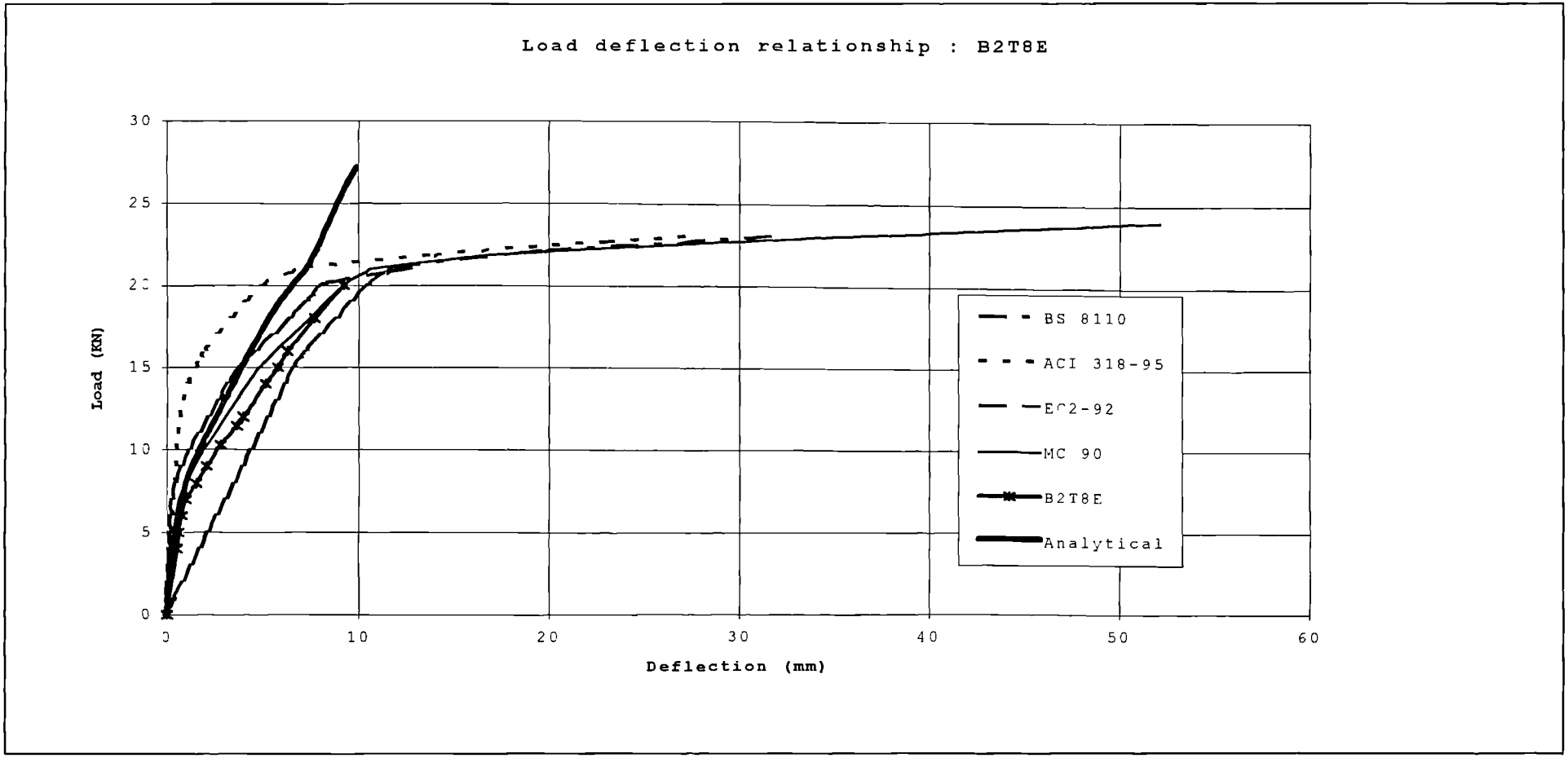

Figure 8-32: B2T8E measured and modelled load deflection curves.

326

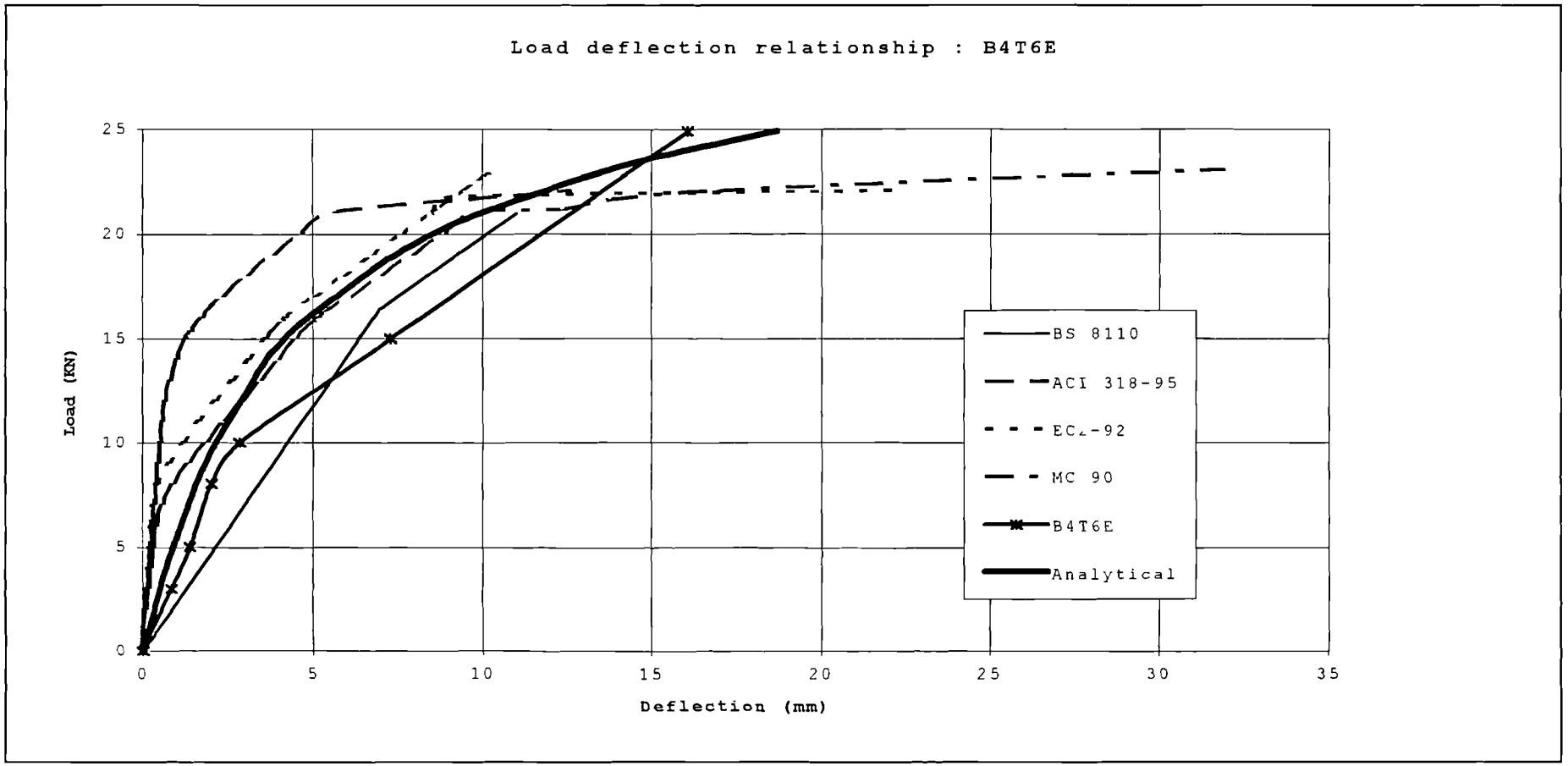

Figure 8-33: B4T6E measured and modelled load deflection curves.

327

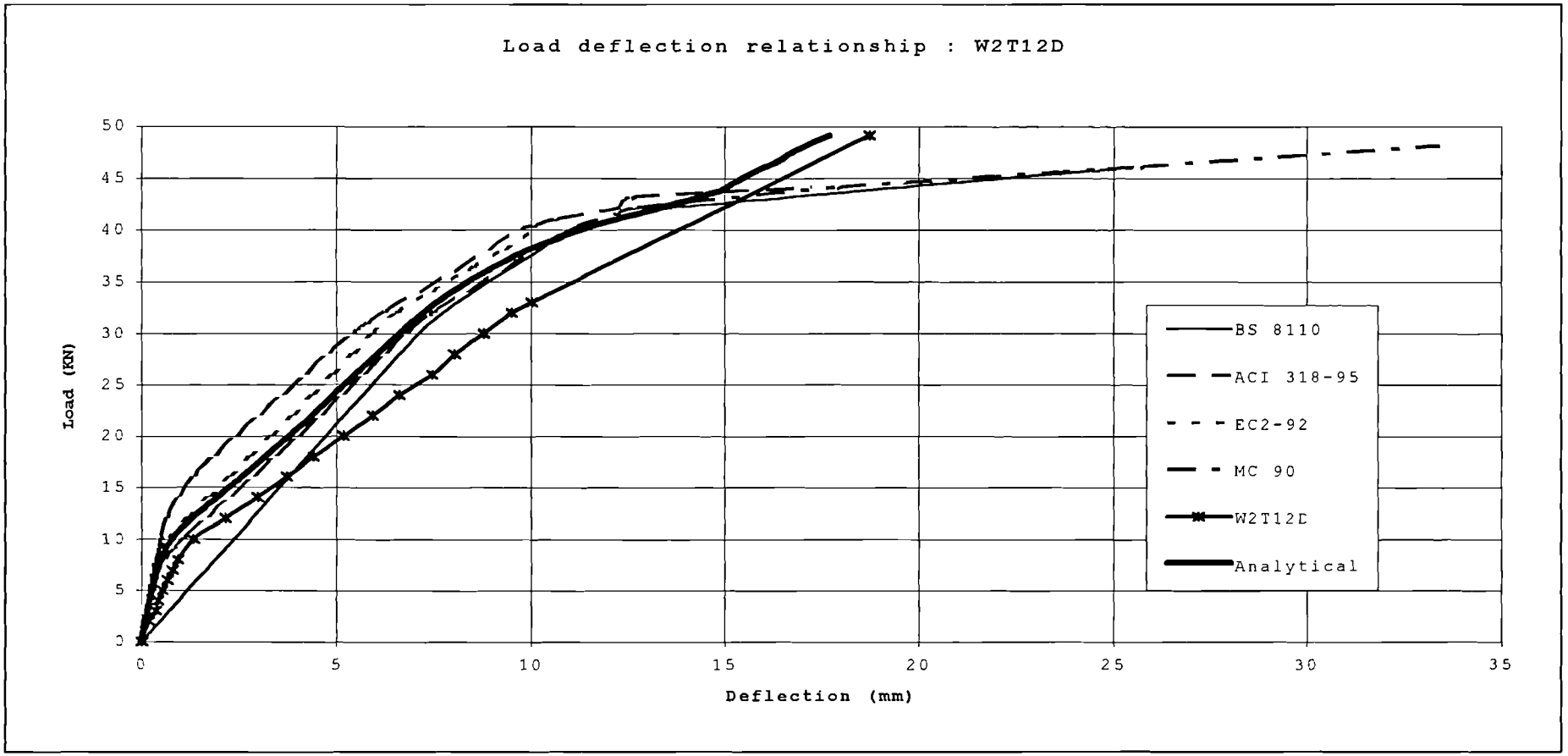

Figure 8-34: W2T12D measured and modelled load deflection curves.

328

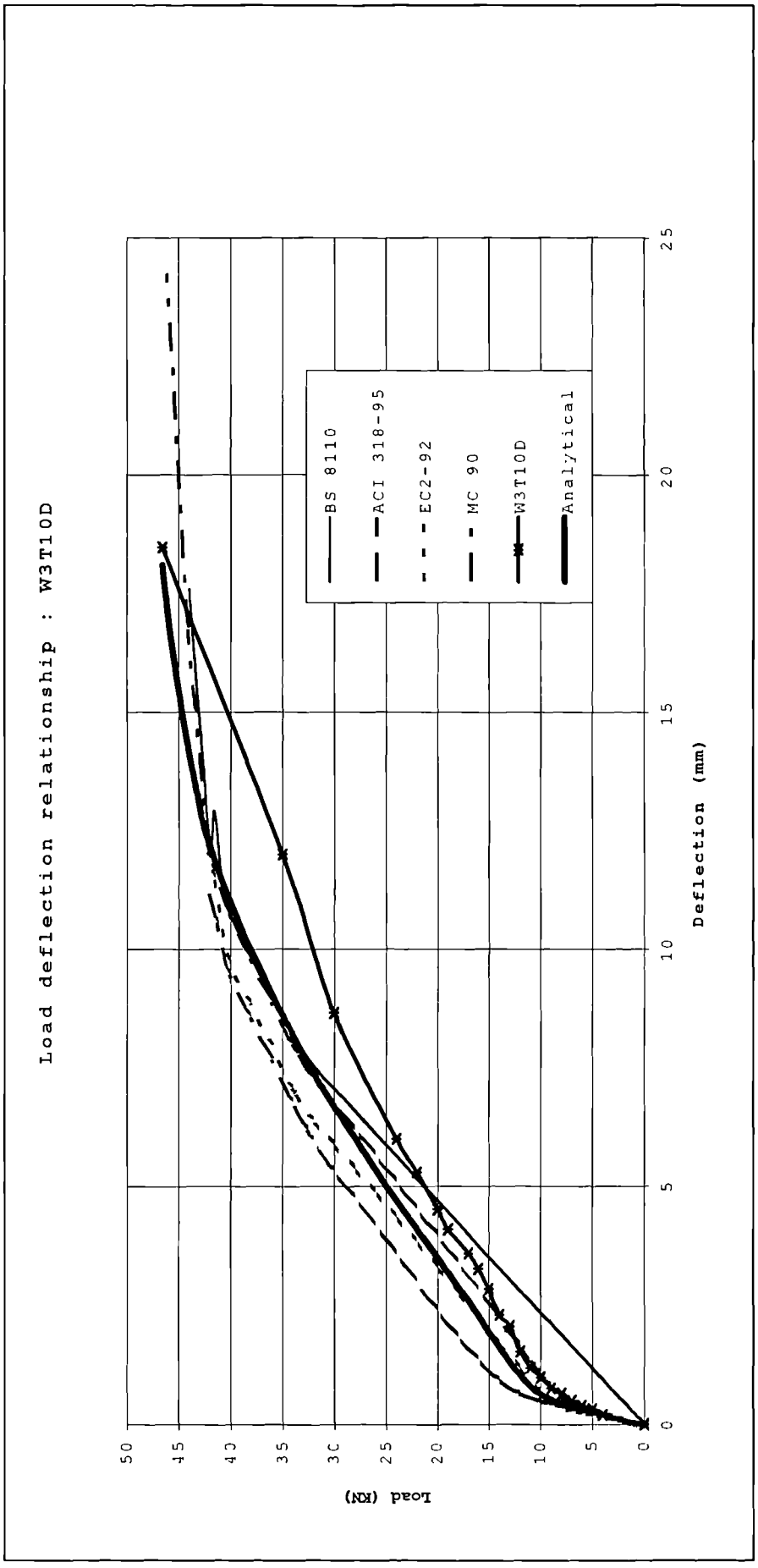
Load deflection relationship : W3T10D
Load (KN)
Deflection (mm)
0
5
10
15
20
25
30
35
40
45
50
BS 8110
ACI 318-95
EC2-92
MC 90
W3T10D
Analytical

Figure 8-35: W3T10D measured and modelled load deflection curves.

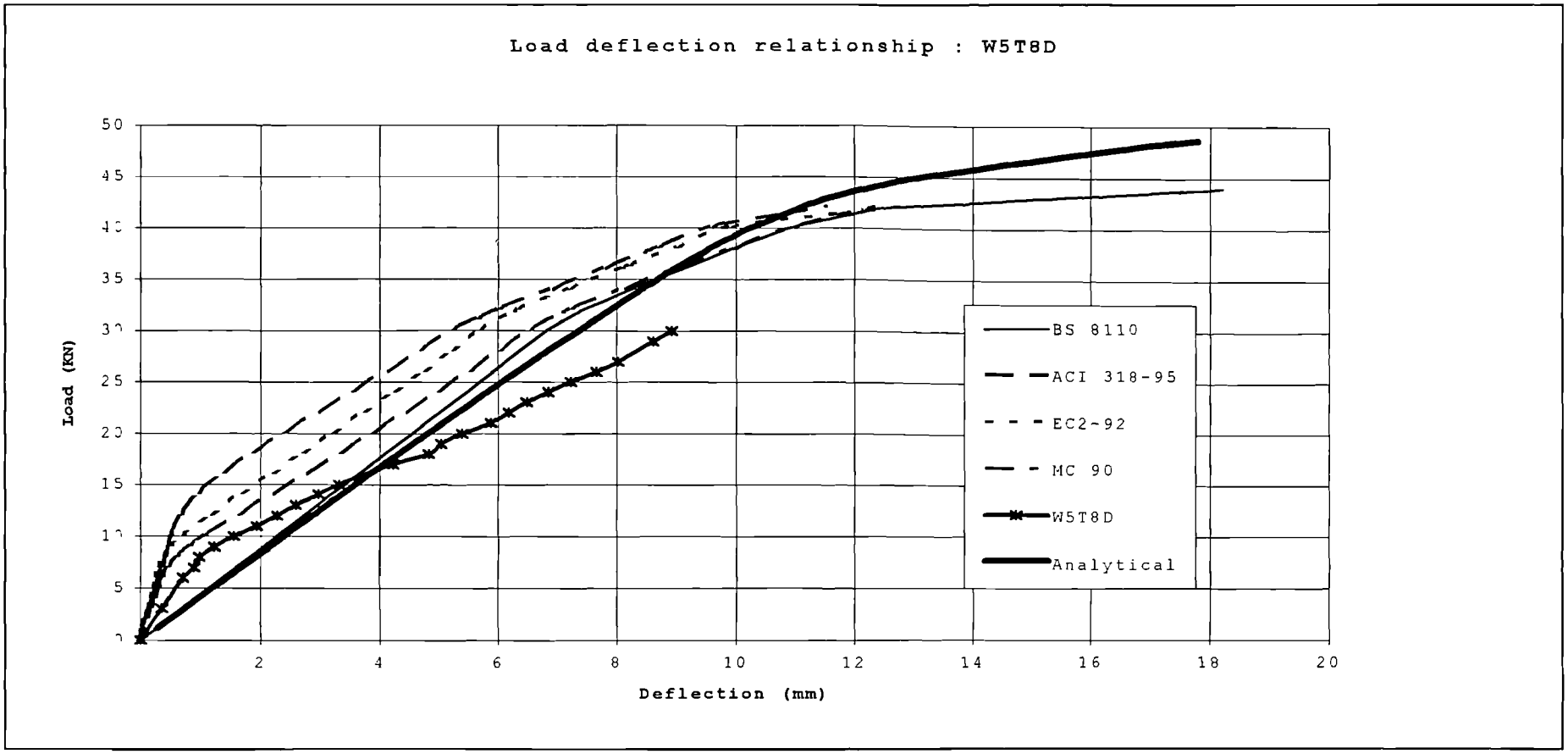

330

Figure 8-36: W5T8D measured and modelled load deflection curves.

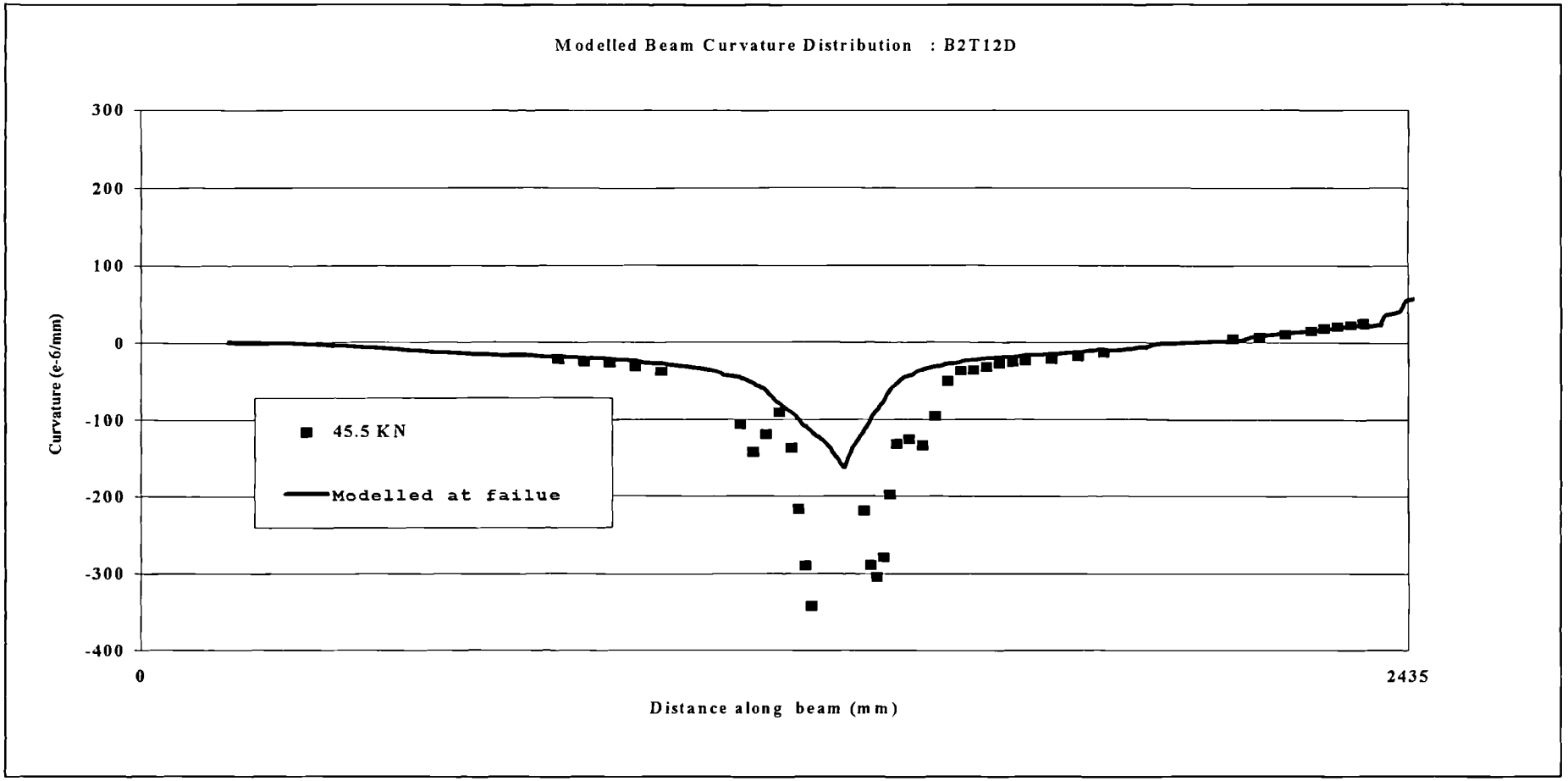

Figure 8-37: B2T12D measured and modelled curvature distributions.

331

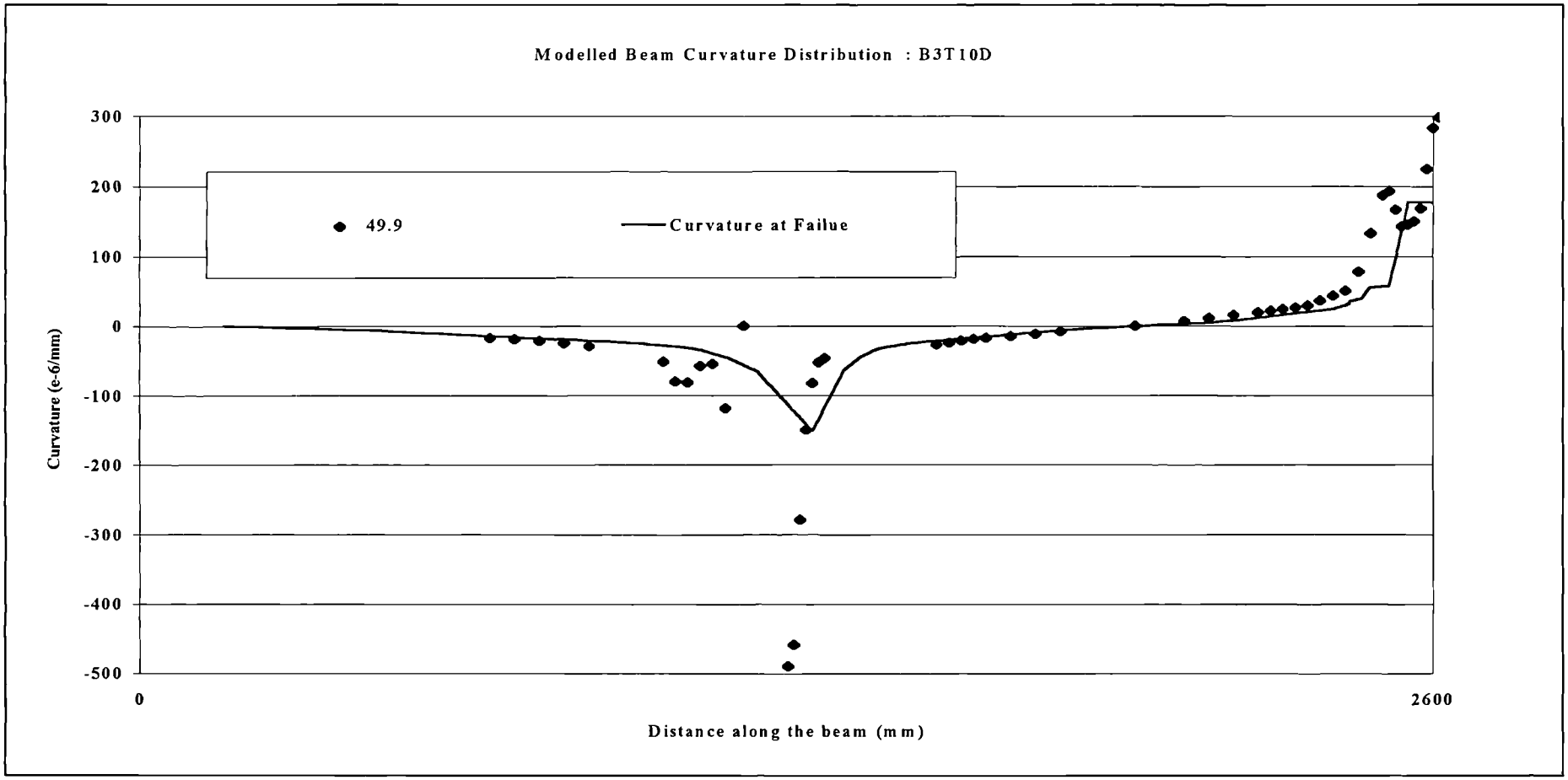

Figure 8-38: B3T10D measured and modelled curvature distributions

332

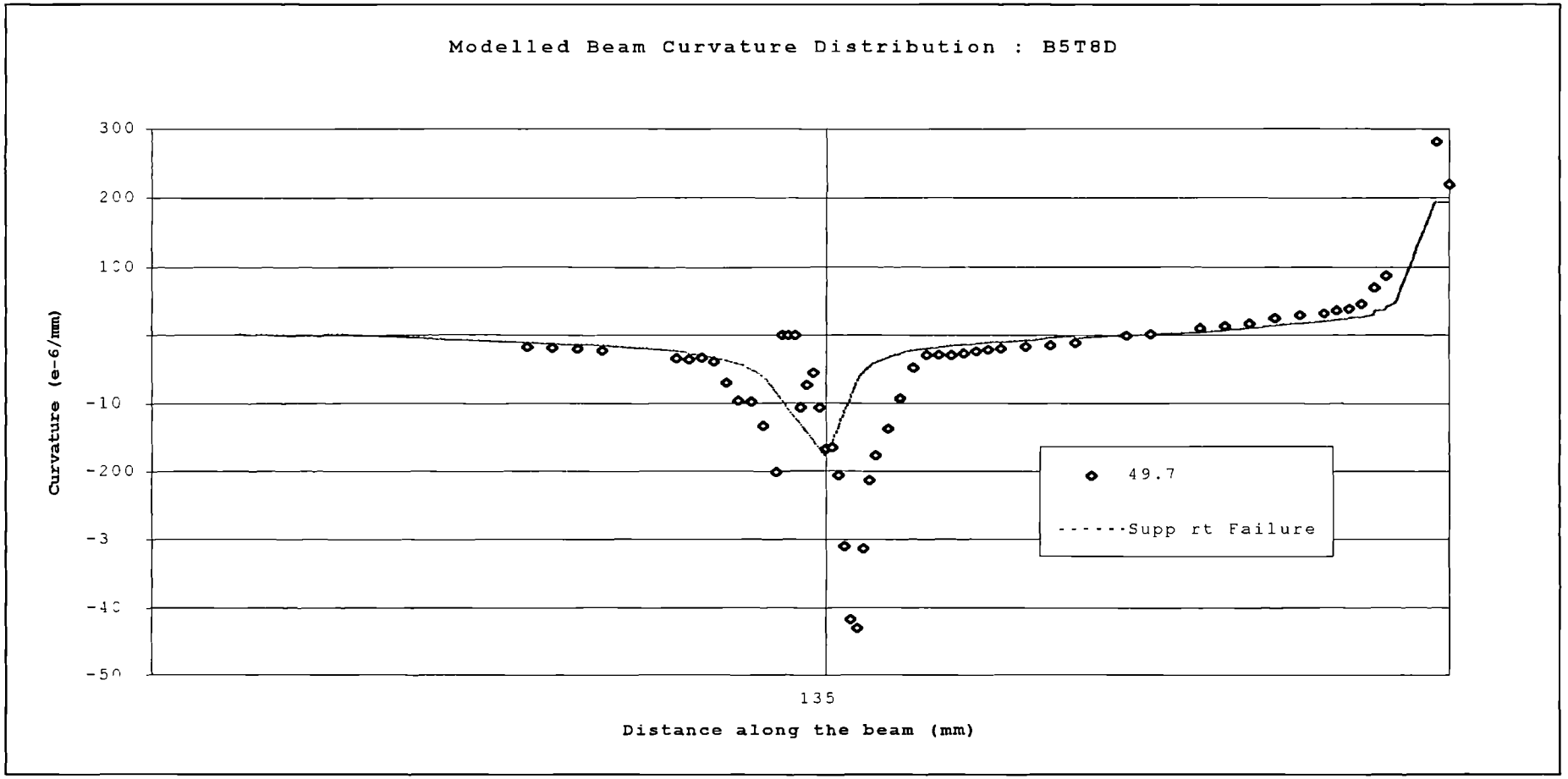

Figure 8-39: B5T8D measured and modelled curvature distributions.

333

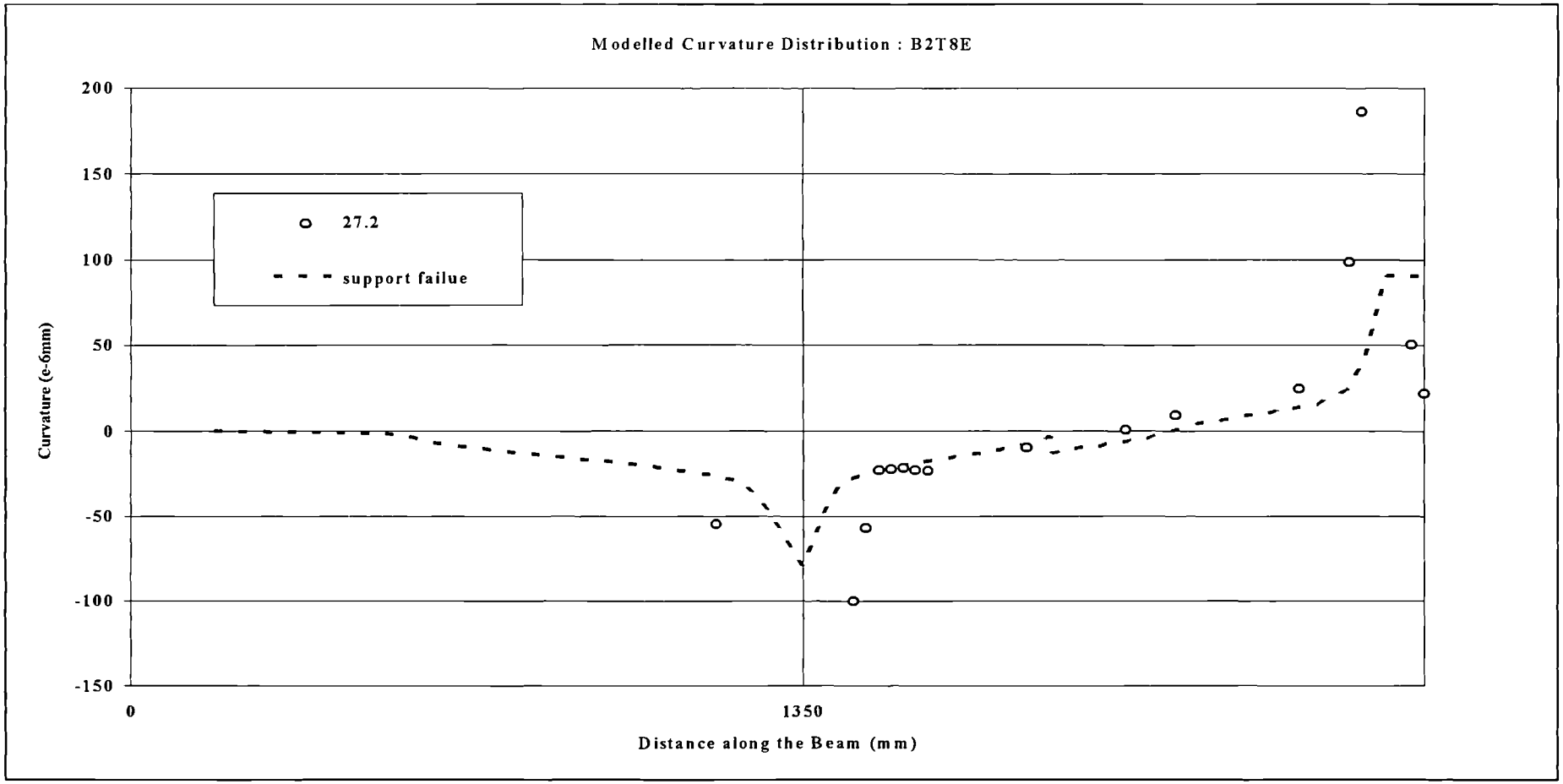

Figure 8-40: B2T8E measured and modelled curvature distributions.

334

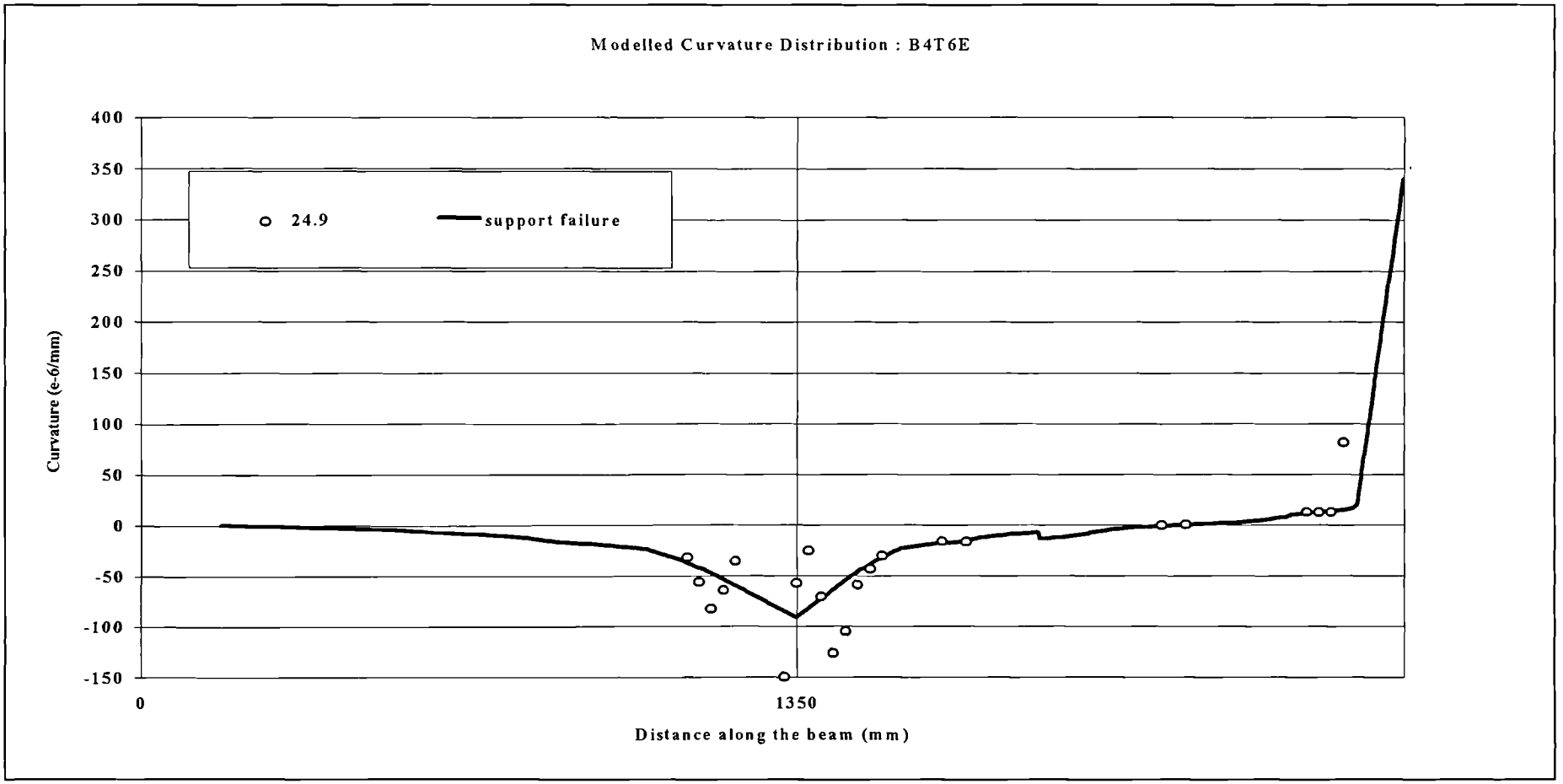

Figure 8-41: B4T6E measured and modelled curvature distributions

335

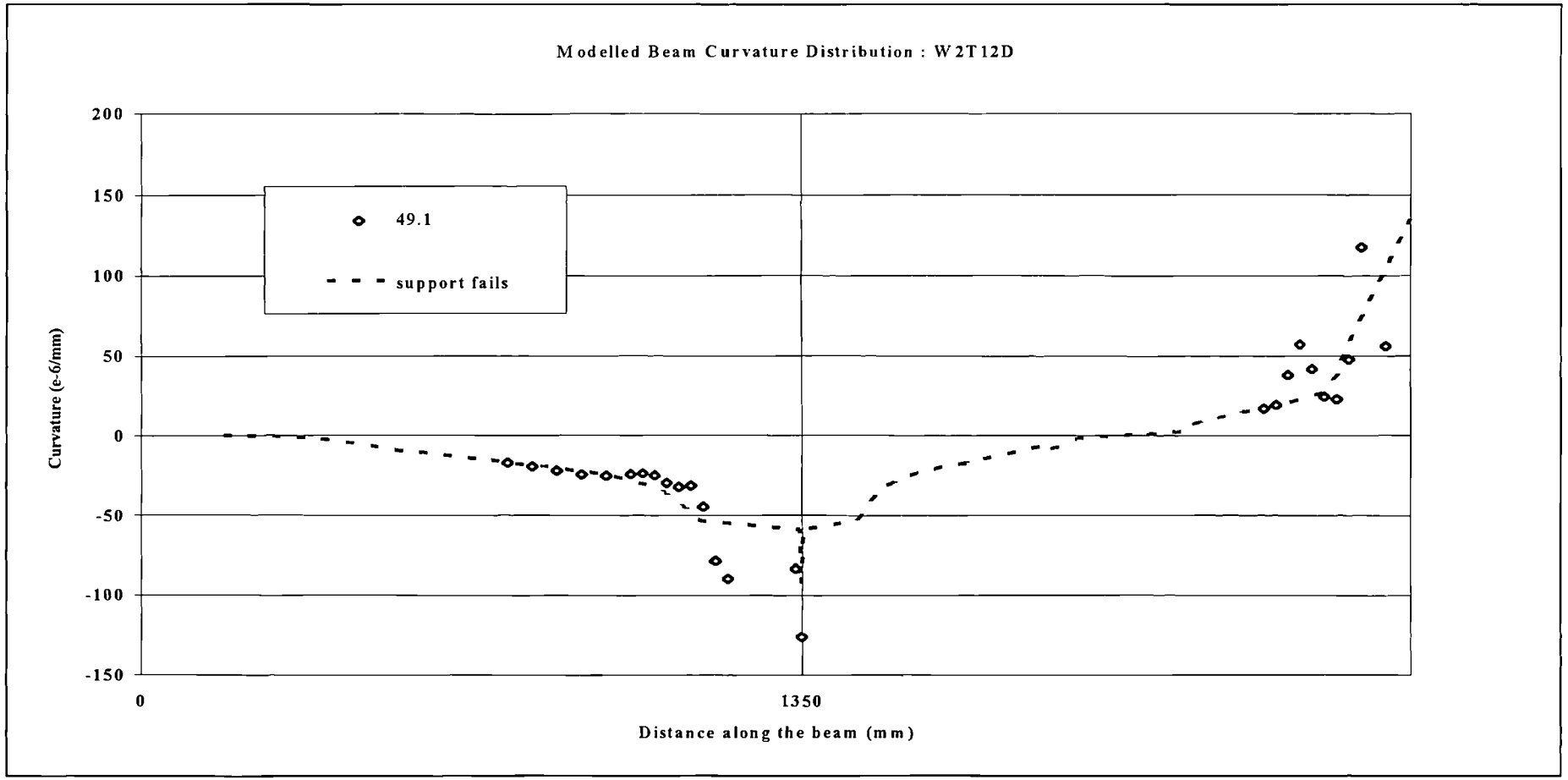

Figure 8-42: W2T12D measured and modelled curvature distributions.

336

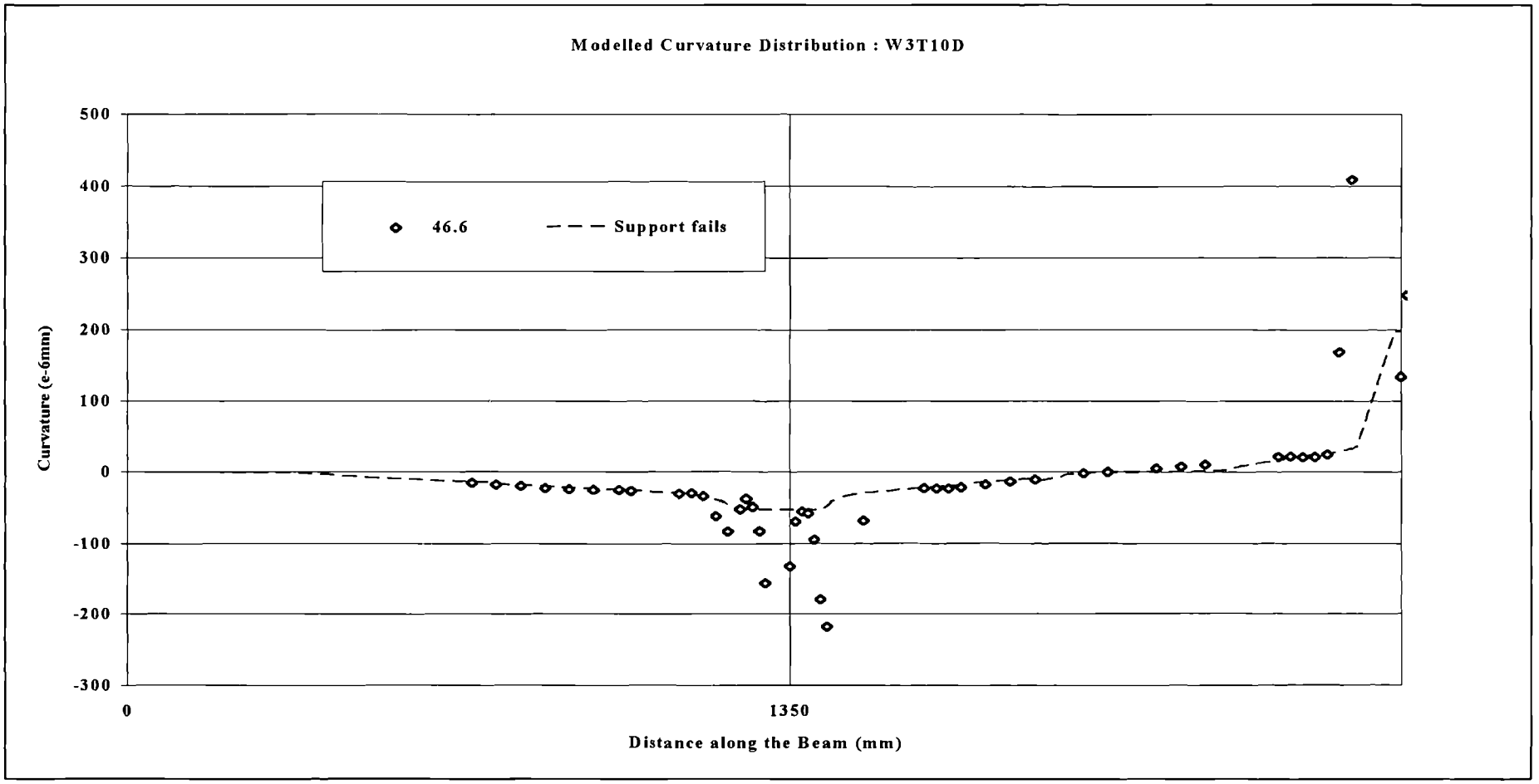

Figure 8-43: W3T10D measured and modelled curvature distributions.

337

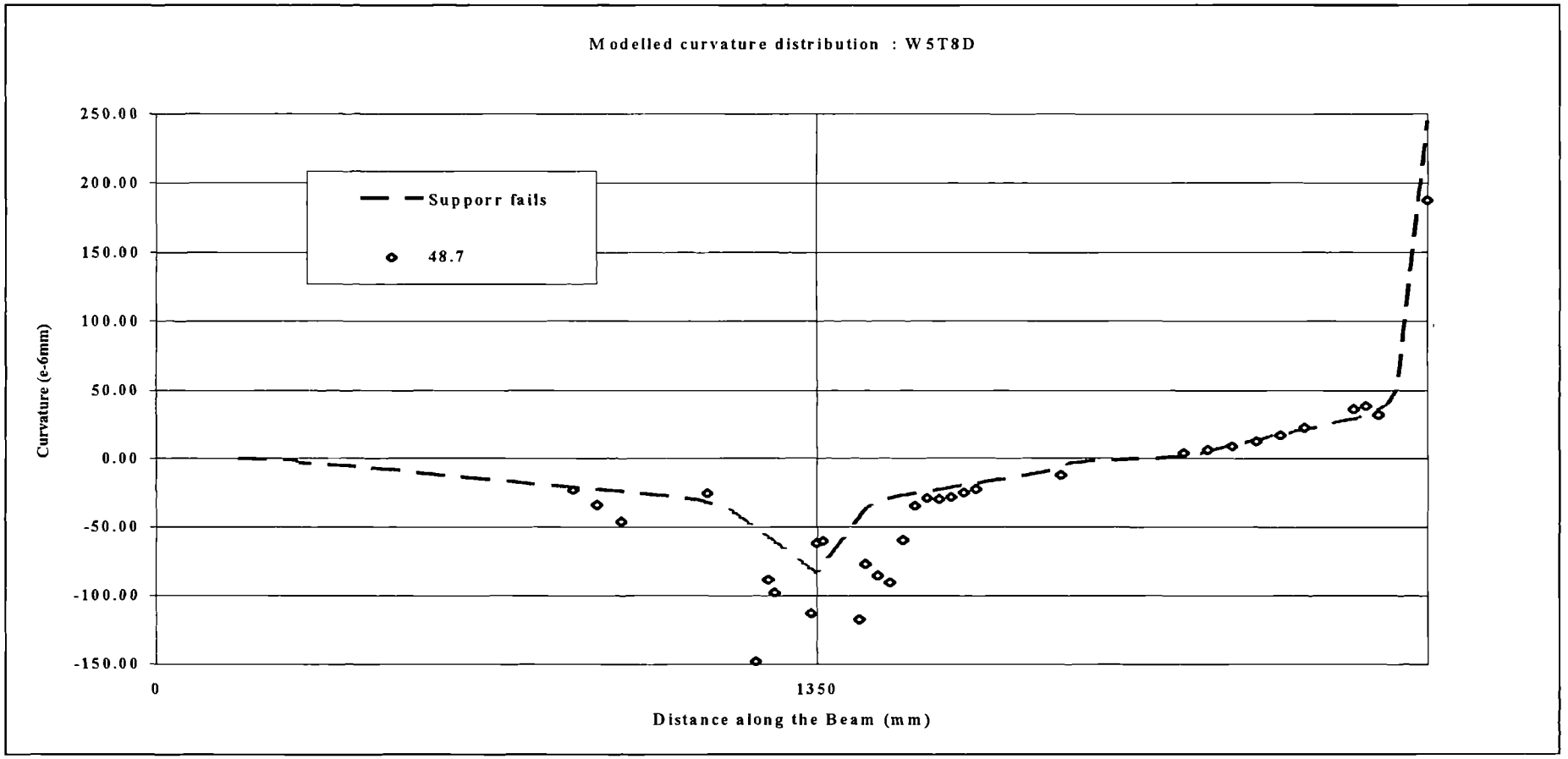

Figure 8-44: W5T8D measured and modelled curvature distributions

338

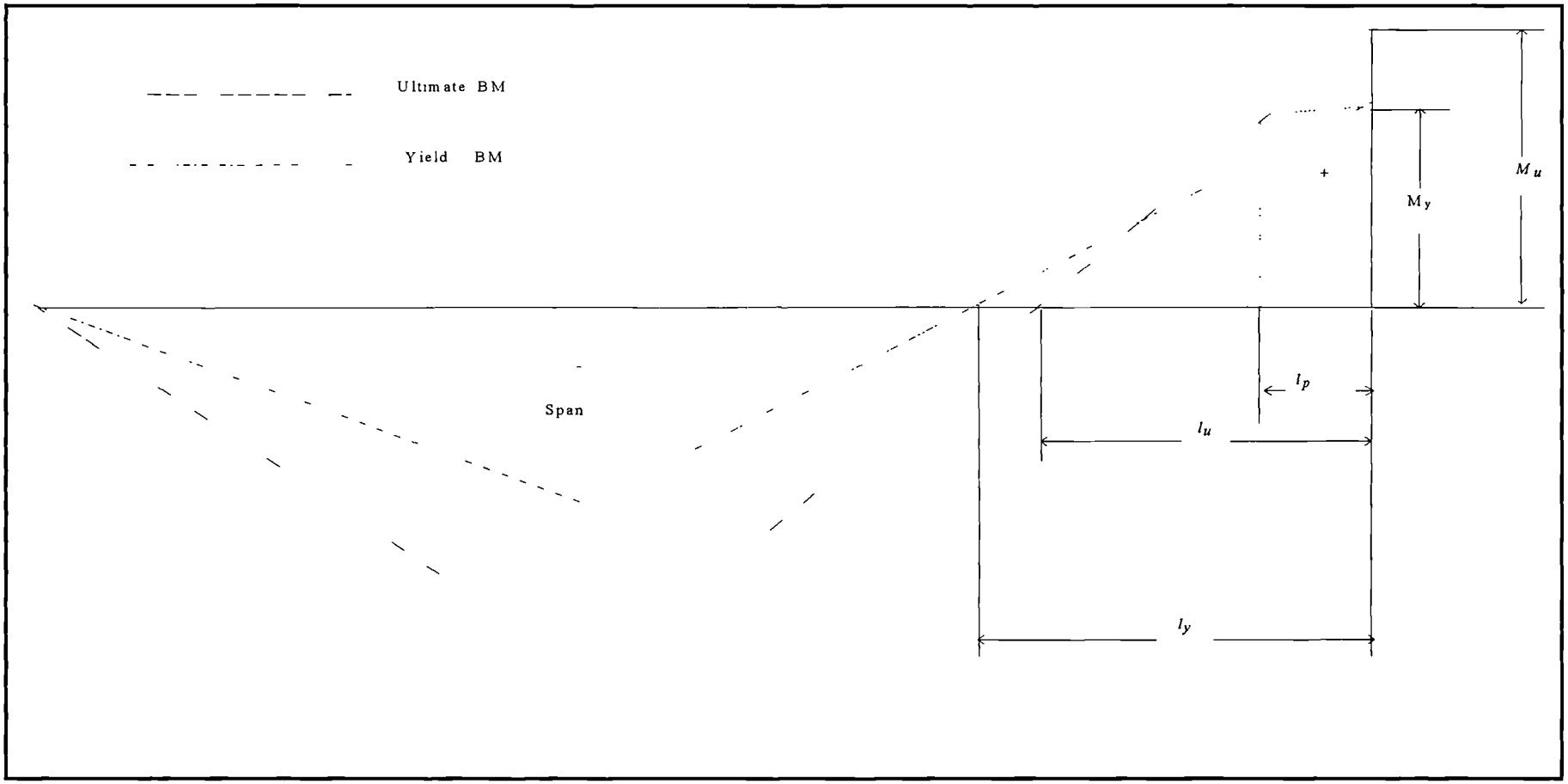

Figure 8-45: Diagram of bending moment distribution at yield and ultimate for the calculation of the modelled plastic hinge length

339

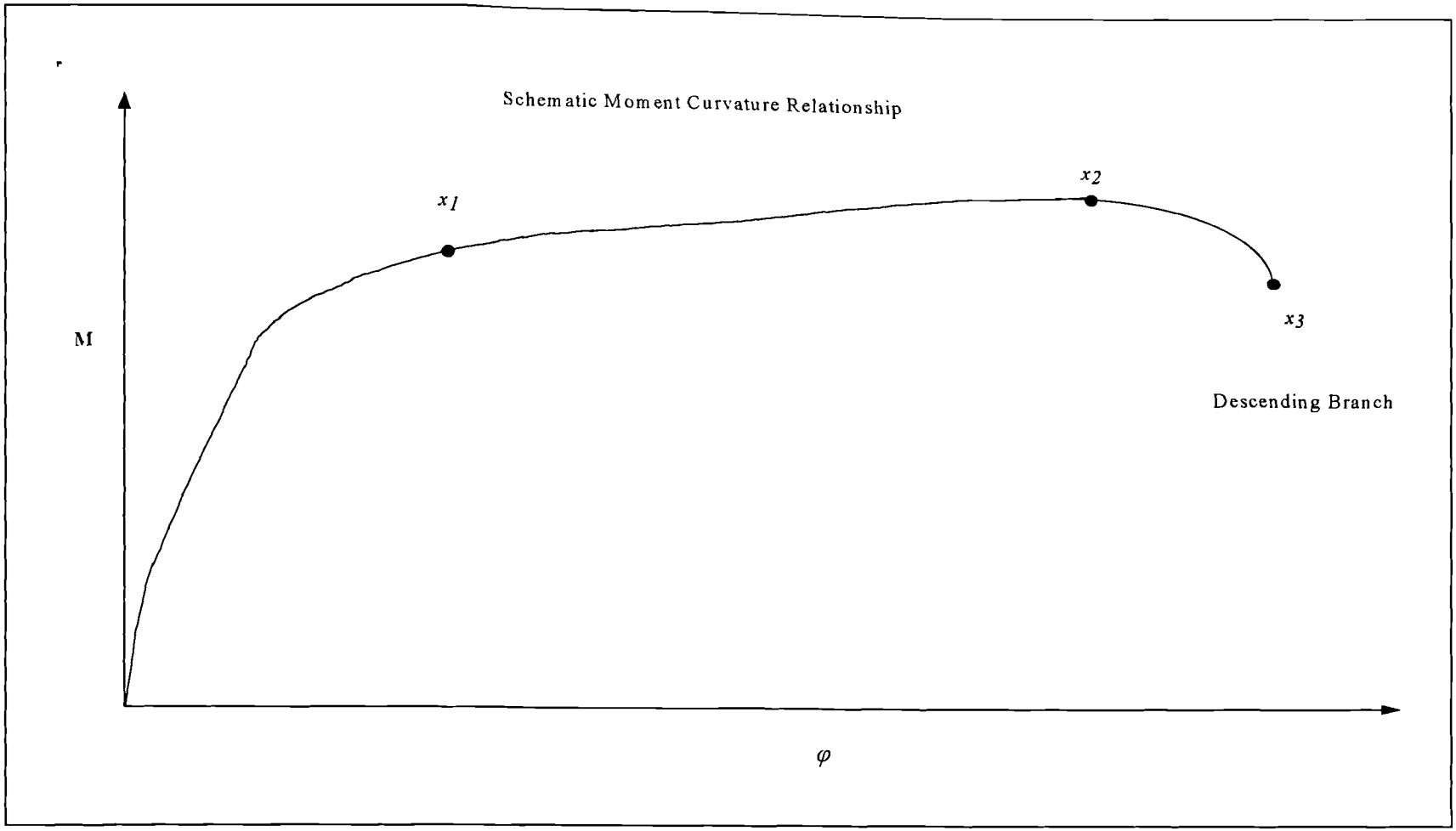

Figure 8-46: Schematic moment curvature relationship showing the various definition of ultimate curvature

340

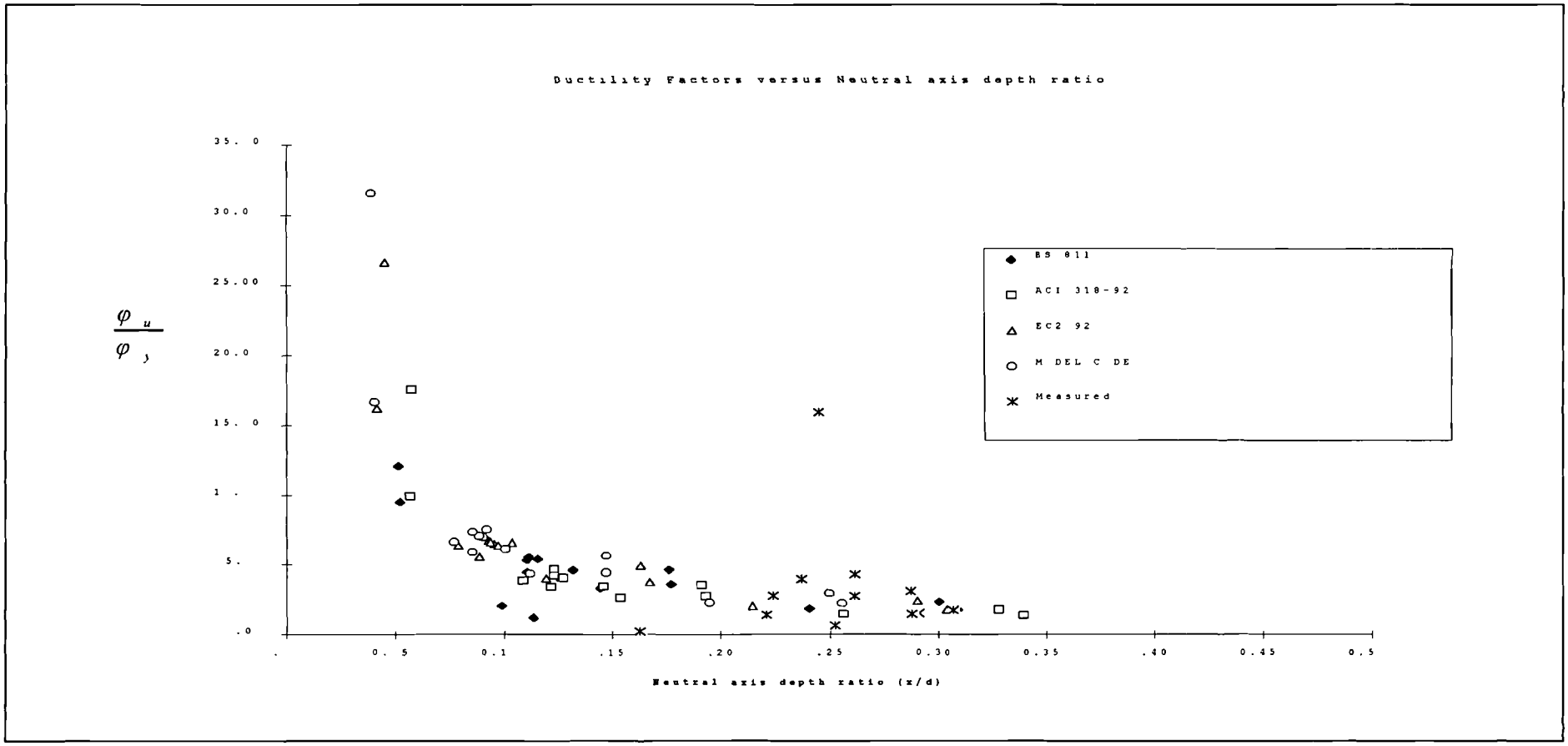

Figure 8-47: Comparison between codes and experimental ductility factors versus neutral axis depth ratio

341

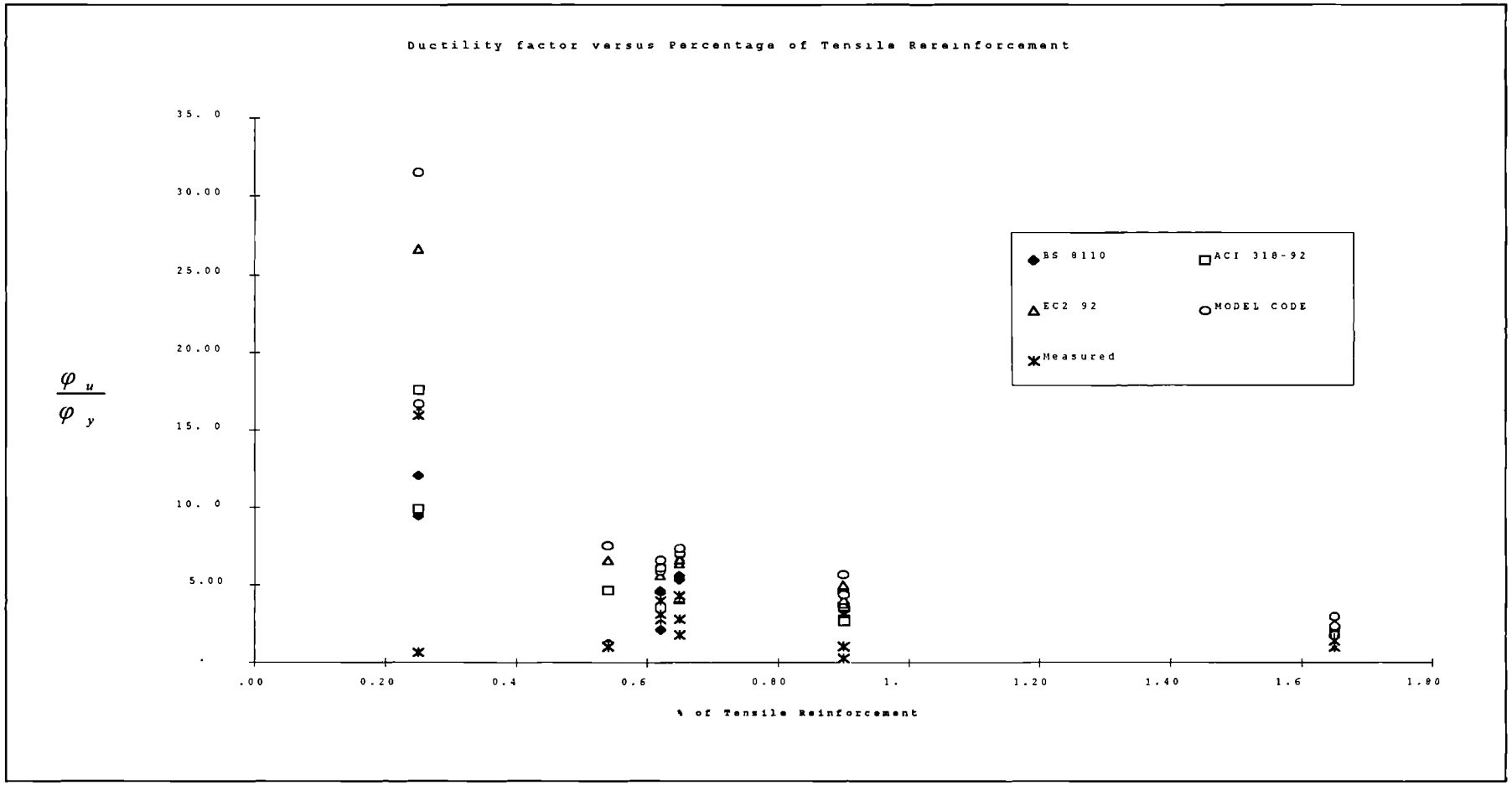

Figure 8-48: Influence of tensile reinforcement ratio on ductility expressed as ductility factor φ_u/φ_y

342

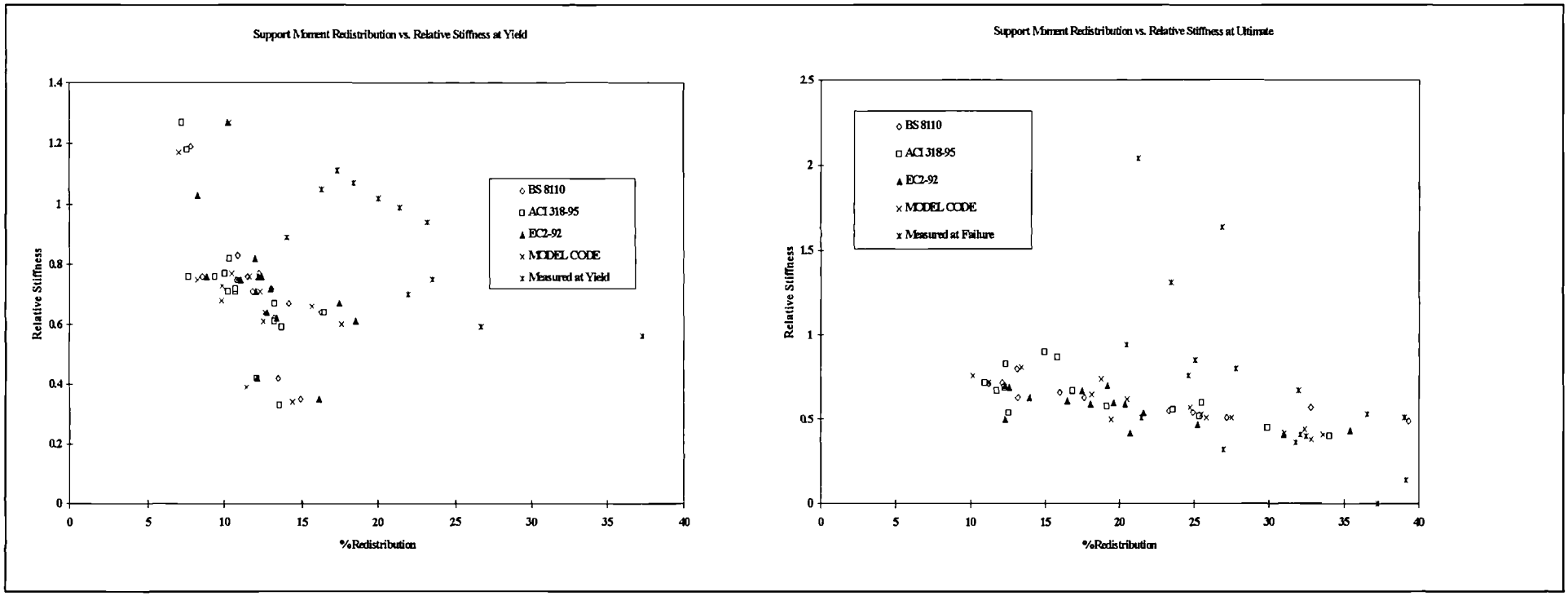

Figure 8-49: Computed and experimental relative stiffness at yield and ultimate

343

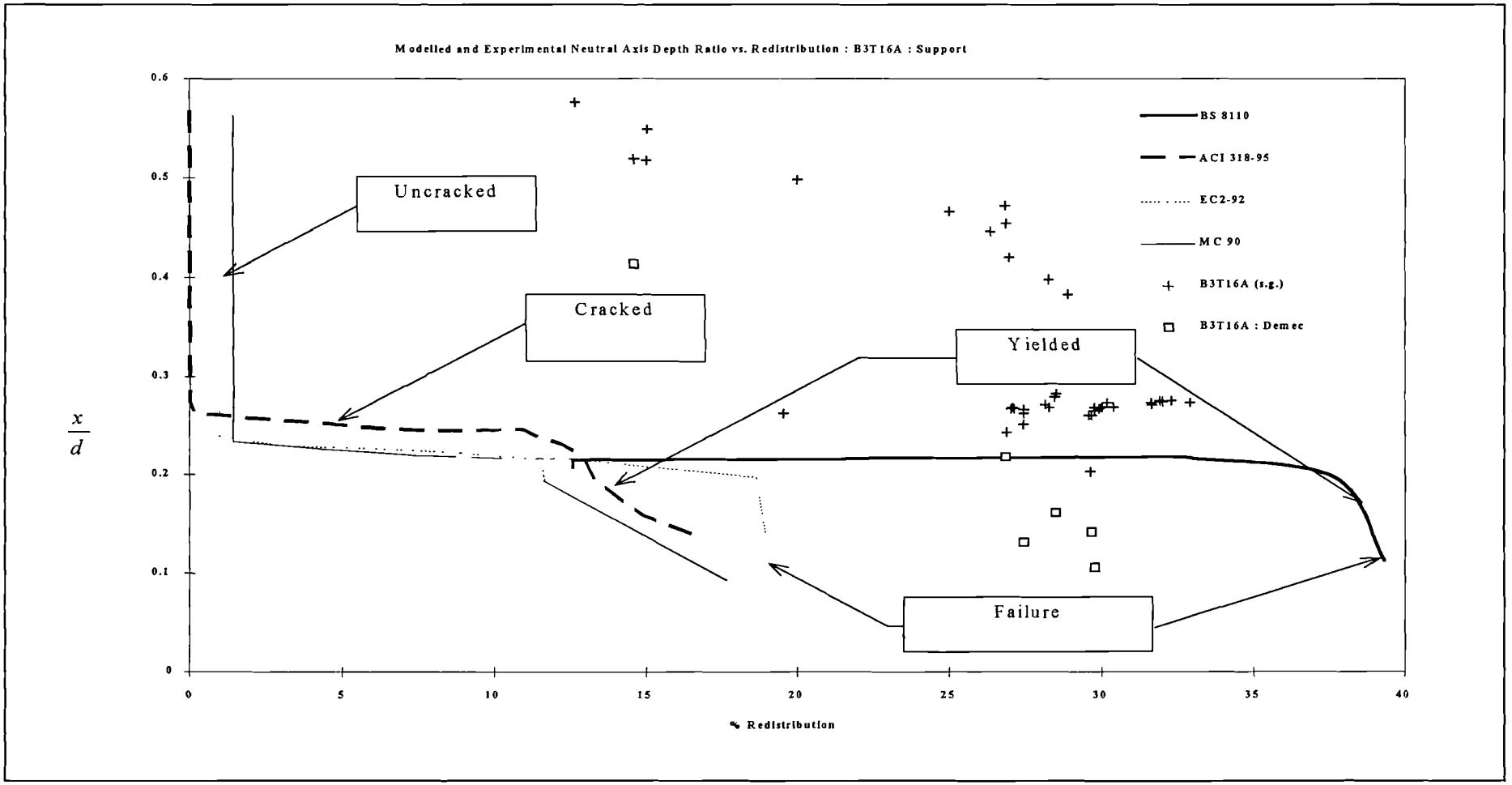

Figure 8-50: Comparison of neutral axis depth development versus redistribution for B3T16A

344

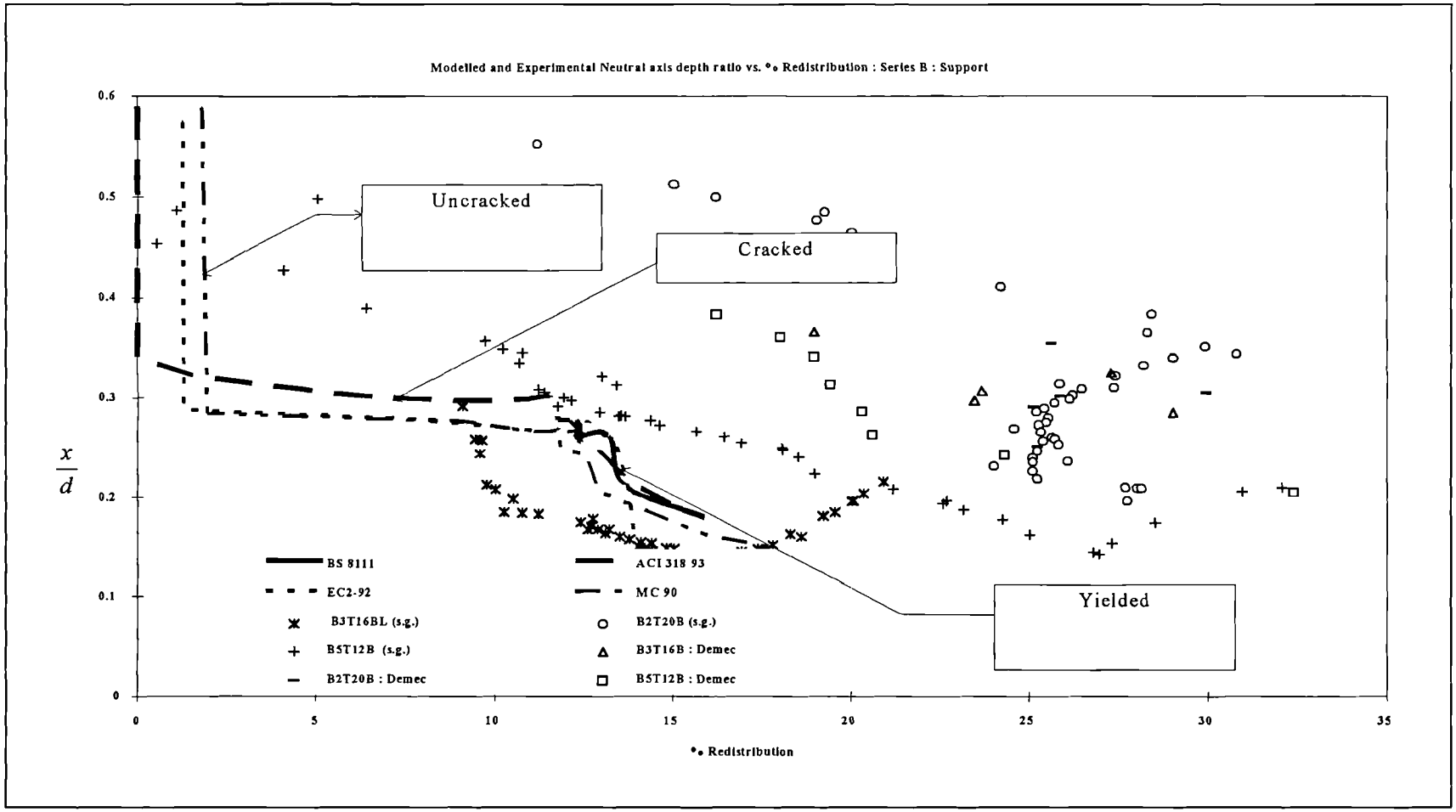

Figure 8-51: Comparison of neutral axis depth ratio development versus redistribution for Series B

345

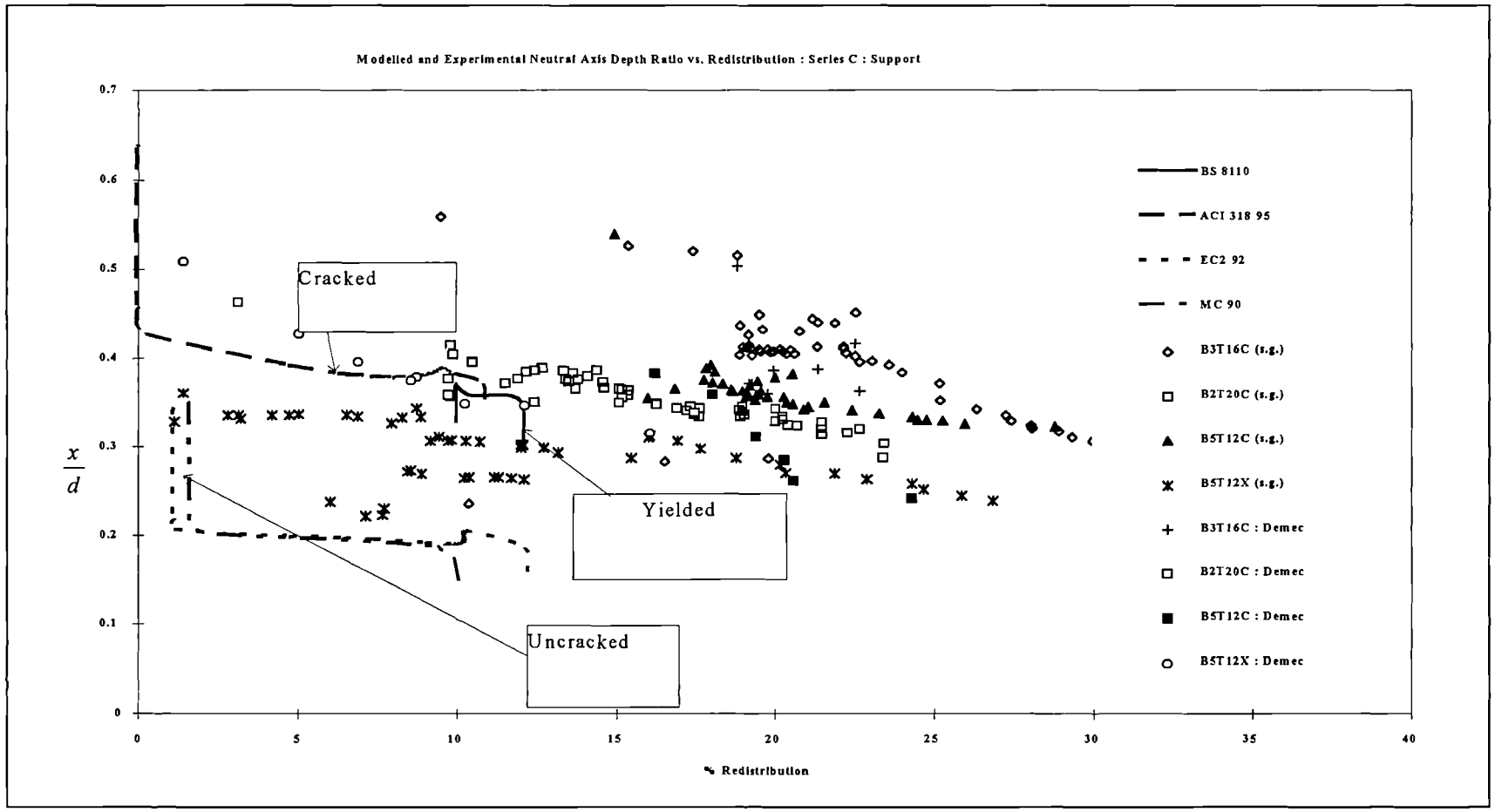

Figure 8-52: Comparison of neutral axis depth ratio development versus redistribution for Series C

346

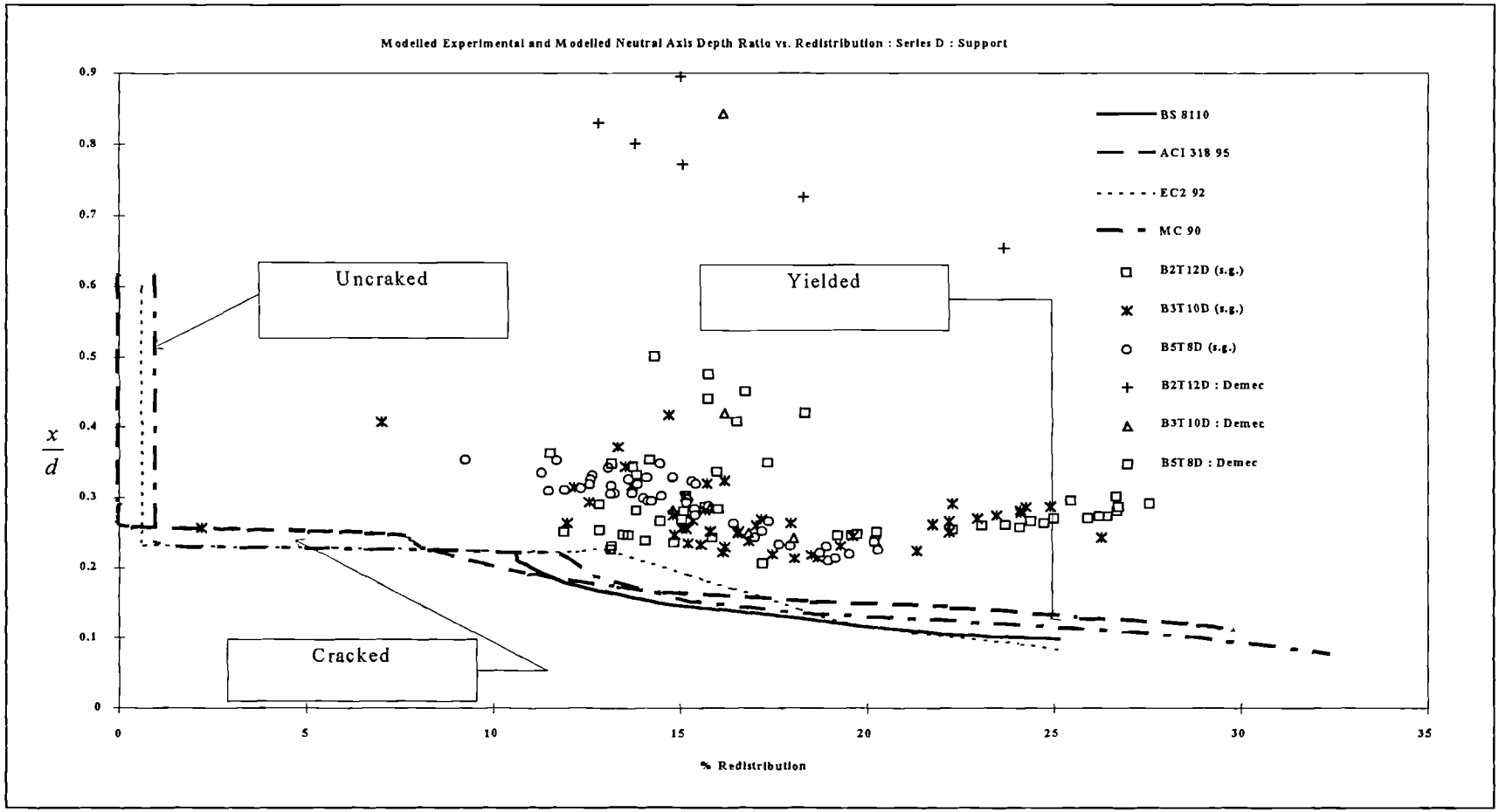

Figure 8-53: Comparison of neutral axis depth ratio development versus redistribution for series D

347

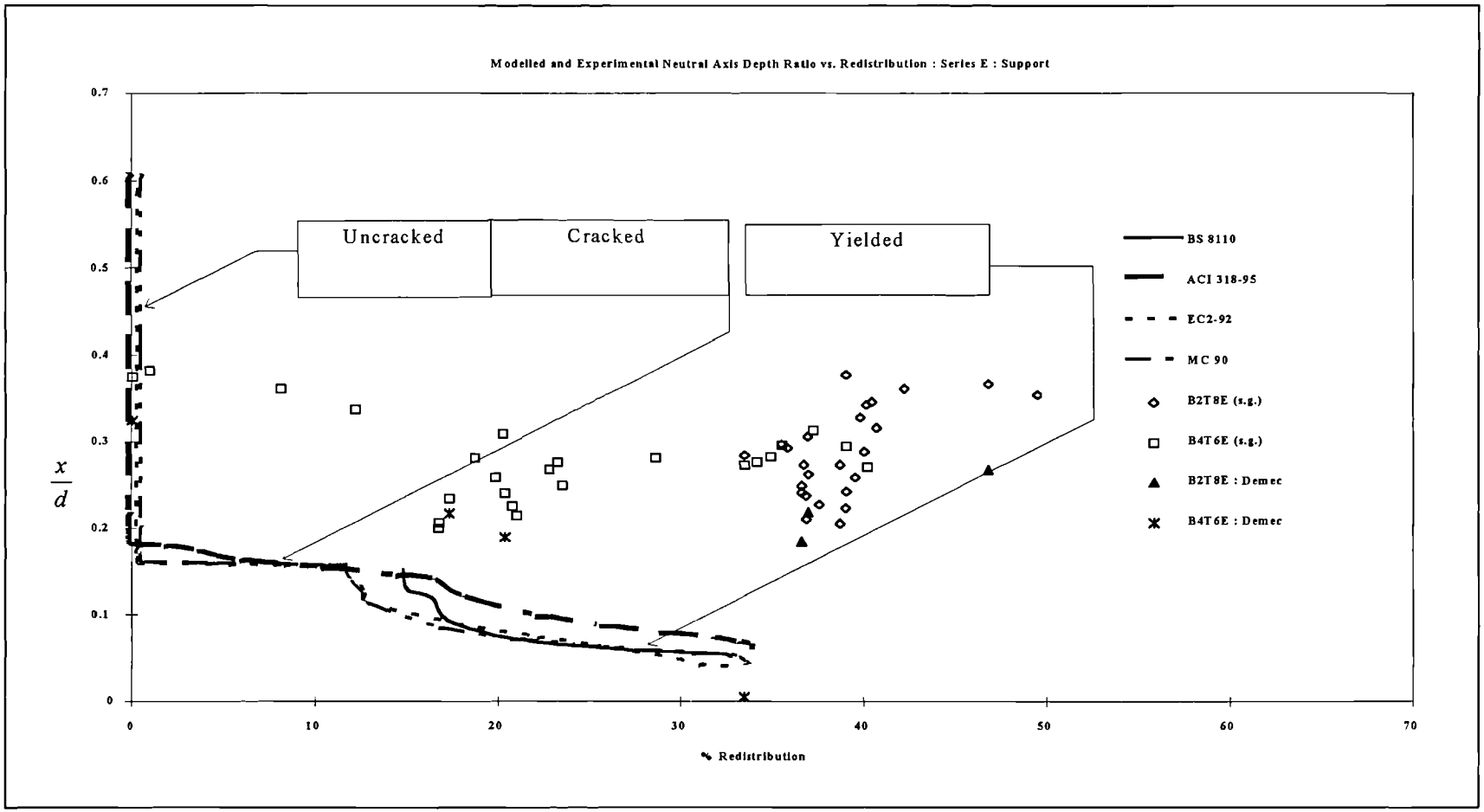

Figure 8-54: Comparison of neutral axis depth ratio development versus redistribution for series E

348

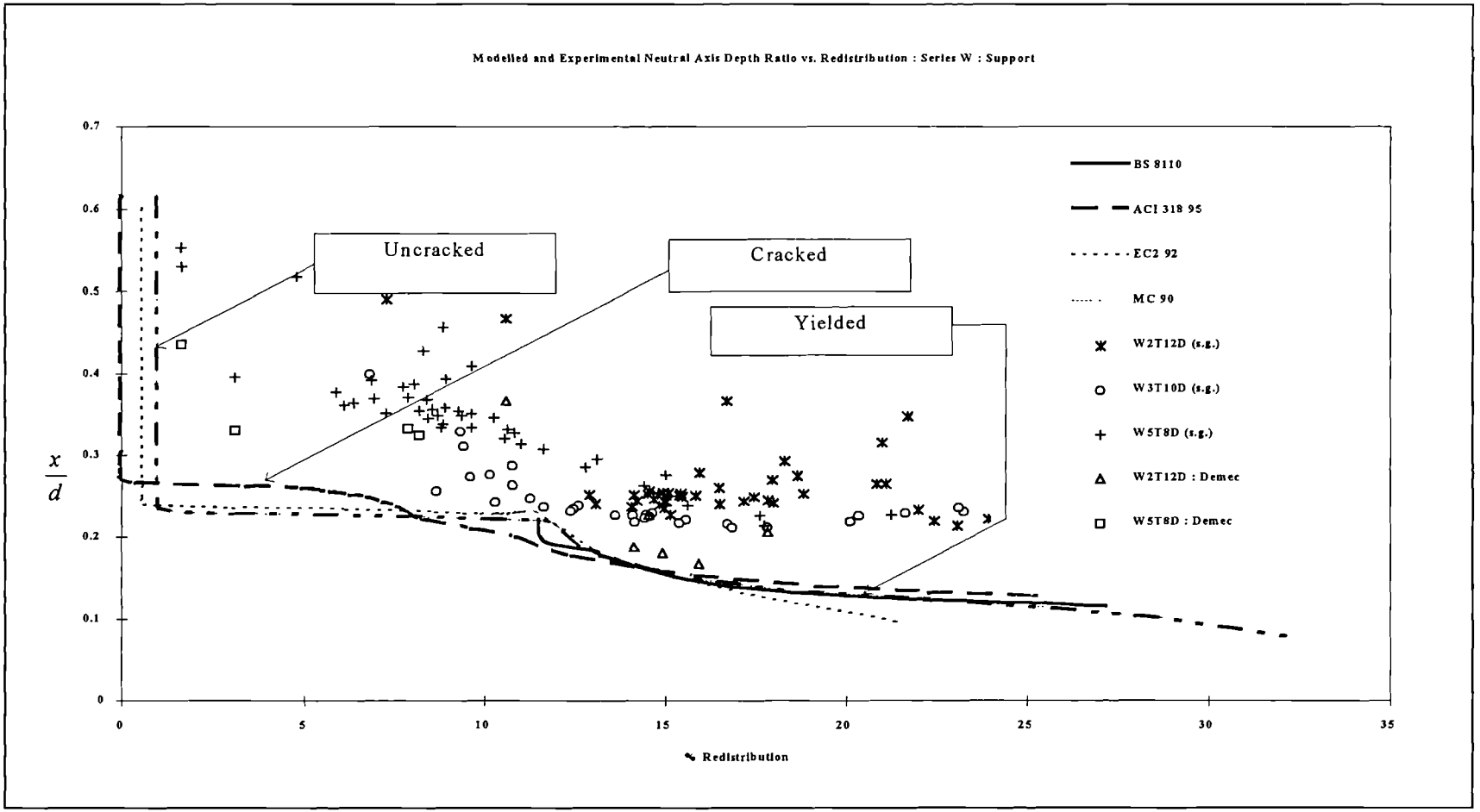

Figure 8-55: Comparison of neutral axis depth ratio development versus redistribution for series W

349

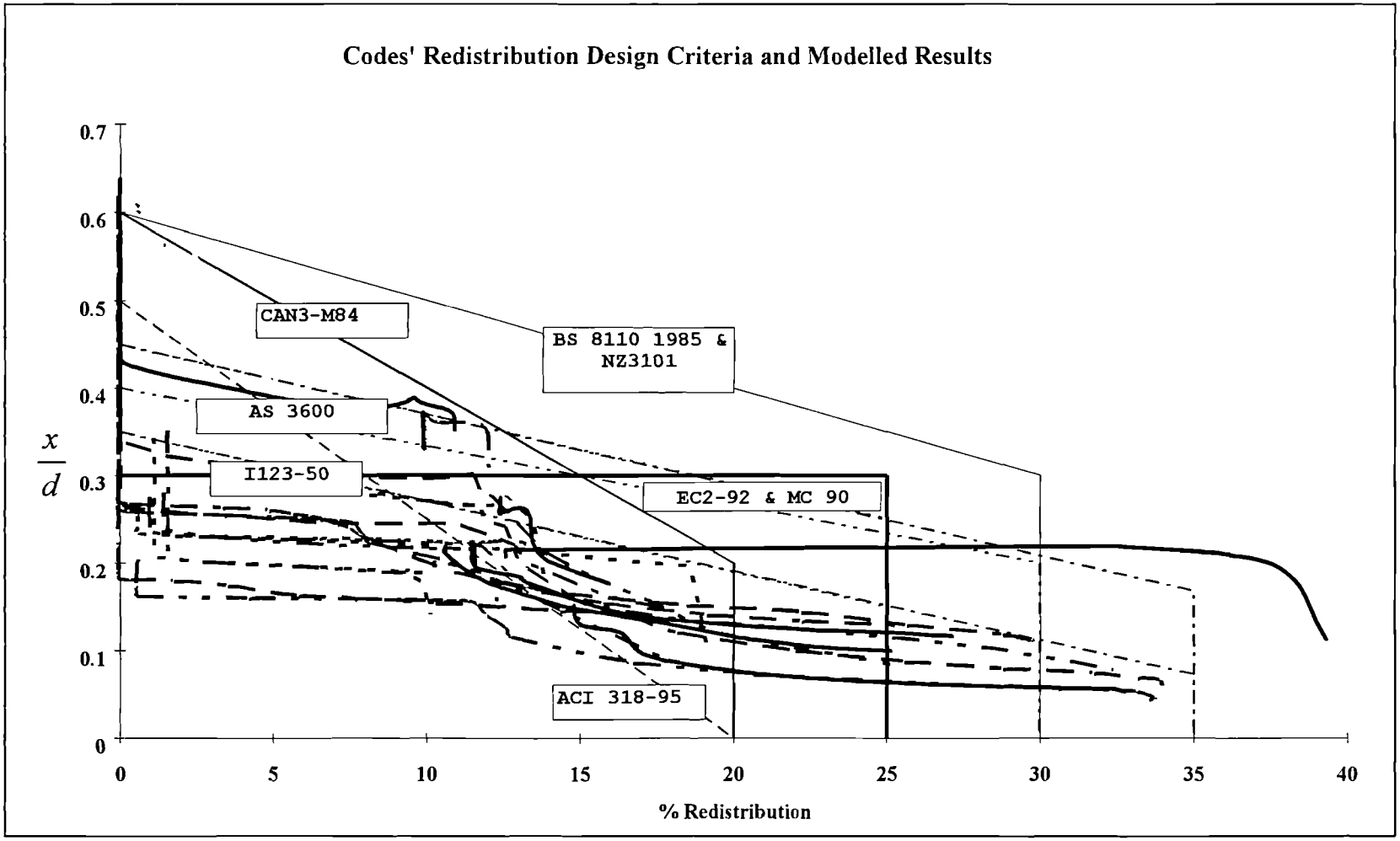

Figure 8-56: Comparison between codes' criteria for redistribution and modelled curves from codes moment curvature relationship

350

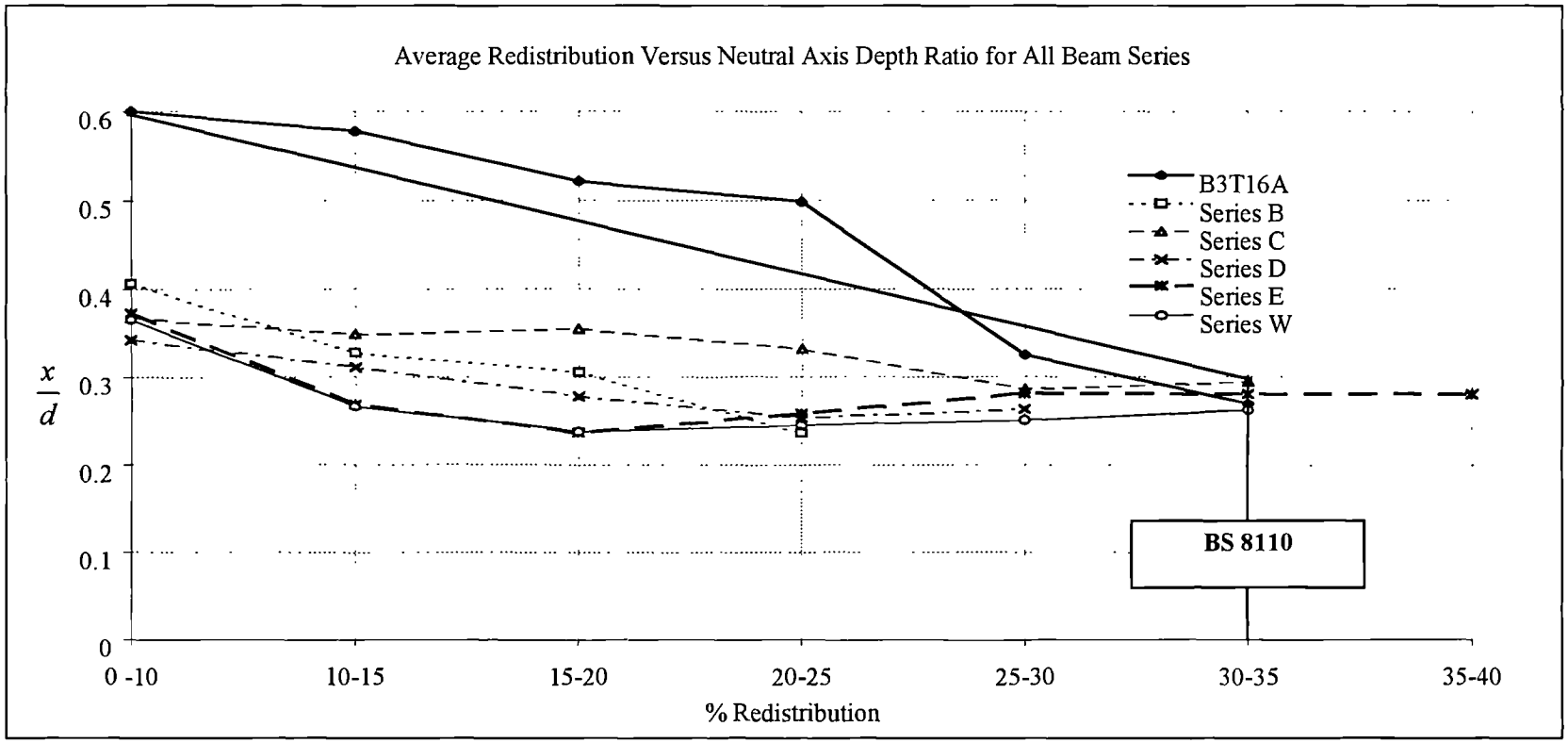

Figure 8-57: Shows a comparison between beam series range of redistribution development with the neutral axis depth ratio

351

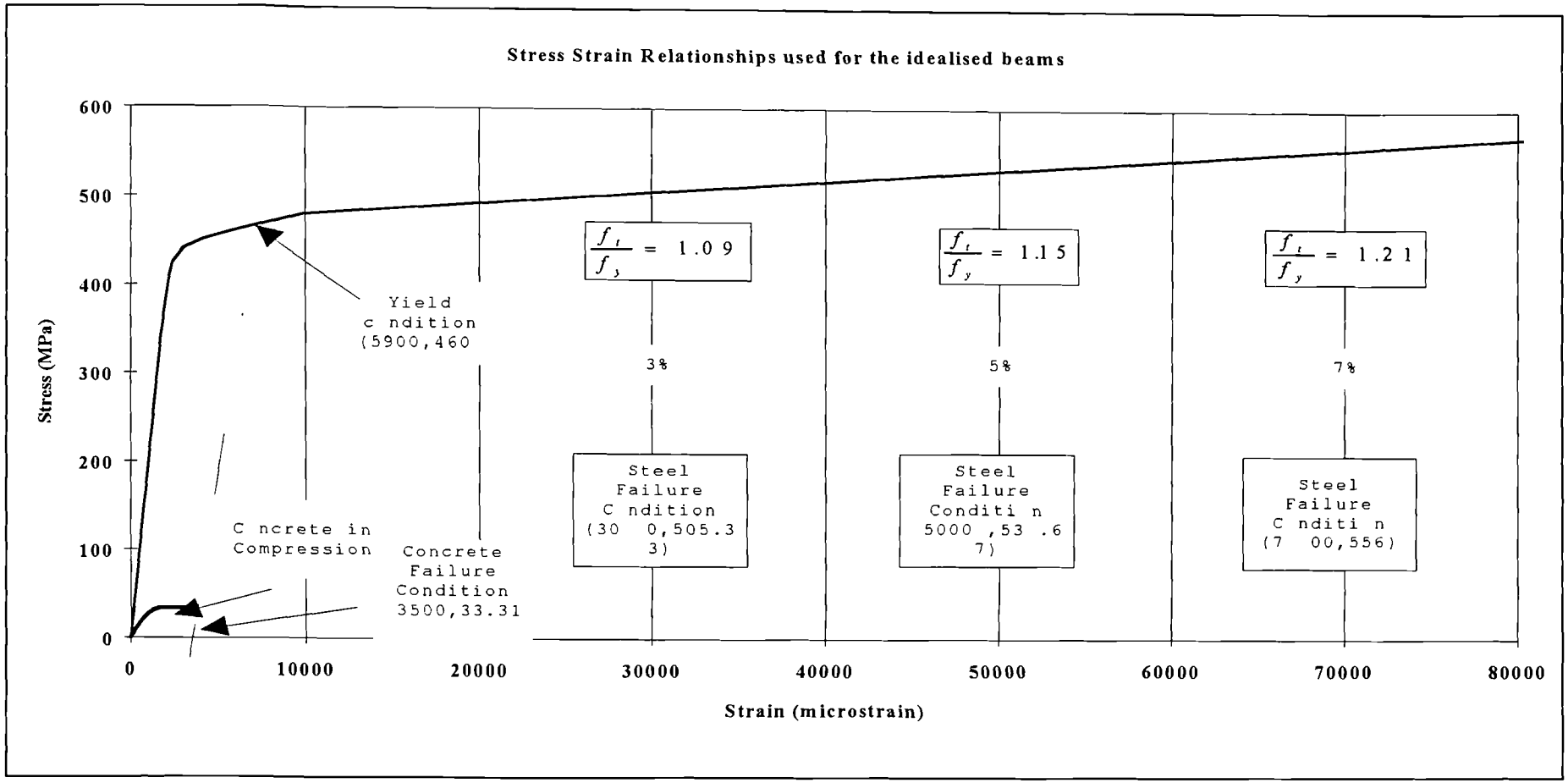

Figure 8-58: Concrete and reinforcement stress strain curves used for modelling the idealised beams.

352

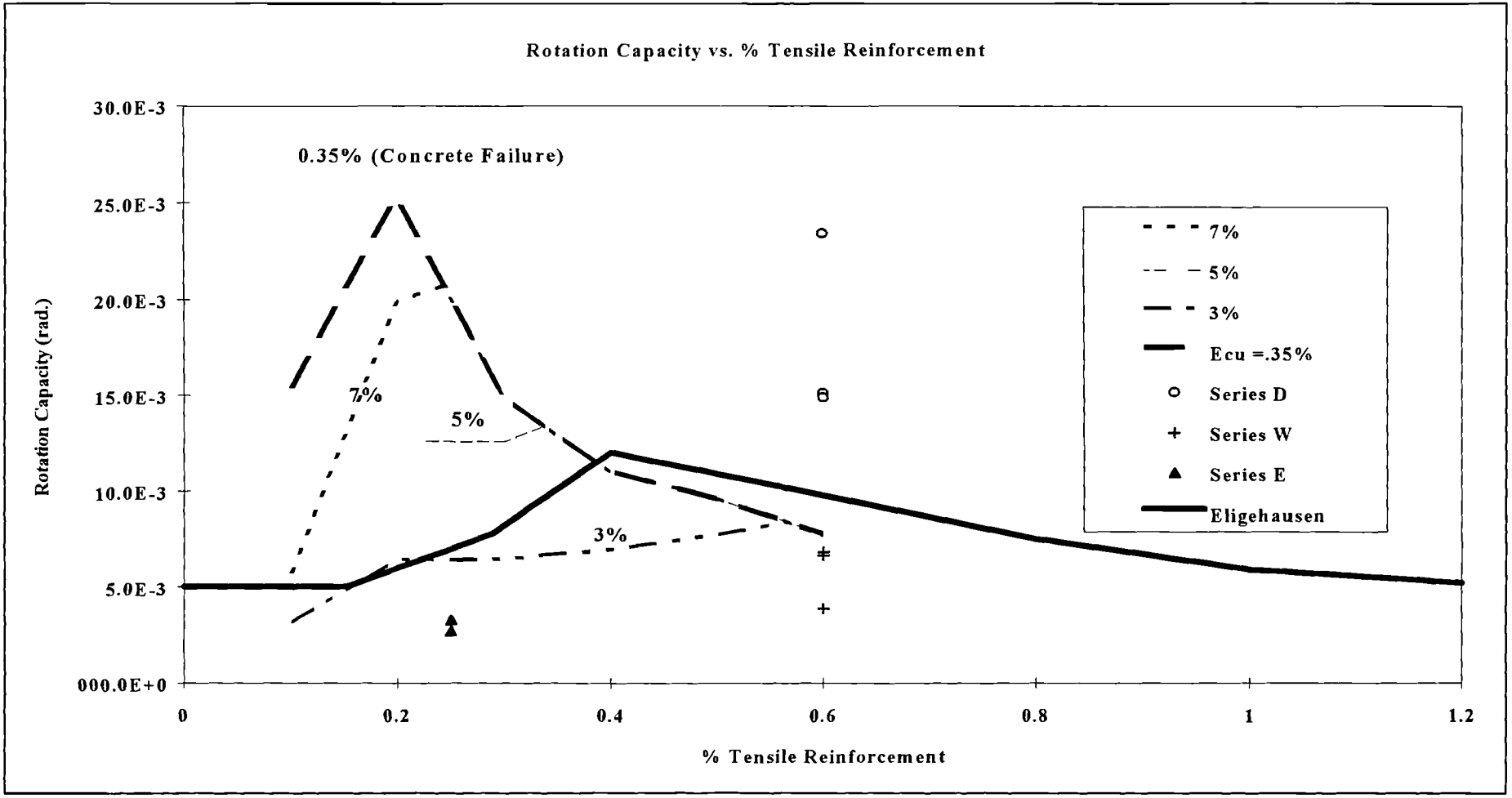

Figure 8-59: Tensile Reinforcement versus rotation capacity at various failure conditions.

353

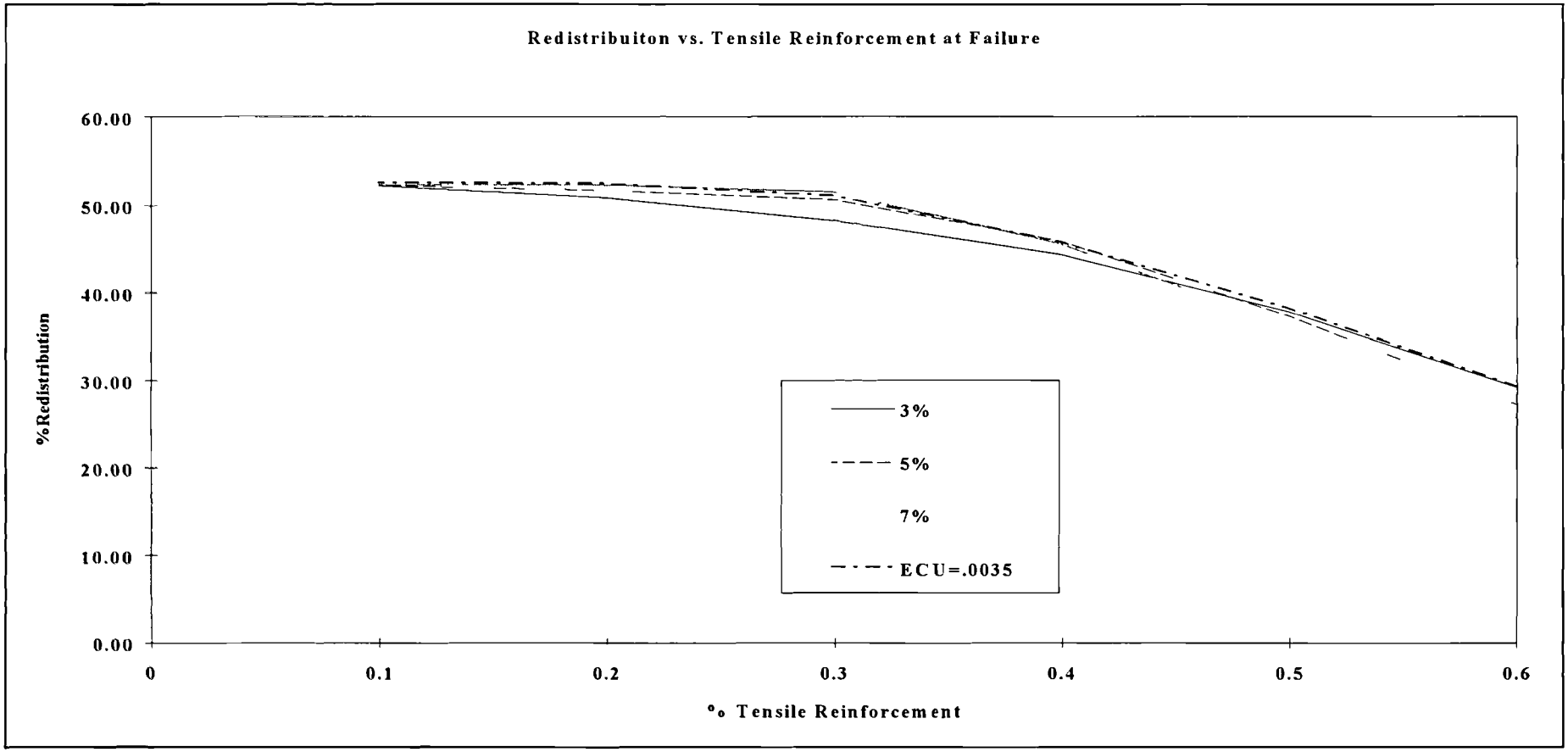

Figure 8-60: Show the relationship between tensile reinforcement to percentage redistribution of idealised beams

CHAPTER NINE

9. CONCLUSIONS

Seventeen two-span continuous beams of reinforced concrete with various ratios of reinforcements were tested to determine the manner and degree of redistribution of moments throughout the load history of the beams. Although the number of specimens was limited, the following conclusions from the experimental results and the modelled ones may be drawn:-

9.1 Experimental Results

1. Redistribution could have started from early load stages even before the beam was cracked due to low initial relative stiffness and unsettled support conditions. However, this redistribution is not significant.
2. Beams with larger bar diameter developed higher redistribution as a result of more crack development along the length of the beams
3. Tension stiffening caused a small decrease in moment redistribution throughout the load history up to yield. After the tension bars yielded, this effect gradually diminished.
4. The relative stiffness of the beams influenced the manner and degree of moment redistribution that took place in the test beams. As the relative stiffness decreased, redistribution increased.
5. Moment redistribution in beams with low reinforcement ratios (i.e. series D, E and W), was mainly caused by the yielding of the tension bars over the support area.
6. Shear failure in a specimen could occur while beam strains are still elastic as did occur in specimen B3T16A.
7. The level of strains exceeding yield strain of the tension bars in the test beams influenced the manner and degree of moment redistribution. As the plastic strains along the tension bars increased, moment redistribution increased.
8. The use of linear regression across section Demec strains gave a clear representation of the strain distribution on the face of the concrete.

9. The investigation demonstrated the practicality of measuring strains using strain gauges embedded in the reinforcement. Results compared well with equivalent Demec gauge readings. Satisfactory agreement between Demec and strain gauge data occurred as long as the section did not crack. After cracking, the severity of cracking controlled the correlation between Demec and strain gauge strains.
10. Neutral axis depth at the support section of the test beams decreased with constant redistribution before the tension bars yielded. Once yielding began, redistribution continued to increase rapidly with decreasing neutral axis depth.
11. The effect of increased moment on the span section due to moment redistribution did not influence the neutral axis depth as was the case in series B and C.
12. Lower reinforced beams of series D, E and W showed lower values of neutral axis depth than series B and C. This indicated that these specimens of series D, E and W were more ductile.
13. Crack formation of the test beams could be classified into two types: shear cracks and flexure cracks. Shear cracks were diagonal and characteristic of specimen B3T16A, series B and C, while flexural cracks of series D, E and W were straight and smaller in number than those of series B and C. The development of cracks in many different manners (shear, flexural and bond slip cracking or shrinkage cracks), always effected an increase in redistribution.
14. If failure in shear or by bond slip can be avoided, the moment capacity can be achieved in the beams in both support and span sections respectively. Furthermore, the failure of one span in shear may cause the other span to fail in bending, but because of the rapid development of shear cracks, this bending failure lacks the mechanism required for the development of a full plastic hinge as was the case in some of the specimens in Series B and C.

9.2 Modelled Results

1. The numerical model developed by the author demonstrated that the elastic bending moment of a propped cantilever reinforced concrete beam, with varying reinforcement layout, can partially be justified for the short lived uncracked portion of the moment curvature relationship. Once cracking occurs, the basic assumption of elastic moments can no longer be held to represent the behaviour in the beam as moment redistribution takes place.

2. Representative moment curvature relationships may be derived from average strain gauge data of the test beam which can be used to model the beam behaviour, i.e. moment redistribution development, curvature, rotation and deflection distribution can be computed.

3. The numerical model developed here is capable of modelling redistribution that takes place even before cracking, due to the varying initial stiffnesses the beam may have.

4. The numerical model developed in this thesis uses multi-linear moment curvature relationships for a propped cantilever. The advantage of this is the flexibility in the analysis and design of continuous beams using any number of moment curvature relationships along the beam based on different reinforcement layout. The model can also be used to model the behaviour of stepped beams. In fact, the program can model the behaviour of any beam regardless of its material composition, (i.e. reinforced concrete or fibre reinforced composite beams) as long as there are sufficient data to formulate the needed moment curvature relationships describing the behaviour of the various sections of the beam.

5. Employing the principles of the second moment area theorem, in which linearised moment curvature relationships of the propped cantilever are known, the actual beam forces can be predicted accurately throughout the loading history. Moment redistribution can be predicted at cracking yield and ultimate cases. Furthermore, the iterative technique used in the

numerical model can also compute the curvature, rotation and deflection profile at any point along the beam.

6. The manner of redistribution was the same for all the beams, but was made of two parts:
    - Redistribution due to cracking over the support
    - Redistribution due to plastic strains developing in the tension reinforcement.
7. Redistribution due to yield increased with decreasing percentage of reinforcement.
8. The degree of moment redistribution developing in the beams using the codes provisions, is governed by the codes flexural stiffnesses assumptions of the sections at both the support and span areas. The higher the concrete modulus of elasticity, the stiffer the beam, therefore redistribution decreases. Similarly, the increase of the concrete tensile strength would decrease redistribution.
9. The numerical model developed here demonstrates its capacity to model small variations of the moment curvature relationship, such as tension stiffening and its effect on redistribution by its ability to calculate redistribution at any point in the load history of the beam.
10. The numerical model developed calculated the plastic hinge length from the movement of the point of contraflexure (point of zero moment) of the modelled bending moment diagram at yield and ultimate. The rotation capacity (total rotation at ultimate) can be determined by integrating the computed (modelled) curvature over the plastic hinge length.
11. Modelled plastic hinge lengths, and consequently rotation capacity are directly proportional to the slope of the moment curvature diagram between yield and ultimate. Both the experimental and modelled results of the plastic hinge length indicate that it may very between *0.6d to 1.1d.* The

author based on experimental results and works by others, suggests an expression for the plastic hinge length may be taken to equal *0.8d*.

12. The assessment of ductility of the reinforced concrete section may be undertaken by evaluating the ratio of ultimate to yield curvatures from the moment curvature relationship of the section. It was found from both the experimental and modelled results, that as the percentage of tensile reinforcement increased, the ductility factor decreased. Similarly, as the tensile reinforcement ratio increased, the neutral axis depth increased, and ductility decreased.

13. From the modelled results, it can be concluded that the relative stiffness of the beam defined by the author as the ratio of support to span stiffness affects the amount of redistribution that takes place in continuous beams. As the relative stiffness approaches unity, redistribution decreases to its minimum.

14. The numerical method presented in this thesis can be used for calculating the complete load-deflection behaviour of the beams. The numerical procedure is based on the specific description of the steel and concrete stress strain relationships and definite failure criteria. The overall accuracy of the results depends on the accuracy of the inputted moment curvature relationship.

15. The results from the numerical model demonstrated that the codes moment curvature relationships overlook the amount of redistribution that may occur at serviceable loads, thus underestimating the ductility continuous beams may possess by allowing an arbitrary redistribution of elastic moments. The amount of redistribution permitted by the various codes varies between 20 and 35%. This cannot be fully justified, and may lead to an underestimation of reinforced concrete ductility due to the limiting concrete ultimate strain to a certain arbitrary value, i.e. (3000 and 3500 microstrain for the ACI and the three other codes respectively).

16. The computed values from the codes moment curvature relationship indicated that the limitations on the neutral axis depth ratio are high, when comparing design curves to computed values. The modelled result suggests that it may be necessary to reduce the neutral axis depth in BS 8110, such that the neutral axis depth ratio should not be greater than 0.25 when designing for maximum redistribution of 30%. The reduction of the neutral axis depth ratio requirement of BS 8110 (although restrictive it may be) at maximum redistribution is in general agreement with the current design practice in both the EC 2 and the CEB-FIP Model Code. The suggested alteration is graphically shown in **Figure 9-1**.

17. Material, geometric and loading conditions affect the degree of rotation capacity that may occur in the beams, thus affecting the ductility of the beams.

18. Ultimate strain levels of the tensile reinforcement may be used as a failure criterion to control the amount of rotation capacity that a beam can undergo.

19. The modelled results of the idealised beams in section 8.13 suggest that there is more than one critical value of the amount of tensile reinforcement when plotted against the rotation capacity of a section. The reason for this being that different failure criteria and different geometric and loading conditions used in the modelling affect the movement of the point of the critical reinforcement ratio of the section. The results suggest that for reinforcement percentages smaller than a critical value, the section may fail due to the rupture of the reinforcement. For this failure mode, the rotation capacity decreases with decreasing reinforcement ratio. For reinforcement ratios larger than a critical value, the beam may fail due to crushing of the concrete. As the results indicated, a specific value for the critical reinforcement ratio cannot be defined. The author sees this as a significant result, since previous modelling done by Eligehausen and Langer (1987) defined only one critical reinforcement ratio. This does not entirely agree with the results obtained here.

9.3 Recommendations for Further Work

Based on the experimental and the modelled results obtained using the numerical model ARMUNY, and the graphs produced in Chapter Eight of percentage of redistribution versus neutral axis depth ratio, the author suggests the following for further work:

Experimental Work

The experimental investigation presented in this thesis in Part One was done on limited reinforcement ratios and one class of concrete. The author suggests that further experimental work should be done on percentages of reinforcement between 0.2 up to 1.2 with 12, 10 and 8 mm bar diameters with varying ratios of compression reinforcement and different concrete grades. The reason for this, in the author's view, is to investigate whether a critical value of reinforcement as Eligehausen and Langer (1987) recommended actually exists. The author further suggests the use of accurate electrolevels in conjunction with strain gauge data to obtain satisfactory measured values of rotations.

Numerical Modelling

A. The model developed by the author is a flexible tool and can be used to model propped cantilevers loaded by a point load at any position along the beam. Therefore, it can be used as the basis for further modelling. The author recommends the model can be further developed to model beams with many point loads and uniformly distributed loads. Such developments will facilitate the use of the model as a parametric tool to investigate and model a variety of beams with different ratios of reinforcement. Furthermore, the author recommends that the two main modelling programs BSECT and ARMUNY, the first being developed by Scott and the latter by the author, can be merged to formulate a comprehensive model.

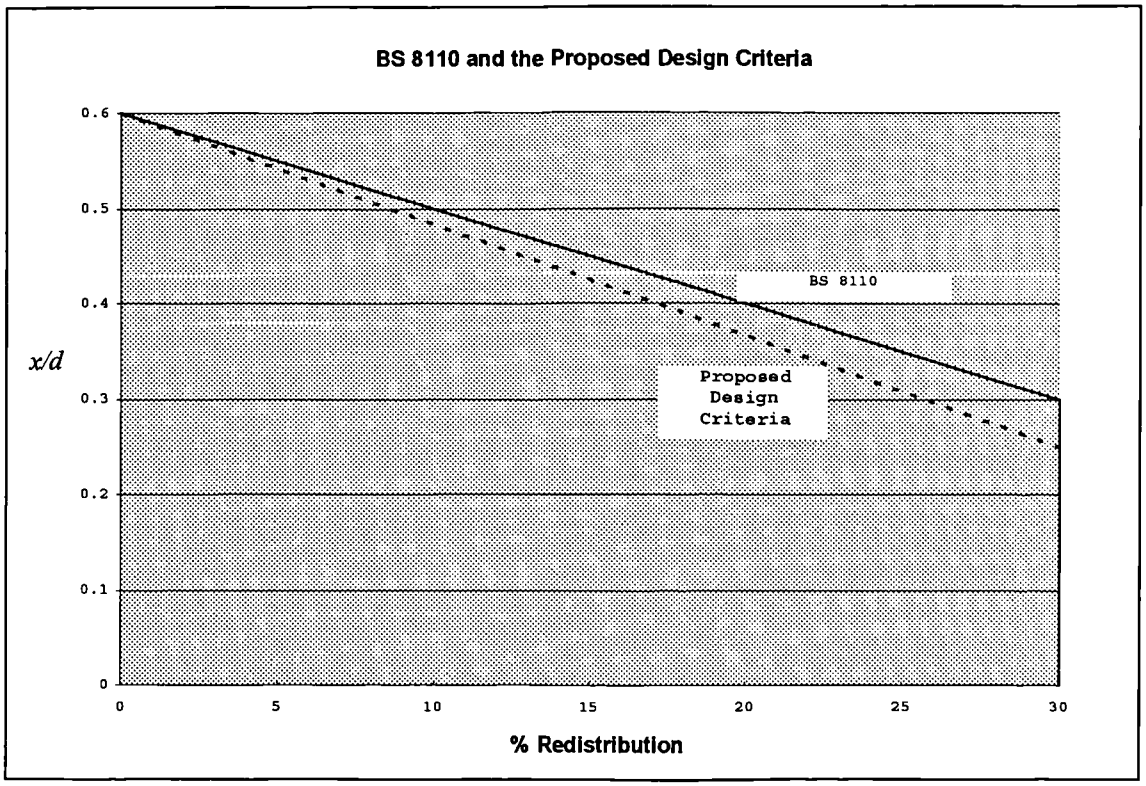

Figure 9-1: Proposed alteration to the BS 8110 redistribution criteria

REFERENCES

American Concrete Institute, (1995), ACI 318-95 Building Code Requirements for Structural Concrete, Detroit.

Australian Code Of Practice, (1988), AS 3600, Section 7.6.8, pp. 44.

Baker, A. L. L., (1949), "A Plastic Theory of Design for Ordinary Reinforced and Prestressed Concrete Including Moment Redistribution in Continuous Members", Magazine of Concrete Research, Vol. 1, No. 2, pp. 57-66.

Baker, A. L. L. and Amarakone, A. M. N., (1964),"Inelastic Hyperstatic Frame Analysis", Proceedings of the International Symposium on Flexural Mechanics of Reinforced Concrete, Miami, pp. 85-142.

Barnard, P. R., (1964), "The Collapse of Reinforced Concrete Beams", Proceedings of the International Symposium on the Flexural Mechanics of Reinforced Concrete, Miami, Fla., November, pp. 501-520.

Barnard, P. R., and Johnson, R. P., (1965), "Plastic Behaviour of Continuous Composite Beams", Proceedings of the Institution of Civil Engineers, Vol. 32, October, pp 180-197.

Bresler, B. and Macgregor, G., (1967), "Review of Concrete Beams Failing in Shear", Journal of the Structural Division, Vol. 93, No. ST1, February, pp. 343-372.

British Standard Institute, (1957), "The Structural Use of Reinforced Concrete in Buildings", Code of Practice, CP114, BSI, London.

British Standards Institution, (1985), "The Structural Use of Concrete" BS8110: Part 1 and 2, B.S.I, London.

Burnett, E. F. P., (1964), "Reinforced Concrete Linear Structures At Ultimate Load", Proceedings of the International Symposium on the Flexural Mechanics of Reinforced Concrete, pp. 29-51.

Burnett, E. F. P., (1972), "Rotation Capacity of Reinforced Concrete Flexural Elements", Inelasticity and Non-linearity In Structural Concrete, Study No. 8, Solid Mechanics Division, University of Waterloo, Waterloo, Canada, pp. 181-210.

Carreira, D. J. and Chu, K-H, (1986), "The Moment-Curvature Relationship of Reinforced Concrete Members", ACI Journal, March-April, pp 191-198.

Chanakya, Arya, (1993), "*Design of Structural Elements: Concrete, Steelwork, Masonry and Timber Design to British Standards and Eurocodes*", E & FN Spon, London, 360 pp.

Clark, L. A. and Thorgood, P., (1985), "Shear Strength of Concrete Beams in Hogging Regions", Proceedings of the Institute of Civil Engineers, Vol. 79, Pt. 2, June, pp 315-326.

Cohn, M. Z. and Ghosh, S. K., (1973), "Ductility of Reinforced Concrete Sections in Bending", Symposium on Inelasticity and Non-Linearity in Structural Concrete, Study No. 8, Solid Mechanics Division, University of Waterloo Press, pp. 111-146.

Ghosh, S. K. and Cohn, M. Z., (1973), "Nonlinear Analysis of Strain Softening Structures", Symposium on Inelasticity and Non-linearity in Structural Concrete, Study no. 8, Paper 12, University of Waterloo Press, pp. 315-332.

Cohn, M. Z. and Gosh, S. K., (1973), "Ductility of Reinforced Concrete Sections in Bending", Inelasticity and Non-Linearity in Structural Concrete, Solid Mechanics Division, University of Waterloo, Study No. 8, pp. 111-180.

Cohn, M. Z. and Lounis, Z, (1991),"Moment redistribution in structural concrete codes", Canadian Journal of Civil Engineering, Vol. 18, pp. 97-108.

Cohn, M. Z., (1979), "Nonlinear Design of Concrete Structures: Problems and Prospects", Nonlinear Design of Concrete Structures, Study No.14, University of Waterloo, Canada, pp. 3-42.

Comité Euro-International Du Beton CEB-FIP (1990), Model Code

Comité Euro-International Du Beton, (1985), Design Manual on Cracking and deformation. CEB, Lausanne.

Conner, H. W. , Kaar, P. H. and Corley, W. G., (1970), "Moment Redistribution in Precast Concrete Frames", Journal of the Structural Division, Proceedings of the ASCE, Vol. 96, no. (ST3), pp 637-661.

Corley, G. "Rotational Capacity of Reinforced Concrete Beams", (1966), Journal of the Structural Division, Proceedings of the American Society of Civil Engineers, Proceedings Paper 4939, Vol. (93,ST2), pp 121-146.

Cranston, W. B., (1965), "A Computer Method for Inelastic Analysis of Plane Frames", Technical Report No. TRA/386, Cement and Concrete Association, London, March, 38 pp.

Eligehausen, R. and Langer, P, (1987), "*Rotation Capacity of Plastic Hinges and Allowable degree of Moment Redistribution*", MSc. Dissertation (English), Stuttgart University, January 41 pp.

Eligehausen, R. and Fabritius, E., (1991), "Tests on Continuous Slabs Reinforced with Welded Wire Mesh", Obtained by the author through private correspondence.

Eligehausen, R. and Longfie, L. I., (1992),"Rotation Capacity of Prestressed Concrete Members", International Conference, "Bond In Concrete, From Research To Practice", Riga Latvia October 15-17, pp 2-58 to 2-67.

Ernest, G. C., (1959), "Ultimate Loads and Deflections", Journal of the American Concrete Institute, June, pp 274-286.

Eurocode 2, EC 2, (1992), *"Design of concrete structures: Part 1. General Rules and Rules for Buildings"*.

Ghosh, S. K. and Cohn, M. Z., (1972), "Ductility of Reinforced Concrete Sections in Combined Bending and Axial Load", Inelasticity and Non-Linearity in Structural Concrete, University of Waterloo Press, pp. 147-180.

Glanville, W. H. and Thomas, F. G. (1935), "The Redistribution of Moments in Reinforced Concrete Beams and Frames", Paper No. 5061, Journal of the Institution of Civil Engineers, London, Vol. 3. pp. 291-329.

Gupta, A. K. and Maestrini, S. R., (1990), "Tension-Stiffening Model for Reinforced Concrete Bars", Journal of Structural Engineering, Vol. 116, No. 3, March pp. 769-167.

Hawkins, N. M., Sozen, M. A. and Siess, C. P., (1964), "Behavior of Continuous Prestressed Beams", Proceedings of the International Symposium on the Flexural Mechanics of Reinforced Concrete, Miami, Fla, Nov. pp 259-293.

Hognestad, E., Hanson, N. W., and Mchenry, D., (1955), "Concrete Stress Distribution in Ultimate Strength Design", Journal of the American Concrete Institute, No. 52-28, December pp 455-479.

Hsu, C. T., (1983), "A Simple Nonlinear Analysis of Continuous Reinforced Concrete Beams", Journal of Engineering and Applied Sciences, Vol. 2, pp. 267-276.

Kemp, A. R., (1981), "Ductility and Moment Redistribution in Reinforced Concrete Beams", Civil Engineering of South Africa, Vol. 23, No. 5, May, pp. 175-177.

Kent, D. C., and Park R., (1971), "Flexural Members with Confined Concrete", Journal of Structural Division, ASCE, (97, ST7), July, pp. 1961-1991.

Kong, F. K. and Evans, R. H., (1990), *"Reinforced and Prestressed Concrete"*, Chapman and Hall, 3rd Edition, Hong Kong, 508 pp.

Kong, F. K. et al., (1983), *"Handbook of Structural Concrete"*, Pitman Books Limited, London, pp. 40-1 to 41-44.

Kraauthammer, T., Shahriar, S. and Shanaa, H. M., (1987), "Analysis of Reinforced Concrete Beams Subjected to Severe Concentrated Load", ACI Structural Journal, Nov-Dec., pp. 473-481.

Lee, L. H. N., (1955), "Inelastic Behaviour of Reinforced Concrete Members", Transactions of the American Society of Civil Engineers, Vol. 120, pp. 181-207.

Macchi, G., (1965), "Elastic Distribution of Moments on Continuous Beams, "Flexural Mechanics of Reinforced Concrete BeamsACI Special Publication", SP-12, pp 237-257.

Mattock, A. H., (1983), "Secondary Moments and Moment Redistribution in ACI 318-77 Code", Proceedings International Symposium on Nonlinearity and Continuity in Prestressed Concrete, Preliminary publication 3, University of Waterloo, Ontario, Canada, pp. 27-48.

Mattock, A. H., (1959), "Limit design for Structural Concrete", Journal of the Portland Cement Association, Research and Development Laboratories, May, pp. 15-24.

Mattock, A. H., (1965), "Rotational Capacity of Hinging Regions in Reinforced Concrete Beams, "Flexural Mechanics of Reinforced Concrete, Proceedings of the International Symposium (ACI Special Publication), SP-12, pp. 143-180.

Mo, Y. L, (1986), "Moment Redistribution in Reinforced Concrete Frames", ACI Journal, Technical Paper, July-August, pp 577-587.

Naaman, A. E. et al., (1986), "Analysis of Ductility in Partially Prestressed Concrete Flexural members", Prestressed Concrete Institute Journal, Vol. 31, No. 3, pp. 64-87.

Nawy, E. G., Danesi, R. F. and Groako, J. J., (1968), "Rectangular Spiral Binders Effect on Plastic Hinge Rotation Capacity in Reinforced Concrete Beams", ACI Journal, December, pp. 1001-1010.

New Zealand Standard, (1982), "The design of Concrete Structures", Part 1, Section 3.5.3.4,.Nz3101, pp. 23.

Nilson, A. H., (1978), "*Design of Prestressed Concrete*", John Wiley and Sons, New York, pp. 286.

Park, R. and Ruitong, D., (1988), "Ductility of Doubly Reinforced Concrete Beam Section", ACI Structural Journal, Mar-Apr., pp. 217-225.

Park, R. and Sampson, R. A., (1971), "Ductility of Reinforced Concrete Columns", Master of Engineering Report, University of Canterbury , Chritchurch, New Zealand, 51 pp.

Popovics, S., (1970), " A Review of Stress-Strain Relationship of Concrete", Journal of the American Concrete Institute, Vol. 67, No. 14, March, pp. 243-248.

Prakhya, G. K. V. and Morley, C. T., (1990), "Tension Stiffening and Moment Curvature Relations of Reinforced Concrete Elements", ACI Structural Journal, Vol. 87, No. 5, Sept-Oct., pp. 597-605.

Rajagopolan, K. S. and Ferguson, P. M.(1968), Explarotary Sheer test emphasizing percentages of Longitudinal Steel, Proceedings of The ACI, Vol. 65, No. 8, pp. 634-638.

Regan, P. E. and Yu, C. W, (1973), *"Limit State Design of Structural Concrete"* Pub. Chatto and Windus, London, pp. 63.

Reynolds, C. E. and Steedman, J. C., (1988), *"Reinforced Concrete Designer Handbook"*, 10th Edition, E and FN Spon, London, pp t136.

Riva, P. and Cohn, M. Z., (1994), "Rotation Capacity of Structural Concrete", Magazine of Concrete Research, Vol. 46, No. 168, September, pp. 223-234.

Riva, P. and Cohn, M. Z., (1989), "Engineering Approach to Nonlinear Analysis of Concrete Structures", Journal of Structural Engineering, Vol. 116, No. 8, June, pp. 2162-2186.

Rosenblueth, E., and Diaz De Cassio, R., (1964), "Instability Considerations in Limit Design of Concrete Frames", Proceedings of the International Symposium on the Flexural Mechanics of Reinforced Concrete, Miami, Fla., November, pp 439-463.

Roy, H. E. H. and Sozen, M. A., (1964), "Ductility of Concrete", Proceedings of the International Symposium on the Flexural Mechanics of Reinforced Concrete, Miami, Fla, November, pp 213-224.

Sakai, Y., Iwase, H., Rokugo, K. and Koyanagi, W., (1984), "Failure Behaviour of Two-span Continuous Beams Under Bending", Transactions of the Japan Concrete Institute, Vol. 6, pp. 711-716.

Scholz, H., (1993), " Contribution to Redistribution of Moments in Continuous Reinforced Concrete Beams", ACI Structural Journal, Mar-Apr., pp 150-155.

Scott, R. H., (1983), "The Short-term Moment Curvature Relationship for Reinforced Concrete Beams", Proceedings of the Institute of Civil Engineers, Vol. 75, Part 2, Dec pp. 725-734.

Scott, R. H. and Gill, P. A. T., (1984), "A modern Data Collection System", Strain, May, pp. 63-68.

Scott, R. H., (1985), "Tension Stiffening Effects in Reinforced Concrete Members", PhD thesis, University of Durham, July, 193 pp.

Scott, R. H. and Gill, P. A. T., (1986), "Techniques in Experimental Stress Analysis for Reinforced Concrete Structures", *Experimental Stress Analysis*, Editor: Wieringa, H., Martinus Nijhoff Publishers, Dordrecht, Netherlands. pp. 87-96.

Scott, R. H., (1989), "The Strain Gauging of Fabric Reinforcement", Report, Apr-Dec. A Development Programme Funded by the Fabric Reinforcement Development Association, 13 pp.

Snowdon, L. C. , (1970), "Classifying reinforcing bars from bond strength", Building Research Station, Current Papers, 36/70 London, April, pp 36-70.

The Institution of Civil Engineers, (1964), "Ultimate Load Design of Concrete Structures", Report of the Research Committee, pp 17.

United Nation Educational Scientific and Cultural Organisation UNISCO (1971), "*Reinforced Concrete: An International Manual*", London: Butterworth, pp. 19-22.

Wang, Chu-Kia, and Salmon, C. G., (1979), "*Reinforced Concrete Design*", 3rd Edition, New York, Harper and Row publishers, 918 pp.

Wilby, C. B., (1991), "*Concrete Materials and Structures: A University Civil Engineering Text*", Cambridge University Press, pp 54-56.

Yu, C. W. and Hognestad, E., (1958), "Review of Limit Design For Structural Concrete", Journal of the Structural Division, Proceedings of the American Society of Civil Engineers, paper 1878, ST 8, December, pp. 1878-1 to 1878-28.